Combustion Research
Gas Phase Chemical Physics Program

DOE Principal Investigators'
Abstracts

May, 2014

Chemical Sciences, Geosciences, and Biosciences Division
Office of Basic Energy Sciences
Office of Science
U.S. Department of Energy

The research grants and contracts described in this document are supported by the U.S. DOE Office of Science, Office of Basic Energy Sciences, Chemical Sciences, Geosciences and Biosciences Division.

Foreword

This collection of active research abstracts illustrates the breadth and depth of basic research supported by the Department of Energy's Office of Basic Energy Sciences (BES) and, in large measure, by the chemical physics program that contributes to the development of a predictive capability for combustion processes. The long-term objective of this effort is the provision of theories, data, and procedures to enable the development of reliable computational models of combustion processes, systems, and devices.

We appreciate the privilege of serving in the management of this research program. In carrying out these tasks, we learn from the achievements and share the excitement of the research of the many sponsored scientists and students whose work is summarized in the abstracts published on the following pages.

We thank all of the researchers whose dedication and innovation have advanced DOE BES research. We look forward to our assembly in 2015 for our 35th annual meeting.

Jeff Krause
Mark Pederson
Wade Sisk

Table of Contents

Table of Contents

Abstracts of Principal Investigator Presentations

The Chemical Dynamics Beamline

Musahid Ahmed, Kevin Wilson & Oleg Kostko
Chemical Sciences Division, Lawrence Berkeley National Laboratory
MS 6R2100, 1 Cyclotron Road, Berkeley, CA-94720, mahmed@lbl.gov

Program Scope: The Chemical Dynamics Beamline, located in the Advanced Light Source (ALS) at Lawrence Berkeley National Laboratory (LBNL), is a national user facility providing state-of-the-art experimental resources for visiting scientists and staff to undertake studies of fundamental chemical processes. Much of the work is related to combustion, energy production and utilization, environmental, and other chemical reactions on interfaces. The beamline is devoted to the study of chemical processes using vacuum ultraviolet (VUV) radiation. Synchrotron based photoionization mass spectrometry on two experimental platforms (molecular beam & aerosol sampling) are applied to a variety of problems of relevance to the Gas Phase Chemical Physics program. A miniature shock tube (Rob Tranter, ANL), pyrolytic reactors (Ralf Kaiser, Hawaii & Barney Ellison, Colorado), and a jet stirred reactor (Steve Leone, Berkeley) have all been incorporated into the molecular beams apparatus. The aerosol mass spectrometer plays a critical role in real time measurements of soot formation chemistry, the results of which are reported by Nils Hansen and Hope Michelson (Sandia, CRF).

Recent Progress and Future Plans:

Formation mechanisms of PAH's- The formation mechanisms of polycyclic aromatic hydrocarbons (PAHs) with indene and naphthalene cores in hydrocarbon-based combustion processes are being examined in collaboration with Ralf Kaiser (Hawaii) in a high temperature 'chemical reactor' where free radicals are reacted with target hydrocarbons. The formation of the aromatic indene molecule via the reaction of the phenyl radical with allene is facile and enhanced compared to its reaction with propyne, enhancement of factor of about 7 was observed for allene vs propyne. In the reaction of phenyl radicals (C_6H_5) with propylene (C_3H_6) it is suggested that the methyl and hydrogen loss are the two major reaction pathways with branching ratios of 86 ± 10% and 14 ± 10%. For the C_8H_8 isomers, Styrene ($C_6H_5C_2H_3$) was found to be the exclusive product, whereas for C_9H_{10} isomers, 3-phenylpropene, cis-1-phenylpropene, and 2-phenylpropene had branching ratios of 96 ± 4%, 3 ± 3%, and 1 ± 1% respectively. The reaction of phenyl radicals (C_6H_5) with 1,3-butadiene ($H_2CCHCHCH_2$) reveals that the atomic hydrogen (H), methyl (CH_3), and vinyl (C_2H_3) losses are open with estimated branching ratios of about 86 ± 4%, 8 ± 2%, and 6 ± 2%, respectively. Analysis indicate the formation of three $C_{10}H_{10}$ isomers (trans-1,3-butadienylbenzene, 1,4-dihydronaphthalene, 1-methylindene), three C_9H_8 isomers (indene, phenylallene, 1-phenyl-1-methylacetylene), and a C_8H_8 isomer (styrene). We also explored the reaction of phenyl radicals (C_6H_5) with acetylene (C_2H_2) to verify the hydrogen abstraction-acetylene addition (HACA) mechanism under controlled combustion-like conditions. Two key products postulated to be formed in the HACA mechanism: phenylacetylene (C_8H_6) and the prototypical PAH naphthalene ($C_{10}H_8$) are identified. Formation of phenylacetylene through hydrogen emission is the first step in the HACA mechanism sequence involving acetylene addition to an aromatic radical, here the phenyl radical. The second HACA mechanism step, a subsequent acetylene addition to either phenylacetylene (C_8H_6) or its intermediate prior to hydrogen emission (C_8H_7) yields the final PAH product naphthalene ($C_{10}H_8$) through cyclization and hydrogen abstraction or addition, respectively. The building blocks of nitrogenated PAH's (NPAH's) are being studied via the reactions of phenyl radicals with vinylcyanide (C_2H_3CN) and acetonitrile (CH_3CN) where pyridine has been identified under combustion like conditions. Future experiments will follow the formation of PAHs with indene and naphthalene cores via reactions of aromatic (AR) and resonantly stabilized free radicals (RSFR) with unsaturated hydrocarbons. The primary focus will be on the phenyl (C_6H_5) and benzyl (C_7H_7) ARs as well as propargyl (C_3H_3) and allyl (C_3H_5) RSFRs with C2 to C4 hydrocarbons. We are enlarging the studies by incorporating nitrogen into the systems to probe the formation of NPAHs. We are proposing to investigate the reactions of aromatic [phenyl (C_6H_5) and benzyl (C_7H_7)] as well as resonantly stabilized free radicals [propargyl (C_3H_3) and allyl (C_3H_5)] with molecular oxygen (O_2) – the *key* process to degrade radicals in combustion systems.

Fundamental Processes in the Thermal Cracking of Biomass- Thermochemical processing of biomass, with the goal of producing synthesis gas (CO and H_2) is an important pathway towards the production of renewable fuels. Understanding of this process is incomplete, however, as even the thermolysis chemistry of many of the organic molecules encountered in these processes is poorly understood or completely unknown. Our strategy is focused on study of the initial molecular processes that occur when the molecular constituents of lignin are heated to temperatures of 1000 K and higher, thereby gaining insight into the physicochemical basis of this emerging and important technology. To this end, we use a miniature, short residence time flow reactor coupled to synchrotron radiation, computational fluid dynamics and theoretical chemistry to determine the identity of the elementary decomposition pathways in collaboration with Barney Ellison (Colorado), John Daily (Colorado) & John Stanton (Texas). We have focused on a molecule that has proven to be a ubiquitous biomass cracking and combustion intermediate – cyclopentadienone (C_5H_4=O), as well as 2,5-dimethylfuran, which is the first legitimate biofuel that we have studied. Specifically, we have determined that C_5H_4=O yields acetylene and vinylacetylene upon thermolysis, but the relative quantities of the two products and chemical mechanisms for these processes are currently being analyzed. Similarly, pyrolysis of 2,5-dimethylfuran leads to an observed set of products rather different from what might be expected based on our earlier work with furan, and indeed are inconsistent with some interpretations already in the literature. In the future we seek to understand the decomposition of a classic "anti-aromatic" organic molecule (C_5H_4=O) and investigate how a "real" biofuel produces energy.

Atmospheric, Combustion and Environmental Chemistry of Particulate Matter

Significant effort by staff and users of the Chemical Dynamics Beamline has been dedicated to understanding heterogeneous free radical chemistry of hydrocarbon droplets and particles. The overall goal of this work is to better elucidate interfacial reaction mechanisms and rates and to determine how surface reactions might differ from analogous processes in isolated gas phase molecules.

Isomer-Resolved Chemistry: Significant efforts have been devoted to combine two dimensional gas phase chromatography with VUV photoionization mass spectrometry (2DVUVMS). This work (done in collaboration with Allen Goldstein's group at UC Berkeley) has revealed new details about complex hydrocarbon samples (fuel) as well as isomer level product distributions of heterogeneous oxidation reactions. The viability of the proposed 2DVUVMS technique was demonstrated for the analysis of diesel fuel—a prototypical environmental pollutant whose chemical complexity itself is a stringent test of any new analytical technique. This technique was used for the analysis of primary organic aerosol collected in the Caldecott tunnel (Berkeley, CA). In this work, unprecedented chemical characterization of primary aerosol was achieved, with a mass closure of 80 ± 30 %. The primary combustion aerosol was characterized by number of carbon atoms (N_C), number of double bond equivalents (N_{DBE}) and degree of molecular branching. This in depth analysis revealed that lubricating oil is the dominant component of particulate pollution for both gasoline and diesel powered vehicles. This compositional analysis of diesel fuel has led to the detailed study of the chemistry of model compounds (branched, linear, and cyclic alkanes) in an effort to examine how molecular structure influence heterogeneous reaction pathways with hydroxyl radicals.

Radical-initiated heterogeneous oxidation can affect the lifetime and chemical composition of organic aerosols in the troposphere. Insights into the influence of molecular structure and thermodynamic phase on chemical mechanisms are obtained by combining two dimensional gas chromatography with mass spectrometry to identify products of the OH-initiated oxidation of submicron particles composed of either *n*-octacosane ($C_{28}H_{58}$, a linear alkane) or squalane ($C_{30}H_{62}$, a highly branched alkane). A common pattern is observed in the positional isomers of octacosanone and octacosanol, with functionalization enhanced towards the end of the molecule. This suggests that relatively large linear alkanes are structured at the surface of submicron particles such that their ends are oriented towards the gas phase. For squalane, positional isomers of first-generation ketones and alcohols form in distinct patterns, which are somewhat consistent with predictions of gas phase H abstraction rates predicted via structure activity relationships. In particular, ketones are favored on carbons immediately adjacent to the tertiary carbons, while hydroxyl groups tend to form towards the end of the carbon backbone. First-generation products also contain some

hydroxyl-containing molecules with two total oxygen atoms. These results suggest that alkoxy radicals are important intermediates and undergo both intramolecular (isomerization) and intermolecular (chain propagation) hydrogen abstraction reactions. Oxidation products with carbon numbers less than the parent alkane are observed to a much greater extent for squalane than for *n*-octacosane oxidation and can be explained by the preferential scission of carbon-carbon bonds involving tertiary carbons (i.e., branching points). Cyclic alkanes also constitute a large fraction of aliphatic hydrocarbon emissions originating from incomplete combustion of diesel fuel and motor oil. To examine the heterogeneous chemistry of this class of compounds, cholestane ($C_{27}H_{48}$) was used as a model system. Analysis of the reaction via 2DVUVMS revealed that the first-generation functionalization products (cholestanones, cholestanals and cholestanols) account for up to 70% by mass of the total speciated compounds. 55% of the cholestanones/cholestanals are found to have the carbonyl group on the rings of the androstane skeleton; while 74% of cholestanols have the hydroxyl group on the rings. These results provided detailed insight into the oxidation chemistry of complex molecules at the isomer level, revealing new details about surface oxidation mechanisms.

Free Radical Chain Propagation Chemistry: A number of current and ongoing studies (with S.R. Leone) are examining the role of radical chain propagation, which is initiated at the surface of particles by hydroxyl radicals. Model systems are used to examine how the number of double bonds in a molecule promote radical chain cycling mechanism (e.g. H abstraction by alkyl and alkoxy radicals). For unsaturated model compounds, such as squalene, radical chain cycling is efficient at a sensitive function of oxygen content in the reactor. These results may indicate the important role that tertiary peroxy and alkoxy radicals might play in free radical chain reactions. Additional experiments have been conducted to isolate the role that alkoxy radicals play in free radical initiated oxidation. For these studies SO_2 is introduced into the reactor, which is observed to react preferentially with peroxy radicals to form a large population of alkoxy radicals with the droplet whose chemistry is examined using the VUV aerosol mass spectrometer located at the beamline. This work is particularly interesting as analogous reactions of SO_2 with gas phase peroxy radicals have been shown to be unfavorable, which might suggest a unique reaction pathways for this chemistry at a hydrocarbon surface.

DOE sponsored research (2011-2013)

N. Hansen, S. A. Skeen, H. A. Michelsen, K. R. Wilson, and K. Kohse-Höinghaus, "Flame Experiments at the Advanced Light Source: New Insights into Soot Formation Processes," (2013) J. Vis. Expt. (In press)

H. Zhang, C. Ruehl, A. Chan, T. Nah, D. Worton, G. Isaacman, A. Goldstein, and K. R. Wilson, "OH- Initiated Heterogeneous Oxidation of Cholestane: A Model System for Understanding the Photochemical Aging of Cyclic Alkane Aerosols," J. Phys. Chem. A. **117**, 12449 (2013)

T. Nah, S. H. Kessler, K. E. Daumit, J. H. Kroll, S. R. Leone and K. R. Wilson, "OH- initiated oxidation of sub-micron unsaturated fatty acid particles," Phys. Chem. Chem. Phys., **15**, 18649 (2013)

K. N. Urness, A. Golan, J. W. Daily, M. R. Nimlos, J. F. Stanton, M. Ahmed, and G. B. Ellison, "Pyrolysis of Furan in a Microreactor," J. Chem. Phys., **139**, 124305 (2013)

F. Bell, Q. N. Ruan, A. Golan, P. R. Horn, M. Ahmed, S. R. Leone, and M. Head-Gordon, "Dissociative Photoionization of Glycerol and its Dimer Occurs Predominantly via a Hydrogen-Bonded Ion Complex," J. Am. Chem. Soc., **135,** 14229 (2013)

A. W. H. Chan, G. Isaacman, K. R. Wilson, D. R. Worton, C. R. Ruehl, T. Nah, D. R. Gentner, T. R. Dallman, T. W. Kirchstetter, R. A. Harley, J. B. Gilman, W. C. Kuster, J. A. de Gouw, J. H. Offenberg, T. E. Kleindienst, Y. H. Lin, C. L. Rubitschun, J. D. Surratt, and A. H. Goldstein, "Detailed Chemical Characterization of Unresolved Complex Mixtures (UCM) in Atmospheric Organics: Insights into Emission Sources, Atmospheric Processing and Secondary Organic Aerosol Formation," J. Geophys. Res., [Atmos.] **118**, 6783 (2013)

C. R. Ruehl, T. Nah, G. Isaacman, D. R. Worton, A. W. H. Chan, K. R. Kolesar, C. D. Cappa, A. H. Goldstein, and K. R. Wilson, "The influence of molecular structure and aerosol phase on the heterogeneous oxidation of normal and branched alkanes by OH," J. Phys. Chem. A., **117**, 3990 (2013)

S. A. Skeen, H. A. Michelsen, K. R. Wilson, D. M. Popolan, A. Violi, and N. Hansen, "Near-threshold Photoionization Mass Spectra of Combustion-Generated High-Molecular-Weight Soot Precursors," J. Aerosol Sci., **58,** 86 (2013)

L. Lee, P. Wooldridge, T. Nah, K. R. Wilson, and R. Cohen, "Observation of Rates and Products in the Reaction of NO_3 with Submicron Squalane Aerosol," Phys. Chem. Chem. Phys., **15**, 882 (2013)

A. Golan, M. Ahmed, A. M. Mebel, and R. I. Kaiser, "A VUV photoionization study of the multichannel reaction of phenyl radicals with 1,3-butadiene under combustion relevant conditions," Phys. Chem. Chem. Phys., **15**, 341 (2013)

D. Gentner, G. Isaacman, D. R. Worton, A. W. H. Chan, T. R. Dallmann, L. Davis, S. Liu, D. A. Day, L. M. Russell, K. R. Wilson, R. Weber, A. Guha, R. A. Harley, and A. H. Goldstein, "Elucidating Secondary Organic Aerosol From Diesel and Gasoline Vehicles Through Detailed Characterization of Organic Carbon Emissions," PNAS., **109**, 18318 *(*2012)

A. Golan and M. Ahmed, "Molecular beam mass spectrometry with tunable vacuum ultraviolet (VUV) synchrotron radiation," J. Vis. Exp., **68**, e50164 (2012)

A. G. Vasiliou, K. M. Piech, B. Reed, X. Zhang, M. R. Nimlos, M. Ahmed, A. Golan, O. Kostko, D. L. Osborn, J. W. Daily, J. F. Stanton, and G. B. Ellison, "Thermal Decomposition of CH_3CHO Studied by Matrix Infrared Spectroscopy and Photoionization Mass Spectroscopy," J. Chem. Phys., **137**, 164308 (2012)

G. Isaacman, A. W. H. Chan, T. Nah, D. R. Worsnop, C. R. Ruehl, K. R. Wilson, and A. Goldstein, "Heterogeneous OH oxidation of motor oil particles causes selective depletion of branched and less cyclic hydrocarbons," Environ. Sci. Technol., **46**, 10632 (2012)

J. H. Kroll, J. D. Smith, D. R. Worsnop, and K. R. Wilson, "Characterisation of lightly oxidized organic aerosol formed from the photochemical aging of diesel exhaust particles," Environ. Chem., **9**, 211 (2012)

F. Zhang, R.I. Kaiser, A. Golan, M. Ahmed and N. Hansen, "A VUV Photoionization Study of the Combustion-Relevant Reaction of the Phenyl Radical (C_6H_5) with Propylene (C_3H_6) in a High Temperature Chemical Reactor," J. Phys. Chem. A., **116**, 3541 (2012)

S. H. Kessler, T. Nah, K. E. Daumit, J. D. Smith, S. R. Leone, C. E. Kolb, D. R. Worsnop, K. R. Wilson, and J. H. Kroll, "OH-initiated heterogeneous aging of highly oxidized organic aerosol," J. Phys. Chem. A., **116**, 6358 (2012)

G. Isaacman, K. R. Wilson, A. W. H. Chan, D. R. Worsnop, J. R. Kimmel, T. Nah, T. Hohaus, M. Gonin, J. H. Kroll, D. R. Worsnop, and A. H. Goldstein, "Improved resolution of hydrocarbon structures and constitutional isomers in complex mixtures using Gas Chromatography-Vacuum Ultraviolet-Mass Spectrometry (GC-VUV-MS)," Anal. Chem., **84**, 2335 (2012)

F. Goulay, A. J. Trevitt, J. D. Savee, J. Bowman, D. L. Osborn, C. A. Taatjes, K. R. Wilson, and S. R. Leone, "Product Detection of the CH Radical Reaction with Acetaldehyde," J. Phys. Chem. A., **116**, 6091 (2012)

K. R. Wilson, J. D. Smith, S. H. Kessler, and J. H. Kroll, "The Statistical Evolution of Multiple Generations of Oxidation Products in the Photochemical Aging of Chemically Reduced Organic Aerosol," Phys. Chem. Chem. Phys., **14**, 1468 (2012)

D. Ghosh, A. Golan, L. K. Takahashi, A. I. Krylov, and M. Ahmed, "A VUV Photoionization and Ab Initio Determination of the Ionization Energy of a Gas Phase Sugar (Deoxyribose)," J. Phys. Chem. Lett., **3,** 97 (2012)

F. Zhang, R. I. Kaiser, V. V. Kislov, A. M. Mebel, A. Golan and M. Ahmed, "A VUV Photoionization Study of the Formation of the Indene Molecule and Its Isomers," J. Phys. Chem. Lett., **2**, 1731 (2011)

S. H. Kessler, T. Nah, A. Carrasquillo, J. T. Wayne, D. R. Worsnop, K. R. Wilson, and J. H. Kroll, "Formation of Secondary Organic Aerosol from the Direct Photolytic Generation of Organic Radicals," J. Phys. Chem. Lett., **2**, 1295 (2011)

C. D. Cappa, D. L. Che, S. H. Kessler, J. H. Kroll, and K. R. Wilson, "Variations in Organic Aerosol Optical and Hygroscopic Properties Upon Heterogeneous OH Oxidation," J. Geophys. Res., [Atmos.], **116**, D15204 (2011)

A. G. Vasiliou, K. M. Piech, X. Zhang, M. R. Nimlos, M. Ahmed, A. Golan, O. Kostko, D. L.Osborn, J. W. Daily, J. F. Stanton, and G. B. Ellison, "The Products of the Thermal Decomposition of CH_3CHO," J. Chem. Phys., **135**, 014306 (2011)

C-L. Liu, J.D. Smith, D.L. Che, M. Ahmed, S.R. Leone, and K.R. Wilson, "The Direct Observation of Secondary Radical Chain Chemistry in the Heterogeneous Reaction of Chlorine Atoms with Submicron Squalane Droplets," Phys. Chem. Chem. Phys., **13**, 8993 (2011)

L. K. Takahashi, J. Zhou, O. Kostko, A. Golan, S.R. Leone, and M. Ahmed, "Vacuum-Ultraviolet Photoionization and Mass Spectrometric Characterization of Lignin Monomers Coniferyl and Sinapyl Alchohols," J. Phys. Chem. A, **115**, 3279 (2011)

C.D. Cappa and K. R. Wilson, "Evolution of organic aerosol mass spectra upon heating: implications for OA phase and partitioning behavior," Atmos. Chem. Phys., **11**, 1895 (2011)

J. H. Kroll, N. M. Donahue, J. L. Jimenez, S. H. Kessler, M. R. Canagaratna, K. R. Wilson, K. E. Altieri, L. R. Mazzoleni, A. S. Wozniak, H. Bluhm, E. R. Mysak, J. D. Smith, C. E. Kolb, D. R. Worsnop, "Carbon oxidation state as a metric for describing the chemistry of atmospheric organic aerosol," Nature Chem., **3**, 133 (2011)

Kinetic processes of importance in combustion

Millard H. Alexander (mha@umd.edu),[1] Lifang Ma,[†] Jacek Klos[‡]
Department of Chemistry and Biochemistry, University of Maryland, College Park, MD 20742-2021
Paul J. Dagdigian (pjdagdigian@jhu.edu)[§] and Qianli Ma[†]
Department of Chemistry, The Johns Hopkins University, Baltimore, MD 21218-2685

I. Program Scope

Our group studies inelastic and reactive collisions of small molecules, focusing on radicals important in combustion environments. Our goal is the better understanding of kinetic processes that may be difficult to access experimentally. An essential component is the accurate determination of potential energy surfaces (PESs). After fitting[1] the *ab initio* points to obtain global PESs, we treat the dynamics using time-independent (close-coupling) methods. Cross sections and rate constants for collisions of are determined with our Hibridon program suite.[2]

II. Recent Progress and Future Work

A. Rovibronic collisional relaxation of methylene

As a prerequisite to our recently published investigation of the rotational relaxation of CH_2 in its ground (^3X) state, we determined the dependence of the CH_2–He PES on the bending vibration of the molecule. By then averaging over the product of wavefunctions for two different bending vibrational levels, we can model ro-vibrational relaxation. This is less efficient by a factor of ~50. In addition, as shown in Fig. 1, here is no clear-cut dependence on the energy gap.

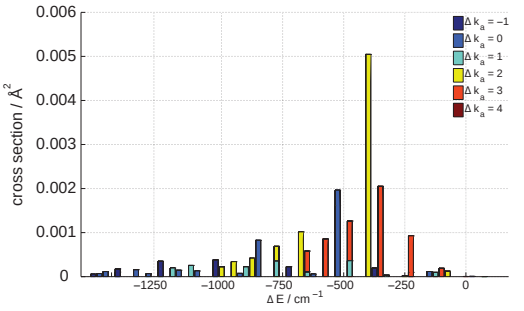

Fig. 1. Cross sections for relaxation out of the $NK_aK_c=5_{15}$ rotational level of the (0,1,0) vibrational manifold of $CH_2(X)$ into rotational levels of the ground (0,0,0) vibrational manifold. The colors differentiate transitions into different K stacks.

B. Collision-induced intersystem crossing in methylene.

The first excited ($^1\tilde{a}$) state of CH_2 lies close enough to the ground state that there exist several near-degeneracies between rotational levels, as shown in Fig. 2. Bley and Temps[3] suggested that

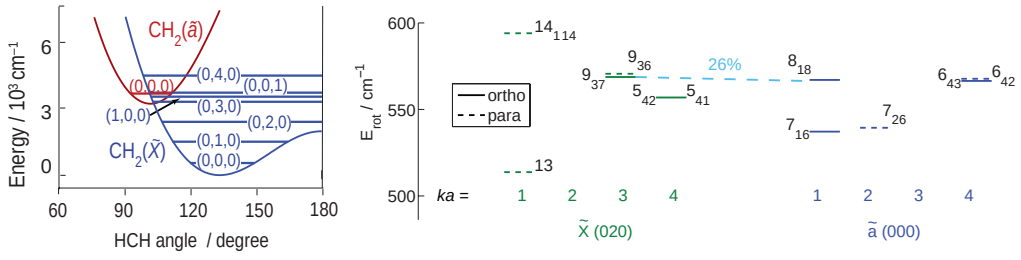

Fig. 2. (Left panel) relative positions of bend-stretch levels of the ground and first excited states of CH_2. (Right panel) High resolution illustration of the near degeneracy between the $\tilde{a}(000)$ 8_{18} and $X(020)$ 9_{37} rotational levels of *o*-CH_2.

spin-orbit mixing of these near degenerate could result in substantial collisional coupling. This

[1] Principal investigator; [†]Graduate student; [‡]Research Assistant Professor; [§]Senior investigator.

"gateway" mechanism was first proposed by Gelbart and Freed. [4]

We have applied this approach to transitions between the ^3X and $^1\tilde{a}$ states of CH_2. We have concentrated on the mixed $\tilde{a}\ 8_{18}$ and $X\ 9_{37}$ levels (See. Fig. 2). Work at Brookhaven, by Hall and Sears,[5] has shown that relaxation out of the $\tilde{a}\ 8_{18}$ level is anomalously slow, and a consequence of mixing with the $X\ 9_{37}$ level, which is less anisotropic. We are modeling relaxation in the presence of this gateway, making use of our recent work on solution of the master equation.[6]

C. Angularly resolved scattering of methyl radicals

Stimulated by our recent work,[7] Orr-Ewing (Bristol, UK) has applied molecular beam and velocity mapping imaging to the determination of differential cross sections for scattering of He by a photolytically- enerated beam of CD_3. REMPI detection of the scattered CD_3 allowed resolution of the rotational angular momentum n, but averaged over a subset of the projection quantum numbers.

Figure 3 shows the excellent agreement between experimental and our theoretical differential cross sections (from close-coupled calculation) for representative transitions involving n=2 levels. Approach of the perturber along and perpendicular to the symmetry axis of a nonlinear polyatomic leads to two anisotropies. The dynamics are correspondingly richer than for the scattering of a diatomic. We are exploring which features of the PES influence the scattering into various final levels. We also compared with scattering of He with another symmetric top molecule, ND_3,[8] for which DCS in collisions with He have recently been measured.[9]

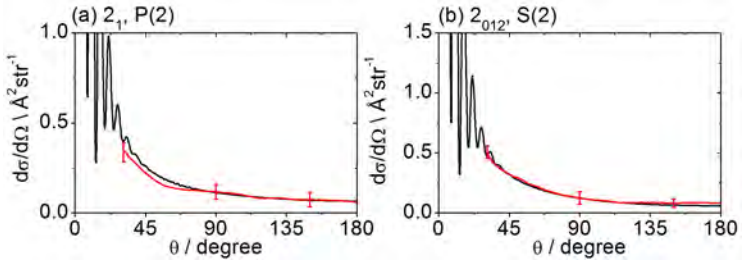

Fig. 3. DCSs for inelastic scattering of CD_3 radicals into (left panel) final rotational levels nk=21 and (right panel) 20+21+22. The REMPI line employed for detection is indicated, along with the range of k' projection levels contributing to the signal. Red curves: experiment; black curves: theory.

D. Exact determination of transport properties

Chemical kinetic models require knowledge of the relevant transport properties for an accurate description of the temporal and spatial dependence of the species concentrations, as well as for the calculation of flame velocities and the production of pollutants in combustion media. We have carried out a series of quantum scattering calculations on exemplary systems to assess the accuracy of simple isotropic Lennard-Jones (LJ) potentials to estimate transport properties.[10-12]

Two issues are of interest: (1) the reliability of the assumption of an isotropic potential and (2) the accuracy of the repulsive wall; the latter affects the temperature dependence of the collision integrals. For the OH–He and H–H_2O systems,[10, 12] inclusion of the full anisotropy leads to differences of only a few percent when compared with spherically averaged potentials. The latter are found to be significantly less repulsive than a LJ 12-6 potential; a LJ 9-6 potential is more realistic. For CH_2, especially in the low-lying excited $\tilde{a}$ state, the anisotropy of the PES significantly affects the transport properties.[11] This is a consequence of the low-lying LUMO, an effect that will be important in similar molecules, such as the BH_3 radical.

We are now studying transport properties for systems that possess deeply bound wells. Here the scattering calculations must be modified. We are adapting the quantum statistical capture theory of Manolopoulos and co-workers.[13] Our first application is to the H–O_2 system, which has both an attractive ($^2A''$) and a repulsive ($^4A''$) PES.

III. Interaction with Other Groups and DOE Synergy

Alexander and Dagdigian maintain a close interaction with Hall and Sears at Brookhaven. In addition to their collaborative work on collisional relaxation of CH_2, we are investigating pressure broadening cross sections and rates to complement the BNL measurements[14] on CN and to compare with forthcoming measurements on the OH $A - X$ transition by Ritchie at Oxford, UK. As discussed above, Alexander and Dagdigian continue to work with the group of Orr-Ewing on the determination of CD_3 differential cross sections in collisions with other species. Alexander's group has also collaborated closely with Chandler's group at Sandia Livermore on the inelastic scattering of the NO radical. Our current interest in transport properties was stimulated through extensive conversations with Brown (LBL) and Wagner (ANL).

IV. Publications and Submitted Journal Articles Supported by this Project (2011–2013)

1. L. Ma, M. H. Alexander, and P. J. Dagdigian, "Theoretical investigation of rotationally inelastic collisions of $CH_2(\tilde{a})$ with helium," J. Chem. Phys. 134, 154307 (13 pages) (2011)
2. M. H. Alexander, G. Hall, and P. J. Dagdigian, "The Approach to Equilibrium: Detailed Balance and the Master Equation," J. Chem. Educ. 88, 1538–1540 (2011).
3. P. J. Dagdigian and M. H. Alexander, "Theoretical investigation of rotationally inelastic collisions of the methyl radical with helium", J. Chem. Phys. **135**, 064306 (9 pages) (2011).
4. L. Ma, M. H. Alexander, and P. J. Dagdigian, "Theoretical investigation of rotationally inelastic collisions of $CH_2(\tilde{X})$ with helium," J. Chem. Phys. **136**, 224306 (9 pages) (2012).
5. P. J. Dagdigian and M. H. Alexander, "Exact quantum scattering calculation of transport properties for free radicals: OH($X\ ^2\Pi$)–helium," J. Chem. Phys. **137**, 094306 (7 pages) (2012).
6. Q. Ma, P. J. Dagdigian, and M. H. Alexander, "Theoretical study of the vibrational relaxation of the methyl radical in collisions with He," J. Chem. Phys. **138**, 104317 (10 pages) (2013).
7. P. J. Dagdigian and M. H. Alexander, "Exact quantum scattering calculations of transport properties: $CH_2(X\ ^3B_1, a\ ^1A_1)$–helium," J. Chem. Phys. **138**, 164305 (7 pages) (2013).
8. P. J. Dagdigian, "Theoretical investigation of collisional energy transfer in polyatomic intermediates," Int. Rev. Phys. Chem. **32**, 229–265 (2013).
9. P. J. Dagdigian and M. H. Alexander, "Exact quantum scattering calculations of transport properties for the H_2O–H system," J. Chem. Phys. **139**, 194309 (8 pages) (2013).
10. P. J. Dagdigian and M. H. Alexander, "Exact quantum scattering calculations of transport properties for the H_2O–H system," J. Chem. Phys. **139**, 194309 (8 pages) (2013).
11. Ondrej Tkáč, A. J. Orr-Ewing, P. J. Dagdigian, M. H. Alexander, J. Onvlee, and A. van der Avoird, "Collision dynamics of symmetric top molecules: A comparison of the rotationally inelastic scattering of CD_3 and ND_3 with He," J. Chem. Phys. **140**, xxxxxx (2014).

V. References

1. P. J. Dagdigian, "Theoretical investigation of collisional energy transfer in polyatomic intermediates," Int. Rev. Phys. Chem. **32**, 229–265 (2013).
2. HIBRIDON is a package of programs for the time-independent quantum treatment of inelastic collisions and photodissociation written by M. H. Alexander, D. E. Manolopoulos, H.-J. Werner, B. Follmeg, P. J. Dagdigian, Q. Ma, and others. More information and/or a copy of the code can be obtained from the website http://www2.chem.umd.edu/groups/alexander/hibridon/.
3. U. Bley and F. Temps, "Collision-induced intersystem crossing of CH_2 from a^1A_1 to $X\ ^3B_1$: A case-study of the mixed–state model," Journal of Chemical Physics **98**, 1058–1072 (1993).

4. W. M. Gelbart and K. F. Freed, "Intramolecular perturbations and quenching of luminescence in small molecules," Chem. Phys. Lett. **18**, 470–475 (1973).
5. A. V. Komissarov, A. Lin, T. J. Sears, and G. E. Hall, "State-resolved thermalization of singlet and mixed singlet-triplet states of CH_2," J. Chem. Phys. **125**, 084308 (084305 pages) (2006).
6. M. H. Alexander, G. Hall, and P. J. Dagdigian, "The Approach to Equilibrium: Detailed Balance and the Master Equation," J. Chem. Educ. **88**, 1538–1543 (2011).
7. O. Tkáč, A. K. Sage , S. J. Greaves, A. J. Orr-Ewing, P. J. Dagdigian, Q. Ma, and M. H. Alexander, "Rotationally inelastic scattering of CD_3 and CH_3 with He: comparison of velocity map-imaging data with quantum scattering calculations," Chem. Sci. **4**, 4199 – 4211 (2013).
8. O. Tkac, A. J. Orr-Ewing, P. J. Dagdigian, M. H. Alexander, J. Onvlee, and A. van der Avoird, "Collision dynamics of symmetric top molecules: A comparison of the rotationally inelastic scattering of CD_3 and ND_3 with He," J. Chem. Phys. **140**, xxxxxx (2014).
9. O. Tkac, A. K. Saha, J. Onvlee, C.-H. Yang, G. Sarma, C. K. Bishwakarma, S. Y. T. van de Meerakker, A. van der Avoird, D. H. Parker, and A. J. Orr-Ewing, "State-to-state resolved differential cross sections for rotationally inelastic scattering of ND_3 with He," Phys. Chem.Chem. Phys. **16**, 477–488 (2014).
10. P. J. Dagdigian and M. H. Alexander, "Exzact quantum scattering calculations of transport properties for free radicals: OH($X^2\Pi$)-helium," J. Chem. Phys. **137**, 094306 (2012).
11. P. J. Dagdigian and M. H. Alexander, "Exact quantum scattering calculations of transport properties: CH2(X^3B_1,a^1A_1)-helium," J. Chem. Phys. **138**, 164305 (2013).
12. P. J. Dagdigian and M. H. Alexander, "Exact quantum scattering calculations of transport properties for the H_2O-H system," J. Chem. Phys. **139**, 194309 (2013).
13. E. J. Rackham, T. Gonzalez-Lezana, and D. E. Manolopoulos, "A rigorous test of the statistical model for atom-diatom insertion reactions," J. Chem. Phys. **119**, 12895–12907 (2003).
14. D. Forthomme, C. P. McRaven, T. J. Sears, and G. E. Hall, "Argon-induced pressure broadening, shifting, and narrowing in the CN $A^2\Pi$–$X^2\Sigma^+$ (1–0) band," J. Phys. Chem. A **117**, 11837–11846 (2013).

Theoretical Studies of Elementary Hydrocarbon Species and Their Reactions

Wesley D. Allen and Henry F. Schaefer III
Center for Computational Quantum Chemistry and Department of Chemistry
University of Georgia, Athens, GA 30602-2525
E-mail: wdallen@uga.edu and ccq@uga.edu; Phone: (706) 542-7729

Resolution of the Structural Enigma of the HO_3 radical

In a collaboration with the experimental group of Gary Douberly, inertial dipole moment components were obtained from Stark spectra of the *trans*-HO_3 radical in superfluid helium nanodroplets, and these quantities were used to resolve the controversy over the structure of this species. Initially computed CCSD(T)/CBS equilibrium dipole moment components disagreed qualitatively with the experimental values. The role of large-amplitude motion and vibrational averaging was then assessed by computing the ground-state vibrational wave function on a relaxed, two-dimensional potential surface for the H–O–O–O torsion and central O–O bond stretch [r(O–O)]. The experimental and theoretical μ_0 values agreed only after shifting the potential along r(O–O), indicating that CCSD(T)/CBS theory considerably underestimates the equilibrium O–O distance by about 0.08 Å. Subsequently, the *trans*-HO_3 geometry was fully optimized at the composite all-electron CCSDT(Q)/CBS level of theory. The inclusion of full triples and a perturbative treatment of quadruple excitations increases r_e(O–O) to 1.65 Å (Figure 1), only 0.01 Å below the empirical distance derived from microwave rotational constants. The CCSDT(Q)/CBS dipole moment was found to be (μ_a, μ_b) = (–0.78, 1.64) D at the corresponding equilibrium geometry, in excellent agreement with experiment once zero-point vibrational averaging was included. The CCSDT(Q)/CBS dissociation energy was D_0(HO–O_2) = 3.01 kcal mol^{-1}, which is within the error bars of the 2.94(7) kcal mol^{-1} value derived from supersonic flow experiments.

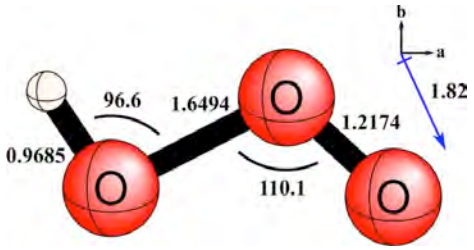

Figure 1. Equilibrium *trans*-HO_3 structure and dipole moment computed at the composite, all-electron CCSDT(Q)/CBS level of theory.

The Intricate Internal Rotation Surface and Fundamental Vibrations of the n-Propyl Radical

Although the *n*-propyl radical is an archetypical intermediate in combustion chemistry, only four of its vibrational modes have been observed via infrared spectroscopy. Three of these modes are C–H stretches, while the fourth near 530 cm^{-1} has been assigned to pyramidal bending of the easily distorted radical center. Both ESR spectroscopy and electronic structure theory have been used to study large-amplitude internal rotation in the *n*-propyl radical, but there is disagreement over the key features of the underlying potential energy surface.

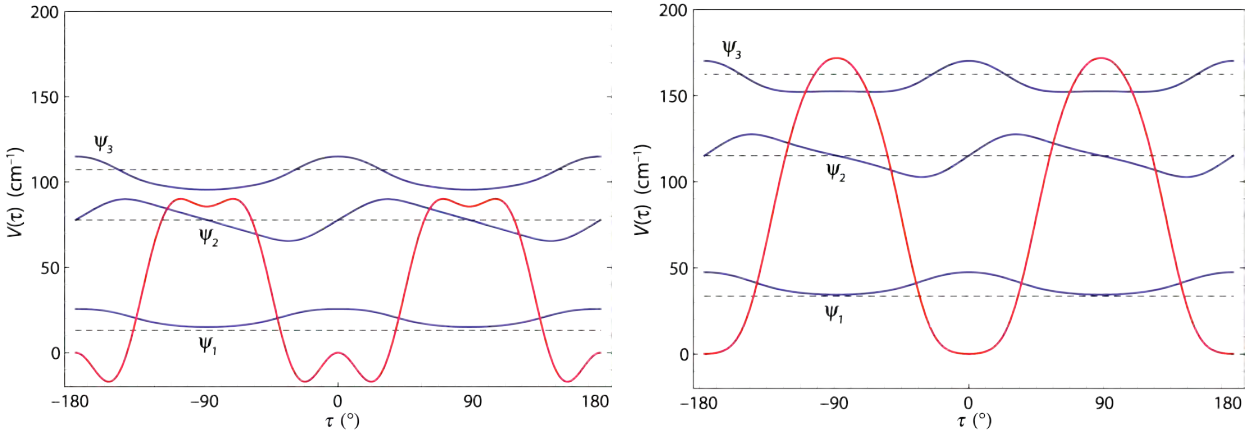

Figure 2. Potential energy (V) and converged vibrational wave functions (ψ) vs. H_2C–C–C torsion angle (τ) for internal rotation in *n*-propyl radical. Left panel: bare CCSD(T)/cc-pVQZ; right panel: final FPA potential with zero-point vibrational corrections.

To promote its definitive spectroscopic characterization, all stationary points of *n*-propyl were optimized with CCSD(T)/cc-pVTZ theory, and focal point analyses (FPA) targeting the CBS limit of CCSDT(Q) were executed to pinpoint the relative energetics. Anharmonic vibrational frequencies were then computed by applying second-order vibrational perturbation theory (VPT2) to a force field assembled from CCSD(T)/ANO1 quadratic and CCSD(T)/ANO0 cubic and quartic terms. As shown in Figure 2 (left panel), the bare internal rotation surface exhibits multiple local minima, owing to the coupling between CH_2 out-of-plane bending at the radical center and the H_2C–C–C torsional motion. However, when the zero-point vibrational energy of the complementary modes is included, a striking transformation takes place (right panel, Figure 2). In particular, $V(\tau)$ collapses to a single minimum every 180°, and the barrier height increases by about 70%! Far-infrared measurements of transitions between the highly anharmonic torsional states of *n*-propyl would not only have diagnostic merit but would also provide fundamental tests of vibrational adiabaticity for a multimode system.

Reaction profiles for radical-radical abstraction via multireference coupled cluster theory

Radical-radical hydrogen abstractions in combustion chemistry are disproportionation reactions that are generally exothermic with little or no barrier, yet are underappreciated and poorly studied. Prototypically these reactions begin with two open-shell reactants and end with two closed-shell products, and thus the electronic transformation is intrinsically multireference in nature. Such challenging electronic structure problems have been tackled using our recently developed state-specific multireference coupled cluster methods Mk-MRCCSD and Mk-MRCCSD(T), as well as the companion perturbation theory Mk-MRPT2 and the popular MRCISD, MRCISD+Q, and CASPT2 approaches. Reaction paths were investigated for five prototypes involving radical-radical hydrogen abstraction: H + BeH → H_2 + Be, H + NH_2 → H_2 + NH, CH_3 + C_2H_5 → CH_4 + C_2H_4, H + C_2H_5 → H_2 + C_2H_4, and H + HCO → H_2 + CO. Selected results are plotted in Figures 3 and 4. Full configuration interaction (FCI) benchmark computations for the H + BeH, H + NH_2, and H + HCO reactions prove that the Mk-MRCCSD(T) potential energy curves display superior accuracy, with mean absolute errors of only 0.2 kcal mol^{-1}. To facilitate studies of combustion kinetics in collaboration with Stephen Klippenstein and Larry Harding at Argonne, energetics for the CH_3 + C_2H_5, H + C_2H_5, and H + HCO reactions were computed at each level of theory with correlation-consistent basis sets (cc-pV*X*Z, *X* = T, Q, 5) and extrapolated to the complete basis set (CBS) limit. The rigorous Mk-MRCCSD(T)/CBS results demonstrate unequivocally that these three reactions proceed with no barrier in the entrance channel, contrary to some earlier predictions. Mk-MRCCSD(T) also reveals that the economical CASPT2 method performs well for large interfragment separations but may deteriorate substantially at shorter distances.

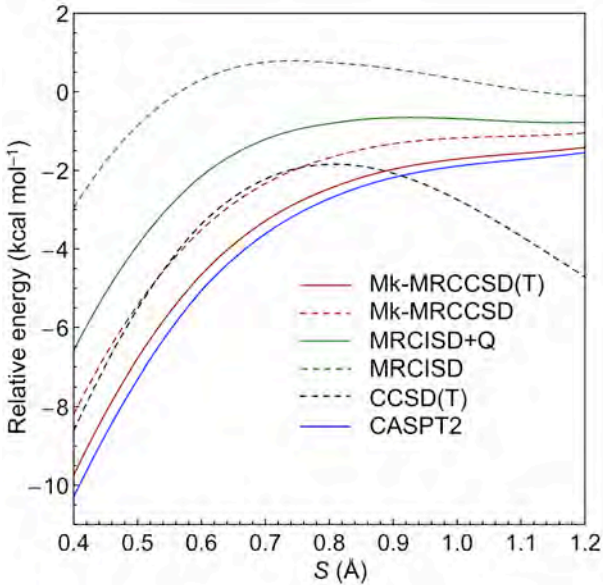

Figure 3. Potential energy curves for the CH_3 + C_2H_5 entrance channel computed at numerous levels and extrapolated to the CBS limit. The reaction coordinate *S* is the difference between C–H distances of the forming and breaking bonds.

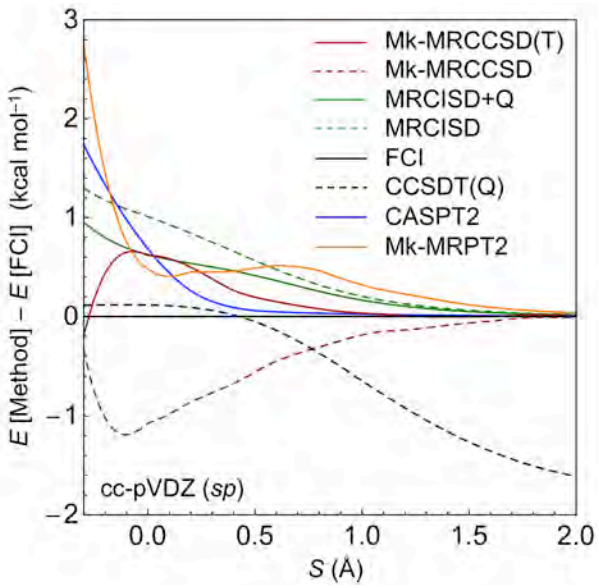

Figure 4. For the entrance channel of H + HCO, energy deviations are plotted with respect to FCI for different levels of theory with the cc-pVDZ(*sp*) basis set.

Publications Supported by DOE: 2011-2014

1. Y. Yamaguchi and H. F. Schaefer, "Analytic Derivative Methods in Molecular Electronic Structure Theory. A New Dimension to Quantum Chemistry and its Applications to Spectroscopy," in *Handbook of High Resolution Spectroscopy*, editors M. Quack and F. Merkt (Wiley, Chichester, 2011), pp. 325-362.
2. D. S. Hollman, A. C. Simmonett, and H. F. Schaefer, "The Benzene + OH Potential Energy Surface: Intermediates and Transition States," *Phys. Chem. Chem. Phys.* **13**, 2214 (2011).
3. J. J. Wilke and H. F. Schaefer, "Spin-Restricted Explicitly Correlated Coupled Cluster for High-Spin Open-Shell Molecules. The *Z*-Averaged CCSD-R12 Approach," *J. Chem. Theory Comput.* **7**, 2416 (2011).
4. J. C. Hargis, E. Vöhringer-Martinez, H. L. Woodcock, A. Toro-Labbe, and H. F. Schaefer, "Characterizing the Mechanism of the Double Proton Transfer in the Formamide Dimer," *J. Phys. Chem. A* **115**, 2650 (2011).
5. H. Feng, W. Sun, Y. Xie, and H. F. Schaefer, "Structures and Energetics of the *t*-Butyl Cation: The Final Answer or a Never-Ending Story," *Chem. Eur. J.* **17**, 10551 (2011).
6. H. M. Jaeger, H. F. Schaefer, E. G. Hohenstein, and C. D. Sherrill, "Protonated Benzene Dimer: Demystifying Intermolecular Interactions of Complex Systems," *Computational and Theoretical Chemistry* **973**, 47 (2011).
7. J. M. Turney, A. C. Simmonett, R. M. Parrish, E. G. Hohenstein, F. Evangelista, J. T. Fermann, B. J. Mintz, L. A. Burns, J. J. Wilke, M. L. Abrams, N. J. Russ, M. L. Leininger, C. L. Janssen, E. T. Seidl, W. D. Allen, H. F. Schaefer, R. A. King, E. F. Valeev, C. D. Sherrill, and T. D. Crawford, "Psi4: An Open-Source *Ab Initio* Electronic Structure Program," *WIREs Comput. Mol. Sci.* **2**, 556 (2012).
8. J. Agarwal, J. M. Turney, and H. F. Schaefer, "Reaction Energetics for the Abstraction Process $C_2H_3 + H_2 \rightarrow C_2H_4 + H$," *J. Phys. Chem. Lett.* **2**, 2587 (2011).
9. G. Koleva, B. Galabov, J. Kong, H. F. Schaefer, and P. R. Schleyer, "Electrophilic Aromatic Sulfonation with SO_3: Concerted or Classical S_EAr Mechanism," *J. Am. Chem. Soc.* **133**, 19094 (2011).
10. P. R. Schreiner, H. P. Reisenauer, D. Ley, D. Gerbig, C.-H. Wu, and W. D. Allen, "Methylhydroxycarbene: Tunneling Control of a Chemical Reaction," *Science* **332**, 1300 (2011).
11. H. Feng, W. Sun, Y. Xie, and H. F. Schaefer, "Is There an Entrance Complex for the $F + NH_3$ Reaction?" *Chem. Asian J.* **6**, 3152 (2011).
12. B. S. Narendrapurapu, A. C. Simmonett, H. F. Schaefer, J. A. Miller, and S. J. Klippenstein, "Combustion Chemistry: Important Features of the C_3H_5 Potential Energy Surface, Including Allyl Radical, Propargyl + H_2, Allene + H, and Eight Transition States," *J. Phys. Chem. A* **115**, 14209 (2011).
13. D. S. Hollman and H. F. Schaefer, "In Search of the Next Holy Grail of Polyoxide Chemistry: Explicitly Correlated *Ab Initio* Full Quartic Force Fields for HOOH, HOOOH, HOOOOH, and Their Isotopologues," *J. Chem. Phys.* **136**, 084302 (2012).
14. U. Bozkaya, J. M. Turney, Y. Yamaguchi, and H. F. Schaefer, "The Lowest-Lying Electronic Singlet and Triplet Potential Energy Surfaces for the HNO-NOH System: Energetics, Unimolecular Rate Constants, Tunneling and Kinetic Isotope Effects for the Isomerization and Dissociation Reactions," *J. Chem. Phys.* **136**, 164303 (2012).
15. M. Morrison, J. Agarwal, H. F. Schaefer, and G. E. Douberly, "Infrared Laser Spectroscopy of the CH_3OO Radical Formed from the Reaction of CH_3 and O_2 within a Helium Nanodroplet," *J. Phys. Chem. A.* **116**, 5299 (2012).
16. N. J. DeYonker and W. D. Allen, "Taming the Low-Lying Electronic States of FeH," *J. Chem. Phys.* **137**, 234303 (2012).
17. J. Agarwal, A. C. Simmonett, and H. F. Schaefer, "Fundamental Vibrational Frequencies and Spectroscopic Constants for the Methylperoxyl Radical $^{13}CH_3O_2$ and Related Isotopologues $^{13}CH_3OO$, $CH_3{}^{18}O{}^{18}O$, and CD_3OO," *Mol. Phys.* **110**, 2419 (2012).
18. G. Li, L. Zhou, Q.-S. Li, Y. Xie, and H. F. Schaefer, "The Entrance Complex, Transition State, and Exit Complex for the $F + H_2O \rightarrow HF + OH$ Reaction. Definitive Predictions. Conventional Density Functional Methods Fail an Important Test," *Phys. Chem. Chem. Phys.* **14**, 10891 (2012).
19. Y. Zhang, D. S. Hollman, and H. F. Schaefer, "From Strong van der Waals Complexes to Hydrogen Bonding: From $CO\cdots H_2O$ to $CS\cdots H_2O$ and $SiO\cdots H_2O$ Complexes," *J. Chem. Phys.* **136**, 244305 (2012).
20. A. Yu. Sokolov, S. Mittal, A. C. Simmonett, and H. F. Schaefer, "Characterization of the *t*-Butyl Radical and its Elusive Anion," *J. Chem. Theory Computation* **8**, 4323 (2012).

21. D. S. Hollman and H. F. Schaefer, "Arbitrary Order El'yashevich-Wilson B Tensor Formulas for the Most Frequently Used Internal Coordinates in Molecular Vibrational Analyses," *J. Chem. Phys.* **137**, 164103 (2012).
22. H. Feng, W. Sun, Y. Xie, H. F. Schaefer, "Moving on from F + H_2: The More Challenging Reaction between Atomic Fluorine and Methylamine," *Chem. Phys. Chem.* **14**, 896 (2013).
23. J. Guan, K. R. Compaan, H. F. Schaefer, and H. Li, "Formylmethylene: The Triplet Ground State and the Lowest Singlet State," *J. Phys. Chem.* **117**, 2152 (2013).
24. P. L. Raston, J. Agarwal, J. M. Turney, H. F. Schaefer, and G. E. Douberly, "The Ethyl Radical in Superfluid Helium Nanodroplets: Rovibrational Spectroscopy and *Ab Initio* Computations," *J. Chem. Phys.* **138**, 194303 (2013).
25. G. Li, Q. S. Li, Y. Xie, and H. F. Schaefer, "The F + H_2O Dimer Reaction: The Second Water Removes the Barrier," *J. Phys. Chem. A* **117,** 11979 (2013).
26. Q. Fan, H. Li, H. Feng, W. Sun, T. Lu, A. C. Simmonett, Y. Xie, and H. F. Schaefer, "New Potential Energy Surface Features for the Li + HF → LiF + H Reation," *J. Phys. Chem. A* **117,** 10027 (2013).
27. Y. Guo, M. Zhang, Y. Xie, and H. F. Schaefer, "Some Critical Features of the Potential Energy Surface for the Cl + H_2O → HCI + OH Forward and Reverse Reactions," *J. Chem. Phys*. **139**, 041101 (2013).
28. L. Horny, H. F. Schaefer, F. Ünlü, and M. Willeke, "Theoretical Investigation of the Cyclopropene Cation $C_3H_4^{+\bullet}$: Structure, Energetics and Spectroscopic Properties," *Mol. Phys.* **111,** 2306 (2013).
29. Y. Qiu, A. Y. Sokolov, Y. Yamaguchi, and H. F. Schaefer, "$BeCH_2$: The Simplest Metal Carbene. High Levels of Theory," *J. Phys. Chem. A* **117,** 9266 (2013).
30. S. R. Barua, W. D. Allen, E. Kraka, P. Jerabek, R. Sure, and G. Frenking, "Nearly Degenerate Isomers of $C(BH)_2$: Cumulene, Carbene, or Carbone?" *Chem. Eur. J.* **19**, 15941 (2013).
31. A. Yu. Sokolov, D. B. Magers, J. I. Wu, W. D. Allen, P. v. R. Schleyer and H. F. Schaefer, "Free Cyclooctatetraene Dianion: Planarity, Aromaticity, and Theoretical Challenges," *J. Chem. Theory Comput.* **9,** 4436 (2013).
32. T. Liang, D. B. Magers, P. L. Raston, W. D. Allen, and G. E. Douberly, "Dipole Moment of the HOOO Radical: Resolution of a Structural Enigma," *J. Phys. Chem. Lett.* **4**, 3584–3589 (2013).
33. D. S. Hollman, H. F. Schaefer, and E. F. Valeev, "Semi-Exact Concentric Atomic Density Fitting: Reduced Cost and Increased Accuracy Compared to Standard Density Fittings," *J. Chem. Phys.* **140,** 064109 (2014).
34. Q. Fan, H. Feng, W. Sun, Y. Xie, C.-H. Wu, W. D. Allen, and H. F. Schaefer, "The Li···HF van der Waals Minimum and the Barrier to the Deep HF–Li Potential Well," *Mol. Phys*. **112**, 770 (2014).
35. Y. Hao, J. Gu, Y. Guo, M. Zhang, Y. Xie, and H. F. Schaefer, "Spin-Orbit Corrected Potential Energy Surface Features for the I ($^2P_{3/2}$) + H_2O → HI + OH Forward and Reverse Reactions," *Phys. Chem. Chem. Phys.* **16,** 2641 (2014).
36. X. Feng, J. Gu, Q. Chen, Y. Xie, and H. F. Schaefer, "How Small Can a Catenane Be?" *J. Chem. Theory Comput.* **10**, 1511 (2014).
37. S. R. Barua, H. Quanz, M. Olbrich, P. R. Schreiner, D. Trauner, and W. D. Allen, "Polytwistane," *Chem. Eur. J.* **20**, 1638 (2014).
38. G. Li, H. Wang, Q.-S. Li, Y. Xie, and H. F. Schaefer, "The Exothermic HCl + $OH^\bullet$ (H_2O) Reaction. Removal of the HCl + OH Barrier by a Single Water Molecule," *J. Chem. Phys.* **140**, 124316 (2014).
39. X. Wang, W. E. Turner, J. Agarwal, and H. F. Schaefer, "Twisted Triplet Ethylene: Anharmonic Frequencies and Spectroscopic Parameters for C_2H_4, C_2D_4, and $^{13}C_2H_4$," *J. Phys. Chem. A*, doi: 10.1021/jp502282v, published online April 2, 2014.
40. J. D. Mosley, J. W. Young, J. Agarwal, H. F. Schaefer, P. v. R. Schleyer, and M. D. Duncan, "Structural Isomerization of the Gas Phase 2-Norbornyl Cation Revealed with Infrared Spectroscopy and Computational Chemistry," *Angew. Chem. Int. Ed.* (2014).
41. C. Li, J. Agarwal, C.-H. Wu, W. D. Allen, and H. F. Schaefer, "The Intricate Internal Rotation Surface and Fundamental Vibrations of the *n*-Propyl Radical," *Phys. Chem. Chem. Phys.* (2014).
42. C. -H. Wu, D. B. Magers, L. B. Harding, S. J. Klippenstein, and W. D. Allen, "Reaction profiles for radical-radical hydrogen abstraction via multireference coupled cluster theory," *J. Chem. Theory Comput*. (2014).

Turbulence-Chemistry Interactions in Reacting Flows

Robert S. Barlow
Combustion Research Facility
Sandia National Laboratories, MS 9051
Livermore, California 94550
barlow@sandia.gov

Program Scope

This program is directed toward achieving a more complete understanding of turbulence-chemistry interactions in gaseous flames and providing detailed measurements for validation of combustion models. In the Turbulent Combustion Laboratory (TCL) simultaneous line imaging of spontaneous Raman scattering, Rayleigh scattering, and two-photon laser-induced fluorescence (LIF) of CO is applied to obtain spatially and temporally resolved measurements of temperature, the concentrations of all major species, mixture fraction, and reaction progress, as well as gradients in these quantities in hydrocarbon flames. The instantaneous three-dimensional orientation of the turbulent reaction zone is also measured by imaging of OH LIF or Rayleigh scattering at 355 nm in two crossed planes, which intersect along the laser axis for the multiscalar measurements. These combined data characterize both the thermo-chemical state and the instantaneous flame structure, such that the influence of turbulent mixing on flame chemistry may be quantified. Our experimental work is closely coupled with international collaborative efforts to develop and validate predictive models for turbulent combustion. This is accomplished through our visitor program and through the TNF Workshop series. In recent years the workshop and this program have expanded their scope to address a broad range of combustion modes, including premixed, stratified, partially premixed, and nonpremixed flames. We are also working to extend our quantitative multiscalar diagnostics to more complex hydrocarbon fuels. Entry into these new research areas has prompted developments in both hardware and methods of data analysis to achieve unprecedented spatial resolution and precision of multiscalar measurements. Within the CRF we collaborate with Jonathan Frank, who applies advanced imaging diagnostics to turbulent flames, and with Joe Oefelein, who performs high fidelity large-eddy simulations (LES) of our experimental flames in order to gain greater fundamental understanding of the dynamics of multi-scale flow-chemistry interactions.

Recent Progress

New Capabilities in Raman Scattering Diagnostics

The capability to simultaneously acquire two orthogonal components of the Raman spectrum has been added to the Raman/Rayleigh/CO-LIF line imaging system in the Turbulent Combustion Laboratory. This allows multiscalar measurements to be made in hydrocarbon flames with high levels of fluorescence interference from soot precursors. Raman scattering mainly retains the polarization of the laser beam, while the interfering fluorescence is unpolarized and contributes equally to both polarization components. Therefore, interference is largely eliminated by subtraction of simultaneously measured signals from the two detectors. A second complete, three camera detection system was built as a mirror image of the first. Both systems use high-

speed (21,000 rpm) rotating slits to provide gating of 3.9 μs for the Raman measurements, rejecting flame luminosity. These custom built shutter wheels are PLL controlled with a relative phase error of less than 70 ns (rms), allowing simultaneous measurements within the fully-open period for both rotating shutter.

This new capability for single-shot, spatially-resolved Raman polarization separation and subtraction was demonstrated by performing measurements of all major species and temperature in laminar and turbulent methane/air jet flames (3/1 molar ratio), which produced levels of fluorescence interference roughly 20 times that which could be tolerated in previous measurements [Magnotti & Barlow (accepted)]. Figure 1 shows the laboratory configuration and example averaged spectra acquired in the maximum interference region of the laminar methane/air jet flame for the two polarization components and the difference spectrum. Single-shot measurements are acquired by binning (on-chip) the spectral regions marked in the figure. The precision is reduced compared to that obtained in Raman friendly flames using a single detector without polarizer because some signal is sacrificed and there is residual noise after subtraction of the fluorescence interference. However, this new capability will allow significant expansion of the types of hydrocarbon flames that can be studied in the future.

An alternate configuration of the second Raman spectrometer has also been tested, which uses a high-dispersion grating to achieve better separation of spectral features from different small hydrocarbons within the C-H stretch region of the Raman scattering spectrum. There is work in progress to directly measure the main stable hydrocarbon intermediates in DME flames, using this dual resolution approach combined with experimentally generated Raman spectral libraries for the small hydrocarbons of interest.

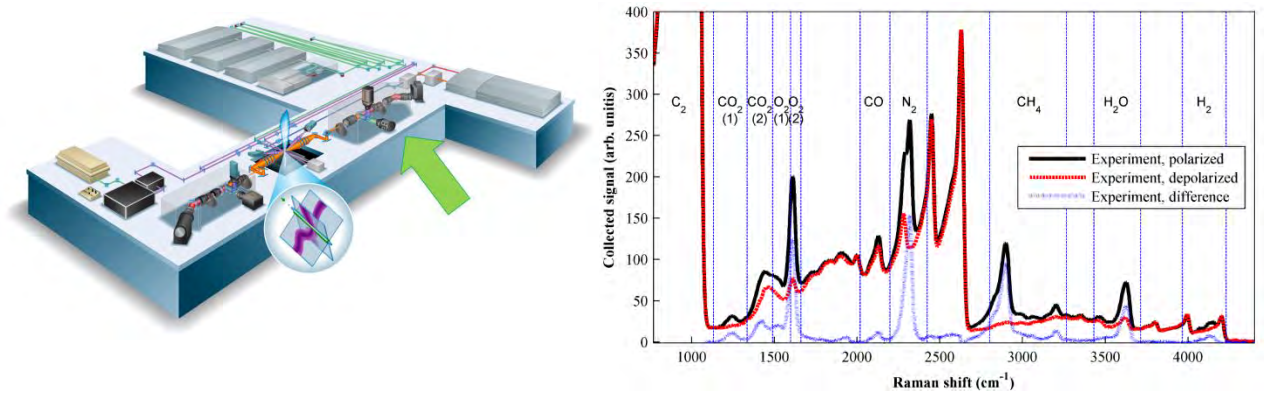

Figure 1. Illustration of the new setup (left) and example averaged spectra (polarized, depolarized and difference) from the fuel-rich region of a methane/air jet flame.

Bluff-Body Stabilized Premixed Flames

Investigations of bluff-body stabilized premixed flames were continued in order to better understand the effects of preferential species transport and shear in this important class of flames. Fuel-lean ($\phi = 0.75$) and fuel-rich ($\phi = 1.23$) methane/air flames operated at three flow conditions (low, intermediate, and high ratios of reactant velocity to laminar flame speed) were mapped, using full radial profiles at six axial distances above the burner surface. Experimental

results confirmed a previous computational finding from Katta (*Proc. Combust. Inst*. 2013) that preferential diffusion effects are greatest near the corner of the bluff-body, where the flame is anchored. These experiments, which included measurements of instantaneous flame orientation by crossed-planar imaging of Rayleigh scattering, also showed that flame thickness increases significantly with increasing reactant velocity for the fuel-rich case, as the flame is forced into the high-shear region of the flow adjacent to the bluff-body recirculation zone. This flame thickening is reflected by decreases in the measured 3D gradient and 3D dissipation of the reaction progress variable based on temperature, as shown in Figure 2.

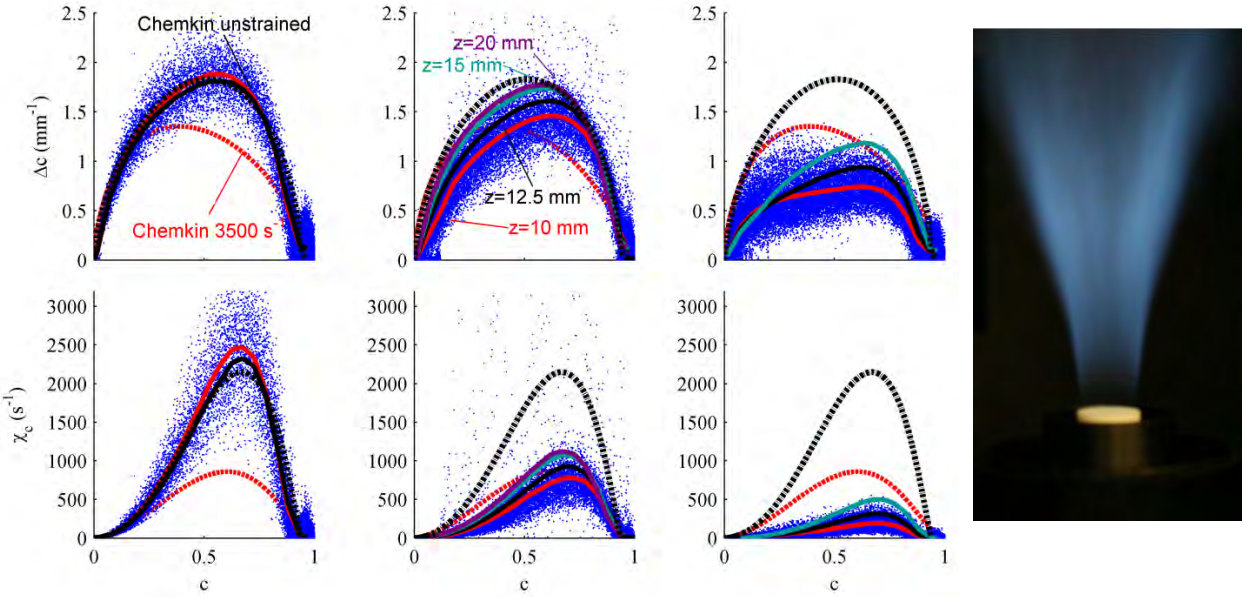

Figure 2. 3D progress variable gradient (upper row) and 3D dissipation (lower row) for ϕ = 1.23 at three values of the ratio of reactant velocity to laminar flame speed (U_b/S_L = 5.5, 9.3, 26). The photo shows the U_b/S_L = 26 flame.

Multi-mode Combustion in Nonhomogeneous Piloted Jet Flames

A new version of the Sydney piloted jet flame burner has been developed, which has a retractable 4-mm diameter tube within the 7.4-mm main tube. Experiments at Sydney University showed a significant increase in blow-off velocity (a measure of comparative flame stability) in partially-premixed methane/air jet flames when the fuel was introduced through the inner tube, and the recess distance of the inner tube was set within an optimum range between 75 mm and 100 mm below the exit plane. Air flows through the annulus around the inner tube. Recent multiscalar measurements at Sandia have revealed that this enhanced stability comes two factors related to the mixing process upstream of the nozzle exit. First, fluid at the edge of the jet is within the premixed flammability limits for the first few jet diameters downstream of the exit plane. This fluid burns in a premixed mode, providing additional heat release that augments the stabilizing effect of the pilot flame. Second, the mixing profile across the jet yields mixture-fraction dissipation levels within the flame zone that are much lower in the optimally-recessed nonhomogeneous case than in the normal piloted flame with homogeneous jet fluid. In the nonhomogeneous flame, the transition from a stratified premixed combustion mode to a diffusion flame mode occurs within a few nozzle exit diameters. These flames should comprise an interesting challenge for combustion models.

Future Plans

Priorities for the next year are to: i) obtain direct single-shot measurements of stable hydrocarbon intermediates along with all major species in the series of turbulent DME jet flames developed by J. Frank and previously studied using approximations to account for hydrocarbon intermediates; ii) fully analyze recent data from the nonhomogeneous jet flames; iii) apply our latest methods to selected cases of the Sydney bluff body flames, which have been an important model test case but have only pointwise scalar data from 1995, iv) and bring online a programmable pulsewidth Nd:YAG laser that will allow measurements of enclosed flames.

BES Supported Publications (2012 - present)

Barlow, R.S.; Dunn, M.J.; Sweeney, M.S.; Hochgreb, S., Effects of preferential transport in turbulent bluff-body-stabilized lean premixed CH_4/air flames. *Combust. Flame* **2012**, *159*, 2563-2575.

Fuest, F.; Barlow, R.S.; Geyer, D.; Seffrin, F.; Dreizler, A., Raman/Rayleigh scattering and CO-LIF measurements in laminar and turbulent jet flames of dimethyl ether, *Combust. Flame* **2012**, *159*, 2533-2562.

Sevault, A.; Dunn, M.J.; Barlow, R.S.; Ditaranto, M., On the structure of the near field of oxy-fuel jet flames using Raman/Rayleigh laser diagnostics, *Combust. Flame* **2012**, *159*, 3342-3352.

Sweeney, M.S.; Hochgreb, S.; Dunn, M.J.; Barlow, R.S., The structure of turbulent stratified and premixed methane/air flames I: Non-swirling flows, *Combust. Flame* **2012**, *159*, 2896-2911.

Sweeney, M.S.; Hochgreb, S.; Dunn, M.J.; Barlow, R.S., The structure of turbulent stratified and premixed methane/air flames II: Swirling flows, *Combust. Flame* **2012**, *159*, 2912-2929.

Sweeney, M.S.; Hochgreb, S.; Dunn, M.J.; Barlow, R.S., Multiply conditioned analyses of stratification in highly swirling methane/air flames, *Combust. Flame* **2012**, *160*, 322-334.

Dunn, M.J.; Barlow, R.S.; "Effects of preferential transport and strain in bluff body stabilized lean and rich premixed CH_4/air flames," *Proc. Combust. Inst.* **2013** , *34*, 1411-1419.

Zhou, R.; Balusamy, S.; Sweeney, M.S.; Barlow, R.S.; Hochgreb, S., Flow field measurements of a series of turbulent premixed and stratified methane/air flames, *Combust. Flame* **2013**, *160*, 2017-2028.

Ma, B.; Wang, G.; Magnotti, G.; Barlow, R.S.; Long, M.B., Intensity-ratio and color-ratio thin-filament pyrometry: Uncertainties and accuracy, *Combust. Flame* **2014**, *161*, 908-916.

Rankin, B.A.; Magnotti, G.; barlow, R.S.; Gore, J.P., Radiation intensity imaging measurements of methane and dimethyl ether turbulent nonpremixed and partially premixed jet flames, *Combust. Flame* (accepted).

Fuest, F.; Magnotti, G.; Barlow, R.S.; Sutton, J.A., Scalar structure of turbulent partially-premixed dimethyl ether/air jet flames, *Proc. Combust. Inst.*(accepted).

Magnotti, G.; Geyer, D.; Barlow, R.S., Interference-free spontaneous Raman spectroscopy for measurements in rich hydrocarbon flames, *Proc. Combust. Inst.*(accepted).

TNF Workshop Information: http://www.sandia.gov/TNF

Predictive Large-Eddy Simulation of Supercritical-Pressure Reactive Flows in the Cold Ignition Regime

Josette Bellan
Mechanical and Civil Engineering Department, California Institute of Technology
Pasadena, CA 91125
Josette.Bellan@jpl.nasa.gov
DOE Award Numbers: **DE-FG02-09ER16107 and 02_GR-ER16107-14-00**
STRIPES award number: **SC0002679**

I. Program Scope

This study addresses issues highlighted in the Basic Energy Needs for Clean and Efficient Combustion of 21st Century Transportation Fuels (DOE BES, 2006) under the topic of Combustion under Extreme Pressure. It is there noted that "the most basic concepts of thermal autoignition" are "based on experience and theory at near atmospheric pressures" and that "as pressure increases significantly…, many of these conceptual pictures begin to change or disappear". It is also stated "A better description of the coupling and interaction of high pressure flow and molecular transport processes with chemistry is also necessary", particularly because "Ignition and flame propagation of alternative and renewable fuels, as well as of the changing feed stocks of conventional fossil-based fuels, are very likely to be much different at very high pressures than under the more familiar, lower pressure conditions of current engines." Recognizing that "Under such *(increasing pressure)* conditions distinctions between gas and liquid phases become moot, new equations of state must be used…", it is immediately apparent that there must be "a re-examination of the basic assumptions that govern the physics and chemistry related to combustion; and the need for this type of re-examination increases as the combustion pressure increases." This recognition is also stated under the topic of Multiscale Modeling since due to the new equations of state "The combination of unexplored thermodynamic environments and new physical and chemical fuel properties results in complex interactions among multiphase *(according to the above, the multiphase distinction becomes moot with increasing pressure)* fluid dynamics, thermodynamic properties, heat transfer, and chemical kinetics that are not understood even at a fundamental level." From the theoretical viewpoint for "systems at high pressure, fluid dynamic time scales can be comparable to chemical time scales." and therefore "completely diffusion-controlled reactions … can become important".

Thus, the objective of this study is the investigation of the coupling among thermodynamics, transport properties, intrinsic kinetics and turbulence under the high-pressure and the relatively (with respect to combustion) low-temperature conditions typical of the auto-ignition regime, with particular emphasis on the manifestation of this coupling on the effective kinetic rate. As planned, we established collaboration with Dr. Joseph Oefelein of the Combustion Research Facility at Sandia Livermore to work together towards implementing the models developed in this research into the high-pressure Large Eddy Simulation (LES) code (named RAPTOR) under development by him at Sandia.

II. Recent Progress

This report contains results obtained during the last year of study. There were two foci of research during this year: (i) to understand the impact of the identified phenomenon of molecular reverse diffusion observed in Direct Numerical Simulations (DNS) realizations [i]

on the required Subgrid-Scale (SGS) modeling for LES, and (ii) to undertake reactive flow DNS so as to understanding the turbulence/reaction coupling in the high-pressure regime.

To address the first focus, we have post-processed transitional-state DNS realizations described in [i] by spatially filtering (at 2 filter widths) and analyzing them; we examined the effects of the initial Reynolds number (Re_0) and of pressure (p) on the domain-averaged magnitude and plane-averaged distribution of the SGS terms in all conservation equations. We found that similar to previous results from binary-species mixing [ii, iii], the (negligible under atmospheric-p conditions) SGS pressure-gradient term in the momentum equation and the SGS heat-flux term in the energy equation were similar in magnitude to that of resolved leading-order terms in those equations, and thus could not be neglected. But here, unlike the situation in [ii,iii], the SGS species mass fluxes were also of comparable magnitude to the resolved terms. The conclusion was that these terms must be modeled in order to achieve LES accuracy. Two models were analyzed: one based on the Approximate Deconvolution Model (ADM), the other based on explicit filtering (EF). Figure 1 illustrates the plane-average RMS of the difference between the species-flux filtered term in the LES equations and the model for it; ideally, that difference should be null. Depicted are: (a) the standard model in which the filtered species flux is replaced by that computed as a function of the filtered field (F), (b) the flux computed according to ADM followed by explicit filtering (ADMEF) and (c) the flux computed using the filtered field and then the flux being explicitly filtered (FEF). Clearly, the latter two models are considerably better than the standard model, as they both minimize the difference between the actual term and model. Since the last model is the least expensive among the latter two, it is that recommended. Current studies are devoted to showing the effect of using the additional SGS models in the LES equations in terms of predicting the filtered-and-coarsened DNS which is the template for LES. We are particularly interested in the prediction of the reverse-diffusion of H_2O and CO_2 because, as it was shown in [i], reverse diffusion regions exhibit species gradients which act akin to a solid mesh in producing turbulence during mixing and also during combustion, as will be seen next.

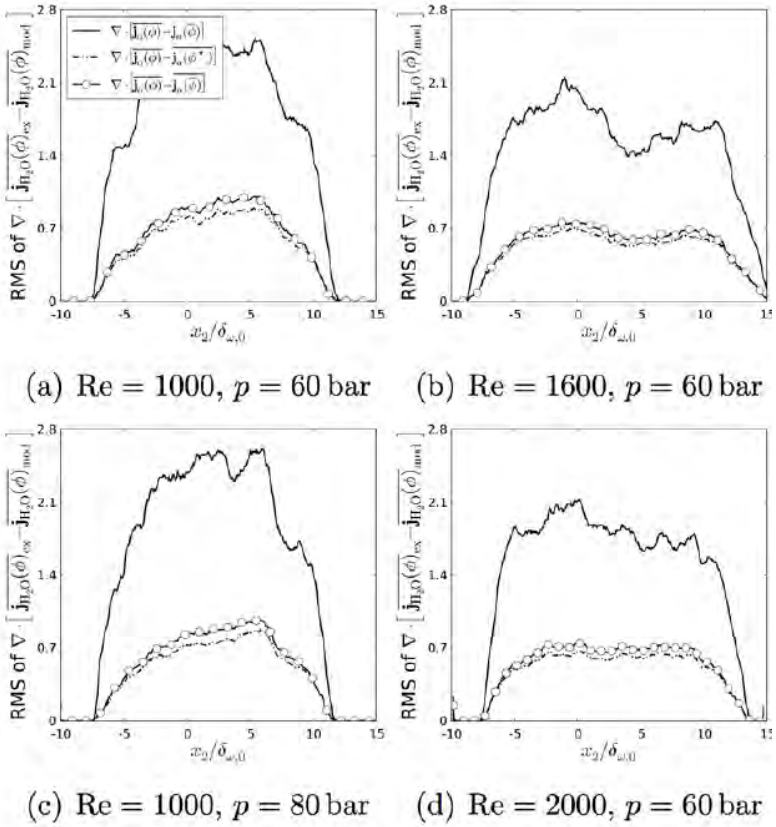

Figure 1. The plane-average RMS of the difference between the actual species-flux term in the LES equations and the proposed model for it, plotted versus the non-dimensional cross-stream coordinate. The difference is evaluated using the DNS database for the species H_2O. Re and p represent the initial Reynolds number and free-stream pressure. --- standard model (F); -- · · -- ADM (ADMEF); --o--o-- (FEF).

The supercritical-p reactive-flow study was initiated by conducting DNS. Considering that DNS is a tool to understand the fundamentals of the reaction/turbulence coupling under high-p conditions, it was natural to consider here a single reaction rather than a set of reactions as one would in LES which is a computational tool for obtaining accurate results pertaining to a situation of immediate practical interest. We fist created a DNS database to understand the requirements of SGS modeling by examining the dissipation (i.e. the irreversible entropy production) and then used this opportunity to examine exhaust gas recirculation (EGR) effects. Each DNS was conducted up to a transitional state and it is this state which was analyzed. Shown in Fig. 2 are the temperature (T) and the flame index (G_{FO}) under high-p conditions. Lack of EGR (Figs. 2e and 2f) promotes a geometrically more complex main flame and results in regions of high T that are more spatially extensive in both upper and lower parts of the mixing layer, consistent with more robust burning. According to G_{FO}, the main flame is of diffusion type (G_{FO} <0) but premixed regions (G_{FO} >0) are observed away from the main flame, and to substantial extent the most intense G_{FO} >0 delineate the extent of the flame from regions only containing unreacted species. As p increases, the most intense G_{FO} >0 region generally draws closer to the diffusion flame, however, some large values G_{FO} >0 regions penetrate deeper into the fuel stream; thus, generally, the flame becomes thinner with increasing p, but this is not uniformly the case. Absence of EGR promotes the formation of strong premixed flames on both sides of the diffusion flame. Displayed in Fig. 3 are the H_2O mass fraction (Y_{H2O}) and an effective water mass-diffusion coefficient (D_{H2O}). For the cases with EGR, the initially uniform Y_{H2O} distribution now appears very non-uniform due primarily to reaction but also to diffusion. The maximum Y_{H2O} is by a factor of 10 larger than the initial-condition value mostly due to combustion. In the main flame region, because D_{H2O}<0 at some locations, some water concentrated there is due to reverse mass diffusion. Most reverse diffusion occurs in the lower part of the mixing layer, but very thin reverse-diffusion regions are also observed at the very top of the mixing layer; in the upper part of the main flame region, increasing p results in decreased D_{H2O} values over the entire layer. The result of reverse diffusion is the formation of regions of high concentration, so that effectively at D_{H2O}<0 locations, H_2O tends to separate from the other species in the mixture. Similar results hold for CO_2. In combustion regions where the formed Y_{H2O} and Y_{CO2} are in excess of their initial values, reverse diffusion does not

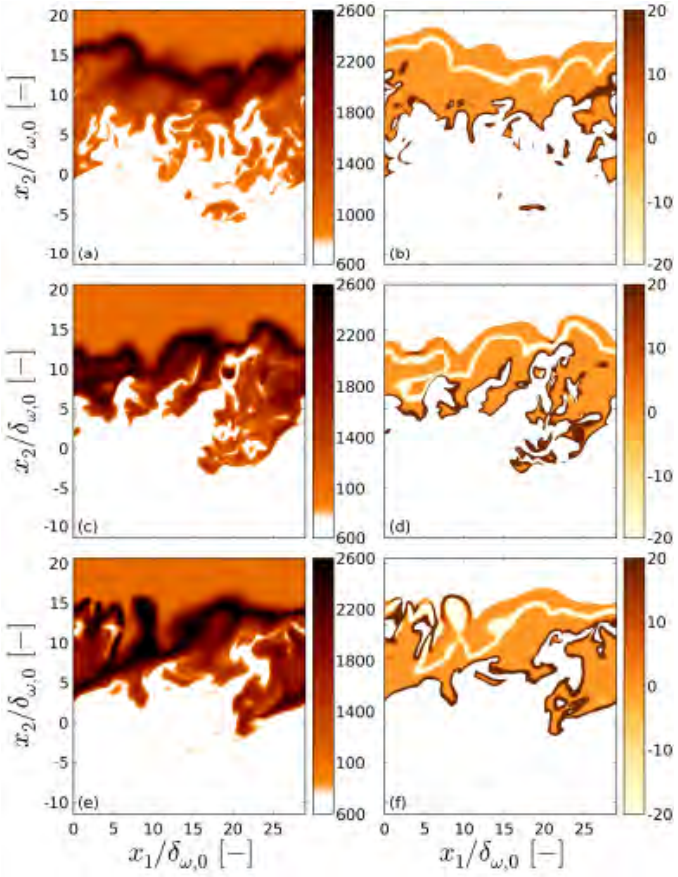

Figure 2. T (a,c,e) and G_{FO} (b,d,f) visualizations in a spanwise plane for p=60 bar with EGR (a,b); p=80 bar with EGR (c,d); and p=60 bar without EGR (e,f). Units for T are K, and for G_{FO} are m^{-2}.

have a large impact, but in other regions of the mixing layer the gradients formed through reverse diffusion enhance turbulence [i]. When EGR is absent, reverse diffusion is greatly minimized, although it is still present at some locations in the flame region where H_2O (and CO_2) are produced. The small-scale complexity of D_{H2O} is absent without EGR, indicating the beneficial aspect of EGR at supercritical pressure in terms of creating a more turbulent flow.

Examination of the dissipation indicated that out of the four modes of dissipation (viscous, heat, mass and reaction), the chemical dissipation is the largest by an order of magnitude. However, because each mode of dissipation is operative in different regions of the flow, all modes must be accurately modeled in LES in order to reproduce the spatial distributions which are so important in reactive flows.

The PI has continued the collaboration with Dr. Oefelein who will modify RAPTOR once we have developed the methodology of LES for high-p flows.

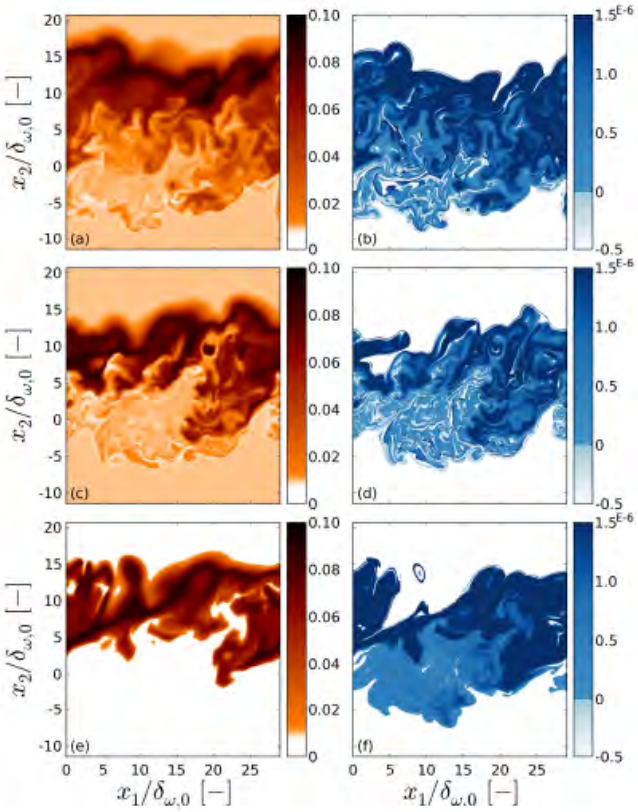

Figure 3. Y_{H2O} (a,c,e) and D_{H2O} (b,d,f) for the same cases as in Fig. 2. D_{H2O} is in m^2/s.

III. Future Plans

The following activities are planned:

- Develop the explicitly-filtered LES methodology for high-p flows.
- Analyze *a priori* the reacting-flow database and propose subgrid-scale models for the turbulent reaction terms.

IV. References

i. Masi, E.; Bellan, J.; Harstad, K.; Okong'o, N. *J. Fluid Mech.* **2013,** *721*, 578

ii. Taşkinoğlu, E. S.; Bellan, J., *J. Fluid Mech.*, **2010**, *645*, 211

iii. Taşkinoğlu, E. S.; Bellan, J., *J. Fluid Mech.*, **2011**, *679*, 156

V. Publications, presentations and submitted articles supported by this project during 2011- 2013

[1] Masi, E. and Bellan, J., The subgrid-scale scalar variance under supercritical pressure conditions, *Phys. Fluid*s, 23(8), doi:085101 (22 pages), 2011

[2] Masi, E. and Bellan, J., The subgrid scalar variance equation under supercritical pressure conditions, paper 1C04, 7th US National Combustion Meeting, Atlanta, GA., 3/21-3/23, 2011

[3] Masi, E., Bellan, J., Harstad, K. and Okong'o N., Multi-species turbulent mixing under supercritical-pressure conditions: modeling, Direct Numerical Simulation and analysis revealing species spinodal decomposition, *J. Fluid Mech.*, 721, 578-626, 2013

[4] Masi, E., Bellan, J. and Harstad, K., Pressure effects from Direct Numerical Simulation of high-pressure multispecies mixing, paper 2013-0711, 51th Aerospace Sciences Meeting, Dallas, TX, 1/7-1/10, 2013

[5] Borghesi, G. and Bellan, J., Irreversible entropy production rate in high-pressure turbulent reactive flows, submitted *Proc. of the Comb. Inst.*, 11/19/2013

Towards predictive simulations of soot formation: from surrogate to turbulence

Guillaume Blanquart
Department of Mechanical Engineering
California Institute of Technology
1200 E. California Blvd., Pasadena, CA 91125

Objectives

The combustion of hydrocarbon fuels, including kerosene, gasoline, and diesel, leads to the formation of soot particles which are known to be the source of several health problems and environmental issues.

The objective of the proposed work is to reduce the gap in the present understanding and modeling of soot formation both in laminar and turbulent flames. This effort spans several length scales from the molecular level to large scale turbulent transport. More precisely, the objectives are three fold: 1) develop a *single combined chemical and soot model* validated for all relevant components usually found in real fuel surrogates; 2) develop a framework able to *explain the complete evolution of soot particles* from cluster of PAHs to oxidation of large fractal aggregates; 3) *understand and model the interplay* between unsteady chemistry, differential diffusion, and turbulent transport.

Recent progress

This year, Large Eddy Simulations (LES) have been performed on an ethylene/air piloted turbulent non-premixed sooting jet flame to quantify the importance of aromatic chemistry-turbulence interactions. Aromatic species are of primary importance since their concentrations control directly the soot nucleation rates.

This work has been accepted recently for publication in the Proceedings of the Combustion Institute [1].

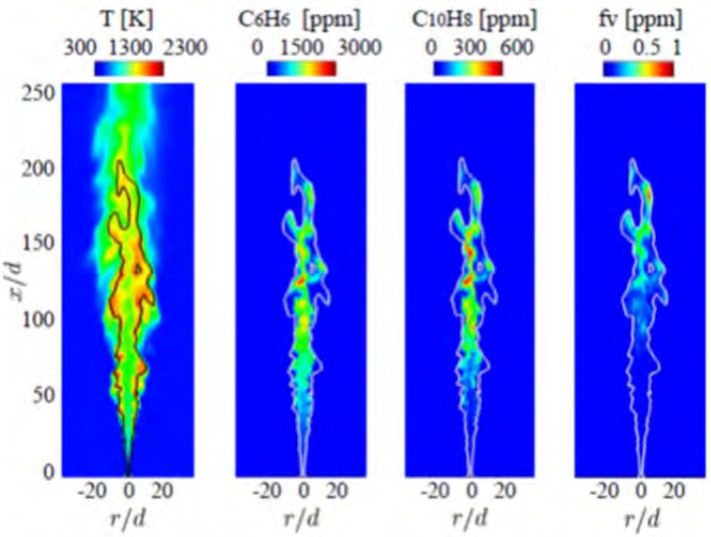

Figure 1. Instantaneous fields of temperature, benzene mass fraction, naphthalene mass fraction, and soot volume fraction. The iso-contour of stoichiometric mixture fraction is shown in solid line.

Numerical algorithms

The proposed simulation framework relies on four major components: a gas-phase chemistry model, a turbulence closure model, a PAH relaxation model, and finally a soot model.

First, the combustion processes are described using the flamelet/progress variable (FPV) approach, extended to include radiative heat losses in the limit of optically thin medium. In the LES, all sub-filter fluxes are closed using a dynamic Smagorinsky model with Lagrangian averaging techniques. The filtered thermochemical quantities are obtained from the equation of state by convolution with a joint sub-filter PDF. Soot formation depends critically on the concentrations of its precursors, namely

aromatic species, which exhibit substantial transient effects due to turbulent unsteadiness. To account for these effects, transport equations are solved for their mass fractions. The chemical source terms for these transported aromatic species are closed using a recently developed ***relaxation*** model [2]. Finally, the geometry of fractal soot aggregates is described using a bi-variate description based on its total volume V and total surface area S. The evolution of soot particles is described, from a statistical point of view, by solving the transport equations for several key moments, and their source terms are closed using the Direct Quadrature Method of Moments (DQMOM).

Details of Sandia Flame

The described models are integrated into LES of a non-premixed ethylene/air piloted turbulent jet flame, experimentally investigated at Sandia National Laboratories by Dr. Shaddix. This flame is selected over other experimentally studied turbulent non-premixed flames, for its relatively large soot yield, high Reynolds number, and well-defined boundary conditions. The burner consists of two concentric tubes, with high-speed fuel injection in the inner one, and low-speed injection of fuel/air mixture in the outer one (pilot flame). While the fuel jet delivers pure ethylene, premixed ethylene/air mixture at an equivalence ratio of 0.9 is supplied as pilot stream.

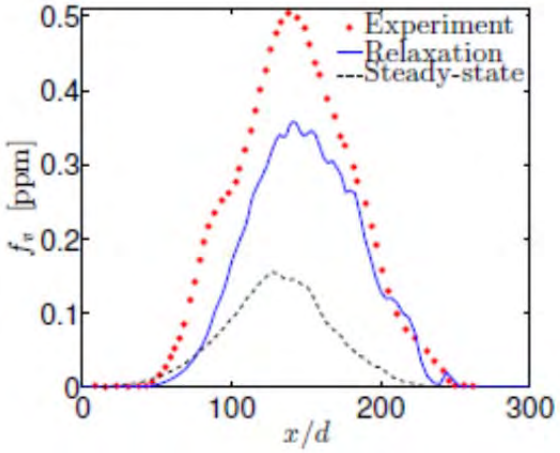

Figure 2. Mean soot volume fraction on the flame centerline.

Results

As expected, the yield of aromatic species and soot is predominant in fuel rich regions (see Fig. 1). The formation of benzene is shown to initiate at x/d=15, while naphthalene is observed to form only after x/d=30. Soot formation occurs at locations even more downstream at x/d=50. These lags in formation locations reflect the combined effects of the sequential formation of aromatic species and soot, and the large time scales governing their formation.

Figure 2 shows the time-averaged soot volume fractions on the flame center-line from both LES and from laser-induced incandescence measurements. Comparison between LES data and experimental results indicates that the relaxation LES predicts the mean soot distribution reasonably accurately. On the other hand, the steady-state LES predicts a lower soot yield and a slightly shifted soot profile towards the burner exit.

Turbulence-chemistry interaction impacts not only mean quantities, but also the fluctuations in soot, as shown in Fig. 3. Both the mean value and the magnitude of fluctuations

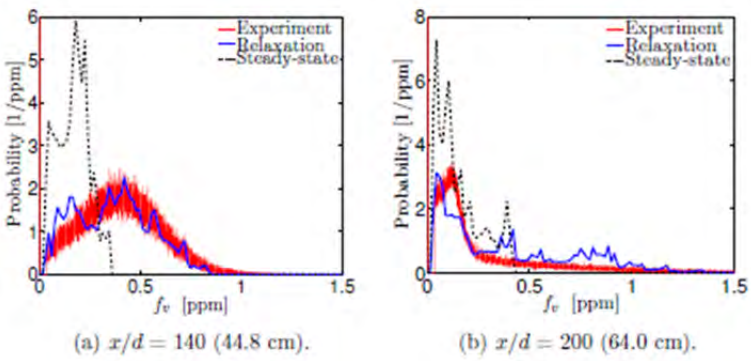

Figure 3. PDFs of soot volume fraction at two locations on the flame centerline.

(width of the PDF) are well captured by the relaxation LES; although occurrence of low soot volume fractions (fv < 0.2 ppm) is slightly over-predicted. In contrast, the steady-state LES predicts a lower mean, as aforementioned, and significantly smaller fluctuations (narrower PDF).

Current and future work

Direct Numerical Simulations of turbulent sooting flames

Simultaneously to the development of the chemistry and soot models, we have set up (and are running) Direct Numerical Simulations of soot formation. The focus is placed on two elements: 1) developing an accurate and robust numerical scheme for the transport of soot quantities in a highly turbulent flow field, and 2) identifying the most relevant initial conditions to study the inception of soot in a turbulent flow field.

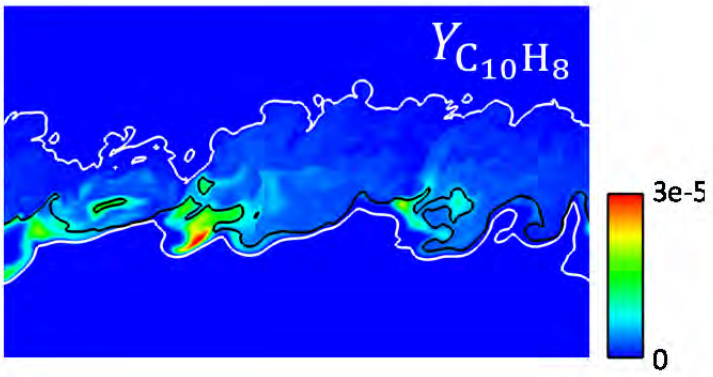

Figure 4. Preliminary results of the DNS of a turbulent mixing layer. Profile of naphthalene mass fraction.

Preliminary results (see Fig. 3) show a strong effect of turbulent unsteadiness on the yield of soot precursors (such as naphthalene) consistently with the analysis performed in laminar flames and in the LES [1,2].

Publications

Xuan, Y., Blanquart, G., « *A flamelet-based relaxation model for polycyclic aromatic hydrocarbons in turbulent flames* », Combust. Flame (2014).

Xuan, Y., Blanquart, G., « *Effects of aromatic chemistry-turbulence interactions on soot formation in a turbulent non-premixed flame* », Proc. Comb. Inst. (2014) accepted.

Theoretical Studies of Combustion Dynamics (DE-FG02-97ER14782)

Joel M. Bowman
Cherry L. Emerson Center for Scientific Computation and Department of Chemistry, Emory University Atlanta, GA 30322, jmbowma@emory.edu

Program Scope. The research supported by this grant focuses on the development of rigorous computational methods to model and predict the basic chemical and physical processes of importance in gas-phase combustion reaction dynamics. This includes the development of full-dimensional, *ab initio*-based potential energy surfaces (PESs) that describe complex unimolecular and bimolecular reactions and energy transfer, as well as anharmonic, coupled vibrational dynamics. Applications are made using quasiclassical, semiclassical and quantum treatments of the nuclear motion. The choice of system to study is typically stimulated by state-of-the-art experiments that advance basic understanding of combustion reaction dynamics and which can benefit from theoretical collaborations.

Recent Progress: The following projects have been completed and written up: Potential energy surfaces and dynamics calculations of the bimolecular reactions $O+NO_2$, OH+CO, X(X=O, F, Cl) $+CH_4$ and $O(^3P)+C_2H_4$, and unimolecular dissociation reactions CH_2CH_2OH, C_3H_5, and CH_3CHO. In addition, an extension of so-called 1G Gaussian binning, which makes use of exact quantum vibrational energies and assignments, was reported and successfully applied to the final vibrational distribution of H_2O in the reactive quenching of OH* by H_2. The most recent work has been on the OH+HBr reaction and a new research direction on calculations of energy transfer in molecules for which accurate full dimensional potential energy surfaces have been previously obtained. Progress in this most recent work is described next. **OH+HBr.** An *ab initio* global PES and quasiclassical trajectory calculations of k(T) over the temperature range 5 to 500 K was completed. The PES is a permutationally invariant fit to 26 000 spin-free UCCSD(T)-F12a/cc-pVDZ energies. A schematic of the PES along the reaction path is shown below at the left. As seen the reaction is highly exoergic with a negative-energy saddle point and pre and post-reaction

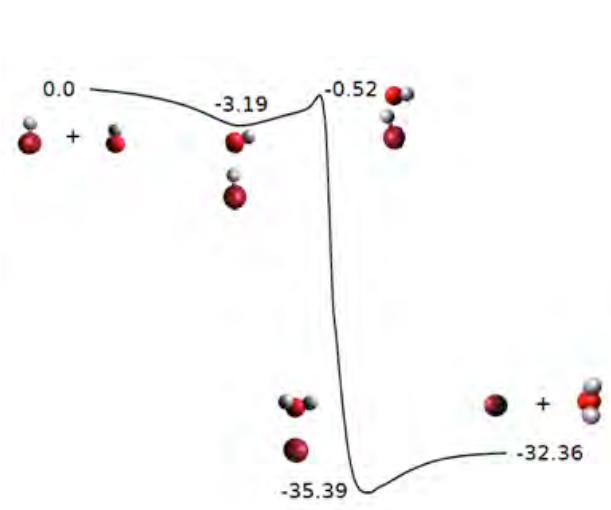

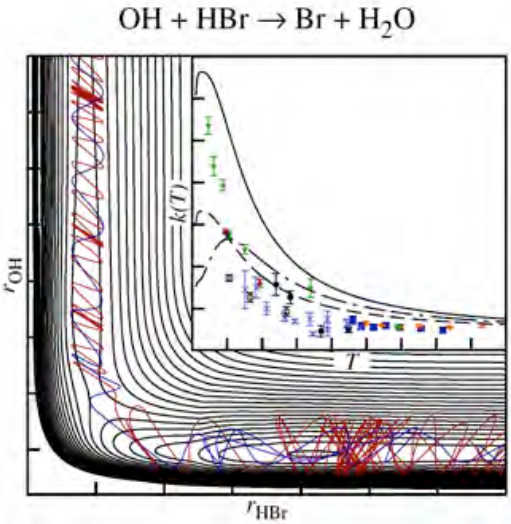

wells. To the right is a relaxed potential energy contour plot with a representative trajectory superimposed. The comparison between the calculated and experimental k(T) is also given. The various calculations come from different quantum mechanical treatments of the OH rotational partition function, Note the unusual behavior of k(T) with T and the unprecedented agreement with experiment. This work has just appeared in J. Phys. Chem. Lett. **Energy transfer in $H+C_2H_2$, Ar+allyl, and Ar+HOCO.** Classical trajectory calculations

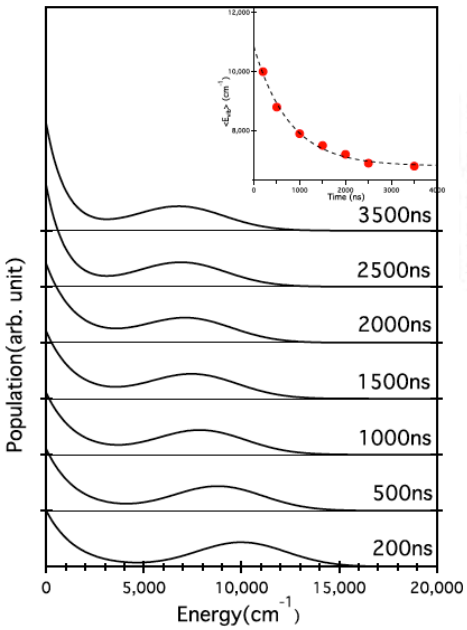

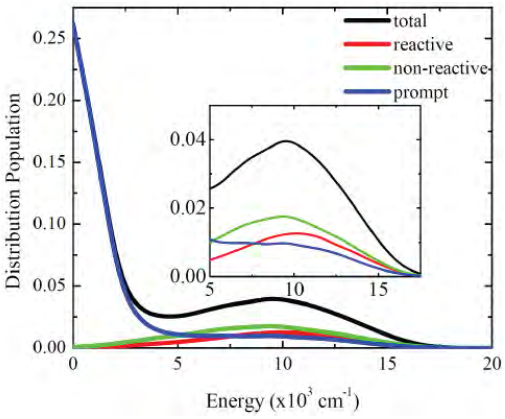

of energy transfer in fast H-atom collisions with ground vibrational state C_2H_2 were performed using an *ab initio* PES. This work was done in collaboration with the group at Temple (J. Smith and H.-L. Dai) who performed analogous experiments and probed the internal energy distribution of the post-collision C_2H_2 via emission spectroscopy. The experimental energy transfer was shown to have a very large component and agreement between experiment, shown in the left panel and theory, shown in the right panel, in the figure to the right is excellent. Notably, the experimental results at the shortest time after collision (200 ns) show a peak in the internal energy of 10 000 cm^{-1} in agreement with the calculated peak at the same initial relative kinetic energy of 1.6 eV. Examination of trajectories reveals the important role of transient complex formation of C_2H_3 for very large energy-transfer collisions. (This work has just appeared as a JACS Communication.) Energy transfer studies have been initiated in the allyl radical, using a full dimensional *ab initio* PES. In the first studies, the collision partner was Ar and an *ab initio* interaction potential was calculated at the MP2/aug-cc-pVTZ level, with counterpoise correction. This interaction potential was represented by a standard sum-of-pairs form (using the sophisticated two-body functional form suggested by Varandas and Rodrigues, J. Chem. Phys. **106**, 9647(1997)) and fit to 286 electronic energies. The pairwise fit gave RMS fitting errors of 22 cm^{-1} for the (negative energy) attractive region, 150 cm^{-1} for energies up to around 1200 cm-1, and 650 cm^{-1} for energies up to roughly 8000 cm^{-1} Thus, this fit is realistic, if not highly precise. Energy transfer calculations were done for allyl initially non-rotating and and in the lowest energy isotopomer configuration. The results in the form of ΔE (up and down) distributions for a number of collision energies have been published.[P27] Simultaneous with the Ar + allyl project, a project investigating energy transfer in Ar+HOCO is underway. This project makes use of a global, high-level *ab initio* global potential surface for HOCO and the calculation of the interaction potential. In this case, the goal was to obtain a benchmark quality interaction potential. This was done by using permutationally invariant (PI) fitting to roughly 12 500 CCSD(T)-F12/aug-cc-pVDZ energies. The RMS fitting error is 28 cm^{-1} for this data set which spans a range from -250 to 12 000 cm^{-1}. The data set was also fit using the pairwise form used for Ar-allyl and novel compact PI form. All three fits were used in preliminary calculations of energy transfer and an initial report of the results has just been accepted for publication as Communication in J. Chem. Phys. **Rovibrational energies of polyatomic molecules.** The code MULTIMODE has been extended and applied to perform essentially exact rovibrational calcuations of polyatomic molecules. An application to *cis* and *trans*-HOCO has recently been done, using an accurate semi-global PES that spans both isomers. A corresponding *ab initio* dipole moment surface has been used to obtain "line-list" quality spectra of these isomers. That work is being written up for publication with the aim to assist experimental determination of the as-yet-unreported OH-stretch energy of *cis*-HOCO. Calculations indicate that that state is heavily mixed.

Future Plans. Further work on energy transfer calculations in both Ar+HOCO and Ar+allyl is planned. Both molecules have isomeric forms and we plan to investigate the dependence of the energy transfer on the isomer. Both molecules (and the PESs describing them) can dynamically isomerize and dissociate to a variety of products subsequent to a collision with Ar. These aspects of the collision dynamics will be examined in the next year. Further development and applications of the MULTIMODE code will also be done. This work will include new coding to parallelize the evaluation of the potential matrix over the n-mode grids.

PUBLICATIONS SUPPORTED BY THE DOE (2011-2013)

1. Dynamics of the Reaction of Methane with Chlorine Atom on an Accurate Potential Energy Surface, G. Czakó and J. M. Bowman, Science **334**, 343 (2011).
2. Quasiclassical Trajectory Calculations of the Dissociation Dynamics of CH_3CHO at High Energy Yield Many Products Y-C Han, B. C. Shepler, and J. M. Bowman J. Phys. Chem. Lett. **2**, 1715 (2011).
3. Communication: Probing the Entrance Channels of the X + CH_4 → HX + CH_3 (X = F, Cl, Br, I) Reactions via Photodetachment of X^-–CH_4, M. Cheng, Y. Feng, Y. Du, Q. Zhu, W. Zheng, G. Czakó, and J. M. Bowman, J. Chem. Phys. **134**, 191102 (2011).
4. The Dynamics of Allyl Radical Dissociation, C. Chen, B. Braams, D. Y. Lee, J. M. Bowman, P. L. Houston, and D. Stranges, J. Phys. Chem. A **115**, 6797 (2011).
5. Three-State Trajectory Surface Hopping Studies of the Photodissociation Dynamics of Formaldehyde...", B. Fu, B. C. Shepler, and J. M. Bowman, J. Am. Chem. Soc. **133**, 7957 (2011).
6. Are Roaming and Conventional Saddle Points for H_2CO and CH_3CHO Dissociation to Molecular Products Isolated from Each Other? B. C. Shepler, Y. Han, and J. M. Bowman, J. Phys. Chem. Lett. **2**, 834 (2011).
7. An *Ab Initio* Spin-Orbit-Corrected Potential Energy Surface and Dynamics for the F + CH_4 and F + CHD_3 Reactions, G. Czakó and J. M. Bowman, Phys. Chem. Chem. Phys. **13**, 8306 (2011).
8. Invited Perspective: High-dimensional *Ab Initio* Potential Energy Surfaces for Reaction Dynamics Calculations, J. M. Bowman, G. Czakó, and B. Fu, Phys. Chem. Chem. Phys. **13**, 8094 (2011).
9. Roaming Radicals, J. M. Bowman and B. C. Shepler, Annu. Rev. Phys. Chem. **62**, 531 (2011).
10. Roaming reactions: The Third Way, J. M. Bowman and A. G. Suits, Phys. Today **64**, 33 (2011).
11. Accurate *Ab Initio* Potential Energy Surface, Thermochemistry, and Dynamics of the Cl(^{2}P, $^2P_{3/2}$) + CH_4 → HCl + CH_3 and H + CH_3Cl Reactions, G. Czakó and J. M. Bowman, J. Chem. Phys. **136**, 044307 (2012).
12. Communication: A Chemically Accurate Global Potential Energy Surface for the HO + CO → H + CO_2 Reaction, J. Li, Y. Wang, B. Jiang, J. Ma, R. Dawes, D. Xie, J. M. Bowman, and H. Guo, J. Chem. Phys. **136**, 041103 (2012).
13. Large-Amplitude Dynamics in Vinyl Radical: The Role of Quantum Tunneling as an Isomerization Mechanism, A. R. Sharma, J. M. Bowman, and D. J. Nesbitt, J. Chem. Phys. **136**, 034305 (2012).
14. Overtone-Induced Dissociation and Isomerization Dynamics of the Hydroxymethyl Radical (CH_2OH and CD_2OH). I. A theoretical Study, E. Kamarchik, C. Rodrigo, J. M. Bowman, H. Reisler, and A. I. Krylov. J. Chem. Phys. **136**, 084304 (2012)
15. Mode Selectivity for a "Central" Barrier Reaction: Eight-Dimensional Quantum Studies of the O(^{3}P) + CH_4 → OH + CH_3 Reaction on an *Ab Initio* Potential Energy Surface, R. Liu, M. Yang, G. Czakó, J. M. Bowman, J. Li, and H. Guo, J. Phys. Chem. Lett. **3**, 3776 (2012).
16. Theoretical Study of the Validity of the Polanyi Rules for the Late-Barrier Cl+CHD_3 Reaction, Z. Zhang, Y. Zhou, D. H. Zhang, G. Czakó, and J. M. Bowman, J. Phys. Chem. Lett. **3,** 3416 (2012).

17. First-Principles Calculations of Rovibrational Energies, Dipole Transition Intensities and Partition Function for Ethylene using MULTIMODE, S. Carter, A. R. Sharma, and J. M. Bowman, J. Chem. Phys. **137**, 154301 (2012).
18. Translational Energy Dependence of the Cl+CH_4(v_b=0, 1) Reactions: A Joint Crossed-Beam and Quasiclassical Trajectory Study, B. Zhang, Kopin L., G. Czakó and J. M. Bowman, Mol. Phys. **110**, 1617 (2012).
19. Quasi-Classical Trajectory Study of the HO + CO → H + CO_2 Reaction on a New *Ab Initio* Based Potential Energy Surface, J. Li, C. Xie, J. Ma, Y. Wang, R. Dawes, D. Xie, J. M. Bowman, and H. Guo, J. Phys. Chem. A **116**, 5057 (2012).
20. Quasiclassical Trajectory Study of Fast H-atom Collisions with Acetylene, Y.-C. Han, A. R. Sharma, and J. M. Bowman, J. Chem. Phys. **136**, 214313 (2012).
21. Dynamics of the O(^{3}P)+CHD_3(v_{CH} = 0,1) Reactions on an Accurate *Ab Initio* Potential Energy Surface, G. Czakó and J. M. Bowman, Proc. Natl. Acad. Soc. U.S.A **109**, 7997 (2012).
22. MULTIMODE Calculations of Rovibrational Energies of C_2H_4 and C_2D_4, S. Carter, J. M. Bowman, and N. C. Handy, Mol. Phys. **110**, 775 (2012).
23. Intersystem Crossing and Dynamics in the O(^{3}P)+C_2H_4 Multichannel Reaction: Experiment Validates Theory, B. Fu, Y.-C. Han, J. M. Bowman, L. Angelucci, N. Balucani, F. Leonori, and P. Casavecchia, Proc. Natl. Acad. Soc. U.S.A., **109**, 9733 (2012).
24. Three-State Surface Hopping Calculations of Acetaldehyde Photodissociation to CH_3+HCO on *Ab Initio* Potential Energy Surfaces, B. Fu, Y-C. Han, and J. M. Bowman, Faraday Discuss. **157**, 27 (2012).
25. Dipole Surface and Infrared Intensities for the *cis*- and *trans*-HOCO and DOCO Radicals, X. Huang, R. C. Fortenberry, Y. Wang, J. S. Francisco, T. D. Crawford, J. M. Bowman, and T. J. Lee, J. Phys. Chem. A **117**, 6932 (2013).
26. Variational Calculations of Vibrational Energies and IR Spectra of *trans* and *cis*-HOCO Using New *ab initio* Potential Energy and Dipole Moment Surfaces, Y. Wang, S. Carter, and J. M. Bowman, J. Phys. Chem. A **111**, 9343 (2013).
27. Classical Trajectory Study of Energy Transfer in Collisions of Highly Excited Allyl Radical with Argon, R. Conte, P. Houston, and J. M. Bowman, J. Phys. Chem. A **117**, 14028 (2013).
28. A novel Gaussian Binning (1GB) analysis of vibrational state distributions in highly excited H_2O from reactive quenching of OH* by H_2, R. Conte, B. Fu, E. Kamarchik, and J. M. Bowman, J. Chem. Phys. **139**, 044104 (2013).
29. Effects of High Angular Momentum on the Unimolecular Dissociation of CD_2CD_2OH: Theory and Comparisons with Experiment, B. G. McKown, M. Ceriotti, C. C. Womack, E. Kamarchik, L. J. Butler, and J. M. Bowman, J. Phys. Chem. A **117**, 10951 (2013).
30. Quasiclassical Trajectory Studies of ^{18}O(^{3}P) + NO_2 Isotope Exchange and Reaction to O_2 + NO on D_0 and D_1 Potentials, B. Fu, D. H. Zhang, and J. M. Bowman, J. Chem. Phys. **139**, 024303 (2013).

Dynamics of Product Branching in Elementary Combustion Reactions: OH + Alkenes and Nitrogen Chemistry

Laurie J. Butler
The University of Chicago, The James Franck Institute
5640 South Ellis Avenue, Chicago, IL 60637
L-Butler@uchicago.edu

I. Program Scope

While the total rate constant for many elementary reactions is well-characterized, understanding the product branching in complex reactions presents a formidable challenge. To gain an incisive probe of such reactions, our experiments directly investigate the dynamics of the product channels that arise from long-lived radical intermediates along the bimolecular reaction coordinates. Our work[1-4] uses the methodology developed in my group in the last fourteen years, using both imaging and scattering apparatuses. The experiments generate a particular isomeric form of an unstable radical intermediate along a bimolecular reaction coordinate and study the branching between the ensuing product channels of the energized radical as a function of its internal rotational and vibrational energy under collision-less conditions.

The experiments use a combination of: 1) measurement of product velocity and angular distributions in a crossed laser-molecular beam apparatus, with electron bombardment detection in my lab in Chicago or 2) with tunable vacuum ultraviolet photoionization detection at Taiwan's National Synchrotron Radiation Research Center (NSRRC), and 3) velocity map imaging using state-selective REMPI ionization, single photon ionization, and now tunable vacuum ultraviolet photoionization of radical intermediates and reaction products. In the third funding period we finished our experiments on two radical intermediates in the reaction of OH + propene. We also completed our theoretical study, in collaboration with Joel Bowman (Emory), Michele Ceriotti (EPFL) and Eugene Kamarchik (Sandia), of the results our experiments on the OH + ethene radical intermediate, CD_2CD_2OH, and our experimental study, joint with Terry Miller (Ohio State), on the photodissociation of $BrCH_2CH_2ONO$ at 351 nm and the unimolecular dissociation of the nascent $BrCH_2CH_2O$ radicals. The results develop insight on product channel branching in reactions that proceed via an addition/elimination mechanism and provide a key benchmark for emerging electronic structure and dynamics calculations on polyatomic reactions that proceed through unstable radical intermediates.

II. Recent Progress

A. Photoproduct Channels from $BrCH_2CH_2ONO$ at 351 nm

Terry Miller's group has been interested in studying the spectroscopy of substituted alkoxy radicals, so had photolyzed at 351nm a series of substituted alkyl nitrites, XCH_2CH_2ONO (X=F, Cl, Br, OH) and obtained spectra of the observed products. They reported (J. Phys. Chem. A, 116, 12032 (2012)) that only for X=F did they observe the spectrum of substituted alkoxy radical, XCH_2CH_2O; for all systems they observed electronic transitions of formaldehyde and vinoxy radical, CH_2CHO. We completed and published our experimental work in this system this year, characterizing the primary photodissociation channels of $BrCH_2CH_2ONO$ at 351 nm and examining the unimolecular dissociation of the nascent $BrCH_2CH_2O$ radicals. Using electron bombardment ionization, we detected stable $BrCH_2CH_2O$ radicals that dissociatively ionized to CH_2CO^+, Br^+ and $BrCH_2^+$, identifying the signal in those spectra from stable $BrCH_2CH_2O$ radicals by momentum matching with the NO co-product signal; the stable radicals did not give observable signal at parent ion, only at these daughter ions. The only unimolecular dissociation

channel of the radicals detected was the expected channel $BrCH_2CH_2O \rightarrow BrCH_2 + CH_2O$, the source of Miller's formaldehyde signal.

Particularly important to the success of the work was the use of tunable vacuum ultraviolet (VUV) photoionization in our imaging apparatus. Electron bombardment ionization results in signal at m/e=93 (see Fig. 1) from two sources: CH_2Br products (green-dashed line fit) from the secondary dissociation of $BrCH_2CH_2O$ radicals and additional signal CH_2Br^+ from dissociative ionization of the stable $BrCH_2CH_2O$ radicals (blue fit). Tunable VUV photoionization at 8.78 eV allowed us to detect the CH_2Br from the $BrCH_2CH_2O \rightarrow CH_2Br + H_2CO$ product channel without contribution from signal from dissociative ionization of $BrCH_2CH_2O$ radicals.

The other results in this publication are described in the 2013 abstract book.

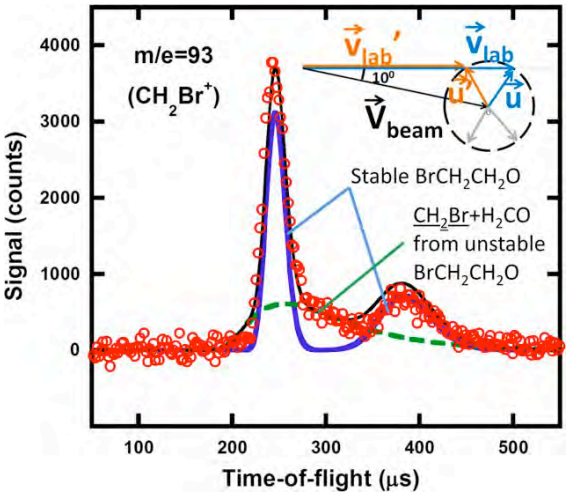

Figure 1. Signal at CH_2Br^+

B. Theoretical Study of the Dissociation Dynamics and Product Branching of the Partially Deuterated Radical Intermediate, CD_2CD_2OH, of the OH + ethene reaction

In this year we also completed our collaborative work with J. Bowman, E. Kamarchik, and M. Ceriotti (EPFL) on the unimolecular dissociation of CD_2CD_2OH radicals imparted with high angular momenta (~127$\hbar$). Our prior experimental work had measured the branching between three product channels expected from RRKM predictions and one, vinyl + water, that results from what Bowman identified as a roaming mechanism. My students Ben McKown and Carrie Womack carefully characterized the distribution of angular momenta imparted to the CD_2CD_2OH radical and Ben wrote the additional code to allow Bowman's QCT code to correctly include the initial angular momentum imparted to the radical intermediate. We also corrected our model for estimating the rotational energy in the radical from the measured recoil kinetic energy distribution for the C-Br bond photofission that generates the radical. The revised model may be used in the general case where the radical's rotation is not about a principle axis. Figure 2 below shows the derived distribution of J in the nascent radicals from the trans photolytic precursors, with an individual plot at one of the lower recoil kinetic energies that generates radicals with high

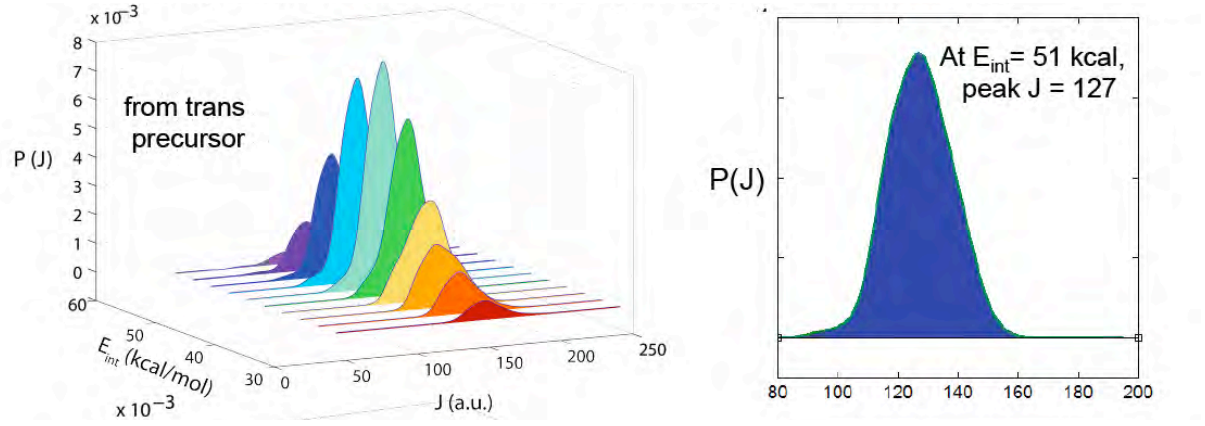

Figure 2: Representative angular momenta derived from expt for classical trajectory calculations.

enough internal energies to dissociate. Our trajectory results did not correctly reproduce the experimental branching ratios, but they did give an excellent prediction for the measured recoil

kinetic energy between the OH and ethene products from the high rotational energy CD_2CD_2OH radicals. This validates our model for deriving the distribution of energy between rotation and vibration in the nascent radical intermediates

We explored three dimensionality reduction methods to understand the trajectory results. Ceriotti's sketch maps (M. Ceriotti et al, PNAS 108, 13023 (2011)), originally developed for protein folding, gave us new physical insight on the unexpected H_2O + vinyl product channel from this addition intermediate. The left frame of Figure 3 plots the carbon−

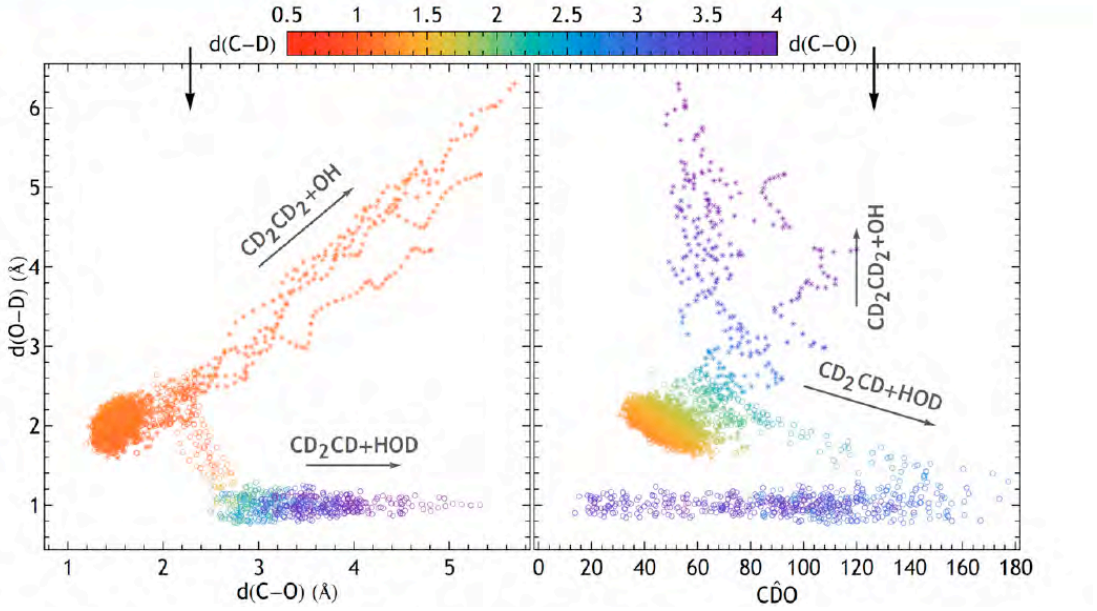

Figure 3. Bifurcation of trajectories en route to OH + ethene

oxygen distance versus the oxygen-abstracted deuterium distance, colored according to the C−D distance. At a carbon−oxygen distance and an oxygen−deuterium distance of 2.0−2.5 Å, the reaction path bifurcates. The right frame plots the oxygen-abstracted deuterium distance against the carbon-abstracted deuterium−oxygen bond angle with the points colored according to the carbon−oxygen bond distance. When the C−OH distance reaches 2.0−2.5 Å, the figure shows that the CDO bond angle drives the bifurcation. Small bond angles preferentially branch to the hydroxyl + ethene channel, while those with large bond angles branch to the vinyl + water product state.

B. Radical Intermediates in the Addition of OH to Propene

Finally, we submitted for publication our newly completed experiments which investigate the photolytic production of two radical intermediates in the reaction of OH with propene, one from addition of the hydroxyl radical to the terminal carbon and the other from addition to the center carbon. In a collision-free environment, we photodissociate a mixture of 1-bromo-2-propanol and 2-bromo-1-propanol at 193 nm to produce these radical intermediates. The data show two primary photolytic processes occur: C-Br photofission and HBr photoelmination. Using a velocity map imaging apparatus, we measured the speed distribution of the recoiling bromine atoms, yielding the distribution of kinetic energies of the nascent C_3H_6OH radicals + Br. Resolving the velocity distributions of $Br(^2P_{1/2})$ and $Br(^2P_{3/2})$ separately with 2+1 REMPI allows us to determine the total (vibrational + rotational) internal energy distribution in the nascent radicals. Using an impulsive model to estimate the

rotational energy imparted to the nascent C_3H_6OH radicals, we predict the percentage of radicals having vibrational energy above and below the lowest dissociation barrier, that to OH + propene; it accurately predicts the measured velocity distribution of the stable C_3H_6OH radicals. In addition, we use photofragment translational spectroscopy to detect several dissociation products of the unstable C_3H_6OH radicals: OH + propene, methyl + acetaldehyde, and ethyl + formaldehyde.

There is one exciting theoretical result in this work. For decades researchers have measured the energy imparted to recoil kinetic energy when radicals dissociate, but comparison of the measured distribution with theory required a global potential energy surface or dynamics-on-the-fly calculations that were only practical for very small molecular systems. Our new model uses the angular momenta of the unstable radicals and the tensor of inertia of each to **predict** the recoil kinetic energy and angular distributions when the C_3H_6OH radicals dissociate to OH + propene; the prediction gives an excellent fit to the data. The only required input is the measured recoil kinetic energies in the C-halogen bond photofission reaction that prepares the highly rotationally excited radical intermediate. As long as the initial photodissociation is via a repulsive excited state and radical dissociates with no barrier beyond the endoergicity, the model we developed accurately predicts the distribution of energies imparted to relative kinetic energy as the radical dissociates.

Figure 4. OH + Propene TOF spectra

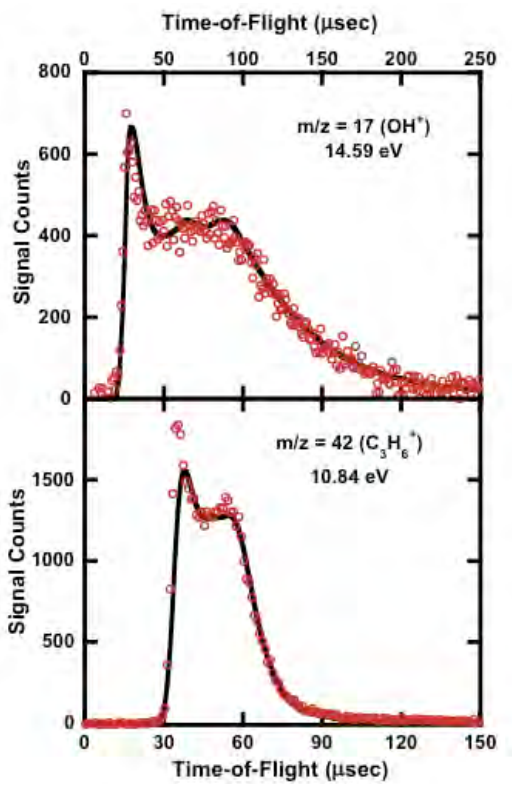

III. Publications Acknowledging DE-FG02-92ER14305 (2012 or later)

1. Photoproduct channels from $BrCD_2CD_2OH$ at 193 nm and the HDO + vinyl products from the CD_2CD_2OH radical intermediate, C. C. Womack, B. J. Ratliff, L. J. Butler, S. –H. Lee, and J. J. Lin, J. Phys. Chem. A 116, 6394-6407 (2012).

2. Effects of high angular momentum on the unimolecular dissociation of CD_2CD_2OH: Theory and comparisons with experiment, B. G. McKown, M. Ceriotti, C. C. Womack, E. Kamarchik, L. J. Butler, and J. M. Bowman, J. Phys. Chem. A 117, 10951-63 (2013).

3. Imaging and scattering studies of the unimolecular dissociation of the $BrCH_2CH_2O$ radical from $BrCH_2CH_2ONO$ photolysis at 351 nm, L. Wang, C. –S. Lam, R. Chhantyal-Pun, M. D. Brynteson, L. J. Butler, and T. A. Miller, J. Phys. Chem. A, 118, 404-416 (2014).

4. Radical Intermediates in the Addition of OH to Propene: Photolytic Precursors and Angular Momentum Effects, M. D. Brynteson, C. C. Womack, R. S. Booth, S. –H. Lee, J. J. Lin, and L. J. Butler, J. Phys. Chem. A, in press (2014).

Crossed-Molecular-Beam Studies of Energy Transfer.

David W. Chandler
Combustion Research Facility
Sandia National Laboratory
Livermore, CA 94551-0969
Email:chand@sandia.gov

Program Scope:

My research focuses on the field of chemical dynamics of gas phase molecular species. I define chemical dynamics as the detailed study of the motion of molecules and atoms on inter- or intra-molecular potential energy surfaces in order to learn about the details of the surface as well as the dynamics of their interactions. We have tested simple bimolecular potential energy surfaces by the careful study of collisional energy transfer processes in crossed molecular beam arrangements utilizing Velocity Mapped Ion Imaging techniques. Last year we reported on our study of electronically excited state collisions of NO(A). This year we report on an extension of these studies. We report a study to the collision-induced dissociation of NO_2 by an atomic collision partner. We use laser light to state-selectively excite the reagents and detect the products of collisional energy transfer / collision induced dissociation processes. We do this with high velocity resolution and with single quantum-state resolution of the product molecules. We have also been working on developing multiplexed spectroscopic techniques for detection of multiple species with microsecond time resolution.

Chemical Dynamics Progress Report: Collision Induced Dissociation of NO_2:

Over the last few years we have been exciting atoms and molecules into transient excited states at the crossing of two particle beams and observing the scattering induced by collisions at the crossing point of the beams. Our first project was studying elastic collisions of Kr atoms [1], then we studied the rotational energy transfer dynamics of NO (A) with atomic partners [2,3] and now we are vibrationally exciting NO_2 to within a few tens of wavenumbers below its dissociation energy and then monitoring the dissociation of the NO_2 after a single collision with an Ar atom. The collision induces translational to rotation and translation to vibration energy transfer. These ro-vibraionally hot molecules then dissociate producing NO(X, J <15) state molecules and a ground state O atom. By measuring the velocity distribution of each of the NO(X, J) states produced and the dissociation branching ratio of NO_2 into each rotational state of the NO as a function of NO_2 internal energy we are able to determine the shape of the Energy Transfer Function, P(E) for this very vibratonally hot molecule. One other study trying to measure the P(E) function for this CID process has been performed by the Reisler group [4,5,6] and our work is complimentary to the work they published.

In Figure 1 is shown a schematic of the experiment. Panel (a) shows the spatial configuration of the experiment. A 398-nm photon intersects a 5%NO_2 / Ar molecular beam before the crossing point with a second supersonic Ar beam. This 398-nm light electronically excites NO_2 to an energy just below the dissociation energy of the NO_2 molecule (we refer to this laser excited NO_2 as NO_2*) as is shown in panel (b). The scattering event produces many velocities (and correlated internal excitation) of NO_2 due to inelastic scattering (we refer to this doubly excited, photon plus collision, NO_2 as NO_2**), it is this velocity distribution that we want to extract from the

data. Following excitation the NO_2** will dissociate into many rotational quantum states of the NO molecule.

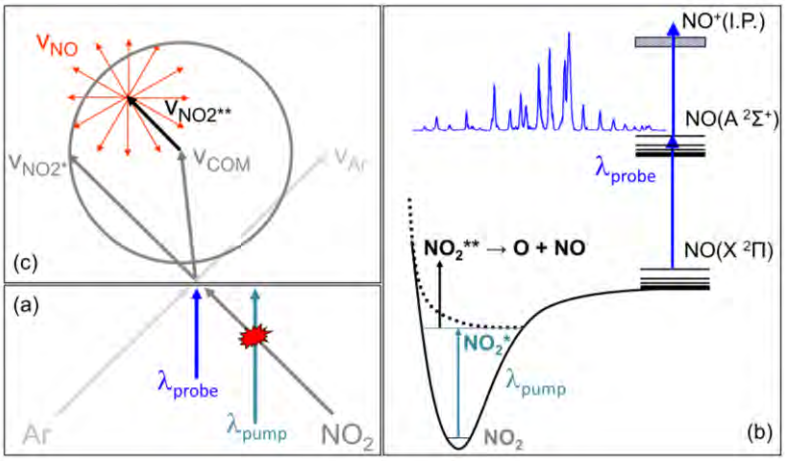

Figure 1. Schematic representation of the experiment. Panel (a) shows the spatial configuration, panel (b) shows the relative energetics, and panel (c) illustrates the key velocity components of the experiment. The Newton diagram shown in panel (c) shows the velocity components of the NO fragment as emanating from the velocity vector of the inelastically scattered NO_2** molecule.

The "Newton diagram" in panel (c) shows the velocity components of the NO fragment as emanating from the velocity vector of the inelastically scattered NO_2** molecule; the dynamics of NO_2* + Ar scattering are centered about the center-of-mass velocity, v_{COM}. We resonantly ionize the NO products and image them onto a position sensitive detector with a velocity mapped imaging apparatus. From this data we are able to determine the velocity distribution of each rotational state of the NO. This information along with the knowledge of the branching ratio of NO_2** into the NO rotational states as a function of energy is all that is required to extract the initial velocity distribution of the NO_2* + Ar collision. The branching ratio of the NO_2** is determined by photoexcitation of the NO_2 to particular energies and measuring the branching ratio into the NO rotational states as a function of excitation energy. We, as well as several groups previously, have measured this distribution and find that the NO(J) states are statistically populated.

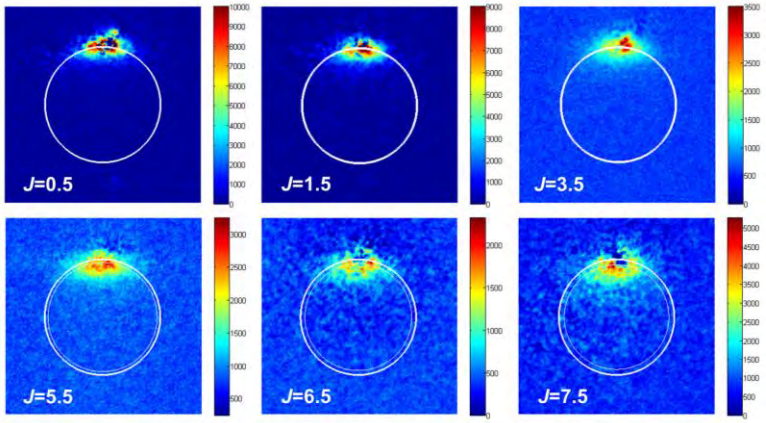

Figure 2. Raw images of velocity distributions from select NO(J) states. NO molecules are produced from collisional dissociation resulting from NO_2* + Ar inelastic scattering. NO_2* forward scattering is shown at the vertical position. The outer white circle shows the elastic scattering radius for NO_2 and the inner white circle shows the reduction of velocity equivalent to the degree of energy required to excite the given NO(J) rotational state from the NO + O dissociation threshold.

The velocity-mapped images of Figure 2 display the velocity of the NO products from the collision induced dissociation process. The velocity of each NO J state is sensitive to energy transfer in a region equal to and above its energetic threshold. By determining the difference between the expected velocity distribution if all energies were equally populated in the NO_2* + Ar collision and statistically distributed to the observed distribution one can determine the average energy transfer function that led to each NO rotational state. Figure 3 displays these averages along with the calculated averages and the previous measurement of Dr. Reisler's group. Their data is sensitive to large energy transfer (>250 cm^{-1}) and ours is sensitive to lower energy transfer (<250 cm^{-1}). At low energy there is strong agreement between the theory and experiment at large energy transfer the theory over-predicts the amount of energy transfer that is observed.

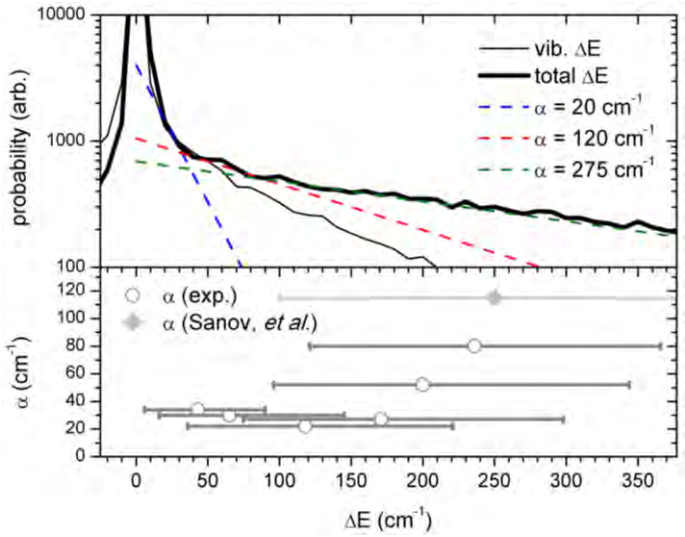

Figure 3. A comparison of experimentally-determined and calculated P(E) distributions. The calculated results in the upper panel are accompanied by three approximate single-exponentials spanning the energy region that the current experimental study is sensitive to. The best fit single-exponential P(E) function is shown in panel (a) for each J-state as the vertical position of a horizontal line. The open circle shows the "center-of-mass" of the J-state's "window", and the length of the line corresponds to the extent of that particular J-state "window" used to interrogate the NO2 P(E). Also shown is the experimental result from a previous experimental study of Sanov, *et al.* (5), with the corresponding energy range that was interrogated.

Present and Future work:

Scattering:

We are building a merged molecular beam scattering apparatus such that two, short (30 microsecond initial opening time), velocity-chirped beams will collided with approximately 7 degrees of angle between the beams. With this arrangement we believe we can scan the velocity distribution of the collisions between about 5 cm-1 of collision energy and 50 cm-1 of collision energy. At these energies and sufficient velocity resolution orbiting resonances for many systems are predicted[7]. We will first investigate collisions with NO as a collision partner. Calculations on OH +H2 and He as well as NH + He are also predicted to show significant resonance behavior. The energetic location of the resonances is a very stringent test of the long-range part of the potential energy surface for the collision partners and will be compared to theory. This orbiting dynamics is the same as what is predicted to account for the long lifetimes required to explain many three-body recombination reactions at high pressures.

Spectroscopy:

We have developed a new type of frequency comb spectrometer using two etalons of slightly different path lengths. By measuring the interference between the outputs of the two etalons one can determine the absorption of molecules within the etalon cavities. We are continuing the development of this spectrometer and have recently built a monolithic spectrometer where both etalon cavities are contained in a single block of invar. With this design and a infrared OPO we will be attempting to obtain time resolved high resolution (150 MHz) spectrum in the infrared potion of the spectrum. When successfully developed this spectrometer will allow one to obtain time-resolved spectra over the bandwidth of the OPO from a single laser shot.

References:

1) Cold Atoms by Kinematic Cooling, J.J. Kay, J. Klos, M. H. Alexander, K. E. Strecker, D. W. Chandler, Phys. Rev. A Vol.82 (3), 032709 (2010)
2) Direct Angle Resolved Measurements of Collision Dynamics with Electronically Excited State Molecules: NO(A2S+)+Ar, J. J. Kay, G Paterson, M. L. Costen, K. E. Strecker, K.G. McKendrick, D. W. Chandler., J Chem. Phys. 134, 091101 (2011)
3) Collisions of Electronically Excited Molecules: Differential Cross-Sections for Rotationally Inelastic Scattering of NO($A^2\Sigma^+$) with Ar and He,: J. J. Kay, J. D. Steill, J. Kłos, G. Paterson, M. L. Costen, K. E. Strecker, K. G. McKendrick, M. H. Alexander and D. W. Chandler, Molecular Physics 00268976.2012.670283. (2012)
4) C. R. Bieler, A. Sanov, M. Hunter and H. Reisler, Gas-Phase Collision-Induced Dissociation of Highly Excited NO2, J. Phys. Chem. 1994,98, 1058-1060.
5) A. Sanov, C. R. Bieler, and H. Reisler, Dissociation of Highly Excited NO_2 Induced by Collisions with Ar, CO, and O_2, J. Phys. Chem. **99**, 7339 (1995).
6) C. R. Bieler, A. Sanov, C. Capellos and H. Reisler, Molecular Beams Studies of the Dissociation of Highly Excited NO2 Induced by Molecular Colliders, J. Phys. Chem. 1996, 100, 3882-3887.
7 Cold and Unltracold Molecules: Spotlight on orbiting resonances: Chandler D. W., J. of Chem . Phys. Vol 132(11) 110901 (2010)

Publications 2012-2014:

1) Dual-Etalon Frequency-Comb Cavity-Ring-Down Spectrometer: D. W. Chandler and K. E. Strecker: J. Chem. Phys. 136,154201 (2012).
2) Collisions of electronically excited molecules: differential cross-sections for rotationally inelastic scattering of NO($A^2\Sigma^+$) with Ar and He,: J. J. Kay, J. D. Steill, J. Kłos, G. Paterson, M. L. Costen, K. E. Strecker, K. G. McKendrick, M. H. Alexander & D. W. Chandler, Molecular Physics DOI 10.1080/00268976.2012.670283. (2012)
3) Rotational Alignment of NO (A(2)S+ from Collisions with Ne: Steill, J. D., Kay J. J., Paterson G., Sharples T. R., Klos J., Costen M. L., Strecker K. E., McKendrick K. G., Alexander M. H., Chandler D. W., J. of Phys. Chem. Vol 117 (34), 8163-8174 (2013).
4) Determination of the Energy Transfer Function From the Collision Induced Dissociation of NO_2 + Ar. Steill JD, Strecker K. E. and Chandler D. W., manuscript in preparation. (2014).

Petascale Direct Numerical Simulation and Modeling of Turbulent Combustion

Jacqueline H. Chen (PI) and Sgouria Lyra
Sandia National Laboratories, Livermore, California 94551-0969
Email: **jhchen@sandia.gov**

Program Scope

In this research program we have developed and applied massively parallel three-dimensional direct numerical simulation **(**DNS) of building-block, laboratory scale flows that reveal fundamental turbulence-chemistry interactions in combustion. The simulation benchmarks are designed to expose and emphasize the role of particular phenomena in turbulent combustion. The simulations address fundamental issues associated with chemistry-turbulence interactions at atmospheric pressure that underly practical combustion devices: extinction and reignition, premixed and stratified flame propagation and structure, flame stabilization in autoignitive coflowing jet flames and reactive jets in crossflow, and flame propagation in boundary layers. In addition to the new understanding provided by these simulations, the resultant DNS data are used to develop and validate predictive mixing and combustion models required in engineering Reynolds-Averaged Navier Stokes (RANS) and large-eddy (LES) simulations.

Recent Progress

In the past year, computer allocations from a DOE Innovative and Novel Computational Impact on Theory and Experiment (INCITE) grant have enabled us to perform several petascale three-dimensional DNS of turbulent flames with detailed chemistry. These joint DNS/experimental studies focused on understanding: 1) the structure and stabilization of hydrogen-rich transverse jets in a vitiated turbulent flow [1], and 2) velocity and reactive scalar spectra from turbulent premixed flames [2]. DNS data were also used to develop and assess a new boundary layer flashback model [3]. Highlights of our accomplishments in the past year are summarized below, followed by a summary of future research directions.

Structure and stabilization of hydrogen-rich transverse jets in a vitiated turbulent flow [1]

Fuel rich hydrogen transverse jets in high temperature vitiated fully developed turbulent channel flow under inert and chemically reacting conditions are studied in a joint experimental and DNS study. Simultaneous stereoscopic PIV, OH-PLIF, three-dimensional dynamic pressure measurements and results from DNS with detailed H2/CO-air chemistry show the effects of the elevated temperature, composition and broadband turbulence of the vitiated cross-flow on the transverse jet, the mixing and flow field, flame stabilization, structure and combustion mode. The three dimensional DNS results of the inert and reacting JICFs show good agreement with the measured mean velocity fields. The mean flame location demarcated by the OH concentration is well captured.

Instantaneously, the inert and reacting shear layers are unstable, characterized by the formation of Kelvin-Helmholtz vortical structures responsible for the fuel-oxidant mixing. In the inert JICF the vortex roll-up has a pronounced preferred shedding frequency, whereas the shedding is more broadband when reactions are initiated. Dilatational effects induced by the density drop in the presence of the flame are important contributors to the increased jet width. Frequency spectra of the span-wise vorticity at distinct locations along the windward shear layer of the reacting JICF from the DNS show strong, narrow-band peaks at both the fundamental and the subharmonic instability frequencies, with the subharmonic becoming dominant further downstream by $y/d_j=3$. These observations are consistent with the findings of previous low density non-reacting JICF and suggest that the presence of significant near-field heat release and a fully-developed turbulent cross-flow does not alter the jet's stability properties, *i.e.* that the jet is globally unstable.

The propensity of the mixture to ignite prior to ignition and the global structure of the resultant burner attached diffusion flame is investigated using both CEMA and the Takeno flame index. The mixture is found to be highly explosive prior to ignition and after reactions are activated, a diffusion flame establishes anchored at the stagnation point in the wind-ward side and at the low velocity region in the lee-ward side.

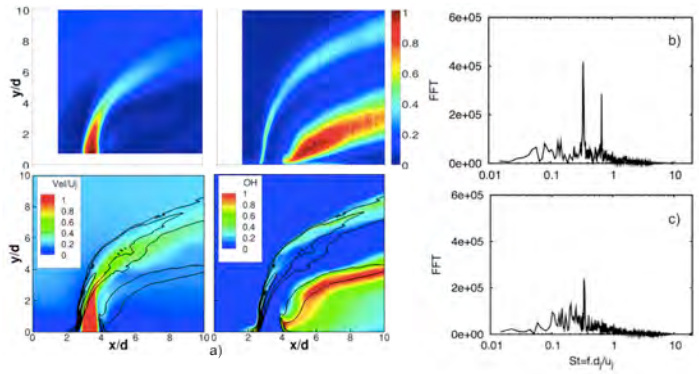

Figure 1. a) Reynolds-averaged velocity magnitude normalized by u_j (left) and normalized OH mass fraction (right), top: experiment, bottom: DNS from the reacting JICF. Iso-lines of the mean heat release rate between 10% and 90% (black) are overlaid on the DNS, and vorticity spectra at DNS probes along the windward shear layer of the reactive JICF at b) y/d = 1, and c) y/d = 3.

Velocity and reactive scalar spectra in turbulent premixed flames [2]

Turbulent combustion models rely on some implicit or explicit assumptions about the dynamics of turbulence-scalar mixing and associated scalar spectra. For instance, the widely used laminar flamelet model for non-premixed turbulent combustion relies on representing the thermo-chemical manifold with a single scalar whose evolution equations employ models based on passive scalar mixing assumptions. While such assumptions are strictly valid for purely passive scalars in incompressible homogeneous isotropic turbulence, it is unclear what the consequences of variable density, finite rate chemical kinetics and differential species diffusion are on the evolution of scalar spectra. Indeed, even the assumption of universality of velocity spectra in the so called dissipation range may be questionable for flows with strong local density change and dilatation, such as turbulent premixed flames, although it is routinely used for closing sub-grid Reynold's stresses in large eddy simulations (LES). While spectra of passive scalars have been widely studied, spectra of reactive scalars have thus far received limited attention.

Kinetic energy and reactive scalar spectra in turbulent premixed flames are studied from compressible three-dimensional DNS of a temporally evolving rectangular slot-jet premixed flame, a statistically one-dimensional configuration. The flames correspond to a lean premixed hydrogen-air mixture at an equivalence ratio of 0.7, preheated to 700 K and at 1 atmosphere and three DNS are considered with a fixed jet Reynolds number of 10000, turbulent Reynolds number varying between 500 and 1000, and a jet Damköhler number varying between 0.13 and 0.54 [4]. For the study of spectra, motivated by the need to account for density change which can be locally strong in premixed flames, a new density-weighted definition for two-point velocity/scalar correlations is proposed. The density weighted two-point correlation tensor retains the essential properties of its constant density (incompressible) counterpart and recovers the density weighted Reynolds stress tensor in the limit of zero separation. Using the density-weighted two-point velocity/scalar correlation, balance equations for velocity and scalar spectrum functions in wavenumber space are derived that illuminate physics unique to combusting flows. In particular, the pressure-dilatation correlation is found to be a source of kinetic energy at high wavenumbers and, analogously, reaction rate-scalar fluctuation correlation is a high wavenumber source of scalar energy. These results are verified by the spectra constructed from the DNS data. The kinetic energy spectra show a distinct inertial range with a $-5/3$ scaling followed by a 'diffusive-reactive' range at higher wavenumbers. The exponential drop-off in this range shows a distinct plateau in the wavenumber range corresponding to a laminar flame thickness and this is attributed to the contribution from the pressure-dilatation term in the energy balance in wavenumber space. Likewise, a clear spike in spectra of major reactant species - hydrogen - arising from the reaction rate term is observed at wavenumbers close to the laminar flame thickness. It appears that in the inertial range classical scaling laws for the spectra involving Kolmogorov scale are applicable, but in the high wavenumber range where chemical reactions have a strong signature the laminar flame thickness produces a better collapse. It is

suggested that a full scaling may involve not only the density weighted Kolmogorov scale, but also laminar flame thickness, density jump, Damköhler number and Karlovitz number.

Modeling of mean flame shape during premixed flame flashback in turbulent boundary layers [3]

Recent studies involving high-resolution experimental measurements and DNS [5,6], focused on the characterization of flashback for premixed, preheated hydrogen-air flames in turbulent boundary layers, and have shown that one of the principal assumptions behind the widely-used flashback model of Lewis and Von Elbe [7] is flawed. Indeed, this pioneering model, dating back to 1943, erroneously assumes that the premixed flame, during its flashback in the wall boundary layer, has no effect on the approaching flow of the reactants while recent DNS have revealed the presence of flow reversals, induced by the flame in the viscous layer, located immediately upstream of the flame surface regions that are convex towards the reactants [6]. The implications of this finding range from a radically different mechanism of boundary layer flashback to re-examination of a near-wall flame propagation model that accounts for the flame-flow coupling. Hence, a new model is proposed that describes the mean turbulent flame brush shape for premixed combustion in wall boundary layers and an *a priori* validation of the model is performed based on DNS data. The new model is able to capture the main features of the flame shape, though additional validation is required at higher Reynolds numbers.

Future Work:

Reactive Velocity and Scalar Spectra Scaling

Spectra are very difficult to measure in experiments since they typically require well-resolved three-dimensional spatio-temporal measurements that are quite challenging. DNS offer a unique way to study spectra in a rigorous manner. Recent results from DNS of turbulent premixed flames reveal that a density change induced by the flame occurring at a characteristic flame scale induces changes to the kinetic energy spectra with a significant deviation from the Kolmogorov scaling, particularly in the high wavenumber range. Furthermore, a dependence of the scaling on a Damköhler number (Da) – ratio of flow time scale to flame time scale – was discerned. A new theoretical framework to study spectral energy balance for variable density flows was proposed that clearly explained the cause of this deviation. However to fully ascertain the proper scaling and to study the balance of energy in the spectral space further DNS spanning a broader range of the relevant parameters, Da and density jump ratio, are required. Two new DNS are proposed, one with a higher Da (1.0) and another with a higher density jump ratio (6) to establish the scaling more clearly. The simulations will be performed using the Sandia DNS code S3D and in the same configuration as previous simulations, i.e. a temporally evolving turbulent premixed jet flame. A dimensional analysis will also be performed to understand the importance of the contribution of terms in the balance equations for the velocity and scalar spectrum functions in wavenumber space for combusting flows.

References:

1. S. Lyra, B. Wilde, H. Kolla, T. Lieuwen, J. H. Chen, "Structure and stabilization of hydrogen-rich transverse jets in a vitiated turbulent flow," submitted to *Proc. Comb. Inst.* Vol. 35, 2014.
2. H. Kolla, E. R Hawkes, A. Kerstein, N. Swaminathan, J. H. Chen, "On velocity and reactive scalar spectra in highly turbulent premixed flames," submitted to *J. Fluid Mech*., 2014.
3. A. Gruber, A.Kerstein, D. Valiev, H. Kolla, J. H. Chen, "Modelling of mean flame shape during premixed flame flashback in turbulent boundary layers," submitted to *Proc. Comb. Inst.* Vol. 35, 2014.
4. E. R. Hawkes, O. Chatakonda, H. N. Kolla, and J. H. Chen, "A petascale DNS study of the modelling of flame wrinkling for large-eddy simulations in intense turbulence," *Combust. Flame* **159(8)** (2012), 2690-2703.
5. C. Eichler and T. Sattelmayer, "Premixed flame flashback in wall boundary layers studied by long distance micro-PIV," *Exp. Fluids* **52 (2)** (2012),347-360.
6. A. Gruber, J. H. Chen, D. Valiev, C.K. Law, "Direct numerical simulation of premixed flame boundary layer flashback in turbulent channel flow," *J. Fluid Mech*., **709** (2012), 516-542.
7. B. Lewis and G. von Elbe, "Stability and structure of burner flames," *J. Chem. Phys*. **11** (1943), 75-97.

BES Publications (2012-2014):

1. Z. Luo, C. S. Yoo, E. Richardson, J. H. Chen, C. K. Law, T. Lu, "Chemical explosive mode analysis for a turbulent lifted ethylene jet flame in highly-heated coflow," *Combust. Flame* **159** (2012), 265-274.
2. E. R. Hawkes, O. Chatakonda, H. N. Kolla, and J. H. Chen, "A Petascale DNS study of the modelling of flame wrinkling for LES in intense turbulence," *Combust. Flame* **159(8)** (2012), 2690-2703.
3. E. S. Richardson and J. H. Chen, "Probability density function modelling of molecular mixing in flames with differential diffusion," *Combust. Flame* **159(7)** (2012), 2398-2414.
4. H. Kolla, R. Grout, A. Gruber, J. H. Chen, "Mechanisms of flame stabilization and blowout in a reacting turbulent hydrogen jet in cross-flow," *Combust. Flame* **159(8)** (2012), 2755-2766.
5. A. Gruber, J. H. Chen, D. Valiev, and C. K. Law, "Direct numerical simulation of premixed flame boundary layer flashback in turbulent channel flow," *J. Fluid Mech.* **709** (2012), 516-542.
6. R. W. Grout, A. Gruber, H. Kolla, P.-T. Bremer, J. C. Bennett, A. Gyulassy and J. H. Chen, "A direct numerical simulation study of turbulence and flame structure in transverse jets analysed in jet-trajectory based coordinates," *J. Fluid Mech.* **706** (2012), 351-383.
7. E. Knudsen, E. S. Richardson, E. M. Doran, H. Pitsch, and J. H. Chen, "Modeling scalar dissipation and scalar variance in LES: algebraic and transport equation closures," *Phys. Fluids* **24** 055103 (2012).
8. Shan R., Yoo C.S., Chen J.H., Lu T., "Computational diagnostics for n-heptane flames with chemical explosive mode analysis," *Combustion and Flame* **159(10)**, (2012), 3119-3127.
9. Y. Yang, H. Wang, S. B. Pope, J. H. Chen, "Large-eddy simulation/probability density function modeling of a non-premixed CO/H2 temporally evolving jet flame," *Proc. Comb. Inst.* **34** (2013), 1241-1249.
10. N. Chakraborty, H. Kolla, R. Sankaran, E. R. Hawkes, J. H. Chen, and N. Swaminathan, "Determination of three-dimensional quantities related to scalar dissipation rate and its transport from two dimensional measurements: Direct Numerical Simulation based validation," *Proc. Comb. Inst.* **34** (2013), 1151-1162.
11. C. M. Kaul, V. Raman, E. Knudsen, E. S. Richardson, J. H. Chen**,** "Large eddy simulation of a lifted ethylene flame using a dynamic nonequilibrium model for subfillter scalar variance and dissipation rate," *Proc. Comb. Inst.* **34** (2013), 1289-1296.
12. O. Chatakonda, E. R. Hawkes, A. Aspden, A. Kerstein, H. Kolla, J. H. Chen, "On the fractal characteristics of low Damkohler number flames," *Combustion and Flame*, **160** (2013) 2422-2433.
13. Y. Yang, S. B. Pope, J. H. Chen, "Empirical low-dimensional manifolds in composition space," *Combustion and Flame*, **160(10)** (2013) 1967-1980.
14. D. M. Valiev, M. Zhu, G. Bansal, H. Kolla, C. K. Law, J. H. Chen, "Pulsating instability of externally forced premixed counterflow flame," *Combustion and Flame* **160(2**), (2013) 285-294.
15. H. Zhang, E. R. Hawkes, J. H. Chen, S. Kook, "A numerical study of the autoignition of dimethyl ether with temperature inhomogeneities," *Proceedings of the Combustion Institute* **34(1),** (2013) 803-812.
16. C. S. Yoo, Z. Luo, T. Lu, H. Kim, J. H. Chen, "A DNS study of ignition characteristics of a lean iso-octane/air mixture under HCCI and SACI conditions," *Proceedings of the Combustion Institute* **34(2)** (2013) 2985-2993.
17. A. Gruber, P. Salimath, J. H. Chen, "Direct numerical simulation of laminar flame-wall interaction for a novel H2-selective membrane / injector configuration" (2014) in press, *International Journal of Hydrogen Energy*, http://dx.doi.org/10.1016/j.ijhydene.2014.01.148.
18. A. Bhagatwala, T. Lu, and J. H. Chen, "Direct numerical simulations of HCCI/SACI with ethanol," (2014) in press, *Combustion and Flame* http://dx.doi.org/10.1016/j.combustflame.2013.12.027
19. A. Krisman, J. Tang, E. R. Hawkes, D. Lignell, and J. H. Chen, "A DNS evaluation of mixing models for transported PDF modelling of turbulent nonpremixed flames," (2014) in press, *Combustion and Flame* http://dx.doi.org/10.1016/j.combustflame.2014.01.009.
20. Y. Xin, C. S. Yoo, J. H. Chen, C. K. Law, "A DNS study of self-accelerating cylindrical hydrogen-air flames with detailed chemistry," submitted *Proc. Combust. Inst.*, **35**, 2014.
21. A. Bhagatwala, T. Lu, H. Shen, J. Sutton, J. H. Chen, "Numerical and experimental investigation of turbulent DME jet flames," submitted *Proc. Combust. Inst.*, **35**, 2014.
22. A. Krisman, E. R. Hawkes, M. Talei, A. Bhagatwala, J. H. Chen, "Tribrachial, tetrabrachial and pentabrachial structures in dimethyl ether edge-flames at NTC conditions," submitted *Proc. Combust. Inst.*, **35**, 2014.
23. A. Gruber, A. Kerstein, D. Valiev, H. Kolla, J. H. Chen, "Modelling of Mean Flame Shape During Premixed Flame Flashback in Turbulent Boundary Layers," submitted *Proc. Combust. Inst.*, **35**, 2014.
24. R. A. C. Griffiths, J. H. Chen, H. Kolla, R. S. Cant, W. Kollmann, "Three-dimensional topology of turbulent premixed flame interaction," submitted *Proc. Combust. Inst.*, **35**, 2014.

Dynamics and Energetics of Elementary Combustion Reactions and Transient Species

Grant DE-FG03-98ER14879

Robert E. Continetti (rcontinetti@ucsd.edu)
Department of Chemistry and Biochemistry, University of California San Diego
9500 Gilman Drive, La Jolla, CA 92093-0340

I. Program Scope

This research program focuses on studies of transient neutral species and collision complexes relevant to combustion phenomena and fundamental elementary reactions. The experimental approach combines photoelectron and photofragment translational spectroscopies in coincidence to provide photoelectron-photofragment coincidence (PPC) measurements of the dissociative photodetachment (DPD) of anionic precursors. This yields a direct measure of the stability and dissociation dynamics of energy-selected reactive intermediates and neutral collision complexes. In the last year, significant advances were made in the studies of benchmark elementary reactions ($F + H_2O \rightarrow HF + OH$ and isotopologs), techniques for vibrational excitation of precursor anions and preliminary results on the effects of vibrational excitation on the $F + H_2O$ reaction. These new results build on the techniques described in the *Review of Scientific Instruments* (DOE pub. 3), in particular the integration of an electrostatic ion beam trap (EIBT) into the apparatus, and the experiments carried out on the HOCO radical and the $OH + CO \rightarrow H + CO_2$ reaction (DOE pubs. 2, 4) and ref. (*1*). In the following sections, recent progress will be reviewed in more detail, followed by a brief discussion of future work.

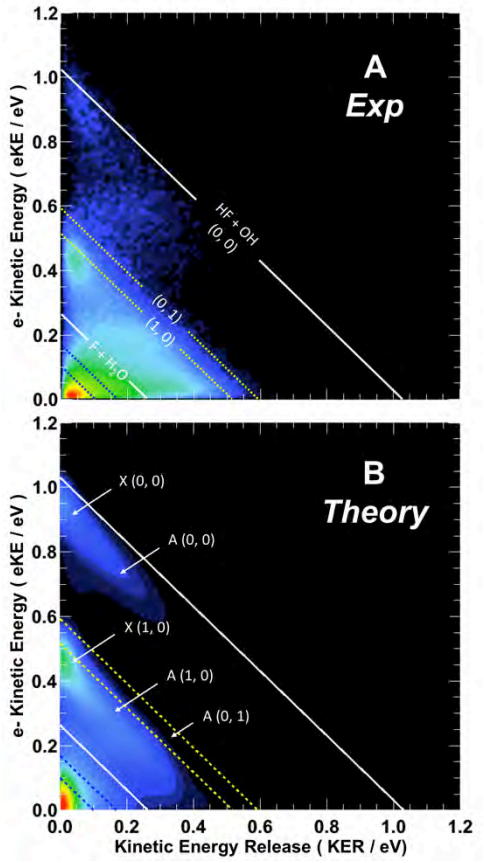

Fig. 1: Top Frame: PPC spectrum for the DPD of F (H_2O). The diagonal line at 1.05 eV denotes the maximum kinetic energy for dissociation into HF(v=0) + OH(v=0) + e^-. The dashed lines correspond to different (vHF,vOH) final states. The X and A designations indicate assignments to the ground, X, state and the first excited A state. Finally, the white line at 0.27 eV corresponds to the threshold for $F + H_2O + e^-$. Bottom Frame: 6-D quantum dynamics simulations of the PPC spectrum (see DOE pub. 6 and supplementary information for labeling).

II. Recent Progress

A. Imaging Dynamics of the $F + H_2O \rightarrow OH + HF$ Reaction from Wells to Barriers

The exothermic reaction $F+H_2O \rightarrow HF+OH$ represents a benchmark four-atom reaction at the frontier of current theoretical and experimental methods. The ground state potential energy surface has been extensively characterized (*2-5*) and global potential energy surfaces have been calculated for both the ground and first excited states.(*6*) The interaction of the F atom with water gives rise to three different PESs, two of which correlate with the $F(^2P_{3/2})$ ground state. In the adiabatic limit the lower-lying ground (*X*) state corresponds to $HF+OH(^2\Pi_{3/2})$ while the higher-lying excited (*A*) state leads to $HF+OH(^2\Pi_{1/2})$ products. Both of these surfaces feature a reaction barrier that separates van-der-Waals complexes on the entrance and exit channel side of the reaction.

In collaboration with Hua Guo's group at the University of New Mexico, we reported on a combined experimental and theoretical study on the FH_2O system, capturing the dynamics of the $F + H_2O \rightarrow HF + OH$ reaction at energies ranging from the reactant and product van der Waals wells to the top of the barrier (DOE pub. 6). In these studies, a PPC experiment using a photon energy of 4.80 eV was carried out to measure the DPD of F (H_2O). The experimental data and corresponding theoretical predictions of the coincidence spectrum are shown in Fig.

1. Using the coincidence technique, a wide range of observables was captured in a single experiment, including details on the dissociation dynamics on the two lowest-lying electronic states. Although the configuration of the nascent FH_2O is more "reactant-like" the spectra show that a majority of all events proceed to form HF + OH products. In addition to the dissociative channels a distinct photoelectron spectrum of stable FH--OH complexes was observed (not shown here) and attributed to long-lived stable and metastable states. Full dimensional (6-D) quantum mechanical wave packet calculations revealed that the dissociation dynamics of the FH_2O system involve both direct processes as well as a significant role for long-lived Feshbach resonances, localized in the FH(v′)--OH van-der-Waals complexes. Long lifetimes of these dynamical resonances of up to 5 μs were inferred from the delay after which stable FH_2O particles were detected in the experiments.

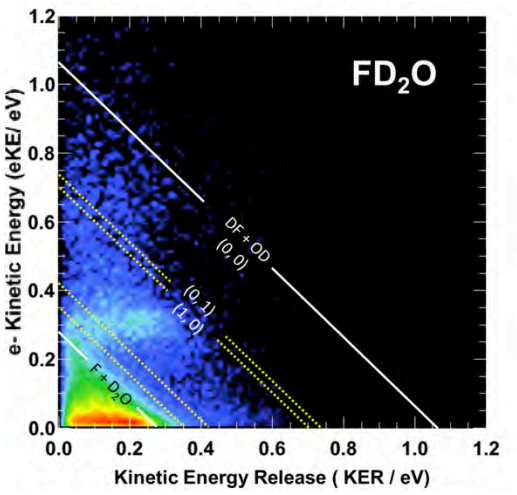

Fig. 2: PPC spectrum for the $F^-(D_2O)$ dissociation at a photon energy of 4.80eV. Energetic limits as in Figure 1, but for the perdeuterated products.

We have also carried out measurements on the $F^-(D_2O)$ and $F^-(HOD)$ isotopologs. The experimental results for $F^-(D_2O)$ are shown in Fig. 2, and reveal some important differences from the $F^-(H_2O)$ data in Fig. 1. In particular in the DF(v=0)+OD(v=0) region of the spectrum there is evidence for more significant product rotational excitation, and the anisotropic product distribution seen in this range for $F^-(H_2O)$ is missing. In the DF(v=1)+OD(v=0) region of the spectrum there is less intensity in the region of the spectrum approaching eKE = 0 (the highest excitations possible on the neutral potential energy surface) and the corresponding high KER products extending out to the maximum limit, KER ~ 0.7 eV. This indicates again a preference for increased excitation of product rotational degrees of freedom. The most striking feature, however, is the horizontal 'stripe' centered around eKE = 0.3 eV, extending out to the DF(v=1)+OD(v=0) limit. This feature is consistent with a metastable state decaying over the 5 μs time of flight (TOF) to the particle detector, and in the stable photoelectron spectrum (not shown), it is found that this feature correlates with resonance states with lifetimes exceeding 5 μs. A detailed comparison of these results as well as those for $F^-(HOD)$ with quantum dynamics calculations done by Guo and co-workers is underway and will be reported on in the current year.

B. Vibrational Excitation of Molecular Anions

An important advance made during the last year was demonstration of efficient vibrational excitation of anions prior to injection into the EIBT. These experiments involve a Nd:YAG-pumped mid-IR OPO/OPA system (LaserVision), providing IR radiation in the 2000 – 5000 cm^{-1} range that is injected into the ion source region and counterpropagates relative to the ion beam using a mirror the ion beam 'jumps' over. This allows excitation of the full ensemble of ions produced in the 10 Hz ion source. As described in DOE pub. 7, we demonstrated up to 90% excitation in the bound-free photodetachment of NO^-, and were also able to record an action spectrum of the transient autodetaching excited vibrational states of NO^-. Of course in excitation of bound vibrational states we will be limited to 50% excitation at saturation. This advance has allowed us to obtain results on the F + $H_2O \rightarrow$ HF + OH reaction by excitation of the proton transfer mode F-H-O in $F^-(H_2O)$ as will be discussed in the next section.

C. Effects of Vibrational Excitation on the Dynamics of the F + H_2O → OH + HF Reaction

A substantial set of data examining the impact of excitation of the first overtone of the proton transfer vibration in F^--H-OH has been obtained. The data shown in Figure 3 shows clear evidence for an effect of the vibrational excitation. In the left frame, the difference PPC spectrum shows an increase in intensity for the in the region where HF(v=1/0)+OH(v=0/1) is energetically allowed and F+H_2O opens up. There is a significant depletion of signal at the lowest eKE, in regions that comparison with

Figure 1 shows corresponded to production of F + H_2O and HF(v=1/0)+OH(v=0/1) at high KER in the vibrationless case. An approximate 'pure' vibrationally excited coincidence spectrum, assuming 20% vibrational excitation is shown in the right frame, revealing some further details. In particular it is seen that there is evidence for a significant increase in the region of the HF(v=2/0) + OH(v=0/2), HF(v=1) + OH(v=1) (limit not shown) and F + H_2O product channels. It is also interesting to note the signal between the diagonal lines at 1.4 and 1.0 eV. This is the easiest part of the spectrum to assign, as energetically it must arise from vibrational excited parent anions that yield HF(v=0)+OH(v=0) products. The most interesting feature to note is that there appears to be a stepped structure as KER increases, indicative of increasing rotational excitation induced by the dissociation of vibrationally excited complexes higher on the repulsive potential energy surface. The alternative explanation is that on the 50 ms timescale of these experiments there is significant IVR in the $F^-(H_2O)$ target anion and vibrational energy has redistributed or radiated into other degrees of freedom yielding a range of total energies. This set of data will once again profit from comparison with high level theory, and with the already existing studies of the vibrational structure of the $F^-(H_2O)$ anion (*7, 8*) and the potential energy surface for $F^-(H_2O)$ calculated by Guo and co-workers (DOE pub. 6), we look forward to comparing to quantum dynamics calculations on this system as well in the near future.

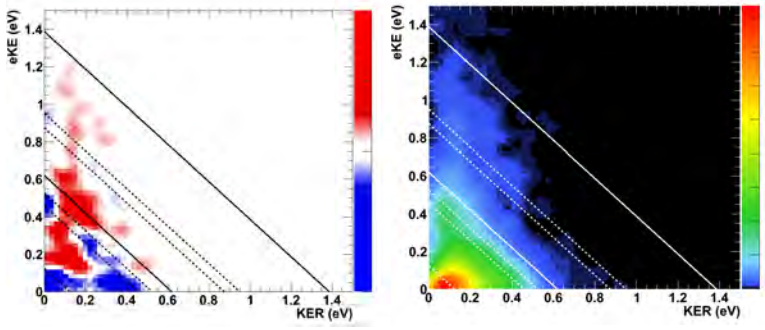

Figure 3: Left Frame: Difference PPC spectrum (IR on – IR off) for F (H_2O) with IR = 2885 cm^{-1} and photodetachment at 4.80 eV. Blue regions show depletion, red regions enhancement, and the energetic limits have been shifted up by 2885 cm^{-1} relative to Figure 1 to reflect the total available energy. Right Frame: Approximate vibrationally excited coincidence spectrum, assuming 20% vibrational excitation in the parent ion beam.

D. Energetics and Dissociation Dynamics of Oxygenated Radicals

We have continued our studies of oxygenated radicals over the last year. A study of the state-resolved dissociation dynamics of the deuterated formyloxyl radical was reported in DOE pub. 5, making use of the sequential DPD of DCO_2^- at a photon energy of 4.27 eV. Photodetachment yields the three lowest-lying electronic states of DCO_2 with substantial excitation in the O-C-O bending mode. These bend-excited states of the radical predissociate, yielding a vibrational inversion in the CO_2 bend. One interesting aspect of these results is that they provide a critical probe of another region of the OH + CO -> H + CO_2 potential energy surface, and comparison of these results with the very low vibrational excitation predicted by QCT calculations of Ma and Guo on the LTSH potential energy surface further confirm the deficiencies of applying that surface to problems beyond the kinetics experiments it was optimized to model.(*9*)

More complex oxygenated organic radicals are of considerable interest owing to their role as combustion intermediates in the oxidation of new fuel stocks, in particular biofuels. A manuscript has been submitted on the photodetachment of tert-butoxide with both non-deuterated and deuterated precursors, $(CH_3)_3CO^-$ and $(CD_3)_3CO^-$. The experiments provided confirmation that the primary stable product is the tert-butoxy radical, but also revealed a dissociative photodetachment channel, involving the loss of a methyl radical. There are two possible reaction pathways for dissociation by loss of a methyl radical: from the carbanion isomer: (a) $(CH_3)_2COHCH_2^- + h\nu \rightarrow CH_3 + CH_3COHCH_2$ or tert-butoxide: (b) $(CH_3)_3CO^- + h\nu \rightarrow CH_3 + (CH_3)_2CO$ (acetone). Theoretical energetics utilizing the CBS-Q//B3 level of theory for the transition state barrier and energetics for each dissociative pathway are consistent with DPD of the carbanion isomer yielding the observed DPD products. The carbanion isomer is considerably less stable than the alkoxide in this case. However, we have shown that much less stable anionic precursors can be isolated, an example being $HOCO^-$ vs. HCO_2^-, where the difference in electron affinities is ~2 eV.

We have also extended our studies of carboxyl free radicals to examine the dissociation dynamics of the propiolyl radical ($HC{\equiv}CCO_2$) and the related isomer $C{\equiv}CCO_2H$ taking advantage of the DPD of $HC{\equiv}CCO_2^-$ and photodetachment of the isomeric carbanion, $^-C{\equiv}CCO_2H$, that is also produced in the ion source. One interesting observation is that dissociation of $HC{\equiv}CCO_2$ yielding $HC_2 + CO_2$ also reveals resolved CO_2 product bending vibrations, similar to the much simpler HCO_2 radical. One aspect that makes these spectra more difficult to interpret are the two low-lying isomeric forms of the carbanion (syn- and anti-), and we are continuing to work on theoretical predictions to assist in the interpretation.

III. Future Work

In the coming year we will finish the preliminary studies of vibrational excitation in the $F + H_2O$ system and initiate similar measurements on HOCO. The measurements on HOCO will require acquisition of a wavelength extender for the IR OPO to permit direct excitation of the HO-CO bond. We are also extending our studies of the reaction dynamics of the hydroxyl radical to progressively larger systems, with the six-atom system $OH + NH_3$ providing preliminary results. Additional improvements to the apparatus will focus on implementation of a new ion source with a cryogenically cooled RF accumulator trap so internal excitation even in infrared-inactive and rotational modes can be quenched, prior to injection in the EIBT and carrying out PPC measurements. This will be important as we seek to extend these studies to larger molecular systems including larger carboxyl radicals relevant to the combustion of biofuels.

IV. References

1. C. J. Johnson, R. E. Continetti, *J. Phys. Chem. Lett.* **1**, 1895 (2010).
2. G. Li, L. Zhou, Q.-S. Li, Y. Xie, H. F. Schaefer, *Phys. Chem. Chem. Phys.* **14**, 10891 (2012).
3. J. Li, R. Dawes, H. Guo, *J. Chem. Phys.* **137**, 094304 (2012).
4. G. Li, Q.-S. Li, Y. Xie, H. F. Schaefer, *J. Phys. Chem. A* **117**, 11979 (2013).
5. L. Nguyen, J. Li, R. Dawes, J. F. Stanton, H. Guo, *J. Phys. Chem. A*, (2013).
6. J. Li, B. Jiang, H. Guo, *J. Chem. Phys.* **138**, 074309 (2013).
7. S. Horvath, A. B. McCoy, J. R. Roscioli, M. A. Johnson, *J. Phys. Chem. A* **112**, 12337 (2008).
8. E. Kamarchik, D. Toffoli, O. Christiansen, J. M. Bowman, *Spectrochimica Acta Part A* **119**, 59 (2014).
9. J. Ma, H. Guo, *Chemical Physics Letters* **511**, 193 (2011).

V. DOE-supported publications by this project 2011-2014

1. B.L.J. Poad, C.J. Johnson and R.E. Continetti, *Photoelectron-photofragment coincidence studies of NO^--X clusters ($X=H_2O$, CD_4)*, Discussions of the Faraday Society **150**, 481-492 (2011).
2. C.J. Johnson, B.L.J. Poad, B.B. Shen and R.E. Continetti, *Communication: New insight into the barrier governing CO_2 formation from OH + CO*, J. Chem. Phys. **134**, 171106-1-4 (2011).
3. C.J. Johnson, B.B. Shen, B.L.J. Poad and R.E. Continetti, *Photoelectron-photofragment coincidence spectroscopy in a cryogenically cooled electrostatic ion beam trap*, Rev. Sci. Instrum. **82**, 105105-1-9 (2011).
4. C.J. Johnson, M.E. Harding, B.L.J. Poad, J.F. Stanton and R.E. Continetti, *Communication: The electron affinities, well depths and vibrational spectroscopy of cis- and trans-HOCO*, Journal of the American Chemical Soc. **133**, 19606-19609 (2011).
5. A.W. Ray, B.B. Shen, B.L.J. Poad and R.E. Continetti, *State-resolved predissociation dynamics of the formyloxyl radical*, Chem. Phys. Lett. **592**, 30-35 (2014).
6. R. Otto, J. Ma, A.W. Ray, J.S. Daluz, J. Li, H. Guo and R.E. Continetti, *Imaging dynamics on the $F + H_2O \rightarrow HF + OH$ potential energy surfaces from wells to barriers*, Science, **343**, 396-399 (2014)
7. R. Otto, A.W. Ray, J.S. Daluz and R.E. Continetti, *Direct IR excitation in a fast ion beam: Application to NO^- photodetachment cross sections*, EPJ Techniques and Instrumentation (In Press) (2014).

Vibrational Dynamics and Dissociation of Ground- and Excited-State Clusters

F.F. Crim
Department of Chemistry
University of Wisconsin–Madison
Madison, Wisconsin 53706
fcrim@chem.wisc.edu

Our research investigates the chemistry of vibrationally excited molecules. The properties and reactivity of vibrationally energized molecules are central to processes occurring in environments as diverse as combustion, atmospheric reactions, and plasmas and are at the heart of many chemical reactions. The goal of our work is to unravel the behavior of vibrationally excited molecules and to exploit the resulting understanding to determine molecular properties and to control chemical processes. A unifying theme is the preparation of a molecule in a specific vibrational state using one of several excitation techniques and the subsequent photodissociation of that prepared molecule. Because the initial vibrational excitation often alters the photodissociation process, we refer to our double-resonance photodissociation scheme as *vibrationally mediated photodissociation.* In the first step, fundamental or overtone excitation prepares a vibrationally excited molecule, and then a second photon, the photolysis photon, excites the molecule to an electronically excited state from which it dissociates. Vibrationally mediated photodissociation provides new vibrational spectroscopy, measures bond strengths with high accuracy, alters dissociation dynamics, and reveals the properties of and couplings among electronically excited states.

Our recent research on vibrational dynamics in clusters has produced new insights into ammonia clusters, one of the prototypical hydrogen-bonded systems. We have determined the dissociation energy of the dimer very precisely (660±20 cm^{-1}) and obtained an experimental estimate of the dissociation energy of the trimer (1600±100 cm^{-1}). The dynamics we probe show selective coupling of vibrational energy during the dissociation of the dimer. These studies have led us into new studies of ammonia-containing complexes that build on our previous investigations, and we have obtained intriguing results on vibrationally induced isomerization in the complex of ammonia with a substituted phenol.

Ammonia Clusters

The measurements on the ammonia oligomers begin with their formation in a supersonic expansion of ammonia seeded in He followed by infrared laser excitation of their N-H stretching vibrations. Flow of energy from the initially excited N-H stretch dissociates the oligomer to produce vibrationally and rotationally excited ammonia fragments. We detect individual rovibrational states of NH_3 by (2+1) resonance enhanced multiphoton ionization (REMPI) through the $\tilde{B}$ state, as illustrated on the left-hand side of Fig. 1. The right-hand side of the figure shows the infrared-action spectrum obtained by observing NH_3 fragments with one quantum of excitation in the umbrella bending vibration (ν_2). As the lower trace in the figure shows, these features are consistent with the transitions observed in He droplets by Vilesov and coworkers [M. N. Slipchenko, *et al.,* J. Phys. Chem. A **111**, 7460 (2007)] and show that excitation of either the symmetric N-H stretch or the antisymmetric N-H stretch initiates vibrational predissociation.

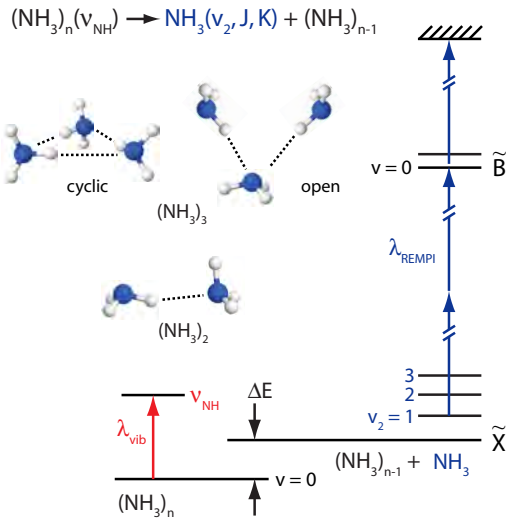

Figure 1

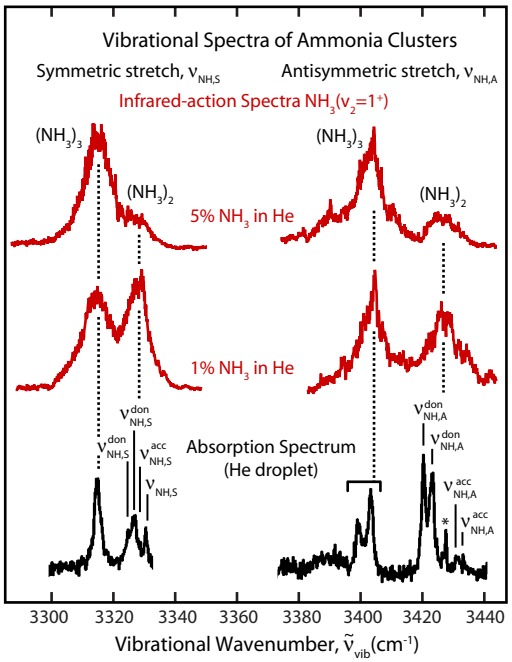

Features corresponding to higher-order clusters appear in the infrared-action spectra in the regions of the intramolecular symmetric N-H stretching vibration ($\nu_{NH,S}$) and the intramolecular antisymmetric N-H stretching vibration ($\nu_{NH,A}$) shown in Fig. 1. The spectra illustrate the influence of expansion conditions on the relative intensities of the features in the spectrum. Because higher seed ratios should favor the formation of larger clusters, the changes between the spectra suggest that the lower energy feature comes from the trimer and that the higher energy feature comes from the dimer, in agreement with the assignments from the He droplet spectra.

Removing an NH_3 fragment from the cyclic trimer, illustrated in Fig. 1, requires breaking two hydrogen bonds. Thus, the dissociation into a monomer and a dimer,

$$(NH_3)_3 + h\nu_{IR} \rightarrow (NH_3)_2 + NH_3(\upsilon,\ J,\ K),$$

consumes more energy than cleaving the single hydrogen bond of the dimer. As the left hand side of Fig. 2 shows, the trimer feature is prominent in the infrared-action spectrum for detection of $NH_3(v_2 = 1^+, J = 1, K = 0)$ but is essentially absent for detection of $NH_3(v_2 = 3^+, J = 3, K = 0)$. The relative intensities of the dimer and trimer features in the infrared-action spectra depend on the amount of energy available for breaking the hydrogen bonds in the cluster, a quantity that depends on the energy content of the detected fragment. Infrared-action spectra for ammonia fragments with large amounts of internal energy have almost no trimer component because there is not enough energy available to break two bonds in the cyclic trimer *and* populate the detected state of the NH_3 fragment. By contrast, infrared-action spectra for fragments with low amounts of internal energy have a substantial trimer component.

The right-hand side of the figure shows a quantitative analysis of the trimer contribution compared to that of the dimer in the action spectra. Fitting the two features in the action spectra with Gaussian functions gives a measure of the relative intensity of the dimer and trimer components. The growth in the trimer contribution suggests that fragmentation of the trimer into a monomer and dimer requires an energy of

about 1600 cm^{-1}, a range that is consistent with several theoretical estimates falling within the grey bar in the figure.

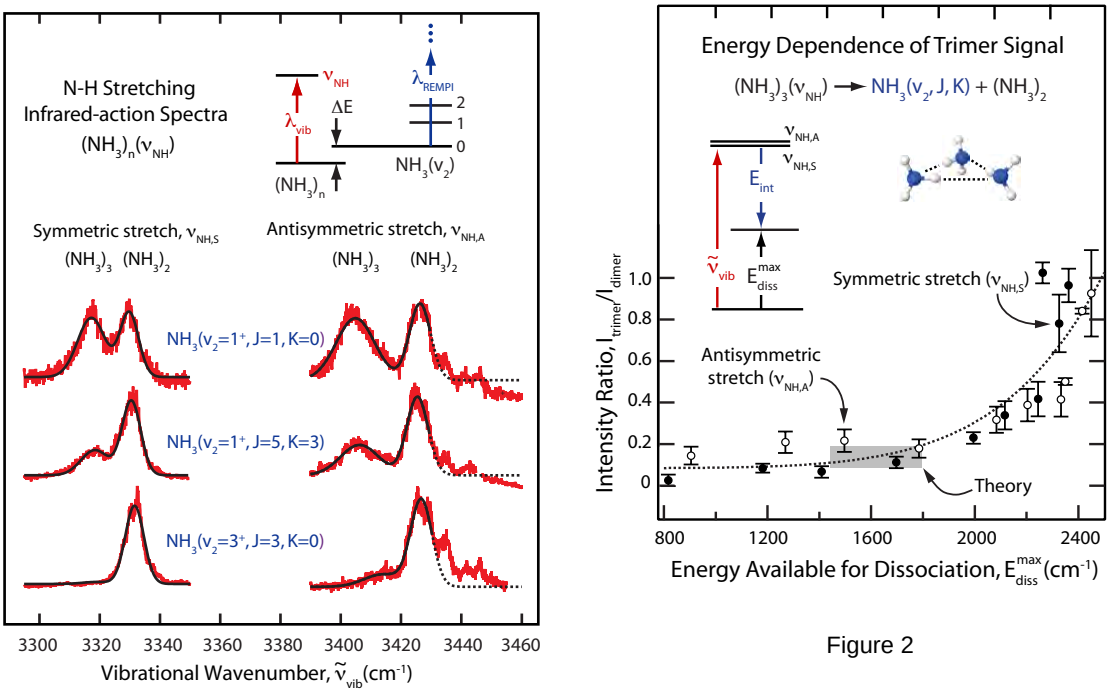

Figure 2

Aminophenol-Ammonia Complexes

We have begun studying the complex of 3-aminophenol with ammonia to understand its bond-strength and its vibrational predissociation as we move toward studying its excited-state dissociation. There are two conformers of 3-aminophenol corresponding to different orientations of the O-H bond. The structures in the top portion of Fig. 3 illustrate the slightly higher energy *cis* conformer and the lower energy *trans* conformer. The spectrum in the top of Fig. 3 is the (1+1) REMPI spectrum of 3-aminophenol with the *cis* and *trans* origins marked. [W. Y. Sohn, *et al.*, Phys. Chem. Chem. Phys. 13, 7006 (2011).] The spectrum in the bottom of the figure is that of the complex, in which the *trans* origin appears about 65 cm^{-1} below that of the bare 3-aminophenol, but the *cis* isomer does not appear, possibly because of interconversion between the two conformers during the formation of the complex. We have recently observed the influence of vibrational excitation on the complex by obtaining the REMPI spectrum after exciting the N-H stretch of the 3-aminophenol in the complex. That action spectrum contains a new feature whose location strongly suggests that it is the origin transition of the *cis* complex. Our preliminary conclusion is that the added vibrational energy induces isomerization of the complex. This observation as well as our detection of a smaller signal upon excitation of the O-H stretch reflects

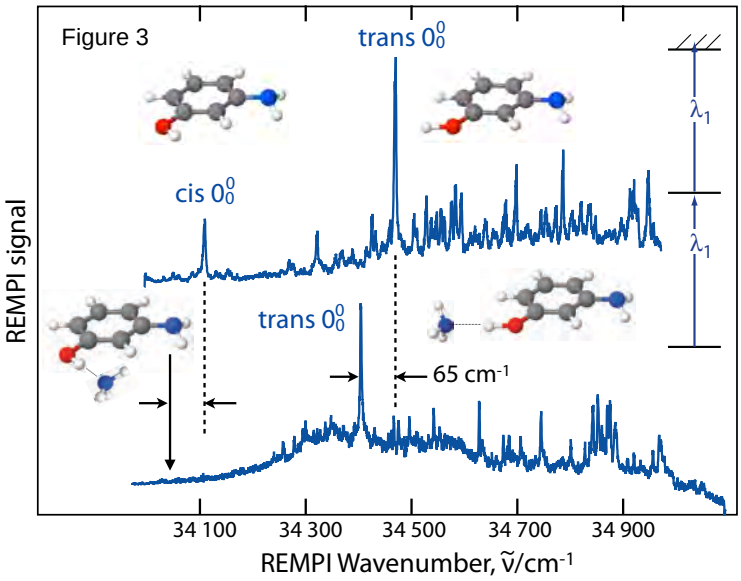

the coupling of the zero-order stretching state to other motions, likely torsions, that promote isomerization.

Future Directions

We are now in the midst of exploring the influence of vibration on the dynamics of a complex. Our future work goes in two directions. One is similar experiments in other complexes, and the other is to observe the effect of vibrational excitation and the presence of an adduct on the dissociation of electronically excited complexes. We have proven that vibrational excitation of NH_3 drastically alters its dissociation by changing the behavior at a conical intersection. Now we can understand that behavior in different complexes where an adduct will influence the dynamics also.

PUBLICATIONS SINCE 2011 SUPPORTED BY DOE

A. S. Case, C. G. Heid, S. H. Kable, and F. F. Crim, *Dissociation energy and vibrational predissociation dynamics of the ammonia dimer,* J. Chem. Phys. **135**, 084312 (2011).

A. S. Case, C. G. Heid, C. M. Western, and F. F. Crim, *Determining the dissociation threshold of ammonia trimers from action spectroscopy of small clusters,* J. Chem. Phys. **136**, 124310 (2012).

Molecular Reaction Dynamics Across the Phases: Similarities and Differences. F. Fleming Crim, Faraday Discussions **157**, 1 (2012).

Theory and Modeling of Multiphase Reacting Flow Dynamics in Simulations and Experiments

Rainer N. Dahms
Combustion Research Facility, Sandia National Laboratories
Livermore, CA 94551-0969
Rndahms@sandia.gov

I. Program Scope

This theoretical and modeling effort on multiphase reacting flow dynamics is based on three primary objectives. The first is to establish a physically-based understanding of improved turbulent mixing and combustion models in multiphase flows. Many of the relevant fluid flow processes take place on time and length scales which are not feasible to resolve directly in simulations. Therefore, sophisticated sub-grid scale models have to be developed. This requires a comprehensive understanding of the fundamental processes of the underlying relevant phenomena. In this context, a major focus is the development of more general regimes that incorporate broader ranges of combustion modes and a more complete set of non-dimensional parameters. The second objective is to develop techniques and methods to understand data sets obtained from high-fidelity Large-Eddy simulations (Oefelein) and measurements performed in the Advanced Imaging Laboratory (Frank) and in the Turbulent Combustion Laboratory (Barlow) in a meaningful manner. The fundamental issues of comparing, validating, and understanding advanced combustion data sets will become even more important as we attempt to understand the dynamics of turbulence-flame interactions using data sets that capture the temporal evolution of turbulent flames. The third objective is to understand the implications of the conclusions obtained from well-controlled experiments in the context of advanced power and propulsion systems including gas turbines, automotive engines, and liquid rockets. This effort has to consider the poorly understood effect of elevated pressure on the fundamentals of multiphase combustion phenomena. It builds on the developed theoretical framework, which establishes a meaningful set of major scaling parameters. Combined with the identification of relevant ranges of combustion regimes and non-dimensional parameters in modern transportation and power systems, the framework will serve the general objective of this program to accelerate the development and validation of science-based, predictive computational models for turbulent combustion systems.

II. Recent Progress

Understanding and quantifying multiphase reacting flow phenomena in fundamental experiments and modern transportation and energy systems is widely recognized as a critical research area for future combustion design. The importance to develop a basic science foundation for predictive models has been consistently highlighted over many years in a variety of industry, government, and academic forums including recent DOE workshops such as the *Workshop to Identify Research Needs and Impacts in Predictive Simulations for Internal Combustion Engines* (PreSICE),[1] and the *Workshop on Clean and Efficient Combustion of 21st Century Transportation Fuels*.[2] Liquid injection processes largely determine the mixture preparation process which ultimately governs the detailed evolution of chemical kinetic processes and their interaction with the turbulent flow field.

Liquid injection in systems at elevated operating pressures is not well understood. Imaging (such as those performed by Mayer *et al*.[3-5]) has long shown that under some high-pressure conditions, the presence of discrete two-phase flow dynamics may become diminished. Then, the characteristic processes

of primary and secondary atomization, multi-component evaporation, and liquid ligament and drop formation do not occur. As a consequence, the widely acknowledged drop formation and breakup regimes (see Lasheras and Hopfinger[6]), which establish the conceptual foundations of most spray simulation models, do not apply anymore. Modern theory has long lacked a first-principle explanation to understand and quantify the observed phenomena (see a recent review by Cheroudi[7]).

Initial studies aimed to quantify the conditions under which a specific n-dodecane–nitrogen mixture, relevant for diesel engine operation, transitions between classical spray atomization and diffusion-dominated dense-fluid mixing dynamics without the presence of surface tension forces. A comprehensive modeling framework, based on theories of extended corresponding states and capillary flows, was developed for the analysis of molecular two-phase interface dynamics. A modified 32-term Benedict-Webb-Rubin equation of state is used to predict the pressure-volume-temperature behavior of the liquid phase, saturated vapor mixtures, and gas phase properties. This real-fluid model is combined with theories of vapor-liquid equilibrium and capillary flows. Gradient theory (see for example the pioneering work of van der Waals[8] and Cahn and Hilliard[9]) facilitates the calculation of representative two-phase molecular interface structures.

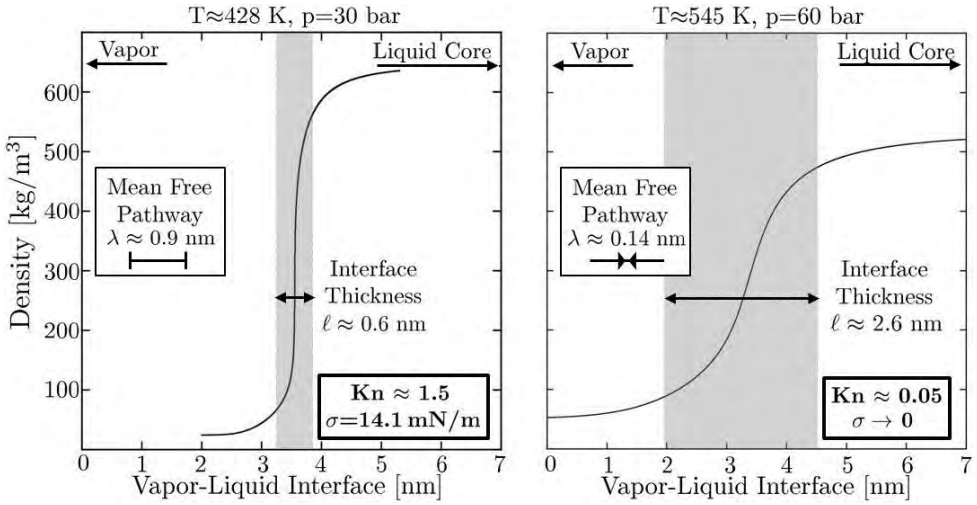

Figure 1: Molecular gas-liquid density profiles and thicknesses for (left) lower-pressure conditions and (right) device-relevant high-pressure conditions, as calculated by gradient theory (see Dahms *et al.*[1,2]). Corresponding mean free pathways are shown for reference. Interestingly, the Knudsen-number criterion (Kn=λ/L) indicates that the device-relevant condition falls within the fluid-mechanic continuum regime (Kn<0.1) where widely assumed classical spray atomization processes do not occur anymore.

Figure 1 shows representative results of this study. Molecular two-phase interfacial density profiles have been calculated for two different flow conditions which are shown on a 1D coordinate system normal to the liquid surface. At the lower pressure and temperature conditions (left), the interface is characterized by a thickness of L≈0.6 nm. The analysis showed that this thickness is smaller than the local mean free path λ. An applied Knusen-number criterion Kn=λ/L demonstrated that related interfacial phenomena are dictated by molecular dynamics (since Kn>0.1). Then, classical two-phase theory applies and this interface exhibits surface tension forces and is expected to lead to the widely recognized spray breakup phenomena. At device-relevant higher pressure and temperature conditions (right), however, the situation becomes markedly different. The interfacial structure has widened substantially and the same Knudsen-number criterion (Kn≈0.05) revealed a major finding. This interface falls within the fluid mechanic continuum length scale regime (since Kn<0.1). As a consequence, interfacial processes are not governed by molecular dynamics anymore. The interfacial region develops nearly-linear gradients over molecular distances. Then, iso-scalar assumptions of vapor-liquid equilibrium and classical two-phase

theory do not apply. The thermodynamic value of surface tension diminishes as the thickness of this interface substantially increases. At this point, the interfacial region becomes a continuous gas-liquid mixing layer that is significantly affected by single-phase real-fluid thermodynamics and transport properties. This dense-fluid mixing layer cannot support classical breakup or drop formation phenomena. Hence, injected liquids evolve in the presence of exceedingly large but continuous thermo-physical gradients in a manner that is markedly different from the classical assumptions.

This theory was corroborated by applying high-speed long-distance macroscopic imaging using an ultra-fast LED source with a diffuser background behind the jet (see Manin *et al*.[5]). At conditions shown in Fig.1 (left), imaging demonstrated characteristic events of classical sprays such as individual ligaments, which stretch and finally separate into distinct drops. Those observations provided evidence of existing surface tension forces. At conditions shown in Fig.1 (right) which are relevant to diesel engines, however, no evidence of existing ligaments or drops was found. Instead, the transition from liquid to gaseous states appeared continuous without a sharp interface separating the gas from the liquid. These findings were consistent with the theoretical predictions. Informed by this theory, a high-fidelity Large-Eddy simulation was performed at device-relevant conditions using a dense-fluid approximation instead of a classical spray model (see Oefelein *et al.*[4,7]). The simulations successfully reproduced key experimental features such as the flow structure and spatial evolution.

This developed and validated framework on two-phase interface dynamics was then applied over a wide range of characteristic flow conditions. The Knudsen-number criterion then served to identify operating conditions where classical spray phenomena are being replaced by dense-fluid mixing dynamics. Such conditions, when compared with well-established conditions during diesel engine fuel injection processes, revealed a major finding. Contrary to conventional wisdom, the analysis suggested that dense-fluid mixing dynamics, instead of classical spray formation, occurs under diesel engine injection conditions. As a consequence, widely used models based on the conceptual view of spray atomization do not necessarily apply at high-pressure diesel engine conditions where dense-fluid jets form with no drops or fuel evaporation present. This understanding has important implications from the standpoint of design and for the development of predictive combustion and emission models.

III. Future Work

The fundamental approach described above will be further developed with an emphasis on interrelated areas of research. A close collaboration between the Large-Eddy simulation program and the experimental flow research program will be maintained. A significant effort on the generalization of the proposed initial theory will be initiated. Such efforts include the improvement and assessment of model accuracy and the investigation of effects of multi-component fuels for liquid jet breakup regimes and turbulent combustion processes at elevated system pressures. The objective is to develop a predictive first-principle model framework suitable for high-fidelity combustion simulations. This framework will also increase our understanding of implications, drawn from conclusions obtained from well-controlled fundamental experiments, in the context of general power and propulsion systems including gas turbines, automotive engines, and liquid rockets.

IV. Literature Cited

1. A Workshop to Identify Research Needs and Impacts in Predictive Simulation for Internal Combustion Engines. http://science.energy.gov/~/media/bes/pdf/reports/files/PreSICE_rpt.pdf, 2011;

Sponsored by the Office of Basic Energy Sciences, Office of Science and the Vehicle Technologies Program, Office of Energy Efficiency and Renewable Energy, U.S. Department of Energy
2. Basic Research Needs for Clean and Efficient Combustion of 21st Century Transportation Fuels. http://www.osti.gov/scitech/servlets/purl/935428, 2006; Report of the Basic Energy Sciences Workshop on Clean and Efficient Combustion of 21st Century Transportation Fuels, U.S. Department of Energy.
3. W. Mayer and H. Tamura. Propellant injection in a liquid oxygen/gaseous hydrogen rocket engine. *Journal of Propulsion and Power* 12:1137-1147, 1996.
4. W. Mayer, A. Schik, B. Vieille, C. Chaveau, I. Gokalp, D. Talley, and R. Woodward. Atomization and breakup of cryogenic propellants under high-pressure subcritical and supercritical conditions. *Journal of Propulsion and Power* 14:835-842, 1998
5. W. Mayer and J.J. Smith. Fundamentals of supercritical mixing and combustion of cryogenic propellants. *Progress Aeronautics and Astronautics* 200:339-367, 2004.
6. J.C. Lasheras and E.J. Hopfinger. Liquid jet instability and atomization in a coaxial gas stream. *Annu. Rev. Fluid Mech*. 32:275-308, 2000. doi: 10.1146/annurev.fluid.32.1.275
7. B. Chehroudi. Recent experimental efforts on high-pressure supercritical injection for liquid rockets and their implications. *Intl. J. Aerospace Engineering* 2012:1-31, 2012. doi: 10.1155/2012/121802
8. J.D. van der Waals. Square gradient model. *Verhandel Konik Akad Weten Amsterdam* 1:8-15, 1893.
9. J.W. Cahn and J.E. Hilliard. Free energy of a nonuniform system. I. Interfacial free energy. *J. Chem. Phys*. 28:258-267, 1958

V. BES Sponsored Publications (2012-2014)

1. R.N. Dahms and J.C. Oefelein. Non-equilibrium interface dynamics in high-pressure liquid injection systems, *Proc. Combust. Inst*., 2014. Submitted.
2. R.N. Dahms and J.C. Oefelein. On the transition between two-phase and single-phase interface dynamics in multicomponent fluids at supercritical pressures. *Phys. Fluids* 25, 092103, 2013. doi: 10.1063/1.4820346
3. R.N. Dahms, J. Manin, L.M. Pickett, and J.C. Oefelein. Understanding high-pressure gas-liquid interface phenomena in diesel engines. *Proc. Combust. Inst.* 34:1667-1675, 2013. doi: 10.1016/j.proci.2012.06.169
4. R.N. Dahms and J.C. Oefelein. Theory and analysis of liquid-oxygen-hydrogen interface dynamics in liquid rockets at supercritical pressures, *49th AIAA/ASME/SAE/ASEE Joint Propulsion Conference*, July 15-17, 2013. San Jose, CA. doi: 10.2514/6.2013-3716
5. J.C. Oefelein, R.N. Dahms, G. Lacaze, and A. Ruiz. Modeling and numerical treatment of liquid injection processes at high-pressure supercritical conditions. *14th Intl. Conference on Numerical Combustion*, April 8-10, 2013. San Antonia, TX.
6. J. Manin, M. Bardi, L.M. Pickett, R.N. Dahms, and J.C. Oefelein. Development and mixing of diesel sprays at the microscopic level from low to high temperature and pressure conditions. *Proceedings of the 7th THIESEL Conference on Thermo- and Fluid-Dynamic Processes in Direct Injection Engines,* September 11-14, 2012. Valencia, Spain.
7. J.C Oefelein, R.N. Dahms, G. Lacaze, J. Manin, and L.M. Pickett. Effects of pressure on the fundamental physics of fuel injection in diesel engines. *Proceedings of the 12th International Conference on Liquid Atomization and Spray Systems*, September 2-6, 2012. Heidelberg, Germany. ISBN 978-88-903712-1-9
8. J.C. Oefelein, R.N. Dahms, and G. Lacaze. Detailed modeling and simulation of high-pressure fuel injection processes in diesel engines. *SAE Intl. J. Engines* 5(3):1410-1419, 2012. doi: 10.4271/2012-01-1258

Bimolecular Dynamics of Combustion Reactions

H. Floyd Davis
Dept. of Chem. and Chem. Biology, Cornell University, Ithaca NY 14853-1301
hfd1@cornell.edu

I. Program Scope:

The aim of this research program is to better understand the mechanisms and product energy disposal in elementary bimolecular reactions fundamental to combustion chemistry. Using the crossed molecular beams method, the angular and velocity distributions of neutral products from single reactive collisions are measured using VUV laser ionization methods.

II. Recent Progress and Future Plans:

During the current funding period, we have further developed VUV generation by four-wave mixing of collimated (*i.e.*, unfocussed) nanosecond laser pulses.[1] Using our rotatable source crossed beams apparatus, we employ universal pulsed photoionization detection, typically using ~0.1 mJ pulses at 9.9 eV (125 nm).[2] We have recently studied the reactions of C_6H_5 (phenyl) radicals C_3H_6 (propene) and C_4H_8 (trans 2-butene)[3] and with O_2.[4]

We have developed a technique for producing radiation extending into the extreme ultraviolet (XUV; λ < 110 nm) with higher conversion efficiencies than previously reported.[5] Our method involves noncollinear phasematching of focused lasers in laser vaporized mercury (Hg) at room temperature. This approach easily facilitates windowless operation. Furthermore, using noncollinear phasematching, the short wavelength radiation is spatially isolated from the residual UV and visible beams without need for lossy optical elements such as windows, lenses, and gratings.

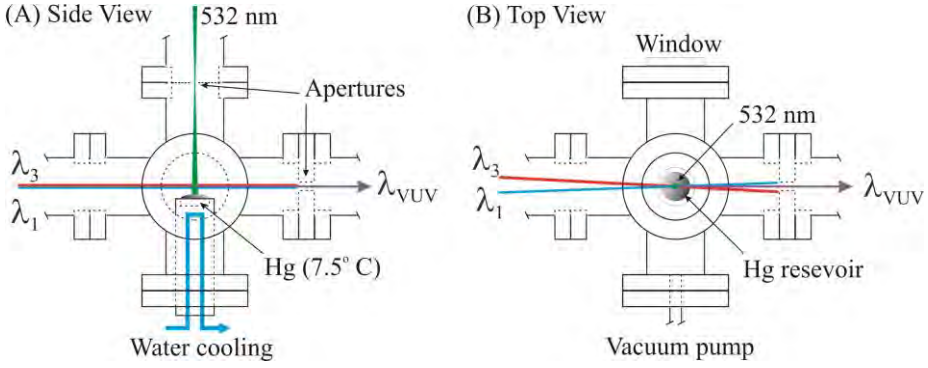

Fig. 1: Side and top view of laser vaporization cell with noncollinear phasematching.

Our approach using "soft" single photon pulsed ionization allows product molecules to drift to a triply differentially pumped detector (10^{-10} Torr) before ionization, spreading out due to their velocities. This method is well suited for experiments using pulsed radical sources. In contrast to ion imaging or Rydberg tagging, where VUV is introduced into the high-pressure molecular beam crossing region, no interference from photodissociation or ion-molecule reactions is observed. As illustrated in our studies of phenyl radical reactions, the high ionization efficiency and low background leads to quite high signal to noise ratios. However, the need to scan the laser delay to measure product TOF distributions represents the key remaining limitation. To address this, we have initiated the development of a new detection method employing *coaxial universal photoionization* of products from crossed beam reactions within an ion guide. This method

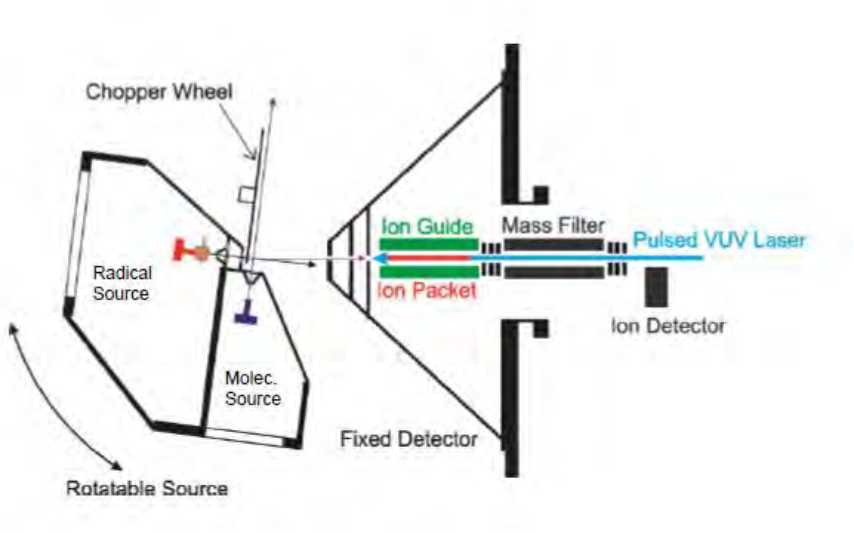

Fig. 2: Rotatable source apparatus with coaxial VUV ionization.

promises to dramatically improve detection sensitivity, with a factor of 30-100 improvement in reactive signal intensities anticipated with no increase in background signals.[2] We plan to implement this method during the upcoming funding period for studies of combustion-related free radical reactions including alkyl radicals with O_2, and hydroxyl radicals with alkenes. The primary challenge in implementing the coaxial ionization method is to ensure that the entire packet of neutrals is detected with constant (or at least known) sensitivity. To date we have explored the use of a ¾"quadruple mass filter in RF-only mode as an ion guide. In this case, the ions produced by photoionization are born at different positions along the quadrupole axis, depending upon their neutral velocities and laser delay. After photoionization, ions drift with their nascent (neutral) velocities down the quadrupole axis to an acceleration region, einzel lens, through a quadruple mass filter, and are then detected. We are also testing a gradiant field approach, consisting of 33 parallel plates each located 1.0 cm apart and connected in series by 1 MΩ resistors. By applying a DC potential to each end of the stack (e.g., + 40V and + 30V), the ions, formed at various locations along the axis, are accelerated by a uniform field towards the quadruple mass filter. This approach has the advantage that the ions are actively accelerated.

Finally, using our fixed-source, rotatable detector apparatus, O atom Rydberg time-of-flight (ORTOF) spectroscopy has been combined with the vastly improved 130 nm VUV light source. We have carried out preliminary experiments on the H + O_2 → OH + O reaction and the results have been very encouraging. This work will be continued during the upcoming funding period.

III. References (Numbers 1-3 are publications since 2011 citing DOE support):

1. D.R. Albert, D.L. Proctor, and H.F. Davis, "High-Intensity Coherent Vacuum Ultraviolet Source Using Unfocussed Commercial Dye Lasers", *Rev. Sci Instrum.* **84**, 063104 (2013).
2. D.R. Albert and H.F. Davis "Experimental Studies of Bimolecular Reaction Dynamics Using Pulsed Tabletop VUV Photoionization Detection", invited perspective article, *Phys. Chem. Chem. Phys.* **15**, 14566-14580 (2013).
3. D.R. Albert, M.A. Todt, and H.F. Davis, "Crossed Molecular Beam Studies of Phenyl Radical Reactions with Propene and 2-Butene" *J. Phys. Chem. A* **117**, 13967-13975 (2013).
4. D.R. Albert and H.F. Davis "Collision Complex Lifetimes in the Reaction C_6H_5 + O_2 → C_6H_5O + O", *J. Phys. Chem. Lett.* **1**, 1107 (2010).
5. M.A. Todt, D.R. Albert, H.F. Davis, "High Intensity VUV and XUV Generation by Noncollinear Phasematching in Laser Vaporized Media", in preparation.

Exploration and validation of chemical-kinetic mechanisms

Michael J. Davis

Chemical Sciences and Engineering Division
Argonne National Laboratory
Argonne, IL 60439
Email: davis@tcg.anl.gov

The focus of the work is on exploration and theoretical validation of chemical-kinetic mechanisms, which combines global sensitivity analysis with the exploration of the characteristics of the sensitivity analysis over the physical and chemical parameters. In the last two years we have made modifications to our algorithm for global sensitivity analysis so that it is accurate with small sample sizes, allowing for its use in device modeling.

Recent Progress

Global Sensitivity Analysis with Small Sample Sizes

In collaboration with W. Liu, a project was initiated in the past two years to improve our algorithm for doing global sensitivity analysis (GSA). It was made more efficient, so that smaller sample sizes could be used. We extended this further by incorporating sparse regression techniques to limit the sample size even more. A preliminary account of this approach is given in [P6].

Our previous implementation of GSA relied on a high-dimensional model representation. The present approach expands the response in terms of all the reactions simultaneously.

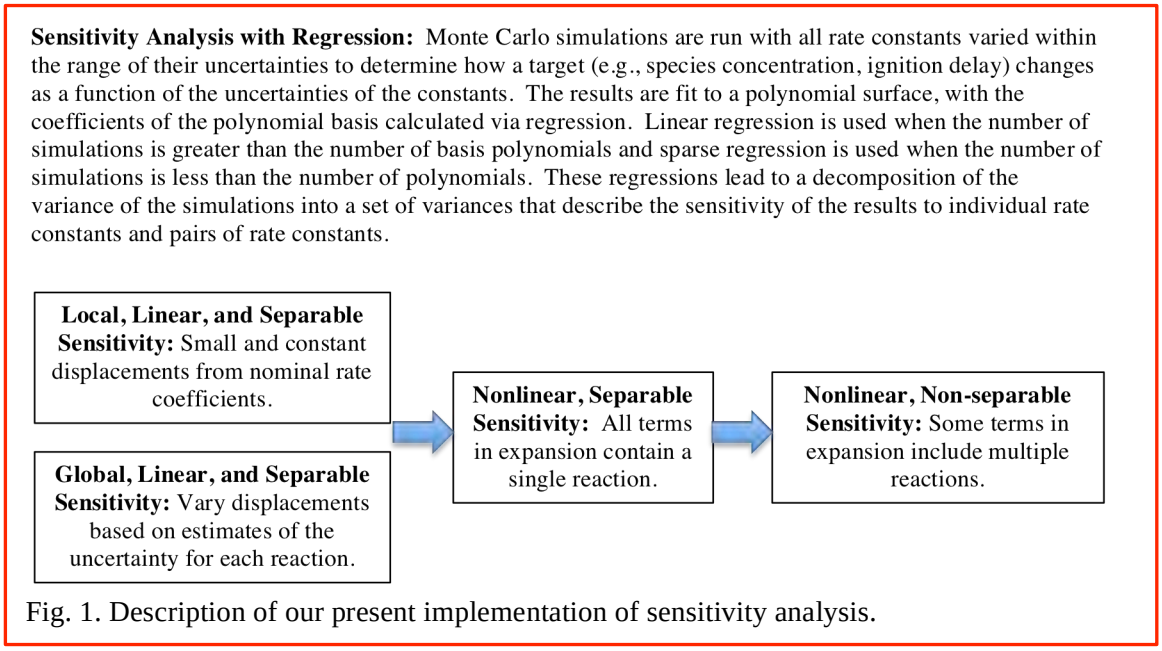

Fig. 1. Description of our present implementation of sensitivity analysis.

Although this requires considerably more computer memory to implement efficiently, our experience is that it requires many less runs to obtain the same accuracy as with the previous approach. This algorithm can also be used to obtain local sensitivity coefficients, which is now being implemented in collaboration with Sivaramakrishnan. In addition, both the local and global versions of sensitivity analysis with this approach can readily incorporate nonlinearity and correlations among reactions, with pair-wise correlations incorporated so far. In the previous

algorithm convergence of these cross-terms was excessively slow. Figure 1 provides a summary of our approach to sensitivity analysis.

Two different versions of the polynomial response surfaces have been studied, as indicated in Eqns. (1a) and (1b), with Eqn. (1c) providing a compact summary:

$$\tau^{(1)}(\{u_i\}) = \sum_{i=1}^{m}\sum_{k=0}^{n} a_{ik} u_i^k \qquad (1a)$$

$$\tau^{(2)}(\{u_i\}) = \sum_{i=1}^{m}\sum_{k=1}^{n} a_{ik} u_i^k + \sum_{i=1}^{p}\sum_{k=1}^{s} b_{ikr} u_i^k u_j^r,\ k+r \le n \qquad (1b)$$

$$\tau(\{u_i\}) = \sum_{i=1}^{L} c_j g_j \qquad (1c)$$

Regression is accomplished by minimizing the following error function:

$$E(\mathbf{c}) = \frac{1}{2}\sum_{k=1}^{M}\left(t_k - \sum_{i=1}^{L} c_j g_j(\mathbf{u}_k) \right)^2 + \lambda \sum_{j=1}^{L} |c_j| \qquad (2).$$

When $\lambda = 0$, the minimization of the function in Eq. (2) is commonly referred to as ordinary least squares fitting, and when $\lambda > 0$ the regression is referred to as l_1-penalized regression, or the lasso. For cases where L in Eq. (1c) is less than the number of input data points, it is expected that Eq. (2) is minimized for $\lambda = 0$, but if the number of input points is less than L, minimization will occur for $\lambda > 0$, because many of the coefficients in the expansion are set exactly to 0. The accuracy of this procedure is contingent on the sparsity of the solution $\{c_i\}$ in Eq. (1c), that is many of the coefficients are very small, a common occurrence in our implementations of global and local sensitivity analysis, and is generally common in high-dimensional regression problems.

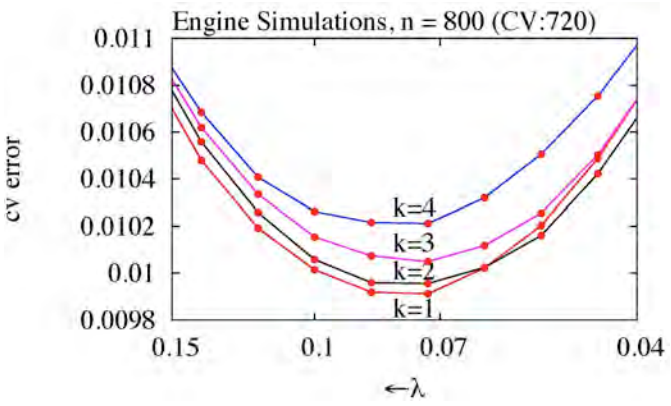

Fig. 2. Cross-validation error calculated from minimization of Eq. (2) using the polynomial model in Eq. (1a).

The penalty parameter λ is chosen by minimizing a cross-validation error, with 10-fold cross validation used here. Ten fits are made with $1/10^{th}$ of the sample left out. The fit is then tested on this set and an error is calculated. The sum of all ten errors defines the cross-validation error. Figure 2 shows the cross-validation errors for Eq. (2) using the form in Eq. (1a) for the engine simulations summarized below. The sample size in all fits was 800, the number of engine simulations. Because there are 914 reactions in the mechanism used to generate the results in Fig. 2, a k = 4 expansion using Eq. (1a) includes 3656 terms, k = 3 includes 2742 terms, etc.

GSA for Compression Ignition Engine Simulations, with Analysis of the In-Cylinder Chemistry

Figure 2 demonstrates that the lowest cross-validation error is for k =1 and this is the model that is used for the global sensitivity analysis of the engine simulations described here, which is a collaboration with Som, Liu, Magnotti, Sivaramakrishnan, and Longman. A detailed description of the simulations is presented in [P7] and [P9], with the larger of the two chemical mechanisms in [P7] studied here (914 reactions), which describes the combustion of a mixture of n-heptane and methyl butanoate.

Results of the GSA for ignition delay for the engine simulations are presented in Table 1. The reactions are ordered (column 2) by their sensitivity coefficients that are listed in column 4.

Table. 1: GSA Results for the engine simulations.

Reaction[a]	Engine Rank	Homogeneous[b] Rank	Eng. Sens. Coeff.
C7H15O2-2=C7H14OOH2-4 (-)	1	1	0.0636
PC4H9O2=C4H8OOH1-3 (-)	2	4	0.0593
NC7H16+OH=C7H15-3+H2O (-)	3	6	0.0406
C4H8OOH1-3O2=NC4KET13+OH (-)	4	7	0.0308
C7H15O2-4=C7H14OOH4-2 (-)	5	3	0.0305
C7H14OOH2-4O2=NC7KET24+OH (-)	6	2	0.0289
PC4H9=C2H5+C2H4 (+)	7	11	0.0212
PC4H9O2=PC4H9+O2 (+)	8	12	0.0211
NC7H16+HO2=C7H15-3+H2O2 (-)	9	9	0.0177
OH+OH(+M)=H2O2(+M) (-)	10	8	0.0166
C7H15O2-3=C7H14OOH3-5 (-)	11	13	0.0161
C7H14OOH4-2O2=NC7KET42+OH (-)	12	5	0.0154
HO2+HO2=O2+H2O2 (+)	13	15	0.0152
Sum of Squares mis-rank		**135**	

[a] (-): Ignition delay decreases with increasing rate; (+): Ignition delay increases with increasing rate

[b] Constant Pressure: P = 77.8 atm, T_0 = 867 K, ϕ_0 = 2.3. Best match to engine ranks.

In order to understand what type of conditions lead to the ordering of reactions in column 2, a series of homogeneous, constant pressure ignition simulations were undertaken at a series of initial temperatures, equivalence ratios, and fixed pressures. Latin Hypercube sampling was used to define these conditions that were chosen to be in the following ranges: P, 70 – 90 atm; T_0, 820 – 940 K; ϕ_0, 1.0 – 3.0. The results were interpolated using the Gaussian process model (Kriging) and the results were examined as demonstrated in Fig. 3. Column 3 in Table 1 shows reaction rankings for a constant pressure simulation near the minimum in Fig. 3.

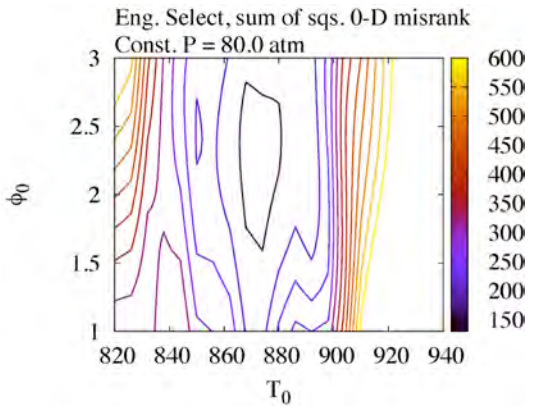

Fig. 3. Difference between reaction rankings in constant P simulations at 80 atm and engine simulations for a set of T_0's and ϕ_0's.

Table 1 and Fig. 3 led to an investigation of the chemistry within the cylinder in the engine simulations and Fig. 4 shows one result. The comparisons in Table 1 and Fig. 3 suggested that the temperature range that contributed to the reaction sensitivities was narrow and centered near 870 K. Cut planes through the cylinder are shown in the two plots in the upper right of Fig. 4. Six temperature contours are

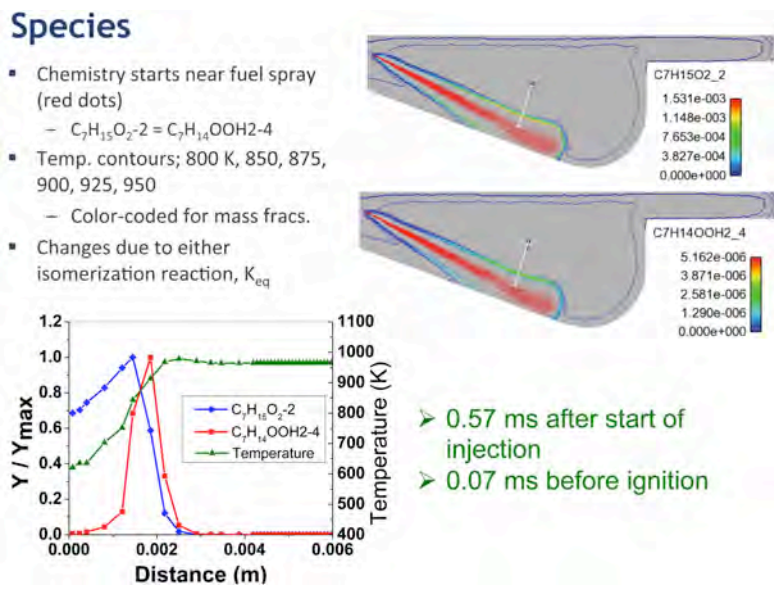

Fig. 4. The location of the two species in the most sensitive reaction (Table 1) for one of the engine simulations.

plotted from 800 K, nearest to the fuel spray, to 950 K, lying away from the fuel spray, nearly the T of the air in the cylinder. Examination of the two plots on the right of Fig. 4, along with the 1-D slice in the bottom left (taken along the white line) demonstrates that this reaction starts near the fuel spray and that the RO_2 species appears closest to the fuel spray followed by the QOOH species, indicative of either the time-evolving reaction or the change in K_{eq} as T increases along the line.

Future Plans

Applications of GSA for engine simulations will be extended to simpler fuels, which will allow a more detailed examination of the chemistry. The sparse algorithm will be extended to other types of fitting. In collaboration with Skodje (Colorado), a new project has been initiated to compare reaction pathway analysis to global sensitivity analysis.

Publications

1. R. Sivaramakrishnan, W. Liu, M. J. Davis, S. Som, and D. E. Longman, "A high temperature model for the combustion of methylbutanoate", East. States Section of the Comb. Instit. (2011).
2. R. L. Miller, L. B. Harding, M. J. Davis, and S. K. Gray, "Bi-fidelity fitting and optimization", J. Chem. Phys. 136, 074102-1 – 074102-11 (2012).
3. D. D. Y. Zhou, K. Han, P. Zhang, L. B. Harding, M. J. Davis, and R. T. Skodje, "Theoretical Determination of the Rate Coefficient for the $HO_2 + HO_2 \rightarrow H_2O_2+O_2$ Reaction: Adiabatic Treatment of Anharmonic Torsional Effects", J. Phys. Chem. 116, 2089-2100 (2012).
4. W. Liu, R. Sivaramakrishnan, M. J. Davis, S. Som, and D. E. Longman, "Development of a Reduced Biodiesel Surrogate Model for Compression Ignition Engine Modeling", Central States Section of the Combustion Institute (2012).
5. W. Liu, R. Sivaramakrishnan, M. J. Davis, S. Som, D. E. Longman and T. F. Lu, "Development of a reduced biodiesel surrogate model for compression ignition engine modeling", Proc. Combust. Inst. 34 401-409 (2013).
6. D. D. Y. Zhou, R. T. Skodje, W. Liu, and M. J. Davis, "Multi-Target Global Sensitivity Analysis of n-Butanol Combustion", Proceedings of the 8th US National Technical Meeting of the Combustion Institute, University of Utah (2013).
7. W. Liu, S. Som, D. D. Y. Zhou, R. Sivaramakrishnan, D. E. Longman, R. T. Skodje, and, M. J. Davis, "The Role of Individual Rate Coefficients in the Performance of Compression Ignition Engine Models", Proceedings of 8th US National Technical Meeting of the Combustion Institute, University of Utah (2013).
8. D. D. Y. Zhou, M. J. Davis, and R. T. Skodje, "Multi-Target Global Sensitivity Analysis of n-Butanol Combustion", J. Phys. Chem. A 117, 3569-3584 (2013).
9. S. Som, W. Liu, D. D. Y. Zhou, G. M. Magnotti, R. Sivaramakrishnan, D. E. Longman, R. T. Skodje, and M. J. Davis, "Quantum Tunneling Affects Engine Performance", J. Phys. Chem. Lett 4, 2021-2025 (2013).
10. Y. Pei, R. Shan, S. Som, T. Lu, D. E. Longman, and M. J. Davis, "Global Sensitivity Analysis of a Diesel Engine Simulation with Multi-Target Functions", Proceedings of the Society of Automotive Engineers (SAE) World Congress, 2014, SAE Paper 2014-01-1117.

Multiple Coupled Potential Energy Surfaces with Application to Combustion

Richard Dawes
Missouri University of Science and Technology
400 W. 11th Street, Rolla, MO 65409
dawesr@mst.edu

Program Scope: Hydrocarbon combustion involves the dynamics of numerous small radicals such as HO_2, HCO, and HOCO. HOCO is an intermediate in the HO + CO → H + CO_2 reaction which is the last and heat releasing step in hydrocarbon combustion and the subject of many ongoing studies. Accurate calculations of their potential energy surfaces (PESs) are possible using traditional quantum chemistry methods such as MRCI. However, multistate and non-adiabatic processes can be important, and tunneling effects may supersede the more common kinetic or thermodynamic control of rates and branching ratios. Significant fractions of molecular products can also result from radicals roaming far from conventional minimum energy paths and tight transition states. Dynamical calculations for these relatively simple systems are very sensitive to the detailed topography of their global potential energy surfaces (PESs).

This project combines developments in the areas of PES fitting and multistate multireference quantum chemistry to allow spectroscopically and dynamically/kinetically accurate investigations of key molecular systems (such as those mentioned above), many of which are radicals with strong multireference character and have the possibility of multiple electronic states contributing to the observed dynamics. A main goal is to develop general strategies for robustly convergent electronic structure theory for global multichannel reactive surfaces. Combining advances in ab initio methods with automated interpolative PES fitting allows the construction of high-quality PESs incorporating thousands of high level data to be done rapidly through parallel processing on high-performance computing (HPC) clusters. New methods and approaches to electronic structure theory will be developed and tested through applications. Some effort will be applied to the development of Quantum Monte Carlo (QMC) and working to apply these methods in the context of global PESs. The feasibility of capturing a larger fraction of the correlation energy than is possible with traditional electronic structure approaches will be tested on suitable combustion related systems. Strategies will be developed to generate QMC data in the context of a *distributed high-throughput computing* model in which 10s or even 100s of thousands of processors are used.

Recent Progress: This section describes progress achieved along various directions of the project occurring over the past 8.5 months since the project start date of 07-15-2013.

Non-Born-Oppenheimer molecular dynamics of the spin-forbidden reaction of $O(^3P) + CO(X^1\Sigma^+) \rightarrow CO_2(\tilde{X}^1\Sigma_g^+)$.[1] A set of three PESs were developed for this system as well as fully geometry-dependent coupling surfaces. The coupled PESs were used with Ahren W. Jasper (Sandia) in non-Born-Oppenheimer molecular dynamics calculations (NBO MD) of the reaction rate. Specifically the coherent switches decay of mixing (CSDM) method was used. To make the PESs the method of dynamically-weighted state-averaged CASSCF[2,3] including electronic 8 states was used as a reference to compute three states at the MRCI/CBS level (1 singlet and 2 triplets). These were iteratively refined into usable fitted PESs by an automated IMLS-based PES generation scheme running in parallel on an HPC cluster.[4,5] The spin-orbit (SO) coupling surfaces were generated the same way using the Breit-Pauli operator method in

Molpro. Geometries, frequencies, well depths and gaps between states were all found to be very accurate at the MRCI/CBS level when compared with experiment. The dynamically weighted multistate electronic structure calculations were found to be very robust and well-behaved allowing the mean estimated fitting error to be converged to just a few cm^{-1} for the three PESs and even less for the coupling surfaces. The magnitude of SO coupling long the crossing seams is only 45 – 80 cm^{-1} and the results were found to be quite sensitive to the coupling strength.

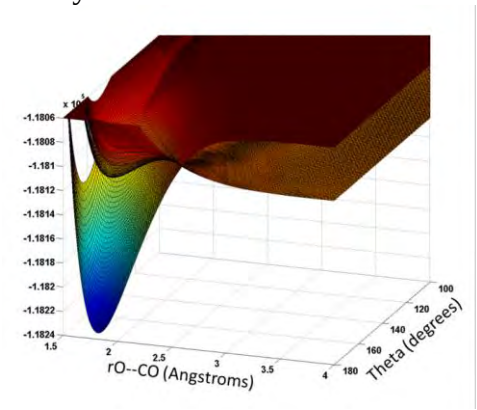

Figure 1. The spin-forbidden chemistry of the $O(^3P)$ + $CO \rightarrow CO_2$ reaction is studied using three automatically generated PESs. Two frustrated triplet states which correlate with ground state $O(^3P)$ have shallow wells hanging above the deep singlet CO_2 well. The spin-forbidden reaction occurs via spin-orbit coupling between the surfaces.

The association kinetics was calculated using the CSDM trajectory method. Both triplet states were found to contribute non-negligibly to the total association rate coefficient. The total CSDM rate coefficient is 7–35 times larger than the values often used in combustion kinetic models. An error sensitivity analysis assigns uncertainty of ~40% to the predicted values (mainly from the SO-coupling strength). An analysis of the dynamics indicated direct and indirect mechanisms with different behaviors with respect to the seam crossings.

A classical trajectories study of the intramolecular dynamics, isomerization and unimolecular dissociation of HO_2.[6] A PES for the ground state of HO_2 was constructed using the method of dynamically-weighted state-averaged CASSCF including all 18 asymptotically degenerate molecular states correlating to separated ground state atoms. The DW-SA-CASSCF reference was used to calculate MRCI/CBS data, fit into a PES by automated IMLS-based fitting. Including 18 states resulted in greatly improved robustness of convergence as no such problems as previously noted by the group of H. Guo were encountered. 1609 automatically generated data at the MRCI/CBS level produced a spectroscopically accurate PES with excellent geometric parameters, vibrational levels and thermochemistry. The PES was used in a trajectories study by A. F. Wagner and the group of D. L. Thompson. Rates of IVR on the new PES were found to be similar (within a factor of 2) to those predicted by the XXZLG PES of Guo et al.,[7] both of which are much different than prediction of an older (1990) PES due to Varandas et al. known as DMBE-IV.[8]

Theoretical/Experimental Comparison of Deep Tunneling Decay of Bound H(D)OCO to H(D)+CO_2. A survey of the use of multireference methods in the HOCO system was performed. Calculations at the CASPT2 level were included in a study of deep tunneling spearheaded by A. F. Wagner to help interpret experiments by the group of R. E. Continetti.[9]

Experimental and theoretical studies of the electronic transitions of MgC. In a previous study of BeC,[10] vibronic calculations were able to help assign and interpret electronic spectra of that system recorded by the group of Michael C. Heaven (Emory). Heaven's recent efforts to observe similar transitions in MgC have so far been unsuccessful. New vibronic calculations were performed for the MgC system using the dynamically weighted multistate scheme to produce MRCI/CBS quality potential curves. A diabatization procedure was used

along with a DVR method including a complex absorbing potential (CAP) to solve for the vibronic levels and their lifetimes/widths.

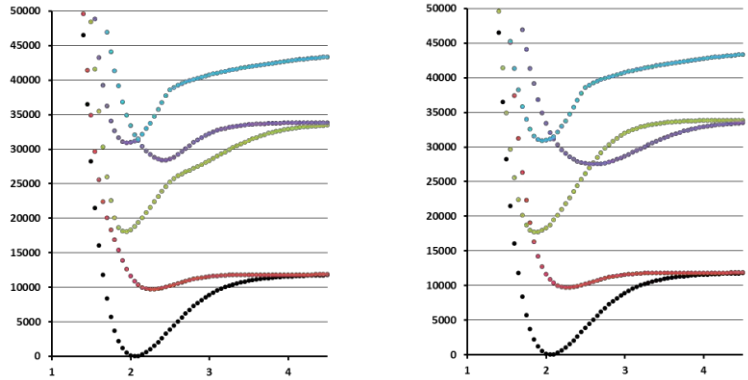

Figure 2. Electronic states of MgC plotted in adiabatic (left) and diabatic representations (right). The zero of the energy is the minimum of the $X^3\Sigma^-$ electronic ground state (shown in black).

The new calculations are promising and perhaps provide an explanation for the failed experiments since no states with significant Franck-Condon factors and life-times are predicted in the spectral range of the initial search. Three good candidate states were identified and new experiments are underway to confirm the predictions.

Level	E(n) (cm^{-1})	E(n)-ZPE(GS) (cm^{-1})	% 1-pi	% 2-pi	% 3-pi	% 4-pi	<r> (Å)	$(<1/r^2>)^{-1/2}$ (Å)	Width (cm^{-1})	FC
44	31166.44	30873.29	0.000	0.257	0.475	99.268	1.9736	1.9698	2.99E-07	0.453
49	31780.33	31487.19	0.000	1.323	1.210	97.467	2.0074	1.9944	1.88E-06	0.360
55	32405.07	32111.93	0.006	1.620	1.273	97.101	2.0162	1.9955	9.34E-04	0.110

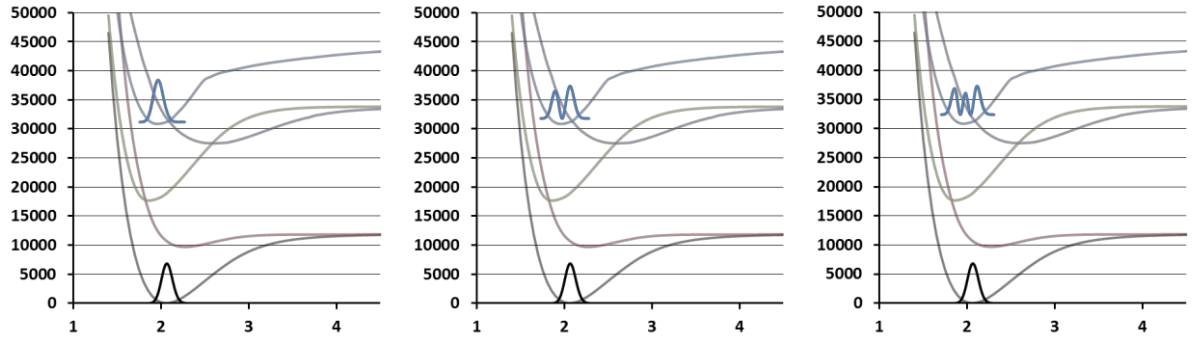

Figure 3. Three predicted vibronic states of predominantly 4-pi character have favorable FCFs and lifetimes for experimental observation.

3D printing of PES models. A procedure was developed for 3D printing of plastic models of PESs. Matlab scripts process the data from a surface plot and add specified thickness to create an object file that can be sent to a 3D printer for construction. A web tutorial was produced: http://chem.mst.edu/facultyandstaff/rdawes/ and an article describing the procedure was submitted to J. Chem. Ed.[11]

Future Plans: Two new directions are underway for the **CO + O system.** First a study of pressure effects on the spin-forbidden kinetics with Ahren W. Jasper. Secondly, a study into isotope exchange reactions including spin quenching effects is providing theoretical support for experiments by K. Boering (Berkeley) and J. Lin (Sinica). This project includes new PESs by the PI and contributions from Jasper as well as the group of H. Guo. The PESs discussed above were

recently extended substantially in their energy and coordinate ranges for the new studies. Remarkably the dynamically weighted electronic structure scheme provided consistent energies that went into a new fit now covering some 500 kcal/mol of energy. The larger coordinate ranges are necessary to fully resolve final product state distributions in the new studies. Preliminary results indicate that the non-adiabatic CSDM trajectory method provides remarkably accurate branching ratios and angular distributions for spin-forbidden ^{18}O exchange reactions.

IMLS-PIP fitting. A large set of ~100,000 high-level multireference data were computed for **methane**. Accurate single expansion fits using the NN-PIP method by the group of H. Guo combined with full 9D vibrational calculations by T. Carrington confirm that the data is of spectroscopic quality. We are currently using this as a test and validation set to implement a version of our automated IMLS-based PES fitting using PIP type basis functions. Preliminary results indicate that the method will be effective to produce fits with negligible fitting error in cases with high permutation symmetry. Methane is not very challenging for fitting since it is semi-rigid and single-welled, so we will soon move to another fitting test set of A. F. Wagner and D. L. Thompson composed of ~400,000 data for **ethyl radical**. This system combines a more complex topography, higher dimensionality and additional permutation symmetry.

$O+H_2O$. A set of three global multichannel PESs are in progress for the $O(^3P) + H_2O$ system using explicitly correlated MRCI-F12 in collaboration with the group of H. Guo. Nominally describing collisions of $O(^3P)$ with H_2O (and the three triplet states that are degenerate at that channel), the PESs also include the $H_2 + O_2$, OH + OH, $H + HO_2$ and separated atoms channels. 36 triplet states are degenerate for separated atoms and are included using the dynamically weighted multistate procedure. Fits will be obtained by the NN-PIP method of Guo and the IMLS-PIP method mentioned above. A series of classical and quantum dynamics studies will employ the new PESs.

QMC. We have been developing scripts and testing methods to use multi-configurational trial wavefunctions in VMC/DMC calculations of PECs for small molecules. We now have some of the methods working and are starting to produce results that can be compared to standard quantum chemistry and experimental spectroscopy.

References (* denotes publications supported by the DOE)

[1] * A. W. Jasper and R. Dawes, *J. Chem. Phys.* **139**, 154313 (2013).

[2] M. P. Deskevich, D. J. Nesbitt and H.-J. Werner, *J. Chem. Phys.* **120**, 7281 (2004).

[3] R. Dawes, A. W. Jasper, C. Tao, C. Richmond, C. Mukarakate, S. H. Kable, S. A. Reid, *J. Phys. Chem. Lett.* **1**, 641 (2010).

[4] R. Dawes, A. F. Wagner, D. L. Thompson, *J. Phys. Chem. A.* **113**(16) 4709-4721 (2009).

[5] R. Dawes, X.-G. Wang, A. W. Jasper, T. Carrington Jr., *J. Chem. Phys.* **133**, 134304 (2010).

[6] * J. W. Perry, R. Dawes, A. F. Wagner D. L. Thompson, *J. Chem. Phys.* **139**, 084319 (2013).

[7] C. Xu, D. Xie, P. Honvault, S. Y. Lin, H. Guo, J. Chem. Phys. **127**, 024304 (2007).

[8] M. R. Pastrana, L. A. M. Quintales, J. Brandão, and A. J. C. Varandas, *J. Chem. Phys.* **94**, 8073 (1990)

[9] * A. F. Wagner, R. Dawes, R. E. Continetti, H. Guo, "Theoretical/Experimental Comparison of Deep Tunneling Decay of Bound H(D)OCO to H(D)+CO_2" (submitted to *J. Chem. Phys.*).

[10] B. J. Barker, I. O. Antonov, J. M. Merritt, V. E. Bondybey, M. C. Heaven, R. Dawes, *J. Chem. Phys.* **137**, 214313 (2012)**.**

[11] * P. Lolur, R. Dawes, "3D Printing of Molecular Potential Energy Surface Models" *J. Chem. Ed.* (submitted, ed-2014-00199m).

Dynamics of Radical Reactions in Biodiesel Combustion

Theodore S. Dibble
Department of Chemistry, SUNY-Environmental Science and Forestry
Syracuse, NY, 13210
tsdibble@esf.edu

I. Program Scope

The ignition of diesel fuel depends on isomerization of peroxy radicals (ROO•) via a hydrogen shift reaction:

$$ROO^{\bullet} \rightarrow QOOH \quad (1)$$

Production of OH radicals (chain propagation and branching) following reaction (1) leads to autoignition. Processes such as reaction (2):

$$ROO^{\bullet} \rightarrow \text{Products} + HOO \quad (2)$$

compete with chain branching. Experimentalists face several difficulties in gaining an understanding of this chemistry, and no QOOH species has ever been detected by experiment! This has inspired many computational studies of these processes.

Biodiesel fuel is increasingly being used worldwide. Although we have a fair understanding of the molecular details of the chemistry of peroxy radicals derived from alkanes, biodiesel fuels contain ester and olefin groups which significantly impact the thermodynamics and kinetics of biodiesel ignition.[1] The broader goal of this research is to carry out systematic computational studies of the elementary kinetics of peroxy radical chemistry from compounds that are models for biodiesel ignition. This includes not only reactions (1) and (2), but also reactions leading to chain branching. In addition, the research will include rigorous treatments of tunneling effects, quantify the effect of chemically activated processes, and synthesize the results into structure-activity relations (SARs)

More recently, we have been investigating cyclization reactions of unsaturated hydrocarbon radicals that can decyclize to yield isomers of the parent radical. These reactions would change the hydrocarbon radical pool, leading to different decomposition alkyl and peroxy radicals in pyrolysis and combustion. The goal is to determine SARs for these reactions to be used in constructing kinetic models.

II. Recent Progress

A) Exploring Unusual Chemistry in Model QOOH Systems

The studies of unimolecular reactions of QOOH from methyl butanoate inspired us to investigate a range of unimolecular reactions of simpler QOOH, specifically $CH_3C{\bullet}HCH_2OOH$ and $\bullet CH_2CH(OOH)CH_3$. Results of these calculations for $CH_3C{\bullet}HCH_2OOH$ are presented in Figure 1 (next page). This work tends to confirm that there are no important reactions missing from models of QOOH chemistry.

B) Autoignition Mechanism of Methyl Butanoate (MB)

Methyl butanoate (MB) is composed of a methyl ester group and a short alkyl group (see Scheme1). MB oxidation mechanism has been studied as the starting point for understanding biodiesel combustion for a decade.[6] The CBS-QB3 composite method is used to determine reaction energies and activation barriers to reactions of peroxy radicals and the corresponding QOOH species. We include all four peroxy radicals formed from H-abstraction from MB (sites 1-3 and 5 in Scheme1). Reactions treated include H-shift and HO_2 elimination of ROO•, and decomposition of QOOH by C-C, C-O, and O-O scission.

Potential energy profiles have been obtained for all four peroxy radicals. As can be seen in Table 1, three of the four ROO• will tend to form QOOH rather than eliminate HO_2. An quite surprising finding was that the 1,8 H-shift (of R5OO) possesses a lower barrier than the 1,6 H-shift, and even the 1,7 H-shift has a lower barrier than 1,6 H-shift. Due to entropic factors (a higher Arrhenius pre-exponential term), the 1,6 H-shift will likely compete with the 1,7 and 1,8 H-shift at temperatures most relevant to diesel ignition.

Figure 1. QOOH Reactions Potential Energy Surface at M052x/6-311+G(2df, 2p)

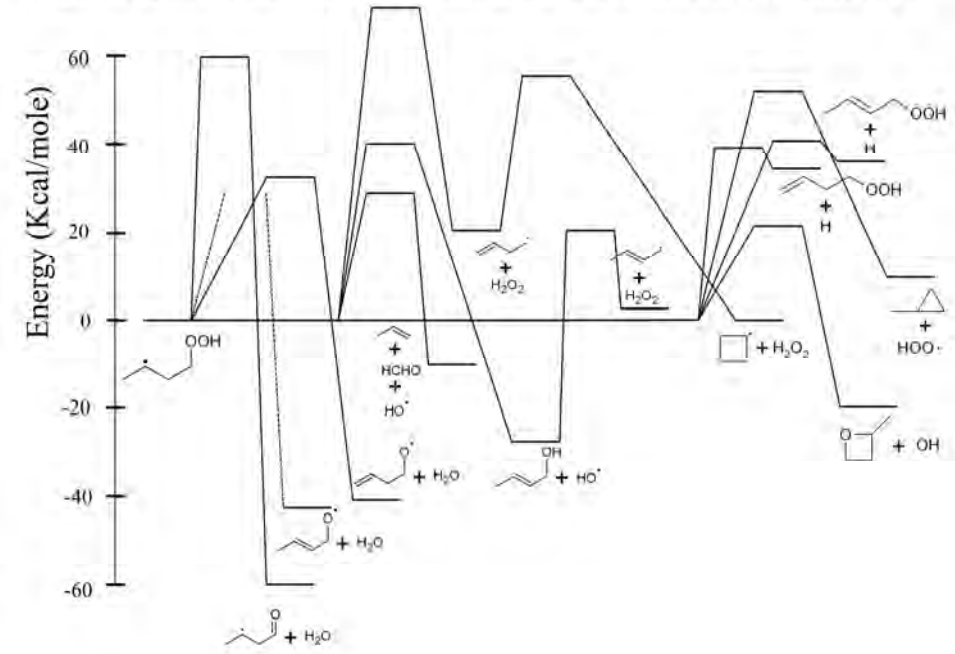

Scheme 1

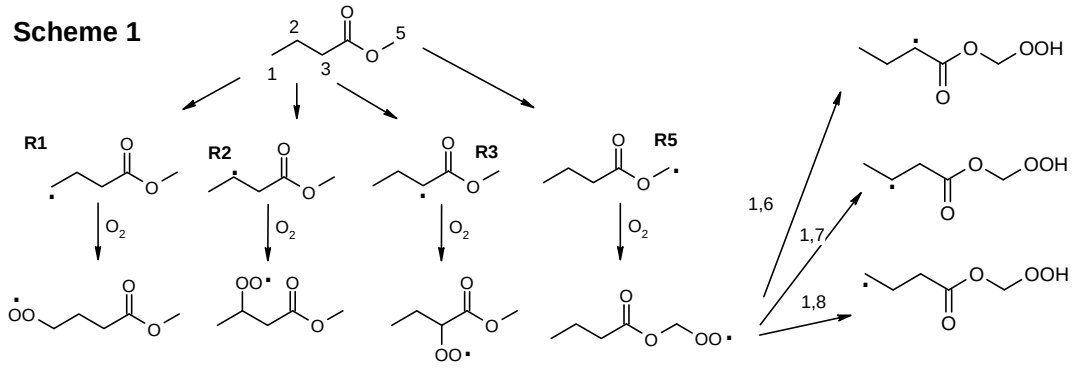

Table 1. CBS-QB3 energy barrier ($\Delta H^{\ddagger}_{0K}$) of H-migration and HO_2 loss reaction of MB-OO• in kcal mole^{-1}, with lowest barriers of respective MB-OO• highlighted in bold. A "-" means the reaction is not applicable. The lowest energy conformer of H-migration transition states possessing multiple conformations is identified using the nomenclature that follows: "mn" indicates the types of radical sites for the product and reactant (p=primary and s=secondary). The superscript A or E indicates axial or equatorial geometries for substituents of secondary radicals in reactants or products.

Peroxy radical	Reaction type					
	1,4-H shift	1,5-H shift	1,6-H shift	1,7-H shift	1,8-H shift	HO_2 loss
R1OO•	32.8	**19.9 (s^Ep)**	-	-	25.4 (pp)	31.4
R2OO•	35.4[a] (ps^E) 32.5[b] (s^Es^E)	-	-	27.8 (ps^E)	-	32.1[a] **26.9[b]**
R3OO•	31.6 (s^As^E)	**22.2 (ps^A)**	30.2 (ps^E)	-	-	29.1
R5OO•	-	-	26.3 (s^Ep)	22.3 (s^Ap)	**20.6 (pp)**	-

a. Hydrogen atom is transferred or lost from the methyl group (site 1).
b. Hydrogen atom is transferred or lost from the methylene group (site 3).

C) Cyclization-Decyclization Reactions of Unsaturated Hydrocarbon Radicals

Cyclization reactions of unsaturated radicals are well known in the organic chemistry literature, and famously through Baldwin's rules.[2] Baldwin's rule discuss exo and endo cyclizations (as illustrated in Scheme 2, below). For the cases below, Baldwin predicted the exo cyclization to be favored over the endo, and the limited literature[3] agrees with that.

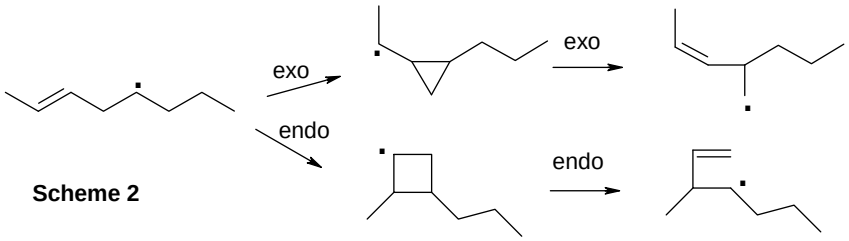

Scheme 2

We initiated a survey of a broad range of reactions, only a few of which are shown here. This survey used one of the newest functionals (MN12-SX),[4] and will be checked with CBS-QB3 calculations. As can be seen from the right side of Figure 2, below, the exo cyclization and decyclization reactions are strongly favored, kinetically, over the endo cyclization, even though the enthalpy changes are almost identical. Moreover, the cyclization reactions seem to have lower barriers than the H-shift reactions, the reactions of which are commonly included in detailed combustion mechanisms. At combustion temperatures, it seems likely that the *n*-alkenyl reactant in Scheme 2 could achieve quasi-equilibrium with the product of exo reactions.

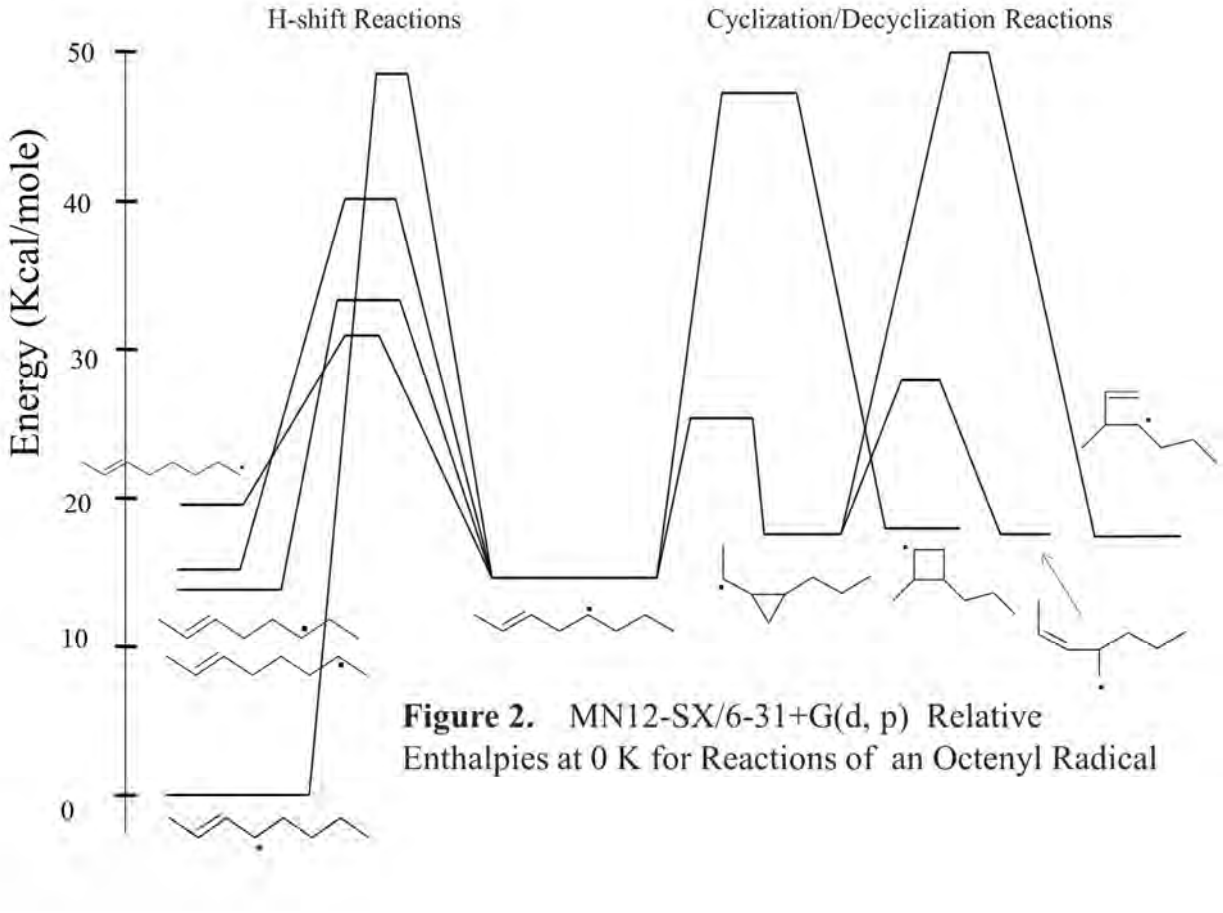

Figure 2. MN12-SX/6-31+G(d, p) Relative Enthalpies at 0 K for Reactions of an Octenyl Radical

III. Future Work

We will compute high-pressure limiting rate constants for reactions of ROO, QOOH and OOQOOH from methylbutanoate, and ROO from $CH_3C{\bullet}HCH_2OOH$ and $\bullet CH_2CH(OOH)CH_3$. We will refine calculations on unsaturated hydrocarbon radicals and extend calculations to competing dissociation reactions of reactants and products. RRKM-Master Equation calculations will be carried out on this large system to determine how the cyclization-decyclization (net isomerization) reactions affect the pool of hydrocarbon radicals.

IV. References

[1] Sumathi, R.; Green W. H., *Phys. Chem. Chem. Phys*. **2003**, *5*, 3402.

[2] Baldwin, J. E. *J. C. S. Chem. Comm*. **1976**, 734-736.

[3] Furxhi, E.; Horner, J. H., Newcomb, M., *J. Org. Chem*. **1999**, *64*, 4064.

[4] Peverati, R.; Truhlar, D. G. *Phys. Chem. Chem. Phys.* **2012**, *14*, 16187.

V. Publications and submitted journal articles supported by this project 2010-2014

T. S. Dibble, Y. Sha, W. F. Thornton, and F. Zhang. Cis-trans isomerization of chemically activated 1-methylallyl radical and fate of the resulting 2-buten-1-peroxy radical, *J. Phys. Chem. A.* **2012**, *116*, 7603–7614.

F. Zhang and T. S. Dibble. Impact of Tunneling on hydrogen-migration of n-propylperoxy radical. *Phys. Chem. Chem. Phys.*, **2011**, *13*, 17969-77.

F. Zhang and T. S. Dibble, Effects of ester and olefin functional groups on kinetics of unimolecular reactions of peroxy radicals, *J. Phys. Chem. A.* **2011**, *115*, 655-663.

T. S. Dibble and Yue Zeng, Potential energy profiles for the N + HOCO reaction and products of the chemically activated reactions N + HOCO and H + HOCO. *Chem. Phys. Letts.*, **2010**, *495*, 170-174.

Vibrational Spectroscopy of Transient Combustion Intermediates Trapped in Helium Nanodroplets (DE-FG02-12ER16298)

Gary E. Douberly
University of Georgia, Department of Chemistry, 1001 Cedar St., Athens, GA 30602-1546

Program Scope

The objective of this research is to isolate and stabilize transient intermediates and products of prototype combustion reactions. This will be accomplished by Helium nanodroplet isolation (HENDI) spectroscopy, a novel technique where liquid helium nanodroplets freeze out high energy metastable configurations of a reacting system, permitting infrared spectroscopic characterizations of products and intermediates that result from hydrocarbon radical reactions with molecular oxygen and other small molecules relevant to combustion environments. A major aim of this work is to directly observe the elusive hydroperoxyalkyl radical (QOOH) and its oxygen adducts (O2QOOH), which are important in low temperature hydrocarbon oxidation chemistry.

Recent Projects

Tunneling Dynamics of Helium-Solvated Vinyl Radical

The vinyl radical ($H_2C_\beta=C_\alpha H$) has been produced by the pyrolysis of di-vinyl sulfone and trapped in liquid He nanodroplets (Ref. 1). At 0.4 K, the entire population of nuclear spin isomers is cooled to either the 0_{00}^+ (ortho) or 0_{00}^- (para) rotovibrational level. IR spectra in the fundamental CH stretch region reveal three bands that are assigned to the symmetric CH_2 (ν_3), antisymmetric CH_2 (ν_2) and lone α-CH (ν_1) stretch bands. The vinyl radical CH stretch band origins in He droplets differ from the VCI calculations of J. Bowman and co-workers by ≈1, 2 and 10 cm^{-1} for the ν_3, ν_2 and ν_1 modes, respectively. Each band consists of *a*-type and *b*-type transitions from the 0_{00} level, and each of these is split by either the *difference in* or *sum of* the v=0 and v=1 tunneling splittings. Comparing the He droplet spectra to previous high-resolution spectroscopy of the ν_3 band (D.J. Nesbitt and co-workers), we find that the A'-B' rotational constant for this mode is reduced to 89% of its gas phase value, and the tunneling splittings (ground and ν_3 excited states) are both reduced by ≈20%. In addition, the relative intensities of

the ν_3 transitions indicate 4:4 spin statistics for ortho and para nuclear spin isomers, suggesting a facile interchange mechanism for all *three* H atoms within the ≈1200 K pyrolysis source, prior to the pick-up and cooling of the hot vinyl radical by the He droplet. The ≈20% reduction in the ground and ν_3 excited state tunneling splittings is due to two contributing effects from the He solvent. The He droplet can modify both the tunneling barrier and the effective reduced mass for motion along this coordinate. We have estimated that either an ≈40 cm^{-1} increase in the effective barrier height or an ≈5% increase in the effective mass of the tunneling particles (both as upper limits) is sufficient to account for the observed ≈20% tunneling splitting reduction. Future theoretical work will be required to assess the extent to which each of these effects contribute to the overall modification of the vinyl radical tunneling dynamics upon solvation in liquid He.

High Resolution Stark Spectroscopy of the Helium-Solvated Ethyl Radical

The ethyl radical has been isolated and spectroscopically characterized in He droplets (Ref. 2). The five fundamental CH stretch bands are observed near 3 μm and have band origins shifted by < 1 cm^{-1} from those reported for the gas phase species (D.J. Nesbitt and co-workers). The symmetric CH_2 stretching band (ν_1) is rotationally resolved, revealing nuclear spin statistical weights predicted by G_{12} permutation-inversion group theory. The first measurement of this radical's permanent electric dipole moment (0.28 (2) D) is obtained via the Stark spectrum of the ν_1 band. In addition to the five fundamentals, three A_1' overtone/combination bands are observed and have resolved rotational substructure. These are assigned to $2\nu_{12}$, $\nu_4+\nu_6$, and $2\nu_6$ through comparisons to anharmonic frequency computations at the CCSD(T)/cc-pVTZ level of theory (in collaboration with H.F. Schaefer and co-workers) and via an analysis of the rotational substructure observed for each band.

Reaction of O_2 with Resonantly Stabilized Free Radicals within Helium Droplets

We spectroscopically probed the outcome of the reaction between the propargyl radical (C_3H_3) and O_2 within He droplets [Ref. 4]. A pick-up technique was employed where He droplets doped with a propargyl radical (generated by pyrolysis of 1-butyn-4-nitrite) were sequentially doped with an O_2 molecule. The reaction carried out at 0.4 K resulted exclusively in the formation of the acetylenic-*trans*-propargyl peroxy radical (HC≡C–CH_2–OO•). This work helped to elucidate

the shape of the entrance channel on the potential energy surface, as it was unclear whether or not there exists a small barrier to formation of the peroxy species. The rapid cooling afforded by the He droplets motivates the conclusion that if a barrier does indeed exist, it is too small to kinetically stabilize a van der Waals complex between C_3H_3 and O_2. MRCI computations carried out in collaboration with Stephen Klippenstein and co-workers indicate that the reaction is barrierless, similar to alkyl + O_2 reactions.

High resolution infrared spectra were obtained for the allyl radical (C_3H_5) and the products of the He-mediated reaction between allyl and O_2 [Ref. 5]. In the IR spectrum of He-solvated allyl, we observed rovibrational bands near the reported band origins in high resolution gas-phase studies carried out by D.J. Nesbitt and co-workers and R. Curl and co-workers. In addition to the fundamental CH stretching modes, four other bands were assigned to the allyl radical using a consistent set of rotational constants. Indeed, it was observed in the previous gas-phase studies that the CH stretch bands are heavily perturbed, but no explanation was given as to the nature of the perturbations. The lower temperature of the He droplets greatly decreases the number of populated rovibrational levels, and aided by anharmonic frequency computations and the resolved rotational substructure, we assigned the ν_1 (a_1), ν_3 (a_1), ν_{13} (b_2) fundamentals and the $\nu_{14}/(\nu_{15}+2\nu_{11})$ (b_2) and $\nu_2/(\nu_4+2\nu_{11})$ (a_1) Fermi dyads, in addition to an unassigned resonant polyad near the ν_1 mode.

Five stable conformers are predicted for the allyl peroxy radical, and a computed two-dimensional potential surface for rotation about the CC–OO and CC–CO bonds revealed multiple isomerization barriers greater than ≈300 cm^{-1}. Nevertheless, the C–H stretch IR spectrum is consistent with the presence of a single conformer following the allyl + O_2 reaction within He droplets. This is similar to the observation for the propargyl peroxy system, and from this we can infer a cooling mechanism for the vibrationally hot reaction products (R-OO•) that is consistent with both sets of data. The mechanism assumes that the more closely spaced torsional levels (<100 cm^{-1}) relax more efficiently in comparison to the higher frequency vibrations, allowing the system to funnel into the lowest energy conformational minimum as it cascades down the ladder of excited stretching/bending levels.

Ongoing Work

We are modifying our pyrolysis source to increase the upper temperature that can be achieved in our experiments. With a higher temperature, the range of precursor systems that can be pyrolyzed to create radicals will be vastly expanded. This involves incorporating a resistively heated silicon carbide (SiC) tube, similar to those reported by P. Chen and co-workers and B. Ellison and co-workers that can be heated up to ~2100 K (Figure 1). Because the pick-up efficiency of the He droplets is quite large, for example, compared to the molecular densities needed for matrix isolation spectroscopy, we can work in a regime where we can isolate transient species while minimizing secondary reactions within the pyrolysis source, such as recombination reactions between two radicals.

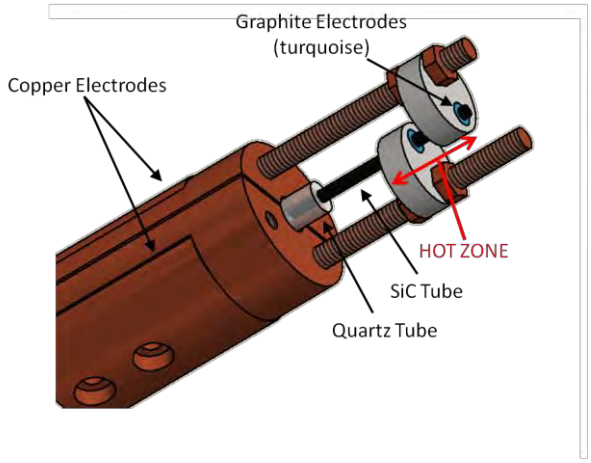

Figure 1. A schematic drawing of our SiC high temperature pyrolysis source. The length of the hot zone can be adjusted.

Publications acknowledging DOE support (2013-present):

1. Paul L. Raston, Tao, Liang and Gary E. Douberly, "Infrared spectroscopy and tunneling dynamics of the vinyl radical in ^{4}He Nanodroplets" *Journal of Chemical Physics*, **138**, 174302 (2013). Published: May 7, 2013.

2. Paul L. Raston, Jay Agarwal, Justin M. Turney, Henry F. Schaefer III and Gary E. Douberly, "The Ethyl Radical in Superfluid Helium Nanodroplets: Rovibrational Spectroscopy and Ab Initio Computations" *Journal of Chemical Physics*, **138**, 194303 (2013). Published: May 21, 2013.

3. Alexander M. Morrison, Paul L. Raston and Gary E. Douberly, "Rotational Dynamics of the Methyl Radical in Superfluid ^{4}He nanodroplets" *Journal of Physical Chemistry A* **117**, 11640-11647 (2013). Published: November 21, 2013.

4. Christopher P. Moradi, Alexander M. Morrison, Stephen J. Klippenstein, C. Franklin Goldsmith and Gary E. Douberly, "Propargyl + O_2 Reaction in Helium Droplets: Entrance Channel Barrier or Not?" *Journal of Physical Chemistry A* **117**, 13626-13635 (2013). Published: December 19, 2013.

5. Christopher M. Leavitt, Christopher P. Moradi, Bradley W. Acrey and Gary E. Douberly, "Infrared Laser Spectroscopy of the Helium-Solvated Allyl and Allyl Peroxy Radicals" *Journal of Chemical Physics* **139**, 234301 (2013). Published: December 21, 2013.

Spectroscopic and Dynamical Studies of Highly Energized Small Polyatomic Molecules

Robert W. Field
Massachusetts Institute of Technology
Cambridge, MA 02139
rwfield@mit.edu

I. Program Scope

The fundamental goal of this program is to develop the experimental techniques, diagnostics, interpretive concepts, spectrum-assignment strategies, and pattern-recognition schemes needed to reveal and understand how large-amplitude motions are encoded in the vibration-rotation energy level structure of small, gas-phase, combustion-relevant polyatomic molecules. We are focusing our efforts on unimolecular isomerizations in several prototypical systems, including the acetylene↔vinylidene isomerization and the acetylene *cis*↔*trans* conformational isomerization on the S_1 excited state surface. Work has been extended to characterization of atmospherically-relevant molecules such as the dihydroxycarbene intermediate and SO_2.

II. Recent Progress

A. Characterization of the acetylene S_1 potential energy surface

The S_1 state of C_2H_2 is a prototype for documentation of the spectroscopic signatures of *cis-trans* conformational isomerization. The S_1(*cis*)-S_0 transition is electronically forbidden. As a result, this transition has only recently been identified by observation of transitions into *cis* vibrational levels that acquire some spectroscopically bright *trans* state character via tunneling through the *cis-trans* isomerization barrier.

These observations have enabled the construction of a nearly complete set of vibrational assignments for both *trans* and *cis* conformers up to the expected energy of the transition state. Our recent IR-UV double resonance spectra of the ungerade vibrational levels of S_1 C_2H_2 in the region 46900-47200 cm^{-1} complete the final step toward characterization of all S_1(*trans*) vibrational levels that lie below the *cis-trans* isomerization barrier. This concludes the current experimental phase of our S_1 acetylene project.

1. IR-UV double-resonance experiment in the region 46900-47200 cm^{-1}

Nearly all vibration-rotation levels observed in the 46900-47200 cm^{-1} region are predissociated and have short fluorescence lifetimes (~20 ns, compared with ~300 ns for lower-lying levels of S_1(*trans*) acetylene, which corresponds to a ~7% fluorescence quantum yield). The rotational structure has been assigned. Vibrational assignments are based on predictions from our *trans*-conformer polyad fit model as well as on the relative intensities of the fluorescence-detected transitions and the radiative lifetime of the state. *K*-staggering, a group theoretical signature of *cis-trans* isomerization, is observed for the $3^2 5^1$ state (+0.93 cm^{-1}) as well as for the $3^4 6^1$ component (+29 cm^{-1}) of the 3^4B^1 polyad. It is difficult to assign most of the other observed states in this region, because the *trans*-bent level-structure in our polyad model becomes distorted by the isomerization process. However, it is interesting to see that relatively long-lived *K*=0, 1, and 2 states (~100 ns lifetime) are observed within 4 cm^{-1} of where corresponding states of the predominantly $2^3 6^1$ component of the 2^3B^1 polyad are predicted (Figure 1). We believe that the $2^3 6^1$ state is both less strongly predissociated and more resistant to isomerization, due to the absence of excitation in mode 3, which is an active promoter of both *cis-trans* isomerization (in combination with mode 6) and predissociation. Even though a few of the states described by our polyad model are not yet observed, we believe that there are several cases where more vibrational levels are observed than are predicted by the polyad model. This suggests the presence of additional S_1(*cis*) vibrational levels. More definite conformer and complete vibrational assignment of the observed interloper levels is in progress.

2. Determination of *cis-trans* isomerization barrier height

Our comprehensive examination of the vibrational energy level structure of the *cis-trans* isomerization has led to the development of a universal, model-independent, spectroscopic diagnostic of transition state energies. We believe that it is possible to generalize the concept of effective vibrational frequency as an indicator of qualitative dynamical changes, previously used for diatomic dissocation (Birge-Sponer, LeRoy-Bernstein) and quasi-linear triatomics ("Dixon dip"), by applying it to the determination of the isomerization barrier height in an asymmetric double minimum potential. We can determine the transition

state energy to high accuracy by fitting the observed vibrational energy level pattern to the empirical formula $\omega^{eff} = \omega_0(1-E/E_{ts})^{1/n}$, where E_{ts} is the transition state energy.

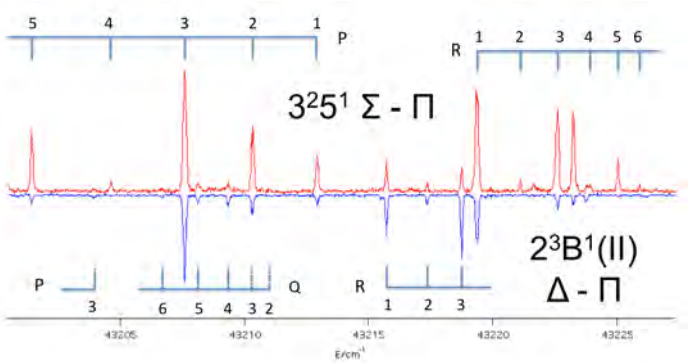

Figure 1. IR-UV double-resonance spectrum of C_2H_2 in the region 47097-47124 cm^{-1} (the energy scale is that of the UV photon). The IR radiation was tuned to the Q branch head of the ($\nu_3+\nu_4$)" band of the ground electronic state. The upper trace (red) includes fluorescence intensity between 0 to 40 ns (early gate) after the laser pulse; the lower trace (blue) includes fluorescence intensity between 40 to 160 ns (late gate). Nearly all vibration-rotation levels observed in the 46900-47200 cm^{-1} region are predissociated and almost all of their fluorescence intensity appears in the upper (early) trace (e.g. the $3^2 5^1$ K=0 state in the figure). States that have more intensity in the lower (late) trace than the upper (early) trace have longer lifetimes and are less strongly predissociated (e.g. the 2^3B^1(II) K=2 state). This is an example where vibrational assignments can be guided by radiative lifetime.

3. *Ab initio* rovibrational variational calculations for S_1 acetylene

The global rovibrational dynamics and energy level structure of an isomerizing system pose challenges for traditional effective Hamiltonian spectroscopic models, which are not easily extended to asymmetric, multi-well potential energy surfaces. Key qualitative dynamical patterns that result from the S_1 C_2H_2 isomerization process, such as rotational level K-staggerings and the dips in effective vibrational frequency discussed above, can be addressed by high level *ab initio* rovibrational variational calculations. In our most recent work we have reproduced much of the bending, torsion, and rotational structure of the S_1 state. Important results include predictions of K-staggerings to good qualitative accuracy and demonstration that large K-staggerings can result from K-dependent *cis-trans* tunneling interactions (Figure 2). These insights will prove useful in the analysis of irregular spectroscopic patterns near the transition state barrier energy region.

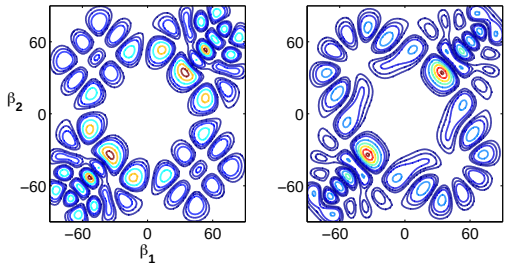

Figure 2. K-dependent *cis—trans* interactions in the *trans* $3^4 6^2$ vibrational level. The *ab initio* vibrational wavefunctions for even K (left) and odd K (right) are plotted as a function of the two CCH angles, $\beta_{1,2}$. The different K levels of this *trans* vibrational level interact with different *cis* vibrational states, as shown by the distinct nodal patterns in the upper left and lower right quadrants (*cis* geometries). This leads to dramatically K-dependent *cis-trans* interactions and energy level shifts.

4. Full-dimensional Franck-Condon Calculations

Full-dimensional Franck-Condon calculations have been performed for the acetylene $\tilde{A} \leftrightarrow \tilde{X}$ transition. In addition to explaining several key features in observed intensity patterns, the calculations provide insight into strategies for accessing large amplitude local bending levels of S_0 acetylene, relevant to the acetylene—vinylidene isomerization. As a result of the isolation of ν_4' (torsion) from Duschinsky rotation effects, the calculation predicts that transitions to local bending levels of S_0 are dominant from S_1 levels with high excitation of the torsional ν_4' mode (Figure 3). This result contrasts with semiclassical arguments made previously that the *cis*-bend ν_6' mode would grant the best access to the local bend.

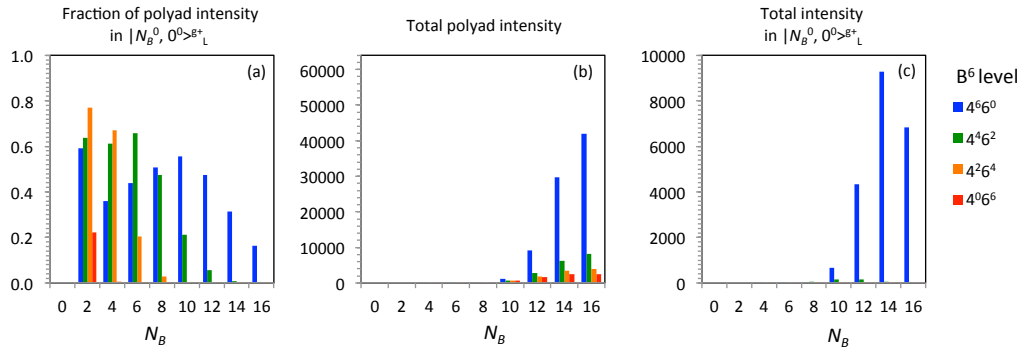

Figure 3. Emission intensity from a_g levels of the B^6 polyad of S_1 acetylene to pure-bending polyads of S_0 with l=0 and g^+ symmetry. The total intensity into each bending polyad is shown in the middle panel, and the fraction of that intensity into the pure local bending level, denoted $|N_B^0,0^0>^{g+}_L$, is shown in the left panel. The right panel shows the total intensity into the pure local bending level. For high-lying B^n polyads of S_1, the dominant emission intensity is from the level with the most torsional character (4^n6^0) to highly excited local bend states.

III. Experimental challenges and future work

Two experimental challenges in extending the spectroscopic characterization of the acetylene S_1 isomerization are (i) the reduced fluorescence quantum yield due to predissociation (as mentioned previously) and (ii) access to high-K rotational sub-manifolds, measurements of which are necessary to reveal and understand isomerization K-staggering patterns, but such high-K levels are usually unobservable due to restrictive rotational propensity rules. We have addressed both challenges recently and new experimental schemes are proposed here.

To overcome the low fluorescence quantum yield, we have constructed a REMPI-TOF spectrometer to record high-resolution H-atom action spectra of S_1 acetylene. Initial spectra yield important measurements on isomerizing states (Figure 4). Using our current REMPI-TOF setup, we plan to develop an acetylene-isotopologue multiplexed H-atom REMPI-TOF scheme, by which high-resolution spectra of several isotopologues of S_1 acetylene can be simultaneously recorded. This will greatly facilitate vibrational assignments in the increasingly complicated high-energy region of the S_1 acetylene potential energy surface. At the same time, we are considering alternate methods to detect the photofragment hydrogen atom, such as via 3d←←1s two-photon excited H-atom 3d→2p fluorescence. The fluorescence-based detection method can be carried out with a larger number density of acetylene molecules than our current ion-detected REMPI-TOF scheme, in addition to being more readily adaptable for experiments in static cell conditions (e.g. a null-cell H-atom fluorescence dip SEP experiment).

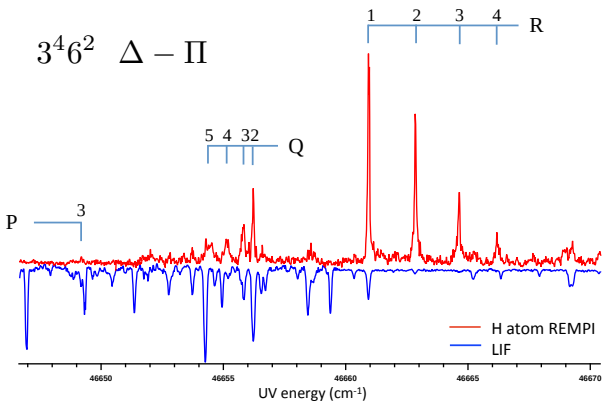

Figure 4. H-atom action (red, upper trace) and LIF (blue, lower trace) spectra of 3^46^2 K=2. J'' assignments are shown with tie-lines. The relative strength of the R branch in the H-atom detection channel over the weak LIF channel demonstrates there is significant predissociation. Measurement of this band via H-atom action REMPI-TOF spectra has enabled the determination of the isomerization K-staggering for this vibrational level.

To address the need for high-K measurements, we have demonstrated hot band-pumped IR-UV double resonance spectroscopy using a hyperthermal, supersonic molecular beam source. This greatly increased the vibrational temperature (~100K) of the beam, while still maintaining cold rotational temperature (~5K). This populates high-l vibrational levels of the electronic ground state, thus permitting transitions to high-K levels of the S_1 state (Figure 5).

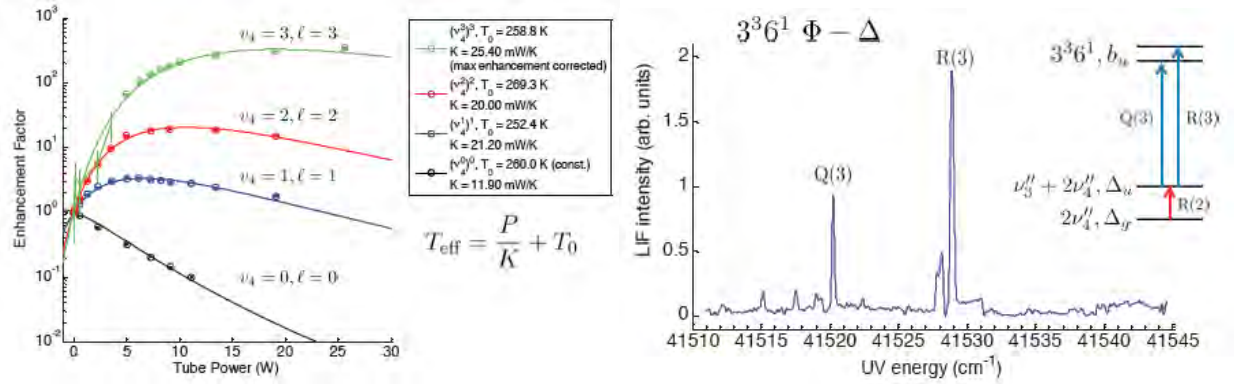

Figure 5. Hot band-pumped IR-UV double resonance LIF spectrum of $3^3 6^1$ K=3 (right panel), demonstrating spectroscopic access to high-K states of S_1 acetylene. The excitation scheme is shown in the diagram on the right. Vibrational population enhancements in the hyperthermal molecular beam source are shown in the left panel.

The combination of high-resolution H-atom detected action spectra and hot band-pumped IR-UV double resonance spectra enables exploration of the near- and above-barrier regions of the S_1 potential energy surface. The H-atom detection scheme will also enable us to better understand the predissociation mechanism(s) of S_1 acetylene. In addition, our near-complete knowledge of the S_1 acetylene rotation-vibration levels below the *cis-trans* isomerization barrier maximum, together with our new full-dimensional Franck-Condon calculations for the acetylene S_1-S_0 electronic band system (including polyads in both the S_1 and S_0 electronic states), puts us in a unique position to carry out SEP experiments that will selectively sample S_0 acetylene↔vinylidene barrier-proximal local-bender states.

Publications supported by this project 2012-2014

1 J. Baraban, P. Changala, A. Merer, A. Steeves, H. Bechtel and R. W. Field, "The $\tilde{A}\ ^1A_u$ state of acetylene: ungerade vibrational levels in the region 45800 – 46550 cm^{-1}," *Mol. Phys.* **110**, 2707-2723 (2012). http://dx.doi.org/10.1080/00268976.2012.706329

2. J. Baraban, J. Stanton, A. Merer and R. W. Field, "Anharmonic force fields of *cis*- and *trans*-S_1 C_2H_2" *Mol. Phys.* **110**, 2725-2733 (2012). http://dx.doi.org/10.1080/00268976.2012.706328

3. H. Lee, J. Baraban, R. W. Field and J. F. Stanton, "High-Accuracy Estimates for the Vinylidene-Acetylene Isomerization Energy and the Ground State Rotational Constants of :C=CH_2," *J. Phys. Chem. A* **117**, 11679-11683 (2013). http://dx.doi.org/10.1021/jp400035a

4. K. Prozument, R. G. Shaver, M. A. Ciuba, J. S. Muenter, G. B. Park, J. F. Stanton, H. Guo, B. M. Wong, D. S. Perry and R. W. Field, "A New Approach Toward Transition State Spectroscopy," *Farad. Disc.* **163**, 33-57 (2013). DOI: http://dx.doi.org/10.1039/C3FD20160K

5. P. Bryan Changala, "Reduced dimension rovibrational variational calculation of the S_1 State of C_2H_2. I. Methodology and implementation", *J. Chem. Phys.* **140**, 024312 (2014). http://dx.doi.org/10.1063/1.4859875

6. P. Bryan Changala, J. H. Baraban, J. F. Stanton, A. J. Merer and R. W. Field, "Reduced dimension rovibrational variational calculations of the S_1 state of C_2H_2. II. The S_1 rovibrational manifold and the effects of isomerization", *J. Chem. Phys.* **140**, 024313 (2014). http://dx.doi.org/10.1063/1.4859876

7. P. Bryan Changala, J. H. Baraban, A. J. Merer and R. W. Field, "Probing *cis-trans* isomerization in the S_1 state of C_2H_2 via H-atom action and hot band-pumped IR-UV double resonance spectroscopies", (*in preparation)*.

8. J. Jiang, J. H. Baraban, G. B. Park, M. L. Clark, and Robert W. Field "Laser-Induced Fluorescence Study of the S_1 State of Doubly-Substituted ^{13}C Acetylene and Harmonic Force Field Determination," *J. Phys. Chem. A* **117**, 13696–13703 (2013). http://dx.doi.org/10.1021/jp407755m.

9. K. Prozument, G. B. Park, R. G. Shaver, A.K. Vasiliou, J. M. Oldham, D. E. David, J. S. Muenter, J. F. Stanton, A. G. Suits, G. B. Ellison, and Robert W. Field, "Chirped-pulse millimeter-wave spectroscopy for dynamics and kinetics studies of pyrolysis reactions," *Phys. Chem. Chem. Phys.*, DOI:10.1039/C3CP55352C.

10. G. B. Park, R. W. Field, "Full-dimensional Franck-Condon calculations for the acetylene $\tilde{A} \leftrightarrow \tilde{X}$ transition in the harmonic basis," (*in preparation*).

Quantitative Imaging Diagnostics for Reacting Flows

Jonathan H. Frank
Combustion Research Facility
Sandia National Laboratories
Livermore, CA 94551-0969
jhfrank@sandia.gov

Program Scope

The primary objective of this project is the development and application of quantitative laser-based imaging diagnostics for studying the interactions of fluid dynamics and chemical reactions in reacting flows. Imaging diagnostics provide temporally and spatially resolved measurements of species, temperature, and velocity distributions over a wide range of length scales. Multi-dimensional measurements are necessary to determine spatial correlations, scalar and velocity gradients, flame orientation, curvature, and connectivity. Current efforts in the Advanced Imaging Laboratory focus on studying the detailed structure of both isolated flow-flame interactions and turbulent flames. The investigation of flow-flame interactions is of fundamental importance in understanding the coupling between transport and chemistry in turbulent flames. These studies require the development of imaging diagnostic techniques to measure key species in the hydrocarbon-chemistry mechanism as well as mixture fraction, rates of reaction and dissipation. Recent studies on flow-flame interactions have focused on localized extinction and re-ignition as well as effects of stratification. Diagnostic development includes efforts to extend measurement capabilities to a broader range of flame conditions and combustion modes, including combustion of hydrocarbon fuels beyond methane and stratified premixed combustion. We continue to develop our diagnostic capabilities for measuring the temporal evolution of turbulent flames using high-repetition rate imaging techniques.

Recent Progress

High-speed imaging of turbulent flame dynamics

Understanding the dynamics of interactions between turbulent flows and flames requires high-repetition rate imaging diagnostic techniques. We recently demonstrated the feasibility of high-repetition rate tomographic particle image velocimetry (TPIV) in turbulent flames. The TPIV technique provides volumetric, three-component velocity field measurements that enable determination of the complete velocity gradient tensor. Our experiments reveal the three-dimensional temporal evolution of key fluid dynamic quantities, such as vorticity and strain rate, at multi-kHz rates. Three-dimensional imaging also resolves ambiguities that occur in the interpretation of high-speed planar imaging measurements. Initial studies have focused on piloted jet flames and the stabilization region of a lifted jet flame. Figure 1a shows a single frame of the three-dimensional velocity field that was measured using 10-kHz TPIV at the base of a lifted DME/air jet flame. Simultaneous high-speed TPIV and OH-LIF imaging measurements can be used to track flow structures as they interact with the flame. For example, Fig. 1b shows a sequence of frames that track the structure of a vortex tube as it approaches the base of the lifted flame. The center of the vortex is used as the origin of the reference frame moving with the vortex. We view the velocity field in this moving frame of reference by subtracting the velocity at the center of the vortex from the velocities that were measured in the laboratory frame of reference. The temporal evolution of the enstrophy isosurfaces shows that

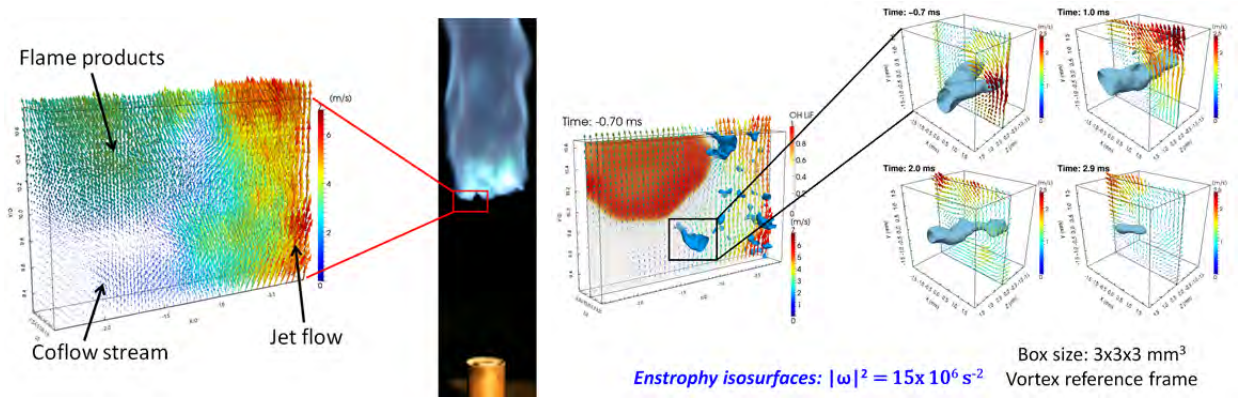

(a) (b)

Fig. 1: (a) Single frame of the three-dimensional velocity field from a 10-kHz tomographic PIV measurement at the base of a lifted DME/air jet flame. (b) Single frame of simultaneous high-speed velocity field and OH-LIF imaging measurements and four frames from a time sequence of the TPIV measurement tracking a vortex tube as it approaches the flame and dissipates. Only 1 out of 64 vectors are displayed for clarity.

the vortex tube initially consists of two branches that merge into a single vortex tube. The strength of the vortex tube dissipates as the vortex approaches the flame reaction zone, which is consistent with the effects of increased viscous dissipation in the vicinity of the flame. Further measurements and statistical analysis are underway to quantify the effects of flames on the temporal evolution of enstrophy and strain rate fields in jet flames.

Turbulent partially-premixed DME/air jet flames

We have established a new series of piloted partially-premixed dimethyl ether/air jet flames as target flames for experimental and modeling studies in the TNF Workshop. This series includes flames with differing degrees of localized extinction and the same stoichiometric mixture fraction as the analogous Sandia piloted CH_4/air jet flame series that has been studied extensively. DME flames represent a step forward in chemical complexity and a good starting point for systematic studies of turbulent flames with oxygenated fuels. Our initial studies include measurements of the velocity, OH, and CH_2O fields using stereoscopic PIV and LIF imaging. Analysis thus far has focused on the relative distributions of formaldehyde and OH. Measurements revealed that at many downstream locations, the instantaneous spatial distributions of these radicals can be separated by significant distances, as shown in Fig. 2a.

We have coupled the imaging measurements with large eddy simulations combined with conditional moment closure (LES-CMC) performed at University of Stuttgart by O. Stein and A. Kronenburg. Figure 2a shows an instantaneous realization of OH and CH_2O LIF signals that were computed using temperature and species data from the LES-CMC calculation. The LES-CMC results capture the gaps between the OH and CH_2O distribution. The probability density function of the measured radial separation distance between the boundaries of the CH_2O and OH fields is shown in Fig. 2b. The PDFs have a tail that extends towards large separation distances. This tail increases significantly as a function of downstream position until approximately x/D = 20. These gaps may produce highly intermittent consumption rates of formaldehyde by OH that results in significant departures from flamelet models in turbulent jet flames. Our ongoing studies are investigating this issue further. Plans also include refinement the

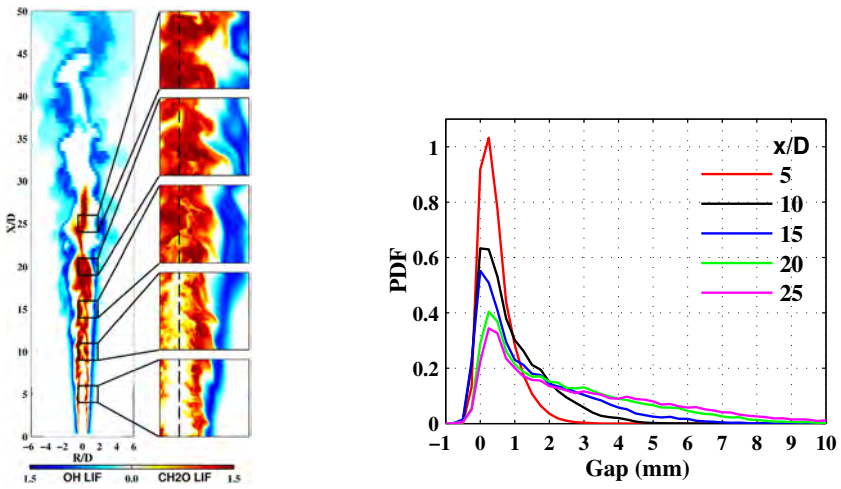

(a) (b)

Fig. 2: OH and CH_2O distributions in a turbulent partially-premixed DME/air jet flame: (a) Composite image of computed OH-LIF and CH_2O-LIF signals from an instantaneous realization of the LES calculations (left). Composite images of single-shot OH-LIF and CH_2O-LIF measurements at different downstream positions (right). (b) Probability density function of measured radial separation distance between boundaries of the CH_2O and OH fields.

formaldehyde LIF measurements, additional analysis of the velocity-scalar field coupling, and performing high-speed imaging measurements to study dynamics of localized extinction and re-ignition in these flames. Results will be coupled with complementary species and temperature measurements by R. Barlow (Sandia) and high-fidelity large eddy simulations performed at Sandia by J. Oefelein.

Soft x-ray absorption spectroscopy of flames

We continue to investigate the development of in situ soft x-ray measurement techniques for combustion with the eventual goal of studying flames under conditions that are not amenable to traditional diagnostic techniques. X-rays promise advantages over traditional laser diagnostic techniques that use UV and visible radiation to probe flame species via laser-induced fluorescence and Raman scattering. Experimental studies of soft x-ray absorption spectroscopy in flames are performed at the Molecular Science Beamline of the Advanced Light Source (ALS) synchrotron of LBNL in collaboration with David Osborn (Sandia), Hendrik Bluhm (LBNL), and Andrey Shavorskiy (LBNL). Recently, we developed a gas filter that significantly reduced the temporal drift in absorption of the x-ray beam by the silicon nitride window that separates the flame chamber from the beamline. We demonstrated that this gas filter significantly improved the reliability of carbon K-edge absorption measurements of carbonaceous species in a low-pressure laminar acetylene jet flame. We plan to extend measurements to larger hydrocarbon fuels and to test the feasibility of measuring total carbon concentrations using the far-edge region of the carbon K-edge absorption spectrum.

Future Plans

A major thrust of our research plans is the investigation of the dynamics of flow-flame interactions in turbulent premixed, non-premixed, and stratified modes of combustion. We

propose to build on our initial demonstration of high-speed tomographic PIV by expanding the high-speed imaging facility in the Advanced Imaging Laboratory and performing extensive studies of turbulent flame dynamics. In particular, we plan to work on a series of turbulent flame studies that focus on the dynamics of localized extinction and re-ignition, stabilization mechanisms in lifted jet flames, turbulent transport of combustion intermediates, and turbulent mixing in stratified combustion. We are also working to understand the effects of heat release on the dynamics of the turbulent flows by comparing temporal evolution of turbulent non-reacting jets and jet flames. Our planned high-speed imaging effort includes optimization of TPIV analysis and further evaluation of uncertainties, investigation of methods for noise reduction, and the development of efficient methods for analyzing large sets of imaging data. We plan to work closely with J. Oefelein in the development of a framework for comparing measurements and simulations of turbulent flame dynamics.

We also plan to improve the quantification of LIF measurements of formaldehyde and krypton. Improved formaldehyde LIF measurements are needed to better understand formaldehyde transport in turbulent DME flames and to resolve discrepancies in predicted formaldehyde concentrations. The krypton LIF work is aimed at advancing the use of a noble gas as a chemically inert tracer for mixing studies in reacting flows. Most previous mixture fraction imaging techniques have used combined measurements of chemically reactive species and temperature to construct a conserved scalar. The advantage of this new approach is that the tracer gas remains chemically inert in a wide range of conditions. We plan to refine this diagnostic technique for a broader range of flame conditions and fuel mixtures. A key refinement for both krypton and formaldehyde LIF measurements will be extending measurements of collisional quenching rates over a wider range of conditions.

BES-supported publications and submitted journal articles (2012-present)

B. Coriton, J.H. Frank, A. Gomez, "Effects of strain rate, turbulence, reactant stoichiometry and heat losses on the interaction of turbulent premixed flames with stoichiometric counterflowing combustion products," *Combust. Flame*, **160,** 2442-2456 (2013).

B. Coriton, J.H. Frank, "High-speed tomographic PIV measurements of strain rate intermittency and clustering in turbulent partially premixed jet flames," *Proc. Combust. Inst.*, submitted.

B. Coriton, M. Zendehdel, S. Ukai, A. Kronenburg, O.T. Stein, S-K Im, M. Gamba, J.H. Frank, "Imaging measurements and LES-CMC modeling of a partially-premixed turbulent dimethyl ether/air jet flame," *Proc. Combust. Inst.*, submitted.

A.M. Steinberg, B. Coriton, J.H. Frank, "Influence of combustion on principal strain-rate transport in turbulent premixed flames," *Proc. Combust. Inst.*, submitted.

J. Weinkauf, P. Trunk, J. H. Frank, M.J. Dunn, A. Dreizler, B. Böhm, "Investigation of flame propagation in a partially premixed jet by high-speed stereo PIV and acetone PLIF," *Proc. Combust. Inst.*, submitted.

B. Coriton, A.M. Steinberg, J.H. Frank, "High-speed tomographic PIV and OH PLIF measurements in turbulent reactive flows," *Exp. Fluids*, submitted.

J.H. Frank, A. Sharvorskiy, H. Bluhm, B. Coriton, E. Huang, D.L. Osborn, "In-situ soft x-ray absorption spectroscopy of flames," *Appl. Phys. B*, submitted.

Computer-Aided Construction of Chemical Kinetic Models

William H. Green
Department of Chemical Engineering, M.I.T.
Cambridge, MA 02139
whgreen@mit.edu

I. Program Scope

The combustion chemistry of even simple fuels can be extremely complex, involving hundreds or thousands of kinetically significant species. The most reasonable way to deal with this complexity is to use a computer not only to numerically solve the kinetic model, but also to construct the kinetic model in the first place. Because these large models contain so many numerical parameters (e.g. rate coefficients, thermochemistry) one never has sufficient data to uniquely determine them all experimentally. Instead one must work in "predictive" mode, using theoretical values for many of the numbers in the model, and as appropriate refining the most sensitive numbers through experiments. Predictive chemical kinetics is exactly what is needed for computer-aided design of combustion systems based on proposed alternative fuels, particularly for early assessment of the value and viability of proposed new fuels. Our research effort is aimed at making accurate predictive chemical kinetics practical; this is a challenging goal which necessarily includes a range of science advances. Our research spans a wide range from quantum chemical calculations on individual molecules and elementary-step reactions, through the development of improved rate/thermo calculation procedures, the creation of algorithms and software for constructing and solving kinetic simulations, the invention of methods for model-reduction while maintaining error control, and finally comparisons with experiment. Many of the parameters in the models are derived from quantum chemistry, and the models are compared with experimental data measured in our lab or in collaboration with others.

II. Recent Progress

A. Methodology for Computer-Aided Kinetic Modeling

The main focus of this research project continues to be the development of advanced methods for automatically constructing, reducing, and solving combustion simulations.[9] We are constantly adding functionality and additional types of chemistry to the open-source Reaction Mechanism Generator (RMG) software package. We currently distribute RMG version 4.0.1 (http://rmg.mit.edu), which includes organosulfur chemistry, a new method for computing thermochemistry of fused cyclic molecules [6], an improved method for automatically identifying and computing the rates of chemically-activated reactions [1,2], and automatic estimation of solvent effects for reactions in liquid phase [i]. We recently developed a new version which can also predict organonitrogen chemistry, and we are preparing to distribute it.

We continue to make progress on improved numerical methods to make it easier to use high-fidelity chemistry models in combustion simulations. This year we developed a new operator-splitting method for solving reacting flows whose splitting-error rapidly vanishes as the system approaches steady-state [ii]; in contrast solutions obtained using the conventional Strang splitting contain significant splitting errors even when it has converged to a steady solution (i.e. the converged solution can be very inaccurate[iii]).

This computer-aided kinetic modeling approach is having a broad impact. With the Brezinsky group we modeled how alkene chemistry depends on the position of the double bond, an issue relevant to biodiesel combustion.[13] We continue to distribute the mechanism construction software to many research groups, and to train and support the new users. In the past year researchers from Chicago, Belgium, China, France, and Germany have visited my group for training in how to use the RMG software. Several companies are also now using the software. Developers outside of my research group have begun to add functionality to this open-source software; among the most active developers are

researchers at Northeastern University and the University of Ghent. These independently funded external efforts leverage the funding provided by this program.

RMG applications funded separately

The work described above which is funded by this grant is even more heavily leveraged by large application-oriented projects funded separately, which provide demonstrations of the utility of computer-aided modeling of combustion chemistry and tests of the accuracy of RMG. Some of these projects fund addition of new features to RMG.

The largest and most important of these related projects is the DOE Combustion Energy Frontier Research Center, which funded development of models for all four isomers of butanol, many experimental tests of the predictions of these models by other researchers, and many quantum chemistry calculations by our collaborators or by us which have been incorporated into the RMG database. That project has provided excellent comprehensive tests of the capabilities and accuracy of RMG; in several cases the model predictions (made before the experiments were done) are quantitatively accurate [iv]. Discrepancies observed in other cases have led to the identification and correction of flaws in some of the rate and thermochemistry estimates or databases, and to the discovery of new types of reactions.[v]

We also participated in a DOE-funded collaboration with Craig Taatjes involving researchers in Florida, Montana, Germany, and China, building kinetic models for the chemistry of ketones and other proposed alternative fuels synthesized from biomass by fungi.[vi]

With separate industrial funding, the new capability of RMG to handle sulfur chemistry was tested by building models for fuel desulfurization in supercritical water, and comparisons with experimental data [vii] on those systems. Several more organosulfur manuscripts are now in preparation. Industrial funding into the fundamentals of diesel fuel injector fouling allowed us to include solvent effects in RMG.[i]

B. Quantum Calculations of Reaction Rates and Thermochemistry

Historically, the accuracy of rate and equilibrium calculations for combustion were almost always limited by the uncertainties in the computed potential energy surface, due to the need to use approximate electronic structure methods and small basis sets. Modern quantum chemistry methods, such as explicitly-correlated coupled-cluster methods (e.g. CCSD(T)-F12) have made it practical to significantly reduce these errors in computed PES's and molecular enthalpies. As the energy calculations improve, we find that the accuracy of our equilibrium and rate calculations is now often limited by other aspects of the overall calculation. This has led us (and many others, including Don Truhlar and Stephen Klippenstein) to invest significant efforts in improving on the traditional rate and thermochemistry computation methodology, which is based on several approximations which are not really accurate.

This year we focused on developing an alternative method for rate calculations, which avoids many of the approximations associated with traditional TST calculations. We created and distributed an efficient software implementation [viii] of the new RPMD method for computing reaction rates. We demonstrated that RPMD is an attractive way for computing accurate rates and isotope-effects for systems too large for exact quantum rate calculations (i.e. bigger than $H+CH_4$), but small enough that constructing a fairly accurate full-dimensional PES is practical. To test and demonstrate the new rate-calculation method we used this new software, often in collaboration with Hua Guo, to compute rate coefficients for several reactions of the type $X + CH_4$ (e.g. X=OH, O, Cl, H, D, Mu).[7,8,10,12] Overall, the tests demonstrated that RPMD is relatively easy to use and that it is pretty accurate; its main drawback is that it requires a full PES, not just the PES at/near the stationary points required by conventional transition state theory (TST).

During our calculations of this relatively small set of relatively simple reactions, we ran into two cases (Cl+CH4, OH+CH4) where there are unexpectedly large differences between the rate computed by RPMD and by a standard TST approach.[12,ix] It appears that the anharmonic shape of the PES near the saddle point leads to pretty large (~ factor of 4) errors in rates computed using the conventional canonical

variational transition-state-theory. (Independently, Don Truhlar also discovered this anharmonicity issue at about the same time in a more complicated reaction, and he has submitted a paper about this topic to JACS). Anharmonicity is apparently even more important for rate calculations than previously appreciated, and methodology for dealing with this needs improvement.

As we pointed out a few years ago [x], anharmonicity associated with coupled torsions (e.g. in molecules with more than one polar functional group) can also lead to significant errors in conventional rate and thermo calculations, particularly for reactions which involve cyclic transition states. We worked with Don Truhlar, using his MS-T method to calculate the torsional anharmonicity, to calculate a particularly interesting and important example, the isomerization of γ-ketohydroperoxides ($RC(O)CH_2CH(OOH)R'$) into cyclic peroxides (which then spontaneously fragment to form the acids and methyl ketones observed as major products from low-temperature oxidations by O_2).[v]

We also showed that secondary ozonides undergo similar fragmentation chemistry as the cyclic peroxides, with implications for Criegee Intermediate chemistry and atmospheric chemistry.[11] We are currently measuring and computing a number of CH_2OO reactions (see e.g. [xi]).

III. Future Work

We recently incorporated nitrogen chemistry into RMG, so we can model cetane improvers (for diesel fuel), dispersants/detergents (all liquid fuels), organonitrogen species in shale oil and biomass, and propellants. There are a large number of rather different N-containing functional groups, and in general this chemistry is not as well-characterized as C/H/O chemistry, so it is an interesting challenge to get this all correct so that we can make high-accuracy predictions.

We continue to work on improving the treatment of coupled hindered rotors, which is a major issue in the ignition chemistry of oxygenated fuels, where intramolecular hydrogen bonds are common.

As we push to higher molecular weight fuels, and include more heteroatoms, we will parallelize the model construction process, and also develop new methods that naturally apply tighter tolerances to the sensitive chain-branching reactions than to the ordinary propagation reactions.

IV. References

i. A. Jalan, R.H. West, and W.H. Green, "An Extensible Framework for Capturing Solvent Effects in Computer Generated Kinetic Models", *J. Phys. Chem. B* **117**, 2955-2970 (2013).

ii. Raymond L. Speth, Shev MacNamara, William H. Green, and Gilbert Strang, "Balanced Splitting and Rebalanced Splitting", *SIAM J. Numerical Analysis* **51**(6), 3084–3105 (2013).

iii. D.A. Schwer, P. Lu, W.H. Green, and V. Semiao, "A Consistent-Splitting Approach to Computing Stiff Steady-State Reacting Flows with Adaptive Chemistry", *Combustion Theory and Modelling* **7**, 383-399 (2003).

iv. N. Hansen, Shamel S. Merchant, Michael R. Harper, William H. Green, "The Predictive Capability of an Automatically Generated Combustion Chemistry Mechanism: Chemical Structures of Premixed *iso*-Butanol Flames," *Combustion and Flame* **160**(11) 2343-2351 (2013)

v. A. Jalan, I.M. Alecu, R. Meana-Paneda, J. Aguilera-Iparraguirre, K.R. Yang, S.S. Merchant, D.G. Truhlar, W.H. Green, "New pathways for formation of acids and carbonyl products in low-temperature oxidation: The Korcek decomposition of γ-ketohydroperoxides." *Journal of the American Chemical Society* **135**(30) 11100-11114 (2013).

vi. J.W. Allen, C. Gao, S.S. Merchant, A.M. Scheer, S.S. Vasu, O. Welz, J.D. Savee, D.L. Osborn, C. Lee, S. Vranckx, Z. Wang, F. Qi, R.X. Fernandes, W.H. Green, M.Z. Hadi, C.A. Taatjes, "Concerted Development of Biofuel Production and Utilization: A Coordinated Investigation of Diisopropyl Ketone, a Prototypical Biofuel", *Combustion & Flame* **161**, 711-724 (2014).

vii. Y. Kida, C. A. Class, A.J. Concepcion, M.T. Timko, and W.H. Green, "Combining Experiment and Theory to Elucidate the Role of Supercritical Water in Sulfide Decomposition", *Phys. Chem. Chem. Phys.* (2014, accepted).

viii. Y.V. Suleimanov, J.W. Allen, and W.H. Green, "RPMDrate: bimolecular chemical reaction rates from ring polymer molecular dynamics", *Comp. Phys. Comm.* **184**(3), 833-840 (2013).

ix. E. Gonzalez-Lavado, J.C. Corchado, Y.V. Suleimanov, W.H. Green, J. Espinosa-Garcia, "Theoretical Kinetics Study of the $O(^3P) + CH_4/CD_4$ Hydrogen Abstraction Reaction: The Role of Anharmonicity and Quantum Mechanical Effects", *J. Chem. Phys.* (submitted).

x. S. Sharma, S. Raman, and W.H. Green, **"**Intramolecular Hydrogen Migration in Alkylperoxy and Hydroperoxy-alkylperoxy Radicals: Accurate Treatment of Hindered Rotors", *J. Physical Chem. A* **114**, 5689-5701 (2010).

V. Publications and submitted journal articles supported by this project 2012-2014

1. J.W. Allen, C.F. Goldsmith, and W.H. Green, "Automatic Estimation of Pressure-Dependent Rate Coefficients", *Physical Chemistry Chemical Physics* **14**, 1131 - 1155 (2012).
2. J.W. Allen and W.H. Green, 'Reply to Comment on "Automatic estimation of pressure-dependent rate coefficients" (J.W. Allen, C. F. Goldsmith, and W. H. Green, Phys. Chem. Chem. Phys, 2012, 14, 1131-1155)', *Physical Chemistry Chemical Physics* **14**, 8434 (2012)
3. C.F. Goldsmith, W.H. Green, & S.J. Klippenstein, "On the Role of O_2 + QOOH in low-temperature ignition of propane I: Temperature and Pressure Dependent Rate Coefficients", *Journal of Physical Chemistry A* **116**, 3325-3346 (2012).
4. R. Kaiser, M. Goswami, F. Zhang, D. Parker, V.V. Kislov, A.M. Mebel, J. Aguilera-Iparraguirre, W.H. Green. "Crossed Beam Reaction of Phenyl and D5-Phenyl Radicals with Propene and Deuterated Counterparts – Competing Atomic Hydrogen and Methyl Loss Pathways", *Physical Chemistry Chemical Physics* **14**, 720–729 (2012).
5. V. Kislov, A. Mebel, J. Aguilera-Iparraguirre, and W.H. Green, "Reaction of Phenyl Radical with Propylene as a Possible Source of Indene and Other Polycyclic Aromatic Hydrocarbons: An Ab Initio/RRKM-ME Study", *Journal of Physical Chemistry A* **116**, 4176-4191 (2012).
6. G.R. Magoon and W.H. Green, "Design and implementation of a next-generation software system for on-the-fly quantum and force field calculations in automated reaction mechanism generation", *Computers in Chemical Engineering* **52**, 35-45 (2013).
7. Y. Li, Y.V. Suleimanov, M.-H. Yang, W.H. Green, and H. Guo, "Ring Polymer Molecular Dynamics Calculations of Thermal Rate Constants for the $O(^3P) + CH_4 \rightarrow OH + CH_3$ Reaction: Contributions of Quantum Effects", *Journal of Physical Chemistry Letters* **4**, 48 (2013).
8. Y. Li, Y.V. Suleimanov, J. Li, W.H. Green, and H. Guo, "Rate coefficients and kinetic isotope effects of the $X + CH_4 \rightarrow CH_3 + HX$ (X = H, D, Mu) reactions from ring polymer molecular dynamics", *Journal of Chemical Physics* **138**, 094307 (2013).
9. Edward Blurock, Federique Battin-Leclerc, Tiziano Faravelli, and William H. Green, "Automatic generation of detailed mechanisms" in *Cleaner Combustion: Developing Detailed Chemical Kinetic Models*, ed. by F. Battin-Leclerc, J. Simmie, and E. Blurock (Springer-Verlag, London, 2013).
10. J.W. Allen, W.H. Green, Y. Li, H. Guo, and Y.V. Suleimanov, "Full dimensional quantum rate coefficients and kinetic isotope effects from ring polymer molecular dynamics for a seven-atom reaction $OH + CH_4 \rightarrow CH_3 + H_2O$", *J. Chem. Phys.* 138, 221103 (2013).
11. A. Jalan, J.W. Allen, and W.H. Green, "Chemically activated formation of organic acids in reactions of the Criegee intermediate with aldehydes and ketones", *Phys. Chem. Chem. Phys.* **15**, 16841-16852 (2013).
12. Y. Li, Y.V. Suleimanov, W.H. Green, and H. Guo, "Quantum Rate Coefficients and Kinetic Isotope Effect for the Reaction $Cl + CH_4 \rightarrow HCl + CH_3$ from Ring Polymer Molecular Dynamics", *Journal of Physical Chemistry A* (2014, accepted).
13. A. Fridlyand, S.S. Goldsborough, K. Brezinsky, S.S. Merchant, and W.H. Green, "Influence of the Double Bond Position on the Oxidation of Decene Isomers at High Pressures and Temperatures", *Proceedings of the Combustion Institute* (2014, accepted).

Quantum Dynamics of Elementary Chemical Reactions

Hua Guo (hguo@unm.edu)

Department of Chemistry and Chemical Biology, University of New Mexico, Albuquerque, NM 87131

Program scope

To understand the quantum dynamics of elementary chemical reactions in the gas phase.

Recent progress

We have made significant advances in a number of fronts, including kinetic and dynamical studies of several combustion reactions. For example, we have collaborated with Bill Green on the calculation of rate coefficients and kinetic isotope effects for the OH/Cl + CH_4 reactions using the ring-polymer molecular dynamics (RPMD) method.[1-2] The applicability of the RPMD method has also been explored for insertion reactions.[3] The RPMD method has been found to give accurate rate coefficients.

A major effort has been devoted to develop accurate multidimensional global potential energy surfaces (PESs) for elementary reactions. For the F + H_2O reaction, for example, we have carried out extensive high-level ab initio calculations in collaboration with John Stanton and Richard Dawes to obtain benchmark values for the barrier height, which helped to construct a more accurate PES using external correlation correction.[4] This new PES has been shown[5] to provide a better agreement with the measured integral cross section of Nesbitt and coworkers.[6] In addition, we have also developed PESs for the O(^{3}P) + H_2O and Cl + H_2O reactions.[7-8] These PESs were fit with the permutation invariant polynomial (PIP) approach of Joel Bowman.[9] To further advance our ability to accurately represent a large number of ab initio points, we have recently proposed a novel, simple, and rigorous method to impose permutation symmetry in fitting PESs with neural networks (NN). The idea is to use a sufficient number of PIPs as the symmetry functions in the input layer of the NN. This new PIP-NN method has been demonstrated in fitting PESs for reactive systems with three,[10] four,[11-12] and five atoms.[13] It is robust, accurate and efficient.

The availability of these accurate PESs opened doors for us to investigate many key issues in bimolecular reactions. For example, the relative efficacies of various reactant modes have been studied and a predictive model (SVP or sudden vector projection) has been proposed to understand the mode

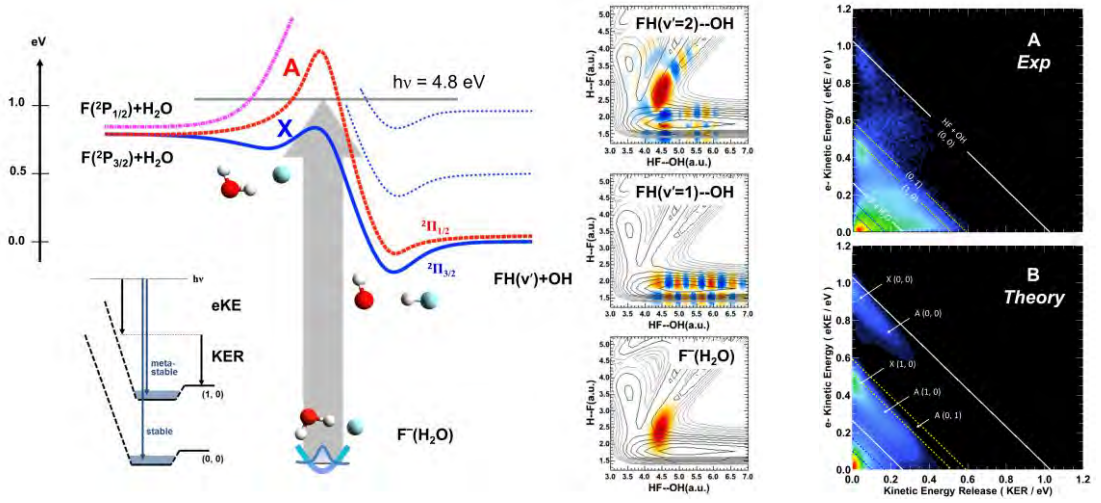

Figure 1. Schematic PESs of the F + H_2O → HF + OH reaction involved in the photodetachment of FH_2O^- (left panels). The wavefunctions for the anion and neutral species (Feshbach resonances) are superimposed on the X-state PES (middle panels). The comparison between the measured and calculated photoelectron photofragment coincidence (PPC) spectra (right panels).

selectivity and product energy disposal.[14-15] Very recently, we have collaborated with Bob Continetti to map out the photodetachment dynamics for FH_2O^-, which revealed various dissociation channels on two lowest PESs with full product quantum state resolution.[16] As shown in Fig. 1, the agreement between theory and experiment is excellent. More importantly, theory provided insights of the dynamics near the transition state for the F + H_2O reaction and identified numerous long-lived Feshbach resonances as well as bound states.

We have extended our dynamical studies to reactions involving more than four atoms. In collaboration with Gabor Czako, Joel Bowman, and Minghui Yang, we investigated the $O(^3P)$ + CH_4 reaction using a reduced-dimensional quantum model and quasi-classical trajectory method.[17-18] The agreement with experimental data of Kopin Liu was quite satisfactory, and additional insights have been gained on the mode selectivity. We have also investigated the effect of reactant rotational excitation for the OH + CH_4 reaction using a reduced-dimensional quantum model.[19]

The roaming pathway in many uni and bimolecular reactions has attracted much recent attention.[20-21] However, few have addressed the quantum mechanical nature of this important dynamical phenomenon. We have recently investigated the roaming channel in the H + MgH bimolecular reaction on an accurate PES,[22] which bears many similarities with the H_2CO system. It is shown that the roaming dynamics is associated with clearly definable roaming resonances, which follow the shallow roaming minimum energy path to the roaming saddle point, as shown in Fig. 2. However, these resonances often possess extensive excitations in the perpendicular modes.

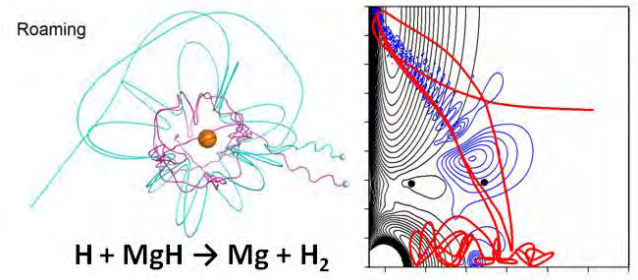

Figure 2. A representative trajectory in the roaming channel of the H + MgH reaction (left) and a roaming resonance superimposed on the MgH_2 PES with one Mg-H bond fixed and a roaming trajectory.

Finally, we have been involved in several other PES,[23-26] spectroscopic,[27] kinetic,[28-30] and dynamic studies.[31-37] Some of the studies are collaborations with Millard Alexander, Richard Dawes, Joaquin Espinosa-Garcia, Bob Field, Kevin Hickson, Shuhei Ono, Al Viggiano, and Daiqian Xie. The details of these studies are not provided here due to space limitations.

Future plans

In the next year, we plan to continue to pursue our proposed research in the areas of chemical dynamics and kinetics. The focus will be placed on the following areas: i). to develop efficient method to obtain state-to-state scattering information for bimolecular reactions, particularly those with four atoms; ii). to construct accurate PESs for such reactions, and iii). to perform quantum scattering and quasi-classical trajectory calculations on these PESs.

References (* indicates DOE funded work in the past year):

*1 J. W. Allen, W. H. Green, Y. Li, H. Guo and Y. V. Suleimanov, J. Chem. Phys. **138**, 221103 (2013).
*2 Y. Li, Y. V. Suleimanov, W. H. Green and H. Guo, J. Phys. Chem. A **in press** (2014).
*3 Y. Li, Y. V. Suleimanov and H. Guo, J. Phys. Chem. Lett. **5**, 700 (2014).
*4 T. L. Nguyen, J. Li, R. Dawes, J. F. Stanton and H. Guo, J. Phys. Chem. A **117**, 8864 (2013).
*5 J. Li and H. Guo, Chin. J. Chem. Phys. **26**, 627 (2013).
6 A. M. Zolot and D. J. Nesbitt, J. Chem. Phys. **129**, 184305 (2008).
*7 J. Li and H. Guo, J. Chem. Phys **138**, 194304 (2013).
*8 J. Li, R. Dawes and H. Guo, J. Chem. Phys. **139**, 074302 (2013).

9 J. M. Bowman, G. Czakó and B. Fu, Phys. Chem. Chem. Phys. **13**, 8094 (2011).
*10 B. Jiang and H. Guo, J. Chem. Phys. **139**, 054112 (2013).
*11 J. Li, B. Jiang and H. Guo, J. Chem. Phys. **139**, 204103 (2013).
*12 J. Li, J. Chen, D. H. Zhang and H. Guo, J. Chem. Phys. **140**, 044327 (2014).
*13 J. Li and H. Guo, Phys. Chem. Chem. Phys. **in press** (2014).
14 B. Jiang and H. Guo, J. Chem. Phys. **138**, 234104 (2013).
15 B. Jiang and H. Guo, J. Am. Chem. Soc. **135**, 15251 (2013).
*16 R. Otto, J. Ma, A. W. Ray, J. S. Daluz, J. Li, H. Guo and R. E. Continetti, Science **343**, 396 (2014).
*17 R. Liu, M. Yang, G. Czakó, C. T. Bowman, J. Li and H. Guo, J. Phys. Chem. Lett. **3**, 3776 (2012).
*18 G. Czakó, R. Liu, M. Yang, J. M. Bowman and H. Guo, J. Phys. Chem. A **117**, 6409 (2013).
*19 H. Song, J. Li, B. Jiang, M. Yang, Y. Lu and H. Guo, J. Chem. Phys. (2014).
20 J. M. Bowman and B. C. Shepler, Annu. Rev. Phys. Chem. **62**, 531 (2011).
21 A. G. Suits, Acc. Chem. Res. **41**, 873 (2008).
*22 A. Li, J. Li and H. Guo, J. Phys. Chem. A **117**, 5052 (2013).
*23 C. Xie, X. Hu, L. Zhou, D. Xie and H. Guo, J. Chem. Phys. **139**, 014305 (2013).
*24 J. Li, Y. Li and H. Guo, J. Chem. Phys. **138**, 141102 (2013).
*25 A. Li, Y. Li, H. Guo, K.-C. Lau, Y. Xu, B. Xiong, Y.-C. Chang and C. Y. Ng, J. Chem. Phys. **140**, 011102 (2014).
*26 R. Dawes, P. Lolur, A. Li, B. Jiang and H. Guo, J. Chem. Phys. **139**, 201103 (2013).
*27 K. Prozument, R. G. Shaver, M. A. Ciuba, J. S. Muenter, G. B. Park, J. F. Stanton, H. Guo, B. M. Wong, D. S. Perry and R. W. Field, Faraday Discuss. **163**, 33 (2013).
*28 J. J. Melko, S. G. Ard, J. A. Fournier, J. Li, N. S. Shuman, H. Guo, J. Troe and A. A. Viggiano, Phys. Chem. Chem. Phys. **15**, 11257 (2013).
*29 J. Daranlot, X. Hu, C. Xie, J.-C. Loison, P. Caubet, M. Costes, V. Wakelam, D. Xie, H. Guo and K. M. Hickson, Phys. Chem. Chem. Phys. **15**, 13888 (2013).
*30 S. G. Ard, J. J. Melko, B. Jiang, Y. Li, N. S. Shuman, H. Guo and A. A. Viggiano, J. Chem. Phys. **139**, 144302 (2013).
*31 L. Zhou, B. Jiang, D. Xie and H. Guo, J. Phys. Chem. A **117**, 6940 (2013).
*32 A. Li, H. Guo, Z. G. Sun, J. Kłos and M. H. Alexander, Phys. Chem. Chem. Phys. **15**, 15347 (2013).
*33 X. Hu, C. Xie, D. Xie and H. Guo, J. Chem. Phys. **139**, 124313 (2013).
*34 A. R. Whitehill, C. Xie, X. Hu, D. Xie, H. Guo and S. Ono, Proc. Natl. Acad. Sci. USA **110**, 7697 (2013).
*35 J. C. Corchado, J. Espinosa-Garcia, J. Li and H. Guo, J. Phys. Chem. A **117**, 11648−11654 (2013).
*36 B. Jiang and H. Guo, J. Chem. Phys. **139**, 224310 (2013).
*37 L. Zhou, D. Xie, Z. Sun and H. Guo, J. Chem. Phys. **140**, 024310 (2014).

Gas-Phase Molecular Dynamics: High Resolution Spectroscopy and Collision Dynamics of Transient Species

Gregory E. Hall
Chemistry Department, Brookhaven National Laboratory
Upton, NY 11973-5000
gehall@bnl.gov

Program Scope

This research is carried out as part of the Gas-Phase Molecular Dynamics program in the Chemistry Department at Brookhaven National Laboratory. Chemical intermediates in the elementary gas-phase reactions involved in combustion chemistry are investigated by high resolution spectroscopic tools. Production, reaction, and energy transfer processes are investigated by transient, double resonance, polarization and saturation spectroscopies, with an emphasis on technique development and connection with theory.

Recent Progress

A. Speed-dependent effects in pressure broadening and optical-optical double resonance

A Doppler-resolved velocity group of a probed molecular state undergoes collisions at an average rate that increases with Doppler detuning from line center. This effect is best known in the context of pressure broadening, where at pressures intermediate between the low-pressure Doppler limit and the high pressure Lorenzian limit, deviations from a simple Voigt convolution can be described as a Gaussian weighted sum of Lorenzians that are broader in the Doppler wings than at line center. A physically distinct but phenomenologically similar Dicke narrowing mechanism is also considered in comprehensive models of pressure broadening: velocity changing collisions that replace an inhomogeneous distribution of Doppler shifts with an effective average over a sequence of Doppler shifts experienced by a single molecule undergoing "optical diffusion" during resonant excitation. We are interested in investigating these collisional effects on pressure broadening, connecting the phenomena with state-resolved sub-Doppler kinetics and first principles quantum scattering calculations on a rare gas + diatomic radical system for which modern state-to-state collision studies and accurate scattering calculations can be compared.

Inspired by frequency-comb-referenced pressure broadening studies on acetylene lines described in Trevor Sears' abstract elsewhere in this book, we have measured accurate frequency modulated lineshapes for selected CN *A*-*X* transitions as a function of added Ar pressure, extracting pressure-dependent broadening, narrowing, and shifting parameters.[1] Since this work was published, we have been collaborating with Paul Dagdigian and Millard Alexander to compare the pressure broadening measurements with scattering calculations on the Ar + CN (*X*) and Ar + CN (*A*) potential energy surfaces, using the formalism of Shafer and Gordon[2]. The magnitudes and rotational state dependence of the measured and calculated pressure broadening coefficients are in generally good agreement. The pressure dependent frequency shifts are in serious disagreement, for reasons we do not understand. If the narrowing parameters are attributed to the speed-dependence of the broadening, we can compare the experimental values with appropriate velocity-weighted averages of the collision energy-dependent pressure broadened cross section, finding modest but not compelling agreement. Further work is underway to assess the conditions under which pressure broadening serves as a reliable proxy for

rotationally inelastic scattering, and the connections among elastic dephasing and inelastic contributions to pressure broadening, particularly in electronic transitions of diatomic radicals.

Related speed-dependent effects can be observed in the time domain, at pressures below the onset of measureable pressure broadening, with optical-optical double resonance techniques. The same Ar + CN (*X*) system has been studied by Doppler-resolved saturation recovery kinetics. A translationally and rotationally thermalized sample of CN (*X*, v=0) is prepared by photolysis of CH_3COCN at 193 nm, after a 10-15 μsec delay. A few mJ from a red ns dye laser depletes the full Doppler spectrum of a chosen rotational state of CN (*X*, v=0) using transitions in the (4-0) band of the *A*-*X* system. Recovery kinetics as a function of probe laser detuning across the Doppler-broadened line are recorded by transient FM spectroscopy to probe the collisional redistribution of the hole in the Boltzmann rotational distribution. The recovery is characterized by an approximately single-exponential decay to a non-zero equilibrium amplitude, where the observed decay rate has a form resembling the Doppler-selected average relative velocity: $k(x_D) = k_0\sqrt{1+\beta\, x_D^{\,2}}$. Here the recovery rate is expressed as a function of the Doppler shift x_D and the recovery rate at line center, k_0. The phenomenological parameter β is typically smaller than the kinematic value expected simply from the relative masses of the probed molecule and the collision partner, and can additionally depend on the competition between inelastic collisions and velocity randomizing collisions, as well as the collision energy dependence of the total inelastic cross section. Correcting for polarization effects, integrating the velocity dependence over the initial thermal speed distribution and extrapolating to the initial recovery rate gives an experimental value for the J-dependent thermal rate constants for rotational energy transfer. Figure 1 contrasts He and Ar data for high and low rotational states of CN. Note the large and J-dependent intercepts due the precursor, and the very different J-dependent slopes for He vs. Ar. We find good agreement with the quantum scattering results of Lique *et al.*[3] in He and Dagdigian in Ar,[4] but surprising disagreement with previous experimental work on total removal rate constants by He from Fei *et al.*[5], particularly for low rotational states, which evidently have an unrecognized sensitivity to inelastic scattering by the photolytic precursor. Additional analysis of the depolarization kinetics and saturation transfer is in progress, with theoretical support from Alexander and Dagdigian.

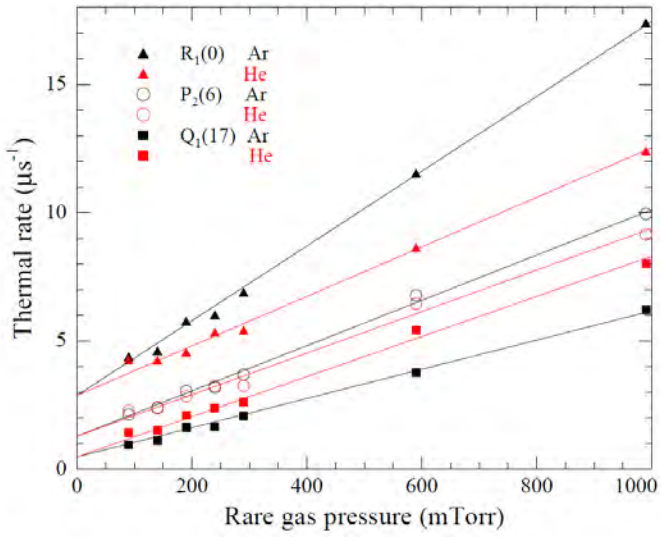

Figure 1. Initial recovery rate vs. rare gas pressure with 10 mTorr photolytic precursor CH_3COCN

B. Sub-Doppler transient saturation spectroscopy

A two-color sub-Doppler saturation recovery kinetics experiment was set up to further investigate speed-dependent relaxation kinetics in the presence of elastic velocity-changing collisions. The collisional time evolution of a sub-Doppler hole in a rotational absorption line should provide a highly informative probe of competing elastic, inelastic, and depolarizing collisions, when compared to analogous time and frequency domain measurements of recovery following saturation of an entire

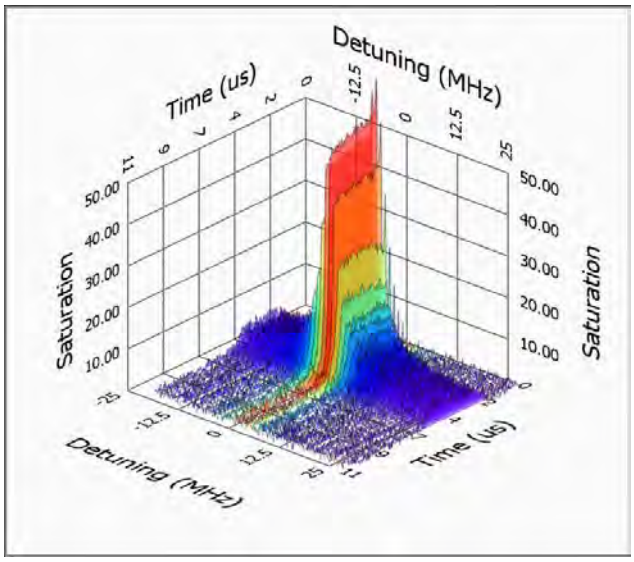

Figure 2 Two-color sub-Doppler saturation and recovery signal in CN

Doppler-broadened line, as described above. Figure 2 illustrates a background-subtracted transient signal on an isolated hyperfine sub-Doppler feature in the $P_2(6)$ line in the CN *A-X* (1-0) band, when exposed to a square 4 μs pulse of bleach light from a different CW laser tuned to the corresponding line of the *A-X* (2-0) band. In order to keep the relative frequencies of the two lasers stable enough for such two-color sub-Doppler spectroscopy, we have used a transfer cavity and a tunable sideband offset lock scheme to track the fluctuations and drift in the bleach laser frequency with the tunable probe laser.[6] The stabilization scheme works well, but only for collinear propagating bleach and probe beams, where the frequency correction has the correct sign. Unfortunately for the kinetics experiment, the collinear interaction of the two beams in a fully resonant three-level system drives a coherent Raman processes that contributes to the transient probe response in addition to the incoherent collision-dependent processes we seek to monitor. Such effects were observed and characterized by Feld[7] and Duclay[8] long ago, in the context of saturation lineshapes and free-induction decay in coupled Doppler-broadened transitions of gas lasers. That part of the probe transient due to the coherent process terminates quickly when the bleach field is turned off – faster than the collisional time scale at low pressures, making the recovery kinetics as shown in Figure 2 not ideal for collision studies. The two-color stabilization scheme is, however, very good for high resolution sub-Doppler spectroscopy, and we exploited the experimental configuration to extend and refine the hyperfine spectroscopy of the CN *A* state in v = 1 and 2, as described in the abstract of Trevor Sears, elsewhere in this book.

Future Work

A. Sub-Doppler saturation recovery in CN radicals

We intend to pursue the two-color sub-Doppler saturation recovery kinetics studies introduced above in a counter-propagating geometry, where the coherent Raman signal is not a complication. This will require absolute frequency stabilization rather than the relative stabilization used in the collinear studies described above. A new laser system has been acquired and is being put into service that should enable this application. Such studies with sub-Doppler saturation recovery kinetics probed by independently tunable sub-Doppler probe spectroscopy can more directly address the conditions under which velocity changing collisions contribute to pressure broadened line shapes. Preliminary work performed with one laser, split into counterpropagating amplitude modulated bleach and frequency modulated probe beams, has shown that the dark recovery rate of a sub-Doppler bleach signal is dominated by rotationally inelastic collisions, at least for low rotational states of CN. One-color saturation spectroscopy is generally sensitive to the collision dynamics on both upper and lower potential energy surfaces, complicating the interpretation of the saturation recovery kinetics. The use of hyperfine crossover resonances, (a three-level, one color, double resonance condition) selectively isolates upper or lower state effects, but only for low rotational states where crossover resonances have significant intensity, and only for the Doppler-free

velocity group near line-center. Using an independently tunable and rapidly extinguished bleach laser will allow analogous measurements of sub-Doppler saturation recovery for different velocity groups and any rotational state, and specifically sensitive to either *A* state or *X* state collisions, for example, with pump laser saturation on the (2-0) band and the probe laser measurement by either gain on the (2-1) band or absorption on the (1-0) band of the red *A*-*X* system. Having access to a range of rotational states will be important, as the relative contribution of velocity changing collisions is expected to increase as the rotational spacing increases and the inelastic cross sections decrease. Comparison with scattering calculations on realistic potentials will be an important part of the program.

Publications supported by this project since 2012

Collinear two-color saturation spectroscopy in CN *A*–*X* (1–0) and (2–0) bands
D. Forthomme, C. P. McRaven, T.J. Sears and G.E. Hall
J. Molec. Spectrosc. **296**, 36-42 (2014)

Temperature-dependent, nitrogen-perturbed line shape measurements in the $\nu_1+\nu_3$ band of acetylene using a diode laser referenced to a frequency comb
M. J. Cich, D. Forthomme, C. P. McRaven, G. V. Lopez, G. E. Hall, T. J. Sears and A. W. Mantz
J. Phys. Chem. A **117**, 13908-13918 (2013)

Argon-induced pressure broadening, shifting and narrowing in the CN $A\ ^2\Pi - X\ ^2\Sigma^+$ (1-0) band
D. Forthomme, C. P. McRaven, T. J. Sears and G. E. Hall
J. Phys. Chem. A **117,** 11837-11846 (2013)

Hyperfine structures in the v=1-0 vibrational band of the $B\ ^3\Pi_g - A\ ^3\Sigma^+_u$ of N_2
D. Forthomme, C. P. McRaven, G. E. Hall, and T. J. Sears
J. Molec. Spectrosc. **282**, 50-55 (2012)

Broadband laser enhanced dual-beam interferometry
V. V. Goncharov and G. E. Hall
Optics Letters **37** 2406-2408 (2012)

What is the Best DFT Functional for Vibronic Calculations? A Comparison of the Calculated Vibronic Structure of the S_1-S_0 Transition of Phenylacetylene with Cavity Ringdown Band Intensities
G. Lopez, C.-H. Chang, P. Johnson, G.E. Hall, T. J. Sears, B. Markiewicz, M. Milan and A. Teslja
J. Phys. Chem. A **116** 6750-6758 (2012)

Cited References

[1] D. Forthomme, C. P. McRaven, T. J. Sears, and G. E. Hall, J. Phys. Chem. A **117**, 50 (2013).
[2] R. Shafer, and R. G. Gordon, J. Chem. Phys. **58**, 5422 (1973).
[3] F. Lique, A. Spielfiedel, N. Feautrier, I. F. Schneider, J. Klos, and M. H. Alexander, J. Chem. Phys. **132**, 024303 (2010).
[4] P. Dagdigian, personal communication (2013).
[5] R. Fei, H. M. Lambert, T. Carrington, S. V. Filseth, and C. M. Sadowski, J. Chem. Phys. **100**, 1190 (1993).
[6] D. Forthomme, C. P. McRaven, T. J. Sears, and G. E. Hall, J. Mol. Spectrosc. **296**, 36 (2014).
[7] M. S. Feld, and A. Javan, Phys. Rev. **177**, 540 (1969).
[8] M. Ducloy, J. R. R. Leite, and M. S. Feld, Phys. Rev. A **17**, 623 (1978).

Flame Chemistry and Diagnostics

Nils Hansen
Combustion Research Facility, Sandia National Laboratories, Livermore, CA 94551-0969
Email: nhansen@sandia.gov

SCOPE OF THE PROGRAM

In this program, we seek to understand the detailed chemistry of combustion through a unique scheme of diagnostics development and experimental studies of simple flames. Our goal is to provide reliable experimental data on the chemical composition of laboratory-scale model flames through state-of-the-art diagnostics. The experiments are designed to serve as benchmarks for the development and validation of detailed chemical kinetic models. In particular, we study laminar premixed flames, which are stabilized on a flat-flame burner under a reduced pressure of ~15-30 Torr and laminar opposed-flow diffusion flames at low and atmospheric pressure. We implement mainly mass spectrometer techniques and our experimental data in the form of species identification and quantification serve as stringent tests for the development and validation of any detailed chemical kinetic mechanisms. Over the past years, the overall objective of this program has been to elucidate the chemistry of soot precursors in hydrocarbon flames. Studying this complex combustion chemistry with an unprecedented level of detail requires determining the chemical structures and concentrations of species sampled from sooting or nearly-sooting model flames.

PROGRESS REPORT

1-Hexene Combustion Chemistry: The speciation in three premixed 1-hexene flames has been studied under a reduced pressure of 20-30 mbar applying flame-sampling molecular-beam time-of-flight mass spectrometry and photoionization by tunable vacuum-ultraviolet synchrotron radiation. Mole fraction profiles of 40 different species for each flame have been measured. This data was used by the Mauß group (Cottbus) to validate a new kinetic scheme that was augmented to capture the flame chemistry of 1-hexene under stoichiometric and fuel rich conditions including benzene formation pathways. A good agreement of modeling results with the experimentally observed mole fraction profiles has been found for all flame conditions providing a sound basis for analyzing benzene formation pathways during 1-hexene combustion. The analysis clearly shows that benzene formation via the fulvene intermediate is a very important pathway for 1-hexene, which is different to previous findings based on the same kinetic model for fuel rich C_2-C_4 flames. The reason for this interesting behavior is probably the unimolecular chemistry, *i.e.* a prompt formation of C_3 species (allyl and *n*-propyl) by C-C fission.

PAH Formation and Soot Morphology in Flames of C_4 Fuels: In collaboration with the group of Kohse-Höinghaus (Bielefeld), we described experimental studies on the formation of polycyclic aromatic hydrocarbons (PAH's) in opposed-flow atmospheric-pressure flames of *n*-butane, *i*-butane, *i*-butene, and *i*-butanol and on the morphology of nascent soot particles sampled from premixed atmospheric-pressure flames of the same fuels. To identify the major contributors to the molecular growth mechanism in the opposed-flow flames, we employed flame-sampling molecular-beam mass spectrometry with electron ionization (EI) and *in-situ* gas-chromatography (GC) with mass spectrometric detection. The EI- and GC-EI mass spectra indicate that several pathways with different building blocks can contribute to molecular growth. Besides the commonly accepted hydrogen-abstraction-C_2H_2-addition steps, we found reactions of the methyl radical to be important steps. This observation is also supported by the complexity of the mass spectra which indicates that at least one of the building blocks is rather small. The importance of phenyl radicals as building blocks seems to be limited. We also used helium-ion microscopy to unravel the influence of the fuel structure on the morphology of nascent soot particles and we found that the observed differences in shape and size of the sampled soot particles are a likely due to a combined effect of temperature, residence time, and chemical nature of the fuel.

Soot Precursor Formation and Limitations of the Stabilomer Grid: Together with K.R. Wilson (LBNL), H.A. Michelsen (Sandia), and A. Violi (Michigan) we have performed flame-sampling aerosol mass spectrometry with vacuum-ultraviolet photoionization of an Ar-diluted C_2H_2/O_2 flame using a near-atmospheric pressure (700 Torr) opposed-flow burner. We recorded aerosol mass spectra at different distances from the fuel outlet for fixed ionization energies and in a fixed position while tuning the photoionization energy. Recorded mass spectra contain a wide variety of peaks, highlighting the importance of small building blocks and showing a variety of chemical species that extends beyond the traditional classification of PAH species based on thermodynamic stability. Experimental results showed that peaks in the observed mass spectra generally consisted of a mixture of PAH isomers. The results also highlight the importance of odd-carbon numbered species and complex growth paths. We observed species of higher masses being built up ahead of species of lower masses.

OUTLOOK

Experimental Studies on the Molecular-Growth Chemistry of Soot Precursors in Combustion Environments: Now that the goal of the research program has shifted towards the formation of larger species in combustion environments, it is the goal of our future studies to directly address the molecular-growth chemistry from small combustion intermediates to larger and larger PAH's. The underlying chemistry will be investigated by a combination of different experiments. The centerpiece of all experiments is a simple, *i.e.* laminar, premixed or opposed-flow flame, and analyzing the chemical

composition of such model flames will provide guidance and benchmarks needed to improve and test theoretical models describing soot-formation chemistry with predictive capabilities. We plan to investigate the chemical composition of these flames in unprecedented detail by flame-sampling mass spectrometry with electron ionization (EI), resonance-enhanced multiphoton ionization (REMPI), single-photon VUV ionization, and gas chromatography (GC/MS). REMPI experiments can be used to great benefit in the flame-structure analysis, as it usually causes less ion fragmentation than electron ionization. In addition, REMPI processes are wavelength-dependent and molecule-specific and can therefore be used for selective and sensitive detection of a given species. In an additional experimental approach, it is proposed to employ gas chromatography equipped with mass spectrometry (GC/MS). The coupling of MBMS with GC is very promising. In spite of its inability to detect reactive compounds, its potential of detailed, even isomer-specific, separation of stable compounds is remarkable. Its sensitivity and its selectivity are very well suited to access small and large aromatics. It is the intention to provide isomer-specific information for PAH species, which is not available from the other MBMS experiments alone.

Although our current set-up allows for a pressure between 30 and 700 Torr, sampling from sooting flames at atmospheric pressure will eventually lead to clogging of the small opening (a few μm) in the microprobe. We therefore propose to rebuild the mass spectrometer and to add an additional stage of pumping.

The systems proposed to study are flames fueled by acetylene (C_2H_2), allene/propyne (C_3H_4), and the C_4 fuels, butane and *iso*-butane (C_4H_{10}), 1-butene and *iso*-butene (C_4H_8), and 1,3-butadiene (1,3-C_4H_6). These fuels are of special interest, because these molecules are potential precursors for the resonance-stabilized propargyl, allyl, and *i*-C_4H_5 radicals. Contributions towards PAH growth via resonantly stabilized free radicals should be enhanced in these flames, thus making them a perfect test case for further model development.

PUBLICATIONS ACKNOWLEDGING BES SUPPORT 2012-PRESENT

1. B. Yang, J. Wang, T. A. Cool, N. Hansen, S. Skeen, D. L. Osborn, "Absolute Photoionization Cross-Sections of Some Combustion Intermediates", *Int. J. Mass Spectrom.*, **309,** 118-128 (2012).
2. F. Zhang, R. I. Kaiser, A. Golan, M. Ahmed, N. Hansen, "A VUV Photoionization Study of the Combustion-Relevant Reaction of the Phenyl Radical (C_6H_5) with Propylene (C_3H_6) in a High-Temperature Chemical Reactor", *J. Phys. Chem. A,* **2012,** 116(14), 3541-3546.
3. N. Hansen, J. A. Miller, S. J. Klippenstein, P. R. Westmoreland, K. Kohse-Höinghaus, "Exploring Formation Pathways of Aromatic Compounds in Laboratory-Based Model Flames of Aliphatic Fuels", *Combust. Expl. Shock Waves*, **2012,** 48(5), 508-515.
4. C. K. Westbrook, B. Yang, T. A. Cool, N. Hansen, K. Kohse-Höinghaus, "Photoionization Mass Spectrometry and Modeling Study of Premixed Flames of Three Unsaturated $C_5H_8O_2$ Esters", *Proc. Combust. Inst.,* **2013,** 34(1), 443-451.
5. A. W. Jasper and N. Hansen, "Hydrogen-Assisted Isomerizations of Fulvene to Benzene and of Larger Cyclic Aromatic Hydrocarbons", *Proc. Combust. Inst.*, **2013,** 34(1), 279-287.

6. S. A. Skeen, B. Yang, H. A. Michelsen, J. A. Miller, A. Violi, N. Hansen, "Studies of Laminar Opposed-Flow Diffusion Flames of Acetylene at Low Pressures with Photoionization Mass Spectrometry", *Proc. Combust. Inst.,* **2013,** 34(1), 1067-1075.
7. N. J. Labbe, V. Seshadri, T. Kasper, N. Hansen, P. Oßwald, K. Kohse-Höinghaus, P. R. Westmoreland, "Flame Chemistry of Tetrahydropyran as a Model Heteroatomic Biofuel", *Proc. Combust. Inst.,* **2013,** 34(1), 259-267.
8. S. A. Skeen, H. A. Michelsen, K. R. Wilson, D. M. Popolan, A. Violi, N. Hansen, "Near-Threshold Photoionization Mass Spectra of Combustion-Generated High-Molecular-Weight Soot Precursors", *J. Aerosol Sci.,* **2013,** 58(1), 86-102.
9. N. Hansen, S.S. Merchant, M. R. Harper, W. H. Green, "The Predictive Capability of an Automatically Generated Combustion Chemistry Mechanism: Chemical Structures of Premixed *iso*-Butanol Flames", Combust. Flame, **2013,** 160(11), 2343-2351.
10. N. Hansen, S. A. Skeen, H. A. Michelsen, K. R. Wilson, K. Kohse-Höinghaus, "Flame Experiments at the Advanced Light Source: New Insights into Soot Formation Processes", *J. Vis. Exp.,* in press.
11. F. N. Egolfopoulos, N. Hansen, Y. Ju, K. Kohse-Höinghaus, C. K. Law, F. Qi, "Advances and Challenges in Experimental Research of Combustion Chemistry in Laminar Flames", *Prog. Energy Combust. Sci.,* submitted.
12. A. Nawdiyal, N. Hansen, T. Zeuch, L. Seidel, F. Mauß, "Experimental and Modelling Study of Speciation and Benzene Formation Pathways in Premixed 1-Hexene Flames", *Proc. Combust. Inst.,* accepted for presentation.
13. N. Hansen, M. Braun-Unkhoff, T. Kathrotia, A. Lucassen, B. Yang, "Understanding the Reaction Pathways in Premixed Flames Fueled by Blends of 1,3-Butadiene and n-Butanol", *Proc. Combust. Inst.,* accepted for presentation.
14. A. Lucassen, S. Park, N. Hansen, S.M. Sarathy, "Combustion Chemistry of Alcohols: Experimental and Modeled Structure of a Premixed 2-Methylbutanol Flame", *Proc. Combust. Inst.,* accepted for presentation.
15. M. Schenk, N. Hansen, H. Vieker, A. Beyer, A. Gölzhäuser, K. Kohse-Höinghaus, "PAH Formation and Soot Morphology in Flames of C_4 Fuels", *Proc. Combust. Inst.,* accepted for presentation.
16. D. Felsmann, K. Moshammer, J. Krüger, A. Lackner, A. Brockhinke, T. Kasper, T. Bierkandt, E. Akyildiz, N. Hansen, A. Lucassen, P. Oßwald, M. Köhler, G.A. Garcia, L. Nahon, P. Hemberger, A. Bodi, T. Gerber, K. Kohse-Höinghaus, "Electron Ionization, Photoionization and Photoelectron/Photoion Coincidence Spectroscopy in Mass-Spectrometric Investigations of a Low-Pressure Ethylene/Oxygen Flame", *Proc. Combust. Inst.,* submitted.
17. S. M. Sarathy, P. Oßwald, N. Hansen, K. Kohse-Höinghaus, "Alcohol Combustion Chemistry", *Prog. Energy Combust. Sci.,* submitted.

Kinetics and Spectroscopy of Combustion Gases at High Temperatures

R. K. Hanson, C. T. Bowman
Department of Mechanical Engineering, Stanford University
Stanford, CA 94305-3023
rkhanson@stanford.edu, ctbowman@stanford.edu

I. Program Scope

This program involves two complementary activities: (1) development and application of cw laser absorption methods for the measurement of concentration time-histories and fundamental spectroscopic parameters for species of interest in combustion; and (2) shock tube studies of reaction kinetics relevant to combustion. Species currently being investigated in the spectroscopic portion of the research include formaldehyde and acetaldehyde. Recent reaction kinetics work has advanced on two fronts. First, we are have made direct high-temperature shock tube/laser absorption measurements of the reaction rate constants for OH + aldehydes and alcohols, including formaldehyde, acetaldehyde, propionaldehyde, n-butyraldehyde, ethanol, and tert-butanol. Second, we have investigated the decomposition of cyclohexene, which is commonly used in single-pulse shock tube studies as a chemical thermometer.

II. Recent Progress: Spectroscopy

Aldehyde Detection using 306 nm UV and 3.4 micron IR Laser Absorption

Laser absorption diagnostic methods were developed for the quantitative measurement of formaldehyde and acetaldehyde at high temperatures in shock tube kinetic studies. Investigation of the high-temperature CH_2O spectrum has shown that the optimal wavelength for CH_2O detection using commercially available lasers is near 2896 cm^{-1}. By exploiting the structural difference between the absorption spectra of CH_2O and that of broadband interfering species, a two-color (2895.92 cm^{-1} and 2895.60 cm^{-1}) interference-free detection scheme for CH_2O sensing in a combustion environment was developed. A third color (32601.10 cm^{-1}) has also been added to develop a UV/IR detection scheme for combined CH_3CHO/CH_2O measurements. To implement these schemes, aldehyde cross-sections at all three colors were measured behind reflected shock waves over a wide span of temperatures and pressures, and the diagnostic schemes were validated using two controlled experiments with well-established chemistry. Applications of these diagnostics were also demonstrated in shock tube pyrolysis experiments of 1,3,5-trioxane, CH_2O and CH_3CHO. Important applications of these diagnostics include monitoring formaldehyde and acetaldehyde during pyrolysis and oxidation of oxygenated fuels. Further details can be found in Publication 1.

II. Recent Progress: Chemical Kinetics

Rate Constant Measurements of the Reactions of C1-C4 Aldehydes with OH

The overall rate constants for the reactions of hydroxyl radicals with a series of aldehydes, formaldehyde (Figure 1), acetaldehyde (Figure 2), propionaldehyde and n-butyraldehyde, were studied under pseudo-first-order conditions behind reflected shock waves at temperatures of 950 - 1400 K and pressures of 1 - 2 atm. OH radicals were produced by rapid thermal decomposition of tert-butyl hydroperoxide, and OH time-histories were monitored by narrow-linewidth UV laser absorption near 306.7 nm. The overall rate constants were inferred by fitting simulated OH profiles to the measured OH time histories using detailed mechanisms, though the OH decay was nearly first-order.

No pressure dependence was observed in these measurements. The measured rate constant for the formaldehyde + OH reaction is consistent with previous experimental studies. For C2-C4 aldehydes + OH, this study provides the first direct rate constant measurement at high temperatures. More general rate constant expressions covering a much wider temperature range (200 - 1600 K) were also determined by combining current measurements with existing low temperature data in the literature. Further details can be found in Publication 2.

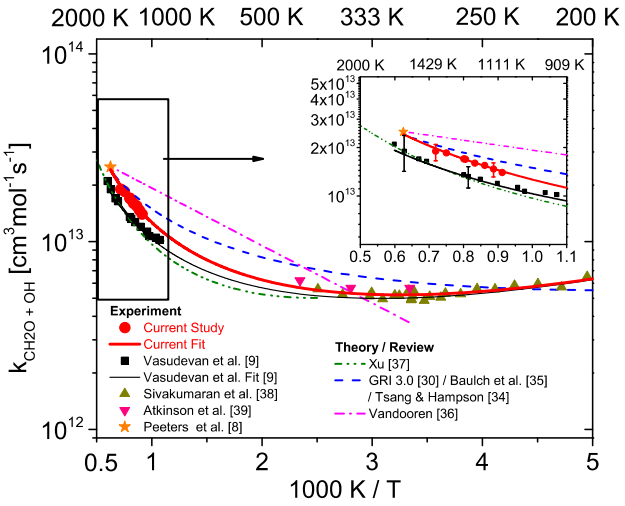

Figure 1. Arrhenius plot of CH_2O+OH = products. See publication 2.

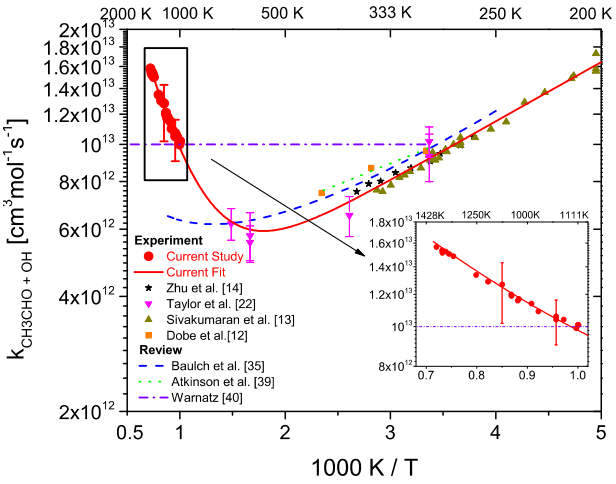

Figure 2. Arrhenius plot of CH_3CHO+OH = products. See publication 2.

Rate Constant Measurements of the Reaction of tert-butanol + OH using Isotopic Labeling

The overall rate constant for the reaction tert-butanol + OH → products was determined experimentally behind reflected shock waves by using ^{18}O-substituted tert-butanol (tert-butan^{18}ol) and tert-butyl hydroperoxide (TBHP) as a fast source of ^{16}OH (Figure 3). The products of the title reaction include the tert-C_4H_8OH radical which is known to have two major β-scission decomposition channels, one of which produces OH radicals. Experiments with the isotopically-labeled tert-butan^{18}ol also lead to an experimental determination of the branching ratio for the primary β-scission pathways of the tert-C_4H_8OH radical by comparing the measured pseudo-first-order decay rate of ^{16}OH in the presence of excess tert-butan^{16}ol, with the respective decay rate of ^{16}OH in the presence of excess tert-butan^{18}ol. The two decay rates of ^{16}OH as a result of reactions with the two forms of tert-butanol differ by approximately a factor of five, due to the absence of ^{16}OH-producing pathways in experiments with tert-butan^{18}ol. This indicates that 80% of the ^{16}OH molecules that react with tert-butan^{16}ol will produce another ^{16}OH molecule through β-scission of the resulting tert-$C_4H_8{}^{16}OH$ radical. Further details can be found in Publication 3.

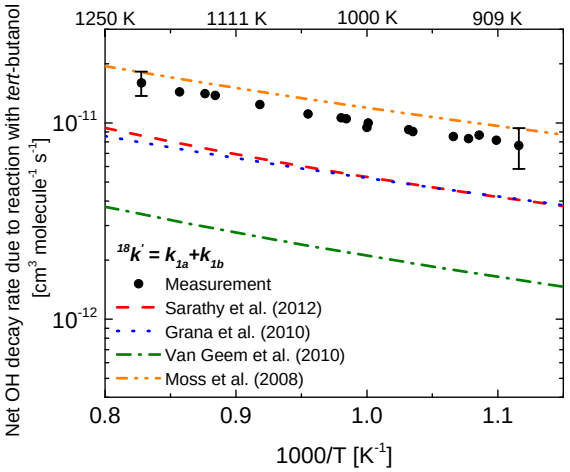

Figure 3: Comparison of the measured overall tert-butanol + OH reaction rate with values used in mechanisms from the literature. See publication 3.

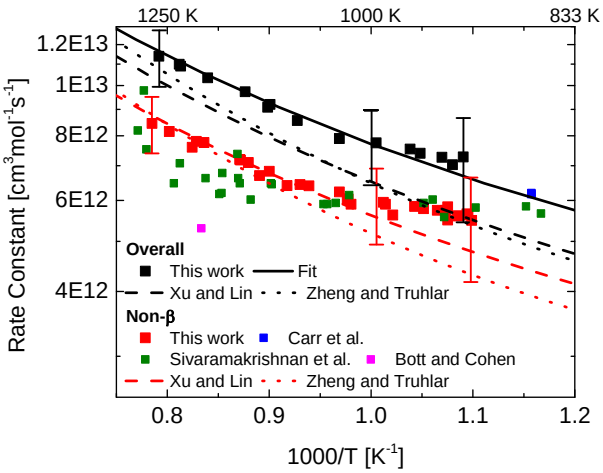

Figure 4. Comparison of the measured overall and non-β rate constants for ethanol+OH with previous theoretical and experimental work at high temperatures. See publication 4.

Rate Constant Measurement of the Reaction of Ethanol + OH

The rate constant for the overall reaction ethanol + OH → products was also determined experimentally from 900-1270 K behind reflected shock waves (Figure 4) using the same TBHP precursor experimental strategy as with tert-butanol+OH experiments. Ethan[18]ol was utilized for these measurements in order to avoid the recycling of OH radicals following H-atom abstraction at the β-site of ethanol. Similar experiments were also performed with unlabeled ethan[16]ol in order to infer the rate constant that excludes reactivity at the β-site. The two data sets were used to directly infer the branching ratio for the reaction at the β-site. Measurements indicate that the branching ratio of the β-site is between 20-25% at the conditions studied. Further details can be found in Publication 4.

Rate Constant Measurement of Reaction Cyclohexene -> Ethylene + 1,3-Butadiene

The cyclohexene decomposition rate is commonly used as a temperature reference in shock tube studies. This rate is currently known to within a factor of two. We have recently measured the rate with a reduced uncertainty, of ±25%, using the latest laser absorption/shock tube techniques.

The rate constant for the reaction cyclohexene → ethylene + 1,3-butadiene was determined by monitoring the formation of ethylene during the pyrolysis of cyclohexene behind reflected shock waves (Figure 5). Ethylene mole-fraction time-histories were measured using direct laser absorption at 10.532 μm. Measurements do not indicate any pressure dependence at these conditions. The data are best-fit by an Arrhenius expression k [s^{-1}] = 4.84 × 10^{14} exp (−31 900 [K]/T) with uncertainties of ±19–36%, depending on the temperature. This appears to be the most accurate determination to date of the rate constant for cyclohexene decomposition. Discrepancies with previous work in the measured rate constant for this reaction correspond to variations in the inferred temperature using the chemical thermometry method of approximately 20 K. Further details can be found in Publication 5.

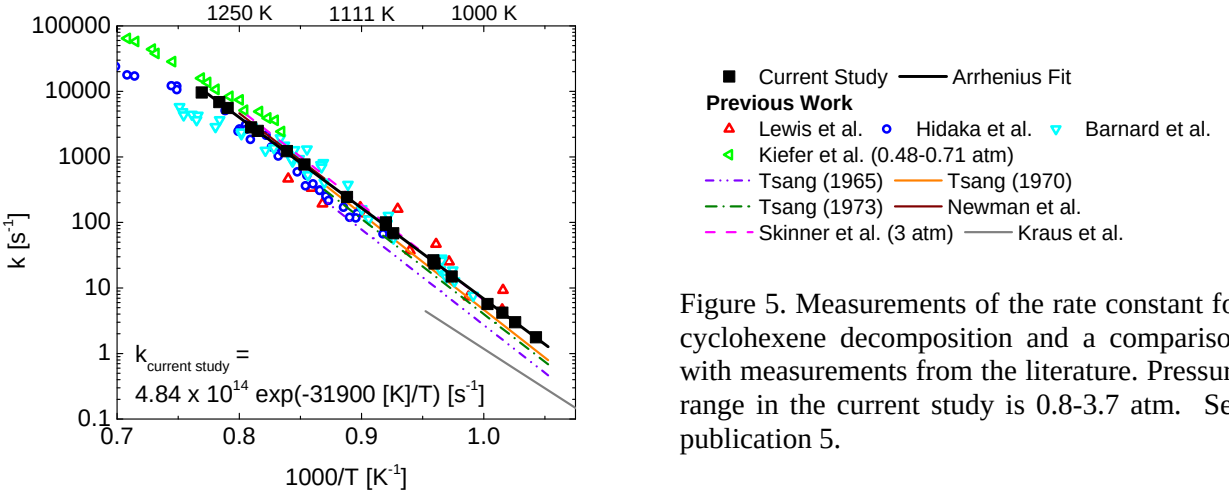

Figure 5. Measurements of the rate constant for cyclohexene decomposition and a comparison with measurements from the literature. Pressure range in the current study is 0.8-3.7 atm. See publication 5.

III. Future Work

Spectroscopic experimental work continues on the development of the multi-color IR-UV aldehyde laser absorption diagnostic, and exploration of mid- and far-IR detection of acetylene and larger alkenes (e.g., propene and butene), respectively. Reaction kinetics studies will focus on measurement of the rate constant for the reaction of CH_2O+H and the acetaldehyde decomposition roaming reaction, as well as alkene decomposition reactions forming acetylene.

IV. Major Publications Attributed to this Grant 2012-2014

1. S. Wang, D. F. Davidson, R. K. Hanson, "High Temperature Laser Absorption Diagnostics for CH_2O and CH_3CHO and Their Application to Shock Tube Kinetics Studies," Combustion and Flame 160 (2013) 1930-1938, DOI 10.1016/j.combustflame.2013.05.004.

2. S. Wang, D. F. Davidson, R. K. Hanson, "High Temperature Measurements for the Rate Constants of C1-C4 Aldehydes with OH in a Shock Tube," submitted to the Proceedings of the Combustion Institute, November 2013.

3. I. Stranic, G. A. Pang, R. K. Hanson, D. M. Golden, C. T. Bowman, "Shock Tube Measurements of the tert-Butanol + OH Reaction Rate and the tert-C_4H_8OH Radical beta-Scission Branching Ratio Using Isotopic Labeling," Journal of Physical Chemistry A 117 (2013) 4777-4784, DOI 10.1021/jp402176e.

4. I. Stranic, G. A. Pang, R. K. Hanson, D. M. Golden, C. T. Bowman, "Shock Tube Measurements of the Rate Constant for the Reaction Ethanol + OH," Journal of Physical Chemistry A 118 (2014) 822-828, DOI 10.1021/jp410853f.

5. I. Stranic, D. F. Davidson, R. K. Hanson, "Shock Tube Measurements of the Rate Constant for the Reaction Cyclohexene -> Ethylene + 1,3-Butadiene," Chemical Physics Letters 584 (2013) 18-23, DOI 10.1016/j.cplett.2013.07.067.

6. K.-Y. Lam, D.F. Davidson and R.K. Hanson, "A Shock Tube Study of H_2+OH $\rightarrow$ H_2O+H using Laser Absorption," Int. J. Chem. Kinetics 45 (2013) 363-373, DOI 10.1002/kin.20771. (With additional support from NSF.)

7. K.-Y. Lam, D. F. Davidson, R. K. Hanson, "High-Temperature Measurements of the Reactions of OH with small Methyl Esters: Methyl Formate, Methyl Acetate, Methyl Propanoate, and Methyl Butanoate," J. Phys. Chem. A 116 (2012) 12229-12241, DOI 10.1021/jp310256j.

8. K.-Y. Lam, D.F. Davidson and R.K. Hanson, "High Temperature Measurements of the Reaction of OH with a Series of Ketones: Acetone, 2-Butanone, 3-Pentanone and 2-Pentanone," J. Phys. Chem. A 116 (2012), 5549–5559, DOI 10.1021/jp303853h.

9. G.A. Pang, R. K. Hanson, D. M. Golden and C. T. Bowman, "Experimental Determination of the High-Temperature Rate Constant for the Reaction of OH with sec-Butanol," J. Phys. Chem. A, 116 (2012), 9607-9613, DOI 10.1021/jp306977e.

10. G. A. Pang, R. K. Hanson , D. M. Golden and C. T. Bowman, "High-Temperature Rate Constant Determination for the Reaction of OH with iso-Butanol," J. Phys. Chem. A 116 (2012) 4720-4725, DOI 10.1021/jp302719j.

11. G.A. Pang, R.K. Hanson, D.M. Golden and C.T. Bowman, "Rate Constant Measurements of the Overall Reaction of OH+1-Butanol$\rightarrow$ Products from 900 to 1200K," J. Phys. Chem. A 116 (2012) 2475-2483, DOI 10.1021/jp211885p. (With additional support from DOE-EFRC.)

12. G.A. Pang, "Experimental determination of rate constants for reactions of the hydroxyl radical with alkanes and alcohols," Ph.D. Thesis, Mechanical Engineering Dept. Stanford University, CA (2012).

13. K.-Y. Lam, W. Ren, Z. Hong, D.F. Davidson and R.K. Hanson, "Shock Tube Measurements of 3-Pentanone Pyrolysis and Oxidation," Comb.and Flame 159 (2012) 3251-3263, DOI 10.1016/j.combustflame.2012.06.012.

Theoretical Studies of Potential Energy Surfaces*

Lawrence B. Harding
Chemical Sciences and Engineering Division
Argonne National Laboratory, Argonne, IL 60439
harding@anl.gov

Program Scope

The goal of this program is to calculate accurate potential energy surfaces for both reactive and non-reactive systems. Our approach is to use state-of-the-art electronic structure methods (CASPT2, MR-CI, CCSD(T), etc.) to characterize multi-dimensional potential energy surfaces. Depending on the nature of the problem, the calculations may focus on local regions of a potential surface or may cover the surface more globally. A second aspect of this program is the development of techniques to fit multi-dimensional potential surfaces to convenient, global, analytic functions suitable for use in dynamics calculations.

Recent Progress

R + O_2: Reactions of radicals with molecular oxygen are among the most important reactions in combustion. These reactions typically proceed via barrierless additions forming peroxy radicals. These R + O_2 addition reactions present significant challenges to electronic structure theory. The electronic wavefunctions in the bottleneck regions of the potential surfaces are highly multi-reference in nature and, as a result, commonly used single reference methods such as CCSD(T) predict spurious barriers to addition. Multi-reference methods also have problems with these reactions. Last year we reported that the internal contraction scheme in the MOLPRO implementation of multi-reference configuration interaction (MRCI) leads to significant errors in the bottleneck region for the H+O_2 addition. Comparisons to small basis set, full CI calculations on H+O_2 suggest that uncontracted MRCI calculations, without a Davidson-type correction for higher order excitations, also yield a potential that is not sufficiently attractive, while the addition of a Davidson-type correction makes the potential too attractive. CASPT2 calculations are also found to yield potentials that are too attractive. This year, in collaboration with Klippenstein and Goldsmith, we have begun exploring the use of a hybrid multi-reference/CCSD(T) approach for these R+O_2 reactions. This is an extension of an approach that we have used in the past to treat transition states having a large degree of multi-reference character. This approach relies on the idea that when one is in a region of a potential surface in which the ground state wavefunction is highly multi-reference in character, there will generally be a low-lying, higher spin, excited state, of similar orbital character, which is not highly multi-reference. Our approach uses CCSD(T) to calculate the energy of the high spin state relative to the appropriate asymptote and MRCI (or CASPT2) to calculate the splitting between the high spin and low spin states. The assumption is that because the orbital structure of the high spin and low spin states are similar the high-order, dynamical correlation for the two states will also be similar.

An example of this approach is shown in Figure 1. These plots illustrate MEP's for the H+O_2 addition calculated with a variety of multi-reference methods. The red curves come from internally contracted MRCI calculations, the blue from uncontracted MRCI calculations (the

dashed red and blue lines include a Davidson correction), and the yellow and green lines are CASPT2 results with and without (respectively) the IPEA shift of Ghigo et al. The curves in the

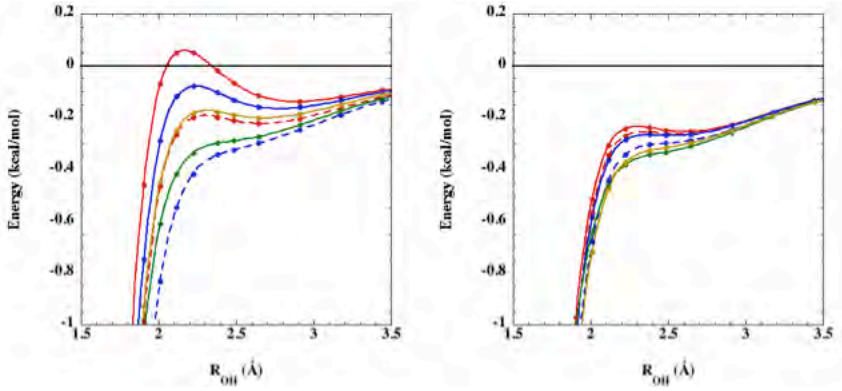

Figure 1

plot on the left are direct calculations of the interaction energies using each of these methods while the plot on the right shows the results with the new hybrid approach. Here the multi-reference methods are used to calculate the energy of the attractive ^{2}A" state relative to the repulsive ^{4}A" state while the energy of the ^{4}A" state relative to the asymptote is determined using CCSD(T). The two plots show that, for example at a distance of 2.1Å, the direct multi-reference calculations give a spread of 0.6 kcal/mol while the new hybrid approach reduces this spread to just 0.2 kcal/mol. The good agreement between all six calculations give us confidence in the accuracy of the results and also provides justification for the use of the much less expensive CASPT2 based calculations to study larger R+O_2 reactions.

We have now used this approach in conjunction with Variable Reaction Coordinate Transition State Theory (VRCTST), to calculate the high-pressure limit for the vinyl+O_2 addition. The results are shown in Figure 2. The dashed red and blue curves employ direct CASPT2 and MRCI interaction energies, respectively, while the solid lines represent the corresponding hybrid methods. From this plot it can be seen that the direct MRCI calculation (including the Davidson correction) leads to a predicted rate that is a factor of two below the experimental results over the entire temperature range. In contrast, the VRCTST calculations based on the raw CASPT2, hybrid CASPT2 and hybrid MRCI calculations all yield predicted rates within ~20% of the experimental results over this temperature range.

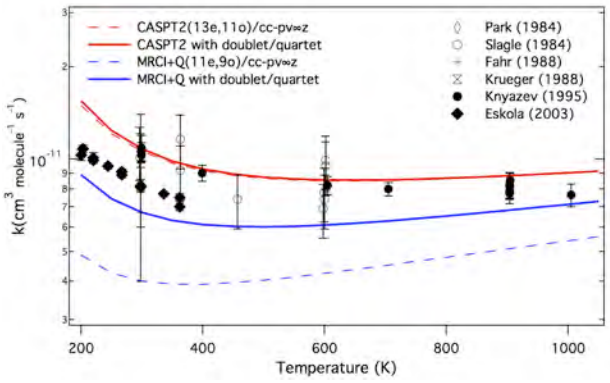

Figure 2

NH_2+NO_2: The reaction of NH_2 with NO_2 has been identified as a key step in the selective noncatalytic reduction (SNCR) of NO using amines. Two pathways have been identified for this reaction involving barrierless additions of the NH_2 to either the N atom of NO_2 or one of the O atoms. Addition to one of the O atoms of NO_2 results in the formation of H_2NONO which decomposes directly to H_2NO+NO. Addition to the N atom results in the formation of H_2NNO_2 which then decomposes via a series of isomerizations to form H_2O+N_2O. Last year we completed a study of the kinetics of these reactions in a combined theoretical/experimental collaboration involving Klippenstein, Glarborg and Marshall. The calculated and observed overall rates are in

excellent agreement. The calculated high temperature rate is significantly below previous estimates. The calculated branching ratio between the two channels is in good agreement with experiment at high temperatures but tend to overestimate the H_2O+N_2O channel at low temperatures.

Roaming Mechanisms for Decomposition of Alcohols: We have begun a study of roaming radical pathways in the decomposition of alcohols. We find the lowest roaming paths generally involve cleavage of the CC bond adjacent to the OH group, followed by abstraction of either the OH hydrogen by the nascent hydrocarbon fragment or abstraction of a hydrogen from the nascent hydrocarbon fragment by the nascent OH containing fragment. For most alcohols these roaming pathways are not very important due to the existence of competing, lower energy, tight transition states for H_2O elimination. However, for alcohols with no beta hydrogens (such as neopentanol) these roaming paths may be important.

Future Plans

We plan to continue our studies of $R+O_2$ reactions and roaming radical pathways.

Acknowledgement: This work was performed under the auspices of the Office of Basic Energy Sciences, Division of Chemical Sciences, Geosciences and Biosciences, U.S. Department of Energy, under Contract DE-AC02-06CH11357.

PUBLICATIONS (2011 - Present):

Uncertainty Driven Theoretical Kinetics Studies for CH_3OH Ignition: HO_2+CH_3OH and O_2+CH_3OH
S. J. Klippenstein, L. B. Harding, M. J. Davis, A. S. Tomlin, R. T. Skodje
33nd Symposium (International) on Combustion, **33**, 351-357 (2011)

The Role of NNH in NO Formation and Control
S. J. Klippenstein, L. B. Harding, P. Glarborg, J. A. Miller
Combustion and Flame, **158**, 774-489 (2011)

Roaming Radicals in the Thermal Decomposition of Dimethyl Ether: Experiment and Theory
R. Sivaramakrishnan, J. V. Michael, A. F. Wagner, R. Dawes, A. W. Jasper, L. B. Harding, Y. Georgievskii, S. J. Klippenstein, Combustion and Flame, **158**, 618-632 (2011)

Shock Tube and Theoretical Studies on the Thermal Decomposition of Propane: Evidence for a Roaming Radical Channel
R. Sivaramakrishnan, M.-C. Su, J. V. Michael, L. B. Harding, S. J. Klippenstein
J. Phys. Chem. A **115**, 3366-3379 (2011)

Near-threshold H/D Exchange in CD_3CHO Photodissociation
B. R. Heazlewood, A. T. Maccarone, D. U. Andrews, D. L. Osborn, L. B. Harding, S. J. Klippenstein, M. J. T. Jordan, and S. H. Kable, Nature Chemistry **3**, 443-448 (2011)

A Statistical Theory for the Kinetics and Dynamics of Roaming Reactions
S. J. Klippenstein, Y. Georgievskii and L. B. Harding
J. Phys. Chem. A 115, 14370-14381(2011)

Bi-fidelity Fitting and Optimization
R. L. Miller, L. B. Harding, M. J. Davis, and S. K. Gray, J. Chem. Phys. 136, 074102(2012)

Theoretical Determination of the Rate Coefficient for the HO_2+HO_2→ H_2O_2+O_2 Reaction: Adiabatic Treatment of Anharmonic Torsional Effects
D. D. Y. Zhou, K. Han, P. Zhang, L. B. Harding, M. J. Davis and R. T. Skodje
J. Phys. Chem. A **116**, 2089-2100 (2012)

Shock Tube Explorations of Roaming Radical Mechanisms: The Decomposition of Isobutane and Neopentane
R. Sivaramakrishnan, J. V. Michael, L. B. Harding and S. J. Klippenstein
J. Phys. Chem. A **116**, 5981-5989 (2012)

Separability of Tight and Roaming Pathways for Molecular Decomposition
L. B. Harding, S. J. Klippenstein, and A. W. Jasper
J. Phys. Chem. A **116**, 6967-6982 (2012)

A Quantitative Explanation for the Apparent Anomalous Temperature Dependence of OH + HO_2 → H_2O + O_2 through Multi-Scale Modeling
M. P. Burke, S. J. Klippenstein, L. B. Harding, Proc. Comb. Inst. **34**, 547-555 (2013)

Unconventional Peroxy Chemistry in Alcohol Oxidation: The Water Elimination Pathway
O. Welz, S. J. Klippenstein, L. B. Harding, C. A. Taatjes, J. Zador
J. Phys. Chem. Letters **4**, 350-354 (2013)

Rate Constant and Branching Fraction for the NH_2 + NO_2 Reaction
S. J. Klippenstein, L. B. Harding, P. Glarborg, Y. Gao, H. Hu, P. Marshall
J. Phys. Chem. A **117**, 9011 (2013)

Predictive Theory for the Addition Insertion Kinetics of $^1CH_2$ Reacting with Unsaturated Hydrocarbons
D. Polino, S. J. Klippenstein, L. B. Harding, Y. Georgievski
J. Phys. Chem. A **117**, 12677-12692 (2013)

Comparison of Multireference Configuration Interaction Potential Energy Surfaces for H + O_2 → HO_2: The Effect of Internal Contraction
L. B. Harding, S. J. Klippenstein, H. Lischka, R. Shepard
Theoretical Chemical Accounts **133**,1429 (2013)

CHEMICAL ACCURACY FROM AB INITIO MOLECULAR ORBITAL CALCULATIONS

Martin Head-Gordon
Department of Chemistry, University of California, Berkeley, and,
Chemical Sciences Division, Lawrence Berkeley National Laboratory,
Berkeley, CA 94720.
mhg@cchem.berkeley.edu

1. Scope of Project.

Short-lived reactive radicals and intermediate reaction complexes play central roles in combustion, interstellar and atmospheric chemistry. Due to their transient nature, such molecules are challenging to study experimentally, and our knowledge of their structure, properties and reactivity is consequently quite limited. To expand this knowledge, we develop new theoretical methods for reliable computer-based prediction of the properties of such species. We apply our methods, as well as existing theoretical approaches, to study prototype radical reactions, often in collaboration with experimental efforts. These studies help to deepen understanding of the role of reactive intermediates in diverse areas of chemistry. They also sometimes reveal frontiers where new theoretical developments are needed in order to permit better calculations in the future.

2. Summary of Recent Major Accomplishments.

2.1 An improved density functional.

Range-separated hybrids (RSH) reduce self-interaction errors (SIE) and in 2008 we developed the ωB97 family of RSH functionals, that reduce SIE by about 66%, relative to B3LYP. Over the last few years, we've been seeking the limit of transferable accuracy that can be achieved with generalized gradient approximations (GGA's) and corrections for long-range dispersion interactions. We've shown [20] that RSH's are more accurate than global hybrids on a diverse test set of roughly 1200 relative energies, when trained consistently on another set of roughly equal size. We also show that Van der Waals (-V) functionals out-perform atom-atom dispersion (-D) corrections for long-range correlation. Our third key result is that the best functionals (in the sense of most transferable [20]) have significantly fewer adjustable parameters than has been common in the literature.

We have self-consistently trained a new RSH-V functional based on the same protocol. The resulting functional [21], named ωB97X-V, contains only 10 adjustable parameters (e.g. versus 15 for our 2008 functional, ωB97X-D, or about 30 for M06-2X). On our test data, ωB97X-V reduces RMS errors in non-bonded interactions by about 40% relative to ωB97X-D, while matching its performance for thermochemistry. M06-2X slightly outperforms it for thermochemistry (10% lower RMS error), while ωB97X-V is greatly superior to M06-2X for non-bonded interactions (60% lower RMS error).

2.2 Approximate Brueckner Orbital Methods.

Usually second order Moller-Plesset (MP2) theory or coupled cluster theory are evaluated using Hartree-Fock orbitals. However, the best orbitals are those that minimize

the energy in absence of single excitations, which are termed Brueckner orbitals. For approximate methods like MP2, use of Brueckner orbitals can make a very large difference. This is illustrated by our study of the soliton defect in polyene radicals [2], where use of Brueckner orbitals is essential to obtain realistic estimates of the size of the radical defect, as well reasonable values of $<S^2>$. For example, for the ground doublet state of $C_{41}H_{43}$, $<S^2>$=6.8 for MP2, versus 0.78 for a Brueckner orbital based MP2 method (the O2 approach), versus the exact value of 0.75.

One problem with OO-MP2 and O2 is that the energy is not bounded from below: it can diverge in the limit of small gaps and restricted orbitals. This can be avoided in practice by using an unrestricted initial guess to converge to a higher energy local minimum. Even better, we have shown that the topology of the OO-MP2 energy surface in orbital space can be tamed by regularizing the equations for the perturbed amplitudes [14]. We introduce a penalty function that is quadratic in the magnitude of the amplitudes. The penalty function prefactor becomes a static level shift, and values of 400 mH or above render the spin polarized solution as the global minimum for stretched bond problems. Remarkably, this large level shift also improves bonded and non-bonded relative energies. This method, δ-OO-MP2 [18], thus improves on both formal and practical aspects of the parent OO-MP2 method. Regularization may also be useful for new orbital optimized double hybrid density functionals [14].

2.3 Intermolecular interactions.

Second order Moller-Plesset (MP2) theory in finite basis sets typically overestimates intermolecular binding energies due to basis set superposition error (BSSE). Even at the complete basis set (CBS) limit, MP2 theory often overestimates interactions because of too-large C6 coefficients. Motivated by these facts, we have explored the effect of attenuating the coulomb operator in MP2 theory, using a single parameter for the attenuation length scale. In the small aug-cc-pVDZ basis, with the attenuation parameter set to 1.05Å, errors in calculated intermolecular interactions can be reduced by about a factor of 5 (!) relative to conventional MP2/aug-cc-pVDZ [8]. For dispersion-sensitive systems, the attenuated aug-cc-pVDZ results are better than MP2/CBS, as well as being hundreds of times faster. We have demonstrated that even higher accuracy can be obtained by attenuated MP2 in the larger aug-cc-pVTZ basis (with similar improvements over conventional MP2 in the same basis) [15,19]. Attenuated MP2 theory is a useful alternative for reasonably accurate calculations of intra- and inter-molecular interactions when higher accuracy coupled cluster methods are unfeasible.

2.4 Valence bond vs coupled cluster for strong electron correlations.

Spin-coupled valence bond (SCVB) theory takes a simple product of *n* non-orthogonal spatial orbitals and spin-couples those orbitals together in all possible ways (the number grows exponentially with *n*). It is possible to exactly reproduce the SCVB limit for fully broken bonds with only quadratic degrees of freedom (provided that the final state is describable by unrestricted Hartree-Fock). Taking this limit as a model defines what we call the coupled cluster valence bond (CCVB) method [4]. CCVB is well suited for describing strong spin correlations such as the antiferromagnetic coupling of high spin electrons at two different centers. Bond dissociations and some types of metal complexes are in this class. We have developed quite exciting theory [4] that re-expresses the CCVB

model as a novel form of coupled cluster doubles theory in which the doubles operator is complex. Its real part involves the singlet coupling between two pairs of electrons, whilst the imaginary part contains quintet coupling between two pairs of electrons. The latter affects the quadruples, and allows correct separation of two electron pairs within a spin-restricted theory. This suggests a generalization of CCVB as a coupled cluster theory, CCVBSD, that recovers all the usual orbital invariances and ionic excitations of CCSD, whilst retaining the beautiful ability of CCVB to correctly separate multiple electron pairs within a spin-restricted active space.

2.5 Intermolecular interactions involving radicals.

An absolutely localized MO energy decomposition analysis (ALMO-EDA) based on stepwise release of variational constraints has been formulated and implemented for intermolecular interactions involving radicals [12]. This ALMO-EDA separates frozen interactions (permanent electrostatics and Paul repulsion) from induced electrostatics, and donor-acceptor charge transfer (CT). It is applicable to any density functional, and is a useful interpretative tool for electronic structure calculations. We have also shown that the CT contribution obtained in the ALMO-EDA is effectively a lower bound, and have explored whether it is possible to formulate an upper bound [10]. These results validate the use of the ALMO-EDA in its present form, and offer hints for future improvements.

2.6 Fundamental studies of chemical bonding.

In addition to studies of hydrocarbon polyene radicals [2] to explore the soliton defect, we have also explored the photodissociation of glycerol, in collaboration with experimental measurements from the Ahmed and Leone groups at LBNL. The ALMO-EDA [12] described above proved very useful in unraveling intermolecular interactions in the key intermediate: a triplex between vinyl alcohol radical cation, water and formaldehyde. Contrary to conventional wisdom, there is a strong charge transfer contribution to these hydrogen-bridged ion-molecule interactions. Other applications have recently been completed, including the tetraradicaloid states associated with the singlet fission process in polycyclic aromatic hydrocarbons such as pentacene [13], and the association process for C2 hydrocarbons and their cations [9].

3. Summary of Research Plans.

- Formulation of improved density functionals: Extending our protocol for the development of less parameterized yet more transferable density functionals to other classes of functionals is an interesting challenge that we are tackling.
- An efficient implementation of CCVB has been completed, and an extension of the method to radicals is underway.
- New studies of radicals and radical reactions will be pursued as opportunities arise.

4. Publications from DOE Sponsored Work, 2012-present.

[1] "An energy decomposition analysis for intermolecular interactions from an absolutely localized molecular orbital reference at the coupled-cluster singles and doubles level", R.J. Azar and M. Head-Gordon, J. Chem. Phys. **136**, 024103 (2012)

[2] "Exploring the competition between localization and delocalization of the neutral soliton defect in polyenyl chains with the orbital optimized second order opposite spin method", W. Kurlancheek, R. Lochan, K.V. Lawler, and M. Head-Gordon, J. Chem. Phys. 136, 054113 (2012) (11 pages).

[3] “A computational and experimental study of the mechanism of hydrogen generation from water by a molecular molybdenum-oxo pentapyridine catalyst”, E.J. Sundstrom, X. Yang, V.S. Thoi, H.I. Karunadasa, C.J. Chang, J.R. Long and M. Head-Gordon, J. Am. Chem. Soc. 134, 5233-5242 (2012).
[4] “A fusion of the closed-shell coupled cluster singles and doubles method and valence-bond theory for bond breaking”, D.W. Small and M. Head-Gordon, J. Chem. Phys. 137, 114103 (2012) (13 pages).
[5] “Refined energetic ordering for sulfate-water (n=3-6) clusters using high-level electronic structure calculations”, D.S. Lambrecht, L. McCaslin, S.S. Xantheas, E. Epifanovsky, and M. Head-Gordon, Mol. Phys. 110, 2513-2521 (2012).
[6] “Examination of the Hydrogen-Bonding Networks in Small Water Clusters (n=2-5,13,17) using Absolutely Localized Molecular Orbital Energy Decomposition Analysis”, Erika A. Cobar, Paul R. Horn, R.G. Bergman, and M. Head-Gordon, Phys. Chem. Chem. Phys. 14, 15328-15339 (2012).
[7] “Restricted Active Space Spin-Flip Configuration Interaction: Theory and Examples for Multiple Spin Flips with Odd Numbers of Electrons”, P.M. Zimmerman, F. Bell, M. Goldey, A.T. Bell, and M. Head-Gordon, J. Chem. Phys. 137, 164110 (2012) (11 pages).
[8] “Attenuating away the errors in inter and intra-molecular interactions from second order Møller-Plesset calculations in the small aug-cc-pVDZ basis set”, Matt Goldey and M. Head-Gordon, J. Phys. Chem. Lett. 3, 3592−3598 (2012).
[9] “Association Mechanisms of Unsaturated C2 Hydrocarbons With Their Cations: Acetylene and Ethylene”, P.P. Bera, M. Head-Gordon, and T.J. Lee, Phys. Chem. Chem. Phys. 15, 2012-2023 (2013).
[10] “Useful lower limits to polarization contributions to intermolecular interactions using a minimal basis of localized orthogonal orbitals: Theory and analysis of the water dimer”, R. Julian Azar, Paul R. Horn, Eric J. Sundstrom, and M. Head-Gordon, J. Chem. Phys. 134, 084102 (2013).
[11] “The Performance of Current Density Functionals for Sulfate-Water Clusters”, Narbe Mardirossian, Daniel S. Lambrecht, Laura McCaslin, Sotiris S. Xantheas, and M. Head-Gordon, J. Chem. Theory Comput. 9, 1368–1380 (2013).
[12] “Unrestricted Absolutely Localized Molecular Orbitals for Energy Decomposition Analysis: Theory and Applications to Intermolecular Interactions Involving Radicals”, Paul R. Horn, Eric J. Sundstrom, Thomas Baker and M. Head-Gordon, J. Chem. Phys. 138, 134119 (2013) (14 pages).
[13] “A Correlated Electron View of Singlet Fission”, P.M. Zimmerman, C.B. Musgrave, and M. Head-Gordon, Acc. Chem. Res. 46, 1339-1347 (2013).
[14] “Orbital optimized double hybrid density functionals”, R. Peverati and M. Head-Gordon, J. Chem. Phys. 139, 024110 (2013).
[15] “Attenuated second order Moller-Plesset theory: Assessment and performance in the aug-cc-pVTZ basis”, M. Goldey, A.D. Dutoi and M. Head-Gordon, Phys. Chem. Chem. Phys. 15, 15869-15875 (2013).
[16] “Dissociative photoionization of glycerol and its dimer occurs predominantly via a ternary hydrogen-bridged ion-molecule complex”, F. Bell, Q.N. Ruan, A. Golan, P.R. Horn, M. Ahmed, S.R. Leone, and M. Head-Gordon, J. Am. Chem. Soc. 135, 14229-14239 (2013).
[17] “Characterizing and understanding the remarkably slow basis set convergence of several Minnesota density functionals for intermolecular interaction energies”, N. Mardirossian and M. Head-Gordon, J. Chem. Theor. Comput. 9, 4453–4461 (2013).
[18] “Regularized orbital optimized second order perturbation theory”, D. Stück and M. Head-Gordon, J. Chem. Phys. 139, 244109 (2013) (7 pages).
[19] “Open Multi Processing Parallel Implementation of Resolution-of-the-Identity Second Order Møller-Plesset Perturbation Theory with Attenuated and Unattenuated Results for Intermolecular Interactions between Larger Molecules”, M. Goldey, R.A. DiStasio, Jr., Y. Shao, and M. Head-Gordon, Mol. Phys. 112, 836-843 (2014).
[20] “Exploring the limit of accuracy for density functionals based on the generalized gradient approximation: Local, global hybrid and range-separated hybrids with and without dispersion corrections”, N. Mardirrosian, and M. Head-Gordon, J. Chem. Phys. 140, 18A527 (2014).
[21] “ωB97X-V: A 10 parameter range separated hybrid density functional including non-local correlation, designed by a survival of the fittest strategy”, N. Mardirossian and M. Head-Gordon, Phys. Chem. Chem. Phys. (2014); doi: 10.1039/C3CP54374A.

Laser Studies of Combustion Chemistry

John F. Hershberger

Department of Chemistry and Biochemistry
North Dakota State University
NDSU Dept. 2735, PO Box 6050
Fargo, ND 58108-6050
john.hershberger@ndsu.edu

Time-resolved infrared diode laser absorption and laser-induced fluorescence spectroscopy are used in our laboratory to study the kinetics and product channel dynamics of chemical reactions of importance in the gas-phase combustion chemistry of nitrogen-containing species. This program is aimed at improving the kinetic database of reactions crucial to modeling of combustion processes, with emphasis on NO_x chemistry. When feasible, we perform quantitative measurement of both total rate constants and product branching ratios.

1) HCNO Photochemistry

In previous years, we have extensively studied the kinetics of radical-molecule reactions involving HCNO, fulminic acid. This molecule is produced in combustion primarily by the HCCO + NO reaction. Reactions previously studied include O + HCNO, OH+HCNO, CN+HCNO, and NCO+HCNO. In all of these reactions, we used infrared spectroscopy to detect reaction products. Depending on the photolysis wavelength used, we typically detected signals for product molecules even in the absence of the radical precursor, suggesting that HCNO was itself absorbing UV light and undergoing photochemistry. In previous studies, those signals were treated as background signals, but in the past year we have begun to study the photochemistry of HCNO explicitly.

We determined the following UV absorption cross sections for HCNO:
σ (193 nm) = 5.39×10^{-19} cm^2 $molecule^{-1}$.
σ (248 nm) = $(1.52 \pm 0.15) \times 10^{-19}$ cm^2 $molecule^{-1}$.
σ (266 nm) = 1.42×10^{-19} cm^2 $molecule^{-1}$.

We then used infrared spectroscopy to detect and quantify several product species, including HCN, DCN, CO_2, CO, DCN, NH, and HNCO. At 248 nm, energetically possible photolysis channels include

$$\text{HCNO} + h\nu\ (248\ \text{nm}) \rightarrow \text{O} + \text{HCN} \quad (1a)$$
$$\rightarrow \text{H} + (\text{NCO}) \quad (1b)$$
$$\rightarrow \text{OH} + \text{CN} \quad (1c)$$

$$\rightarrow CO + NH(a^1\Delta) \qquad (1d)$$

$$\rightarrow HNCO \qquad (1e)$$

In order to suppress and/or redirect secondary chemistry, additional reagents were often added. For example, if channel (1b) is active, the NCO produced can react with HCNO:

$$NCO + HCNO \rightarrow HCN + CO + NO \qquad (2)$$

which would interfere with our HCN detection experiment. Addition of NO reagent can suppress this reaction, as NCO+NO is fast and does not produce HCN. CN radicals in channel (1c) are more problematic, however:

$$CN + HCNO \rightarrow NO + HCCN \qquad (3)$$
$$HCCN + NO \rightarrow HCN + NCO \qquad (4)$$

Our solution was to use labeled $^{15}N^{18}O$ reagents (the ^{15}N labeling is crucial, the ^{18}O labeling is not), so that $HC^{15}N$ is produced in (4), while we detected the unlabeled HCN from (1a).

To detect channel (1b), we directly detected the NCO radical, but without an absolute calibration. We determined the yield of (1b) by including $^{15}N^{18}O$, and detecting the mixed isotope $OC^{18}O$ produced from NCO + $^{15}N^{18}O$ (here, the ^{18}O labeling is helpful, because any NCO produced via secondary chemistry, reactions (3) and (4), would be $NC^{18}O$, and would therefore react with $^{15}N^{18}O$ to produce double labeled $^{18}OC^{18}O$.

To quantify channel (1c), we detected DCN produced upon addition of C_2D_6:

$$CN + C_2D_6 \rightarrow C_2D_5 + DCN \qquad (5)$$

Similar approaches were used to determine absolute quantum yields of all of the photolysis channels (details are in the publication). We obtain ϕ_{1a} (O+HCN) = 0.39 ± 0.07, ϕ_{1b} (H+(NCO)) = 0.21 ± 0.04, ϕ_{1c} (CN+OH) = 0.16 ± 0.04, ϕ_{1d} (CN+NH($a^1\Delta$)) = 0.19 ± 0.03, and ϕ_{1e} (HNCO) = 0.05 ± 0.02. The quantum yields sum to unity, indicating that we have accounted for all major channels.

Current and ongoing work involves determination of quantum yields at 193 nm photolysis wavelength. This is complicated by the possibility of a sixth photolysis channel, CH + NO. If present, additional secondary chemistry due to the highly reactive CH radical will have to be considered. Preliminary results suggest that this channel is very minor.

2) CN + Alcohols

There is a fairly extensive literature on the kinetics of the CN radical, including reactions with saturated and unsaturated hydrocarbons, O_2, NO, NO_2, etc. Our program is interested in extending this literature to lesser-studied reactions. For example, there is no published literature on reactions of CN with alcohols:

$CN + CH_3OH$	$\rightarrow HCN + CH_2OH$	(6a)
	$\rightarrow HCN + CH_3O$	(6b)
$CN + CH_3CH_2OH$	$\rightarrow HCN + CH_2CH_2OH$	(7a)
	$\rightarrow HCN + CH_3CHOH$	(7b)
	$\rightarrow HCN + CH_3CH_2O$	(7c)
CN + n-propanol	$\rightarrow$ products	(8)

We have used time-resolved infrared laser detection of CN produced by 266-nm photolysis of ICN to measure total rate constants (at 296 K) using standard pseudofirst order kinetics methods:

$k_6 = (1.03 \pm 0.2) \times 10^{-11}$ cm^3 $molecule^{-1}$ s^{-1}
$k_7 = (2.84 \pm 0.78) \times 10^{-11}$ cm^3 $molecule^{-1}$ s^{-1}
$k_8 = (7.57 \pm 2.0) \times 10^{-11}$ cm^3 $molecule^{-1}$ s^{-1}

We find that k_6 has very little temperature dependence over the modest range 298-450 K. Furthermore, in reaction (1), we have used selectively deuterated methanol to examine the branching between alkyl and hydroxyl hydrogen abstraction:

$CN + CH_3OD$	$\rightarrow HCN + CH_2OD$	(9a)
	$\rightarrow DCN + CH_3O$	(9b)
$CN + CD_3OH$	$\rightarrow DCN + CD_2OH$	(10a)
	$\rightarrow HCN + CD_3O$	(10b)

We find that kinetic isotope effects on the total rate constant are very small. In addition, we detect HCN by infrared laser spectroscopy near 3240 cm^{-1}. We find that in reaction (9), using CH_3OD reagents, a large amount of HCN is observed, channel (9a), as expected if alkyl abstraction dominates. Somewhat surprisingly, however, a small amount of HCN is detected using CD_3OH, channel (10b), indicating a small but detectable amount of hydroxyl abstraction. This is in contrast to literature on Cl +

CH_3OH, which seems to indicate that only alkyl abstraction takes place. We find that the HCN yield in (9) is about 80-90% of that in (6), while only the HCN yield in (10) is only about 10% of that in (6). We have also detected small amounts of DCN produced in channel (9b) and larger amounts in(10a). We therefore conclude that that alkyl abstraction represents 80-90% of the reaction, while hydroxyl abstraction contributes ~10%.

Students/postdocs involved in project: Wenhui Feng, Erik Janssen.

Publications acknowledging DOE support (2011-present)

1. "Kinetics of the CN + CS_2 and CN + SO_2 Reactions", W. Feng and J.F. Hershberger, J. Phys. Chem. A 115, 286 (2011).
2. "Kinetics of the NCCO + NO_2 Reaction", W. Feng and J.F. Hershberger, J. Phys. Chem. A 115, 12173 (2011).
3. "Kinetics of the O + ICN Reaction", W. Feng and J.F. Hershberger, J. Phys. Chem. A 116, 4817 (2012).
4. "Product Channels of the CN + HCNO Reaction", W. Feng and J.F. Hershberger, J. Phys. Chem. A 116, 10285 (2012).
5. "Experimental and Theoretical Study of the Product Channels of the C_2H + NO Reaction", W. Feng and J.F. Hershberger, J. Phys. Chem. A 117, 3585 (2013).
6. "Quantification of the 248 nm Photolysis Products of HCNO (Fulminic Acid)", W. Feng and J.F. Hershberger, J. Phys. Chem. A 118, 829 (2014).
7. "Kinetics of CN Reactions with Alcohols", E. Janssen and J.F. Hershberger, manuscript in preparation.

Breakthrough Design and Implementation of Electronic and Vibrational Many-Body Theories

So Hirata (principal investigator: DE-FG02-11ER16211)
Department of Chemistry, University of Illinois at Urbana-Champaign,
600 South Mathews Avenue, Urbana, IL 61801
sohirata@illinois.edu

Program Scope

Predictive chemical computing requires hierarchical many-body methods of increasing accuracy for both electrons and vibrations. Such hierarchies are established, at least conceptually, as configuration-interaction (CI), many-body perturbation (MP), and coupled-cluster (CC) methods, which all converge at the exact limit with increasing rank of a hierarchical series. These methods can generate results of which the convergence with respect to various parameters of calculations can be demonstrated and which can thus be predictive in the absence of experimental information.

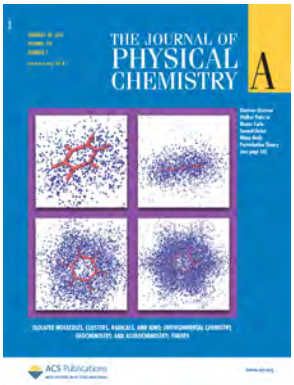

The wide use of the hierarchical electronic and vibrational many-body methods has, however, been hindered (1) by the immense cost of *executing* the calculations with these methods and, furthermore, the nonphysical rapid increase of the cost with increasing system or computer size; in other words, the conventional matrix-algebra-based algorithms of these methods are fundamentally non-scalable, (2) by the complexity and cost of *developing* some of the high-rank members of these methods, and (3) by the slow convergence of electronic energies and wave functions with respect to one-electron basis set sizes, which further drives up the cost of execution. For applications to large molecules and solids, the additional difficulties arise by the lack of (4) size consistency in some methods (whose energies and other observables scale nonphysically with size) and of (5) efficient methods that work for metallic and superconducting states as well as for electronic and/or vibrational strong correlation.

We aim to address all of these difficulties for electrons and vibrations with a view to establishing accurate and systematic computational methods for condensed-phase systems, which go beyond the usual density-functional approximations for electrons and harmonic approximation for vibrations.

Recent Progress

Publications

Fifteen (15) papers[2-9,11,13,14,16-19] and one submitted paper[20] have resulted from this award since 2011, acknowledging this DOE support. They include a Feature Article in *Journal of Physical Chemistry A* with a cover art (left figure) and an account (under review) in *Account of Chemical Research*. There are three (3) additional papers[10,12,15] that do not acknowledge any funding support. One book chapter[1] in *Annual Reviews of Physical Chemistry* has also resulted from this project.

The PI has served as a guest editor of the 50th-year Anniversary Issue of *Theoretical Chemistry Accounts* **131** (2012) with regular editors, D. G. Truhlar and C. J. Cramer (University of Minnesota), and five other guest editors. The PI was also a guest editor with G. Beran (University of California, Riverside) of the Special Issue on "Fragment and Localized Orbital Methods for Electronic Structure Theory" in *Physical Chemistry Chemical Physics* **14** (2012) (the cover figure shown on the right was prepared by Beran). Together, nineteen (19) papers (including one under review), one book chapter, proceedings, and two journal special issues are fully or partially ascribed to this grant since 2011.

Size-consistency theorems.[1-3,13,14,18] Every thermodynamic observable is either extensive or intensive. An extensive quantity such as correlation energy is asymptotically proportional to volume, while an intensive quantity such as excitation energy is asymptotically constant. An electron-correlation theory is considered *size-consistent* (*size-extensive*) if it yields a correlation energy that is extensive. Only a size-consistent method can be usefully applied to larger molecules, solids, and liquids.

We have conducted a thorough analysis of size consistency, dispelling some of the widespread confusions about its mathematical definition and existing criteria for judging whether a method is size-consistent. We have introduced the ***normalization theorem***, which reveals the different size dependence of excitation amplitudes in wave functions that are normalized or intermediately normalized. On this basis, we have put forward the ***extensive and intensive diagram theorems***, which provide unambiguous conditions for size consistency of a method for extensive and intensive quantities, respectively, stipulated in terms of diagrammatic topology and vertex makeup. Although the extensive diagram theorem is part of the well-known linked diagram theorem of Goldstone, the intensive diagram theorem is new. Together, they clarify the hitherto unrecognized role of two normalization schemes: A wave function must be (intermediately) normalized in a method that describes an intensive (extensive) quantity. We have also derived the ***extensive-intensive consistency theorem***, which stipulates the exact balance between the spaces spanned by extensive and intensive operators in a method that is intended to describe extensive and intensive quantities simultaneously.

On the basis of these theorems, we have put forth a conjecture stating that an *ab initio* electron-correlation method, which thus excludes the Hartree-Fock (HF) method, cannot be simultaneously *variational* and *size consistent*. This is, again, understood in terms of the different roles of the two normalization schemes: A variational method must normalize its wave function, whereas a size-consistent method must use an intermediately normalized wave function, and these two requirements are mutually exclusive.

Monte Carlo MP2 and Monte Carlo explicitly correlated MP2.[1,4,5,8] The conventional algorithms of *ab initio* electron-correlation theories are based on matrix algebra, which is fundamentally non-scalable with respect to the system size or the number of processors in a modern supercomputer. We have sought to completely redesign these algorithms into ones that are more naturally parallel and efficient for larger molecules. As an example of such redesign, we have proposed Monte Carlo (MC) integrations of the correlation energies of MP2. In this ***MC-MP2 method***, the canonical expressions of the perturbation corrections, which are long sums of products of two-electron integrals, are recast into sums of a few high-dimensional integrals, using a Laplace transform. These integrals are then evaluated by the MC method with sampling points generated randomly by the Metropolis algorithm according to a suitably chosen weight function.

The MC-MP2 method eliminates the hotspot of the conventional algorithms, namely, the atomic-orbital-to-molecular-orbital transformation of two-electron integrals, the operation and memory costs of which grow as $O(n^5)$ and $O(n^4)$, respectively, with the number of orbitals (n). By virtue of this elimination, the size dependence of the operation cost of MC-MP2 is drastically reduced to $O(n^2)$ or nearly $O(n^1)$ in the actual observation, while the memory cost also becomes negligibly small. It can be easily and efficiently parallelized into an algorithm nearly free of inter-processor communications, as demonstrated in our initial parallel calculation on the NCSA's Blue Waters supercomputer. This can be viewed as a new branch of quantum Monte Carlo (QMC), perhaps the first diagrammatic and rigorously size-consistent QMC variant, but unlike the conventional variants, it can compute energy differences (such as correlation and self-energies) directly and not as small differences of two noisy total energies and does

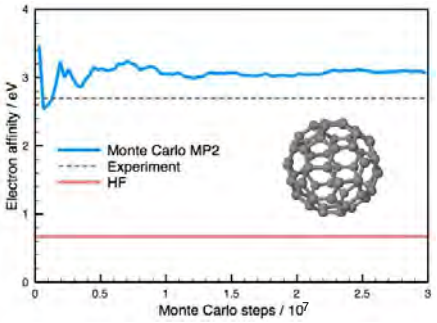

Convergence of the electron affinity of C_{60} evaluated by redundant-walker MC-MP2 for self-energies as a function of Monte Carlo steps. This calculation was run on 320 processors of the Blue Waters supercomputer.

not suffer from the fermion sign problem or related fixed-node errors. While inspired by recent studies that wed *ab initio* wave function theory and QMC (such as projector QMC of Ohtsuka and Nagase), MC-MP2 has the distinct advantage of not having to compute or store the two-electron integrals in any basis.

In collaboration with J. Zhang and E. F. Valeev (Virginia Tech), we have extended this MC algorithm to explicitly correlated MP2 (MP2-F12). This work has been published as Ref. 4.

Research Highlights II. Vibrational Structure Theory

Size-extensive vibrational self-consistent-field (XVSCF) methods.[7,11,16] We have developed diagrammatically size-consistent variants of the vibrational self-consistent-field (VSCF) methods: ***XVSCF(n)*** and ***XVSCF[n]***. Both are based on a Taylor series PES truncated at the *n*th-order force constants and include the connected and thus size-consistent anharmonic contributions to the energy and frequencies of VSCF. XVSCF[*n*] additionally includes the effect of the connected anharmonic contributions to the geometry. We have shown that the one-mode potentials of the XVSCF methods are effectively harmonic with its force constants including the effects of a certain class of even-order force constants. This means that XVSCF does not need any basis functions to expand one-mode functions, a quadrature to evaluate the matrix elements over these functions, or a matrix diagonalization to determine the expansion coefficients, all of which are necessary in VSCF. We have demonstrated, both numerically and analytically, that XVSCF[*n*] and VSCF give the same results in the bulk limit, with the former being orders of magnitude faster than the latter.

We have also introduced the new mathematical constructs of the ***first-order Dyson coordinates and geometry*** in this context. The former are a unitary transformation of the normal coordinates and the anharmonic vibrational counterpart of the Dyson orbitals in electronic structure theory. The first-order Dyson coordinates bring the sums of the harmonic force constants and the first-order diagrammatic perturbation corrections, which are identified as the first-order Dyson self-energies and related to the XVSCF one-mode potentials, to a diagonal form. The first-order Dyson geometry has no counterpart in electronic structure theory and a completely new concept. It is the geometry at which the sums of the energy gradients and the first-order diagrammatic perturbation corrections vanish and is identified as the XVSCF[*n*] geometry. These constructs provide a unified view of the relationship between VSCF and its size-consistent analogues, XVSCF(*n*) and XVSCF[*n*], as well as the so-called self-consistent phonon method widely used in solid-state physics.

Size-extensive vibrational MP2 (XVMP2).[6] We have extended the diagrammatic vibrational method to the second order of many-body perturbation theory. Our new method, ***XVMP2***, solves the vibrational Dyson equation of individual modes self-consistently, taking into account the frequency dependence of the self-energy (the right figure). This is contrasted with conventional vibrational MP2 (VMP2), which is based on the Rayleigh–Schrödinger perturbation theory and calculates the frequencies as differences of the total energies between the ground and excited states. VMP2, therefore, often suffers from divergences in the presence of Fermi resonances, whereas XVMP2 can directly evaluate the frequencies from the self-energy diagrams and resist divergences thanks to the recursive structure of the Dyson equation. The Dyson equation for one mode can also have multiple roots, all of which are meaningful as overtones, combinations, or counterparts of Fermi resonances. It also gives relative intensities as the residues of the poles at those frequencies.

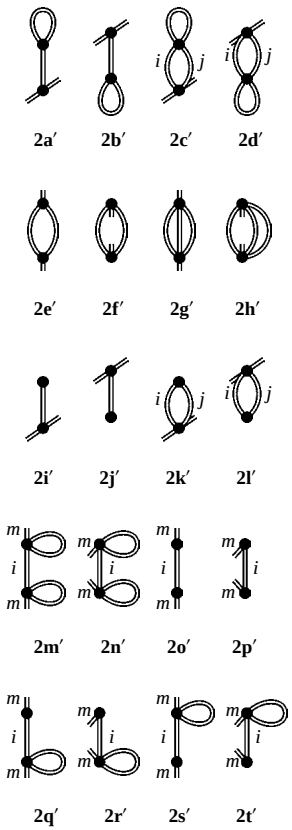

Self-energy diagrams in XVMP2.

Publications of DOE Sponsored Research (2011–Present)

Book chapters

1. S. Hirata, M. Keçeli, Y.-Y. Ohnishi, O. Sode, and K. Yagi, *Annual Reviews of Physical Chemistry* **63**, 131-153 (2012), "Extensivity of energy and size-consistent electronic and vibrational structure methods for crystals."

Refereed articles (reviews, perspectives, and editorials in bold letters)

2. S. Hirata, X. He, M. R. Hermes, and S. Y. Willow, *The Journal of Physical Chemistry A* **118**, 655-672 (2014) [an invited Feature Article], "**Second-order many-body perturbation theory: An eternal frontier**."
3. S. Hirata and I. Grabowski, *Theoretical Chemistry Accounts* **133**, 1440 (2014) (9 pages) [Thom Dunning Special Issue], "On the mutual exclusion of variationality and size consistency."
4. S. Y. Willow, J. Zhang, E. F. Valeev, and S. Hirata, *The Journal of Chemical Physics* (*Communications*) **140**, 031101 (2014) (4 pages), "Stochastic evaluation of explicitly correlated second-order many-body perturbation energy."
5. S. Y. Willow, M. R. Hermes, K. S. Kim, and S. Hirata, *Journal of Chemical Theory and Computation* **9**, 4396-4402 (2013), "Convergence acceleration of parallel Monte Carlo second-order many-body perturbation calculations using redundant walkers."
6. M. R. Hermes and S. Hirata, *The Journal of Chemical Physics* **139**, 034111 (2013) (21 pages), "Second-order many-body perturbation expansions of vibrational Dyson self-energies."
7. M. R. Hermes and S. Hirata, *The Journal of Physical Chemistry A* **117**, 7179-7189 (2013) [Joel M. Bowman Festschrift], "First-order Dyson coordinates and geometry."
8. S. Y. Willow, K. S. Kim, and S. Hirata, *The Journal of Chemical Physics* **137**, 204122 (2012) (5 pages), "Stochastic evaluation of second-order many-body perturbation energies."
9. K. Yagi, M. Keçeli, and S. Hirata, *The Journal of Chemical Physics* **137**, 204118 (2012) (16 pages), "Optimized coordinates for anharmonic vibrational structure theories."
10. R. D. Thomas, I. Kashperka, E. Vigren, W. Geppert, M. Hamberg, M. Larsson, M. af Ugglas, V. Zhaunerchyk, N. Indriolo, K. Yagi, S. Hirata, and B. J. McCall, *Astrophysical Journal* **758**, 55 (2012), "Dissociative recombination of vibrationally cold CH_3^+ and interstellar implications."
11. M. R. Hermes, M. Keçeli, and S. Hirata, *The Journal of Chemical Physics* **136**, 234109 (2012) (17 pages), "Size-extensive vibrational self-consistent field method with anharmonic geometry corrections."
12. G. J. O. Beran and S. Hirata, *Physical Chemistry Chemical Physics* **14**, 7559-7561 (2012) [Guest Editorial in Special Issue on "Fragment and Localized Orbital Methods in Electronic Structure Theory"], "**Fragment and localized orbital methods in electronic structure theory**," (Top 10 most read in May, 2012).
13. S. Hirata and Y.-Y. Ohnishi, *Physical Chemistry Chemical Physics* **14**, 7800-7808 (2012) [Special Issue on "Fragment and Localized Orbital Methods in Electronic Structure Theory"], "Thermodynamic limit of the energy density in a crystal," (A Hot Article)
14. Y.-Y. Ohnishi and S. Hirata, *Chemical Physics* **401**, 152-156 (2012) [Debashis Mukherjee Special Issue], "Charge-consistent redefinition of Fock integrals."
15. S. Hirata, *Theoretical Chemistry Accounts* **131**, 1071 (2012) (4 pages) [an introductory article in the 50th Anniversary Issue], "**Electronic structure theory: Present and future challenges**."
16. M. Keçeli and S. Hirata, *The Journal of Chemical Physics* **135**, 134108 (2011) (11 pages), "Size-extensive vibrational self-consistent field method."
17. Y.-Y. Ohnishi and S. Hirata, *The Journal of Chemical Physics* **135**, 094108 (2011) (10 pages), "Hybrid coupled-cluster and perturbation method for extended systems of one-dimensional periodicity."
18. S. Hirata, *Theoretical Chemistry Accounts* [an invited Feature Article] **129**, 727-746 (2011),"**Thermodynamic limit and size-consistent design**."
19. D. G. Patel, Y.-Y. Ohnishi, Y. Yang, S.-H. Eom, R. T. Farley, K. R. Graham, J. Xue, S. Hirata, K. S. Schanze, and J. R. Reynolds, *Journal of Polymer Science Part B: Polymer Physics* **49**, 557-565 (2011),"Conjugated polymers for pure UV light emission: Poly(*meta*-phenylenes)."

Submitted articles

20. S. Hirata, K. Gilliard, X. He, J. Li, and O. Sode, *Accounts of Chemical Research* (under review, 2014), "**Ab initio molecular crystal structures, spectra, and phase diagrams**."

Generalized Van Vleck Variant of Multireference Perturbation Theory

Mark R. Hoffmann
University of North Dakota
Chemistry Department
Grand Forks, ND 58202-9024
Email: mhoffmann@chem.und.edu

I. Project Scope

There is a continuing need to develop new, cutting edge theoretical and computational electronic structure methods to support the study of complex potential energy surfaces (PESs). While standard methods of computational chemistry are usually adequate for studying the ground electronic states of molecular species near their equilibrium geometries, reaction intermediates, transition states and excited states generally require advanced methods that take into account their multiconfigurational nature. Multireference (MRPT) and quasidegenerate (QDPT) perturbation theories have been demonstrated to be efficient and effective for the description of electron correlation in essentially arbitrarily complex molecules. Recent work demonstrated that the mathematically robust and physically correct structures in our MRPT, called Generalized van Vleck Perturbation Theory (GVVPT), are amenable to highly efficient algorithms. Specifically, second- and third-order approximations of GVVPT (i.e., GVVPT2 and GVVPT3) utilize routines in common with our efficient macroconfiguration-based, configuration-driven MRCISD[1]. Consequently, theoretical and computational development can proceed by first addressing the structurally simpler equivalent CI problem. Chemical problems that are not addressed readily by other theoretical methods become accessible to MRPT or QDPT: problems such as the descriptions of large regions of excited electronic state PESs of polyatomics, especially when the characters of the excited states are doubly excited relative to the ground state, and the characterizations of multiple PESs of the same symmetry in close proximity. Within the scope of this grant, we apply these theoretical techniques primarily to combustion-relevant Group 15 and 16 oxides, and to develop their descriptions of derivative and spin-orbit nonadiabatic couplings.

II. Recent Progress

A.1. GVVPT2 Molecular Derivatives and Nonadiabatic Coupling Terms. The fully variational Lagrangian functional formalism[2] provided, in past reporting periods, the framework to construct analytical formulas for GVVPT2[LoP1, LoP2] and MRCISD[3] molecular gradients and nonadiabatic coupling terms. Efforts to scale-up beyond transformation-based approaches, to iterative techniques, continue to be faced with puzzling convergence issues that manifested themselves in the need to use unfeasibly large Lanczos or Arnoldi subspaces. It was thought, and reported in the 2013 Abstract, that the source of the instability was the commonly used parameterization of the CI vectors in the MCSCF space and the affiliated constraint equation and that a reparametrization in which the MCSCF space responses are parameterized in terms of state rotations will resolve the difficulty. Unfortunately, after extensive numerical experiment in this past year, this proved to be false.

In the past year, our analysis shows that the source of the instability is likely due to the use of numerical techniques appropriate to convex surfaces (e.g. the Lagrangian multiplier approach or, equivalently, constrained variational approach) to an inherently non-convex surface.[4] It appears that this class of problem has not been previously addressed (or at least not widely discussed) in the molecular electronic structure literature. In words, the problem is that none of the wave function parameters (with the exception of the rather trivial configuration amplitudes of the effective Hamiltonian) are stationary with respect to energy. This contrasts strongly with the situation in MRCISD, in which the MCSCF parameters are non-stationary (with respect to the MRCISD energy), but the CI amplitudes are not only stationary but strict minima.

Efforts to understand the topology of the space of wave function parameters for GVVPT2 has led to the development of randomized single valued decomposition[5] approaches to electronic structure. In

completed studies, we have shown that randomized SVD produces meaningful and accurate solutions for an asymptotically stable (in the Lyapunov sense) series, such as produced by garden-variety, closed-shell MP2 or even by a quartically confined hydrogen atom. Work is underway to develop programs to support the large-scale (i.e., high dimensionality) vector spaces of relevance to GVVPT2.

A.2. Relativistic Effects. Two types of relativistic effects are considered within the scope of this project. One is the scalar (or spin-free) contribution and the other is spin-orbit coupling. The standard approach starts with approximations to the spin-free relativistic Hamiltonian (such as the second-order Douglas-Kroll-Hess (DKH) approximation or the zero-order regular approximation (ZORA)), and grafts onto such calculations spin-orbit coupling (often using some approximation to the Breit-Pauli operator). This protocol, while useful in many respects, is not entirely satisfactory.[6] Finite order approximations to the kinematic (or scalar relativistic) effects can have slow convergence, especially for heavier elements. Achievement of a model chemistry appropriate to the entire periodic table recommends that an alternative procedure be pursued. During the past year, we have realized a spin-free exact two-component (X2C)[7] within our GVVPT2 approach.[8] Although the approach is yet to be demonstrated on Group 15 and 16 oxides, we have used it successfully on some highly problematic first- and second-row transition metal dimers (including the ever popular Cr_2). In particular, we have generated the first-ever complete potential energy curves of the lowest three states of Y_2, which correlate to the same asymptotic atomic states. Our implementation of sf-X2C for MCSCF and GVVPT2 appears robust and, unless some hitherto unsuspected problem arises, can be considered completed.

The situation with spin-dependent relativistic effects is much less clear. Contrary to expectations, spin-dependent X2C converges slowly (albeit monotonically) with order.[7] Evidence suggests that a partitioning that is reminiscent of Douglas-Kroll-Hess, but with a different unperturbed operator, produces quite satisfactory results in low order.[7] In the past year, work has been refocused from producing an effective one-electron spin-orbit operator (for use in GVVPT2) that is derived from rigorous separation of the spin-dependent part from the spin-independent parts of the X2C operator to one that is obtained from the Douglas-Koll-Hess-like representation of spin dependence. It is conjectured that an effective one-electron spin-orbit operator can be developed that is related to the full spin-dependent DKH-like treatment in much the same manner that atomic mean field integrals[9] (AMFI) are derived from the Breit-Pauli operator will be efficacious. Calculation of the true one-electron contribution (i.e., essentially the pVp-type integral with the scalar product replaced by a vector product) using efficient Obara-Saika recursion has been refined in the preceding year for our software platform. Particular attention was paid to the symmetry properties, as the effective one-electron integrals that include the two-electron contributions through AMFI, will have the same symmetries.

B.1. Selenium Oxides GVVPT2 calculations on the monoselenium oxides (SeO, SeO_2 and SeO_3) and some of their dimers (Se_2O_3 and Se_2O_5) were completed last year and the results published.[LoP4] Since the selenium oxide studies were emphasized in last year's Abstract, this Abstract only summarizes the new findings. In particular, it was recently found that the thermodynamics of the selenium oxides favor production of the dimers from the monomers and that the more highly oxidized Se_2O_5 was more stable than the less oxidized Se_2O_3.

$SeO + SeO_2 \rightarrow Se_2O_3$	-7.4 kcal/mol
$SeO_2 + SeO_3 \rightarrow Se_2O_5$	-19.4 kcal/mol
$Se_2O_3 + O_2 \rightarrow Se_2O_5$	-49.5 kcal/mol

As barriers for the formation of the diselenium oxides were not prohibitive, our work was the first (either experimental or theoretical) to identify the accretion of this trace element as a factor that models of coal combustion should consider including.

B.2. Arsenic Oxides With the completion of the selenium oxide work, and with the caveat that we still wait for experimental studies that may call for additional studies, focus has shifted in the past year to examining another major trace element of coal combustion, namely arsenic. Based on the completed selenium oxide work, and earlier work on nitrogen oxides, studies of plausible oxides containing one or two arsenic were performed.[LoP5] The studies followed much the same protocol as did the selenium oxides study. Specifically, geometries were optimized as the B3LYP level, with verification of suitability against GVVPT2 and CR-CC(2,3)[10] for a select number of compounds, followed by single point energy calculations using GVVPT2, with comparison with CR-CC(2,3) for a number of the more traditionally bound isomers.

The active orbitals for the dimeric arsenic oxides were also divided into two subgroups as were the monomers and the selenium oxides. The high (single point) energy occupied orbitals and the low energy unoccupied orbitals comprised the two groups. The model space was generated by allowing all one and two electron excitations from the first to the second group. This procedure, which used our macroconfiguration-based configuration generation program, allowed us to generate a small active space than nonetheless spanned the most important configurations of a large number of orbitals. Specifically, the energy calculations of the isomers and transition states of As_2O_3 used 20 active orbitals (i.e., the 2s and 2p of O, and the 4s and 4p of As) which contained 28 electrons (28e, 20o) that were distributed as G_1 = (13-18a_1 5a_2 6-9b_1 11-13b_2, in C_{2v} symmetry for isomer 1 (see Figure), 23-31a' 10-14a", in C_s symmetry for isomer 2, or simply 32-45a in C_1 symmetry) and G_2 = (19-20a_1 6a_2 10b_1 14-15b_2, in C_{2v} symmetry, 32-35a' 15-16a", in C_s symmetry, or simply 46-51a in C_1 symmetry). For isomer 4 of As_2O_3, the MCSCF calculation used 17 active orbitals (i.e., the 2p of O, and the 4s and 4p of As) which contained 22 electrons (22e, 17o) that were distributed as G_1 = (27-33a' 9-12a") and G_2 = (34-38a' 13a"), while in the GVVPT2 treatment, the oxygen 2s dominated molecular orbitals were correlated which introduced three additional orbitals into the GVVPT2 occupied space (24-26a", in C_s symmetry). GVVPT2 calculations were then performed allowing all one and two electron excitations from all active orbitals plus those from the lower energy occupied orbitals (i.e., "core") to the higher energy unoccupied orbitals (i.e., "virtual"). Excitations from the core to the active, as well as all semi-internal excitations, were also allowed at the GVVPT2 stage.

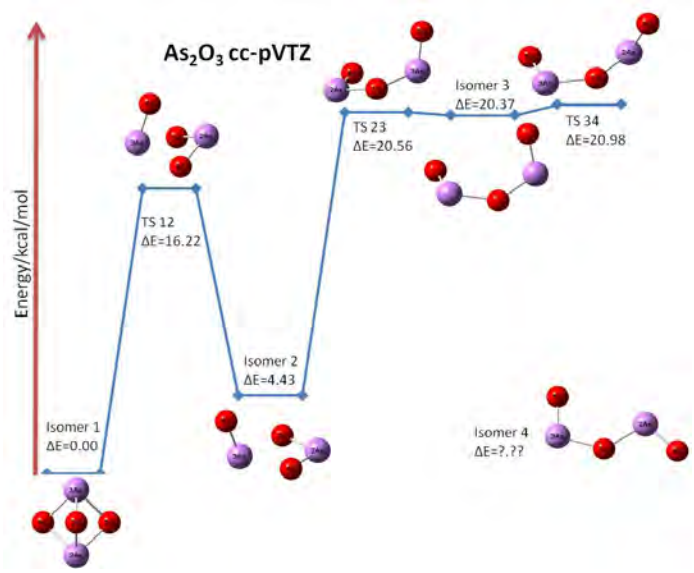

III. Future Work

We expect continued progress in both the advancement of nuclear derivative and relativistic effects for GVVPT2 and MRCISD in applications to primarily Group 15 and 16 oxides. The highest priority vis-à-vis GVVPT2 continues to be resolution of the scale-up issue for gradients. However, as was determined in the previous year, the problem is not a simple programming issue, but will require exploration of appropriate non-convex numerical algorithms. Progress on scale-up of determination of the GVVPT2 nonadiabatic coupling matrix

elements is expected to follow, since the response matrix is identical between GVVPT2 gradients and nonadiabatic couplings. Using the in-house configuration-driven UGA code, spin-dependent Douglas-Kroll-Hess-like effective one-electron spin-orbit coupling matrix elements should become better integrated with our program suite ("undmol"). This framework should provide a theoretically more consistent alternative to the widely used Breit-Pauli operator based approach, and will be compared. Together with the recently realized inclusion of spin-free exact two-component (X2C) treatment of kinematic effects, robust relativistic MRCISD and GVVPT2 computer programs, appropriate for much of the periodic table, will be pursued. As production computer codes become available, we intend to refine the Se_mO_n and As_mO_n potential energy surfaces, and develop corresponding Sb_mO_n surfaces, with inclusion of nuclear derivative and spin-orbit nonadiabatic coupling. Similarly, our studies on O_3 (and now HO_3) and the NO+NO surfaces, which were examined earlier by us at the GVVPT2 level using only energy calculations, will be re-examined as the new spin-orbit and nonadiabatic coupling codes become available. Plans are to consider dynamical and kinematical features of the surfaces.

IV. References

[1] W. Jiang, Y. G. Khait, and M. R. Hoffmann, *J. Phys. Chem. A* **113**, 4374 (2009).

[2] T. Helgaker and P. Jørgensen, *Adv. Quantum Chem.* **19**, 183 (1988); *Theor. Chim. Acta* **75**, 111 (1989).

[3] Y. G. Khait, D. Theis, and M. R. Hoffmann, *Mol. Phys.* **108**, 2703-2716 (2010).

[4] A. Y. Azimov and R. N. Gasimov, *Cybern. Syst. Anal.* **38**, 412 (2002).

[5] N. Halko, P. G. Martinsson and J. A. Tropp, arXiv:09094061v2 [math.NA] (2010).

[6] W. Liu, *Mol. Phys.* **108**, 1679 (2010).

[7] Z. Li, Y. Xiao, and W. Liu, *J. Chem. Phys.* **137**, 154114 (2012).

[8] P. K. Tamukong, M. R. Hoffmann, Z. Li, and W. Liu, *J. Phys. Chem. A* **118**, 1489 (2014).

[9] B. A. Hess, C. M. Marian, U. Wahlgren, and O. Gropen, *Chem. Phys. Lett.* **251**, 365 (1996).

[10] P. Piecuch, M. Wloch, J. R. Gour, and A. Kinal, *Chem. Phys. Lett.* **418**, 467 (2006).

V. Publications and Submitted Journal Articles Supported by this Project 2011-2013

[LoP1] D. Theis, Y. G. Khait, and M. R. Hoffmann, GVVPT2 energy gradient using a Lagrangian formulation, *J. Chem. Phys.* **135**, 044117/1–14 (2011).

[LoP2] Y. G. Khait, D. Theis, and M. R. Hoffmann, Nonadiabatic coupling terms for the GVVPT2 variant of multireference perturbation theory, *Chem. Phys.* **401**, 88–94 (2012).

[LoP3] T. J. Dudley, J. J. Howard, and M. R. Hoffmann, Generalized Van Vleck Perturbation Theory Study of Chlorine Monoxide, *AIP Conf. Proc.* **1504**, 582-585 (2012).

[LoP4] R. M. Mokambe, J. M. Hicks, D. Kerker, W. Jiang, D. Theis, Z. Chen, Y. G. Khait, and M. R. Hoffmann, GVVPT2 Multireference Perturbation Theory Study of Selenium Oxides, *Mol. Phys.* **111**, 1078–1091 (2013).

[LoP5] J. Hicks, Theoretical Studies of Oxides Relevant to the Combustion of Fossil Fuels, M.S. Thesis, Grand Forks, December 2013.

Theoretical Methods for Pressure Dependent Kinetics and Electronically Nonadiabatic Chemistry

Ahren W. Jasper
Combustion Research Facility, Sandia National Laboratories
Livermore, CA 94551-0969
ajasper@sandia.gov

I. Program Scope

In favorable cases, elementary chemical kinetics calculations can aid in the interpretation of experimental rate measurements and inform the development of comprehensive and detailed models of combustion. The predictive accuracy of chemical kinetics calculations is improving and generally approaching so-called "kinetic accuracy," defined as a factor of 2 in the calculated rate coefficient. This term may be compared with the 1990s realization of "chemical accuracy" (~1 kcal/mol) in thermochemistry, when calculated thermochemistry began to be accurate enough to be used alongside experimental values. A similar situation is emerging in chemical kinetics thanks to ongoing improvements in computational power and theoretical methods. The principal goal of this project is to develop and validate new theoretical methods designed to broaden the applicability and improve the accuracy of theoretical chemical kinetics and to aid in the realization of kinetic accuracy for applications throughout combustion. The model developments we are presently focused on are: (1) predicting pressure dependence in elementary reactions using detailed master equation models of energy transfer informed by classical trajectories, (2) more accurately characterizing spin-forbidden kinetics using both multistate trajectory methods and statistical theories, and (3) predicting anharmonic vibrational properties for polyatomic molecules at combustion temperatures via Monte Carlo phase space integration.

II. Recent Progress

Ensembles of classical trajectories were used to calculate moments of the total energy and total angular momentum transferred due to the collisions for several systems. As we are principally interested in low-order moments, we may expect the classical approximation to be a good one. The dominant source of error in these calculations instead likely arises from the choice of the potential energy surface. These calculations require full-dimensional potential energy surfaces, and we have pursued two strategies for obtaining them.

We have carried out direct dynamics collisional energy transfer trajectory calculations, where the potential energy surface was calculated using MP2 and double-ζ basis sets. The quality of the MP2 potentials was validated by comparing cuts through the interaction potential with those from higher-level quantum chemistry methods and then optimizing details of the basis set and/or scaling the correlation energy. This MP2-based approach accurately reproduces anisotropies in the interaction potentials while remaining efficient enough for the trajectory calculations. This approach is particularly useful for systems with strongly anisotropic interaction potentials, such as $CH_4 + H_2O$.

For systems with weaker interactions and/or with less anisotropy, simple pairwise interaction potentials are often accurate. We have used direct dynamics trajectory results for CH_4 + He, Ne, and H_2, C_2H_5 + He, and C_2H_6 + He to test the accuracy of the pairwise approximation for the interaction potential. We further tested the accuracy of using the interaction potentials obtained for CH_4 + M for systems larger than methane, i.e., we tested the accuracy of using methane's interaction parameters as universal C_xH_y + M interaction parameters. For the systems we considered, results obtained using the universal C_xH_y + M potentials were found to agree with direct dynamics results within the statistical uncertainties of the calculations, except near 300 K where the universal C_xH_y + M potentials somewhat

over-predicted the direct dynamics results (by ~20%). The resulting universal potentials are very efficient relative to direct dynamics and may be used to study systems with dozens of C atoms.

We used the universal C_xH_y + M potential to evaluate Troe's collision efficiency (and an approximation to it) for seven atomic and diatomic baths and for molecules and radicals as large as octane. In total, 266 systems were studied, including normal, branched, cyclic, and unsaturated hydrocarbon molecules, as well as hydrocarbon radicals interacting with the seven baths. These collision efficiencies are simple functions of the first moment of the energy transferred in deactivating collisions, $<\Delta E_d>$. We also considered the *rotational* collision efficiency for several systems by calculating the first moment of the angular momentum transferred in deactivating collisions, $<\Delta J_d>$. Trends in the collision efficiencies with respect to the bath gas, its temperature, and the size and chemical structure of the hydrocarbon target were quantified and discussed.

Collisional energy transfer for the CH_4 + H_2O system was studied in detail, and the results for this bath were compared with those for atomic and diatomic baths considered previously. For example, the collision efficiency of water relative to argon was found to depend on temperature and to vary from 3 at 300 K to 7 at 2000 K. We also quantified the kinetic effect of incomplete rotational collision efficiency for the different baths. We found that water completely equilibrated rotations only at low temperatures, and that none of the other baths completely equilibrated rotations at any of the temperatures considered. Nonetheless, low-pressure rate coefficients calculated using a model that assumes statistically equilibrated rotations were shown to be accurate at combustion temperatures and for the heavier baths at all temperatures. At low temperatures and for He, however, weak-collider-in-*J* effects were found to reduce the predicted low-pressure-limit rate coefficients by a factor of 2.

Several simple methods for predicting Lennard-Jones parameters for use as transport parameters in detailed chemical kinetics models and for calculating collision rate coefficients in elementary kinetics calculations were tested. The "one-dimensional minimization" method was found to be both accurate and efficient. In this method, the two interacting species are randomly oriented with respect to one another, and the interaction potential is minimized for this fixed orientation. The process is repeated for several orientations, and the resulting set of minimum energies and optimized center-of-mass separations are then averaged to obtain the Lennard-Jones parameters. Collision rates predicted using this method agree well with those based on tabulated parameters (typically within ~10%) for a wide variety of systems.

The high-pressure limit rate coefficient for the spin-forbidden reaction O + CO $\rightarrow$ CO_2 was characterized in detail using a combination of high-level ab initio calculations, diabatic potential energy surface fitting, and electronically nonadiabatic trajectory calculations. The dynamic weighted MRCI method with a large basis set and near full valence active space was used to characterize the lowest-energy singlet and two lowest-energy triplet surfaces. The interpolated moving least squares (IMLS) method was used to fit accurate global analytic representations of the MRCI surfaces along with geometry-dependent calculated spin-orbit coupling surfaces. The coherent switches with decay of mixing semiclassical trajectory method was then used to calculate spin-forbidden rate coefficients corresponding to the high pressure limit. Dynamical details of the coupled-state trajectories were used to analyze the appropriateness of typical assumptions appearing in spin-forbidden statistical models.

Efficient and accurate strategies for performing classical Monte Carlo phase space integrals (MCPSI) for calculating vibrational properties at combustion temperatures have been developed. We showed that the classical phase space integration could be done more efficiently using natural (z-matrix, curvilinear) coordinates instead of Cartesian normal mode coordinates. A general and convenient strategy for using curvilinear coordinates for molecular systems was obtained via numerical evaluations of Jacobian. For methane, we compared our classical anharmonic MCPSI partition functions with those obtained via quantum mechanical VCI calculations. The classical MCPSI results are fairly accurate at combustion temperatures and can be made quantitative via simple Pitzer-Gwinn corrections to the classical anharmonic partition functions.

To better enable practical MCPSI calculations for large molecular systems, we have approximated the full-dimensional phase space integral via a hierarchy of expressions based on so-

called "*n*-mode intrinsic" state densities. The 2-mode (pairwise) intrinsic state density, for example, is defined for a pair of vibrational coordinates as the vibrational state density not represented by the convolution of the one-dimensional state densities for each of the coordinates. The low-order state densities used to define the intrinsics are evaluated via MCPSI and contain all of the anharmonicity within the modes considered, i.e., no Taylor's series truncation of the potential is required, and so the method may be applied to nonlocal motions such as torsions. The full-dimensional state density is then approximated via convolutions of the intrinsic state densities with low-order state densities for remaining degrees of freedom. We found that very accurate full-dimensional anharmonic state densities could be recovered by considering only pairwise intrinsic state densities. The computational cost scales much better with respect to the size of the system via this pairwise approximation relative to full-dimensional MCPSI.

The H-assisted isomerization kinetics of fulvene → benzene was studied in detail, and the importance of similar processes involving isomers of naphthalene was discussed. These fast isomerizations proceed via a cyclopropylcarbinyl intermediate—a substituted cylcopropyl group adjacent to a radical carbon—that provides a facile route for carbon bonding rearrangement. If sufficiently fast in larger systems, such processes may promote thermodynamic equilibrium among isomeric PAHs, thus simplifying the development of detailed reaction mechanisms for PAH growth.

We have analyzed the applicability of transition state theory for the nontrivial case of roaming radical reactions. The conditions under which competing tight processes (e.g., those with conventional 3-center transition state geometries) and roaming processes for molecular elimination may be accurately treated as dynamically separable were analyzed, and a formal foundation for understanding this separability was developed. We showed that tight and roaming mechanisms may be treated as separable to a good approximation, and we identified features of the potential energy landscape that serve as mechanism dividers (second order saddle points or minimum energy points on conical intersections). Importantly, competing mechanisms may be *dynamically* separable even when the two regions are not energetically separated and even when there is no intrinsic feature of the potential energy surface associated with the mechanism divider.

III. Future Work

We will continue the development of predictive models for pressure dependence in chemical kinetics. We will apply our direct dynamics collisional energy transfer trajectory methods to new classes of targets, including CH_3OH and CH_3Cl. Enhanced energy transfer for halogens and alcohols has been reported, and the trajectory studies will be used to elucidate the dynamical mechanisms of these enhancements. As discussed above, existing models for collisional energy transfer used in master equation calculations ignore the effect of changes in angular momentum due to collisions or use simple models to describe this dependence. We will explicitly include this effect and other trajectory-based details in new models for use in master equation calculations, with parameters obtained via our classical trajectory methods and validated potential energy surfaces. This work is being carried out in collaboration with Miller and Klippenstein at Argonne.

We will continue our ongoing studies of collisional energy transfer in the NO_2* + Ar system. This theoretical work is being carried out in collaboration with CRF experimentalists Chandler and Steill. Detailed theoretical/experimental comparisons will be made, and future work will consider the effect of electronically nonadiabatic transitions due to collisions.

Several elementary chemical kinetics studies will be carried out. For example, H-assisted isomerizations for substituted fulvenes will be studied in collaboration with Argonne experimentalist Tranter. Pressure-dependence in the O + CO reaction will be fully characterized theoretically, as motivated by the recent modeling studies of Haas, Dryer, and co-workers.

The MCPSI method will continue to be applied and developed. We will focus on systems where the accuracy of existing vibrational anharmonicity approaches is not known, such as those involving constrained torsions and rings. We will also adapt our curvilinear *n*-mode MCPSI strategies

for calculating classical fluxes through transition state dividing surfaces, where care must be taken when projecting out the curvilinear reaction coordinate.

We propose to continue to develop and validate theoretical methods for studying electronic state transitions in chemistry. Specifically, we will use short-time multistate trajectories to calculate improved spin-forbidden transition probabilities that, unlike the Landau-Zener approximation, include multidimensional dynamical effects. These multidimensional transition probabilities will be used in statistical calculations, where complex reactions with competing spin-forbidden and spin-allowed pathways can be accurately studied. This proposed work is entirely analogous to the development of modern treatments of tunneling, where it is recognized that there are significant differences in one-dimensional and multidimensional models of this quantum effect. Our preliminary calculations suggest that multidimensional effects can contribute up to an order of magnitude of error in the spin-forbidden transition probabilities. Initial studies are underway for the reactions: O + CO, H + HO_2, H + NCO, and O + alkenes.

IV. AITSTME

The AITSTME project (PI: Klippenstein, Argonne) is part of the Predictive Theory and Modeling component of the Materials Genome Initiative and supports the integration of several chemical kinetics codes actively being developed at Argonne and Sandia. In the past year, we have used our AITSTME funding to develop two published codes. `DiNT` (sandia.gov/~ajasper/dint/) is a general trajectory code capable of nonadiabatic trajectory calculations (including those for the spin-forbidden kinetics reported in Ref. 4) as well as energy transfer calculations (including those reported in Refs. 1 and 3). `OneDMin` (sandia.gov/~ajasper/onedmin/) is a code for efficiently approximating Lennard-Jones parameters from full-dimensional interaction potentials via the "one-dimensional minimization" method described in Ref. 2. Our universal C_xH_y + M potential energy surfaces are distributed as part of both codes. In the next year, we will continue to develop several codes, with the AITSTME-funded goals of generalizing and documenting them such that they can usefully be made available online. Two codes currently being developed are `mcPSI`, a Monte Carlo phase space integral code containing the methods described in Refs. 5 and 6, and `K0`, a two-dimensional master equation code for calculating low-pressure-limit unimolecular rate coefficients using trajectory-based energy transfer functions. This work will be carried out in close collaboration with the chemical kinetics code development of Miller and Klippenstein at Argonne.

V. Publications supported by this project since 2012

1. "Third-body" collision efficiencies for combustion modeling: Hydrocarbons in atomic and diatomic baths, A. W. Jasper, C. M. Oana, and J. A. Miller, *Proc. Combust. Inst.*, 35, accepted.
2. Lennard-Jones parameters for combustion and chemical kinetics modeling from full-dimensional intermolecular potentials, A. W. Jasper and J. A. Miller, *Combust. Flame* 161, 101 (2014).
3. The collision efficiency of water in the unimolecular reaction CH_4 (+ H_2O) $\rightarrow$ CH_3 + H (+ H_2O): One-dimensional and two-dimensional solutions of the low-pressure-limit master equation, A. W. Jasper, J. A. Miller, and S. J. Klippenstein, *J. Phys. Chem. A* 117, 12243 (2013).
4. Non-Born–Oppenheimer molecular dynamics of the spin-forbidden reaction $O(^3P)$ + $CO(X\ ^1\Sigma^+)$ ~> CO_2 ($X\ ^1\Sigma_g^+$), A. W. Jasper and R. Dawes, *J. Chem. Phys.* 139, 154313 (2013).
5. Anharmonic vibrational properties from intrinsic *n*-mode state densities, E. Kamarchik and A. W. Jasper, *J. Phys. Chem. Lett.* 4, 2430 (2013).
6. Anharmonic state counts and partition functions for molecules via classical phase space integrals in curvilinear coordinates, E. Kamarchik and A. W. Jasper, *J. Chem. Phys.* 138, 194109 (2013).
7. Hydrogen-assisted isomerizations of fulvene to benzene and of larger cyclic aromatic hydrocarbons, A. W. Jasper and N. Hansen, *Proc. Combust. Inst.* 34, 279 (2013).
8. Separability of tight and roaming pathways to molecular decomposition, L. B. Harding, S. J. Klippenstein, and A. W. Jasper, *J. Phys. Chem. A* 16, 6979 (2012).

Probing the Reaction Dynamics of Hydrogen-Deficient Hydrocarbon Molecules and Radical Intermediates via Crossed Molecular Beams

Ralf I. Kaiser
Department of Chemistry, University of Hawai'i at Manoa, Honolulu, HI 96822
ralfk@hawaii.edu

1. Program Scope

The major goals of this project are to explore experimentally in crossed molecular beams experiments the reaction dynamics and potential energy surfaces (PESs) of hydrocarbon molecules and their corresponding radical species, which are relevant to combustion processes. The reactions are initiated under single collision conditions by crossing two supersonic reactant beams containing radicals and/or closed shell species under a well-defined collision energy and intersection angle. By recording angular-resolved time of flight (TOF) spectra, we obtain information on the reaction products, intermediates involved, branching ratios of competing reaction channels, reaction energetics, and on the underlying reaction mechanisms. These data are of crucial importance to comprehend the formation of resonantly stabilized free radicals (RSFRs) and (substituted) polycyclic aromatic hydrocarbons (PAHs) together with their hydrogen deficient precursors in combustion flames.

2. Recent Progress

2.1. Formation of Monocyclic Aromatic Molecules

We disseminated the synthetic routes to the formation of the toluene molecule ($C_6H_5CH_3$; C_7H_8) and benzyl radical ($C_6H_5CH_2$; C_7H_7) under single collision conditions via the reactions of the D1-ethynyl radical (CCD) and dicarbon molecules (CC) with isoprene (2-methyl-1,3-butadiene; C_5H_8). Combining the crossed beam experiments with electronic structure and RRKM calculations (Alexander Mebel, FIU), our investigations revealed the very first experimental evidence – contemplated by theoretical studies – that under single collision conditions a methyl-substituted aromatic hydrocarbon molecule (toluene) and its corresponding radical (benzyl) can be formed via reaction of two acyclic molecules involving cyclization processes at collision energies relevant in combustion flames. Further, our studies provided evidence that the replacement of a hydrogen atom by a methyl group within a closed shell unsaturated hydrocarbon reactant (1,3-butadiene versus 2-methyl-1,3-butadiene) can have a profound impact on the reaction dynamics (hydrogen atom loss from the methyl groups) suggesting that the methyl group does not necessarily act as a spectator (P15, P19).

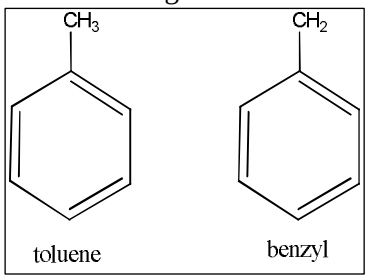

2.2. Formation of Bicyclic Aromatic Hydrocarbon Molecules

Considering our unique capabilities to synthesize bicyclic PAH molecules (indene (P6), naphthalene (P10), dihydronaphthalene (P13)) via reactions of the phenyl radical (C_6H_5) with unsaturated C3 and C4 hydrocarbons under single collision conditions, we have expanded our studies to the next level and are investigating the formation of methyl-substituted PAHs. For this, we generated an intense supersonic beam of p-tolyl (4-methylphenyl) radicals ($C_6H_4CH_3$) and the perdeuterated counterpart ($C_6D_4CD_3$) via photodissociation of p-chlorotoluene (4-chlorotoluene) at 193 nm and probed the reactions with unsaturated C3 to C5 hydrocarbons allene/methylacetylene (C3), vinylacetylene/1,3-butadiene (C4), and isoprene (C5) (P20). These are currently being analyzed and disseminated (Fig. 1). The studies were conducted in collaboration with Prof. Mebel (Florida International University) and Prof. Morakuma (Emory) to investigate the bimolecular reactions computationally.

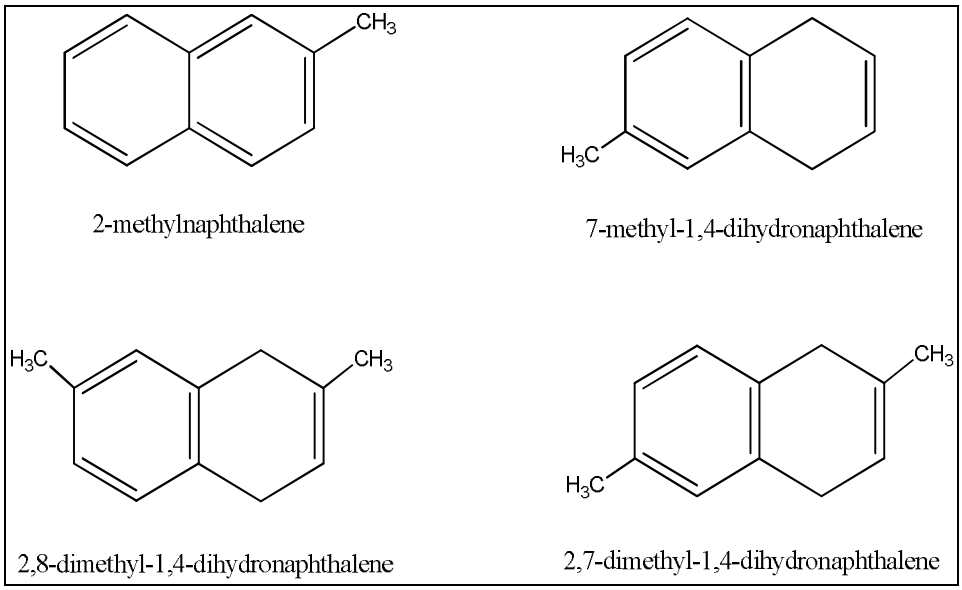

Fig. 1: Formation of methyl substituted PAHs 2-methylnaphthalene [vinylacetylene], 7-methyl-1,4-dihydronaphthalene [1,3-butadiene], as well as 2,8-dimethyl-1,4-dihydronaphthalene and 2,7-dimethyl-1,4-dihydronaphthalene [isoprene] formed via bimolecular reactions of the p-tolyl (4-methylphenyl) radical with unsaturated C4 and C5 hydrocarbons as specified in square parenthesis. The synthesis of methyl-substituted indene species via reaction of the p-tolyl radical with allene and/or methylacetylene is currently under investigation.

2.3. Formation of Resonantly Stabilized Free Radicals (RSFRs)

We also probed the formation of resonantly stabilized C_5H_5 and C_6H_5 radicals via the reaction of dicarbon molecules with propylene (C_3H_6) and with distinct C_4H_6 isomers 1-butyne, 2-butyne, and 1,2-butadiene under single collision conditions (P16, P21). These reactions revealed the synthesis of acyclic doublet radicals, which are isomers of the thermodynamically more stable cyclopentadienyl and phenyl radicals, respectively. These studies were conducted in collaboration with Prof. Mebel (Florida International University) to investigate these bimolecular reactions computationally.

2.4. Growth and Destruction of Aromatic Molecules - Photoionization Studies at the ALS

To yield further insights into the chemistry of the phenyl radical – the key growth species leading to PAH formation - under combustion relevant conditions it is important to unravel not only the molecular growth pathways from reactions with (unsaturated) hydrocarbons, but also the destruction pathways of the phenyl radical upon reaction with molecular oxygen. Here, we expanded our collaboration with Musa Ahmed (LBNL) at the Chemical Dynamics Beamline and probed the outcome of two key reactions of the phenyl radical with acetylene and molecular oxygen in a high temperature 'chemical reactor'. These reactions are conducted in a supersonic molecular beam through reaction of pyrolytically generated phenyl radicals (C_6H_5) with acetylene and oxygen, respectively, inside a heated silicon carbide tube ('chemical reactor'). The products formed are then photoionized by vacuum ultraviolet (VUV) light from the Advanced Light Source at various photon energies from 7.5 to 12 eV to record photoionization efficiency (PIE) curves. Based on known PIE curves of known/calibrated isomers, the recorded PIE curves are then simulated to extract the nature of the products formed and their branching ratios over a range of combustion-relevant reaction vessel temperatures and pressures.

Despite the popularity of the HACA mechanism in PAH formation, this mechanism has not been verified experimentally to date. Exploiting a 'chemical reactor' to simulate combustion conditions, we verified for the first time that the HACA mechanism can produce phenylacetylene (C_8H_6) and the prototypical PAH naphthalene ($C_{10}H_8$) in the reaction of phenyl radicals (C_6H_5) with acetylene (C_2H_2). Formation of

phenylacetylene through hydrogen emission is the first step in the HACA mechanism sequence involving acetylene addition to an aromatic radical, here the phenyl radical. The second step, a subsequent acetylene addition to the C_8H_7 intermediate ultimately yields naphthalene ($C_{10}H_8$) through cyclization and hydrogen abstraction/addition (Fig. 2). – The data of the phenyl – oxygen system are currently being analyzed.

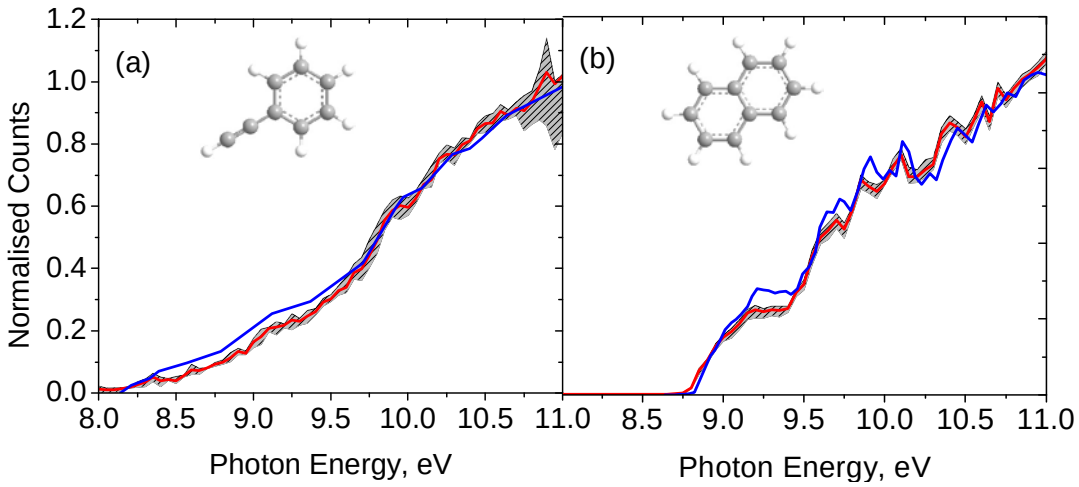

Fig. 2: Experimentally obtained photoionization efficiency (PIE) curves recorded at m/z = 102 and 128 shown as red line along with experimental errors defined as a hatched area. The blue line show the experimentally determined reference PIE curves for (a) phenylacetylene and (b) naphthalene.

3. Future Plans

We planning to expand our studies on the formation of prototype methyl-substituted PAHs with indene and naphthalene cores via reactions of *aromatic* and *resonantly stabilized* C_7H_7 radicals (benzyl; o- and m-methylphenyl) with C2 – C4 hydrocarbons (acetylene, methylacetylene, allene, vinylacetylene, 1,3-butadiene) in collaboration with Prof. Mebel. Further, we continue the elucidation of the formation and destruction of PAHs and their radicals in the pyrolysis reactor in collaboration with Musa Ahmed (LBNL) at the Chemical Dynamics Beamline.

4. Acknowledgements

This work was supported by US Department of Energy (Basic Energy Sciences; DE-FG02-03-ER15411).

5. Publications Acknowledging DE-FG02-03ER15411 (1/2011 – now)

P1 P. Maksyutenko, F. Zhang, X. Gu, R.I. Kaiser, *A Crossed Molecular Beam Study on the Reaction of Methylidyne Radicals [CH($X^2\Pi$)] with Acetylene [$C_2H_2(X^1\Sigma_g^+)$] – Competing C_3H_2 + H and C_3H + H_2 Channels.* Physical Chemistry Chemical Physics 13, 240-252 (2011).

P2 D.S.N. Parker, F. Zhang, Y.S. Kim, R.I. Kaiser, A.M. Mebel. *On the Formation of the Resonantly Stabilized C_5H_3 Radicals - A Crossed Beam and Ab Initio Study of the Reaction of Ground State Carbon Atoms with Vinylacetylene.* The Journal of Physical Chemistry A 115, 593-601 (2011).

P3 F. Zhang, R.I. Kaiser, V. Kislov, A.M. Mebel, A. Golan, M. Ahmed, *A VUV Photoionization Study of the Formation of the Indene Molecule and its Isomers.* The Journal of Physical Chemistry Letters 2, 1731-1735 (2011).

P4 R.I. Kaiser, M. Goswami, P. Maksyutenko, F. Zhang, Y.S. Kim, A.M. Mebel, *A Crossed Molecular Beams and Ab Initio Study on the Formation of C_6H_3 Radicals - An Interface between Resonantly Stabilized (RSFRs) and Aromatic Radicals (ARs).* The Journal of Physical Chemistry A 115, 10251-10258 (2011).

P5 D.S.N. Parker, F. Zhang, R.I. Kaiser, *Phenoxy Radical (C_6H_5O) Formation under Single Collision Conditions from Reaction of the Phenyl Radical (C_6H_5, X^2A_1) with Molecular Oxygen (O_2, $X^3\Sigma_g^-$) – The Final Chapter?* The Journal of Physical Chemistry A 115, 11515-11518 (2011).

P6 D.S.N. Parker, F. Zhang, R. I. Kaiser, V. Kislov, A.M. Mebel, *Indene Formation under Single Collision Conditions from Reaction of Phenyl Radicals with Allene and Methylacetylene – A Crossed Molecular Beam and Ab Initio Study*. Chemistry – An Asian Journal 6, 3035-3047 (2011).

P7 A.V. Wilson, D.S.N. Parker, F. Zhang, R.I. Kaiser, *Crossed Beam Study of the Atom-Radical Reaction of Ground State Carbon ($C(^3P_j)$) with the Vinyl Radical (C_2H_3, X^2A').* Physical Chemistry Chemical Physics 14, 477-481 (2012).

P8 R.I. Kaiser, X. Gu, F. Zhang, P. Maksyutenko, *Crossed Beams Reactions of Methylidyne [$CH(X^2\Pi)$] with D2-Acetylene [$C_2D_2(X^1\Sigma_g^+)$] and of D1-Methylidyne [$CD(X^2\Pi)$] with Acetylene [$C_2H_2(X^1\Sigma_g^+)$].* Physical Chemistry Chemical Physics 14, 575-588 (2012).

P9 R.I. Kaiser, D.S.N Parker, M. Goswami, F. Zhang, V. Kislov, A.M. Mebel, *Crossed Beam Reaction of Phenyl and D5-Phenyl Radicals with Propene and Deuterated Counterparts – Competing Atomic Hydrogen and Methyl Loss Pathways.* Physical Chemistry Chemical Physics 14, 720-729 (2012).

P10 D.S.N Parker, F. Zhang, R.I. Kaiser, V. Kislov, A.M. Mebel, A.G.G.M. Tielens, *Low Temperature Formation of Naphthalene and Its Role in the Synthesis of PAHs in the Interstellar Medium.* Proceedings National Academy of Sciences USA (PNAS) 109, 53-58 (2012).

P11 D.S.N. Parker, F. Zhang, Y. S. Kim, R. I. Kaiser, A. Landera, A. M. Mebel, *On the Formation of Phenyldiacetylene (C_6H_5CCCCH) and D5-Phenyldiacetylene (C_6D_5CCCCH) Studied under Single Collision Conditions.* Physical Chemistry Chemical Physics 14, 2997-3003 (2012).

P12 F. Zhang, R.I. Kaiser, A. Golan, M. Ahmed, N. Hansen, *A VUV Photoionization Study of the Combustion-Relevant Reaction of the Phenyl Radical (C_6H_5) with Propylene (C_3H_6) in a High Temperature Chemical Reactor.* The Journal of Physical Chemistry A 116, 3541-3546 (2012).

P13 R.I. Kaiser, D.S.N. Parker, F. Zhang, A. Landera, V.V. Kislov, A.M. Mebel, *Formation of PAHs and their Derivatives under Single Collision Conditions - The 1,4-Dihydronaphthalene Molecule as a Case Study.* The Journal of Physical Chemistry A 116, 4248-4258 (2012).

P14 A. Golan, M. Ahmed, A. M. Mebel, R.I. Kaiser, *A VUV Photoionization Study on the Formation of Primary and Secondary Products in the Reaction of the Phenyl Radical with 1,3-Butadiene under Combustion Relevant Conditions.* Physical Chemistry Chemical Physics 15, 341-347 (2013).

P15 B.B. Dangi, D.S.N. Parker, R.I. Kaiser, A. Jamal, A.M. Mebel, *A Combined Experimental and Theoretical Study on the Gas Phase Synthesis of Toluene under Single Collision Conditions.* Angew. Chemie Int. Ed. 52, 7186-7189 (2013).

P16 B.B. Dangi, S. Maity, R.I. Kaiser, A.M. Mebel, *A Combined Crossed Beam and Ab Initio Investigation of the Gas Phase Reaction of Dicarbon Molecules (C_2; $X^1\Sigma_g^+/a^3\Pi_u$) with Propene (C_3H_6; X^1A').* The Journal of Physical Chemistry A 117 11783-11793 (2013).

P17 D.S.N. Parker, T. Yang, R. I. Kaiser, A. Landera, A. M. Mebel, *On the Formation of Ethynylbiphenyl ($C_{14}D_5H_5$; $C_6D_5C_6H_4CCH$) Isomers in the Reaction of D5-Phenyl Radicals (C_6D_5; X^2A_1) with Phenylacetylene ($C_6H_5C_2H$; X^1A_1) Under Single Collision Conditions.* CPL (in press 2014).

P18 T. Yang, D.S.N. Parker, B. Dangi, R.I. Kaiser, V.V. Kislov, A.M. Mebel, *Crossed Beam Reactions of the Reaction of Phenyl (C_6H_5; X^2A_1) and D5-Phenyl Radical (C_6D_5; X^2A_1) with 1,2-Butadiene ($H_2CCCHCH_3$; X^1A'),* JPCA (revised version submitted 2013).

P19 B.B. Dangi, D.S.N. Parker, T. Yang, R.I. Kaiser, A.M. Mebel, *A Combined Experimental and Theoretical Study on the Gas Phase Synthesis of the Benzyl Radical ($C_6H_5CH_2$) under Single Collision Conditions.* Angew. Chemie (revised version submitted 2014).

P20 D.S.N. Parker, B. B. Dangi, R.I. Kaiser, A. Jamal, M.N. Ryazantsev, K. Morokuma, A. Korte, W. Sander, *An Experimental and Theoretical Study on the Formation of 2-Methylnaphthalene ($C_{11}H_{10}/C_{11}H_3D_7$) in the Reactions of the Para-Tolyl (C_7H_7) and Para-Tolyl-d7 (C_7D_7) with Vinylacetylene (C_4H_4).* JPCA (submitted 2014).

P21 D.S.N. Parker, S. Maity, B.B. Dangi, R.I. Kaiser, T. Labrador, A. M. Mebel, *Understanding the Chemical Dynamics of the Reactions of Dicarbon with 1-Butyne, 2-Butyne, and 1,2-Butadiene – Toward the Formation of Resonantly Stabilized Free Radicals*. JPCA (submitted 2014).

DYNAMICAL ANALYSIS OF HIGHLY EXCITED MOLECULAR SPECTRA

Michael E. Kellman
Department of Chemistry, University of Oregon, Eugene, OR 97403
kellman@uoregon.edu

PROGRAM SCOPE:

Highly excited vibration-rotation dynamics of small molecular species, including those approaching the threshold of reaction, are crucial to understanding fundamental processes important for combustion. Our goal is to develop theoretical tools to analyze spectra and dynamics of these highly excited systems. A persistent theme is the use of effective spectroscopic fitting Hamiltonians to make the link between experimental data and theoretical dynamical analysis. There are three areas currently under investigation. (1) The role of bifurcations and the "birth of new modes in bifurcations from the low energy normal modes." (2) A more recent focus has been systems approaching and undergoing intramolecular isomerization reactions. We have been developing new generalizations of the effective Hamiltonian, called "polyad-breaking Hamiltonians," to deal with spectra of isomerizing systems. In our most recent work we have extended these investigations to consider time-dependent dynamics, including the isomerization process. (3) Most recently, in a new development in our research program, we have begun an investigation of the "quantum thermodynamics" of a small quantum molecular system immersed in a quantum heat bath. In this report, I will speak briefly of the first two topics, then comment in more detail on our newer recent thrust in quantum thermodynamics.

RECENT PROGRESS AND FUTURE PLANS. Our current research is pursuing three main directions:

CRITICAL POINTS BIFURCATION ANALYSIS OF EFFECTIVE SPECTROSCOPIC HAMILTONIANS.

This work continues with Dr. Vivian Tyng. Ref. 5 was done in collaboration with DOE Combustion PI Hua Guo of the University of New Mexico.

Our emphasis on the critical points bifurcation analysis of effective spectroscopic Hamiltonians has continued in recent years [1-5]. In a project conducted with Dr. Vivian Tyng, we are completing our first bifurcation analysis for a rotation-vibration effective Hamiltonian, using a recent spectroscopic Hamiltonian for CO_2 fit to experimental data.

We have in hand the successful critical points analysis of rotation-vibration dynamics of CO_2 on the effective Hamiltonian fit to experimental data. The analysis gives relatively simple, intelligible dynamics, comparable to but significantly extending what has been obtained with pure vibrational dynamics. At J = 0 there is only the bifurcation tree of normal modes and Fermi resonance modes. Then, as J increases, we find a principal "Coriolis mode" that bifurcates out of one of the Fermi resonance modes at very low J, with further finer branching of the tree into Coriolis modes with increasing J.

The challenge to completing this work has been the physical interpretation of the results of the critical points analysis. What is the physical nature of the rotation-vibration motion in the new bifurcation rotation-vibration "modes" of the molecule? The natural starting point is the standard

picture of the rotation-vibration motion of a symmetric top. In the new Coriolis modes of CO_2 determined in the bifurcation analysis, things will be somewhat but not altogether different from the symmetric top; and also with some similarities to the asymmetric top.

GENERALIZED SPECTROSCOPIC HAMILTONIAN FOR ISOMERIZING SYSTEMS WITH POLYAD BREAKING.

This work has been primarily in collaboration with Dr. George Barnes. The recent focus of our work is systems approaching and even surmounting an isomerization barrier, in which the standard effective spectroscopic Hamiltonian breaks down. The Hamiltonian used in virtually all existing spectral fits invokes an approximate conserved quantity known as the polyad or total quantum number. In a recent step, initiated with two papers [3,4], we showed that it is possible to construct an effective Hamiltonian to encompass multiple potential energy minima in an isomerizing system. As our exemplar, we used one of the most important elementary combustion species is the hydroperoxyl radical HO_2.

A new direction will involve combining the existing bifurcation analysis of our HO_2 effective Hamiltonian with our thrust into entangled system-environment dynamics outlined briefly at the end of the following section.

QUANTUM THERMODYNAMICS OF SMALL MOLECULAR SYSTEMS.

Our DOE work for many years has focused on the dynamics of highly excited molecular systems in isolation. We have recently turned our attention to embedding these systems in an environment. A proper full quantum description involves "entanglement" of a system in some kind of environment, both described quantum mechanically in terms of a Hamiltonian operator, with system-environment interaction. The behavior of small quantum entangled systems is of great interest in many areas of fundamental and applied physics and physical chemistry. The particular questions we have begun investigating fall in the domain of "quantum thermodynamics" of small molecular systems. This is of obvious relevance to combustion systems, where small molecular species are embedded in a thermal, in general non-equilibrium environment. With George Barnes, one paper has been published in J. Chem. Phys. [6] and another is near completion [7].

Thermal behavior in a small quantum entangled system-environment.

In the first of these papers [6], simulations were performed of a small quantum system interacting with a quantum environment. The system consists of various initial states of two harmonic oscillators coupled to give normal modes. The environment is "designed" by its level pattern to have a thermodynamic temperature. A random coupling causes the system and environment to become entangled in the course of time evolution. We examine the time-dependent quantum behavior of various initially prepared pure states as the oscillator system interacts with the quantum environment. The total system + environment "universe"' is in a pure state described by the density matrix ρ_{se}. The statistical behavior of the system is described by the reduced density matrix (RDM) ρ_s = Trace ρ_{se}. Visual insight into the dynamics of the system is obtained by examining spatial density distributions of the system RDM ρ_s.

Approach to a Boltzmann distribution is observed, and effective fitted temperatures close to the designed temperature are obtained. All initial pure states of the system are driven to equilibrium at very similar rates, with quick loss of memory of the initial state. The time evolution of the von Neumann entropy is calculated as a measure of equilibration and of quantum coherence. Spatial

density distribution plots show that quantum interference is eliminated only with maximal entropy, which corresponds thermally to infinite temperature. (See the figure with the spatial density plots following page, where the final density at thermal equilibrium clearly shows quantum interference effects.)

Perhaps the most interesting result of this investigation is the phenomenon of each initial state being driven to equilibrium at essentially the same rate. The symmetric normal mode overtone state, which looks most like the equilibrium distribution, is essentially no different in this regard than the antisymmetric mode, which is orthogonal in coordinate space; or the local mode state, which undergoes time-dependent oscillations between the two local mode overtones in the pure system initial state. Fig. 6 from Ref. [6] below shows the spatial density of the initial local mode state as a function of time. This spatial density is computed as outlined above using the reduced density matrix of the system. The figure shows snapshots of the time evolution of the initial local mode state. Oscillations between local mode states are seen at short time, but density quickly begins to obey a Boltzmann like distribution.

An interesting question is whether this behavior will persist for systems with more complex dynamics than the simple normal mode system considered here. Nonlinear moleuclar systems with strong resonance couplings, such as coupled stretch normal modes in 2:2 resonance, or 2:1 Fermi resonance systems, have marked phase space structure, including stable and unstable modes born in bifurcations. These might be expected to have significantly different dynamics, including decoherence behavior and rates of approach to equilibrium. Clearly, detailed investigation of these nonlinear systems is warranted.

The second law, entropy of the universe, and the second law.

In the second paper with Dr. Barnes [7], we investigate the meaning of the second law of thermodynamics in the context of quantum thermodynamics. The standard statement of the second law in "classical thermodynamics" is that the entropy of the universe is always increasing in a spontaneous process: $\Delta S_{univ} > 0$. The problem is that the standard quantum definition of entropy due to von Neumann yields $S^{vN} = 0$ for a pure quantum state. That means if we consider a small system-environment "universe" to be in a pure quantum state, as is the case in our simulations reported above, the von Neumann entropy of the universe S^{vN}_{univ} is always zero! We take the view that there is an obvious conflict with standard "classical" thermodynamics. To our surprise, this conflict does not seem to have been addressed widely in the small-systems quantum thermodynamics community. We propose seek an alternative definition of the entropy of the universe that is in accord with the second law. For a model quantum system becoming entangled with a quantum environment, we perform simulations of time dependent dynamics. We test the new definition of the entropy of the universe against the standard thermodynamic relation $\Delta F_{sys} = - T \Delta S_{univ}$, calculating the properties of the system using the reduced density matrix and standard von Neumann entropy. Good agreement between the two sides is obtained, showing the compatibility of a definition of entropy for the pure state of a universe with the statements of the second law and the concept of free energy.

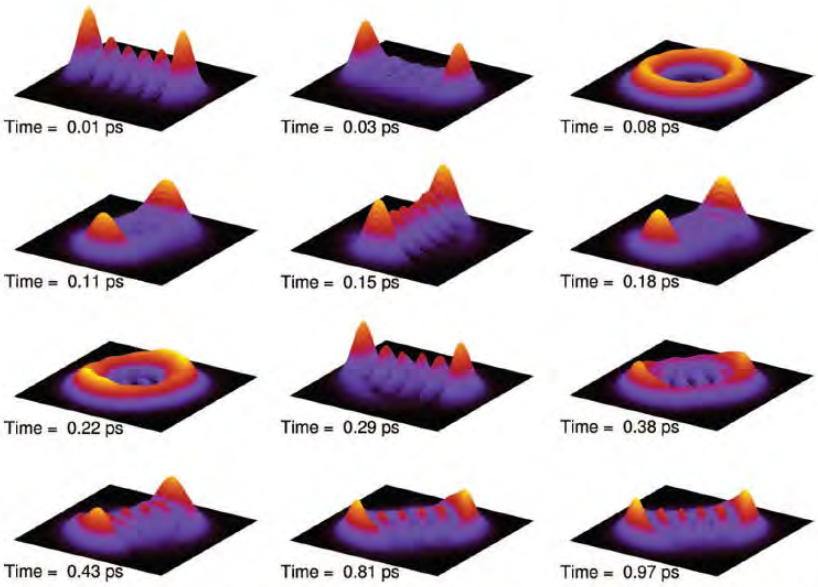

FIG. 6. Snapshots of the time evolution of the total state density for an initial local mode state. Oscillations between local mode states are seen at short time, but density quickly begins to obey a Boltzmann like distribution with fluctuations.

Recent publications referenced above, related to DOE supported research:

1. G. L. Barnes and M.E. Kellman, "Effective Spectroscopic Hamiltonian for Multiple Minima with Above Barrier Motion: Isomerization in HO_2", J. Chem. Phys. 133, 101105 (2010).

2. G.L. Barnes and M.E. Kellman, "Detailed Analysis of Polyad-Breaking Spectroscopic Hamiltonians for Multiple Minima with Above Barrier Motion: Isomerization in HO_2", J. Chem. Phys. 134, 074108 (2011).

3. G.L. Barnes and M.E. Kellman, "Effective Hamiltonian for femtosecond vibrational dynamics" J. Chem. Phys. 135, 144113 (2011).

4. G.L. Barnes and M.E. Kellman, "Visualizing the Zero Order Basis of the Spectroscopic Hamiltonian," J. Chem. Phys. 136, 024114 (2012).

5. J. Ma, D. Xu, H. Guo, V. Tyng, and M.E. Kellman, "Isotope effect in normal-to-local transition of acetylene bending modes" J. Chem. Phys. 136, 014304 (2012).

6. G.L. Barnes and M.E. Kellman, "Time Dependent Quantum Thermodynamics of a Coupled Quantum Oscillator System in a Small Thermal Environment," J. Chem. Phys. 139, 214108 (2013).

7. G.L. Barnes and M.E. Kellman, "Quantum Thermodynamics, Entropy of the Universe, Free Energy, and the Second Law," manuscript in preparation.

Time-Resolved Optical Diagnostics

Christopher J. Kliewer (PI)
Combustion Research Facility, Sandia National Laboratories
P.O. Box 969, MS 9055
Livermore, CA 94551-0969
cjkliew@sandia.gov

Program Scope

This program focuses on the development of innovative laser-based techniques for measuring temperature and concentrations of important combustion species as well as the investigation of fundamental physical and chemical processes that directly affect quantitative application of these techniques. Our development efforts focus on crossed-beam approaches such as time-resolved nonlinear wave-mixing. A critical aspect of our research includes the study of fundamental spectroscopy, energy transfer, and photochemical processes. This aspect of the research is essential to the development of accurate models and quantitative application of techniques to the complex environments encountered in combustion systems. These investigations use custom-built tunable picosecond (ps) and commercial femtosecond lasers, which enable efficient nonlinear excitation, provide high temporal resolution for pump/probe studies of collisional processes, and are amenable to detailed physical models of laser-molecule interactions.

Recent Progress

Accurate time- and spatially resolved measurement of temperature remains a critical focus of combustion diagnostics. The local temperature field and gradient not only govern chemical reaction rates but also physical quantities such as gas expansion and heat transfer.[A] Coherent anti-Stokes Raman spectroscopy (CARS) has been applied for concentration measurements and ro-vibrational thermometry in gas-phase applications for more than three decades, and is often held as the gold standard optical technique for the non-intrusive determination of temperature in gas-phase systems.

2-dimensional coherent Raman imaging for combustion: A significant limitation to the CARS technique during its development has been its applicability as a 0-dimensional technique, allowing the experimenter to obtain a CARS spectrum only at a single point in space during each laser shot. Several recent innovations in this laboratory have enabled the first single-laser-shot 2-dimensional CARS measurements. Two hurdles must be overcome in the application of CARS as a single-laser-shot planar imaging technique. The first concern is phase-matching. Traditionally, the three CARS beams (pump, Stokes, and probe) are overlapped following the BOXCARS configuration for constructive signal growth.[B] However, this phase-matching configuration does not lend itself to planar imaging, as there is no feasible way of combining the three beams to generate a spatially well-resolved 2D signal. However, we have recently explored the phase matching physics involved with performing CARS measurements with just two crossed beams.[6] A broadband laser beam provides both pump and Stokes photons in a single pulse, and a narrowband laser is scattered from the excited coherences at an angle determined for optimal spatial resolution and adequate signal. In this configuration, a single coherence excitation sheet is intersected with an unfocussed probe beam to generate a 2-dimensional CARS signal. The

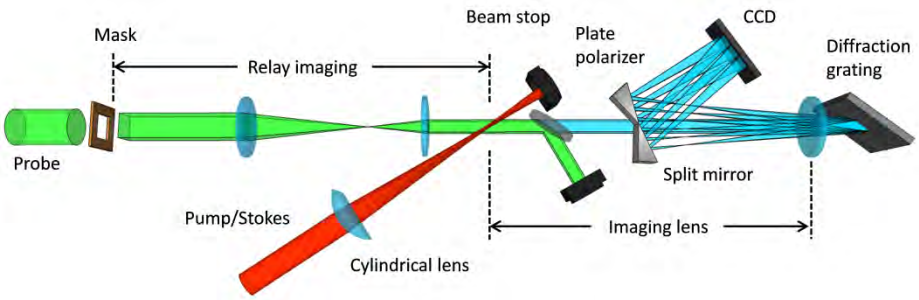

Figure 1. Experimental layout and detection scheme for 2D-CARS

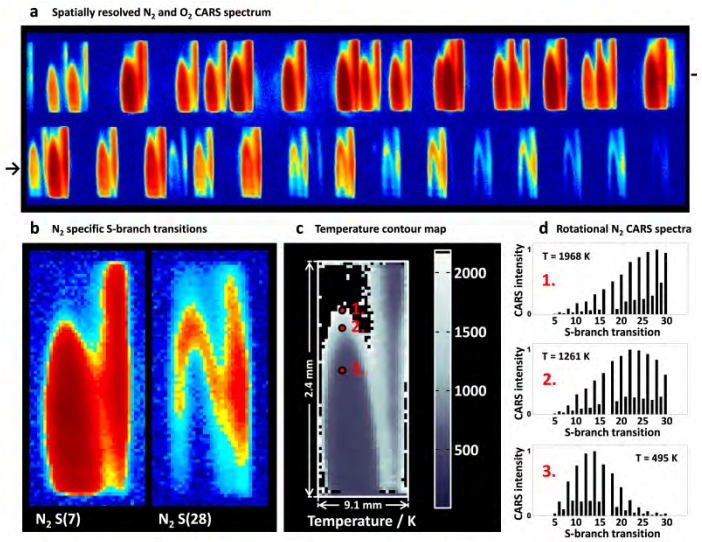

Figure 2. In panel (a), raw 2D-CARS data from a single-laser-shot in a premixed methane/air flame is presented. Signal from a low, S(7), and a high S(28) rotational transition in N_2 are compared in (b), demonstrating the spatially correlated thermal population of higher energy rotational states in the reaction zone. Panels (c) and (d) demonstrate three rotational CARS spectra extracted from the flame.

second hurdle in the development of a 2D-CARS diagnostic regards the spectrally resolved detection of a 2-dimensional signal in a single laser shot. Figure 1 demonstrates the developed imaging spectrometer. The signal generation plane is imaged through a grating at Littrow's angle to the face of a CCD camera, and thus CARS transitions of different frequencies are mapped to different locations on the CCD. The optical system is carefully tuned to the molecular transitions of interest to allow for well-isolated images of populated states. Figure 2 presents pure-rotational 2D-CARS data from a slightly rich premixed laminar methane/air flame. The mask placed in the probe beam allows for spatial calibration of each of the rotational transition images to correct for any distortion through the optical imaging system. For example, a slight astigmatic magnification occurs for transitions diffracted further from Littrow's angle. Figure 2d illustrates the intensity spectra extracted for three separate spatial locations in the 2D image, clearly demonstrating the thermally populated Boltzmann distribution of rotational states which can be fitted for temperature. We have demonstrated measurements of up to 15,000 spatially correlated CARS spectra obtained within a single laser shot with this new technique.

2-beam ultrabroadband CARS: Over the years, many complex dual-pump CARS schemes have been developed with the aim of detecting up to a few molecular species simultaneously, specific to the laser frequencies employed. Similarly, CARS schemes have been developed to simultaneously probe more than one manifold of a molecule, such as the pure-rotational and Q-branch of N_2 with the aim of improved accuracy in mode-specific thermometry. We have recently demonstrated a capability for crossed beam ultrabroadband CARS, allowing for high spatial and spectral resolution, and the simultaneous detection of pure-rotational, and vibrational O-, Q-, and S-branches of any molecules present in significant concentration (>1%) with Raman-active transitions up to 4200 cm^{-1}. The 45 femtosecond output of our laser is sent through a hollow-core fiber filled with Argon inducing a significant amount of spectral broadening primarily through self phase modulation. This pulse is then compressed to ~7 fs using negatively chirped optics. The two-beam CARS phase matching scheme ensures that the ultrashort pump and Stokes fields are automatically overlapped temporally, while allowing for the high spatial resolution of a crossed probe technique. We have demonstrated the technique in single-shot 1D-CARS measurements of N_2, H_2, and CH_4 in Figure 3. Pure-rotational transitions are excited over the entire bandwidth of the ultrabroadband pulse, whereas the signal from methane corresponds to the wings of the pulse. Naturally, this results in very strong signal levels on the pure-rotational side of the spectrum. However, if desired, the relative signal intensities may be tuned using polarization suppression techniques. The spectrum in Figure 3 has not been normalized for the excitation bandwidth, demonstrating the balanced detection of both pure-rotational and vibrational transitions with similar signal intensities. This development imparts the benefit of multiplex detection normally associated with linear Raman to CARS diagnostics. The standard deviation in the determination of relative mole fraction is ~4% for $[H_2]/[N_2]$ and 13% for $[CH_4]/[N_2]$ in the experiment shown.

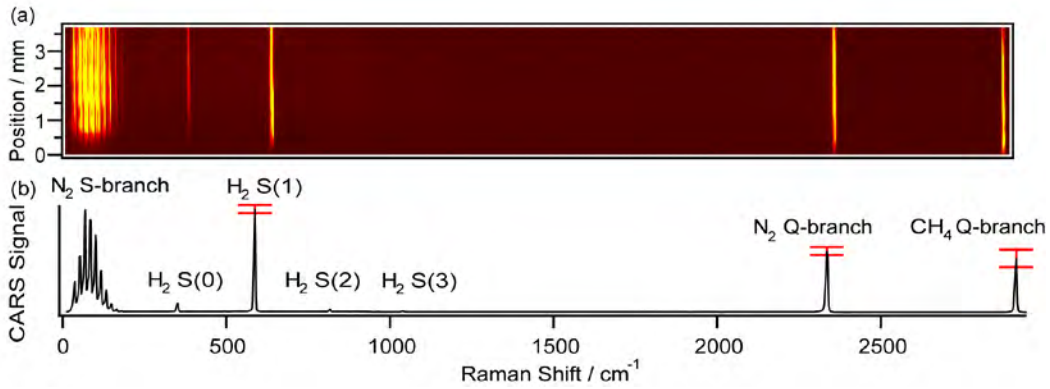

Figure 3. Ultrabroadband 1D-CARS measurement demonstrated in a single-laser-shot recorded in a flowing mixture of H_2, N_2, and CH_4. Error bars indicate the single-shot standard deviation in signal intensity.

Future Work

Application of 1D fs/ps CARS to the study of flame-wall interactions and determination of burner boundary conditions. One of the key advantages of the coherent nature of the CARS signal is the ability to probe very near to scattering interfaces such as a burner nozzle. Whereas linear optical techniques such as filtered Raleigh/Raman scattering may provide excellent thermometry and species concentrations in combustion, these techniques fail near scattering objects such as a burner surface, near a wall, or in sooting environments. However, accurate temperature and species concentration profiles are critical in these locations to set the boundary conditions in numerical simulations of combusting flows. Several projects are planned utilizing our state-of-the-art 1D fs/ps CARS spectrometer. In an ongoing collaboration with Andreas Dreizler of TU Darmstadt, we will continue to study the flame-wall interaction by time-resolved probing of turbulent combusting flows impinging and quenching upon a metal surface. Both steady-state and time-resolved ignition delay studies will be performed to study fluctuations of the instantaneous thermal gradient upon surface quenching. Further, we plan initial experiments with Rob Barlow to obtain single-laser-shot 1D and possibly 2D temperature measurements close to the bluff body flame stabilizer in the annular premixed burner recently constructed in his laboratory. Access to the region within 5 mm of the surface is not possible with the current setup, but in the 2-beam CARS arrangement, the instantaneous temperature field may be acquired to within microns of the surface.

Refinement and implementation of 2D and ultrabroadband CARS. With the recent development of the first 2D-CARS measurements and ultrabroadband CARS, our plan is to continue development on these techniques to yield robust combustion diagnostics. The 2D-CARS spectrometer design has been modified to allow precise matching between the laser sheet height and the desired probe volume to maximize the available irradiance for coherent excitation. Further, a scheme has been developed for significantly increasing the probe pulse irradiance without damaging optics. These improvements should yield the 2D-CARS signal levels adequate for single-shot measurement even in challenging combustion environments, such as in the presence of some turbulence or low air concentration. Further work is needed to benchmark the new 2D-CARS technique in terms of the precision and accuracy it provides. Experiments in heated flows and well-studied and benchmarked flames are planned to validate the veracity of results. Particularly, spatial resolution and averaging effects will be tested in the presence of steep thermal gradients. In the ultrabroadband CARS technique, we are developing a method to simultaneously record the nonresonant excitation profile, thereby correcting for the fluctuating spectrum of the supercontinuum on a single-shot basis. In the end, we aim to combine both ultrabroadband and 2D-CARS into a single diagnostic, enabling the direct CARS imaging of thermometry as well as major

species concentrations. This development will enable mixture fraction imaging, and the extension of measurements to turbulent flame environments is planned.

Direct measurement of N_2-Fuel and N_2-H_2O broadening coefficients. With the successful development of the time-domain technique for acquiring high-accuracy S-branch broadening coefficients, demonstrated thus far for the N_2-N_2 and N_2-H_2 collisional systems, we propose to continue the collaboration with Per-Erik Bengtsson of Lund University, Sweden, to tackle the relative paucity of broadening coefficient data in the literature for air-fuel collisional systems. Initial studies will focus on the collisional broadening of N_2 and O_2 when perturbed by DME, ethane, ethylene, propane, and propylene. Accurate broadening models must be developed for these collisional environments, especially at elevated pressures. We will alter our current time-domain CARS code to implement these new linewidth libraries and test the validity of the model in our newly constructed high-pressure, high-temperature cell.

References

A. Patton, R. A.; Gabet, K. N.; Jiang, N.; Lempert, W. R.; Sutton, J. A., *Appl. Phys. B* **2012,** *108* (2), 377-392.

B. Eckbreth, A. C., BOXCARS - Crossed-beam phase-matched CARS generation in gases. *Appl. Phys. Lett.* **1978,** *32* (7), 421-423.

Journal publications supported by this BES project (2012-2014)

1. A. Bohlin, E. Nordström, B. D. Patterson, P.-E. Bengtsson, and C. J. Kliewer, "Direct measurement of S-branch N_2-H_2 Raman linewidths using time-resolved pure rotational coherent anti-Stokes Raman spectroscopy," J. Chem. Phys. **137**, 074302 (2012).
2. Y. Gao, A. Bohlin, T. Seeger, P.-E. Bengtsson, and C. J. Kliewer, "In situ determination of N_2 broadening coefficients in flames for rotational CARS thermometry," Proc. Combust. Inst. (2012).
3. C. J. Kliewer, A. Bohlin, E. Nordström, B. D. Patterson, P.-E. Bengtsson, and T. B. Settersten, "Time-domain measurements of S-branch N_2–N_2 Raman linewidths using picosecond pure rotational coherent anti-Stokes Raman spectroscopy," Appl. Phys. B. **108**, 419-426 (2012).
4. C. J. Kliewer, "High-spatial-resolution one-dimensional rotational coherent anti-Stokes Raman spectroscopy imaging using counterpropagating beams," Opt. Lett. **37**, 229-231 (2012).
5. A. Bohlin and C. J. Kliewer, "Communication: Two-dimensional gas-phase coherent anti-Stokes Raman spectroscopy (2D-CARS): Simultaneous planar imaging and multiplex spectroscopy in a single laser shot," J. Chem. Phys. **138**, 221101 (2013).
6. A. Bohlin, B. D. Patterson, and C. J. Kliewer, "Simplified two-beam rotational CARS signal generation demonstrated in 1D," J. Chem. Phys. **138**, 081102 (2013).
7. S. P. Kearney, D. J. Scoglietti, and C. J. Kliewer, "Hybrid femtosecond/picosecond rotational coherent anti-Stokes Raman scattering temperature and concentration measurements using two different picosecond-duration probes," Opt. Express **21**, 12327-12339 (2013).
8. B. D. Patterson, Y. Gao, T. Seeger, and C. J. Kliewer, "Split-probe hybrid femtosecond/picosecond rotational CARS for time-domain measurement of S-branch Raman linewidths within a single laser shot," Opt. Lett. **38**, 4566-4569 (2013).
9. A. Bohlin and C. J. Kliewer, "Two-beam ultrabroadband coherent anti-Stokes Raman spectroscopy for high resolution gas-phase multiplex imaging," Appl. Phys. Lett. **104**, 031107 (2014).
10. A. Bohlin and C. J. Kliewer, "Diagnostic Imaging in Flames with Instantaneous Planar Coherent Raman Spectroscopy," J. Phys. Chem. Lett., 1243-1248 (2014).
11. A. Bohlin, M. Mann, B.D. Patterson, A. Dreizler, C. J. Kliewer, “Development of two-beam femtosecond/picosecond one-dimensional rotational coherent anti-Stokes Raman spectroscopy: time-resolved probing of flame wall interactions,” submitted

ARGONNE-SANDIA CONSORTIUM ON HIGH-PRESSURE COMBUSTION CHEMISTRY

Stephen J. Klippenstein (PI), Michael J. Davis, Lawrence B. Harding, Joe V. Michael,
James A. Miller, Branko Ruscic, Raghu Sivaramakrishnan, Robert S. Tranter
Chemical Sciences and Engineering Division, Argonne National Laboratory, Argonne, IL, 60439
sjk@anl.gov
Craig A. Taatjes (PI), Ahren W. Jasper, David L. Osborn, Leonid Sheps, Judit Zádor
Combustion Research Facility, Mail Stop 9055, Sandia National Laboratories
Livermore, CA 94551-0969
cataatj@sandia.gov

Program Scope

The goal of this project is to explore the fundamental effects of high pressure (P) on the chemical kinetics of combustion and to use that knowledge in the development of accurate models for combustion chemistry at the high pressures of current and future engines. We design and implement novel experiments, theory, and modeling to probe high-pressure combustion kinetics from elementary reactions, to submechanisms, to flames. The work focuses on integrating modeling, experiment, and theory (MET) through feedback loops at all levels of chemical complexity. We are currently developing and testing the methodology for propane, small alcohols, and dimethyl ether as key prototype fuels. The consortium expands and enhances collaborations between Argonne's Dynamics in the Gas Phase Group and the Combustion Chemistry Group in Sandia's Combustion Research Facility and also interacts closely with the Princeton-led Combustion Energy Frontier Research Center (CEFRC).

Recent Progress

Experimental Developments

OH + alkenes: These reactions are important in low-temperature (T) autoignition mechanisms of alkanes (unsaturated compounds are major products of alkyl radical oxidation) and alcohols (the production of OH + alkenes is a key decomposition pathway for hydroxyalkyl radical intermediates). We have studied the T and P dependent reaction of hydroxyl radical with *cis*- and *trans*-2-butene (P = 1 – 20 atm, T = 300 – 800 K) by time-resolved OH laser-induced fluorescence (LIF) (manuscript in preparation with Zádor). The measured OH time-histories, shown in Fig. 1, are dominated by the competition between H abstraction pathways, OH addition to the C–C double bond, and back-dissociation of the OH-butene adduct, which is an important quantity for combustion models of butanol.

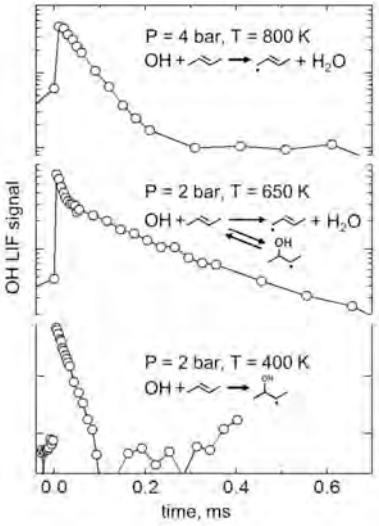

Figure 1. Time-resolved OH LIF traces in the reaction OH + trans-2-butene.

Fundamental autoignition chemistry: We have also made progress in our studies of the P-dependence in low-T oxidation reactions using multiplexed photoionization mass spectrometry (MPIMS). A key experimental advance was the introduction of a fused silica insert into our prototype high-P flow cell, providing a chemically inert reactor surface and dramatically reducing wall reactions. This improvement overcomes a long-standing technical challenge in applying the powerful MPIMS method to high-P systems and ensures that experimental results accurately reflect the gas-phase reaction kinetics.

Propane oxidation. In light of our technical improvement, we revisited our earlier work on propane oxidation by time-resolved MPIMS using tunable synchrotron ionization radiation. We now estimate that our first measurements suffered extensive interference from surface reactions, with wall losses removing ~75% of the initially formed propyl peroxy radicals. In contrast, the latest experiments at P = 1 – 2 atm and T = 600 – 650 K (shown in Fig. 2) yield branching fractions and kinetic traces that are consistent with a negligible role for wall reactions. This new data provided the basis for our multiscale informatics modeling effort. We are currently expanding our studies of propane oxidation to higher pressures and a wider temperature range.

Ketohydroperoxide formation in butane oxidation. Low-T alkane oxidation hinges on the P- and T-dependent competition between unimolecular decomposition of alkyl peroxy radicals and internal H atom transfer to form hydroperoxyalkyl species, QOOH. Although no QOOH have so far been directly observed, we recently detected ketohydroperoxide (KHP), an important product of QOOH + O_2 reactions, in butane oxidation at P up to 2 atm.

Kinetic measurements at varying T and [O_2] confirm KHP as the source of the observed signals, and experiments using deuterated butene isomers allow an assignment of the reaction pathways responsible for KHP production.

High pressure, high repetition rate shock tube (HRRST): The HRRST is a unique, miniature (0.25" bore) shock tube designed for use at synchrotron light sources. Recently, the design was published along with test data [12]. It can be fired at repetition rates up to 4 Hz and generates reproducible reaction conditions of P < 100 bar and 600 < T < 3000 K. The primary diagnostic is time-of-flight mass spectrometry although the apparatus can easily be used with other diagnostics such as W/SAXS and optical techniques. The apparatus has been run in three campaigns at the Advanced Light Source and VUV-PIMS data was obtained for the dissociation of dimethyl ether, DME. Example ensemble averaged (~900 shocks, 10.5eV) mass spectra are shown in Fig. 3 and the expected end products are seen. Some additional fragments are also observed and Ar^+, from the bath gas, which arises due to a small amount of high harmonic light not being filtered out at the beamline. To produce such spectra it is necessary to acquire many identical experiments and considerable effort has been devoted to characterizing the behavior of the HRRST and the reproducibility of reaction conditions. These tests included: using laser schlieren densitometry to confirm that well-formed shock waves are generated; measuring the reflected shock pressure at the end of the driven section to measure the available reaction time and compare the measured pressure with that calculated from ideal shock theory; measuring a state property of the driven gas for comparison with calculated values. For the latter, the density behind incident shock waves in argon with helium driver was measured by X-ray absorption. These experiments were conducted at the Advanced Photon Source and ~ 40,000 shocks were acquired over a range of temperatures and pressures. There is excellent agreement between the calculated and measured densities although the spread of values in calculated temperatures is a little larger than desired. However, rather than trying to constrain the variation in shock temperature to <1% it is more efficient to acquire shocks rapidly and bin them appropriately during data reduction.

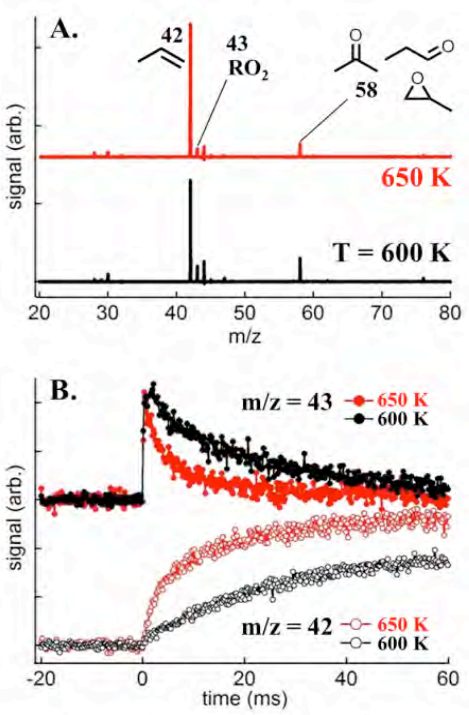

Figure 2. Initial results from propane oxidation at 1 atm. *Panel A*: time-resolved mass spectra at T = 600 and 650 K. *Panel B*: Kinetic time traces of propene, m/z = 42, and propyl peroxy, m/z = 43.

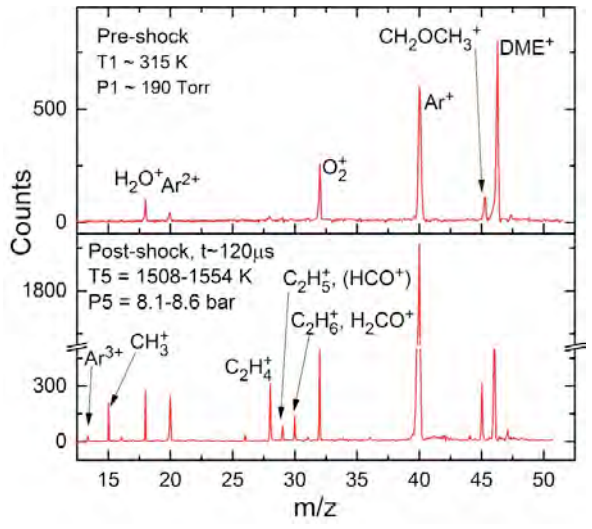

Figure 3: Averaged VUV-PIMS mass spectra (~900) of a 2% DME/Ar mixture dissociating behind reflected shock waves in the HRRST at the ALS.

Theory and Experiment for Rate Coefficients

CH_3 + C_2H_6/C_2H_4/C_2H_2: The reflected shock tube technique with H-ARAS detection has been used to study the reactions of CH_3 radicals with C_2H_6, C_2H_4, and C_2H_2 over the T-range 1100-1350 K. These studies represent a novel implementation of the sensitive technique to measure rate constants for poorly characterized and difficult to isolate "slow" CH_3-radical reactions with stable C_2 hydrocarbons. Biacetyl, $(CH_3CO)_2$, was used as a clean high temperature thermal source for CH_3-radicals for all three reactions studied in this work. For C_2H_6, the measurement of [H]-atoms was used to derive direct high-temperature rate constants for the only bimolecular process that occurs,

H-atom abstraction. TST calculations based on ab-initio properties calculated at the CCSD(T)/CBS//M06-2X/cc-pVTZ level of theory show excellent agreement, within ± 20%, of the measured rate constants.

For C_2H_4, the observations correlate with the sum of the rate constants from two competing processes: addition-elimination, $CH_3 + C_2H_4 \rightarrow C_3H_6 + H$, and direct abstraction, $CH_3 + C_2H_4 \rightarrow C_2H_2 + H + CH_4$. The present results are in excellent agreement with our earlier theoretical kinetics predictions. For C_2H_2 the observations provide direct unambiguous determinations of the rate constant for the addition-elimination, $CH_3 + C_2H_2 \rightarrow p\text{-}C_3H_4 + H$. These results are in good agreement with recent theoretical predictions for this reaction. For both C_2H_4 and C_2H_2 the present study provides the only direct measurement of the high-temperature rate constants for the stated channels.

OH + CH_3OH: Isotopic labeling studies reveal mechanistic features of CH_2OH decomposition: The kinetics of OH + CH_3OH is of relevance to atmospheric and combustion chemistry. Measurements of H/D-atoms (using the ARAS technique) that results from shock heating mixtures of CH_3OH and TBHP (tert-butylhydroperoxide as a thermal source for OH) were used to probe the kinetics of OH + CH_3OD/CD_3OH. H-atom profiles were used to obtain total rate constants for OH + CD_3OH. While kinetics simulations (based on input from ab-initio/theoretical kinetics) for H/D-atom profiles reveals that site-specific abstraction rate constants at the CH_3 and OH site in CH_3OH are indeterminate in these experiments (because of the sequence of reactions $CH_2OH \rightarrow CH_3O \rightarrow$ Products); the H/D-atom profiles provide some constraints for the abstraction branching ratios in the title reaction.

Ketohydroperoxide Decomposition: A T- and P-dependent theoretical kinetic analysis was provided for the decomposition of the KHP derived from n-propyl. The possibility for direct dissociation of the KHP precursor was treated through a coupling of direct dynamical simulations of the energy distribution arising from the dissociation of the O_2QOOH precursor with novel master equation simulations of the hot dissociation.

Non-Boltzmann Effects in Radical Oxidation: We also expanded on this treatment of the KHP decomposition to study the possible role of non-Boltzmann effects for the full $O_2 + O_2$ + propyl sequence of reactions that leads to chain branching. This analysis involved novel implementations of the master equation approach, which were designed to treat the effects of reactions that occur during the vibrational relaxation process. It indicates that while non-Boltzmann reaction sequences are unlikely to substantially alter ignition predictions at higher pressures (at least for propane), there are likely significant effects on the low-pressure experimental measurements commonly used to investigate the R + O_2 and QOOH + O_2 reactions central to engine-relevant ignition behavior.

Modeling Developments

Multiscale modeling: Work on the multiscale informatics based modeling of the low temperature oxidation of propane is now effectively complete. The MPIMS data obtained in the experimental part of this effort provided a key focus for the modeling. The final multi-scale informed model provides a consistent quantitative explanation of *ab initio* calculations and time-resolved measurements for OH, HO_2, *n*-propyl, *i*-propyl, C_3H_6, oxetane, and methyl-oxirane over a wide range of low temperatures and pressures. Perhaps more importantly, it points to key aspects of the kinetics where additional information is required in order to fully understand the overall kinetics.

Comprehensive mechanism: We continue to make progress towards the development of a rigorous, comprehensive chemical kinetic model for the combustion of C0-C3 hydrocarbon and oxygenated hydrocarbon fuels. Numerous theoretical studies of key elementary reaction rates have been performed in response to shortcomings and uncertainties in the model. Furthermore, we have incorporated large-scale updates of the thermochemical and transport properties, which were performed as part of our core-program efforts.

Future Directions

Development of high-pressure MPIMS: We have recently completed the design for an improved high-P MPIMS apparatus that addresses the challenges identified with the current prototype reactor, the chief one being a large drop in experimental signal levels associated with high-pressure operation. The increase in sample P comes solely from higher bath gas concentrations, while the reactant concentrations remain low in order to avoid radical-radical reactions. In contrast to low-P experiments, the relative mole fraction of reactants at high P is exceedingly small ($10^{-7} – 10^{-8}$), pushing the sensitivity limits of conventional mass spectrometry. The new apparatus will implement an innovative mass spectrometer design, where photoionization occurs in a high-density region of the supersonic sampling expansion, followed by sophisticated electrostatic ion guides in order to ensure high collection efficiency. We anticipate that the new apparatus, which will benefit both the flow cell and the HRRST and is to be built within one year, will bring a factor of ~100 increase in detection sensitivity over the current prototype.

Low-temperature autoignition chemistry. We plan to continue our detailed time-resolved studies of low-T autoignition chemistry with a focus on general effects of fuel structure on reactivity. We will broaden the ongoing propane and butane oxidation experiments to include larger branched-chain alkanes, and we plan to study the low-T oxidation of ethers, starting with the simplest linear compound, dimethyl ether (DME), which has also been chosen

as the next target for the theory and modeling efforts. Other experimental target compounds for the near future will be the cyclic ethers tetrahydrofuran (THF) and 2-methyl THF, two next-generation biofuel candidates. The complementary methods of laboratory-based OH LIF detection and synchrotron-based MPIMS will help elucidate the various competing QOOH pathways and provide rigorous constraints for validation of combustion models.

HRRST: The HRRST is being coupled to a new mass spectrometer that can be operated with electron impact or VUV-PI, and which can acquire data at 150 kHz. The higher repetition rate of this spectrometer will now provide sufficient time resolution for kinetic measurements. Initial experiments will examine the pyrolysis of DME and the roaming channel. Later experiments will contribute to other core HPSCC activities.

ARAS Shock Tube Measurements and Modeling: We plan to extend our studies to the determination of site-specific H-abstraction rate constants in simple oxygenated molecules. We envision that these studies will also yield a direct probe of the thermal decompositions of radicals. Abstraction using a thermal source for OH-radicals (TBHP) or O-atoms (O_3) will yield the radical of interest in the shock tube. H/D/O-ARAS and/or OH-multipass absorption diagnostics will then provide time-resolved measurements of the radical decomposition.

DOE Supported Publications, 2012-Present

1. **High-Temperature Rate Constants for H/D + C_2H_6 and C_3H_8**, R. Sivaramakrishnan, J. V. Michael, and B. Ruscic, *Int. J. Chem. Kinet.* **44**, 194-205 (2012).
2. **On the Role of O_2 + QOOH in Low-Temperature Ignition of Alkanes I: Temperature and Pressure Dependent Rate Coefficients,** C. F. Goldsmith, W. H. Green, and S. J. Klippenstein**,** *J. Phys. Chem. A*, **116**, 3325-3346 (2012).
3. **Shock Tube Explorations of Roaming Radical Mechanisms: The Decompositions of Iso-Butane and Neo-Pentane,** R. Sivaramakrishnan, J. V. Michael, L. B. Harding, and S. J. Klippenstein**,** *J. Phys. Chem. A*, **116**, 5981-5989 (2012).
4. **Comment on 'Automatic Estimation of Pressure-Dependent Rate Coefficients'** (J.W. Allen, C. F. Goldsmith, and W. H. Green, Phys. Chem. Chem. Phys, 2011, 14, 1131-1155), J. A. Miller and S. J. Klippenstein, *Phys. Chem. Chem. Phys.* **14**, 8431-8433 (2012).
5. **Uncertainty Propagation in the Derivation of Phenomenological Rate Coefficients from Theory: A Case Study of Propyl Radical Oxidation,** C. F. Goldsmith, A. S. Tomlin, and S. J. Klippenstein**,** *Proc. Comb. Inst.*, **34**, 177-185 (2013).
6. **Unimolecular Dissociation of Hydroxypropyl and Propoxy Radicals**, J. Zádor and J. A. Miller, *Proc. Comb. Inst.* **34**, 519-526 (2013).
7. **Studies of Laminar Opposed-Flow Diffusion Flames of Acetylene at Low Pressures with Photoionization Mass Spectrometry**, S. A. Skeen, B. Yang, H. A. Michelsen, J. A. Miller, A. Violi, N. Hansen, *Proc. Comb. Inst.* **34**, 1067-1075 (2013).
8. **Unconventional Peroxy Chemistry in Alcohol Oxidation – The Water Elimination Pathway,** O. Welz, S. J. Klippenstein, L. B. Harding, C. A. Taatjes, and J. Zádor, *J. Phys. Chem. Lett.*, **4**, 350-354 (2013).
9. **Determining Phenomenological Rate Coefficients from a Time-Dependent, Multiple-Well Master Equation: "Species Reductions" at High Temperatures**, J. A. Miller and S. J. Klippenstein, *Phys. Chem. Chem. Phys*., **15,** 4744-4753 (2013).
10. **The Dissociation of Propyl Radicals and Other Reactions on a C_3H_7 Potential,** J. A. Miller and S. J. Klippenstein, *J. Phys. Chem. A*, **117**, 2718-2727 (2013).
11. **Lennard-Jones Parameters for Combustion and Chemical Kinetics Modeling from Full-Dimensional Intermolecular Potentials,** A. W. Jasper, J. A. Miller, *Combust. Flame*, **161**, 101-110 (2013).
12. **A Miniature High Repetition Rate Shock Tube**, R. S. Tranter, P. T. Lynch, *Rev. Sci. Instrum*. **84**, 094102 (2013).
13. **Direct Measurements of Rate Constants for CH_3 Radicals with C_2H_6, C_2H_4, and C_2H_2 at High Temperatures,** S. L. Peukert, N. J. Labbe, R. Sivaramakrishnan, J. V. Michael, *J. Phys. Chem. A*, **117**, 10228-10238 (2013).
14. **Low-Temperature Combustion Chemistry of n-Butanol: Principal Oxidation Pathways of Hydroxybutyl Radicals,** O. Welz, J. Zádor, J. D. Savee, L. Sheps, D. L. Osborn, C. A. Taatjes, *J. Phys. Chem. A*, **117**, 11983–12001, (2013).
15. **The Collision Efficiency of Water in the Unimolecular Reaction CH_4 ($+H_2O$) → CH_3 + H ($+H_2O$): One-Dimensional and Two-Dimensional Solutions of the Low-Pressure-Limit Master Equation,** A. W. Jasper, J. A. Miller, S. J. Klippenstein, *J. Phys. Chem. A*, **117,** 12243-12255 (2013).
16. **Effect of Non-Thermal Product Energy Distributions on Ketohydroperoxide Decomposition Kinetics,** C. F. Goldsmith, M. P. Burke, Y. Georgievsii, S. J. Klippenstein, accepted for presentation, 35th Comb. Symp. (2014).
17. **Toward a Quantitative Understanding of the Role of Non-Boltzmann Reactant Distributions in Low-Temperature Oxidation,** M. P. Burke, C. F. Goldsmith, Y. Georgievskii, S. J. Klippenstein, acc. for present., 35th Comb. Symp. (2014).
18. **Probing the Low-Temperature Chain-Branching Mechanism for n-Butane Autoignition Chemistry via Time Resolved Measurements of Ketohydroperoxide Formation in Photolytically Initiated n-C_4H_{10} Oxidation**, A. J. Eskola, O. Welz, J. Zádor, I. O. Antonov, L. Sheps, J. D. Savee, D. L. Osborn, C. A. Taatjes, acc. pres., 35th Comb. Symp. (2014).
19. **"Third-body" Collision Efficiencies for Combustion Modeling: Hydrocarbons in Atomic and Diatomic Baths,** A. W. Jasper, C. M. Oana, and J. A. Miller, accepted for presentation, 35th Comb. Symp. (2014).
20. **High Temperature Rate Constants for H/D + n-C_4H_{10} and i-C_4H_{10}**, S. L. Peukert, R. Sivaramakrishnan, J. V. Michael, accepted for presentation, 35th Comb. Symp. (2014).
21. **Adventures on the C_3H_5O potential energy surface: OH + propyne, OH + allene and related reactions,** J. Zádor J.A. Miller, accepted for presentation, 35th Comb. Symp. (2014).

THEORETICAL CHEMICAL KINETICS

Stephen J. Klippenstein
Chemical Sciences and Engineering Division
Argonne National Laboratory
Argonne, IL, 60439
sjk@anl.gov

Program Scope

The focus of this program is the theoretical estimation of the kinetics of elementary reactions of importance in combustion chemistry. The research involves a combination of *ab initio* electronic structure calculations, variational transition state theory (TST), classical trajectory simulations, and master equation calculations. We apply these methods to reactions of importance in various aspects of combustion chemistry including (i) polycyclic aromatic hydrocarbon (PAH) formation, (ii) hydrocarbon oxidation, and (iii) NO_x chemistry. The specific reactions studied are generally motivated by our interactions with combustion modeling efforts. We are also interested in a detailed understanding of the limits of validity of and, where feasible, improvements in the accuracy of specific implementations of transition state theory. Detailed comparisons with experiment and with other theoretical methods are used to explore and improve the predictive properties of the transition state theory models. Dynamics simulations are performed as a means for testing the statistical assumptions, for exploring reaction mechanisms, and for generating theoretical estimates where statistical predictions are clearly inadequate. Master equation simulations are used to study the pressure dependence of the kinetics and to obtain phenomenological rate coefficients for use in kinetic modeling.

A new component of this effort involves the development of an expert state-of-the-art, open-source, user-friendly ab initio transition-state-theory-based master equation (AITSTME) software package for predicting the thermal kinetics of gas phase reactions. Separate funding for this effort is provided by the Predictive Theory and Modeling Component of the Materials Genome Initiative.

Recent Progress

High Level Ab Initio Thermochemistry and Kinetics:

Our work on mapping out the 0 K thermochemistry for small hydrocarbon combustion relevant species (most C_xH_y, $C_xO_yH_z$, $C_xN_yH_z$, and $C_xN_yO_zH_w$ species with 34 electrons or less) is now essentially complete. A publication (with Ruscic and Harding) comparing the high level predictions with a large set of high accuracy values from the active thermochemical tables (ATcT) approach is in preparation. We are now routinely using related high level ab initio methods in our kinetic analyses for small combustion species.

Reactions on the C_3H_6 Surface:

We have mapped out the kinetics of reactions on the C_3H_6 surface using the ab initio transition theory based master equation approach. This study was motivated by the desire to understand the pressure dependence of the branching in the reaction of $^1CH_2$ with C_2H_4. Variable reaction coordinate transition state theory (VRC-TST) was employed to treat the

barrierless channels on the PES, while for channels possessing a distinct barrier, rate coefficients were instead obtained with conventional transition state theory employing rigid-rotor harmonic oscillator assumptions. The properties of the tight transition state were determined with the same high-level electronic structure methods as employed in our ongoing thermochemical analyses. The analysis yields modified Arrhenius rate expressions for the $^1CH_2 + C_2H_4$, $C_2H_3 + CH_3$, $CH_2CHCH_2 + H$, $CH_3CCH_2 + H$, and $CH_3CHCH + H$ recombination reactions as well as for the dissociations and isomerizations of propene and cyclopropane.

$C_2H_3 + O_2$ and $NH_2 + NO_2$:

We have performed detailed ab initio TST based master equation calculations as summarized in the abstract of Harding.

$C_3H_3 + O_2$ van der Waals Complex Stabilization:

In collaboration with Douberly we have examined the question of whether or not there is a minimum on the PES in the van der Waals region for $C_3H_3 + O_2$. The resonance stabilization in propargyl suggests that this radical is more likely to exhibit such minima, and earlier low-level theoretical calculations find a significant minimum. A series of CAS+1+2+QC, CASPT2, and CCSD(T) analyses indicate that there is a shelf in the potential for separations ranging from about 2.2 to 3.0 Å at a potential value of about -2.0 kcal/mol relative to reactants, but that there is no long-range minimum. Meanwhile, IR spectroscopic observations show peaks related to a chemical complex, but also find no evidence for the existence a long-range complex.

Perspectives Article

In collaboration with Truhlar and Pande we wrote a perspectives article for J. Am. Chem. Soc. This article presents a personal overview of the current status of the theory of chemical kinetics and mechanisms for complex processes. We assessed the status of the field for reactions in the gas phase, at gas-solid interfaces, in liquid solutions, and in enzymes and for protein folding. Some unifying concepts such as PES's, master equations, and reaction coordinates occur in more than one area.

AITSTME Code (PAPER):

We have made major progress on the development of our expert AITSTME code (with Jasper, Miller, and Zádor). The effort began with the consideration of an alternative formulation of the master equation for complex-forming chemical reactions with multiple wells and bimolecular products. Within this formulation the dynamical phase space consists of only the microscopic populations of the various isomers making up the reactive complex, while the bimolecular reactants and products are treated equally as sources and sinks. This reformulation yields compact expressions for the phenomenological rate coefficients describing all chemical processes, i.e., internal isomerization reactions, bimolecular-to-bimolecular reactions, isomer-to-bimolecular reactions, and bimolecular-to-isomer reactions and helps understand the relation between various earlier master equation derivations.

Our general code PAPER (Predictive Automated Phenomonelogical Elementary Rates) implementing this formulation now includes a variety of advances beyond other existing codes. These advances include automated merging of species as their equilibration

rates exceed collisional stabilization rates, automatic consideration of all reactions on a given potential energy surface including the generation of PLOG modified Arrhenius fits for all channels, multidimensional quantum and semiclassical treatments of torsions including the variation of secondary vibrations with torsional configuration, anharmonic treatment of umbrella modes, threaded parallelization of the key diagonalization step, a procedure for reducing the matrix dimension through energy dependent species merging (this procedure is also expected to yield more stable results for strongly equilibrated species), a perturbative procedure that yields stable results for low temperature, and a procedure for properly modeling the separation into thermal and direct kinetics for hot initial distributions. Notably, the generation of a complete set of CHEMKIN parameters (representing the temperature and pressure dependence of the rate coefficients) from the input data for a typical multiple well multiple product system now requires only a few minutes of real time. We have begun to share PAPER with select research groups in order to obtain feedback.

Future Directions

Our future work will continue to focus on (i) the further development of PAPER and (ii) the application of this code to the prediction of the kinetics for reactions of key importance in combustion chemistry. One major new code development will involve the generalization to the 2-dimensional master equation and the coupling with codes for performing trajectory simulations of energy transfer. This effort will be carried out in collaboration with Ahren Jasper. Further considerations of anharmonic torsional, linear bending, and umbrella modes and their coupling are also planned. Currently, we are developing a method for treating the coupling of torsional and umbrella motions with the transitional modes for barrierless reactions. The applications will continue to involve coupling with state-of-the-art electronic structure methods in collaboration with Harding. One planned large-scale application will involve the development of standard polynomial based representations of the temperature dependence of the thermochemical properties for the full set of core combustion species.

DOE Supported Publications, 2011-Present

1. **Roaming Radicals in the Thermal Decomposition of Dimethyl Ether: Experiment and Theory,** R. Sivaramakrishnan, J. V. Michael, A. F. Wagner, R. Dawes, A. W. Jasper, L. B. Harding, Y. Georgievskii, and S. J. Klippenstein, *Comb. Flame*, **158**, 618-632 (2011).
2. **The Role of NNH in NO Formation and Control**, S. J. Klippenstein, L. B. Harding, P. Glarborg, and J. A. Miller, *Comb. Flame*, **158,** 774-789 (2011).
3. **Near-Threshold H/D Exchange in CD_3CHO Photodissociation** B. R. Heazlewood, A. T. Maccarone, D. U. Andrews, D. L. Osborn, L. B. Harding, S. J. Klippenstein, M. J. T. Jordan, and S. H. Kable, *Nature Chem.*, **3**, 443-448 (2011).
4. **Insights into the Role of PAH Condensation in Haze Formation in Jupiter's Atmosphere,** L. Biennier, H. Sabbah, V. Chandrasekaran, S. J. Klippenstein, I. R. Sims, and B. R. Rowe, *Astronomy and Astrophysics*, **532,** A40, 10.1051, (2011).
5. **Long-Range Interaction Potential of Open Shell Atoms with Neutral Molecules: Application to the Calculation of the Rate Constant for the $C_2H + O(^3P)$ Reaction** Y. Georgievskii and S. J. Klippenstein *IAU Symp. 280 (The Molecular Universe), Proceedings,* Eds. J. Cernicharo and R. Bachiller, doi:10.1017/S1743921311025129 (2011).
6. **Combustion Chemistry: Important Features of the C_3H_5 Potential Energy Surface, Including Allyl Radical, Propargyl + H_2, Allene + H, and Eight Transition States** B. S. Narendrapurapu,

A. C. Simmonett, H. F. Schaefer III, J. A. Miller, and S. J. Klippenstein, *J. Phys. Chem. A*, **115,** 14209-14214 (2011).

7. **Statistical Theory for the Kinetics and Dynamics of Roaming Reactions** S. J. Klippenstein, Y. Georgievskii, and L. B. Harding, *J. Phys. Chem. A*, **115,** 14370-14381 (2011).
8. **Uncertainty Driven Theoretical Kinetics Studies for CH_3OH Ignition: HO_2 + CH_3OH and O_2 + CH_3OH**, S. J. Klippenstein, L. B. Harding, M. J. Davis, A. S. Tomlin, and R. T. Skodje, *Proc. Comb. Inst.*, **33**, 351-357 (2011).
9. **Separability of Tight and Roaming Pathways to Molecular Decomposition,** L. B. Harding, S. J. Klippenstein, and A. W. Jasper, *J. Phys. Chem. A*, **116**, 6967-6982 (2012).
10. **Comprehensive H_2/O_2 Kinetic Model for High-Pressure Combustion,** M. P. Burke, M. Chaos, Y.-G. Ju, F. L. Dryer, S. J. Klippenstein, *Int. J. Chem. Kinet.*, **44,** 444-474 (2012).
11. **Interception of Excited Vibrational Quantum States by O_2 in Atmospheric Association Reactions,** D. R. Glowacki, J. Lockhart, M. A. Blitz, S. J. Klippenstein, M. J. Pilling, S. H. Robertson, P. W. Seakins**,** *Science*, **337**, 1066-1069, (2012).
12. **Rapid Association Reactions at Low Pressure: Impact on the Formation of Hydrocarbons on Titan,** V. Vuitton, R. V. Yelle, P. Lavvas, and S. J. Klippenstein, *Astrophys. J.*, **744**, 11:1-7 (2012).
13. **Exploring Formation Pathways of Aromatic Compounds in Laboratory-Based Model Flames of Aliphatic Fuels**, N. Hansen, J. A. Miller, S. J. Klippenstein, P. R. Westmoreland, and K. Kohse-Hoinghaus, *Combust. Expl. and Shockwaves*, **48**, 508-515 (2012).
14. **Comment on "Automatic Estimation of Pressure-Dependent Rate Coefficients",** J. A. Miller, S. J. Klippenstein, *Phys. Chem. Chem. Phys*., **14,** 8431-8433 (2012).
15. **A Quantitative Explanation for the Apparent Anomalous Temperature Dependence of OH + HO_2 = H_2O + O_2 through Multi-Scale Modeling,** M. P. Burke, S. J. Klippenstein, L. B. Harding, *Proc. Comb. Inst.*, **34**, 547-555 (2013).
16. **Rate Constant and Branching Fraction for the NH_2 + NO_2 Reaction**, S. J. Klippenstein, L. B. Harding, P. Glarborg, Y. Gao, H. Hu, and P. Marshall, *J. Phys. Chem. A*, **117**, 9011-9022 (2013).
17. **Reformulation and Solution of the Master Equation for Multiple-Well Chemical Reactions**, Y. Georgievskii, J. A. Miller, and S. J. Klippenstein, *J. Phys. Chem. A*, Curt Wittig special issue, **117**, 12146-12154 (2013).
18. **Low Temperature Rate Coefficients for the Reaction CN + HC_3N?** S. C. Sid Ely, S. B. Morales, J.-C. Guillemin, S. J. Klippenstein, and I. R. Sims, *J. Phys. Chem. A*, Curt Wittig special issue, **117**, 12155-12164 (2013).
19. **Predictive Theory for the Addition and Insertion Kinetics of $^1CH_2$ Reacting with Unsaturated Hydrocarbons**, D. Polino, S. J. Klippenstein, L. B. Harding, and Y. Georgievskii, *J. Phys. Chem. A*, feature article, **117**, 12677-12692 (2013).
20. **Propargyl + O_2 Reaction in Helium Droplets: Entrance Channel Barrier or Not?** C. P. Moradi, A. M. Morrison, S. J. Klippenstein, C. F. Goldsmith, and G. E. Douberly, *J. Phys. Chem. A*, Terry Miller special issue, **117**, 13626-13635 (2013).
21. **Comparison of Multireference Configuration Interaction Potential Energy Surfaces for H + $O_2 \rightarrow HO_2$: The Effect of Internal Contraction**, L. B. Harding, S. J. Klippenstein, H. Lischka, and R. Shepard, *Theor. Chem. Acc*., Thom Dunning special issue, **133**, 1429 (2013).
22. **Chemical Kinetics and Mechanisms of Complex Systems: A Perspective on Recent Theoretical Advances**, S. J. Klippenstein, V. S. Pande, and D. G. Truhlar, *J. Am. Chem. Soc.*, perspective article, **136**, 528-546 (2014).
23. **The Role of Prompt Reactions in Ethanol and Methylformate Low-Pressure Flames,** N. J. Labbe, R. Sivaramakrishnan, S. J. Klippenstein, *Proc. Comb. Inst.*, **35**, accepted for presentation (2014).
24. **Pressure-Dependent Branching in the Reaction of $^1CH_2$ with C_2H_4 and other Reactions on the C_3H_6 Potential Energy Surface**, L. L. Ye, Y. Georgievskii, S. J. Klippenstein, *Proc. Comb. Inst.*, **35**, accepted for presentation (2014).

Theoretical modeling of spin-forbidden channels in combustion reactions

Anna I. Krylov
Department of Chemistry, University of Southern California,
Los Angeles, CA 90089-0482
krylov@usc.edu

1 Scope of the project

The goal of our research is to develop predictive theoretical methods, which can provide crucial quantitative data (e.g., rate constants, branching ratios, heats of formation), identify new channels and refine reaction mechanisms. Specifically, we are developing tools for computational studies of spin-forbidden and non-adiabatic pathways of reactions relevant to combustion, and applying these tools to study electronic structure, reactions, and spectroscopy of open-shell and electronically excited species involved in these processes.

2 Summary of recent major accomplishments

During the past year, we conducted several computational studies of open-shell and electronically excited species. The common theme in these studies is interactions between states of different character and intersections between the corresponding potential energy surfaces. We also continued to develop and benchmark computational methods for modeling electronic structure and spectroscopy of open-shell species. Particular emphasis was placed on determining spectroscopic signatures of transient species, to facilitate comparisons with experimental data.

In 2013-2014, the DOE support has been acknowledged in five papers;[1–5] one paper is under review. Some of the recent results are highlighted below.

2.1 Multiple potential energy surfaces and conical intersections

Accurate description of conical intersections is a challenging task for electronic structure methods as it requires balanced description of interacting states. Using a simple model system, PSB3, we investigated the performance of various approaches in the vicinity of a conical intersection,[5] see Fig. 1 (left). We considered multi-reference methods, such as CASSCF, MR-CI with and without Davidson correction, various flavors of MR-PT, as well as spin-flip methods. We found that a balanced description of dynamical and non-dynamical correlation is essential for reproducing the location and energy of conical intersections. As illustrated in

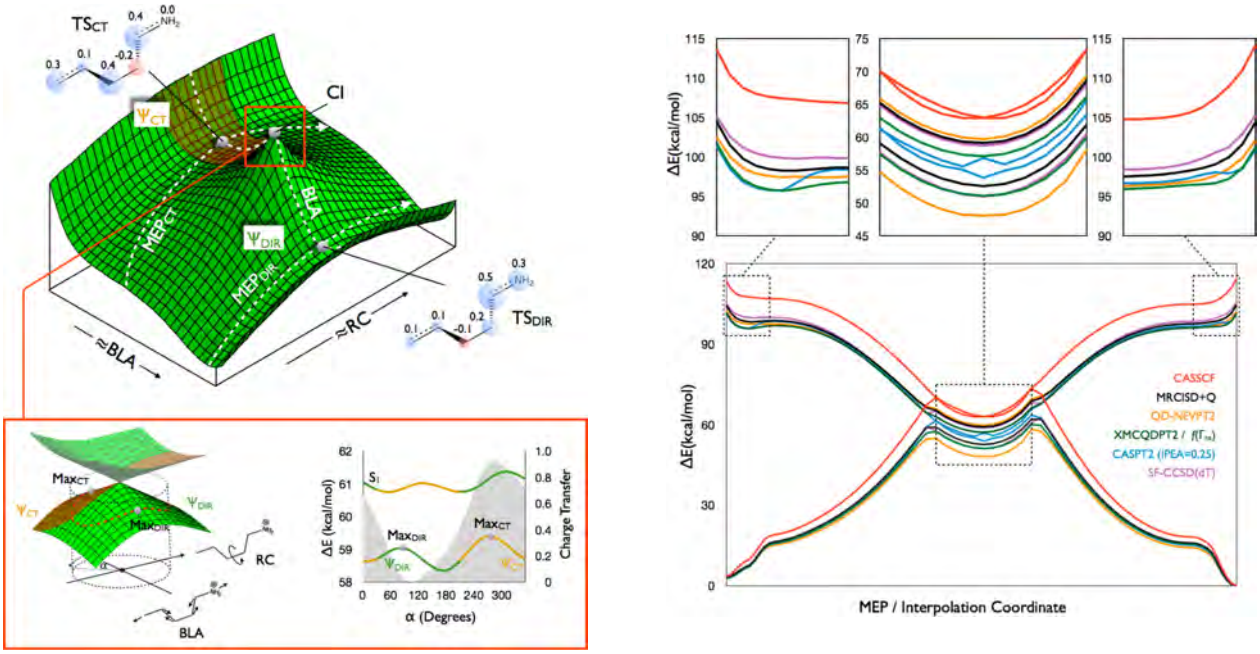

Figure 1: Left: Schematic two-dimensional cut of the ground-state potential energy surface of PSB3. The two coordinates can be described as bond length alternation (BLA) and the C2-C3 twisting reaction coordinate (RC). Around the intersection, the wave function changes its character from charge-transfer (brown) to diradical (green). Three different paths around the intersection (dashed lines) are shown by the dashed lines on the surface. Right: CASSCF (red), MRCISD+Q (black), QD-NEVPT2 (orange), XMCQDPT2 (green), CASPT2 (blue), and SF-CCSD(dT) (violet) energy profiles along the composite CASSCF path comprising MEP_{CIS}, CI seam, and MEP_{TRANS}. The insets show an expansion of the 10 points nearest to each of the cis- and trans-PSB3 structures and of the CI seam.

Fig. 1 (right), dynamical correlation stabilizes the S_1 state along the entire path and, also, stabilizes the S_0 energy of all structures relative to the equilibrium cis and trans structures. While it is not surprising that the CASSCF surfaces are quite far from the reference MR-CISD(Q), the discrepancies between various MR-PT methods are disconcerting. Overall, the performance of XMCQDPT2 is solid, whereas the CASPT2 methods exhibit artifacts in the regions of exact degeneracies. EOM-SF-CCSD provides a qualitatively accurate description of the two PES, however, the triples correction (dT) is needed for quantitatively accurate profiles that are in good agreement with MRCISD+Q.

2.2 Dyson orbitals and photoionization/photodetachment cross sections

Dyson orbitals quantify the difference between N and $N-1$ electron wave functions:

$$\phi^d(x) = < \Psi(N)|\hat{p}|\Psi(N-1) > \quad (1)$$

They are needed for computing photoionization/photodetachment cross sections and angular photoelectron distributions. We completed new and robust implementation of Dyson orbitals

within the EOM-IP-CCSD formalism using new tensor library and EOM/CC codes.[3] We also corrected problems that were present in our earlier pilot implementation (incorrect normalization). In collaboration with Prof. John Stanton, we are now investigating different approaches for improving the description of the free electron, which is required for cross section calculations.

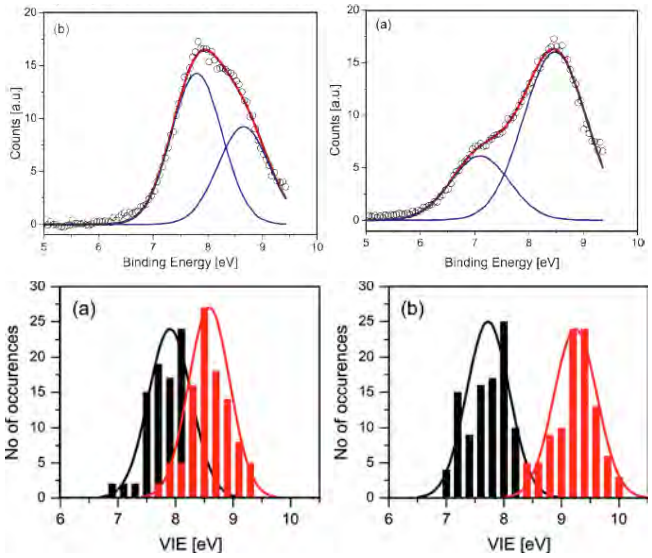

Figure 2: Photoelectron spectra of aqueous phenol and phenolate (top) show two bands. The calculations of ionization energies in bulk solvent (bottom) reproduce the position and the width of the bands, but fail to explain different intensity. Note that in phenol, the intensity of the first band is higher, whereas in phenolate the ratio is reversed. Adapted from Ghosh *et al*, J. Phys. Chem. B **116**, 7269 (2012).

We are applying the new code to photoionization spectra of phenol and phenolate in water (see Fig. 2). Electronic structure calculations that assume identical cross sections for all transitions reproduce well both the positions of the peaks and their widths; however, the trends in the peaks intensities are not captured suggesting that the two ionization bands have different cross sections, and that the respective cross sections are different in phenol and phenolate. Our preliminary calculations of Dyson orbitals reveal that the character of the second ionized state changes considerably upon deprotonation. The calculations of relative weights corresponding to deferent plane waves confirm that the cross sections indeed should be different. For quantitative comparison, we plan to include solvent molecules via the EFP approach.

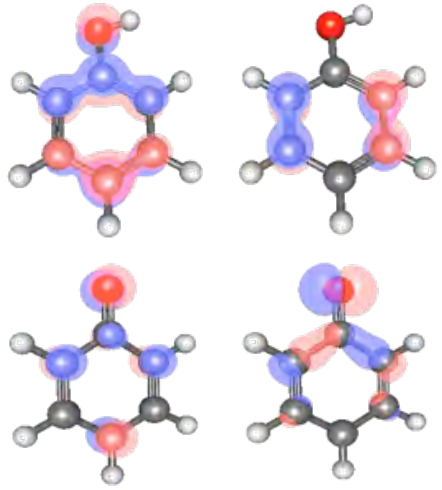

Figure 3: Dyson orbitals corresponding to the two lowest ionized states of phenol (top) and phenolate (bottom). Deprotonation leads to changes in electronic states of the ionized species. While the lowest ionized state is dominated by out-of-plane lp(O) (plus contributions from the π-system) both in phenol and in phenolate, the second ionized state is different in the two species. Consequently, the coefficients of different target states are very different for the second state leading to differences in cross sections.

2.3 Protocols for calculating redox properties and energetics of hydrade transfer reactions

Motivated by the experimental work targeting design of the organic photo-catalysts for hydrade transfer, which is of interest in the context of solar fuels, we investigated ground and excited-state properties of model compounds based on 10-methyl-9-phenyl-9,10-dihydroacridine.[1] We developed and refined computational protocols for computing redox potentials and energetics of hydrade transfer. For reference systems, the computed Gibbs free energies are within 2 kcal/mol from the experimental values. This protocol is now used by the experimentalists (Glusac group) enabling computational screening of a large number of prospective compounds.

3 Current developments and future plans

Currently, we are improving the methodology for calculating cross sections from Dyson orbitals. This will be followed by extensive benchmarking. We are also implementing mean-field approximation to spin-orbit couplings, which will enable calculations for larger systems. Other projects include computational studies of several radicals relevant to combustion and improving numeric stability of analytic gradients for non-collinear SF-TDDFT.

References

[1] X. Yang, J. Walpita, D. Zhou, H.L. Luk, S. Vyas, R.S. Khnayzer, S.C. Tiwari, K. Diri, C.M. Hadad F.N. Castellano, A.I. Krylov, and K.D. Glusac, Towards organic photohydrides: Excited-state behavior of 10- methyl-9-phenyl-9, 10-dihydroacridine, J. Phys. Chem. B **117**, 15290 (2013).

[2] K. Khistyaev, A. Golan, K.B. Bravaya, N. Orms, A.I. Krylov, and M. Ahmed, Proton transfer in nucleobases is mediated by water, J. Phys. Chem. A **117**, 6789 (2013).

[3] E. Epifanovsky, M. Wormit, T. Kuś, A. Landau, D. Zuev, K. Khistyaev, P. Manohar, I. Kaliman, A. Dreuw, and A.I. Krylov, New implementation of high-level correlated methods using a general block-tensor library for high-performance electronic structure calculations, J. Comput. Chem. **34**, 2293 (2013).

[4] K.B. Bravaya and A.I. Krylov, On the photodetachment from the green fluorescent protein chromophore, J. Phys. Chem. A **117**, 2293 (2013).

[5] S. Gozem, F. Melaccio, R. Lindh, A.I. Krylov, A.A. Granovsky, C. Angeli, and M. Olivucci, Mapping the excited state potential energy surface of a retinal chromophore model with multireference and equation-of-motion coupled-cluster methods, J. Chem. Theory Comput. **9**, 4495 (2013).

Radical Reactions and Dynamics in the Gas and Heterogeneous Phases

Stephen R. Leone, Jessica F. Lockyear, Denisia M. Popolan-Vaida, Theodora Nah and Andrew Attar
Lawrence Berkeley National Laboratory and Departments of Chemistry and Physics University of California, Berkeley, California 94720 (510) 643-5467 srl@berkeley.edu

Scope of the Project: In this program a diverse approach to researching combustion chemistry is taken by applying a variety of techniques. This makes it possible unravel a range of unknown aspects of this enormously complex process. Combustion involves innumerable intertwined reactions and processes such as short-lived-radical reactions, highly excited states, fuel transport, heterogeneous chemistry, fluid dynamics, and energy transfer. Decades of research into each of these areas individually have lead to an increased understanding of combustion in real environments and allowed for many technological and chemical advances to be made. Vacuum ultraviolet (VUV) light from the Chemical Dynamics Beamline of the Advanced Light Source is a powerful tool to selectively investigate the individual component processes involved in combustion. Several experimental set-ups have been coupled with the synchrotron light with this goal in mind: a multiplexed photoionization mass spectrometer (MPIMS), which was co-constructed with D. L. Osborn and C. A. Taatjes of the Sandia Combustion Research Facility (CRF), is used to investigate gas-phase chemistry; an aerosol mass spectrometer is used to investigate heterogeneous phase chemistry; and a recently-developed jet-stirred reactor (JSR) is used to investigate high temperature hydrocarbon oxidation. In addition, the latest advances include use of a novel laboratory table-top UV-pump, XUV-probe transient absorption technique to capture ultrafast photochemical dynamics of radicals.

Recent Progress

Gas-Phase Chemistry: Experimental investigations using the MPIMS have considered several reactions of CH and C_2H with straight-chain molecules that result in formation of cyclic species. Specifically, it was found that the reaction between CH and acrolein proceeds *via* addition and H-loss to yield C_4H_4O products with an isomeric composition of (60 ± 12)% 1,3-butadienal and (17 ± 10)% furan. Formation of the heterocyclic 5-membered ring is significant since the reactive pathways that lead to oxygen-heterocycles in combustion are not well understood. Moreover, further evidence has been obtained that shows cyclization reactions compete favorably with direct H-loss that gives straight-chain products. For example, the reaction of CH with 1,3-butadiene, which has a structural motif identical to that of acrolein, yields cyclopentadiene in an analogous pathway to the furan formation in the CH + acrolein reaction. In addition, C_2H reacts with 1,3-butadiene to give approximately 45% fulvene. In contrast with acrolein, the reaction of CH with propanal was found to generate exclusively straight chain products that are predominantly ketenes, such as ketene, methylketene, ethylketene and dimethylketene. Ketenes are known to be important combustion intermediates.

Heterogeneous Chemistry: The kinetics and products of two model heterogeneous reaction systems, OH + squalene ($C_{30}H_{50}$, a branched alkene with 6 C=C double bonds) and OH + unsaturated fatty acid (oleic acid $C_{18}H_{34}O_2$, linoleic acid $C_{18}H_{32}O_2$ and linolenic acid $C_{18}H_{30}O_2$, linear carboxylic acids with 1, 2 and 3 C=C double bonds, respectively), are measured to investigate the effect of molecular structure and chemical functionality on the reaction rates and mechanism in the OH-initiated oxidation of organic particles. In a 10% mixture of O_2 in N_2 in the flow reactor, the effective uptake coefficients (γ_{eff}) for squalene and the unsaturated fatty acids are all larger than unity (measured by loss of the parent aerosol molecules), providing clear evidence for particle-phase chain chemistry.

γ_{eff} for squalene is 2.34 ± 0.07, smaller than γ_{eff} for linoleic acid and linolenic acid (3.75 ± 0.18 and 5.73 ± 0.14, respectively) despite the larger number of C=C double bonds in squalene. This may be attributed to differences in the uptake of OH at the particle surface and particle-phase secondary reactions. In addition, γ_{eff} for squalene increases with $[O_2]$ in the reactor, whereas γ_{eff} values for the unsaturated fatty acids decrease with increasing $[O_2]$. This suggests that the chain-cycling mechanism in these two systems is different since O_2 promotes chain propagation in the OH + squalene reaction but causes chain termination in the OH + unsaturated fatty acid reactions. Elemental analysis of squalene particles shows that particle volatilization only becomes important in the later stages of oxidation at ~ 0 % $[O_2]$, while significant particle volatilization occurs once oxidation is initiated at 10% $[O_2]$. In contrast, elemental analysis of linoleic acid particles shows that $[O_2]$ does not influence the rate of particle volatilization in the OH + linoleic acid reaction.

The reaction of I atoms with squalene and squalane sub-micron droplets was investigated in order to interrogate the effect of C=C bonds. The results show no evidence of product formation with squalane droplets (no C=C bonds). In contrast, squalene droplets (6 C=C bonds) are found to react with I atoms, despite the gas-phase reaction having very low probability. The uptake coefficient for squalene is found to be three orders of magnitude larger than that estimated for squalane. These results emphasize that reactions that have low probability in the gas phase might have an enhanced probability in the heterogeneous phase.

Hydrocarbon Oxidation in a Jet-Stirred Reactor: A high temperature (500-1100 K) JSR system has recently been constructed and successfully interfaced to a molecular-beam mass spectrometer. This experimental arrangement presents a unique approach to monitor chemical transformations in well-defined conditions comparable to those in combustion engines. Oxidation studies of n-butane, partially deuterated n-butane and dimethyl ether have revealed new insights into the oxidation mechanism of these species while the molecular beam sampling approach permitted the detection of fragile intermediates like ketohydroperoxides, which act as important chain branching intermediates in low temperature auto-ignition. These experiments were performed together with the CEFRC project in Princeton, in collaboration with the team lead by N. Hansen of Combustion Research Facility, Sandia National Laboratories, and as part of augmentation support together with C. A. Taatjes of Sandia National Laboratories. The initial experiments also involved principal researchers, S. M. Sarathy (KAUST), K. Kohse-Höinghaus (Bielefeld), P. Dagaut (Orleans), and Y. Ju (Princeton).

XUV Probing of Ultrafast Reaction Dynamics: A novel UV-pump, XUV-probe transient absorption technique utilizing high-harmonic generation to produce XUV pulses with sub-40 fs duration has been applied to capture ultrafast gas-phase photochemical reaction dynamics. The core-to-valence transitions involved in XUV absorption spectroscopy allow for direct probing of the electronic structure of transient species throughout the lifetime of a photochemical reaction. The technique has been applied to track the UV photodissociation of dihalomethanes, CH_2IBr and CH_2I_2, and to probe the formation and electronic structure of halomethyl radicals CH_2Br and CH_2I. These are the simplest of the α-haloalkyl radicals (R-CX, X=Br,I) and can act as key reactive intermediates in combustion chemistry or in the case of CH_2I as a precursor for a Criegee intermediate. The transient absorption XUV spectra of the CH_2Br and CH_2I radicals formed from photodissociation of CH_2IBr and CH_2I_2 have been observed for the first time, revealing 3d(Br)→SOMO (singly occupied molecular orbital) and 4d(I)→SOMO resonances. In

both CH_2I_2 and CH_2IBr, the 266 nm excitation is dominated by $n(I) \rightarrow \sigma^*(C\text{-}I)$ transitions, leading primarily to C-I bond cleavage. However, in the case of CH_2IBr, there is also a minor excitation of the $n(Br) \rightarrow \sigma^*(C\text{-}Br)$ transition leading to C-Br bond cleavage. Dissociation along each reaction coordinate can be separately, yet simultaneously, monitored and the measured time constants of the two dissociation channels are found to be different. The rise times of the I atomic resonances from C-I dissociation and Br atomic resonances from C-Br dissociation are measured as 53 ± 10 fs and 117 ± 17 fs, respectively.

Future Plans: Future directions in the gas-phase efforts involve investigating the recently discovered propensity of CH and C_2H radicals to form cyclic products in reactions with multiply unsaturated hydrocarbons. One aspect of the ring-forming reactions that we plan to explore is the importance of the separation of the unsaturated sites. This will be probed by studying the reaction of CH and C_2H with 1,2-butadiene and 1,4-pentadiene. Another aspect to be investigated is the influence of branching in the reactant molecule on the propensity for CH and C_2H to yield cyclic isomers; to this end, reactions of these radicals with methacrolein and methylvinylketone will be studied. It is also valuable to study the reaction of C_2H with 1,2-butadiene, which has been predicted theoretically to yield predominantly 2-ethynyl-1,3-butadiene, an outcome that can be tested experimentally.

The structural complexity and the low volatility of long hydrocarbon chains of the fatty-acid esters of biodiesel fuels impede studies of their gas-phase oxidation chemistry. Therefore, in the JSR, we plan to investigate the oxidation chemistry of three pairs of fuels with similar structures, but different degrees of unsaturation (methyl butanoate *vs*. methyl crotonate, methyl isobutanoate *vs*. methyl methacrylate, ethyl propanoate *vs*. ethyl propenoate). These molecules are chosen because they contain the structural functional groups expected to account for fuel-specific effects, while their structural simplicities allow quantitative kinetic modelling. The main focus will be on understanding the formation of important low-temperature oxidation intermediates such as ketohydroperoxides.

In most real combustion devices the preparation of the fuel-air mixture is a critical determinant of the overall performance, and the mechanisms of breakup, mixing, and evaporation of liquid fuel (droplet sprays) is a key area of research. A novel set of experiments will be developed to probe the interaction of these physical and chemical processes by introducing heterogeneous flows of particles into a controlled oxidizing environment in a JSR, while monitoring the gas phase products and particle composition. Efforts are underway in collaboration with C. A. Taatjes and co-workers of Sandia's CRF to modify the existing JSR system to make it suitable for the investigation of low-vapor-pressure fuels. First systems will be to measure the oxidation of methyl stearate and methyl linoleate as well as novel biodiesel candidates, bisabolene and bisabolane. The measurements will focus on the important "negative temperature coefficient" region, where the oxidation process becomes slower with increasing temperature. Fuel-structure effects are most prominent in this temperature region. Also, in this range the reactivity difference between resonance-stabilized and non-resonance-stabilized radicals is most dramatic. In these studies special attention will be dedicated to understanding the effect of double bonds and how their presence changes the nature of the ignition process.

On-going and future experiments in the area of XUV radical dynamics aim to address the effects of substituents on the energetics of the SOMO in haloalkyl radicals. Replacing

hydrogen atoms with methyl groups or fluorine atoms, for example, will allow us to evaluate the energetics of the SOMO under the influence of electron donating and withdrawing groups directly through the core-to-SOMO XUV transition energies.

Recent Publications Citing DOE Support (2011-2013)

- J. F. Lockyear, O. Welz, J. D. Savee, F. Goulay, A. J. Trevitt, C. A. Taatjes, D. L. Osborn and S. R. Leone, "*Isomer Specific Product Detection in the Reaction of CH with Acrolein*", J. Phys. Chem. A, *117*, 11013 **(2013)**
- A. J. Trevitt, M. B. Prendergast, F. Goulay, J. D. Savee, D. L. Osborn, C. A. Taatjes and S. R. Leone, "*Product Branching Fractions of the CH plus Propene Reaction from Synchrotron Photoionization Mass Spectrometry*", J. Phys. Chem. A, *117*, 6450, **(2013)**
- J. Bouwman, M. Fournier, I. R. Sims, S. R. Leone and K. R. Wilson, "*Reaction Rate and Isomer-Specific Product Branching Ratios of C_2H + C_4H_8: 1-Butene, cis-2-Butene, trans-2-Butene, and Isobutene at 79 K*", J. Phys. Chem. A, *117*, 5093, **(2013)**
- E. R. Hosler and S. R. Leone, "*Characterization of Vibrational Wave Packets by Core-Level High-Harmonic Transient Absorption Spectroscopy*", Phys. Rev. A, *88*, 023420, **(2013)**
- S. D. Chambreau, J. B. Liu, G. L. Vaghjiani, C. J. Koh, A. Golan, O. Kostko and S. R. Leone, "*Thermal decomposition mechanisms of ionic liquids by direct dynamics simulations and vacuum ultraviolet photoionization mass spectrometry*", Abstracts of Papers of the Am. Chem. Soc., *245*, 206-PHYS, **(2013)**
- T. Nah, M. Chan, S. R. Leone and K. R. Wilson, "*Real Time in Situ Chemical Characterization of Submicrometer Organic Particles using Direct Analysis in Real Time Mass Spectrometry*", Anal. Chem., *85*, 2087, **(2013)**
- T. Nah, S. H. Kessler, K. E. Daumit, J. H. Kroll, S. R. Leone and K. R. Wilson, "*OH-initiated oxidation of sub-micron unsaturated fatty acid particles*", Phys. Chem. Chem. Phys., *115*, 18649, **(2013)**
- S. H. Kessler, T. Nah, K. E. Daumit, J. D. Smith, S. R. Leone, C. E. Kolb, D. R. Worsnop, K. R. Wilson and J. H. Kroll, "*OH-Initiated Heterogenous Aging of Highly Oxidized Organic Aerosol*", J. Phys. Chem. A, *116*, 6358 **(2012)**
- J. Bouwman, F. Goulay, S. R. Leone and K. R. Wilson, "*Bimolecular Rate Constant and Product Branching Ratio Measurements for the Reaction of C_2H with Ethene and Propene at 79 K*", J. Phys. Chem. A, *116*, 3907 **(2012)**
- F. Goulay, A. J. Trevitt, J. D. Savee, J. Bouwman, D. L. Osborn, C. A. Taatjes, K. R. Wilson and S. R. Leone, "*Product Detection of the CH Radical Reaction with Acetaldehyde*", J. Phys. Chem. A, *116*, 6091, **(2012)**
- F. Goulay, S. Soorkia, G. Meloni, D. L. Osborn, C. A. Taatjes and S. R. Leone, "*Detection of Pentatetraene by Reaction of the Ethynyl Radical (C_2H) with Allene ($CH_2=C=CH_2$) at Room Temperature*", Phys. Chem. Chem. Phys. *13*, 20820 **(2011)**
- J. Trevitt, S. Soorkia, J. D. Savee, T. S. Selby, D. L. Osborn, C. A. Taatjes, and S. R. Leone, "*Branching Fractions of the CN + C_3H_6 Reaction Using Synchrotron Photoionization Mass Spectrometry: Evidence for the 3-Cyanopropene Product*", J. Phys. Chem. A *115*, 13467 **(2011)**
- S. Soorkia, C.-L. Liu, J. D. Savee, S. J. Ferrell, S. R. Leone, and K. R. Wilson, "*Airfoil Sampling of a Pulsed Laval Beam with Tunable Vacuum Ultraviolet Synchrotron Ionization Quadrupole Mass Spectrometry: Application to Low Temperature Kinetics and Product Detection*", Rev. Sci. Instrum. *82*, 124102 **(2011)**
- C.-L. Liu, J. D. Smith, D. L. Che, M. Ahmed, S. R. Leone, and K. R. Wilson, "*The Direct Observation of Secondary Radical Chain Chemistry in the Heterogeneous Reaction of Chlorine Atoms with Submicron Squalane Droplets*", Phys. Chem. Chem. Phys. *13*, 8993 **(2011)**

INTERMOLECULAR INTERACTIONS OF HYDROXYL RADICALS ON REACTIVE POTENTIAL ENERGY SURFACES

Marsha I. Lester
Department of Chemistry
University of Pennsylvania
Philadelphia, PA 19104-6323
milester@sas.upenn.edu

I. Program Scope

Hydroxyl radicals are important in combustion and atmospheric environments, where they are often detected by laser-induced fluorescence (LIF) on the $A^2\Sigma^+$–$X^2\Pi$ band system. However, collision partners known to quench electronically excited OH $A^2\Sigma^+$ radicals are ubiquitous in these environments. Thus, great effort has been made to quantify the rates and/or cross sections for collisional quenching, so that its effects on LIF signals may be taken into account. This laboratory has focused on understanding the fundamental chemical dynamics governing quenching of OH $A^2\Sigma^+$ by molecular partners of significance in combustion environments. This is achieved through experimental studies of the dynamical ***outcomes*** following collision quenching of OH $A^2\Sigma^+$ and complementary theoretical investigations. Related work is aimed at developing a sensitive, quantum state-selective ionization scheme for OH radicals, and utilizing this approach for mass-selective time-of-flight and velocity map imaging studies of OH $X^2\Pi$ products from dynamical processes.

II. Recent Progress

A. *Outcomes* of collisional quenching of electronically excited OH $A^2\Sigma^+$ radicals

Our experimental studies of collisional quenching of OH $A^2\Sigma^+$ by molecular partners examine reactive processes that generate chemically distinct products as well as nonreactive processes that return OH $A^2\Sigma^+$ radicals to their ground $X^2\Pi$ electronic state. The experimental observables measured include the branching between reactive and nonreactive decay channels, kinetic energy release to atomic products, and quantum state distributions of the products. These dynamical outcomes reflect the forces acting on the nuclei as the system switches from the electronically excited potential energy surface to products through regions of strong nonadiabatic coupling, known as conical intersections.

Several key trends are emerging from our quenching studies of OH $A^2\Sigma^+$ + M = H_2, N_2, and CO, where both experiment and theory are available.[1] The large cross sections for collisional quenching are associated with fast dynamics and strong coupling between the OH ($A^2\Sigma^+$, $X^2\Pi$) + M potential energy surfaces in very limited regions, e.g. O-side of OH pointing toward M, of the available configuration space. The minimal vibrational excitation of the OH $X^2\Pi$ products shows that the OH bondlength is essentially unchanged as it switches from the excited $A^2\Sigma^+$ to ground $X^2\Pi$ electronic state. On the other hand, the quite significant rotational excitation of the OH $X^2\Pi$ products is indicative of a strong torque placed on the OH radical in the vicinity of the conical intersection. In these same systems, the $\Pi(A')$ Λ-doublet propensity of the OH $X^2\Pi$ products appears to reflect the symmetry of the potentials at the crossing. The kinetic energy

release to H, D, and O-atom reaction products and the corresponding internal energy of the cofragment provides additional insight on the geometric configuration at the conical intersection region, particularly when it differs greatly from the equilibrium structure of the products. In some cases, such as the H_2O products from OH $A^2\Sigma^+ + H_2$, the configuration at the conical intersection maps onto highly vibrationally excited products. Finally, the pitch and tilt of the cone at the intersection influences the branching between nonreactive and reactive quenching events.

Our most recent study involves electronic quenching of OH $A^2\Sigma^+$ by Kr, where we probed the OH $X^2\Pi$ product distribution.[2] Again, we find that the OH $X^2\Pi$ products of quenching exhibit a significant degree of rotational excitation, but minimal vibrational excitation. The OH $X^2\Pi$ (v''=0, N'') distribution exhibits a peak around 9 quanta of rotation, followed by a slight dip and then a second peak around 17 quanta of rotation, with an average rotational energy of 4400 cm^{-1}. The doubly peaked rotational distribution in the OH + Kr system is different than other systems studied, although there is still an overall high degree of rotational excitation. Alexander and coworkers carried out complementary theoretical studies of the OH ($A^2\Sigma^+$, $X^2\Pi$) + Kr potential energy surfaces (PES's), nonadiabatic coupling, and quasi-classical trajectory calculations to elucidate the quenching dynamics.[2] Accurate PES's for the two lowest diabatic states of A′ symmetry are computed along with the angularly dependent coupling between them. Coupling in near linear HO–Kr configurations provides the mechanism for the electronic quenching. A deep attractive well on the OH $A^2\Sigma^+$ – Kr PES facilitates access to this region of strong coupling. Surface-hopping quasi-classical trajectory calculations yield quenching cross sections and OH $X^2\Pi$ product rotational distribution in good accord with our experimental observations.

B. A new spectroscopic window on hydroxyl radicals using UV+VUV resonant ionization

We have carried out a detailed investigation of a new 1+1′ resonance enhanced multiphoton ionization (REMPI) scheme for detection of OH $X^2\Pi$ radicals utilizing a broad range of intermediate $A^2\Sigma^+$ (v=1, 2) levels.[3,4] The intensities of OH A-X (1,0) transitions detected by subsequent fixed-frequency VUV ionization at 118 nm are compared with those obtained by near simultaneous laser-induced fluorescence (LIF) measurements. The ratios of the REMPI to LIF intensities for various OH $A^2\Sigma^+$ (v=1, J, F_i) levels yield enhancement factors that provide information on the VUV excitation step and/or ionization process. The enhancement factors display a peaked profile with total energy indicating that the VUV step accesses the OH [$A^3\Pi$, 3d], v = 0 Rydberg state prior to rapid Auger decay and ionization. The enhancement factors also provide a quantitative guide for using this 1+1′ REMPI scheme for state-selective and mass-specific detection of OH $X^2\Pi$ radicals. The OH A-X transition is well characterized and the fixed-frequency VUV at 118 nm is readily generated from the third harmonic of a Q-switched Nd:YAG laser, making this 1+1′ REMPI scheme ideal for laboratory ionization studies of the OH $X^2\Pi$ radical. This REMPI scheme has already been utilized for detection of OH $X^2\Pi$ products from unimolecular decay of Criegee intermediates.[5,6] Many future experiments are suggested by this work, some of which will be enabled with tunable VUV light.

C. Velocity map imaging studies related to Criegee intermediates

DOE provided supplementary equipment funds that enabled us to construct a new velocity map imaging (VMI) apparatus. Our initial VMI study focused on the photodissociation of CH_2I_2

at 248 nm,[7] which is of renewed interest because subsequent reaction of CH_2I photofragments with O_2 is being utilized to generate the simplest Criegee intermediate CH_2OO for laboratory studies.[8,9] In our VMI study, the I*($^2P_{1/2}$) products are detected by 2+1 REMPI at 313 nm; background one-color I* signal from 313 nm photolysis/ionization alone is subtracted. The resultant image arising from 248 nm photolysis is reconstructed to obtain the velocity and angular distributions of the I* products as well as the corresponding kinetic energy release to products and anisotropy parameter. The dominant feature in the total kinetic energy distribution has a sizable breadth and average translational energy of 2100 cm^{-1}, which corresponds to only 14% of the available energy. This leaves the remaining 86% channeled into the internal excitation of the CH_2I cofragment, where $\langle E_{int} \rangle$ = 12,700 cm^{-1} (36.3 kcal mol^{-1}). This is in accord with a previous investigation of IR emission from CH_2I fragments produced with a combination of I and I* cofragments.[10] Assuming that this high degree of internal excitation of the CH_2I fragment is carried over into CH_2OO in a near thermo-neutral process,[11] the internal energy of the Criegee intermediate produced in the laboratory likely mimics that from alkene ozonolysis in the atmosphere.

Our next VMI study focused on the UV photodissociation dynamics of the simplest Criegee intermediate CH_2OO.[12] Here, the velocity and angular distributions of O ^1D photofragments are characterized following UV excitation of CH_2OO on the $B^1A' \leftarrow X^1A'$ transition.[9] An anisotropic angular distribution indicative of prompt dissociation yields the orientation of the transition dipole moment, which reflects the $\pi^* \leftarrow \pi$ character of the electronic transition associated with the COO group. The total kinetic energy release distributions obtained at several photolysis wavelengths provide detail on the internal energy distribution of the formaldehyde cofragments and the dissociation energy of CH_2OO X^1A' to $O^1D + H_2CO$ X^1A_1. A common termination of the total kinetic energy distributions, after accounting for the different excitation energies, gives an upper limit for the CH_2OO X^1A' dissociation energy of $D_0 \leq 54$ kcal mol^{-1}, which compares favorably with theoretical predictions including high level multi-reference *ab initio* calculations.

III. Future Work

Future studies will expand our investigation of the 1+1′ REMPI detection scheme for OH $X^2\Pi$ radicals, particularly focused on the autoionization process. Tunable VUV light for the valence to Rydberg transition along with photoelectron kinetic energy and angular distribution measurements are needed. We also plan to utilize this novel OH detection scheme in VMI studies of photochemical and unimolecular reactions.

IV. References

1. J. H. Lehman and M. I. Lester, *Ann. Rev. Phys. Chem.* **65**, 537‑55 (2014).
2. J. H. Lehman, M. I. Lester, J. Kłos, M. H. Alexander, P. J. Dagdigian, D. Herráez-Aguilar, F. J. Aoiz, M. Brouard, H. Chadwick, T. Perkins, and S. A. Seamons, *J. Phys. Chem. A* **117**, 13481-90 (2013).
3. J. M. Beames, F. Liu, M. I. Lester and C. Murray, *J. Chem. Phys.* **134**, 241102 (2011).
4. J. M. Beames, F. Liu, and M. I. Lester, *Mol. Phys.* **112**, 897-903 (2014).
5. J. M. Beames, F. Liu, L. Lu, and M. I. Lester, *J. Chem. Phys.* **138**, 244307 (2013).
6. F. Liu, J. M. Beames, A. M. Green, and M. I. Lester, *J. Phys. Chem. A* **118**, 2298–2306 (2014).

7. J. H. Lehman, H. Li and M. I. Lester, *Chem. Phys. Lett.* **590**, 16-20 (2013).
8. O. Welz, J. D. Savee, D. L. Osborn, S. S. Vasu, C. J. Percival, D. E. Shallcross and C. A. Taatjes, *Science* **335**, 204 (2012).
9. J. M. Beames, F. Liu, L. Lu and M. I. Lester, *J. Am. Chem. Soc.* **134**, 20045 (2012).
10. S. L. Baughcum and S. R. Leone, *J. Chem. Phys.* **72**, 6531 (1980).
11. E. P. F. Lee, D. K. W. Mok, D. E. Shallcross, C. J. Percival, D. L. Osborn, C. A. Taatjes and J. M. Dyke, *Chem. Eur. J.* **18**, 12411 (2012).
12. J. H. Lehman, H. Li, J. M. Beames and M. I. Lester, *J. Chem. Phys.* **139**, 141103 (2013).

V. Publications supported by this project (2011-2014)

1. J. H. Lehman and M. I. Lester, "Dynamical outcomes of quenching: Reflections on a conical intersection", *Ann. Rev. Phys. Chem.* **65**, 537‑55 (2014).
2. J. M. Beames, F. Liu, and M. I. Lester, "1+1′ resonant ionization of OH radicals via the $A^2\Sigma^+$ state: Insights from direct comparison with A-X fluorescence detection", *Mol. Phys.* **112**, 897-903 (2014).
3. J. H. Lehman, H. Li, J. M. Beames and M. I. Lester, "Communication: Ultraviolet photodissociation dynamics of the simplest Criegee intermediate CH_2OO", *J. Chem. Phys.* **139**, 141103 (2013).
4. J. H. Lehman, H. Li and M. I. Lester, "Ion imaging studies of the photodissociation dynamics of CH_2I_2 at 248 nm", *Chem. Phys. Lett.* **590**, 16-20 (2013).
5. J. H. Lehman, M. I. Lester, J. Kłos, M. H. Alexander, P. J. Dagdigian, D. Herráez-Aguilar, F. J. Aoiz, M. Brouard, H. Chadwick, T. Perkins, and S. A. Seamons, "Electronic quenching of OH $A^2\Sigma^+$ induced by collisions with Kr atoms", *J. Phys. Chem. A* **117**, 13481-90 (2013).
6. J. H. Lehman, M. I. Lester, and D. H. Yarkony, "Reactive quenching of OH $A^2\Sigma^+$ by O_2 and CO: Experimental and nonadiabatic theoretical studies of H- and O-atom product channels", *J. Chem. Phys.* **137**, 094312 (2012).
7. J. M. Beames, F. Liu, M. I. Lester, and C. Murray, "Communication: A new spectroscopic window on hydroxyl radicals using UV+VUV resonant ionization", *J. Chem. Phys.* **134**, 241102 (2011).
8. J. H. Lehman, J. Bertrand, T. A. Stephenson, and M. I. Lester, "Reactive quenching of OD $A^2\Sigma^+$ by H_2: Translational energy distributions for H- and D-atom product channels", *J. Chem. Phys.* **135**, 144303 (2011).

Theoretical Studies of Molecular Systems

William A. Lester, Jr.
Chemical Sciences Division,
Ernest Orlando Lawrence Berkeley National Laboratory and
Kenneth S. Pitzer Center for Theoretical Chemistry
Department of Chemistry, University of California, Berkeley
Berkeley, California 94720-1460
walester@lbl.gov

Program Scope

This research program is directed at extending fundamental knowledge of atoms and molecules. The approach combines the use of ab initio basis set methods and the quantum Monte Carlo (QMC) method to describe the electronic structure and energetics of systems of primarily combustion interest.

Recent Progress

To assist understanding of combustion processes, we have investigated reactions of methylidyne (CH) with acrolein (CH_2CHCHO) using various ab initio and QMC methods stimulated by experiments and theory of Leone and collaborators. The DFT, MP2 and CASSCF approaches have been carried out and these methods used, in addition, to form the independent-particle part of QMC trial wave functions. Both the variational (VMC) and diffusion (DMC) variants of the QMC method are being used. In agreement with experiment, we found from computations to date that the dominant product channel is the formation of C_4H_6 systems + H with leading products of furan + H and 1,3-butadienal + H. Equilibrium geometries, transition states, heats of reaction, and total energies are being computed using the various approaches as well as reaction barriers and atomization energies.

Future Plans

The present level of development of the two central QMC approaches, VMC and FNDMC, is sufficiently high that they can be used routinely to compute ground state energies of molecular systems. Certain basic and methodological aspects of QMC still need refinement and development, especially for electronically excited states and open-shell systems. Future research incorporates these aspects. The primary direction is system-specific research that focused on issues relevant to experimental investigations carried out by CSD PIs. This direction

is primarily dedicated to utilization of existing QMC methodology for computations of various energetic characteristics of molecules, such as reaction energies, reaction barriers, electron affinities and detachment energies. FNDMC is a reliable source of these values even with the simplest available trial wave functions of Hartree-Fock (HF) or Kohn-Sham (KS-DFT) quality.

DoE Supported Publications (2011-2013)

1. X. You, R. Whitesides, D. Zubarev, W. A. Lester, Jr., and M. Frenklach, "Bay-capping Reactions: Kinetics and Influence on Graphene-Edge Growth," Proc. Combust. Inst. **33**, 685 (2011).
2. D. Yu. Zubarev, X. You, J. McClean, W. A. Lester, Jr., and M. Frenklach, "Patterns of local aromaticity in graphene oxyradicals," J. Mater. Chem. **21**, 3404 (2011).
3. X. You, D. Yu. Zubarev, W. A. Lester, Jr., and M. Frenklach, "Thermal decomposition of pentacene oxyradicals," J. Phys. Chem. A **115**, 14184 (2011).
4. D. Yu. Zubarev, X. You, M. Frenklach, and W. A. Lester, Jr., "Delocalization effects in pristine and oxidized graphene substrates," in *Advances in the Theory of Quantum Systems in Chemistry and Physics* (P. E. Hoggan, E. J. Brändas, J. Maruani, P. Piecuch, and G. Delgado-Barrio, Eds.), Progress in Theoretical Chemistry and Physics, Vol. 22, Springer, Dordrecht, (2012), Chapter 29, p. 553.
5. D. Yu. Zubarev, M. Frenklach, and W. A. Lester, Jr., "From Aromaticity to Self-Organized Criticality in Graphene," Phys. Chem. Chem. Phys. **14**, 12075 (2012). (Communication).
6. E. LeDell, Prabhat; D. Yu. Zubarev, B. M. Austin, and W. A. Lester, Jr., "Classification of Nodal Pockets in Many-Electron Wave Functions via Machine Learning," J. Math. Chem. **50**, 2043 (2012).
7. D. Yu. Zubarev, B. M. Austin, and W. A. Lester, Jr., "Quantum Monte Carlo for the X-Ray Absorption Spectrum of Pyrrole at the Nitrogen K-Edge", J. Chem. Phys. **136**, 144301 (2012).
8. D. Yu. Zubarev, and W. A. Lester, Jr., "Beyond a Single Solvated Electron: Hybrid Quantum Monte Carlo and Molecular Mechanics Approach," ACS Symposium Series "Advances in Quantum Monte Carlo," **1094**, 201 (2012).
9. D. Yu. Zubarev, B. M. Austin, and W. A. Lester, Jr., "Practical Aspects of Quantum Monte Carlo for the Electronic Structure of Molecules," in *Practical Aspects of Computational Chemistry: Methods, Concepts and Applications,* J. Leszczynski and M. K. Shukla, Eds., Springer, 2012, p. 255.
10. B. M. Austin, D. Yu. Zubarev, and W. A. Lester, Jr., "Quantum Monte Carlo and Related Approaches," Chem. Rev. **112**, 263 (2012).
11. D. E. Edwards, X. You, D. Yu. Zubarev, W. A. Lester, Jr., and M. Frenklach, "Thermal Decomposition of Graphene Armchair Oxyradical," Proc. Combust. Inst. **34**, 1759 (2013).
12. D. E. Edwards, D. Yu. Zubarev, W. A. Lester, Jr., and M. Frenklach, "Oxidation of Phenanthrene Radicals by OH," 8th U.S. National Combustion Meeting, Park City, UT, May 19-23, 2013, Paper No. 2B14.

Computational Flame Diagnostics for Direct Numerical Simulations with Detailed Chemistry of Transportation Fuels

Tianfeng Lu
Department of Mechanical Engineering
University of Connecticut, Storrs, CT 06269-3139
tlu@engr.uconn.edu

I. Program Scope

The goal of the proposed research is to create computational flame diagnostics that are rigorous numerical algorithms for systematic detection of critical flame features, such as ignition, extinction, and premixed and non-premixed flamelets, and to understand the underlying physicochemical processes controlling the limit phenomena, flame stabilization, turbulence-chemistry interactions and pollutant emissions etc. The goal will be accomplished through an integrated effort on mechanism reduction, direct numerical simulations (DNS) of flames at engine conditions, computational diagnostics, and DNS data mining.

II. Recent Progress

Mechanism reduction and multi-dimensional flame simulations

Chemistry of practical engine fuels involves a large number of species and reactions, as well as severe chemical stiffness. A necessary step to accommodate realistic chemistry in large-scale flame simulations is to obtain reduced mechanisms with small sizes and satisfactory accuracy. In the recent work, reduced mechanisms were developed for various fossil and renewable engine fuels. The reduction was primarily based on the directed relation graph (DRG) methods, analytically solved linearized quasi steady state approximations, while chemical stiffness was dynamically removed during flame simulations [i]. The reduction methods feature high computational efficiency and rigorous error control. Specifically, a reduced mechanism with 30 transported species was developed for dimethyl ether (DME) as a diesel surrogate, and applied in DNS of a turbulent DME jet flame, and a 28-species reduced mechanism, including NOx formation, was developed for ethanol/air, and was applied for 2-D and 3-D DNS of homogeneous charge compression ignition (HCCI) and spark assisted compression ignition (SACI) of ethanol flames (collaboration with Dr. J.H. Chen at Sandia National Laboratories) [7, 9]. A 116-species reduced mechanism was developed for primary reference fuels (PRF) as a gasoline surrogate, and a 73-species reduced mechanism was developed for a biodiesel surrogate (ternary mixtures of n-heptane, methyl decanoate and methyl-9-decanoate). Both reduced mechanisms were used for 2-D DNS of HCCI combustion involving different flame propagation modes (collaboration with Prof. C.S. Yoo at UNIST) [1,

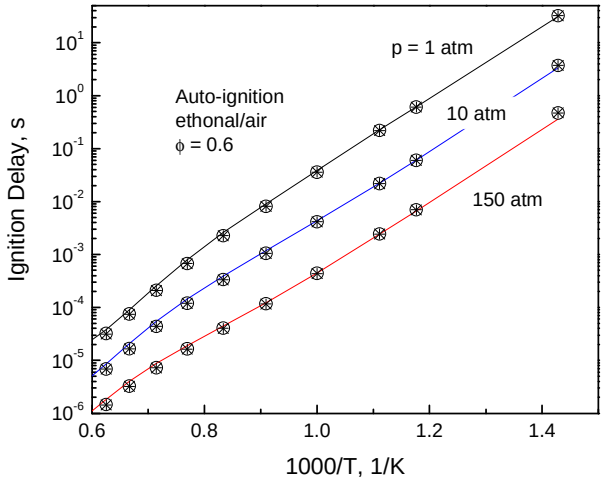

Figure 1. Validation of a 28-species reduced mechanism for ethanol/air [7]. Lines: detailed, Circles: skeletal, Stars: reduced.

10]. Furthermore, a 106-species skeletal mechanism was developed for n-dodecane and applied in RANS simulations of practical diesel engine combustion (collaboration with Dr. W.J. Pitz at Lawrence Livermore National Laboratory and Dr. S. Som at Argonne National Laboratory). The reduced mechanisms feature high chemical fidelity with rigorously controlled worst-case errors, and are amenable for DNS and other multi-dimensional flame simulations. Typical accuracy of the reduced mechanisms is demonstrated in Fig. 1 for ethanol-air.

Computational flame diagnostics with chemical explosive mode analysis (CEMA) and bifurcation analysis (BA)

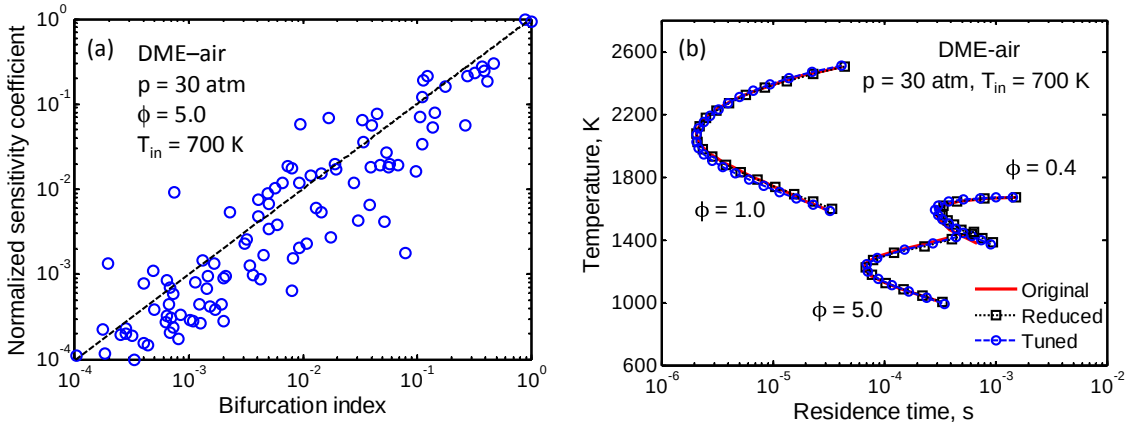

Figure 2. (a) Correlation of the bifurcation index (BI) with the normalized sensitivity coefficients, and (b) strong flame extinction calculated with reactions with large BI values with and without rate parameter tuning, for DME-air in perfectly stirred reactors (PSR).

Ignition and extinction are critical limit flame phenomena and of primary concern in many combustion applications. It is important to systematically identify the underlying chemical processes controlling ignition and extinction to understand and predict relevant flame behaviors at turbulent conditions. A method of bifurcation analysis (BA) [8] was developed based on the description of extinction and ignition states as bifurcation points on the S-curves of steady state combustion. Reactions important to ignition and extinction are identified based on their contributions to the

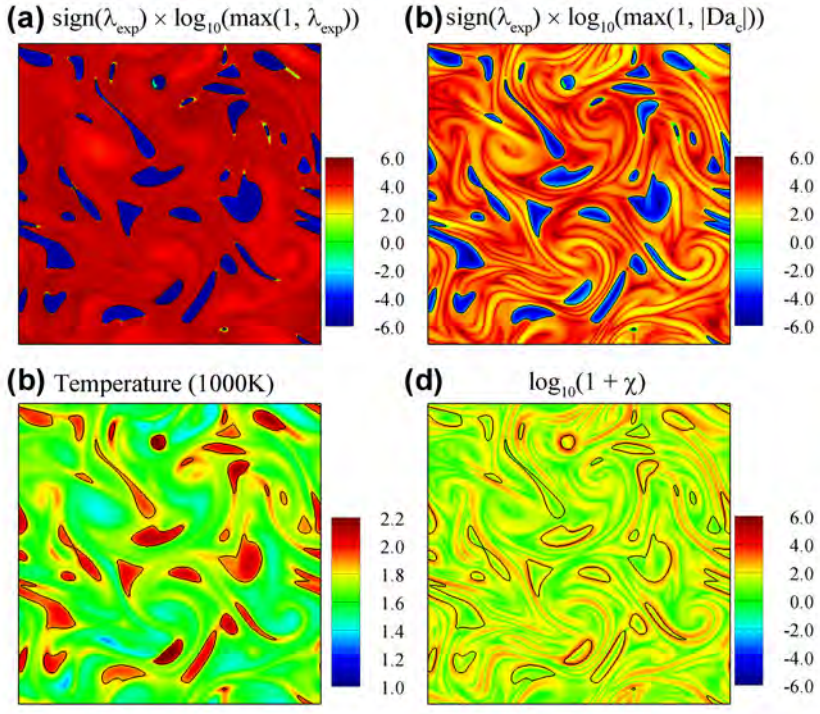

Figure 3. Isocontours of (a) chemical explosive mode timescale, (b) Damköhler number, (c) temperature, and (d) scalar dissipation rate for a 2-D DNS of HCCI combustion of biodiesel/air [10].

bifurcation points, defined as the bifurcation index (BI) [8]. The BA method is validated against and compared with the brute-force global sensitivity analysis, which is probably the most widely used method to numerical identify important species and reactions for ignition and extinction. Figure 2 shows that the BI values are strongly correlated with the global sensitivity as demonstrated by the extinction state of DME-air in perfectly stirred reactors (PSR). Compared with the global sensitivity analysis, the BI values carry clear physical meanings and are significantly more efficient to evaluate in complex flows. It was further found that ignition and extinction of steady state flames are attributed to the competition between mixing and a particular chemical mode associated with positive eigenvalue, which is the central target of the chemical explosive mode analysis (CEMA) [ii]. Local ignition and extinction in complex turbulent flames can be accurately captured with CEMA.

The DNS data obtained for the ethanol, DME, PRF and biodiesel flames are systematically diagnosed with CEMA to extract critical flame features, such as premixed flame fronts, local ignition and extinction. Different premixed flame propagation modes, i.e. the propagation of auto-igniting fronts and the canonical deflagration wave, were further identified with CEMA for the DNS data. A flame structure identified with CEMA is demonstrated in Fig. 3 for the HCCI of biodiesel [10].

Dynamic adaptive chemistry (DAC) for flame simulations

While the size of chemical kinetics of practical fuels can be large, the species and reactions typically do not always remain important in different flame zones and time instances. To exploit this nature of detailed chemistry, a DAC method was developed to expedite time integration of chemically reacting systems based on the DRG method [3,5,11], which rigorously controls the worst-case incurred errors. The DAC method was studied with the Strang splitting schemes, which is widely adopted in CFD simulations involving stiff chemistry, and a second order accuracy in time-integration was achieved as demonstrated with a 1-D freely propagating premixed laminar flame of methane-air, as shown in Fig. 1 [5]. Furthermore, the DAC and *in situ* adaptive tabulation (ISAT) [iii] were combined and compared. It was found that the performance of DAC is mostly independent of the nature of combustion simulations, e.g., steady or unsteady, premixed or non-premixed, and its efficiency increases with the size of the chemistry. A speedup factor of about 30 was achieved using DAC for a simulation of HCCI combustion of iso-octane/air in a partially stirred reactor [3]. Even larger speedup factors were achieved by combining DAC with ISAT.

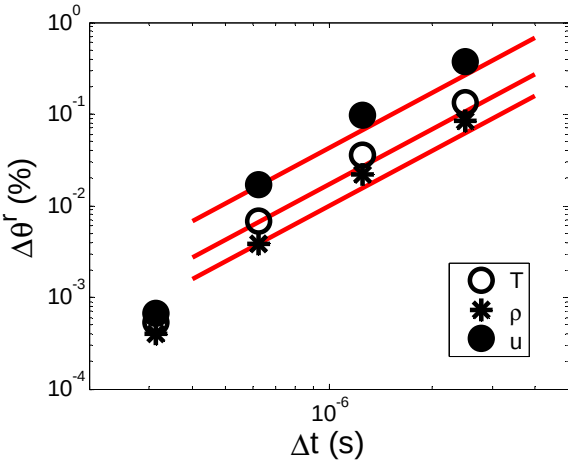

Figure 4. Demonstration of the second-order temporal convergence of the Strang splitting schemes with DAC for temperature, density and velocity in a 1-D premixed flame of methane-air [5]. The solid lines are lines of slope two.

III. Future Work

In the next stage, the methods for mechanism reduction and dynamic adaptive chemistry will be extended to analyze the DNS data for systematic data mining and data reduction. CEMA and bifurcation analysis will be further investigated to obtain flame statistics based on the

rigorously identified critical flame features, which will be subsequently used to create turbulent combustion models for accurate prediction of local ignition and extinction in turbulent flames.

IV. References

i. T. Lu, C. K. Law; *Prog. Energy Combust. Sci.* **2009**, 35(2), 192-215.
ii. Lu, T.F.; Yoo, C.S.; Chen, J.H.; Law, C.K. *J. Fluid Mech.,* **2010** 652 (1) 45–64.
iii. Pope, S.B, *Combust. Theory Model.,* **1997** 1 (1) 41–63.

V. Publications supported by this project: September 2012 – April 2014

1. M.B. Luong, Z. Luo, T.F. Lu, S.H. Chung, C.S. Yoo, "Direct numerical simulations of the ignition of lean primary reference fuel/air mixtures under HCCI condition," *Combustion and Flame*, 160 (10) 2038–2047, 2013.
2. S.M. Sarathy, S. Park, B. Weber, W. Wang, P. Veloo, A.C. Davis, C. Togbe, C.K. Westbrook, O. Park, G. Dayma, Z. Luo, M.A. Oehlschlaeger, F. Egolfopoulos, T.F. Lu, W.J. Pitz, C.J. Sung, P. Dagaut, "A comprehensive experimental and modeling study of iso-pentanol combustion," *Combustion and Flame*, 160 (12) 2712-2728, 2013.
3. Z. Ren, Y. Liu, T.F. Lu, L. Lu, O.O. Oluwole, G.M. Goldin, "The use of dynamic adaptive chemistry and tabulation in reactive flow simulations," *Combustion and Flame*, 161 (1) 127–137, 2014.
4. Z. Ren, H. Yang, T.F. Lu, "Effects of Small-Scale Turbulence on NOx Formation in Premixed Flame Fronts," *Fuel*, 115 241–247, 2014.
5. Z. Ren, C. Xu, T.F. Lu, M.A. Singer, "An Operator Splitting Scheme with Dynamic Adaptive Chemistry for Reactive Flow Simulations," *Journal of Computational Physics*, 263 19–36, 2014.
6. Z. Luo, S. Som, S.M. Sarathy, M. Plomer, W.J. Pitz, D.E. Longman, T.F. Lu, "Development and Validation of an n-Dodecane Skeletal Mechanism for Diesel Spray-Combustion Applications," *Combustion Theory and Modeling*, DOI: 10.1080/13647830.2013.872807, 2014.
7. A. Bhagatwala, J.H. Chen, T.F. Lu, "Direct numerical simulations of HCCI/SACI with ethanol," *Combustion and Flame*, http://dx.doi.org/10.1016/j.combustflame.2013.12.027, 2014.
8. R. Shan, T.F. Lu, "A Bifurcation Analysis for Limit Flame Phenomena of DME/air in Perfectly Stirred Reactors," *Combustion and Flame*, http://dx.doi.org/10.1016/j.combustflame.2013.12.025, 2014.
9. A. Bhagatwala, T.F. Lu, H. Shen, J.A. Sutton, J.H. Chen, "Numerical and experimental investigation of turbulent DME jet flames," *Proceedings of the Combustion Institute*, submitted.
10. M.B. Luong, T.F. Lu, S.H. Chung, C.S. Yoo, "Direct numerical simulations of the ignition of a lean biodiesel/air mixture with temperature and composition inhomogeneities at high pressure and intermediate temperature," *Combustion and Flame*, submitted.
11. Z. Lu, L. Zhou, Z. Ren, T.F. Lu, K.H. Luo, "Transient simulations of an n-heptane spray flame with dynamic adaptive chemistry," *Combustion Theory and Modeling*, submitted.

Advanced Nonlinear Optical Methods for Quantitative Measurements in Flames

Robert P. Lucht
School of Mechanical Engineering, Purdue University
West Lafayette, IN 47907-2088
Lucht@purdue.edu

I. Program Scope

Nonlinear optical techniques such as laser-induced polarization spectroscopy (PS), resonant wave mixing (RWM), and electronic-resonance-enhanced (ERE) coherent anti-Stokes Raman scattering (CARS) are techniques that show great promise for sensitive measurements of transient gas-phase species, and diagnostic applications of these techniques are being pursued actively at laboratories throughout the world. The objective of this research program is to develop and test strategies for quantitative concentration and temperature measurements using nonlinear optical techniques in flames and plasmas. We have continued our fundamental theoretical and experimental investigations of these techniques. We have also initiated both theoretical and experimental efforts to investigate the potential of femtosecond (fs) laser systems for sensitive and accurate measurements in gas-phase media. Our initial efforts have been focused on fs CARS, although the systems will be useful for a wide range of future diagnostic techniques involving two-photon transitions. In the last year we have demonstrated the acquisition of single-shot temperature measurements at data rates of 5 kHz in highly turbulent, swirl-stabilized methane-air flames. The fs CARS measurements exhibited high signal-to-noise ratios and temperatures were extracted from nearly every laser shot.

Over the past year we have continued our two-color PS measurements. We developed and optimized a new laser system for the two-color PS measurements of nitric oxide featuring two injection-seeded optical parametric generator/pulsed dye amplifier (OPG/PDA) systems, both operating near 452 nm. Collision-induced resonances were clearly observed with this system.

We are investigating the physics of both fs CARS and two-color PS by direct numerical integration (DNI) of the time-dependent density matrix equations for the resonant interaction. Significantly fewer restrictive assumptions are required using this DNI approach compared with the assumptions required to obtain analytical solutions. We are concentrating on the accurate simulation of two-photon processes, including Raman transitions, where numerous intermediate electronic levels contribute to the two-photon transition strength. We have made significant progress in the last year on modeling two-color PS of atomic hydrogen, and are obtaining good agreement between experiment and modeling.

We have also developed a new technique for simultaneous pure rotational and vibrational CARS, and we have continued to develop and apply this new technique during the past year. This method takes advantage of a two-beam phase-matching scheme for pure rotational CARS.

II. Recent Progress

A. Femtosecond CARS Calculations and Experiments

The single-shot, chirped-pulse-probe (CPP) fs CARS system for temperature measurements is shown in Fig. 1. Fs CARS offers several major potential advantages compared with nanosecond (ns) CARS; i.e., CARS as usually performed with nanosecond pump

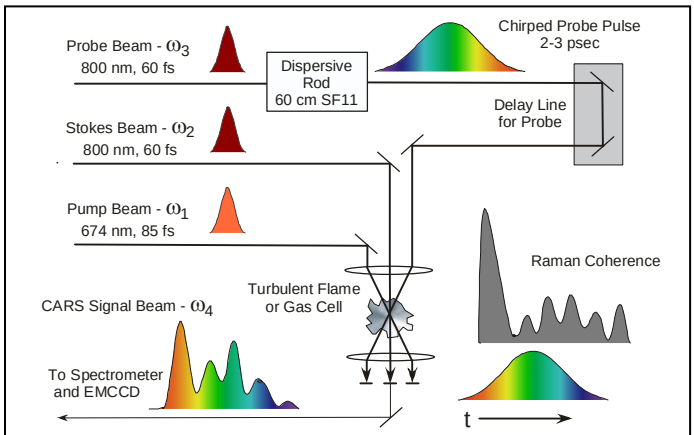

Figure 1. Schematic diagram of CPP fs CARS experiment.

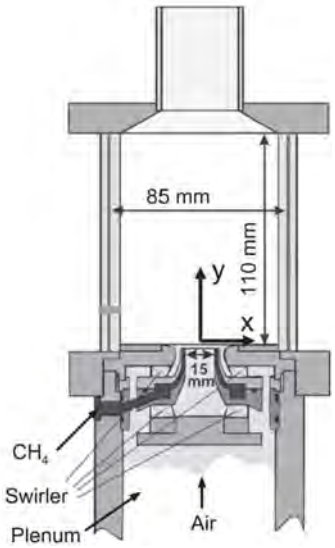

Figure 2. Swirl-stabilized methane/air burner from DLR Stuttgart.

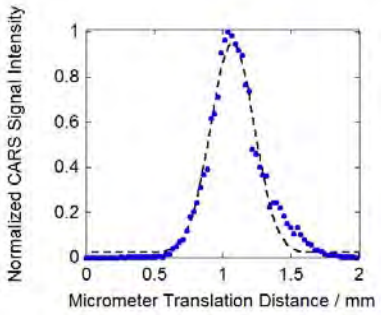

Figure 3. Spatial resolution of the CPP fs CARS system.

and Stokes lasers. These potential advantages include an elimination of collisional effects in the signal generation and the capability of performing real-time temperature and species measurements at data rates of 1 kHz or greater as compared to 10-50 Hz for ns CARS. Our Coherent ultrafast laser system operates at 5 kHz with a fundamental pulse width of 60 fs and energy of over 2 mJ. The fundamental 800-nm pulse is Fourier-transform-limited to within a few percent. The fundamental 800-nm beam is used as the probe beam for our CPP fs CARS experiments. The greatly increased pulse energy of the chirped-pulse-probe beam results in a significant increase in the signal-to-noise ratio of the single-pulse measurements.

The fundamental 800-nm pulse is Fourier-transform-limited to within a few percent. The fundamental 800-nm beam is used as the probe beam for our chirped-pulse-probe (CPP) fs CARS experiments as shown in Fig. 1. The greatly increased pulse energy of the chirped-pulse-probe beam results in a significant increase in the signal-to-noise ratio of the single-pulse measurements.

During the past year single-laser-shot temperature measurements at a data rate of 5 kHz were performed in a highly turbulent, swirl-stabilized burner that has been characterized extensively at DLR Stuttgart. The burner is shown in Fig. 2. Measurements were performed for a so-called "stable" case and for a case with significant thermoacoustic instabilities. Despite the high levels of turbulence in the burner, there were few if any single-shot fs CARS signals that were so weak that temperatures could not be determined from the spectra. The excellent single-shot performance is attributable to the stability of the fs laser spectrum from laser shot to laser shot. In addition, the beams focused very well and our measured spatial resolution was better than 600 microns as shown in Fig. 3. Typical single-shot, 5 kHz time-temperature histories are shown in Fig. 4. These measurements are described in detail in P8.

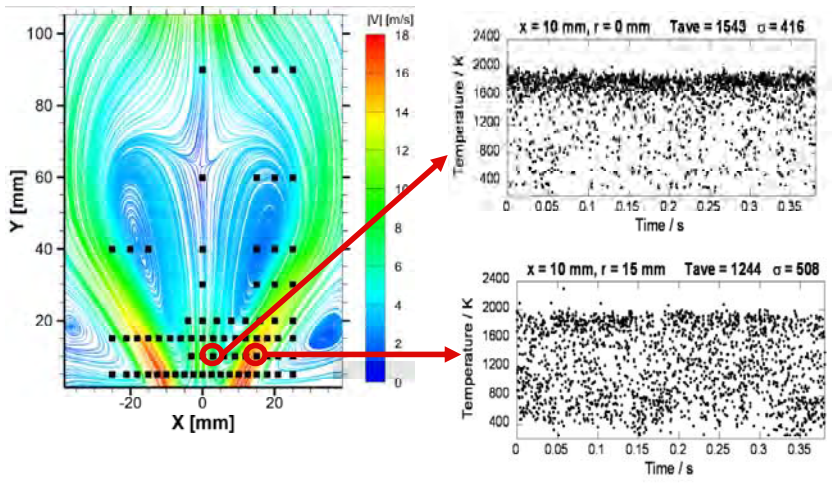

Figure 4. Typical time-temperature histories obtained from CPP fs CARS experiment in the swirl-stabilized burner.

B. Polarization Spectroscopy and Six-Wave Mixing: Experiments and Modeling Efforts

We developed and have continued to apply a new experimental apparatus for high-spectral-resolution PS measurements. The system features two OPG stages that injection

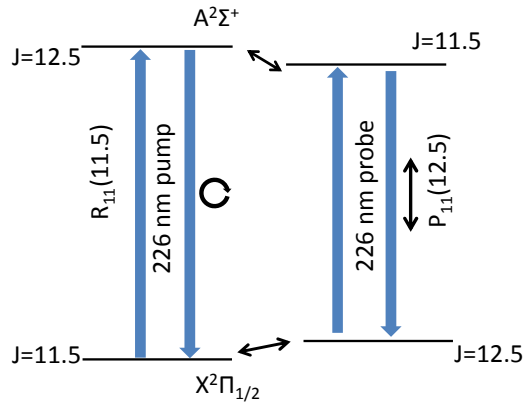

Figure 5. Energy level diagram for a collision-induced resonance in two-color NO PS.

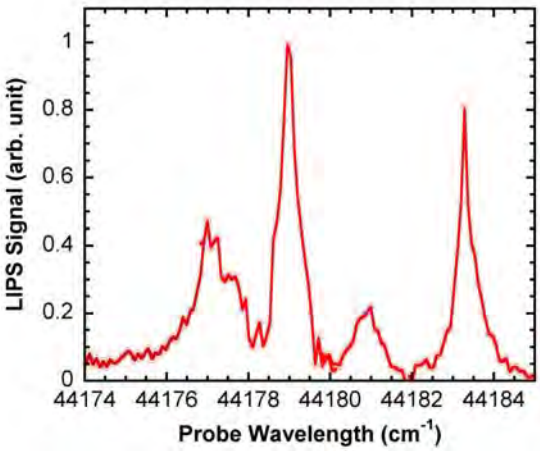

Figure 6. Two-color NO PS probe scan spectrum illustrating both direct [P_{11}(11.5), P_{11}(13.5)] and collision-induced resonances [P_{11}(12.5)]. The pum beam is tuned to the R_{11}(11.5) resonance.

seeded at the idler wavelength and pumped by the 355-nm third harmonic radiation from an injection-seeded Nd:YAG laser. The signal radiation from OPGs is then amplified using two separate pulse dye amplifier stages. During the last year we have concentrated on two-color, single-photon PS of NO. An energy level diagram for the measurements is shown in Fig. 5, and a typical experimental spectrum is shown in Fig. 6. The spectrum shown in Fig. 6 clearly shows transitions resulting from the transfer of anisotropy in the Zeeman state distribution during rotational transfer in either the lower or upper electronic levels for the transition.

We are continuing our collaborative efforts with Dr. Thomas B. Settersten at Sandia's Combustion Research Facility on six-wave mixing (6WM) spectroscopy and PS of atomic hydrogen. The DNI computer code for the calculation of 6WM and PS signals from atomic hydrogen was significantly modified to incorporate all of the different possible photon mixing processes that can potentially contribute to both the 6WM and PS signals. The computer code has been modified recently to compute the PS signal by integrating over the path length of the PS probe beam, a modification that was necessary to account for the saturation of the 2S-3P transition in the experiments. We are obtained good agreement between the experimental spectra that we have obtained (see P4) and our calculated spectra for both ultraviolet pump scans and visible pump scans.

C. Development of a New System for Combined Pure Rotational and Vibrational CARS

We have developed a new scheme for simultaneous generation and detection of pure rotational and vibrational N_2 CARS using two 532-nm pump beams and a 607-nm dye laser beam. The generation of both the pure rotational and the vibrational CARS signals is advantageous because pure rotational CARS is an excellent thermometry technique for temperatures below 1000 K, and vibrational CARS is most accurate for temperatures above 1000 K. The pure rotational CARS signal is generated by the interaction of either 532-nm beam with the 607-nm beam, and is essentially collinear with either 532-nm beam. We have demonstrated the simultaneous detection of both pure rotational and N_2 vibrational CARS in near adiabatic hydrogen/air flames; these measurements and the experimental system are discussed in P7. We have developed a new system for simultaneous pure rotational and dual-pump vibrational CARS and are just starting to perform measurements with this system.

III. Future Work

We will continue to perform fs CARS experiments in our laboratory using the Coherent ultrafast laser system. Our studies of temperature measurements using CPP fs CARS will continue. We

continue to investigate the effect of laser system parameters on the CPP fs CARS spectrum to improve the temperature accuracy of the technique. We will explore the potential for using CPP fs CARS for accurate concentration measurements for water vapor, a very hard species to measure using ns CARS. We will investigate the potential for measuring mixtures of hydrocarbon species. We plan to design and fabricate a high-temperature, high-pressure furnace for fundamental studies of temperature and species measurements.

Our investigation of the physics of single-photon, two-color PS for species such as NO, and two-photon, two-color PS and 6WM for species such as CO will continue. We have developed a new experimental apparatus for these measurements and collected extensive line shape and concentration data for atomic hydrogen, and are in the process of investigating collision-induced resonances for two-color PS of NO. We will be able to explore collisional effects on the PS and 6WM processes in much more detail using a low-pressure cell filled with NO and different buffer gases. We will continue to use the density matrix code to gain insight into the physics of the PS and 6WM processes.

In the future we plan to introduce a dual-pump CARS variant of the technique for sensitive detection of three or more species along with the temperature measurement from both pure rotational and vibrational CARS. We plan to combine the two-beam pure rotational CARS with a dual-beam CARS system where the vibrational spectra for H_2 and N_2 are detected simultaneously.

IV. Refereed publications and submitted journal articles supported by this project 2011-2013

P1. D. R. Richardson, R. P. Lucht, S. Roy, W. D. Kulatilaka, and J. R. Gord, "Single-Laser-Shot Femtosecond Coherent Anti-Stokes Raman Scattering Thermometry at 1000 Hz in a Driven H_2-Air Flame," Proc. Combust. Inst. **33**, 839-845 (2011).

P2. S. Roy, R. P. Lucht, and J. R. Gord, "Orientation and Alignment Dynamics During Generation of Laser-Induced Polarization Spectroscopy (LIPS) Signal," JOSA B **28**, 208-219 (2011).

P3. D. R. Richardson, R. P. Lucht, S. Roy, W. D. Kulatilaka, and J. R. Gord, "Theoretical Modeling of Single-Laser-Shot, Chirped-Probe Pulse Femtosecond Coherent Anti-Stokes Raman Scattering Thermometry," Applied Physics B **104**, 699-714(2011).

P4. A. H. Bhuiyan, A. Satija, S. V. Naik, and R. P. Lucht, "Development of a Two-Color Laser System for High-Resolution Polarization Spectroscopy Measurements of Atomic Hydrogen," *Optics Letters* 37, 3564-3566 (2012).

P5. D. R. Richardson, D. Bangar, and R. P. Lucht, "Polarization Suppression of the Nonresonant Background in Femtosecond Coherent Anti-Stokes Raman Scattering for Flame Thermometry at 5 kHz," *Optics Express* **20**, 21495 (2012).

P6. D. R. Richardson, R. P. Lucht, S. Roy, W. D. Kulatilaka, and J. R. Gord, "Chirped-Probe-Pulse Femtosecond Coherent Anti-Stokes Raman Scattering Concentration Measurements," *Journal of the Optical Society of America B* 30, 188-196 (2013).

P7. A. Satija and R. P. Lucht, "Development of a New Combined Pure Rotational and Vibrational Coherent Anti-Stokes Raman Scattering (CARS) System," *Optics Letters* **38**, 1340-1342 (2013).

P8. C. N. Fineman, C. D. Slabaugh, I. G. Boxx, W. Meier, R. P. Lucht, "Femtosecond Coherent Anti-Stokes Raman Scattering Thermometry at 5 kHz in a Gas Turbine Model Combustor," *Proceedings of the Combustion Institute*, accepted for publication (2014).

V. PhD theses completed by students supported by this project 2011-2013

T1. Aizaz Bhuiyan, "Polarization Spectroscopy Measurements of Atomic Hydrogen in Flames," Purdue University, May 2012.

T2. Daniel R. Richardson, "Femtosecond CARS Spectroscopy for High-Data-Rate Temperature Measurements," Purdue University, July 2012.

Theoretical studies of chemical reactions related to the formation and growth of polycyclic aromatic hydrocarbons and molecular properties of their key intermediates

Alexander M. Mebel
Department of Chemistry and Biochemistry, Florida International University
Miami, Florida 33199. E-mail: mebela@fiu.edu

Program Scope

In this project, we investigate complex chemical mechanisms of PAH formation and growth via theoretical studies of their critical elementary reactions. Our primary objectives include (i) to unravel reaction mechanisms through detailed, accurate, and reliable calculations of pertinent potential energy surfaces (PESs); (ii) to compute rate constants for individual reaction steps and total absolute reaction rate constants and product branching ratios depending on reaction conditions, such as collision energy or temperature and pressure; (iii) to characterize molecular, energetic, and spectroscopic parameters of various possible reaction intermediates and products including their enthalpies of formation, geometric structure, vibrational frequencies and rotational constants, as well as photoionization and photoexcitation spectra. To achieve these goals, we employ chemically accurate ab initio and density functional calculations (using CCSD(T)/CBS, G3, and explicitly correlated methods) of the PESs of these reactions which are then utilized for statistical (TST and RRKM/Master Equation) computations of absolute reaction rate constants and product branching ratios. In the current project period we study the reactions of dicarbon C_2 with unsaturated hydrocarbons producing resonance-stabilized free radicals (RSFR), which in turn can contribute to the formation of aromatic species, the isomer-specific growth of various PAH and CP-PAH molecules beyond the second aromatic ring, and the oxidation of PAH radicals.

Recent Progress

Reaction mechanisms and product branching ratios for the reactions of dicarbon C_2 with unsaturated hydrocarbons. In the last two years, we have studied PESs for the reactions of C_2 in its ground singlet $X^1\Sigma_g^+$ and first excited $a^3\Pi_u$ states with propene C_3H_6, three C_4H_6 isomers (1,2-butadiene, 1-butyne, and 2-butyne), and two C_5H_8 isomers (isoprene and 1,3-pentadiene). The PESs were utilized for calculations of energy-dependent rate constants for individual unimolecular reaction steps, which in turn were used to compute product branching ratios under single-collision conditions. These theoretical studies were carried out in parallel with crossed molecular beams experiments by Kaiser's group at the University of Hawaii. For $C_2 + C_3H_6$, both on the singlet and triplet surfaces, the reactions involve indirect scattering dynamics and are initiated by the addition of the dicarbon reactant to the carbon–carbon double bond of propene. These initial addition complexes rearrange via multiple isomerization steps leading ultimately via atomic hydrogen elimination from the former methyl and vinyl groups to the formation of 1-vinylpropargyl and 3-vinylpropargyl. Both triplet and singlet methylbutatriene species were identified as important reaction intermediates. On the singlet surface, the unimolecular decomposition of the reaction intermediates was found to be barrier-less, whereas on the triplet surface, tight exit transition states were involved. It was concluded that in combustion flames, the acyclic C_5H_5 isomers formed in the $C_2 + C_3H_6$ reactions can undergo a hydrogen-atom assisted isomerization leading ultimately to the thermodynamically most stable cyclopentadienyl isomer. Only a relatively small amount of cyclopentadienyl (up to 20%) can be formed directly in the singlet reaction according to our calculations but this product has not been detected in experiment.

The reactions of C_2 with C_4H_6 isomers 2-butyne, 1-butyne and 1,2-butadiene were found to be indirect, forming C_6H_6 complexes through barrierless additions by dicarbon on the triplet and singlet surfaces. Isomerization of the C_6H_6 reaction intermediate leads to product formation by hydrogen or methyl loss in dicarbon-hydrogen atom or dicarbon-CH_3 exchange mechanisms forming acyclic C_6H_5 or C_5H_3 reaction products through loose exit transition states in overall exoergic reactions. In a sharp contrast to the C_2 + 1,3-butadiene reaction studied by us earlier, the reactions of dicarbon with the other C_4H_6 isomers do not produce aromatic phenyl radicals. Instead, we found that over 10 different acyclic C_6H_5 and C_5H_3 RSFRs are formed highlighting the importance of isomer specific reaction mechanisms. Detailed knowledge of the reaction mechanisms of dicarbon with C_4H_6 isomers 2-butyne, 1-butyne and 1,2-butadiene under combustion conditions are essential to chemical kinetic models to represent combustion process accurately, while so far a common theme in modeling and analyzing combustion processes has been to not treat same mass isomers individually.

We have also discovered that the benzyl radical ($C_6H_5CH_2$) can be formed in the reaction of dicarbon with 2-methyl-1,3-butadiene (isoprene; C_5H_8; X^1A') accessing the triplet and singlet C_7H_8 PESs. Our ab initio and statistical calculations were combined with the experimental crossed molecular beams data to reveal the underlying reaction mechanism and chemical dynamics. On the singlet and triplet surfaces, the reactions involve indirect scattering dynamics and are initiated by the barrier-less addition of C_2 to the carbon–carbon double bond of the 2-methyl-1,3-butadiene molecule. These initial addition complexes rearrange via multiple isomerization steps involving cyclization and hydrogen shifts leading eventually to the formation of C_7H_7 radical species through atomic hydrogen elimination. The benzyl radical ($C_6H_5CH_2$), which presents the thermodynamically most stable C_7H_7 isomer, is determined to be the major product on the triplet PES. This reaction demonstrates the synthesis of the prototype of an aromatic and resonance-stabilized free radical - the benzyl radical - via a previously unknown reaction route involving a single collision. From synthetic point of view, the formation of a cyclic product from two acyclic reactants - dicarbon and isoprene - presents a benchmark system, which opens up future investigations on this reaction class leading to (substituted) phenyl and benzyl-type radicals via a single collision event in the gas phase. For the reaction of C_2 with another C_5H_8 isomer, 1-methyl-1,3-butadiene (1,3-pentadiene), our calculations show that the benzyl radical is only a minor product with a relative yield of less than 10%. The reaction on the singlet surface mostly forms acyclic C_7H_7 isomers, whereas on the triplet surface cyclization is favored but the major products are predicted to be cycloheptatrienyl and *meta*-tolyl radicals.

A theoretical study of the reaction of phenyl radical with phenylacetylene. The reaction of the phenyl radical with phenylacetylene was investigated by *ab initio* calculations in parallel with the experimental study in crossed molecular beams by Kaiser's group. The results show that the reaction proceeds indirectly via the formation of $C_6H_5C_8H_6$ collision complexes through addition of the phenyl radical to the o-, m-, and/or p-position of the phenylacetylene molecule via small barriers of about 5-11 kJ mol^{-1}. A part of these collision complexes hold life times long enough to fly to the detector of the crossed beams machine. The collision complexes also undergo unimolecular decomposition via atomic hydrogen elimination leading to 2-ethynylbiphenyl, 3-ethynylbiphenyl, and/or 4- ethynylbiphenyl ($C_6H_5C_8H_5$) via tight exit transition states in overall slightly (34-47 kJ mol^{-1}) exoergic reactions. No phenanthrene formation is predicted theoretically and this product was not detected experimentally.

A theoretical RRKM-Master Equation study of rate coefficients and product branching ratios for the oxidation of phenyl and naphthyl radicals. Theoretical VRC-TST/RRKM-ME

calculations were performed to evaluate total rate coefficients and product branching ratios for the oxidation of phenyl and 1- and 2-naphthyl radicals with O_2 at temperatures relevant to combustion (1500, 2000, and 2500 K) and pressures of 0.01, 0.1, 1.0, and 10 atm. The results give the rate coefficients in the range of $3.0-5.5\times10^{-11}$ cm^3 $molecule^{-1}$ s^{-1} with slightly positive temperature dependence, activation energies varying within 2.3−3.3 kcal/mol, and pre-exponential factors of $7-10\times10^{-11}$ cm^3 $molecule^{-1}$ s^{-1}. The dominant reaction channel in all three cases is elimination of the oxygen atom from peroxy complexes formed at the initial O_2 addition step and leading to the phenoxy and naphthoxy radical products. The contribution of this channel increases with temperature. Chemically-activated phenoxy and naphthoxy radicals either decompose to the cyclopentadienyl + CO and indenyl + CO products, respectively, or undergo thermal equilibration. The relative yields of the decomposition/equilibration products strongly depend on temperature and pressure in the way that a temperature growth favors decomposition, whereas an increase in pressure favors equilibration. At the lowest temperature considered, 1500 K, the reactions also yield significant amounts of pyranyl + CO (phenyl + O_2) or 1-benzopyranyl + CO (1-naphthyl + O_2). A comparison of the phenyl + O_2 and naphthyl + O_2 reactions reveals that although the general trends in the oxidation kinetics of phenyl and naphthyl radicals are similar, the size and especially the position of the radical site in the aromatic moiety may affect the details of the mechanism and relative product yields.

Future Plans

We will continue investigating PESs, rate constants, and product yields for the reactions relevant to the formation of larger PAH molecules via HACA sequences and other possible mechanisms with the goal to understand relative abundances of various PAH molecules in different isomeric forms in combustion flames and environmental samples. We will also study oxidation reactions of larger PAH radicals, such as those of acenaphthalene, phenanthrene, and pyrene, via ab initio/RRKM-ME calculations. The studies of the reactions of the *p*-tolyl radical with isoprene, 1,2-butadiene, and C_3H_4 isomers, and the reaction of the phenyl radical with isoprene will be performed in conjunction with crossed molecular beams experiments in Kaiser's group. A new collaborative project is underway with Arthur Suite's group on the studies of Cl atoms with alkenes, such as butene isomers 1-butene, 2-butene, and isobutene. The first results for Cl + isobutene indicate that the reaction proceeds via a Cl-addition-HCl-elimination route where the elimination step occurs by a Cl atom roaming mechanism. We will continue studying this interesting reaction class, which promise to reveal new exciting reaction dynamics features.

DOE/BES sponsored publications (2011-2014)

1. Parker D.S.N., Zhang F., Kim, Y.S. Kaiser R.I., Mebel A.M., "On the Formation of Resonantly Stabilized C_5H_3 Radicals -A Crossed Beam and Ab Initio Study of the Reaction of Ground State Carbon Atoms with Vinylacetylene", J. Phys. Chem. A, 2011, 115, 593-601.
2. Zhang F., Kaiser R.I., Kislov V.V., Mebel A.M., Golan A., Ahmed M., "A VUV Photoionization Study of the Formation of the Indene Molecule and Its Isomers", J. Phys. Chem. Lett., 2011, 2, 1731-1735.
3. Kaiser R.I., Goswami M., Maksyutenko P., Zhang F., Kim Y.S., Landera A., Mebel A.M., "A Crossed Molecular Beams and Ab Initio Study on the Formation of C_6H_3 Radicals - An Interface between Resonantly Stabilized (RSFRs) and Aromatic Radicals (ARs)", J. Phys. Chem. A., 2011, 115, 10251-10258.
4. Parker D.S.N., Zhang F., Kaiser R.I., Kislov V.V., Mebel A.M., "Indene Formation under Single Collision Conditions from Reaction of Phenyl Radicals with Allene and Phenylacetylene – A Crossed Molecular Beam and Ab Initio Study", Chem. Asian J., 2011, 6, 3035-3042.

5. Kaiser R.I., Goswami M., Zhang F., Parker D., Kislov V.V., Mebel A.M., Aguilera-Iparraguirre J., Green W.H., “Crossed Beam Reaction of Phenyl and D5-Phenyl Radicals with Propene and Deuterated Counterparts – Competing Atomic Hydrogen and Methyl Loss Pathways”, Phys. Chem. Chem. Phys., 2012, 14, 720-729.
6. Parker D.S.N., Zhang F., Kaiser R.I., Landera A., Kislov V.V., Mebel A.M., Tielens A.G.G.M., “Low Temperature Formation of Naphthalene and its Role in the Synthesis of PAH in the Interstellar Medium”, Proc. Nat. Acad. Sci., 2012, 109, 53-58.
7. Parker D.S.N., Zhang F., Kim Y.S., Kaiser R.I., Landera A., Mebel A.M., “On the Formation of Phenyldiacetylene (C_6H_5CCCCH) and D5-Phenyldiacetylene (C_6D_5CCCCH) Studied under Single Collision Conditions”, Phys. Chem. Chem. Phys., 2012, 14, 2997-3003.
8. Zhou C.-W., Kislov V.V., Mebel A.M., “The Reaction Mechanism of Naphthyl Radicals with Molecular Oxygen. I. A Theoretical Study of the Potential Energy Surface”, J. Phys. Chem. A, 2012, 116, 1571–1585.
9. Kislov V.V., Mebel A.M., Aguilera-Iparraguirre J., Green W.H., “The Reaction of Phenyl Radical with Propylene as a Possible Source of Indene and Other Polycyclic Aromatic Hydrocarbons: An Ab Initio/RRKM-ME Study”, J. Phys. Chem. A, 2012, 116, 4176-4191.
10. Kaiser R.I., Parker D.S.N., Zhang F., Landera A., Kislov V.V., Mebel A.M., “PAH Formation under Single Collision Conditions - Reaction of Phenyl Radical and 1,3-Butadiene to Form 1,4-Dihydronaphthalene”, J. Phys. Chem. A, 2012, 116, 4248-4258.
11. Mebel A.M., Landera A., “Product branching ratios in photodissociation of phenyl radical: A theoretical Ab initio/RRKM study”, J. Chem. Phys., 2012, 136, 234305 (9 pp.).
12. Kaiser R.I., Mebel A.M., Golan A., Ahmed M., “A VUV Photoionization Study on the Formation of Primary and Secondary Products in the Reaction of the Phenyl Radical with 1,3-Butadiene under Combustion Relevant Conditions”, Phys. Chem. Chem. Phys., 2013, 15, 341-347.
13. Kislov V.V., Sadovnikov A.I., Mebel A.M., “Formation Mechanism of Polycyclic Aromatic Hydrocarbons Beyond the Second Aromatic Ring”, J. Phys. Chem. A, 2013, 117, 4794-4816.
14. Dangi B.B., Parker D.S.N., Kaiser R.I., Jamal A., Mebel A.M., “A Combined Experimental and Theoretical Study on the Gas-Phase Synthesis of Toluene under Single Collision Conditions”, Angew. Chem., Int. Ed., 2013, 52, 7186-7189.
15. Dangi B.B., Maity S., Kaiser R.I., Mebel A.M., “A Combined Crossed Beam and Ab Initio Investigation of the Gas Phase Reaction of Dicarbon Molecules (C_2; $X^1\Sigma_g^+/a^3\Pi_u$) with Propene (C_3H_6; X^1A'): Identification of the Resonantly Stabilized Free Radicals 1- and 3-Vinylpropargyl”, J. Phys. Chem. A, 2013, 117, 11783–11793.
16. Wang Q., Dyakov Y.A., Wu D., Zhang D., Jin M., Liu F., Liu H., Hu Z., Ding D., Mineo H., Teranishi Y., Chao S.D., Lin S.H., Kosheleva O.K., Mebel, A. M., “Ionization/dissociation processes of methyl-substituted derivates of cyclopentanone in intense femtosecond laser field”, Chem. Phys. Lett., 2013, 586, 21–28.
18. Parker D.S.N., Yang T., Kaiser R.I., Landera A., Mebel A.M., “On the formation of ethynylbiphenyl ($C_{14}D_5H_5$; $C_6D_5C_6H_4CCH$) isomers in the reaction of D5-phenyl radicals (C_6D_5; X^2A_1) with phenylacetylene ($C_6H_5C_2H$; X^1A_1) under single collision conditions”, Chem. Phys. Lett., 2014, 595-596, 230-236.
19. Dangi B.B., Parker D.S.N., Yang T., Kaiser R.I., Mebel A.M., “ Gas-phase synthesis of the benzyl radical ($C_6H_5CH_2$)”, Angew. Chem., Int. Ed., 2014, in press. DOI: 10.1002/anie.201310612.

FLASH PHOTOLYSIS-SHOCK TUBE STUDIES

Joe V. Michael

Chemical Sciences and Engineering Division
Argonne National Laboratory, Argonne, IL 60439
E-mail: jmichael@anl.gov

The scope of the program is to measure, with the ANL flash photolysis reflected shock tube technique, high-temperature thermal rate constants for use in high-temperature combustion. This year we have concentrated on reactions where H (or D) is either a reactant or product. For both types of studies we used H- or D-atom atomic resonance absorption spectrometry (ARAS) as the detection technique.[1] In this work, we are responding to the specific need to develop chemical mechanisms for biofuels including methyl esters, alcohols, and aldehydes.

Thermal Rate Constants for the Reactions, D with n-butane and iso-butane.[2] The reactions of D/H with n-C_4H_{10} and i-C_4H_{10} have been studied with both shock-tube experiments and ab initio transition state theoretical calculations. D-atom profiles were measured behind reflected shock waves using D-atom atomic resonance absorption spectrometry (ARAS) in mixtures with C_2D_5I (D-atom precursor, <1 ppm) and the alkane of interest in excess (>200 ppm), over the T-range 1063 – 1327 K, at pressures ≅ 0.5 atm. D-atom depletion in the present experiments is sensitive only to the reactions,

$$D + n\text{-}C_4H_{10} \rightarrow \text{products} \qquad (A)$$
$$D + i\text{-}C_4H_{10} \rightarrow \text{products.} \qquad (B)$$

Figure 1 shows a typical D-atom profile for D + i-C_4H_{10}. Simulations of the measured profiles allow for determinations of total rate constants for the processes (A) and (B). The experimental rate constants are well represented by the Arrhenius equations,

$$k_A = 2.11 \times 10^{-9} \exp(-5661\ K/T)\ cm^3\ molecules^{-1}\ s^{-1} \qquad (1074\text{-}1253\ K)$$
$$k_B = 2.57 \times 10^{-9} \exp(-5798\ K/T)\ cm^3\ molecules^{-1}\ s^{-1} \qquad (1063\text{-}1327\ K)$$

The title reactions have also been characterized using electronic structure theory at the CCSD(T)/CBS//M06-2X/cc-pvtz level of theory. Over the T-range of the present experiments, the ab-initio based Transition State Theory (TST) kinetics predictions for the isotope effects, k_D/k_H, are near unity at high temperatures (>1000 K). This suggests that measurements for the deuterium analog afford an appropriate surrogate for probing the kinetics of the corresponding abstraction by H-atoms. The theoretical predictions are in good agreement with the experimental results and can be represented by the modified Arrhenius equations,

$$k_{A,THEORY} = 6.677 \times 10^{-17}\ T^{2.118} \exp(-2700\ K/T)\ cm^3\ molecules^{-1}\ s^{-1} \qquad (500\text{-}2000\ K)$$
$$k_{B,THEORY} = 5.627 \times 10^{-20}\ T^{2.934} \exp(-1225\ K/T)\ cm^3\ molecules^{-1}\ s^{-1} \qquad (500\text{-}2000\ K)$$

To our knowledge, the present experiments are the first direct measurements for the title reactions, and the rate constants from this combined experimental/theoretical effort are recommended for use in combustion modeling. Results from the present studies on n-C_4H_{10} and i-C_4H_{10} along with prior

studies on C_2H_6 and C_3H_8 suggest the applicability of rate rules for H + Alkanes that are based on generic primary, secondary, and tertiary abstraction sites.

Thermal Rate Constants for CH_3 and D with methanol.[3] The shock tube technique has been used to study the hydrogen abstraction reactions and are the first direct results on these abstractions.

$$D + CH_3OH \rightarrow CH_2O + H + HD \quad (A)$$
$$CH_3 + CH_3OH \rightarrow CH_2O + H + CH_4 \quad (B)$$

Reflected shock tube experiments, monitoring the depletion of D-atoms using D-atom ARAS, were performed on reaction (A) using gas mixtures of C_2D_5I and CH_3OH in Kr bath gas. C_2D_5I was used as precursor for D-atoms. For reaction (B), reflected shock tube experiments monitoring H-atom formation with H-atom ARAS, were carried out using gas mixtures of Biacetyl ($(CH_3CO)_2$) and CH_3OH in Kr bath gas. $(CH_3CO)_2$ was used as the source of CH_3-radicals. Detailed reaction models were assembled to fit the D-atom and H-atom time profiles in order to obtain experimental rate constants for reactions (A) and (B).

Total rate constants from the present experiments on D + CH_3OH and CH_3 + CH_3OH can be represented by the Arrhenius equations

$$k_A(T) = 1.51 \times 10^{-10} \exp(-3843\ \text{K}/T)\ \text{cm}^3\ \text{molecules}^{-1}\ \text{s}^{-1} \quad (1016\ \text{K} \leq T \leq 1325\ \text{K})$$
$$k_B(T) = 9.62 \times 10^{-12} \exp(-7477\ \text{K}/T)\ \text{cm}^3\ \text{molecules}^{-1}\ \text{s}^{-1} \quad (1138\ \text{K} \leq T \leq 1270\ \text{K})$$

The experimentally obtained rate constants were compared with available rate data from the literature. In this work, optimized structures and rovibrational properties were obtained from ab initio calculations at the MP2/6-311G** level of theory. Carvalho et al.[4] have also performed a quantum chemical study for the H + CH_3OH abstraction reaction. Structures, barrier heights, and rate constants were calculated with DFT, MP2, and CCSD(T) methods coupled with variational transition state theory (VST). Similar calculations for reaction (B) were also made, and the results from these quantum chemical studies on both reactions were found to be in good agreement with the present experimental results. With respect to the experiments on CH_3 + CH_3OH, the present study is a new implementation of the H-ARAS technique for measuring rate constants of a "slow" reaction ($k \sim 10^{-14}$ $\text{cm}^3\ \text{molecules}^{-1}\ \text{s}^{-1}$).

Thermal Rate Constants involving iso-propanol. Alcohols are increasingly being considered to be suitable alternative fuels. In earlier studies from this laboratory,[5,6] the thermal decompositions and bimolecular reactions of the two simplest alcohols, CH_3OH and C_2H_5OH were studied using atom (H, D-atoms) and radical (OH) diagnostics. These experimental studies were also complemented by state-of-the-art electronic structure based theoretical predictions[7] to provide rate constants over wide temperature and pressure ranges for use in combustion modeling.

We have carried out experiments and theoretical calculations on the next larger homolog, iso-propanol. Direct experimental measurements for iso-propanol decomposition are limited to rate constant determinations[8] for the molecular process, i-$C_3H_7OH \rightarrow C_3H_6 + H_2O$. However, the energetically accessible bond fission channel, i-$C_3H_7OH \rightarrow CH_3 + CH_3CHOH$, is an expected initiation step at high-temperatures. The only literature estimates for this C-C bond fission channel are the G2M theoretical predictions of Bui et al.[9] Our shock tube experiments, in order to characterize this poorly studied decomposition, monitored the formation of H-atoms by using H-atom ARAS over

a temperature range of 1190–1450 K at pressures ranging from 0.2 – 0.85 bar. The measured formation of H-atoms is sensitive to the rate constants for the energetically lowest-lying bond fission channel through the subsequent dissociation (nearly instantaneous) of the radical, $CH_3CHOH \rightarrow H + CH_3CHO$. Figure 2 shows the Arrhenius plot for this bond-fission channel. Since the bimolecular reaction, H + i-C_3H_7OH, is also an important fuel destruction process at high temperatures, rate constants for the reaction, D + i-C_3H_7OH (as a surrogate), were also experimentally determined. Measurements of D-atom profiles using D-ARAS allowed unambiguous rate constant measurements for the reaction D + i-$C_3H_7OH \rightarrow$ Products (980 K ≤ T ≤ 1250 K; P ~ 0.4 bar). These experiments are being extended by performing thermal decomposition studies on selected isotopically substituted iso-propanols, These studies are also expected to be complemented by state-of-the-art electronic structure based theoretical predictions.

This work was supported by the U.S. Department of Energy, Office of Science, Office of Basic Energy Sciences, Division of Chemical Sciences, Geosciences, and Biological Sciences under contract No. DE-AC02-06CH11357.

References

1. S.L. Mielke, K.A. Peterson, D.W. Schwenke, B.C. Garrett, D.G. Truhlar, J.V. Michael, M.-C. Su, and J.W. Sutherland, Phys. Rev. Lett. **91**, 063201-1 - 063201-4 (2003).
2. S.L. Peukert, R. Sivaramakrishnan, and J.V. Michael, Proc. Combust. Inst**. 35**, accepted (2014).
3. S. Peukert and J.V. Michael, J. Phys. Chem. A **117**, 10186-10195 (2013).
4. E.F.V. Carvalho, A.N. Barauna, F.B.C. Machado, and O. Roberto-Neto, Chem. Phys. Lett. **463**, 33-37 (2008).
5. N.K. Srinivasan, M.-C. Su, and J.V. Michael, J. Phys. Chem. A **111**, 3951-3958 (2011).
6. R. Sivaramakrishnan, M.-C. Su, J.V. Michael, S.J. Klippenstein, L.B. Harding, and B. Ruscic, J. Phys. Chem. A **114**, 9425-9439 (2010).
7. A. W. Jasper, S.J. Klippenstein, L.B. Harding, and B. Ruscic, J. Phys. Chem. A **111**, 3932-3950 (2007).
8. C. Rosado-Reyes, W. Tsang, I. M Alecu, S. S. Merchant, W. H. Green, J. Phys. Chem. A **117**, 6724-6736 (2013) and references within.
9. H. Bui, R. S. Zhu, M. C. Lin, J. Chem. Phys. **117**, 11188 (2002).

PUBLICATIONS FROM DOE SPONSORED WORK FROM 2011-2013

- *Experiment and Theory on Methyl Formate and Methyl Acetate Kinetics at High Temperatures: Rate Constants for H-atom Abstraction and Thermal Decomposition*, S. Peukert, R. Sivaramakrishnan, M.-C. Su, and J. V. Michael, Combust. and Flame, **159**, 2312-2323 (2012).

- *High Temperature Rate Constants for H/D + Methylformate and Methylacetate,* S. Peukert, R. Sivaramakrishnan, M.-C. Su, and J.V. Michael, Proc. Combust. Inst. **34**, 463-471 (2013).

- *High Temperature Shock Tube and Theoretical Studies on the Thermal*

Decomposition of Dimethyl Carbonate and its Bimolecular Reactions with H and D -Atoms, S. Peukert, R. Sivaramakrishnan and J.V. Michael, J. Phys. Chem. A, **117**, 3718-3728 (2013)

- *High Temperature Shock Tube Studies on the Thermal Dissociation of O_3 and the Reaction of Dimethyl Carbonate with O-atoms*, S. Peukert, R. Sivaramakrishnan, and J.V. Michael, J. Phys. Chem. A, **117**, 3729-3738 (2013).

- *High Temperature Shock Tube and Modeling Studies on the Reactions of Methanol with D-Atoms and CH_3-Radicals*, S.L. Peukert and J.V. Michael, J. Phys. Chem. A **117**, 10186-10195 (2013).

- *Direct Measurements of Rate Constants for the Reactions of CH_3 radicals with C_2H_6, C_2H_4, and C_2H_2 at High Temperatures* S.L. Peukert, N.J. Labbe, R. Sivaramakrishnan, J.V. Michael, J. Phys. Chem. A **117**, 10228-10238 (2013).

- *High Temperature Rate Constants for H/D + n-C_4H_{10} and i-C_4H_{10}*, S.L. Peukert, R. Sivaramakrishnan, and J.V. Michael, Proc. Combust. Inst., Accepted (2014).

- *Shock tube and theoretical studies on the thermal decomposition of iso-propanol and its reaction with D-atoms*, S.L. Peukert, R. Sivaramakrishnan, S.J. Klippenstein, and J.V. Michael, J. Phys. Chem. A, In preparation (2014).

- *The Decomposition Kinetics of Xylyl Radicals*, D. Polino, C. Cavallotti, R. Sivaramakrishnan, S.J. Klippenstein, and J.V. Michael, J. Phys. Chem. A, preparation (2014).

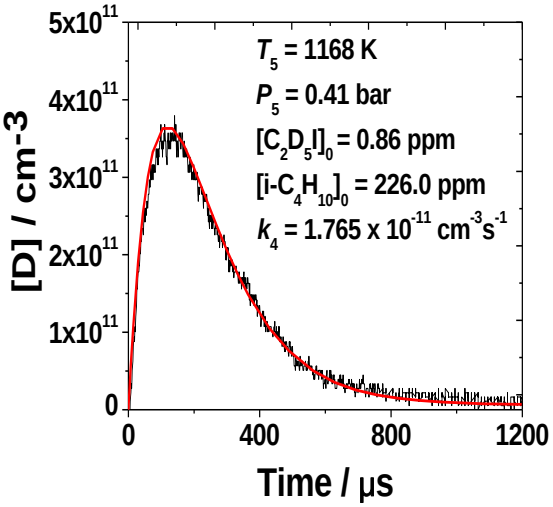

Figure 1: D-atom profile from D + i-C_4H_{10}

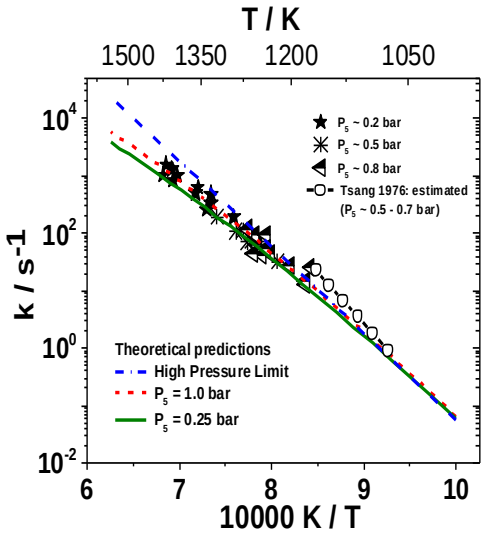

Figure 2: Arrhenius plot for i-C_3H_7OH CH_3 + CH_3CHOH

Particle Diagnostics Development

H. A. Michelsen
Sandia National Labs, MS 9055, P. O. Box 969, Livermore, CA 94551
hamiche@sandia.gov

I. Program Scope

Combustion processes often produce solid carbon particles, i.e., soot. These particles may be oxidized to form gas-phase species or released into the exhaust stream, where they can be coated with liquid coatings. These coatings can be comprised of any of a number of components, including unburned fuel, lube oil, sulfuric acid, water, and other combustion by-products.[1] The research program described here focuses on the development of optical diagnostics for soot particles in combustion environments and combustion exhaust plumes. The goal of this work is *in situ* measurements of volume fraction, size, composition, and morphology of combustion-generated particles with fast time response and high sensitivity. Measurement techniques are targeted for studies of soot formation and evolution and must be versatile enough to probe particles throughout their entire life cycle. Techniques are being developed for detection and characterization of particles in combustion environments from incipient particles that are 2-10 nm in diameter and composed of condensed large organic species to mature soot particles composed of aggregates of carbonaceous primary particles resembling polycrystalline graphite. Diagnostics are also being developed for chemical studies of growth, pyrolysis, and oxidation within combustors and characterization of inhomogeneous particles in exhaust streams.

II. Recent Progress

Our work has focused on developing a detailed understanding of the chemical and physical mechanisms that influence the applicability of laser-based techniques for soot detection under a wide range of conditions. In recent work, we have investigated the optical and physical properties of soot in a flame. We have combined measurements of laser-induced incandescence (LII), extinction, elastic laser scatter, and particle temperature from spectrally and temporally resolved radiative emission to develop a model that describes the energy- and mass-balance equations for laser-heated soot. We have compared the model predictions of time-resolved incandescence signals to observed LII temporal profiles from mature (graphitic) soot and less mature soot, which has significant hydrogen content. We have used this analysis to extend the use of LII for gaining information about soot composition.

We are also working on a SISGR project led by Prof. Angela Viola to develop a validated predictive multiscale model to describe the chemical composition of soot nanoparticles in premixed and diffusion flames. This project closely couples experimental investigations of soot precursors and incipient particle characteristics with the development of a predictive model for the chemical composition of soot nanoparticles. The co-investigators on the project are Prof. Angela Violi (University of Michigan) for model development and Drs. Hope Michelsen (Sandia) and Nils Hansen (Sandia) in collaboration with Dr. Kevin Wilson (LBNL ALS) for experimental investigations.

A. Influence of Soot Maturity on Its Optical and Physical Characteristics

Clean, mature soot is composed of small “primary” particles of polycrystalline graphite 10-50 nm in diameter covalently bound into dendritic aggregates of varying size. Mature soot absorbs strongly and broadly across optical wavelength regions and appears black. Less mature soot maintains some of its original hydrocarbon characteristics and includes significant hydrogen content. Previous studies have suggested that the wavelength dependence of the absorption cross section tends to shift to shorter wavelengths and decreases in magnitude with increasing hydrogen-to-carbon ratio (H/C), i.e., decreasing soot maturity. Very hydrogen rich soot particles often appear brown, rather than black. Mature soot can also be coated with a layer or multiple layers of organic and/or inorganic species, which can also lead to changes in absorption and scattering cross sections.

LII involves heating the particles with a high power laser and measuring the resulting radiative emission. The LII signal strongly depends on particle temperature, and the particle temperature is closely correlated with the absorption cross section. Because of these relationships, the LII signal recorded with different laser wavelengths can be used to directly infer the relative absorption cross section at different wavelengths. This technique has the advantage over extinction measurements because it is directly related to the absorption cross section and does not require any assumptions about, or measurements of, the

scattering cross section whereas extinction is a measure of attenuation by the combination of absorption and scattering. We have used LII fluence curves to derive relative absorption cross sections of soot at 532 and 1064 nm at the center and edge of flames produced by co-flow diffusion burners. Particles in the center are less mature than particles at the edge, where the temperatures and ambient oxygen concentrations are higher. The results indicate that the absorption cross-section ratio $\sigma_{abs}(532nm)/\sigma_{abs}(1064nm)$ increases with decreasing soot maturity, i.e., that less mature particles absorb more strongly at shorter wavelengths.

The fluence curves are shifted to higher fluences in the center relative to the edge region in both flames studied and at both laser wavelengths. Given an absorption cross section that increases with soot maturity, these observations are consistent with less mature soot in the center than in the edge regions, which is consistent with the trends in the absorption cross-section ratio in these regions. This result is supported by comparisons with an LII model that includes a soot-maturity dependent absorption cross section. Figure 1 shows the model results for the peak LII as a function of laser fluence compared with the measurements from the center and edge of one of the flames studied. In Fig. 1a the measurements are reproduced by a model using an absorption cross section that increases with soot maturity. Figure 1b shows the model using an absorption cross section that is independent of soot maturity but constrained to give good agreement with the more mature soot measurements in the edge region. The model does not reproduce the center fluence curves. The poor agreement shown in Fig. 1b demonstrates that differences in ambient temperature, primary-particle size, and aggregate morphology between the center and edge regions are not sufficient to explain the fluence shift between the center and edge data in the fluence curves. The better agreement demonstrated in Fig. 1a indicates that differences in the peak LII signals between the two flame regions can be explained by changes in the wavelength dependence and magnitude of the absorption cross section with soot maturity.

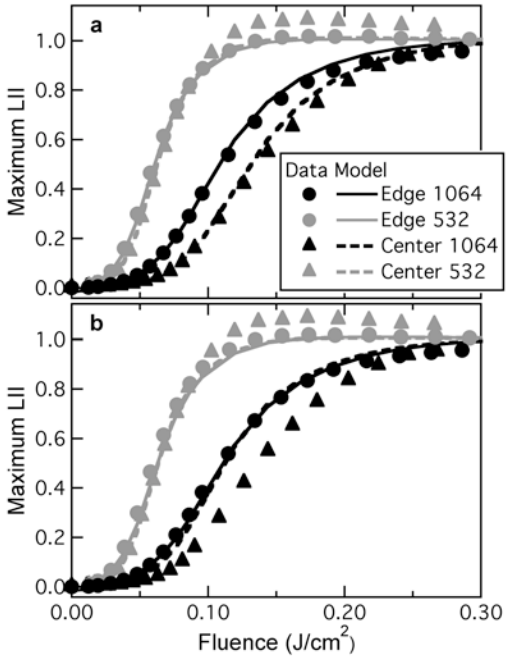

Figure 1. Measured and modeled peak LII signal as a function of fluence. Symbols represent maximum values of the LII temporal profiles measured in the center and edge regions of a co-flow diffusion flame. The laser wavelengths were 532 and 1064 nm, and the detection wavelength was 682 nm. The lines present model predictions using (a) a soot-maturity dependent absorption cross section and (b) an absorption cross section independent of soot maturity.

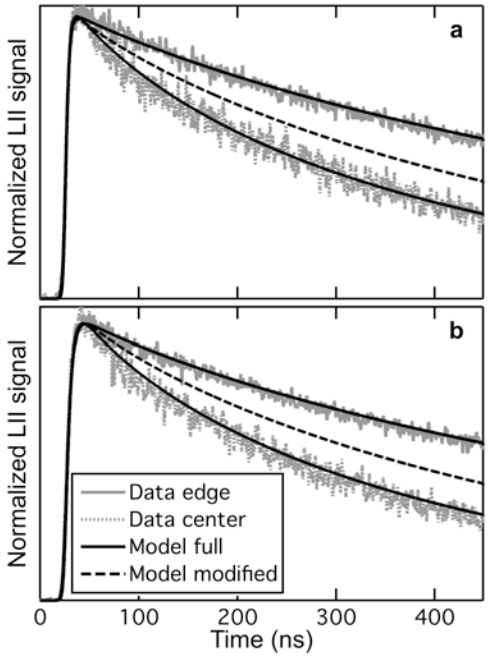

Figure 2. Measured and modeled LII temporal profiles. The solid (edge) and dotted (center) gray lines represent measured profiles. The solid black curves represent the model predictions with a soot-maturity dependent thermal-accommodation coefficient, and the dashed black curves show the model predictions where soot maturity was neglected in the conductive-cooling calculation. Modeled and measured curves were scaled to each other. Data were produced with laser wavelengths of (a) 532 nm (0.048 J/cm^2 for edge, 0.052 J/cm^2 for center) and (b) 1064 nm (0.086 J/cm^2 for edge, 0.110 J/cm^2 for center).

In addition to optical properties, soot maturity and composition can influence other physical properties. Some of these properties, in turn, can influence LII signals. Previous work has indicated that the conductive-cooling rate decreases with increasing soot maturity.[3] This observation is consistent with a decrease in surface roughness and associated decrease in the thermal-accommodation coefficient as hydrogen is removed from the surface and the surface becomes more graphitic and ordered.[4] In addition, theoretical and experimental studies have shown that graphite surfaces pucker when hydrogen is bound to the surface.[5] Because LII is sensitive to these non-optical physical properties of soot particles, understanding the LII signal response to these properties is required for the correct interpretation of these measurements.

Analysis of LII temporal profiles in the center and edge regions of these flames indicates that the thermal-accommodation coefficient decreases with soot maturity. This observation is consistent with results presented by Bladh et al.[3] LII signals decay more slowly in the edge region than at the center for both flames, as shown in Fig. 2 for one of the flames studied. Smaller primary-particle sizes, less compact aggregate morphologies, and lower ambient temperatures can all lead to faster signal decay rates, but differences in these parameters cannot account for the differences in the signal decay rates between the center and edge regions in the flame. Figure 2 shows comparisons between the measured temporal profiles and results from the full LII model (solid black lines), which includes a soot-maturity dependent thermal-accommodation coefficient and demonstrates good agreement with the observations. Figure 2 also demonstrates the discrepancies introduced between the model and the measurements if the soot maturity dependence is neglected in the thermal-accommodation coefficient used in the model (dashed black lines). For the edge, the results from the full model, which includes a maturity-dependent accommodation coefficient, are indistinguishable from the modified model, which neglects soot maturity in accommodation. The dashed black line that lies between the measured temporal profiles shows results of a calculation for the center that accounts for primary-particle size, aggregate morphology, and ambient temperature. The remaining differences between the measured center temporal profiles and this latter calculation can be explained by the enhanced conductive-cooling rate associated with the higher thermal accommodation for less mature soot. This conclusion is demonstrated by the agreement achieved between the measured center temporal profile and the full model.

Our studies have suggested that the absorption cross-section ratio decreases, the absolute absorption cross section increases, and the thermal-accommodation coefficient decreases with increasing soot maturity. Given the sensitivity of LII to these parameters, it may be possible to use a combination of *in situ* measurements of LII fluence curves and temporal profiles to gain information about soot maturity.

III. Future Work

Some of our future work focuses on combustion-generated particles with inorganic and organic coatings representative of particles found in exhaust plumes. In order to simulate exhaust-plume particulates, we have built a flow-tube system to allow controlled deposition of a coating with low volatility on flame-generated soot. The thickness of the coating can be varied, and the particles collected for analysis by transmission electron microscopy (TEM), scanning mobility particle sizing (SMPS), or centrifugal particle mass analyzer (CPMA), or analyzed with an aerosol mass spectrometer that is under construction. Coatings investigated to date have been selected for diagnostic development for diesel exhaust and include sulfuric acid, heptamethylnonane, and oleic acid. We are also preparing our LII model for release as a community-based model in collaboration with Karla Morris, another staff member at Sandia. In addition, we are exploring other laser-based and x-ray optical diagnostics approaches that can be implemented for *in situ* measurements in flames or for *ex situ* analysis on extracted samples and can be used to gain compositional information about particle formation and evolution. Preliminary studies are planned in collaboration with Chris Kliewer (Sandia) and Tony Van Buuren (LLNL).

IV. References

1. (a) Kittelson, D. B., Engines and nanoparticles: A review. *J. Aerosol Sci.* **1998,** *29* (5/6), 575-588; (b) Lighty, J. S.; Veranth, J. M.; Sarofim, A. F., Combustion aerosols: Factors governing their size and composition and implications for human health. *J. Air Waste Manage. Assoc.* **2000,** *50* (9), 1565-1618.
2. (a) Habib, Z. G.; Vervisch, P., On the refractive index of soot at flame temperature. *Combust. Sci. Technol.* **1988**, *59*, 261-274; (b) Dalzell, W. H.; Sarofim, A. F., Optical constants of soot and their application to heat-flux calculations. *J. Heat Transfer* **1969**, 91, 100-104; (c) Minutolo, P.; Gambi, G.; D'Alessio, A., The optical band gap model in the interpretation of the UV-visible absorption spectra of rich premixed flames. *Proc. Combust. Inst.* **1996**, 26, 951-957; (d) Siddall, R. G.; McGrath, I. A., The emissivity of luminous flames. *Proc. Combust. Inst.* **1963**, 9, 102-110; (e) D'Alessio, A.; Beretta, F.; Venitozzi, C., Optical investigations of soot forming methane-oxygen flames. *Combust. Sci. Technol.* **1972**, 5, 263-272.
3. Bladh, H.; Johnsson, J.; Bengtsson, P.-E., Influence of spatial laser energy distribution on evaluated soot particle sizes using two-colour laser-induced incandescence in a flat premixed ethylene/air flame. *Appl. Phys. B* **2009**, 96, 645-656.
4. (a) Rettner, C.T.; Auerbach, D.J.; Tully, J.C.; Kleyn, A.W., Chemical dynamics at the gas-surface interface. *J. Phys. Chem.* **1996**, *100*, 13021-13033; (b) Saxena, S.C.; Joshi, R.K., *Thermal Accommodation and Absorption Coefficients of Gases*. **1981** McGraw-Hill, New York.
5. (a) Sha, X.; Jackson, B., First-principles study of the structural and energetic properties of H atoms on a graphite (0001) surface. *Surf. Sci*. **2002**, *496*, 318-330; (b) Zecho, T.; Güttler, A.; Sha, X.; Jackson, B.; Küppers, J., Adsorption of hydrogen and deuterium atoms on the (0001) graphite surface. *J. Chem. Phys.* **2002**, *117*, 8486-8492.

V. Publications and submitted journal articles supported by this project 2012-2014

1. A. Nanthaamornphong, K. Morris, D. W. I. Rouson, and H. A. Michelsen, "A case study: Agile development in the Community Laser-Induced Incandescence Modeling Environment (CLiiME)", *Comput. Sci. Eng.*, in press (2014).
2. K. O. Johansson, J. Y. W. Lai, S. A. Skeen, K. R. Wilson, N. Hansen, A. Violi, and H. A. Michelsen, "Soot precursor formation and limitations of the stabilomer grid", *Proc. Combust. Inst.*, submitted (2013).
3. X. López-Yglesias, P. E. Schrader, and H. A. Michelsen, "Effects of soot maturity on its absorption cross section and thermal-accommodation coefficient", *J. Aerosol Sci.*, submitted (2013).
4. N. Hansen, S. A. Skeen, H. A. Michelsen, K. R. Wilson, and K. Kohse-Höinghaus, "Flame experiments at the Advanced Light Source: New insights into soot formation processes", *Journal of Visualized Experiments (JoVE)*, in press (2014).
5. R. P. Bambha, M. A. Dansson, P. E. Schrader, and H. A. Michelsen, "Effects of volatile coatings on the laser-induced incandescence of soot", *Appl. Phys. B* **112(3)**, 343-358 (2013).
6. R. P. Bambha, M. A. Dansson, P. E. Schrader, and H. A. Michelsen, "Effects of volatile coatings and coating removal mechanisms on the morphology of graphitic soot", *Carbon* **61**, 80-96 (2013).
7. F. Goulay, P. E. Schrader, X. López-Yglesias, and H. A. Michelsen, "A dataset for validation of models of laser-induced incandescence from soot: Temporal profiles of LII signal and particle temperature", *Appl. Phys. B* **112(3)**, 287-306 (2013).
8. J. M. Headrick, P. E. Schrader, and H. A. Michelsen, "Radial-profile and divergence measurements of combustion-generated soot focused by an aerodynamic-lens system", *J. Aerosol Sci.* **58**, 158-170 (2013).
9. S. A. Skeen, H. A. Michelsen, K. R. Wilson, D. M. Popolan, A. Violi, and N. Hansen, "Near-threshold photoionization mass spectra of combustion-generated high-molecular-weight soot precursors", *J. Aerosol Sci.* **58**, 86-102 (2013).
10. S. A. Skeen, B. Yang, H. A. Michelsen, J. A. Miller, A. Violi, and N. Hansen, "Studies of laminar opposed-flow diffusion flames of acetylene at low pressures with photoionization mass spectrometry", *Proc. Combust. Inst.* **34**, 1067-1075 (2013).

Detection and Characterization of Free Radicals Relevant to Combustion Processes

Terry A. Miller
Laser Spectroscopy Facility, Department of Chemistry
The Ohio State University, Columbus OH 43210, email: tamiller@chemistry.ohio-state.edu

1 Program Scope

Combustion processes have been studied for many years, but the chemistry is very complex and yet to be fully understood. New fuels have introduced modifications to traditional mechanisms. Computer models typically employ hundreds of reaction steps with a comparable number of chemical intermediates. The predictions of such models are obviously limited by the dynamical and mechanistic data that are input. Spectroscopic identifications and diagnostics for the chemical intermediates in the reaction mechanisms constitute an important experimental benchmark for the models, as well as providing molecular parameters that are "gold standards" against which quantum chemistry computations of molecular properties may be judged. Our recent work has emphasized the spectroscopy of organic peroxy radicals which are key intermediates in combustion reactions.

2 Recent Progress

For several years the technique of near-infrared (NIR) cavity ringdown spectroscopy (CRDS) of reactive chemical intermediates has been a mainstay in our laboratory and we have used it to investigate the $\widetilde{A}$ - $\widetilde{X}$ absorptions of simple alkyl peroxy radicals. These studies have created a database which allows structural/spectral relationships to be developed. These relationships provide approximate predictions of spectral shifts for structural changes, e.g. *primary* (*pri*), *secondary* (*sec*), *tertiary* (*tert*) position of the peroxy group, length of the hydrocarbon chain, additional substitutions along the chain, etc. For the most part, these relationships have been based on the spectra of relatively small peroxy radicals, and are both isomer and conformer specific. Most fuels contain a mixture of larger hydrocarbons and we have recently concentrated on obtaining the spectroscopy of their combustion intermediates with the goal of determining how well CRDS can characterize complex peroxy radicals and mixtures of such radicals. A second, related, and new area of CRDS spectral observation combines our alkyl peroxy work with investigations of two chemically closely related species, the halomethyl peroxy radicals, CH_2XO_2 (X=Cl, Br, I) and the very intriguing Criegee intermediate species, CH_2O_2.

A third area of work involves the development of a practical CRDS apparatus to take advantage of the fact that for any absorption spectroscopy, such as CRDS, the observed signal intensity is linearly related to the concentration of the molecular species, in the limit of small absorption. We have constructed a dual wavelength CRDS apparatus (2λ-CRDS) capable of pulsed or CW operation to measure absorption cross-sections and rates of reactions for peroxy radical intermediates.

2.1 Spectroscopic Investigations of C_6-C_{10} Peroxy Radicals

It is well known that larger chain alkanes (>C_5-C_{10}) are important components of gasoline and diesel fuels. Our previous CRDS spectroscopy of combustion intermediates has been limited to the $\tilde{A} - \tilde{X}$ transition of peroxy radicals with $\leq$5 carbon atoms. Recently we have extended our observations to larger chain intermediates, e.g. hexyl, heptyl, octyl, nonyl, and decyl peroxy radicals. In these experiments the peroxy radicals are formed from H atom extraction by Cl

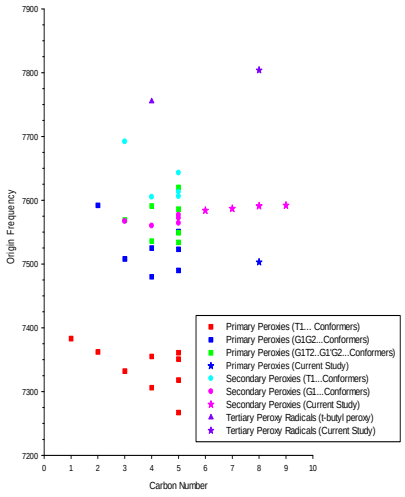

Figure 1: Spectral/structural relationships for origin bands of the conformers and isomers of C_1-C_5 alkyl peroxy radical. New measurements for the C_6-C_{10} alkyl peroxies are indicated by *s and color coded to conform to the assignments of the smaller alkyl peroxies.

atom attack (simulating OH attack in combustion) on the corresponding hydrocarbon followed by reaction with O_2. It is possible to form multiple isomers of peroxy radicals as there are several unique hydrogen atoms that can be abstracted by the Cl atom. Fig. 1 shows the structural/spectral relationships that have been derived from our earlier data on C_1-C_5 hydrocarbons. These relationships allow assignments of the C_6-C_{10} peroxy radical spectra which are mostly too large for accurate predictions from electronic structure calculations.

In Fig. 2 we focus on the spectrum of the peroxy radicals resulting from the oxidation of two isomers of octane, *n*-octane and *iso*-octane, the latter the standard (100) for the rating of commercial gasolines. The combination of the data in Figs. 1 and 2 shows that *n*-octane, like the other larger alkanes studied, produces almost exclusively the *sec* isomers of the corresponding peroxy radical. On the other hand, in the case of *iso*-octane the spectral/structural relations in Fig. 1 indicate that only the *pri* and *tert* isomers are observed. The assignment of the *tert*-octyl peroxy spectrum is further confirmed by the negligible decay of these spectral lines in 1 ms, as shown in the bottom trace of Fig. 2. The *tert*-peroxy isomers are known to have very small rate constants for self-reaction because of the large stearic hinderance around the peroxy moiety and so effectively do not decay on the timescale of the experiment.

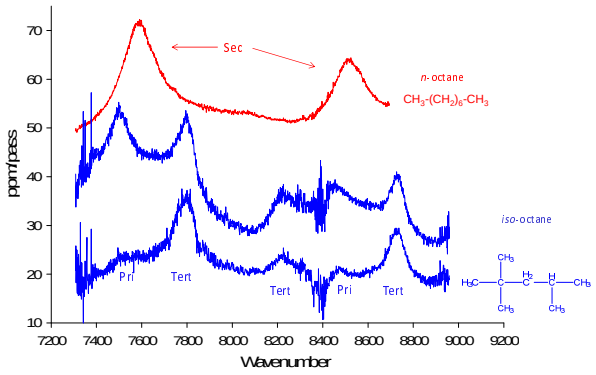

Figure 2: $\tilde{A} - \tilde{X}$ spectra of octyl and isooctyl peroxy radicals. Top (red) trace arises from *n*-octane precursor. The lower (blue) traces are from the *iso*-octane precursor. The bottom trace is taken at a time delay of 1 ms and shows the time evolution of the isooctyl peroxy spectrum. The sharp lines in the isooctyl peroxy traces (≈8290-8420 cm^{-1}) are from incomplete substraction of a precursor band.

2.2 Spectroscopic Investigations of Halogenated Peroxy Radicals and Criegee Intermediates

Following the initial reports from the Combustion Research Facility of a new procedure for producing the Criegee intermediate, CH_2O_2, there has been an explosion of interest in its spectroscopy and reactions. While the protocols of various workers have differed in details the basic idea, as illustrated in Fig. 3, is the same, i.e. photolysis of a CH_2I_2 precursor produces CH_2I which reacts with O_2 to release I and form CH_2O_2. Spectroscopic studies have included reports of a broad UV absorption spectrum, a structured mid-IR vibrational spectrum, and microwave rotational spectra. Each of these spectroscopic techniques has its own advantages and disadvantages for providing a diagnostic for following the reactions of CH_2O_2 and characterizing its geometric and electronic structure.

To complement these studies, we have attempted to observe the $a^3\tilde{A}'-X^1A'$ electronic spectrum of CH_2O_2. The analogous transition has long been known in the isoelectronic O_3 species as the Wulf band. Like the alkyl peroxy $\tilde{A} - \tilde{X}$ electronic transitions it occurs in the NIR. This is not surprising as one of the resonance forms of the Criegee intermediate is the methylene peroxy radical, $\cdot CH_2O_2\cdot$.

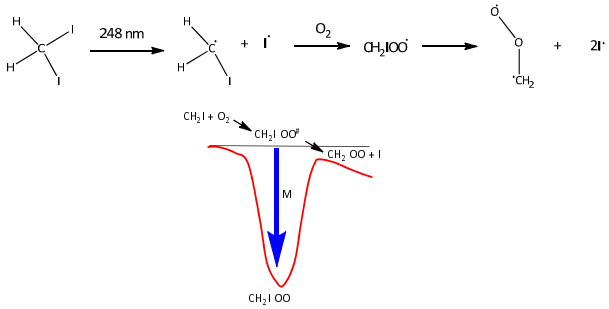

Figure 3: Proposed mechanism (Huang, H.; Eskola, A.; Taatjes, C. A. *J. Phys. Chem. Lett.* 2012, **3**, 3399) for the production of CH_2O_2 indicating a possible second channel producing CH_2IO_2.

Fig. 4 shows the CRDS spectrum in the NIR that we observed using CH_2I_2 photolysis in the presence of O_2. As the figure shows, this spectrum has several characteristics expected of CH_2O_2. Its apparent origin is in the NIR, just below 7000 cm^{-1}, and it clearly exhibits an O-O stretch and combination bands whose frequencies are characteristic, albeit slightly lower, than those in typical alkyl peroxy radicals. However the information available from the spectrum is limited by signal/noise as well as interference from several other species and some spectral features, e.g. the complex structure near the origin, are difficult to understand. While good electronic structure calculations exist for the $\tilde{X}^1A'$ state, there are at present no reliable calculations for the $\tilde{a}^3A'$ state that could aid the detailed assignment of the spectrum.

Fig. 3 shows that another species postulated to be formed from the CH_2I_2 photolysis chemistry is CH_2IO_2. The general characteristics of the observed spectrum in Fig. 4 are also broadly consistent with assignment to CH_2IO_2, whose excited $\tilde{A}$ state likewise is somewhat difficult to calculate reliably due to the need to use a pseudo-potential for the I atom. We have therefore decided to compare the spectrum in Fig. 4 to the

spectra of CH_2ClO_2 and CH_2BrO_2. These species have been generated by photolysis of CH_2ClI or CH_2BrI. (Indistinguishable spectra are also observed when CH_2Cl_2 and CH_2Br_2 respectively are photolyzed.) Energetic considerations should preclude the breaking of the second carbon-halogen bond and hence no CH_2O_2 should be produced with these precursors consistent with each trace in Fig. 4 being unique.

Fig. 5 shows there is also a good deal of similarity among the spectra produced by photolyzing CH_2ClI, CH_2BrI, and CH_2I_2. However it could be argued that the spectrum resulting from CH_2I_2 shows some unique features. Nonetheless at this stage we consider the spectral evidence not to be conclusive as to the carrier of the spectrum in Fig. 4. If anything, the spectral evidence, e.g. rotational contours and the origin structure, probably favors its assignment to CH_2IO_2 although numerous questions also exist with this assignment.

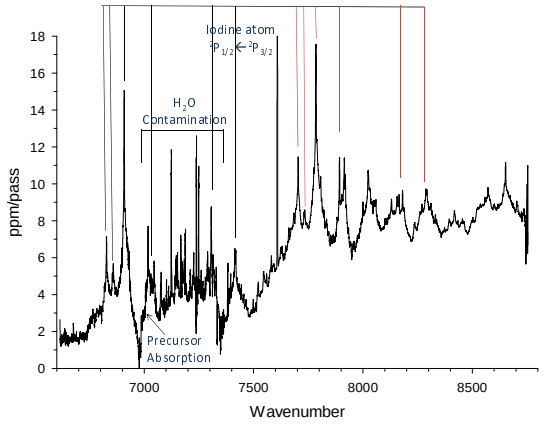

Figure 4: NIR CRDS spectrum observed following photolysis of CH_2I_2 in the presence of O_2. Spacing ($\approx$875 cm^{-1}) between black and red ticks on bar indicates O-O stretch frequency and its combination bands correlated to their fundamentals.

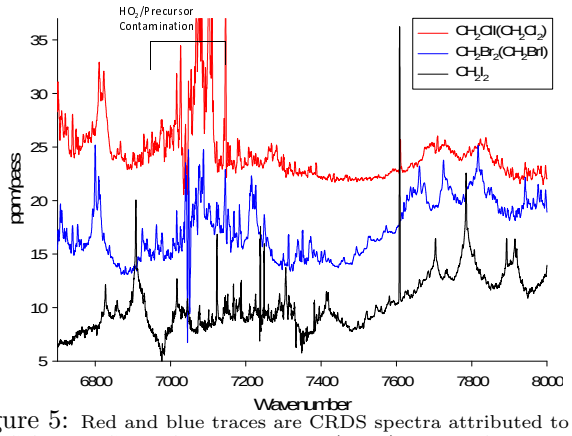

Figure 5: Red and blue traces are CRDS spectra attributed to CH_2ClO_2 and CH_2BrO_2. The bottom (black) trace is from Fig. 4.

In order to help identify the carrier of the spectrum in Fig. 4 chemical arguments can be advanced to differentiate between the CH_2O_2 and CH_2IO_2 carriers. First the production conditions were nearly identical to those used by the Lee group which reported a strong vibrational spectrum for CH_2O_2 but could not detect CH_2IO_2 transitions. Photolyzing of CH_2I_2 in the absence of O_2 results in a baseline iodine atom absorption, that increases when O_2 is present which is consistent with the proposed mechanism of $CH_2I + O_2$ forming CH_2O_2+I. In another experiment the delay time between the NIR probe beam and our photolysis pulse was varied to measure the temporal decay of the spectrum due to self reaction. We estimate a self reaction rate constant of 4 ± 3 x 10^{-10} cm^3 $molecules^{-1}$ s^{-1}, which is consistent with the self-reaction rate constant just-published by the Lee group for CH_2O_2. Finally SO_2 is known to be an effective Criegee scavenger while reacting very slowly with alkyl peroxy radicals. The presence of SO_2 quenched all of the absorption bands shown in Fig. 4, but the same pressure of SO_2 did not affect the spectra attributed to CH_2BrO_2 or CH_2ClO_2. The chemical tests therefore are all consistent with the Criegee intermediate being the carrier of the spectrum in Fig. 4.

2.3 Application of CW 2λ-CRDS to Reaction Rate Constant Measurements

In the past we have reported development of an analytical method for the accurate determination of the absorption cross-section of reactive intermediates by means of a dual wavelength 2λ-CRDS spectrometer. This method utilizes a chemical reaction which photolytically produces, in a well-known stochiometric ratio, a reactive species of interest and a chemically inert byproduct whose absorption cross-section is accurately known. We have applied this technique to the $\tilde{A} \leftarrow \tilde{X}$ electronic transition of $C_2H_5O_2$, and thereby obtained directly its absorption cross section, σ. In the past year we completed work and published results from a 2λ-CRDS experiment which yields a direct measurement of the ratio of the self-reaction rate constant, k_{obs}, and σ for the ethyl peroxy radical. Combination of this new result with the previously measured value of σ allows a direct determination of k_{obs}.

The experiment utilized a CW diode laser whose frequency was periodically tuned across a CRDS cavity resonance generating a rapid succession of ring-down events. This approach allows near-continuous monitoring of the time evolution of the radical sample, and provides two key advantages over traditional shot-to-shot CRDS-based measurements. First, it eliminates experimental uncertainties associated with power variation of the photolysis radiation and resulting variation in sample concentration from shot to shot. Second, it allows for a dramatic increase in the data acquisition rate.

Results from this method are illustrated in Fig. 6, which shows a comparison of the previously available data for k_{obs} (and error bars) with the results of the present measurement. The presently reported value is consistent with most of the previous reports; however, the new measurement enjoys substantially smaller uncertainty.

3 Future Directions

A major goal is to complete the analyses of the CH_2ClO_2 and CH_2BrO_2 spectra. Combining these results with a reliable calculation of the $\tilde{a}^3A'$ state and/or a resolved rotational spectrum should determine the carrier assignment for the observed spectrum from CH_2I_2 photolysis. If the Criegee radical is the carrier, the spectrum will provide a useful new diagnostic for CH_2O_2. If not, then the reported chemistry involving CH_2O_2 will need to be re-examined to understand why the observed spectrum behaves as if the carrier were.

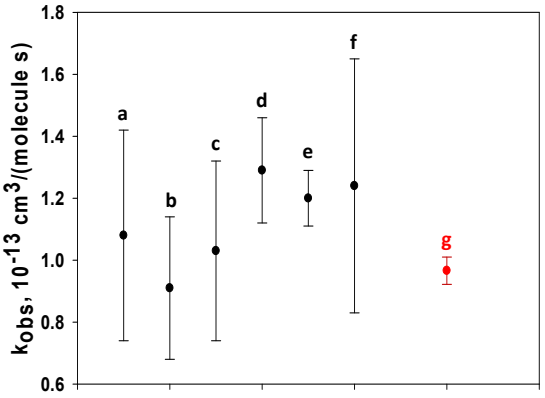

Figure 6: Comparison of the previously available data for k_{obs} (a-f) with the value obtained in the present studies (g) for the self-reaction rate constant of ethyl peroxy. See publication 11 for the details of the present measurement and the previously reported k_{obs} values.

Based upon our work with ethyl peroxy we have now determined that our 2λ-CRDS apparatus is capable of measuring absorption cross sections, and with those in hand corresponding self reaction rates. For the latter measurement we have employed a new version of the 2λ-CRDS experiment that has the potential to greatly improve the speed and accuracy of rate constant measurements. We plan to push this work into two areas. One direction is to extend our measurements to reaction rates between two different peroxy radicals, e.g. CH_3O_2 with $C_2H_5O_2$. Another important direction is to extend our frequency coverage so we can make both cross-section and reaction rate measurements involving HO_2. We are collaborating with our OSU colleague, Walter Lempert, to combine his burst-pulse OPO laser source with our 2λ-CRDS apparatus. This source provides the frequency coverage to observe the HO_2 $\tilde{A} - \tilde{X}$ transition, has a narrower bandwidth (300 MHz) than the HO_2 rotational transitions ensuring quantitatively accurate concentration measurements, and has a high (kHz) repetition rate to take advantage of our new faster experimental protocol for measuring reaction rates. The burst laser is working and soon will be combined with the 2λ-CRDS apparatus.

Publications Supported by DOE (2010-2014)

[1] "Measurement of the Absolute Absorption Cross Sections of the $\tilde{A} \leftarrow \tilde{X}$ Transition in Organic Peroxy Radicals by Dual Wavelength Cavity-Ringdown Spectroscopy," D. Melnik, R. Chhantyal-Pun, and T. A. Miller, *J. Phys. Chem. A* **114**, 11583 (2010).

[2] "The $\tilde{A} - \tilde{X}$ Absorption of Vinoxy Radical Revisited: Normal and Herzberg-Teller Bands Observed Via Cavity Ringdown Spectroscopy," P. S. Thomas, R. Chhantyal-Pun, N. D. Kline, and T. A. Miller, *J. Chem. Phys.* **132**, 114302 (2010).

[3] "Cavity Ringdown Spectroscopy of the NIR $\tilde{A} - \tilde{X}$ Electronic Transition of Allyl Peroxy Radical (H_2C=CH-$CH_2OO\cdot$)," P. S. Thomas and T. A. Miller, *Chem. Phys. Lett.* **491**, 123 (2010).

[4] "Observation of the $\widetilde{A} - \widetilde{X}$ Electronic Transition of the β-Hydroxyethylperoxy Radical," R. Chhantyal-Pun, N. D. Kline, P. S. Thomas, and T. A. Miller, *J. Phys. Chem. Lett.* **1**, 1846 (2010).

[5] "Cavity Ringdown Spectroscopy of Peroxy Radicals: The $\tilde{A} - \tilde{X}$ Absorption of Propargyl Peroxy (H-C=C-$CH_2OO\cdot$)," P. S. Thomas, N. D. Kline, and T. A. Miller, *J. Phys. Chem. A* **114**, 12437 (2010).

[6] "The $\tilde{A} - \tilde{X}$ Absorption of Cyclopentadienyl Peroxy Radical (c-$C_5H_5OO\cdot$): A Cavity Ringdown Spectroscopic and Computational Study," P. S. Thomas and T. A. Miller, *Chem. Phys. Letts.* **514**, 196 (2011).

[7] "The Electronic Transition Moment for the 0_0^0 Band of the $\tilde{A} - \tilde{X}$ Transition in the Ethyl Peroxy Radical," D. Melnik, P. S. Thomas, and T. A. Miller, *J. Phys. Chem. A* **115**, 13931 (2011).

[8] "Spectroscopic Studies of the $\tilde{A} - \tilde{X}$ Electronic Spectrum of the β-Hydroxyethylperoxy Radical: Structure and Dynamics," M.-W. Chen, G. M. P. Just, T. Codd, and T. A. Miller, *J. Chem. Phys.* **135**, 184304 (2011).

[9] "Analysis of the $\tilde{A}-\tilde{X}$ Electronic Tranistion of the 2,1-Hydroxypropylperoxy Radical Uisng Cavity Ringdown Spectroscopy," N. D. Kline and T. A. Miller, *Chem. Phys. Letts.* **530**, 16 (2012).

[10] "Kinetic Measurements of the $C_2H_5O_2$ Radical Using Time-resolved Cavity Ring-down Spectroscopy with a Continuous Source," D. Melnik and T. A. Miller, *J. Chem. Phys.* **139**, 094201, (2013).

[11] "Detection and Characterization of Reactive Chemical Intermediates Using Cavity Ringdown Spectroscopy," N. Kline and T. A. Miller, in *Cavity Enhanced Spectroscopy and Sensing*, G. Gagliardi and P. Loock, eds., Springer-Verlag, Berlin Heidelberg, (2014).

[12] "Observation of the $\tilde{A} - \tilde{X}$ Electronic Transition of C_6-C_{10} Peroxy Radicals," N. D. Kline and T. A. Miller, *Chem. Phys. Lett.* (accepted).

Reaction Dynamics in Polyatomic Molecular Systems

William H. Miller

Department of Chemistry, University of California, and
Chemical Sciences Division, Lawrence Berkeley National Laboratory
Berkeley, California 94720-1460
millerwh@berkeley.edu

I. Program Scope

The goal of this program is the development of theoretical methods and models for describing the dynamics of chemical reactions, with specific interest for application to polyatomic molecular systems of special interest and relevance. There is interest in developing the most rigorous possible theoretical approaches and also in more approximate treatments that are more readily applicable to complex systems.

II. Recent Progress

Effort in recent years has focused on finding ways to add quantum mechanical effects to classical molecular dynamics (MD) simulations, which are now so ubiquitously applied to all types of dynamical processes in complex molecular systems, e.g., chemical reactions in clusters, nano-structures, molecules on or in solids, bio-molecular systems, etc. Since quantum effects in *transitions between different electronic states* can obviously be very significant, one of the most important applications of semiclassical (SC) approaches[1-3] is to these non-adiabatic processes. The first approach that allowed both nuclear and electronic degrees of freedom (DOFs) to be treated by SC, or even classical methods, in a unified and completely consistent fashion was the model introduced by Meyer and Miller[4] (MM), in which each electronic state is characterized by a classical DOF (a harmonic oscillator). [Stock and Thoss[5] (ST) later showed this to be an *exact representation* of a vibronic system.] A variety of applications of this approach has demonstrated its usefulness.[6-8]

The most significant recent development on this topic has been to realize that a modified version of the venerable 'quasi-classical' model for state-to-state quantum transitions provides a surprisingly good description of electronically non-adiabatic processes using the MM model for the electronic DOFs. It should be emphasized that this is a completely classical treatment, where the electronic quantum states are 'quantized' (approximately) by assigning their corresponding classical action variables to histogram 'boxes' initially and finally. It is thus straightforward to apply this approach to any molecular system for which a classical molecular dynamics is feasible.

In the MM model each electronic state k is characterized by a pair of classical action-angle variables (n_k, q_k), and if $(\boldsymbol{P}, \boldsymbol{R})$ are the nuclear momenta and coordinates, the MM classical Hamiltonian for the nuclear and electronic degrees of freedom is

$$H(\boldsymbol{P},\boldsymbol{R},\boldsymbol{n},\boldsymbol{q}) = \frac{\boldsymbol{P}^2}{2\mu} + \sum_{k=1}^{F} n_k\, H_{kk}(\boldsymbol{R}) + 2\sum_{k<k'=1}^{F} \sqrt{(n_k+\gamma)(n_{k'}+\gamma)}\cos\left(q_k - q_{k'}\right) H_{kk'}(\boldsymbol{R}) \qquad (1)$$

where, as indicated, the $F\times F$ diabatic electronic matrix $\left\{H_{kk'}(\boldsymbol{R})\right\}$ is a function of the nuclear coordinates and assumed to come from many-electron 'quantum chemistry.' (There is an equivalent adiabatic version of this Hamiltonian, but the diabatic version is somewhat simpler to describe.) The electronic and nuclear dynamics are determined by computing classical trajectories from this Hamiltonian (by integrating Hamilton's equations) for electronic and nuclear degrees of freedom. This was the primary goal of the MM approach: to have a consistent dynamical description of electronic and nuclear degrees of freedom that treated them in an equivalent framework.

The parameter γ in Eq. (1) was at first equal to 0 in MM's heuristic derivation of this Hamiltonian, but on the basis of semiclassical considerations (a Langer-like modification) they then took it to be 1/2, effectively providing the zero point energy of each electronic degree of freedom. Stock later found[9] in some of his applications that better results were obtained by choosing $\gamma < 1/2$ (suggesting a 'best value' of ~ 1/4), so as to incorporate only a fraction of the zero point energy. Within the quasi-classical approach we take it to be an empirical parameter with a value between 0 and ½; there is theoretical justification for choosing it to be $(\sqrt{3}-1)/2 \sim 0.366$, a value we find to give good results in our symmetrical windowing treatment.

More details of the approach are described in ref. 10, and here some of the examples that demonstrate its performance.

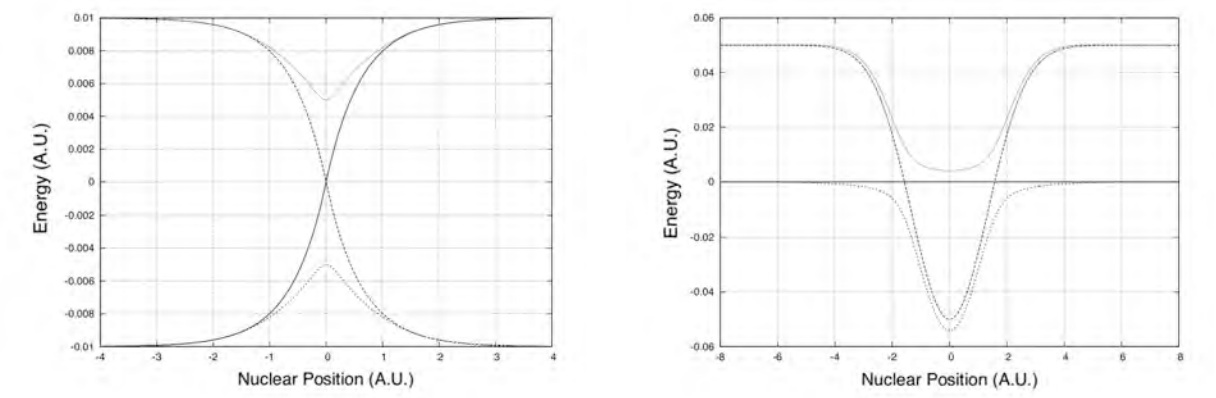

The above figures are the 1d potential curves for two electronic states that were used by Tully[11] to test his 'fewest switches' surface hopping model, and which have been widely used model problems to test non-adiabatic processes in a simple system. The first is a single curve crossing, and the second a model with two curve crossing regions. The transition probabilities (as a function of collision energy) given by the present quasi-classical model are shown below (points), compared to the correct quantum results (solid lines). The agreement is seen to be extremely good, and especially interesting is the double crossing case which shows an oscillatory structure usually attributed to quantum interference effects from crossing at one or the other of

the two crossing regions (Stuekelberg oscillations). One sees that this completely *classical* treatment gives quantitative results.

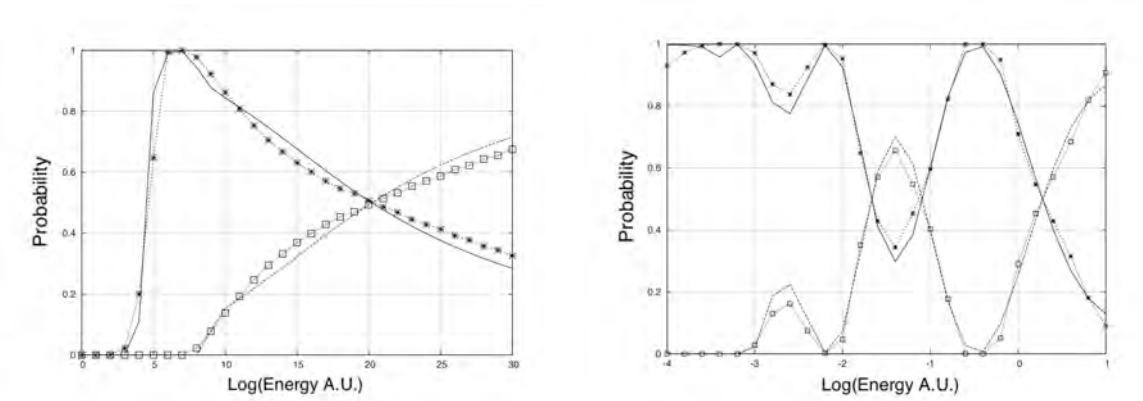

Below are shown results for the spin-boson model (two electronic states for which the diabatic potential energy surfaces are multi-dimensional shifted harmonic potentials). Shown is the population relaxation, the probability of being is state 1 minus that of being in state 2, having begun in state 1. The first two figures are for the symmetric model, the first in the incoherent regime and the second in the coherent regime. (Points are the correct quantum results, and the solid lines the quasi-classical results.) Again note that the coherent structure is well described by the classical model.

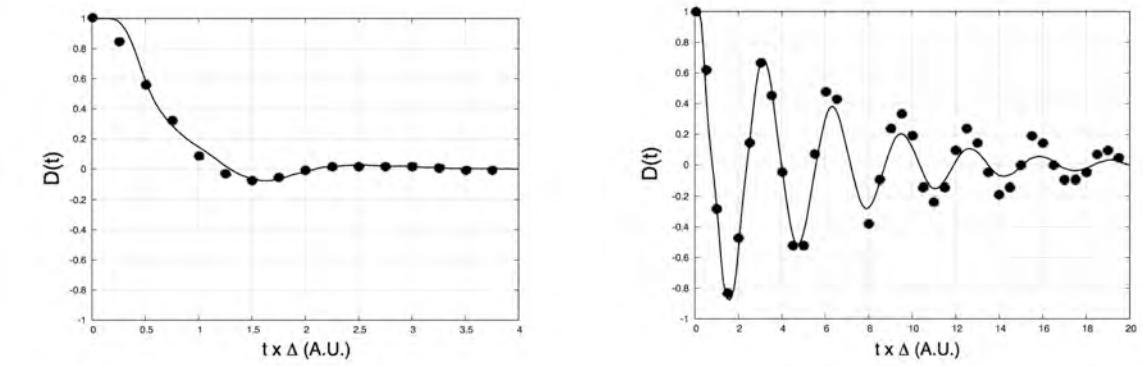

Below are results for the asymmetric spin-boson model, which is much more difficult for various approximations to describe well. One sees that the present quasi-classical approach describes both coherent and incoherent regimes of asymmetric case equally well.

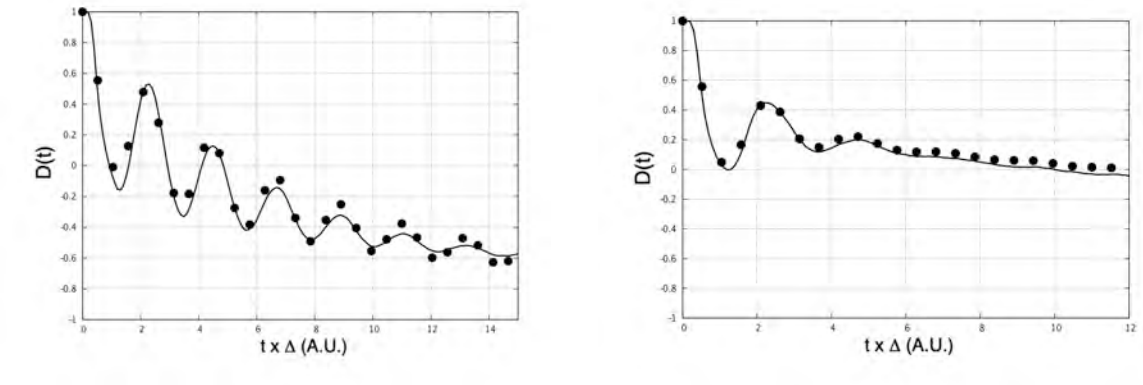

III. Future Plans

Since this quasi-classical model has proved quite reliable for describing electronically non-adiabatic dynamics in these simple model problems, work is in progress to extend its application to more general and complex non-adiabatic processes.

References

1. For reviews, see W. H. Miller, Adv. Chem. Phys. **25**, 69-177 (1974); **30**, 77-136 (1975).
2. W. H. Miller, J. Chem. Phys. **53**, 1949-1959 (1970).
3. For reviews, see (a) W. H. Miller, J. Phys. Chem. A **105**, 2942-2955 (2001); (b) W. H. Miller, Proceedings of the National Academy of Sciences, **102**, 6660-6664 (2005); (c) W. H. Miller, J. Chem. Phys. **125**, 132305.1-8 (2006).
4. H. D. Meyer and W. H. Miller, J. Chem. Phys. **71**, 2156-2169 (1979).
5. G. Stock and M. Thoss, Phys. Rev. Lett. **78**, 578-581 (1997).
6. G. Stock and M. Thoss, Adv. Chem. Phys. **134**, 243 (2005).
7. W. H. Miller, J. Phys. Chem. **113**, 1405-1415 (2009).
8. D. F. Coker and L. Xiao, J. Chem. Phys. **102**, 496-510 (1995).
9. G. Stock, J. Chem. Phys. **103**, 2888-2902 (1995).
10. S. J. Cotton and W. H. Miller, J. Chem. Phys. **139**, 234112.1-9 (2013).
11. J. C. Tully, J. Chem. Phys. **93**, 1061-1071 (1990).

IV. 2012 - 2014 (to date) DOE Publications

1. W. H. Miller, Perspective: Quantum or Classical Coherence?, J. Chem. Phys. **136**, 210901.1-6 (2012).
2. W. H. Miller, Another Resolution of the Identity for Two-Electron Integrals, J. Chem. Phys. **136**, 216101.1-2 (2012).
3. G. Tao and W. H. Miller, Time Dependent Importance Sampling in Semiclassical Initial Value Representation Calculations for Time Correlation Functions. II A Simplified Implementation, J. Chem. Phys. **137**, 124105.1-7 (2012).
4. B. Li and W. H. Miller, A Cartesian Classical Second-Quantized May-Electron Hamiltonian, for Use with the Semiclassical Initial Value Representation, J. Chem. Phys. J. Chem. Phys. **137**, 154107.1-7 (2012).
5. B. Li, T. J. Levy, W. H. Swenson, E. Rabani and W. H. Miller, A Cartesian Quasi-Classical Model to Nonequilibrium Quantum Transport: The Anderson Impurity Model, J. Chem. Phys. **138**, 104110.1-6 (2013).
6. G. Tao and W. H. Miller, Time-Dependent Important Sampling in Semiclassical Initial Value Representation Calculations or Time Correlation Functions. III. A State-Resolved Implementation to Electronically Non-Adiabatic Dynamics, Mol. Phys. **111**, 1987-1993 (2013).
7. S. J. Cotton and W. H. Miller, Symmetrical Windowing for Quantum States in Quasi-Classical Trajectory Simulations, J. Phys. Chem. A **117**, 7190-7194 (2013).
8. S. J. Cotton and W. H. Miller, Symmetrical Windowing for Quantum States in Quasi-Classical Trajectory Simulations: Application to Electronically Non-Adiabatic Processes, J. Chem. Phys. **139**, 234112.1-9 (2013).
9. B. Li, E. Y. Wilner, M. Thoss, E. Rabani and W. H. Miller, A Quasi-Classical Mapping Approach to Vibrationally Coupled Electron Transport in Molecular Junctions, J. Chem. Phys. submitted (2014).

Dynamics of Activated Molecules

Amy S. Mullin
Department of Chemistry and Biochemistry, University of Maryland
College Park, MD 20742
mullin@umd.edu

I. Program Scope

We investigate the microscopic mechanisms for inelastic collisions of molecules with large amounts of internal energy using high-resolution transient IR absorption probing. Collisional energy transfer is ubiquitous in gas-phase chemistry and impacts overall reaction rates and branching ratios. This is particularly true for high energy molecules that are more likely to undergo chemical transformations. Currently, there are no first-principle theories of collisional energy transfer for high energy molecules and the lack of fundamental knowledge often results in cursory and insufficient treatments in reactive models. A goal of my research program is to gain new insights into the microscopic details of relatively large complex molecules at high energy as they undergo quenching collisions and redistribute their energy. This data provides important benchmarks for the development of new models that account for energy partitioning in molecular collisions.

We use state-resolved transient IR absorption to characterize the energy transfer pathways that are responsible for the collisional cooling of high energy molecules. Direct probing of high energy molecules is challenging due to their transient nature, poorly defined spectral signatures and high state densities. Our approach is to develop a molecular level understanding by focusing instead on the small energy-accepting bath molecules that undergo collisions with high energy molecules. We measure the population changes for individual rotational and vibrational states that are induced by collisions and the nascent translational temperatures of the scattered molecules. With this technique, we have performed in-depth spectroscopic studies that provide a greater understanding of high energy molecules and their collisional energy transfer. In 2007, we made a major stride forward by developing the means to characterize the transient behavior for the full range of rotational states for the scattered molecules. Previous measurements had been limited to only the highest energy states, thereby giving information about the "strongest" collisions. Having eyes to also see the so-called "weak" collisions gives us access to characterize the entire energy transfer distribution with unprecedented detail.

In the current grant period, we have made major progress in improving our instrumental capabilities which has opened exciting new research directions. In the past two years, we have incorporated two new generation mid-IR light sources into our high-resolution transient absorption spectrometers. One is a tunable optical parametric oscillator (OPO) and the other is a quantum cascade laser (QCL). The OPO and QCL offer a number of advantages for high resolution transient IR absorption studies. They provide continuous and broad tuning ranges, a high degree of frequency and amplitude stability and relatively high output powers. Our IR tuning range now covers λ=2.5-3.9 μm (OPO) and 4.2-4.5 μm (QCL and lead salt diode). Our first studies using the OPO as our IR probe source focused on the collision dynamics of highly vibrationally excited pyrazine ($C_4H_4N_2$, E=38000 cm^{-1}) with HCl. The high quality of the OPO light enabled us to complete these measurements, whereas diode laser measurements were plagued by low signal to noise levels.

Our ability to measure the full distribution of scattered molecules allows us to ask fundamental questions about the underlying molecular features that are responsible for observed energy transfer behavior. In the past year, we have targeted 3 studies: 1) the collisional energy transfer dynamics of highly vibrationally excited molecules in the presence of strong hydrogen-bonding interactions, 2) the first transient IR absorption studies on methane following collisions with high energy molecules and 3) the experimental sources of asymmetries in transient absorption line profiles. Our recent progress in these studies is described below.

II. Recent Progress

A. Collision dynamics of pyrazine-d_4 (E=38000 cm^{-1}) + HCl

Last year we reported on some extraordinary isotope effects in the collisions of pyrazine-h_4 ($C_4H_4N_2$, E=38000 cm^{-1}) with HCl when compared to collisions with DCl.[1] While the nascent rotational energy distributions for HCl(v=0) and DCl(v=0) were very similar (T_{rot}~900 K), the nascent translational energy distributions for HCl and DCl show opposite J-dependence. For HCl (v=0), the recoil velocities are inversely correlated to J, while for DCl (v=0), the product translational energy increases monotonically with J. Our understanding of the DCl(v=0) scattering data in consistent with an impulsive mechanism for which product rotational and translational energy gains are directly correlated. Stronger collisions impart large amounts of both rotation and translation while gentler collisions yield more modest amounts of both types of energy. There is ample evidence that the primary pathway for quenching by CO_2 involves impulsive collisions, which may be direct single-impact encounters or may be chattering collisions that involve multiple, sequential points of impact. In contrast, the inverted product correlation from HCl collisions shows that the energy transfer does not occur solely from a random distribution of HCl orientations. Instead, we ask how hydrogen bonding interactions influence the energy transfer mechanisms of HCl. The picture is that HCl molecules experience a strong electric field that orients them relative to pyrazine prior to scattering and that the energy transfer occurs via a quasi-complex. The new question becomes why do HCl and DCl have such different scattering?

To gain some insight into this behavior, we considered the body of research on the vibrational predissociation of van der Waals complexes[2] and found evidence for strong sigma-type interactions between HCl and the lone-pair on nitrogen in pyrazine. A near-resonant intermolecular energy transfer mechanism was proposed to explain differences in the vibrational predissociation lifetimes for acetylene-HCl and acetylene–DCl.[3] It is possible that in the presence of strong orienting interactions, collisional energy transfer between pyrazine and HCl involves some type of complex formation followed by near-resonant predissociation. We have explored several ideas to explain these observations. The first was to remove the near-resonant vibrational modes of pyrazine-h_4 and HCl by switching to pyrazine-d_4 as an energy donor. The vibrational frequency of HCl is 2949 cm^{-1} which is fairly close to the C-H stretches of pyrazine-h_4 that lie between 3040 and 3066 cm^{-1}. The C-D stretches of pyrazine-d_4 are much lower and are 2270 and 2290 cm^{-1}. The state-resolved scattering data show that the recoil energies for pyrazine-d_4(E)-HCl collisions are very similar to those for pyrazine-h_4(E), indicating that near-resonant effects are not responsible for the observed dynamics. In addition, measurements of the HCl (v=1) product state distributions for both donors are quite similar. These results indicate that single quantum effects are not influencing the energy transfer dynamics, but leaves open the question as to why HCl energy transfer is so unusual. It may be that failed chemical reactions are involved in some way, based on differences in the basicity of pyridine isotopes.

B. Collisions of high energy molecules and methane: pyrazine (E=38000 cm^{-1}) + CH_4

This year we have developed the instrumentation and expertise to measure collisional dynamics of methane using high-resolution transient IR absorption. Methane is the simplest hydrocarbon and the ability to measure its energy transfer dynamics will lead to a greater understanding of hydrocarbon energy flow in combustion. Our first study targets collisions with highly excited pyrazine, which serves as a prototype high energy molecule for this type of study. This work is a starting place for investigating the dynamics of hydrocarbons in combustion environments.

Despite being the simplest hydrocarbon, methane's IR spectroscopy is remarkably complex. When methane does not rotate or vibrate, it is a spherical top with rotational energies given by BJ(J+1). For all other ro-vibrational states, vibration-rotation coupling and centrifugal distortion of spherical symmetry split the $(2J+1)^2$ degeneracy, resulting in numerous states for each J and numerous IR transitions. Nuclear spin statistics lead to groups of states with A, E and F type symmetry. Each rotational states are identified by J and a symmetry number. The IR probe transitions involve the v_3 asymmetric stretch at λ=3.3 μm. as

shown in Fig. 1a for the P3 A2 transition. Fig. 1b shows a transient absorption signal for methane J=3, measured at line center, following collisions with pyrazine (E). The J=3 state is thermally populated at room temperature and its transient signal at line center (Fig. 2b) is dominated by depletion of thermally populated molecules. In the Doppler-broadened wings of the P3 transition, the transient signal shows overall appearance of J=3 molecules. The average time between collisions in these experiments is 4 μs and nascent signals are collected at t=1 μs following UV excitation of pyrazine.

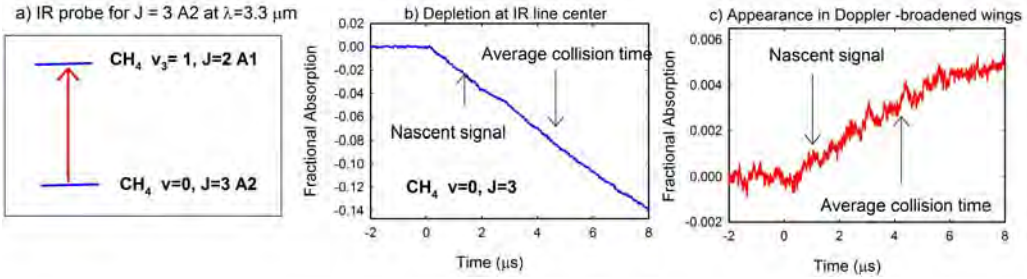

Fig. 1. Wavelength-dependent transient IR absorption signals for CH_4 J=3 following collisions with highly vibrationally excited pyrazine (E=38000 cm-1). Ro-vibrational transitions of the v3 asymmetric stretch at λ=3.3 μm are used to probe rotational states of CH_4 (v=0).

Transient Doppler-broadened line profiles have been measured for methane in v=0 for a number of rotational states up to J=15. Line profiles at t=1 μs are shown below in Fig. 2. Double-Gaussian profiles for simultaneous appearance and depletion of population are observed for states with J≤12. Unconstrained fitting using a double Gaussian function yields nascent temperatures

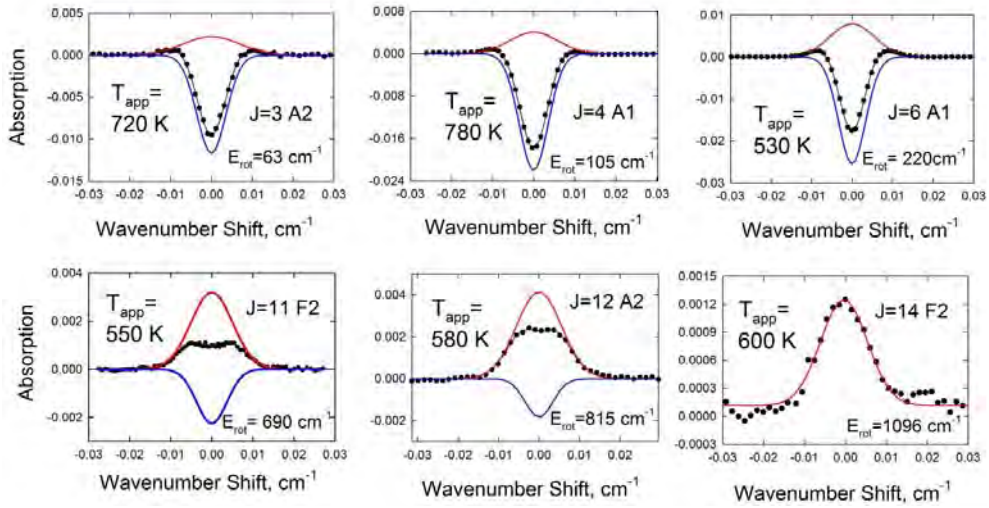

Fig. 2. Nascent Doppler-broadened line profiles for several J states of CH_4 (v=0) scattered via collisions with pyrazine-h_4(E) measured at t=1 μs following excitation of pyrazine with 266 nm light. The blue curves correspond to depletion of thermally populated states and the red curves describe the appearance of product states. J-specific appearance temperatures T_{app} are determined from full-width half maximum line widths.

for appearance and depletion of individual methane states. The nascent appearance temperatures (in the lab frame) range from 530 K to 780 K for methane states with J=2-15. No significant J-dependence is observed. The depletion temperatures range from 250-350 K, corresponding to initial ambient cell temperature. It is interesting to compare the J-dependent recoil energies for methane and CO_2 as they collisionally relax pyrazine (E). Fig. 3 shows the center-of-mass frame translational temperatures as a function of J and a function of energy for methane and CO_2.

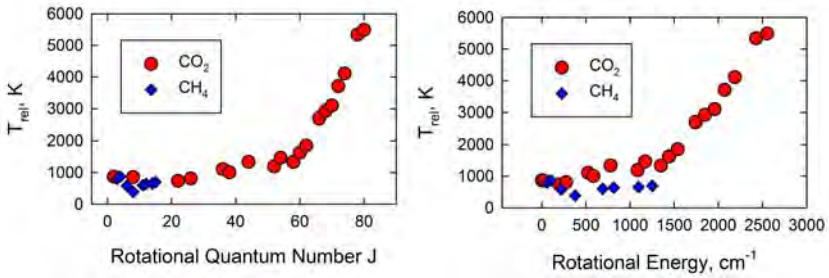

Fig. 3. Comparison of methane and CO_2 as collisional quenchers of pyrazine (E). Small recoil energies are seen for the low rotational angular momentum states of both methane and CO_2. As a function of energy however, CO_2 has a larger translational energy component. .

C. Sources of asymmetry in transient absorption line profiles

The unusual inverse scattering behavior seen for pyrazine-HCl collisions prompted us to repeat a number of line profile measurements. A subset of the full ensemble of data for the low-J states had to be excluded because of asymmetries in the line profiles, leading to an unacceptably large spread in results. Extensive systematic studies concluded that the asymmetry was minimized for pyrazine-HCl collisions by careful optical feedback control of the IR light and optimized pressure conditions. Interestingly, the asymmetry was not present for collisions of HCl with other donors, nor for pyrazine with other acceptors.

III. Future Work

In the short term, we will continue our studies on the energy transfer dynamics in collisions of highly excited molecules with CH_4. Our immediate goals are to characterize the rotational distribution and rate constants for pyrazine collisions and then look at the dynamics for vibrationally excited collision products. We are also gearing up for new studies using the QCL to measure state-to-state dynamics and use saturation spectroscopy for labeling an initial collision partner.

IV. References

1. J. Du, L. Yuan and A. S. Mullin, J. Phys. Chem. A (2007)
2. H. Reisler, Photofragment spectroscopy and predissociation dynamics of weakly bound molecules, Annu. Rev. Phys. Chem. 60, 39 (2009)
3. D. C. Dayton, P. A. Block and R. E. Miller, Spectroscopic evidence for near-resonant intermolecular energy transfer in the vibrational predissociation of C_2H_2-HX and C_2H_2-DX complexes, J. Phys. Chem. A 95, 2881 (1991). L. Oudejans and R. E. Miller, State-to-state vibrational predissociation dynamics of the acetylene-HCl complex, J. Phys. Chem. A 103, 4791 (1999)

V. Publications supported by this project 2012-2013

1. J. Du, N. A. Sassin, D. K. Havey, K. Hsu and A. S. Mullin, "Full energy gain profiles of CO_2 from collisions with highly vibrationally excited molecules. II. Energy dependent pyrazine (E=32700 and 37900 cm^{-1}) relaxation" J. Phys. Chem. A 117, 12104-12115 (2013)
2. G. Echibiri, M. Smarte, W. Walters and A. S. Mullin, "Performance of a high-resolution mid-OR optical parametric oscillator transient absorption spectrometer" Optics Express, submitted.
3. J. Du, D. K. Havey, S. W. Teitelbaum and A. S. Mullin, "Full energy gain profiles of CO_2 from collisions with highly vibrationally excited molecules. III. 2-Methylpyridine, 2,6-dimethylpyridine and 3,5-dimethylpyridine (E~38500 cm^{-1}) relaxation" in preparation.
4. M. Smarte, G. Echibiri, W. Walters, J. Cleveland and A. S. Mullin, "Unusual isotope effects in collisions of pyrazine (E) + HCl and DCl: Evidence of strong interactions", in preparation for the Journal of Physical Chemistry.

Reacting Flow Modeling with Detailed Chemical Kinetics

Habib N. Najm

Sandia National Laboratories
P.O. Box 969, MS 9051, Livermore, CA 94551
hnnajm@sandia.gov

I. Program Scope

The goal of this research program is to improve our fundamental understanding of reacting flow, thereby advancing the state of the art in predictive modeling of combustion. The work involves:

- Developing numerical methods for the efficient solution of reacting flow systems of equations with detailed kinetics and transport, massively parallel codes for computing large scale reacting flow with detailed kinetics, and techniques for analysis of multidimensional reacting flow.
- Using computations to investigate the structure and dynamics of flames using detailed chemical kinetics.
- Developing numerical methods for uncertainty quantification in reacting flow computations.
- Estimation of uncertain chemical model parameters, and calibration/validation of reacting flow models, based on experimental data and computational predictions.
- Uncertainty quantification (UQ) studies in computations of chemical systems and reacting flow.

In the following, recent progress and future plans in this overall area are discussed.

II. Recent Progress

A. Structured adaptive mesh refinement computations of reacting flow

Working with A. Ghoniem's group at MIT, we adapted our earlier-developed structured adaptive mesh refinement (SAMR) reacting flow code to flows with immersed solid objects. The result is a robust second-order SAMR code for simulations of reacting flow around heat-conducting immersed solid objects. The SAMR framework employs a low-Mach number operator-split projection algorithm. A "buffer zone" methodology is introduced to impose the solid-fluid boundary conditions such that the solver uses symmetric derivatives and interpolation stencils throughout the interior of the numerical domain; irrespective of whether it describes fluid or solid cells. Solid cells are tracked using a binary marker function. The no-slip velocity boundary condition at the immersed wall is imposed using the staggered mesh. Near the immersed solid boundary, single-sided buffer zones (inside the solid) are created to resolve the species discontinuities, and dual buffer zones (inside and outside the solid) are created to capture the temperature gradient discontinuities. The development is limited to a two-dimensional Cartesian grid-conforming solid. The code was validated using benchmark simulations documented in the literature. Overall second-order convergence was demonstrated. The code was used to study a methane/air premixed flame stabilized on a channel-confined bluff-body using a detailed chemical kinetics model.

B. Intrusive UQ in chemical systems

In the forward UQ context, one area of significant challenge has been the use of intrusive *global* Polynomial Chaos (PC) methods for forward propagation of uncertainty in chemical ordinary differential equation (ODE) systems. These methods, if they can be made to work effectively, can lead to significant computational savings, avoiding (sparse) quadrature sampling strategies in high-dimensional spaces. On the other hand, we have experienced first hand their instabilities when applied to chemical ignition computations. In was established in subsequent work that one path towards stability involves the use of *local* PC methods, relying on block decomposition of the parametric space and local, spectral-element type, representations. This path, however, while indeed stable, is not viable for high dimensional spaces because of the challenges with meshing in high-D and large computational cost. Accordingly, there is still a strong need for stabilized intrusive global PC constructions employed in ODEs.

We have developed and demonstrated a new method for stabilizing global intrusive ODE computations of chemical ignition. The technique uses a numerical filtering procedure that enforces positivity constraints on the state vector in order to minimize the probability of spurious solutions, resulting from aliasing and high-order truncation errors. The filtering seeks a minimal perturbation to the PC expansion for the state vector in a manner that tries to enforce positivity. This is done using an optimization procedure that minimizes both the probability of negative states (PNS) and the perturbation of the solution, with a chosen relative weighting of each of the two objectives. We successfully demonstrated the construction in the context of a 2-equation ODE system. Results illustrate the nature of the instability problem in the absence of filtering, being related to violation of state positivity, growth of uncertainty, explosive growth of the solution, and aliasing errors. We demonstrated the role of filtering in suppressing the instability by reducing the PNS and eliminating persistent spurious positive eigenvalues and associated growth. While the method is demonstrated to work in this one system, arriving at stable intrusive global PC computations of uncertain ignition, further work is needed to demonstrate it in more detailed chemical kinetic models of practical relevance.

C. Application of DFI to an H_2-O_2 mechanism

We have begun the application of our data free inference (DFI) procedure to the estimation of a joint density on Arrhenius rate coefficients of a H_2-O_2 model based on published data. We are working with data from shock-tube measurements by the Hanson group at Stanford, of OH time history under nearly-isothermal conditions, resulting from the reaction H+O_2=OH+O. This data was used to fit Arrhenius rate coefficients of this reaction, with the published work including nominal values and error bars of $k(T)$ at a number of temperature values. We are working on building efficient surrogates for the system response as a function of time, and the rate parameters, namely $X_{\mathrm{OH}}(t, \ln A, E, n)$ at different temperatures. These surrogates employ a combination of Padé and polynomial approximants to provide a good approximation of the underlying response. They will be used in the likelihood function for Bayesian inference of rate parameters, for proposed DFI data sets.

D. Dynamical analysis in stochastic chemical systems

Stochasticity in chemical kinetics is relevant at small scales, with practical utility *e.g.* in catalytic reactions at microscale surface features. Generally, the modeling of microscale chemical systems, accounting for stochastic noise, is of significant interest because stochastic effects can influence the overall dynamics of the systems. At the same time, these computations can be very expensive. As a result, effective model reduction is of significant interest. Model reduction strategies abound for chemical systems governed by macroscale ordinary or partial differential equation systems. Generally, dynamical strategies for macroscale model analysis and reduction rely on the eigenanalysis of the governing equations, and identification of low dimensional slow manifolds. The corresponding analytical framework for stochastic chemical systems is, on the other hand, much sparser. Accordingly, startegies for model reduction in these systems do not benefit from equivalent capabilities of identification of low dimensional "slow" manifolds as in the macroscale case.

We have worked on the theoretical development for definition and identification of stochastic manifolds in stochastic differential equation (SDE) systems. We outlined in recent work the essential outlines of an analytical framework for this purpose, providing means of deriving equations that define the manifold as a random object. This framework relies on a key transformation of the SDE to a random dynamical system (RDS). The RDS formalism provides the path towards definition and identification of the random slow manifold. We applied the construction to the analysis of a model stiff SDE system involving random noise in both slow and fast processes, arriving at an equation for the random manifold. Simulations of system trajectories were studied, starting from arbitrary initial conditions. Trajectories, superposed with random fluctuations, exhibited fast decay towards the neighborhood defined by the manifold, and proceeded at a slower pace in the manifold neighborhood towards the equilibrium point, sampling different realizations of the random manifold as they proceeded forward. Results clearly indicate the ability of the analysis to accurately predict the random manifold which is followed by the slow evolution of the SDE. In future work, this analysis will be applied to more complex systems, and will be used to provide a basis for deriving measures of (un)importance, as a pre-requisite for robust dynamical-analysis-based model reduction strategies in stochastic chemical systems.

E. Model error in chemical systems

Model error, also known as structural error or model discrepancy, is always present in general, as models are at best an approximation of the truth over a certain range of conditions. While much of the UQ literature focuses on parametric uncertainty, the matter of model uncertainty is understood to be significant, particularly in complex physical systems. In the context of chemical models specifically, it is well appreciated that chemical kinetic models for complex fuels are deficient and largely overfitted, such that statements about model validity are very difficult to make definitively. This is an area where much work remains to be done as far estimating model errors and associated predictive uncertainty.

We have started working in this area, focusing on the estimation of model error in chemical kinetic models. In order to start with simple scenarios, we focused on UQ with model error in the absence of data noise. Specifically, we worked on model calibration for estimation of model errors and associated uncertainty in predictions in a context where a "simple" model is calibrated with respect to a "detailed" model, the latter being considered the truth for present purposes. Conventional statistical methods for model error estimation, where model error is defined as a perturbation on model output observables, have a number of shortcomings when considering the calibration of physically-based models. We employed rather a strategy where model error is embedded in targeted submodels/phenomenology. Using approximate Bayesian computation (ABC) methods applied in a density estimation framework, we demonstrated a strategy for model calibration where uncertainty due to model error is embedded in specific model parameters, such that output predictions are centered on the truth in a least square (LS) sense, and exhibit uncertainty that is consistent with the LS discrepancy from the truth. We illustrated the technique in simple models, and demonstrated its efficacy in the context of calibration of a simple model for methane-air ignition.

F. UQ in LES of turbulent combustion

Working with J. Oefelein and G. Lacaze we have demonstrated initial progress towards UQ in LES computations of 3D turbulent reacting flow in a cylindrical bluff body combustor geometry. The UQ strategy relied on non-intrusive PC with sparse-quadrature sampling in a 3D space comprised of the Smagorinsky constant, the turbulent Schmidt number, and the turbulent Prandtl number. Initial studies focused on the propagation of synthetic uniform distributions on these parameters spanning their ranges of interest, to provide a PC surrogate for the forward model. This surrogate model will be used in future work for data-based calibration of the LES model, arriving at a joint posterior density on the three parameters of interest. The forward UQ for surrogate construction provided also global sensitivity information of specific LES model output quantities of interest to each of the parameters.

III. Future Plans

A. Intrusive UQ in chemical systems

Our demonstrated hitherto progress towards stable intrusive global PC UQ in chemical systems has relied on the design of spectral filters that rely on estimation of the probability of negative states (PNS) by random sampling of the PCE of the system state. This PNS estimation procedure is not cheap, since it seeks the estimation of tail probabilities. Further, the overall time integration strategy employing this filtering approach, while stable, can bear improvement in terms of efficiency and robustness under wider ranges of conditions. Working with H. Matthies of TU Braunschweig, we have identified a path forward toward a potentially more efficient and robust construction that eschews estimation of PDF tails by random sampling, in favor of a functional approach that relies on sampling and lagrange interpolants to preserve positivity of the function. This approach derives from computational mechanics. It relies on time integration of a differential-algebraic system of equations, where the algebraic component is precisely the positivity constraint in our particular context. We will adapt this approach to intrusive globa PC UQ of chemical systems, demonstrating it in a simple 2-equation system to begin with, and comparing its performance to our present construction. This will be followed by application in a hydrogen-oxygen homogeneous ignition context.

B. Model error in chemical systems

We will further develop and extend our ABC/density-estimation method for model calibration accounting for model error. The hitherto demonstration in a data-noise-free context will be extended to allow for data noise. This, more

general, setting will need to address disambiguation of data and model errors. This ought to be non-problematic, as our construction allows for the placement of the two error contributions in different parts of the model, so that they are not simply additive. Further, given that the overall approach remains in the Bayesian context, this will provide natural paths to inclusion of data noise in the density estimation framework.

C. UQ in LES of turbulent combustion

We will continue the above reported progress on UQ in LES of turbulent reacting flow. We will extend the present surrogate construction to include a broader range of observables. We will also begin work towards construction of relevant likelihood functions for purposes of Bayesian inference employing available data on flow observables. Initial steps in this regard will target available point measurements before progressing towards more extensive spatial imaging data. We also plan to extend this work to include additional parameters, including both physical-modeling and numerical-discretization parameters that affect the LES computations.

D. Global sensitivity analysis in reacting flow

In an effort to identify important parameters in both ignition and flame computations, we will employ global sensitivity analysis (GSA) in reacting flow computations. This will rely on random sampling of uncertain kinetic and thermodynamic parameters, and the estimation of Sobol' sensitivity indices. Despite the apparent high-dimensionality of the uncertain input space in this context, the intrinsic dimensionality of the dependence of any given flame observable on input parameters is expected to be small. By default, therefore, random sampling of the higher-dimensional parameter space will provide the requisite sampling, with much better coverage, of the relevant low-dimensional space of important parameters. We will do this first with simple fuels in the context of ignition, to be followed by application in 1D and 2D laminar flames.

E. Application of DFI to an H_2-O_2 mechanism

We will continue working on DFI of chemical parameters in a H_2-O_2 ignition system, based on available shock-tube measurements by Hanson. Efficient surrogates of the OH time history will be used in the inner DFI MCMC chain on the parametric space, while an ABC-based likelihood will be employed in the outer chain. The construction will be used to arrive at a meaningful joint density on the Arrhenius rate coefficients for the $H+O_2$=OH+O reaction. The analysis will include nuisance parameters, being uncertain rate coefficient parameters that are used in the requisite fitting to establish the rate constants of the reaction of interest here.

IV. BES-Supported Published/In-Press Publications [2012-2014]

[1] Najm, H.N., Berry, R.D., Safta, C., Sargsyan, K., and Debusschere, B.J., Data Free Inference of Uncertain Parameters in Chemical Models, *Int. J. for Uncertainty Quantification* (2014) in press.

[2] Prager, J., Najm, H.N., Sargsyan, K., Safta, C., and Pitz, W.J., Uncertainty Quantification of Reaction Mechanisms Accounting for Correlations Introduced by Rate Rules and Fitted Arrhenius Parameters, *Combustion and Flame*, 160:1583–1593 (2013).

[3] Prager, J., Najm, H.N., and Zádor, J., Uncertainty Quantification in the *ab initio* Rate-Coefficient Calculation for the $CH_3CH(OH)CH_3$+OH→$CH_3C^*(OH)CH_3$+H_2O Reaction, *Proc. Comb. Inst.*, 34:583–590 (2013).

[4] Berry, R.D., Najm, H.N., Debusschere, B.J., Adalsteinsson, H., and Marzouk, Y.M., Data-free inference of the joint distribution of uncertain model parameters, *Journal of Computational Physics*, 231:2180–2198 (2012).

[5] Alexanderian, A., Le Maître, O.P., Najm, H.N., Iskandarani, M., and Knio, O.M., Multiscale stochastic preconditioners in non-intrusive spectral projection, *J. Sci. Comp.*, 50:306–340 (2012).

[6] Salloum, M., Alexanderian, A., Le Maître, O.P., Najm, H.N., and Knio, O.M., Simplified CSP Analysis of a Stiff Stochastic ODE System, *Computer Methods in Applied Mechanics and Engineering*, 217-220:121–138 (2012).

Spectroscopy, Kinetics and Dynamics of Combustion Radicals

David J. Nesbitt
JILA, University of Colorado and National Institute of Standards and Technology, and Department of Chemistry and Biochemistry, University of Colorado, Boulder, Colorado

Both the dynamics and spectroscopy of jet cooled hydrocarbon transients have been explored, utilizing i) high resolution IR lasers, ii) slit discharge sources for formation of jet cooled radicals, and iii) high sensitivity detection with direct laser absorption methods near the quantum shot noise limit. The advantage of this experimental combination is that such highly reactive radical transients can be made under high pressures/temperatures characteristic of combustion conditions, with the resulting species rapidly cooled to T ≈10-15K in the slit supersonic expansion for maximal spectroscopic simplification. Four highlights from work over the last year are summarized below.

1) Propargyl Radical: Sub-Doppler Rovibrational/Spin-Rotation Spectroscopy

The formation of benzene molecules from reaction of two propargyl radical (H_2CCCH) has been recently observed in synchrotron based VUV photoionization mass spectrometry in low pressure flames, which showcases the possibly singular importance of such C_3 propargyl radical species in the early growth stages to form larger aromatic structures. This provides strong motivation for detailed understanding of the high resolution spectroscopy and dynamics of propargyl radical, in order to facilitate both unambiguous identification and direct laser based concentration measurements in further experimental studies of such aggregation processes. We have obtained first sub-Doppler infrared spectra of jet cooled propargyl radical in the CCH stretch region, based on formation and rapid cooling in a slit supersonic jet discharge source. The extensive delocalization of this unpaired electron over the entire radical framework proves to be a particularly interesting issue, which has attracted attention from both theoretical and experimental perspectives. The localization or delocalization of this unpair electron result in electronic structure corresponding to either the propargyl form ($H_2C–C≡CH$) or the nominally allenyl form ($H_2C=C=CH$), with a paired electron localized at the methylenic or acetylenic carbon atom, respectively. However, there is evidence that a more balanced intermediate resonance structure [$H_2C–C≡CH \leftrightarrow H_2C=C=CH$] may be the appropriate description for this system, for which the probability density distribution of the unpaired electron can influence the geometry of the radical and vice versa. In the present study, the rovibrational transitions of the acetylenic CH stretching mode of propargyl radical in the vicinity of 3326 cm^{-1} has been investigated in a discharge slit jet expansion under supersonically cooled conditions and with sub-Doppler resolution (~60 MHz). The density of collisions in the slit jet discharge expansion result in efficient rotational cooling of the hot propargyl radical down to the lowest two para/ortho nuclear spin states K_a=0, 1, with fully Boltzmann distributions in J well characterized by T_{rot} = 17 K. Most importantly, sub-Doppler resolution in the

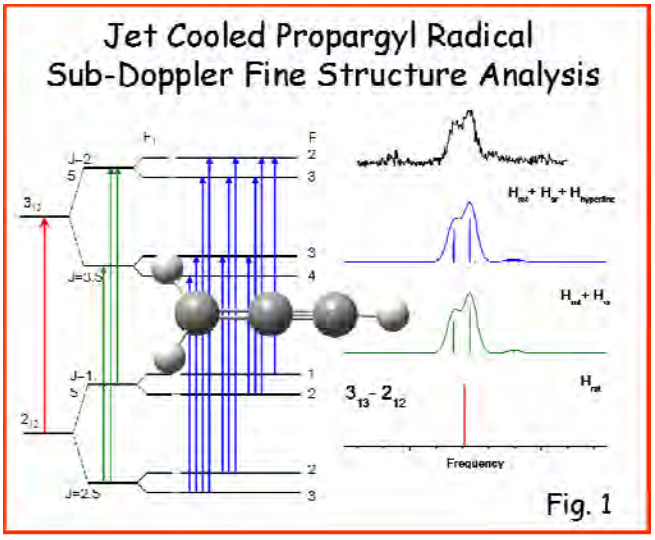

Fig. 1

slit jet expansion geometry permits a first glimpse into fine-structure electron spin-rotation dynamics in propargyl radical for the C–H stretching mode, as well as partial hyperfine information on Fermi contact interactions for the two sets of distinguishable H nuclei.

2. Sub-Doppler Spectroscopy of Diacetylene: Ethynyl Radical Chain Addition

Diacetylene (H-C≡C-C≡CH), the smallest member of the polyyne family, represents an ubiquitous species in combustion/pyrolysis chemistry What makes these linear polyynes so chemically interesting is the fact that they form so readily via chain reaction addition with CCH ethynyl radical, e.g., i) HC≡CH + C≡CH → [H-C≡C(H)-C≡CH] → H-C≡C-C≡CH + H, augmented by ii) H + HCCH → H_2 + CCH. It is worth noting here that the intermediate species of reaction i) is not a high energy transition state but rather an extremely stable radical adduct, > 60 kcals/mol lower in energy than HCCH + CCH reactants, with little or no barrier and therefore resulting in insertion on nearly every collision. This process can therefore continue by subsequent exothermic attack of CCH into one of the diacetylene CC bond, which then forms even higher order polyynes such as triacetylene, tetraacetylene, etc. Indeed, such chain reaction kinetics are extremely rapid under non-oxidizing flame conditions, and therefore diacetylene is thought to be a crucial intermediate in the formation of soot particles. The fundamental anti-symmetric CH stretching mode (ν_4) and its many hot combination bands in the region of 3333 cm^{-1} of di-acetylene (C_4H_2) have been reinvestigated under sub-Doppler jet cooled conditions in a pulsed supersonic slit discharge. Single quantum hot bands ($\Pi \leftarrow \Pi$) due to all 4 degenerate bending vibrations (specifically, the cis C≡C-H bend (ν_6), trans C-C≡C bend (ν_7), trans C≡C-H bend (ν_8) and cis C-C≡C bend (ν_9)) are observed in conjunction with the ν_4 CH stretch fundamental and successfully analyzed. In addition, a clear $\Sigma \leftarrow \Sigma$ hot band built on the strong ν_4 fundamental is observed and unambiguously assigned to single quantum excitation of the low frequency C-C symmetric stretch (ν_3). Furthermore, the combination of i) sub-Doppler line widths and ii) absence of spectral congestion in the slit jet permit weak Coriolis perturbation structure in the ν_4 CH stretch fundamental to be observed and analyzed for the first time. The observation of such extensive hot band structure even under jet cooled slit conditions underscores the presence of highly non-equilibrium dynamics in rovibrational degrees of freedom, with a cold rotational temperature (T_{rot} = 15 K) common to all lower states and yet a highly *superthermal* vibrational temperature on the order of 358(16) K. From a dynamical perspective, a simple Boltzmann population analysis suggests that effective vibrational "temperatures" to be over > 20-25-fold higher than rotation. Indeed, such dramatic levels of bend excitation can be ascribed to i) a highly bent precursor HCCCCH framework, which, as suggested by *ab initio* MOLPRO (CCSD(T)/vdzf12) calculations, tend to funnel energy selectively into low frequency bending coordinates, augmented by ii) far less efficient cooling of vibrations vs. rotations in the normal 2D pinhole expansion.

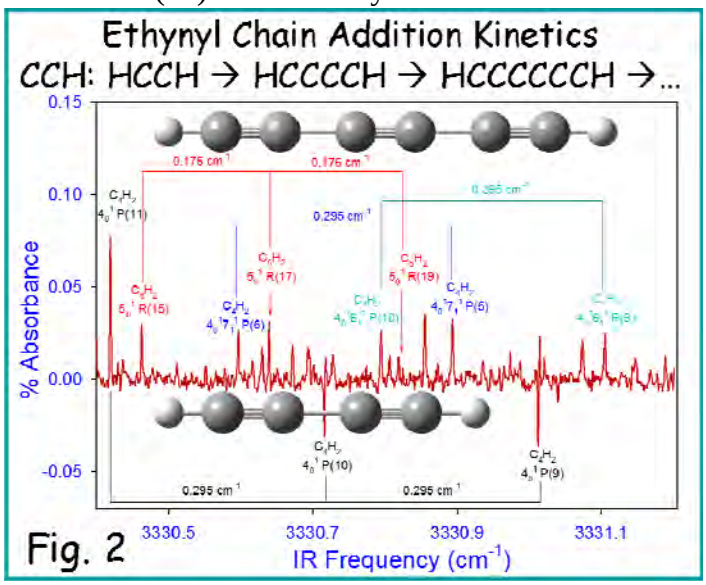

Fig. 2

3. High-Resolution Spectroscopy of Jet-cooled Hydroxymethyl Radical

Hydroxymethyl radical, CH_2OH, plays a critically role as a reactive intermediate in combustion. In addition to fundamental combustion processes, hydroxymethyl radical is an important intermediate for oxidative reactions occurring in the troposphere. For example, atmospheric scrubbing reactions of alkanes, alkenes, and alcohols all involve hydroxymethyl radical as a reactive intermediate. Hydroxymethyl ($^{\bullet}CH_2OH$), is predicted to have a slightly non-planar equilibrium structure with a low barrier across a C_s transition state due to OH internal rotation.[1] This work has profited by the excellent vibrationally tagged double resonance ion depletion (DRID) studies of Reisler and coworkers[2,3] on $^{\bullet}CH_2OH$, which yielded structured rovibrational band contours in the CH and OH stretch regions limited by a 0.4 cm^{-1} laser linewidth. The present studies under sub-Doppler conditions promise to provide over 2 orders of magnitude improvement, which permit complete resolution and analysis of the underlying spectral structure due to end-over-end tumbling, internal OH rotor dynamics as well as coupling with CH/OH vibration modes. We have already made substantial progress, with initial spectral searches for CH_2OH in the symmetric CH_2 stretch region in a methanol doped He/Ne discharge. At sub-Doppler resolution, CH_2OH reveals a surprisingly intense spectrum, with typical S/N of 20:1, and $K_a = 0 \leftarrow 0$ A-type rotational assignments, which provide first precision molecular constants for this oxyradical species. The transitions are fit to a Watson A-reduced symmetric top Hamiltonian to yield first precision experimental values for the ground state rotational constants as well as improved values for the symmetric stretch rotational constants and vibrational band origin. The results both complement and substantially augment previous spectral efforts[3] as well as offer high resolution predictions for astronomical detection of CH_2OH radical in the mm-wave region.

Of particular dynamical interest, however, is the strong evidence in the spectra for large amplitude motion due to strong coupling between the CH_2 flip and COH torsional coordinate, which makes the spectra challenging to analyze without complete rotational resolution yet also provides potentially much more informative with respect to isomerization barrier heights. Again from a simple freshman chemistry perspective, this coupling can be rationalized as arising from valence electron repulsion of radical and lone pair orbitals, amplified by a "soft" barrier between sp^2 and sp^3 hybridization of the C radical center. Indeed, we have performed high level MOLPRO 2D potential surface calculations (CCSD(T)/AVDZ) in torsion and flip coordinates , which elucidate an exceptionally low barrier (≈ 160 cm^{-1}) "valley" as a function of CH_2 wagging angle (at fixed COH torsion angle) as well as a high barrier (≈ 1600 cm^{-1}) "ridge" as a function of COH torsion angle (at fixed CH_2 wagging angle). Analysis of the spectra will require 2D quantum treatment of both large amplitude coordinates, which will provide critical insights into radical isomerization dynamics for such a benchmark open shell oxyhydrocarbon species.

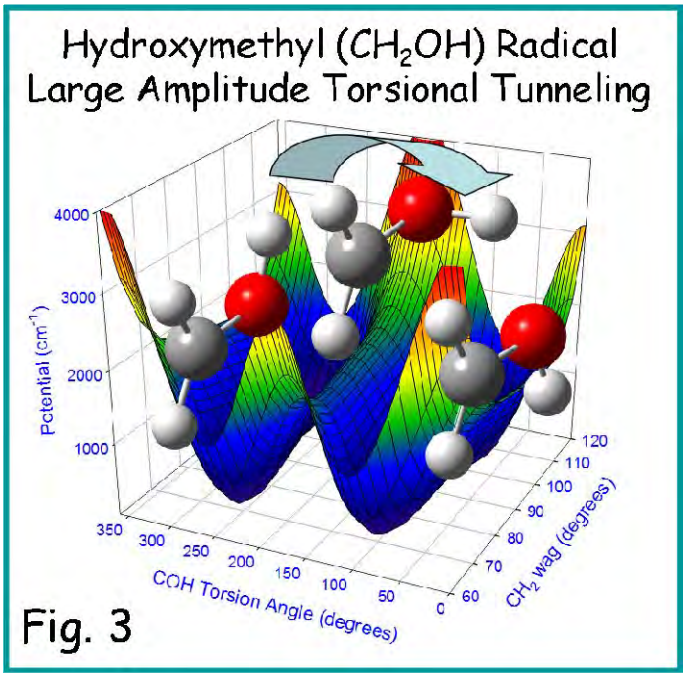

4. Jet-cooled *trans*-HOCO Radical: Sub-Doppler OH Stretch Spectroscopy

The chemical reaction, OH + CO → H + CO_2, is an overall strongly exothermic process and responsible for the final oxidative conversion step of CO to CO_2 which is clearly essential to achieving high efficiency levels of combustion. Indeed, its prominent stature in the combustion community has only been increased by recently being described as the "*second most important combustion reaction*" in a review paper by Miller *et. al.*[4] The unusual nature of this reaction is that it plays a critical and ubiquitous role in oxidative combustion of essentially all hydrocarbons, yet the reaction does not explicitly involve the actual hydrocarbon fuel. Despite its deceptive simplicity, this reaction is clearly far from "elementary" and is known to have multiple barriers, intermediates and pathways along the reaction coordinate. To address some of these issues, rovibrational spectroscopy of the fundamental OH stretching mode of *trans*-HOCO radical has been studied via sub-Doppler high resolution infrared laser absorption in a discharge slit-jet expansion. The *trans*-HOCO radical is formed by discharge dissociation of H_2O to form OH, which then combines with CO and cools in the Ne expansion to a rotational temperature of 13.0(6) K. Rigorous assignment of both *a*-type and *b*-type spectral transitions is made possible by 2-line combination differences from microwave studies, with full rovibrational analysis of the spectrum based on a Watson asymmetric top Hamiltonian. Additionally, fine structure splittings of each line due to electron spin are completely resolved and thus permitting all three ε_{aa}, ε_{bb}, ε_{cc} spin rotation constants to be experimentally determined in the vibrationally excited state. Furthermore, as both *a*- and *b*-type transitions for *trans*-HOCO are observed for the first time, the ratio of transition dipole moment projections along the *a*, *b* principal axes is determined to be μ_a/μ_b = 1.78(5), which is in close agreement with density functional quantum theoretical predictions (B3LYP/6-311++g(3df,3pd), μ_a/μ_b = 1.85). Finally, we note the energetic possibility in the *excited* OH stretch state for predissociation dynamics (i.e., *trans*-HOCO → H + CO_2), with the present sub-Doppler linewidths providing a rigorous upper limit of > 2.7 ns for the predissociation lifetime.

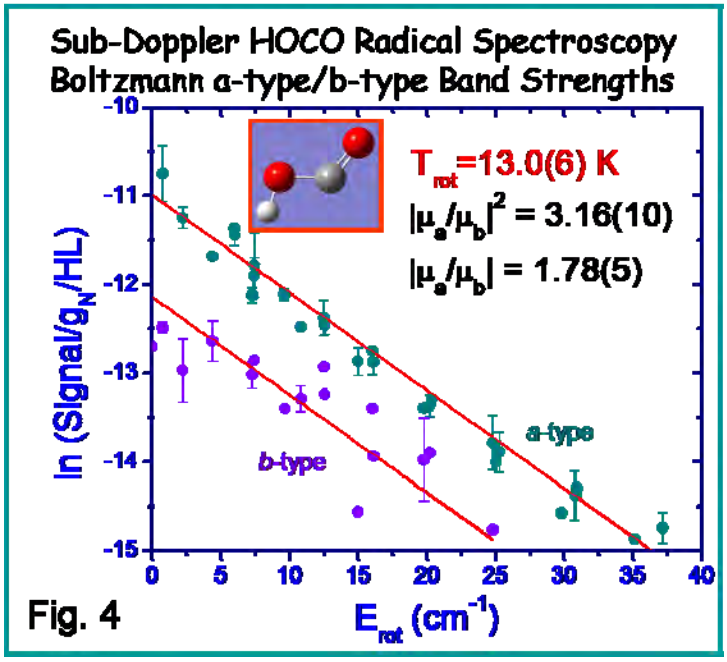

Fig. 4

References:

1 R. D. Johnson and J. W. Hudgens, J. Phys. Chem. **100**, 19874 (1996).

2 J. Wei, B. Karpichev, and H. Reisler, J. Chem. Phys. **125** (2006).

3 L. Feng, J. Wei, and H. Reisler, J. Phys. Chem. A **108**, 7903 (2004).

4 J. A. Miller, R. J. Kee, and C. K. Westbrook, Annu. Rev. Phys. Chem. **41**, 345 (1990).

Radical Photophysics and Photochemistry

Daniel Neumark
Chemical Sciences Division
Lawrence Berkeley National Laboratory
Berkeley, CA 94720

This project applies complementary experimental techniques to study the spectroscopy and photodissociation of free radicals and other transient species, with a particular focus on species that play a key role in combustion chemistry. These experiments also provide fundamental new insights into the chemical dynamics of free radicals. These species, owing to their high reactivity, present unique experimental challenges that are absent for closed shell molecules. The experiments are carried out on two instruments: a fast radical beam instrument (FRBM) and a molecular beam apparatus. In the FRBM instrument, free radicals are formed by photodetaching a fast beam of mass-selected negative ions. The resulting radicals are photodissociated by a second laser. Photofragments are detected in coincidence using a time-and-position sensitive (TPS) detector. In the molecular beam apparatus, radicals are generated by flash photolysis of a suitable precursor and photodissociated. Photofragments are detected with a rotating mass spectrometer. Both experiments yield primary photochemistry along with translational energy and angular distributions for each product channel.

To measure the relative position and arrival time of coincident photofragments in the FRBM experiment, we have recently upgraded our previous TPS detection scheme to a Roentdek Hex80 delay line anode detector. Compared to our previous setup, the delay-line anode has the advantage of much simpler data acquisition and read out while requiring fewer detection components and less alignment for operation. It is also more suitable for investigating three-body dissociation, as shown in more detail below.

Research during the past year has focused on the three-body dissociation of ozone, and on elucidating whether the dissociation dynamics of the phenyl radical (C_6H_5) are statistical. The ozone experiments were carried out on the FRBM instrument. The goal was to measure and characterize the three-body dissociation reaction, $O_3 \rightarrow 3O(^3P)$, (ΔE=6.2 eV) at the photodissociation wavelengths of 193 nm (6.4 eV) and 157 nm (7.8 eV). While the two-body photodissociation of O_3 has been studied in many laboratories, the existence of the three-body channel has been inferred only from quantum yield (QY) measurements at these two wavelengths as well as in some molecular beam photodissociation experiments. The QY measurements suggest that this channel is quite small at 193 nm but is significantly more important at 157 nm.

In our experiment, O_3 was produced by photodetachment of a fast beam of O_3^- and then dissociated at either 157 nm or 193 nm. Both two- and three-fragment channels

were characterized by coincidence detection of the fragments using the Roentdek detector. One issue with this experiment is that the O_3^- has to be photodetached approximately 1 eV above the electron affinity of O_3, because anion photodissociation dominates at lower photon energies closer to the detachment threshold. As a result, the initial O_3 vibrational distribution is essentially the Franck-Condon distribution produced by photodetachment, with significant excitation in the ν_1 symmetric stretch.

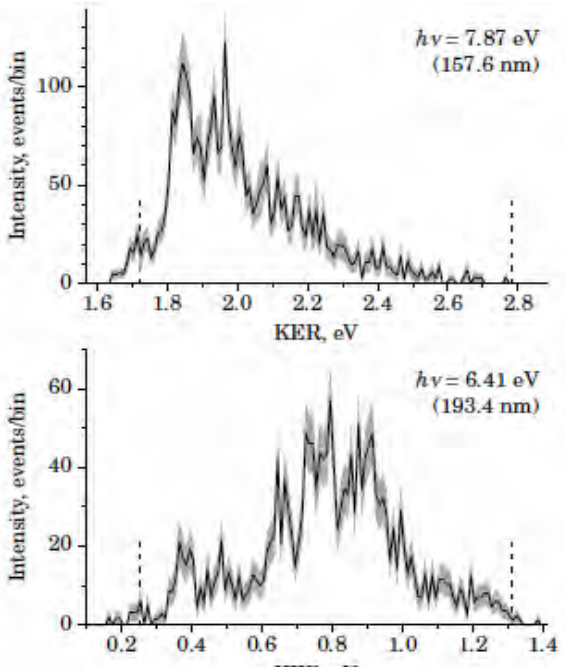

Figure 1. Translational energy distributions for three-body dissociation of O_3.

The translational energy distributions for three-body dissociation are shown in Fig. 1, while Fig. 2 shows Dalitz plots at the two wavelengths. Even though the O_3 is vibrationally excited, the distributions in Fig. 1 are highly structured, with each peak, in principle, corresponding to a particular O_3 vibrational level. However, although the initial O_3 vibrational distributions are the same in both panels of Fig. 1, the translational energy distributions are quite different. The results at 157 nm resemble the initial FC distribution of O_3 level, but at 193 nm it appears that three-body dissociation from high vibrational levels is significantly more important than from lower levels. Analysis of the relevant excited state potential energy surfaces indicates that excitation at 193 nm is enhanced by symmetric stretch excitation of the O_3, consistent with the observed results.

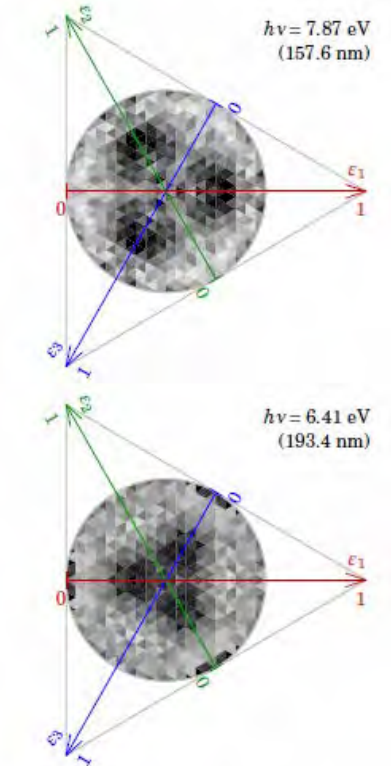

Figure 2. Dalitz plots for three-body dissociation of O_3.

The Dalitz plots in Fig. 2 show how the translational energy released in photodissociation is partitioned among the three fragments. At both wavelengths, but more noticeably at 157 nm, the plots comprise three spots centered on the symmetry axes. Events along those axes correspond to equal energy partitioning in two of the recoiling O atoms, consistent with a synchronous concerted mechanism in which the two O-O bonds in ozone dissociate symmetrically and at the same time.

In previous work on the photodissociation of the phenyl radical, we found that at 248 nm, the only observed

channel was production of C_6H_4 (ortho-benzyne) + H, the lowest energy channel. At 193 nm, however, an additional channel, C_4H_3 + C_2H_2, was observed and found to be the dominant channel. This result was surprising, given that it is a higher energy channel than H atom loss, and was attributed to either non-statistical dissociation or the possibility that the C_4H_3 product was the lower energy i-C_4H_3 isomer (H_2CCCCH). However, recent calculations by Mebel and co-workers have shown that if dissociation at 193 nm is a statistical ground state process, then very little of this isomer should be produced and H-atom loss should dominate. They concluded that for C_2H_2 loss to be a major channel, there must be conical intersections among excited states that direct the dynamics along this pathway.

With this in mind, we re-investigated the photodissociation of C_5H_5 to see how sensitive the product branching was to experimental conditions, in particular those producing excess internal energy in the radical over and above the photon energy used to dissociate it. We focused on optimizing source conditions in the flash pyrolysis radical source to reduce the internal temperature of the radicals, and ran the experiment at considerably lower photodissociation laser fluences to minimize the likelihood of two-photon processes. Under these conditions, we still observed both channels at 193 nm, but found that the H-atom channel was in fact dominant, with branching between the two channels consistent with the expected results for statistical ground state dissociation.

Recent Publications:

W. A. Donald, R. D. Leib, M. Demireva, B. Negru, D. M. Neumark, and E. R. Williams, “Average Sequential Water Molecule Binding Enthalpies of $M(H_2O)_{19\text{-}24}^{2+}$ (M=Co, Fe, Mn, and Cu) Measured with Ultraviolet Photodissociation at 193 and 248nm,” J. Phys. Chem. A. **115**, 2, (2011).

P. E. Crider, A. W. Harrison, D. M. Neumark, “Two-and Three-body Photodissociation Dynamics of the Diiodobromide (I_2Br^-) Anion,” J. Chem. Phys. **134**, 134306, (2011).

B. Negru, G. M. P. Just, D. Park, and D. M. Neumark, "Photodissociation Dynamics of the t-butyl Radical via Photofragment Translational Spectroscopy at 248 nm," Phys. Chem. Chem. Phys. **13**, 8180, (2011).

A. W. Harrison, J. S. Lim, P. E. Crider, D. M. Neumark, “Three-body Photodissociation Dynamics of $I_2^-(CO_2)$, ” Chem. Phys. Lett. **512**, 30, (2011).

G. M. P. Just, B. Negru, D. Park, and D. M. Neumark, “Photodissociation of Isobutene at 193 nm,” Phys. Chem. Chem. Phys. **14**, 675 (2012).

N. C. Cole-Filipiak, B. Negru, G. M. P. Just, D. Park, D. M. Neumark, "Photodissociation dynamics of the methyl perthiyl radical at 248 nm via photofragment translational spectroscopy," J. Chem. Phys. **138**, 054301 (2013).

A. W. Harrison, J. S. Lim, M. Ryazanov, G. Wang, S. Gao, D. M. Neumark, "Photodissociation Dynamics of the Thiophenoxy Radical at 248, 193, and 157 nm," *J. Phys. Chem. A* **117**, 1197 (2013).

Determination of Accurate Energetic Database for Combustion Chemistry by High-Resolution Photoionization and Photoelectron Methods

C. Y. Ng

Department of Chemistry, University of California, Davis, California 95616
E-mail Address: cyng@ucdavis.edu

I. Program Scope

The main goal of this research program is to obtain accurate thermochemical data, such as ionization energies (IEs), 0 K dissociative photoionization thresholds or appearance energies (AEs), 0 K bond dissociation energies (D_0's), and 0 K heats of formation ($\Delta H°_{f0}$'s) for small and medium sizes molecular species and their ions of relevance to combustion chemistry. Accurate thermochemical data determined by high-resolution photoionization and photoelectron studies for selected polyatomic neutrals and their ions are also useful for benchmarking the next generation of *ab initio* quantum computational procedures.

II. Progress in state-to-state photodissociation studies (Publications 1, 3, 10, 13, and 17)

The most significant achievement in our laboratory in the past year is the establishment of the two-color VUV-VUV laser velocity-map-imaging-photoion (VMI-PI) apparatus, which is highlighted below. This apparatus is equipped with two independently tunable VUV lasers and a time-slice VMI-PI detector. By employing the VUV laser photodissociation-pump and VUV laser photoionization-probe approach, this apparatus has been shown to allow state-to-state photodissociation measurements of many small molecules for the first time.

Partly due to the technical difficulty in generating intense tunable VUV photon sources, molecular photodissociation processes involving atmospheric gases have not been investigated in detail. The recent development of the VUV laser time-slice VMI-PI apparatus has made possible systematic state-to-state VUV photodissociation studies of CO, N_2, NO, and CO_2. The broadly tunable VUV laser source has allowed the photoexcitation of the molecule of interest to selected predissociative rovibonic states. We found that the same VUV photolysis laser pulse can also be used for state-selective photoionization sampling of nascent atomic photofragments, making possible the determination of the total kinetic energy release (TKER) spectrum to be obtained by time-slice VMI-PI measurements.

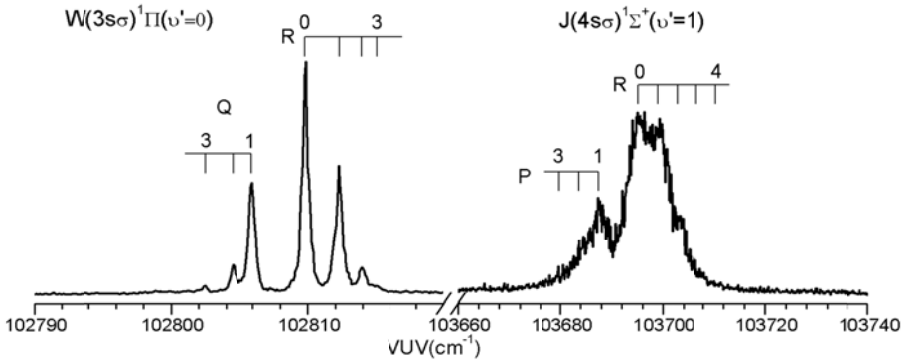

Figure 1. Carbon ion photofragment spectrum for the CO vibronic states $J(4s\sigma)^1\Sigma^+(v'=1)$ and $W(3s\sigma)^1\Pi(v'=0)$. The relative intensities of these states were not normalized to the corresponding VUV intensities.

As an example, we show in Fig. 1, the C^+ ion photofragment spectrum for $C(^1D)$ and $C(^3P)$ formed by predissociation of CO in the excited rovibronic states $W(3s\sigma)^1\Pi(v' = 0)$ and $J(4s\sigma)^1\Sigma^+(v' = 1)$ measured in the VUV range of 102,790-102,820 and 103,660-103,740 cm^{-1}, respectively (35). The rotational assignments are marked on top of the spectra in Fig. 1. The broadening observed for the rotational lines of the $J(4s\sigma)^1\Sigma^+(v' = 1)$ state can be attributed to lifetime broadening. In time-slice VMI-PI measurements, the VUV laser frequency is tuned to one of the rovibronic peaks identified in the C^+ ion photofragment spectra to

collect the time-slice VMI-PI image. Two typical time-slice VMI-PI images and their corresponding TKER spectra for CO predissociation from the R(0) lines or J′ = 1 levels of the $W(3s\sigma)^1\Pi(v' = 1)$ level at 104,578.7 cm^{-1} and the $J(4s\sigma)^1\Sigma^+(v' = 1)$ level at 103,695.8 cm^{-1} are shown in Figs. 2(a)-2(d). Based on the TKER spectra, the $W(3s\sigma)^1\Pi(v' = 1)$ state is found to dissociate into the excited $C(^1D) + O(^3P)$ spin-forbidden channel and the $C(^3P) + O(^3P)$ ground state channel with a branching ratio of $C(^1D) + O(^3P) : C(^3P) + O(^3P) = 25.6 \pm 0.1 : 74.4 \pm 0.1$, whereas the $J(4s\sigma)^1\Sigma^+(v' = 1)$ state dissociates 100% into the ground state channel. These branching ratios for CO photodissociation from the $W(3s\sigma)^1\Pi(v' = 1)$ and $J(4s\sigma)^1\Sigma^+(v' = 1)$ states are found to be independent of J′ for J′ = 0-2 (35). Since the VUV photodissociation energies used are lower than the threshold energy for the formation of $C(^3P) + O(^1D)$ from CO, this product channel cannot be produced in this experiment. Here, the $C(^3P)$ and $C(^1D)$ products are photoionized by the same VUV photolysis laser pulse that is used for exciting CO to the predissociative states. Considering that the duration of the VUV laser pulse is about 5 ns, while the dissociation of CO occurs in $< 10^{-12}$ s, the formation of C^+ can be considered to follow a two-step process, in which neutral C atoms are first produced by the photodissociation of CO induced by the early part of the VUV laser pulse, and then the photoionization of C atoms is promoted by absorbing another VUV photon in the later part of the VUV laser pulse. The relative yields of the product channels deduced from the TKER spectra have been corrected for the photoionization cross sections of $C(^3P)$ and $C(^1D)$. Due to the lack of independent tunability of the VUV photoionization energy, the VUV laser VMI-PI apparatus does not allow the optimization of experimental conditions for state-selective photoionization detection.

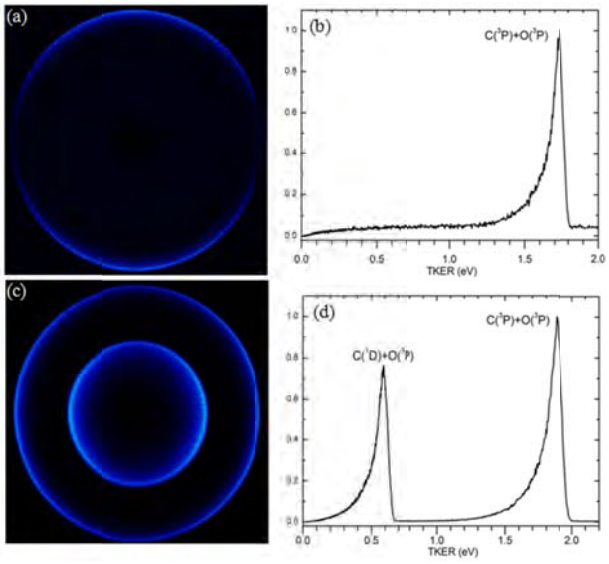

Figure 2. Time-slice VMI-PI images of C^+ and their TKER spectra produced from the VUV predissociation of CO at the R(0) lines of the state $J(4s\sigma)^1\Sigma^+$ (v′=1) ((a) and (b)) at 103,695.8 cm^{-1} and the state $W(3s\sigma)^1\Pi(v'=1)$ ((c) and (d)) at 104,578.7 cm^{-1}. The assignments for each of the peaks are shown in (b) and (d).

We have recently successfully developed the VUV-VUV laser VMI-PI apparatus by implementing a second tunable VUV laser (VUV-II) to the VUV laser VMI apparatus for state-selective photo-ionization sampling together with the original VUV laser (VUV-I) for photodissociation excitation. This implementation has made possible the application of the VUV-UV (1+1′) resonance-enhanced photoionization scheme for state-selective detection of photofragments. The first step of this state-selective detection scheme involves the VUV-II excitation of the photofragment to a Rydberg state. For a Rydberg state formed below the IE of the photofragment, its subsequent ionization can be efficiently promoted by absorbing an additional UV photon, which is also a component of the laser beam. For a Rydberg state formed above the IE of the photofragment, prompt autoionization can readily occur. Since the VUV Rydberg autoionization and the VUV-UV (1+1′) photoionization schemes are mediated by a resonant Rydberg state, they have significantly higher efficiencies for photoionization samplings than that achieved by direct photoionization. The ability to independently tune the energy of the VUV-II photoionization laser was found to enhance the experimental sensitivity by more than two orders of magnitude compared to that observed by using a single VUV laser for both photodissociation excitation and photoionization sampling. Considering that the VUV laser radiation generated by the four-wave mixing schemes is tunable in the range of ≈7-19 eV, which basically covers the IEs of nearly all atomic and molecular species, we conclude that the VUV-UV (1+1′) photoionization and VUV Rydberg autoionization schemes can be generally applicable for photodissociation studies of nearly all molecular systems.

The VUV-VUV laser VMI-PI apparatus has been successfully applied for determining the fine-structure distribution of product $C(^3P_{0,1,2})$ formed by the VUV-I photodissociation of CO at selected rotational lines of the vibronic states $(4s\sigma)^1\Sigma^+(v = 4)$, $(4p\sigma)^1\Sigma^+(v = 3)$, and $(4p\pi)^1\Pi(v = 3)$ at 109,452.6, 109484.7 and 109568.6 cm^{-1}, respectively. The fine structure distributions thus determined are found to be strongly dependent on the predissociative rovibronic states of CO being excited. The branching ratios for $C(^3P_2) + O(^3P_J) : C(^3P_2) + O(^1D_2)$, $C(^3P_1) + O(^3P_J) : C(^3P_1) + O(^1D_2)$, and $C(^3P_0) + O(^3P_J) : C(^3P_0) + O(^1D_2)$, which were determined based on the time-slice VMI-PI measurements of C^+ ions formed by J-state selective photoionization sampling of $C(^3P_{0,1,2})$, also reveal strong dependences on the spin-orbit state of $C(^3P_{0,1,2})$ (36). By combining these measured branching ratios and fine-structure distributions of $C(^3P_{0,1,2})$, we have determined the correlated distributions of $C(^3P_{0,1,2})$ accompanying the formation of $O(^1D_2)$ and $O(^3P_J)$ produced in the VUV photodissociation of CO. These correlated distribution measurements are expected to be highly valuable for benchmarking theoretical dynamical calculations, and thus provide fundamental understanding of the photodissocition dynamics.

In addition to the state-to-state photodissociation study of CO, we also plan to apply the newly established VUV-VUV laser VMI-PI apparatus to perform detailed investigations of the VUV photodissociation of carbon monoxide (CO_2), methoxyl radical (CH_3O), and methyl peroxy radical (CH_3OO).

III. High resolution photoelectron spectroscopic measurements of radicals

We are making excellent progress in VUV-photoion and VUV-PFI-PE measurements of small radicals using the VUV laser photoion-photoelectron apparatuses established in our laboratory. We have been successful in performing high-resolution VUV laser VMI-photoelectron VMI-PE and VMI-threshold photoelectron (VMI-TPE) measurements on selected radicals, such as propargyl (C_3H_3), allyl (C_3H_5), and halogenated hydrocarbon methyl radicals CH_2X, X = Cl and Br. We have demonstrated that the VUV laserVMI-PE and VMI-VMI-TPE methods can achieve higher sensitivity and similar energy resolutions (1-2 cm^{-1}) compared to the PFI-PE) tech. We plan to perform VUV-VMI-PE and VUV-VMI-TPE measurements on selected radicals, including halogenated methyl radicals CH_2X and CHXY (X, Y = F, Cl, Br, and I), CH_3O, CH_3OO, and Criegee intermediates (CH_2OO and CH_3CHOO). With the enhanced experimental sensitivity, we propose to perform two-color IR-VUV-VMI-PE and IR-VUV-VMI-TPE measurements on allyl radical (C_3H_5) as a benchmark experiment on rotationally selected and resolved photoelectron study of combustion radicals.

IV. Publications acknowledged the support of DOE (2011-present)

1. Hong Gao, Yang Pan, Lei Yang, Jingang Zhou, C. Y. Ng, and W. M. Jackson, "Time-sliced velocity-map ion imaging studies of the photodissociation of NO in the extreme vacuum ultraviolet (EUV) region", *J. Chem. Phys.* **136**, 134302 (2012). Selected for the May 2012 issue of Virtual Journal of Ultrafast Science.
2. Xiaoyu Shi, Huang Huang, Brian Jacobson, Yih-Chung Chang, Qing-Zhu Yin, and C. Y. Ng, "A high-resolution photoionization and photoelectron study of ^{58}Ni using a vacuum ultraviolet laser", *Astrophys. J.* **747**, 20 (2012).
3. Hong Gao, Yu Song, Lei Yang, Xiaoyu Shi, Qing-Zhu Yin, Cheuk-Yiu Ng, and William M. Jackson, "Branching ratio measurements of the predissociation of $^{12}C^{16}O$ by time-slice velocity imaging in the energy region from 108,000 to 110,500 cm^{-1}", *J. Chem. Phys*. **137**, 034305 (2012).
4. Yih-Chung Chang, Yuntao Xu, Zhou Lu, Hong Xu, and C. Y. Ng, "Rovibrationally selected ion-molecule collision study using the molecular beam vacuum ultraviolet laser pulsed field ionization-photoion method: charge transfer reaction of $N_2^+(X; v^+ = 0\text{-}2, N^+ = 0\text{-}9) + Ar$, *J. Chem. Phys.* **137**, 104202 (2012).
5. Hong Gao, Zhou Lu, Lei Yang, Jingang Zhou, and C. Y. Ng, "*Communication*: A vibrational study of propargyl cation using the vacuum ultraviolet laser velocity-map imaging photoelectron method", *J. Chem. Phys.* **137**, 161101 (2012).

6. Yuntao Xu, Bo Xiong, Yih Chung Chang, and C. Y. Ng, "*Communication*: Rovibrationally selected absolute total cross sections for the reaction $H_2O^+(X^2B_1; v_1^+v_2^+v_3^+ = 000; N^+_{Ka+Kc+}) + D_2$: Observation of the rotational enhancement effect", *J. Chem. Phys*.**137**, 241101 (2012).
7. Yih-Chung Chang, Huang Huang, Zhihong Luo, and C. Y. Ng, "*Communication*: A vibrational study of titanium dioxide cation using the vacuum ultraviolet laser pulsed field ionization-photoelectron method", *J. Chem. Phys.* **138**, 041101 (2013).
8. Huang Huang, Yih Chung Chang, Zhihong Luo, Xiaoyu Shi, Chow-Shing Lam, Kai-Chung Lau, and C. Y. Ng, "Rovibronically selected and resolved two-color laser photoionization and photoelectron study of cobalt carbide cation", *J. Chem. Phys*., **138**, 094301 (2013).
9. Kai-Chung Lau, Yi Pan, Chow-Shing Lam, Huang Huang, Yih-Chung Chang, Zhihong Luo, Xiaoyu Shi and C. Y. Ng, "High-level *ab initio* predictions for the ionization energy, bond dissociation energies and heats of formation of Cobalt carbide (CoC) and its cation (CoC^+)", *J. Chem. Phys*. **138**, 094302 (2013).
10. Hong Gao, Yu Song, Yih-Chung Chang, Xiaoyu Shi, Qing-Zhu Yin, Roger C. Wiens, William M. Jackson, and C. Y. Ng, "Branching ratio measurements of the photodissociation of $^{12}C^{16}O$ by time-slice velocity-map imaging photoion method in the vacuum ultraviolet region from 102,500 to 106,300 cm^{-1}", *J. Phys*. *Chem. A* (invited), **117**, 6185-6195 (2013).
11. Yuntao Xu, Yih Chung Chang, Zhou Lu, and C. Y. Ng, "Absolute total cross sections and product branching ratios for the vibrationally selected ion-molecule reactions: $N_2^+(X^2\Sigma_g^+; v^+ = 0\text{-}2) + CH_4$", *Astrophys. J.* **72**, 769 (2013).
12. Huang Huang, Zhihong Luo, Yih Chung Chang, Kai-Chung Lau, and C. Y. Ng, "Rovibronically selected and resolved two-color laser photoionization and photoelectron study of titanium monoxide cation", *J. Chem. Phys.* **138**, 174309 (2013).
13. Hong Gao, Yu Song, William M. Jackson, and C. Y. Ng, "*Communication*: State-to-state photodissociation study of $^{12}C^{16}O$ by the VUV-VUV pump-probe Time-Slice Velocity-Map Imaging Photoion Method", *J. Chem. Phys.* **138**, 191102 (2013).
14. Yuntao Xu, Bo Xiong, Yih Chung Chang, and C. Y. Ng, "Translational, rotational, and vibrational energy effects on the chemical reactivity of water cation $H_2O^+(X\ ^2B_1)$ in the collision with deuterium molecule D_2", *J. Chem. Phys.* **139**, 024203 (2013).
15. Yu Song, Hong Gao, Yih Chung Chang, Zhou Lu, C. Y. Ng, and William M. Jackson, "Photodissociation of CO_2 between 13.540 and 13.678 eV", *Phys. Chem. Chem. Phys.*, published on the web Oct. 11, 2013. DOI: (10.1039/3cp53250j).
16. Hong Gao, Yuntao Xu, Lei Yang, Chow-Shing Lam, Hailing Wang, Jingang Zhou, and C. Y. Ng, "Erratum: High-resolution threshold photoelectron study of the propargyl radical by the vacuum ultraviolet laser velocity-map imaging method [*J. Chem. Phys.* 135, 224304 (2011)], *J. Chem. Phys*. **139**, 079902 (2013).
17. Cheuk-Yiu Ng, "State-to-state spectroscopy and dynamics of ions and neutrals by photoionization and photoelectron methods", *Annual Review Physical Chemistry*, **65**, 197-224 (2014).
18. Anyang Li, Yongle Li, Hua Guo, Kai-Chung Lau, Yuntao Xu, Bo Xiong, Yih-Chung Chang, and C. Y. Ng, "Communication: The origin of rotational enhancement effect for the reaction of $H_2O^+ + H_2$ (D_2)", *J. Chem. Phys*. **140**, 011102 (2014)..

Large Eddy Simulation of Turbulence-Chemistry Interactions in Reacting Flows

Joseph C. Oefelein and Guilhem Lacaze
Combustion Research Facility, Sandia National Laboratories
Livermore, CA 94551-0969
oefelei@sandia.gov

Program Scope

Application of the Large Eddy Simulation (LES) technique within the Diagnostics and Reacting Flows program at the CRF is based on two primary objectives. The first is to establish a set of high-fidelity first-principles computational benchmarks that identically match the geometry and operating conditions of selected experimental target flames. The second is to establish a scientific foundation for advanced model development that effectively bridges the gap between the idealized jet flame processes studied under this program and application relevant processes exhibited at the device scale. The goal is to provide direct one-to-one correspondence between measured and modeled results at conditions unattainable using Direct Numerical Simulation (DNS) by performing a series of detailed simulations that progressively incorporate the fully coupled dynamic behavior of reacting flows with detailed thermodynamics, transport, chemistry, and realistic spectrums of turbulence. Our primary focal point is the series of flames that have been studied as part of the Experimental Reacting Flow Research program in collaboration with Barlow and Frank. This represents a direct extension of joint activities being pursued as part of the *International Workshop on Measurement and Computation of Turbulent (Non)premixed Flames*[1] (i.e., the "TNF Workshop"). Complementary information from highly specialized LES calculations, combined with detailed laser-based measurements, provide new opportunities to understand the central physics of turbulence-chemistry interactions in realistic parameter spaces and for the development of accurate predictive models for turbulent combustion. After achieving an adequate level of validation, results from high-fidelity LES provide fundamental information that cannot be measured and a strong link between theory, experiments, and relevant applications. The insights gained provide a basic science foundation for development of models and simulation techniques for state-of-the-art transportation, propulsion, and power devices such as internal combustion engines (e.g., reciprocating, gas turbine, liquid rockets).

Recent Progress

The need for improved error quantification and quality metrics for LES has been recognized now for many years. Activities associated with the TNF Workshop, for example, have identified many issues. In TNF8 (Heidelberg Germany, 2006), attempts to model simple bluff-body flames (the Sydney HM1 case for example) by several different research groups illustrated many ambiguities. Two issues arose from initial comparisons with available experimental data: 1) uncertainty with respect to boundary conditions, and 2) uncertainty with respect to code and simulation parameters (i.e., numerics, grid resolution, time-step, integration time, etc.). Codes with a variety of different numerical schemes and capabilities (e.g., with and without artificial dissipation added for stability) were used. In many cases geometric details of the burner were not resolved, and limited computational resources imposed significant constraints on the levels spatial and temporal resolution applied. The combined uncertainties made it extremely difficult to draw any conclusions regarding the accuracy of the models tested.

Given the myriad of competing interdependencies that affect solution accuracy, time to solution, and the overall confidence in the predictive capabilities of LES, we have devoted significant time to begin to establish robust performance metrics to assess the "quality" of a given simulation in a manner that minimizes potential sources of error and provides a clear set of quantitative implementation requirements for different classes of subgrid models. Initial studies aimed at understanding and improving the accuracy of LES focused on the impact of grid resolution on numerical and model errors. Past criteria have been developed to assess LES quality in simple geometries, under simple conditions (single phase, low turbulence intensity, non-reacting). Similarly, various algebraic error indicators (such as Popes 80 % criterion[2]) have been developed in an attempt to provide some guiding metrics (see for example Gant[3] and Celik *et*

al.[4]). In TNF9 (Montreal Canada, 2009), algebraic error indicators were applied to the Sydney HM1 flame to explore their utility in the context of the observations above. It was shown that these indicators produce anomalous results. In dissipative schemes, for example, measures of the resolved turbulent kinetic energy in an LES can be misleadingly high since dissipative errors incorrectly damp the velocity fluctuations, and thus the total level of turbulent kinetic energy in the system. As a consequence, low values of turbulent viscosity suggest good resolution, when in reality artificial dissipation introduces non-physical damping of the turbulence.

A second focal point in TNF9, followed by TNF10 (Beijing China, 2010), was application of advanced techniques based on multi-objective optimizations to reach an ideal set of simulation parameters (see for example the work of Meyers *et al.*[5]). One such technique known as the error-landscape method was applied to the Sydney HM1 flame by Kempf, Geurts, and Oefelein.[6] Results demonstrated how the method could be used to optimize the widely used Smagorinsky model using a given grid resolution and numerical scheme. Here, small values of the Smagorinsky constant C_s were shown to allow flow structures on order of grid spacing where numerical errors dominate. Large values were shown excessively damp flow structures. An optimal value of C_s = 0.173 was found to provide a compromise, where both numerical and model errors were minimized simultaneously. A novel feature of the error-landscape method is it provides a way to systematically assess the total error that results from the combination of the selected models and numerical methods using available experimental data. This is in contrast to more sophisticated Uncertainty Quantification (UQ) methods that require significantly more input than is typically available from an experiment. However, combined errors are lumped together and the total error cannot be reduced to any arbitrary level.

To further understand how to control errors in LES, we have recently begun a series of collaborations with Khalil and Najm aimed at incorporating advanced UQ methods into LES. Following the approach described above, we performed a new set of studies using the same Sydney HM1 flame. We address the forward UQ problem focusing on parametric uncertainty associated with the Smagorinsky constant and related turbulent Prandtl and Schmidt numbers. To perform this analysis, 25 LES simulations are performed from which Khalil and Najm build a surrogate model using a polynomial chaos expansion for the quantities of interest (see Najm's abstract). This enables global sensitivity analysis and forward propagation of uncertainty, and thus provides marginal and joint distributions on the outputs of interest. Using the non-intrusive polynomial chaos method to construct the surrogate models eliminates the need to modify the LES solver. Results provide insights on the underlying structure of the LES simulation, the impact of different parameters on specific observables, and correlations among different quantities of interest.

LES calculations were performed using the RAPTOR code framework, which is a fully compressible solver that has been optimized to meet the strict algorithmic requirements imposed by the LES formalism. Details related to the baseline formulation and subgrid-scale models are given by Oefelein.[7] In the current study, we are not interested in any particular model, but instead focus on demonstrating the merits of the non-intrusive UQ approach using a simple albeit well-known model. Thus, the subgrid-scale turbulence closure is obtained using the Smagorinsky model and the flamelet approach for the combustion closure. The overall model includes the Leonard and cross-term stresses and provides a Favre averaged generalization of the Smagorinsky eddy viscosity model coupled with gradient diffusion models to account for subgrid-scale mass and energy transport processes. The focal point of our analysis are the model constants C_s, Pr_t, and Sc_t, which represent the Smagorinsky constant and subgrid-scale Prandtl and Schmidt numbers, respectively. In the present configuration, the fuel contains hydrogen making the flame very robust to strain and no extinction zones are experimentally observed in the flame sheet. Since finite-rate chemistry effects are neglected, a one-dimensional look-up table is employed for simplicity based on the tabulation of a single opposed-jet flame using the GRI-Mech 3.0 mechanism.

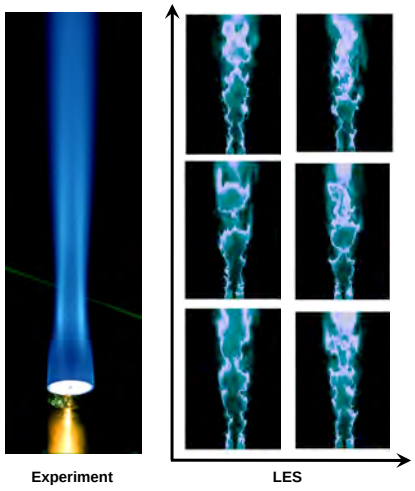

Figure 1: Photograph of the Sydney bluff-body (HM1) flame with a corresponding set of LES results showing the instantaneous median field of temperature as a function of increasing Smagorinsky constant (abscissa) and subgrid-scale Schmidt number (ordinate).

A photograph of the flame and corresponding LES results showing the instantaneous median field of temperature are shown in Fig. 1. The system is composed of a cylindrical bluff-body ($d_{bb} = 50\ mm$ in diameter) placed at the center of a wind tunnel ($d_{co} = 160\ mm$). The fuel is injected at the center of the bluff-body through a $d_j = 3.6\ mm$ nozzle. The air of the external wind tunnel flows at $U_{co} = 35\ m/s$ with a turbulence intensity of 2 %. The fuel is injected at a velocity of $U_j = 108\ m/s$ and assumed to be

fully developed. The device is operated at atmospheric pressure and both fuel and oxidizer streams are injected at room temperature ($T_{co} = T_j = 298\ K$). The non-premixed flame is attached to the rim of the bluff-body between the rich recirculation region downstream of the injection plate and the external air stream. The computational set-up is based on the same dimensions as in the experiment. The domain is a square section parallelepiped ($160 \times 160 \times 200\ mm$). As the flame and velocity gradients are only present in the wake of the bluff-body ($r < 30\ mm$, where r is the radius from the fuel jet axis) the cartesian grid spacing is constant and concentrated in this region ($\Delta_r = \Delta_x = 0.3\ mm$). The grid is smoothly stretched away from the zone of interest. The mesh is composed of 12-million hexahedral cells.

At the inlets, mean profiles are adjusted to match experimental measurements. Turbulent fluctuations are added to the mean profiles using a synthetic correlated signal with a specified intensity. Generally, output uncertainties are impacted by boundary conditions, the numerical method, grid spacing, and initialization. For all present computations, those computational aspects are held constant so that results only depend on tested parameters. In the present analysis, the ranges of model parameters have been extracted from reference studies based on empirical and theoretical approaches. The Smagorinsky constant is varied over a range of $0.065 < C_s < 0.346$. Similarly, the subgrid-scale Prandtl and Schmidt numbers are varied over the ranges $0.5 < Pr_t < 1.7$ and $0.5 < Sc_t < 1.7$. The initial solution from which the UQ study is carried out has been obtained with a parameter triplet taken at the center of this matrix. The initialization follows a simple start-up procedure by running for $300\ ms$ to flush the initial state. Then the simulation is run for an additional $100\ ms$ to acquire converged statistics. All computations are then started from this converged flow field ($t = 400\ ms$) and computed for an additional $30\ ms$, which corresponds to 8 turn-over times of the recirculation zone. This duration has been found to be a good compromise between computational cost and temporal convergence of key flow features. Each case is run on 1024 processors for 62 hours. Hence, the total CPU requirement for generating the data for the UQ analysis (25cases) is 1.6-million CPU hours. A representative set of profiles are presented in Fig. 2 showing the scatter associated with the test matrix.

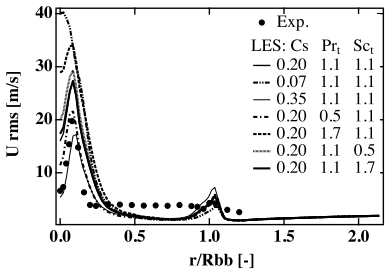

Figure 2: Representative comparison of the RMS of axial velocity between the experimental measurements (symbols) and LES (lines) at $x = 10\ mm$ downstream of the bluff-body.

Using these data, application of the UQ technique by Khalil and Najm shows that the fluctuation of axial velocity is strongly sensitive to the Smagorinsky constant. This response can be anticipated since the turbulent viscosity has a direct impact on the fluctuating flow field contrary to the other two parameters. Interestingly, the mean velocity on the centerline at $x = 30\ mm$ also has a significant sensitivity to the turbulent Prandtl number. One assumption as to why is that dilatation effects mainly depend on Prandlt number, which significantly impacts the shape of the recirculation zone and thus has a major influence on the mean velocity. This coupling is still not fully understood and will require further investigation. Mean mixture fraction and temperature exhibit similar trends with regard to sensitivity, which is a result of the flamelet closure used in the simulation. Mean mixture fraction has a stronger dependence on C_s. A potential explanation is that mixture fraction is predominantly affected by the resolved-scale velocity fluctuations, which are more sensitive to the Smagorinsky constant. Fluctuations in temperature and mixture fraction have comparable responses for the three parameters. This shows that the confidence in the prediction of these quantities relies on the accuracy with which all three parameters are estimated. These results will be extended in future work to provide further improvements in accuracy and to examine other flow/flame observables of interest.

Future Plans

We will continue to use the foundational approach and framework described above with emphasis placed on three interrelated areas of research: 1) Maintain close coordination between LES and the experimental reacting flow research program with emphasis on the collaborative activities of the TNF Workshop to advance our fundamental understanding of turbulent reacting flows. 2) Maintain a significant effort in the development of quality assessment techniques for LES aimed at understanding and controlling the myriad of errors that complicate the development and validation of predictive models. 3) Continue to develop advanced models and simulation techniques aimed at accurate prediction of flame behavior across a broad range of combustion modes, regimes, and fuels. Tasks related to research area 1 will be pursued through close collaborations with Barlow and Frank following the proposed series of experiments outlined in their respective abstracts. Tasks related to research area 2 will be pursued through close collaborations with Najm *et al*. (e.g., see Najm's abstract). Tasks related to research area 3 will continue to focus on advanced model development in a manner that effectively bridges the gap between the idealized jet flame processes studied under this program and application relevant processes exhibited at the device scale.

Literature Cited

1. R. S. Barlow. International workshop on measurement and computation of turbulent (non)premixed flames. www.sandia.gov/TNF, 1996-2014. Sandia National Laboratories, Combustion Research Facility, Livermore, California.
2. S. B. Pope. *Turbulent Flows*. Cambridge University Press, Cambridge, United Kingdom, 2000.
3. S. E. Gant. Reliability issues of LES-related approaches in an industrial context. *Flow, Turbulence and Combustion*, 84(2): 325–335, 2010. doi: 10.1007/s10494-009-9237-8.
4. I. B. Celik, Z. N. Cehreli, and I. Yavuz. Index of resolution quality for large eddy simulations. *Journal of Fluids Engineering*, 127:949–958, 2005.
5. J. Meyers, P. Sagaut, and B. J. Geurts. Optimal model parameters for multi-objective large-eddy simulations. *Physics of Fluids*, 18(095103):1–12, 2006. doi: 10.1063/1.2353402.
6. A. M. Kempf, B. J. Geurts, and J. C. Oefelein. Error analysis of large eddy simulation of the turbulent non-premixed Sydney bluff-body flame. *Combustion and Flame*, 158:2408–2419, 2011. doi: 10.1016/j.combustflame.2011.04.012.
7. J. C. Oefelein. Large eddy simulation of turbulent combustion processes in propulsion and power systems. *Progress in Aerospace Sciences*, 42(1):2–37, 2006.

BES Sponsored Publications (2012–Present)

1. M. Khalil, G. Lacaze, J. C. Oefelein, and H. N. Najm. Uncertainty quantification in LES of a turbulent bluff-body stabilized flame. *Proceedings of the Combustion Institute*, 2015. Submitted.
2. G. Lacaze, A. Misdariis, A. Ruiz, and J. C. Oefelein. Analysis of high-pressure diesel fuel injection processes using LES with real-fluid thermodynamics and transport. *Proceedings of the Combustion Institute*, 2015. Submitted.
3. R. N. Dahms and J. C. Oefelein. Non-equilibrium gas-liquid interface dynamics in high-pressure liquid injection systems. *Proceedings of the Combustion Institute*, 2015. Submitted.
4. R. N. Dahms and J. C. Oefelein. Liquid jet breakup regimes in high-pressure systems. *Journal of Fluid Mechanics*, 2014. Submitted.
5. J. Manin, M. Bardi, L. M. Pickett, R. N. Dahms, and J. C. Oefelein. Microscopic investigation of the atomization and mixing processes of diesel sprays injected into high pressure and temperature environments. *Fuel*, 2014. Submitted.
6. A. Ruiz, G. Lacaze, and J. C. Oefelein. Assessing the accuracy of large eddy simulation in a jet in cross flow configuration. *Proceedings of the 2014 Spring Meeting of the Western States Section of the Combustion Institute*, March 24-25 2014. Pasadena, California.
7. J. Oefelein, G. Lacaze, R. Dahms, A. Ruiz, and A. Misdariis. Effects of real-fluid thermodynamics on high-pressure fuel injection processes. *SAE International Journal of Engines*, 7(3):1–12, 2014. doi: 10.4271/2014-01-1429.
8. R. N. Dahms and J. C. Oefelein. On the transition between two-phase and single-phase interface dynamics in multicomponent fluids at supercritical pressures. *Physics of Fluids*, 25(092103):1–24, 2013. doi: 10.1063/1.4820346.
9. R. N. Dahms, J. Manin, L. M. Pickett, and J. C. Oefelein. Understanding high-pressure gas-liquid interface phenomena in diesel engines. *Proceedings of the Combustion Institute*, 34:1667–1675, 2013. doi: 10.1016/j.proci.2012.06.169.
10. L. Lu, P. M. Najt, T.-W. Kuo, V. Sankaran, and J. C. Oefelein. A fully integrated linear eddy and chemistry agglomeration method with detailed chemical kinetics for studying the effect of stratification on HCCI combustion. *Fuel*, 105:653–663, 2013. doi: 10.1016/j.fuel.2012.09.031.
11. J. C. Oefelein, R. N. Dahms, G. Lacaze, J. L. Manin, and L. M. Pickett. Effects of pressure on the fundamental physics of fuel injection in diesel engines. *Proceedings of the 12th International Conference on Liquid Atomization and Spray Systems*, September 2-6 2012. Heidelberg, Germany. ISBN 978-88-903712-1-9.
12. J. C. Oefelein, R. N. Dahms, and G. Lacaze. Detailed modeling and simulation of high-pressure fuel injection processes in diesel engines. *SAE International Journal of Engines*, 5(3):1–10, 2012. doi: 10.4271/2012-10-1258.
13. R. Knaus, J. Oefelein, and C. Pantano. On the relationship between the statistics of the resolved and true rate of dissipation of mixture fraction. *Flow, Turbulence and Combustion*, 89(1):37–71, 2012. doi: 10.1007/s10494-012-9391-2.
14. G. Lacaze and J. C. Oefelein. A non-premixed combustion model based on flame structure analysis at supercritical pressures. *Combustion and Flame*, 159:2087–2103, 2012. doi: 10.1016/j.combustflame.2012.02.003.
15. B. Hu, M. P. Musculus, and J. C. Oefelein. The influence of large-scale structures on entrainment in a decelerating transient turbulent jet revealed by large eddy simulation. *Physics of Fluids*, 24(045106):1–17, 2012. doi: 10.1063/1.3702901.

KINETICS AND DYNAMICS OF COMBUSTION CHEMISTRY

David L. Osborn
Combustion Research Facility, Mail Stop 9055, Sandia National Laboratories
Livermore, CA 94551-0969
dlosbor@sandia.gov

PROGRAM SCOPE

The goal of this program is to elucidate mechanisms of elementary combustion reactions through the use of multiplexed optical spectroscopy and mass spectrometry. We developed a technique known as time-resolved multiplexed photoionization mass spectrometry (MPIMS), which is used to sensitively and selectively probe unimolecular and bimolecular reactions. This work is in collaboration with Craig Taatjes and many scientists from other institutions in the US and abroad. The Sandia-designed MPIMS instrument utilizes tunable vacuum ultraviolet light from the Advanced Light Source synchrotron at Lawrence Berkeley National Laboratory for sensitive, isomer-specific ionization of reactant and product molecules in chemical reactions.

As a complementary approach, we utilize time-resolved Fourier transform spectroscopy (TR-FTS) to probe multiple reactants and products with broad spectral coverage (> 1000 cm^{-1}), moderate spectral resolution (0.1 cm^{-1}), and a wide range of temporal resolution (ns – ms). The inherently multiplexed nature of TR-FTS makes it possible to simultaneously measure product branching ratios, internal energy distributions, energy transfer, and spectroscopy of radical intermediates. Together with total rate coefficients, this additional information provides further constraints upon and insights into the potential energy surfaces that control chemical reactivity. Because of its broadband nature, the TR-FTS technique provides a global view of chemical reactions and energy transfer processes that would be difficult to achieve with narrow-band, laser-based detection techniques.

RECENT PROGRESS

Isomer-resolved mass spectrometry

The multiplexed chemical kinetics photoionization mass spectrometer operates both at Sandia National Laboratories (using a discharge lamp to create VUV radiation), and at the Chemical Dynamics Beamline of the Advanced Light Source (ALS) synchrotron of LBNL. The chemical reactor is based on the Gutman design,[1] which allows the study of photodissociation and bimolecular reactions at pressures of 1 – 10 Torr and temperatures of 300 – 1000 K.

During past 3-year period, we have applied this apparatus to a broad array of chemical problems, including studies of biofuel oxidation, reactions relevant to Saturn's moon Titan, the chemistry of carbonyl oxides (Criegee Intermediates), and fundamental studies of photoionization dynamics and absolute cross sections.

The propargyl (H_2CCCH) + acetylene (HCCH) reaction sequence

There has been much debate on the mechanism for the formation of the first and second aromatic ring in molecular weight growth chemistry during rich combustion. One mechanism, the Hydrogen Abstraction C_2H_2 Addition (HACA), proposed by Frenklach and co-workers,[2] involves addition of acetylene to free radicals, forming a larger free radical, which may add additional acetylenes in a reaction sequence. Using time-resolved mass spectrometry, Knyazev and Slagle[3] studied the propargyl + acetylene reaction from 800 – 1100 K, which they described with the following sequence of reactions: $C_3H_3 + C_2H_2 \rightarrow C_5H_5 (+C_2H_2) \rightarrow C_7H_7 (+C_2H_2) \rightarrow$

C_9H_8 + H. They measured small rate coefficients (~ 10^{-15} cm^3 $molecule^{-1}$ s^{-1}) for each step even at these high temperatures. Although no isomeric information on the free radicals could be obtained, they inferred that the radicals must be resonance stabilized to persist at such high temperatures.

We have revisited this reaction using MPIMS with tunable synchrotron radiation for photoionization, enabling isomer selectivity at T = 800 K, P = 8 torr, and T = 1000 K, P = 10 torr. Our kinetic traces are very similar to those of Knyazev and Slagle, confirming the same reaction sequence they assigned. At 800 K, the initial step produces two isomers of C_5H_5: the 1-vinyl propargyl radical (HCCCH–C_2H_3), and the cyclopentadienyl radical (the most stable C_5H_5 isomer). These two isomers are formed at the same rate, but vinyl propargyl decays more rapidly than cyclopentadienyl. At the higher temperature of 1000 K, vinyl propargyl's contribution to the C_5H_5 signal is decreased by more than an order of magnitude, implying that it either unimolecularly dissociates or isomerizes rapidly on the timescale of our experiment.

We have recently acquired reference photoionization spectra of both the benzyl (C_6H_5–CH_2) and tropyl (c-C_7H_7) isomers of C_7H_7. With this new information we find clear evidence that the C_7H_7 radical produced from the propargyl + acetylene reaction sequence at 1000 K shows no evidence of the benzyl isomer, but is instead consistent with the seven-membered symmetric ring structure of the tropyl radical. This result is qualitatively consistent with recent calculations of DaSilva and coworkers[4] on this reaction. The data at 800 K shows an additional isomer of the C_7H_7 radical that is as yet unidentified. In the final addition of acetylene to C_7H_7, we do not observe the C_9H_9 radical. Instead, the only product is indene (C_9H_8), a two-ring aromatic compound.

Photoionization dynamics of the formyl radical

The formyl radical (HCO) is a ubiquitous species in flames, and the simplest oxygenated hydrocarbon radical. It has been studied by many spectroscopic techniques, and its ionization energy has been measured accurately,[5] but surprisingly, no photoionization spectrum has been reported in the literature. We have measured the photoionization spectra of HCO and DCO, produced from 308 nm photodissociation of acetaldehyde and acetaldehyde-d_4.

Our photoionization spectrum of the $\tilde{X}^+ (^1\Sigma^+) \leftarrow \tilde{X} (^2A')$ transition shows very poor Franck-Condon overlap in this linear ← bent transition, in agreement with the long progression observed in the photoelectron spectrum from Dyke.[6] At photon energies higher than the first Franck-Condon envelope, we observe two series of autoionizing resonances that appear to converge to the lowest excited triplet state of the cation, which is bent, like the ground state of the neutral. The competition between photodissociation and autoionization in these transitions is complex, as revealed by the contrasting linewidths in the spectra of HCO and DCO. We are pursuing a quantitative model of this process. In addition, we can place the photoionization cross section of HCO on an absolute scale by comparing to the known photoionization cross section of the CH_3 radical that is produced in a 1:1 ratio upon 308 nm photodissociation. These results will be compared with the previous work of Shubert and Pratt[7] and FitzPatrick *et al*.[8]

Photoelectron Photoion Coincidence as a tool for chemical analysis

We and others have made great use of photoionization spectroscopy as a tool for quantitative chemical analysis in complex chemical environments such as flames and time-evolving chemical reactions. Coupled with time-of-flight mass spectrometry (or other multi-mass spectrometry), the technique provides an efficient method to sort a chemical mixture first

by *m*/*z* ratio, and further by ionization energy and spectral shape at each *m*/*z* ratio for isomer identification. However, all techniques have their limits, and in some cases, mixtures of three or more isomers can be difficult or impossible to quantify by this technique.

In the absence of resonances, the photoionization spectrum is essentially the integral of the photoelectron spectrum of a molecule. Detecting peaks in a photoelectron spectrum provides a better molecular fingerprint than the thresholds of a photoionization spectrum. However, photoelectron spectroscopy (where only electrons are detected) has rarely been applied to mixtures of neutral species because it is difficult to correlate multiple overlapping photoelectron spectra with each cation present in a system. For most of the reactions we study, this approach would be hopeless due to the large number of molecular species present.

Photoelectron photoion coincidence (PEPICO) spectroscopy is one solution to this problem, providing an independent photoelectron spectrum for each cation *m*/*z* ratio. In collaboration with Prof. Bálint Sztáray of the University of the Pacific, we have recently shown[9] that modern imaging PEPICO spectroscopy can be used to separate mixtures of many components with significantly increased fidelity compared to photoionization spectroscopy.

Future Plans

In future work we will optimize a new set of ion optics for the unique needs of time-resolved PEPICO spectroscopy, which should enable better molecular fingerprints to help resolve chemical reaction mechanisms that are beyond our capabilities at present.

BES-sponsored publications, 2012 – present

1) Low-Temperature Combustion Chemistry of Novel Biofuels: Resonance-Stabilized QOOH in the Oxidation of Diethyl Ketone, A. M. Scheer, O. Welz, J. Zádor, D. L. Osborn and C. A. Taatjes, Phys. Chem. Chem. Phys. **in press** doi:10.1039/C3CP55468F (2014).
2) Rate Coefficients of C1 and C2 Criegee Intermediate Reactions with Formic and Acetic Acid Near the Collision Limit: Direct Kinetics Measurements and Atmospheric Implications, O. Welz, A. J. Eskola, L. Sheps, B. Rotavera, J. D. Savee, A. M. Scheer, D. L. Osborn, D. Lowe, A. M. Booth, P. Xiao, M. A. H. Khan, C. J. Percival, D. E. Shallcross, and C. A. Taatjes, Angew. Chem. **in press** doi:10.1002/anie.201400964 (2014).
3) A coordinated investigation of the combustion chemistry of diisopropyl ketone, a prototype for biofuels produced by endophytic fungi, J.W. Allen, A.M. Scheer, C. Gao, S.S. Merchant, S.S. Vasu, O. Welz, J.D. Savee, D.L. Osborn, C. Lee, S. Vranckx, Z. Wang, F. Qi, R.X. Fernandes, W.H. Green, M.Z. Hadi, and C.A. Taatjes, Combustion and Flame **161**, 711 (2014).
4) Synchrotron photoionization mass spectrometry measurements of product formation in low-temperature n-butane oxidation: towards fundamental understanding of autoignition chemistry and *n*-$C_4H_9 + O_2$ / *s*-$C_4H_9 + O_2$ reactions, A. J. Eskola, O. Welz, J. D. Savee, D. L. Osborn, and C. A. Taatjes, J. Phys. Chem. A **117**, 12216 (2013).
5) Low-temperature combustion chemistry of *n*-butanol: principal oxidation pathways of hydroxybutyl radicals, O. Welz, J. Zador, J. D. Savee, L. Sheps, D. L. Osborn, and C. A. Taatjes, J. Phys Chem. A **117**, 11983 (2013).
6) Isomer specific product detection in the reaction of CH with acrolein, J. F. Lockyear, O. Welz, J. D. Savee, F. Goulay, A. J. Trevitt, C. A. Taatjes, D. L. Osborn, and S. R. Leone, J. Phys. Chem. A **117**, 11013 (2013).
7) Mass-resolved isomer-selective chemical analysis with imaging photoelectron photoion coincidence spectroscopy, A. Bodi, P. Hemberger, D. L. Osborn, and B. Sztaray, J. Phys. Chem. Lett. **4**, 2948 (2013).
8) Product branching fractions of the CH + propene reaction from synchrotron photoionization mass spectrometry, A. J. Trevitt, M. B. Prendergast, F. Goulay, J. D. Savee, D. L. Osborn, C. A. Taatjes, and S. R. Leone, J. Phys. Chem. A **117**, 6450 (2013).
9) Regional and global impacts of Criegee intermediates on atmospheric aerosol formation, C. J. Percival, O. Welz, A. J. Eskola, J. D. Savee, D. L. Osborn, D. O. Topping, D. Lowe, S. R. Utembe, A. Bacak, G. McFiggans, M. C. Cooke, P. Xiao, A. T. Archibald, M. E. Jenkin, R. G. Derwent, I. Riipinen, D. W. K. Mol, E. P. F. Lee, J. M. Dyke, C. A. Taatjes, and D. E. Shallcross, Faraday Discussions **165**, 45 (2013).
10) Absolute photoionization cross-section of the vinyl radical, J. D. Savee, J. F. Lockyear, S. Borkar, A. J. Eskola, O. Welz, C. A. Taatjes, and D. L. Osborn, J. Chem. Phys. **139**, 056101 (2013).
11) Facile rearrangement of 3-oxoalkyl radicals is evident in low-temperature gas-phase oxidation of ketones, A. M. Scheer, O. Welz, D. Y. Sasaki, D. L. Osborn, and C. A. Taatjes, Journal of the American Chemical Society **DOI:** 10.1021/ja405892y (2013).

12) Absolute photoionization cross-sections of selected furanic and lactonic potential biofuels, J. Czekner, C. A. Taatjes, D. L. Osborn, and G. Meloni, International Journal of Mass Spectrometry **348**, 39 (2013).
13) Directly measuring reaction kinetics of QOOH—a crucial but elusive intermediate in hydrocarbon autoignition, J. Zador, H. Huang, O. Welz, J. Zetterberg, D. L. Osborn, and C. A. Taatjes, Physical Chemistry Chemical Physics **15**, 10753 (2013).
14) Direct measurements of conformer-dependent reactivity of the Criegee intermediate CH_3CHOO, C. A. Taatjes, O. Welz, A. J. Eskola, J. D. Savee, A. M. Scheer, D. E. Shallcross, B. Rotavera, E. P. F. Lee, J. M. Dyke, D. K. W. Mol, D. L. Osborn, and C. J. Percival, Science **340**, 177 (2013).
15) Formation of dimethylketene and methacrolein by reaction of the CH radical with acetone, F. Goulay, A. Derakhshan, E. Maher, A. J. Trevitt, J. D. Savee, A. M. Scheer, D. L. Osborn, and C. A. Taatjes, Physical Chemistry Chemical Physics **15**, 4049 (2013).
16) Phototautomerization of Acetaldehyde to Vinyl Alcohol: A Primary Process in UV-Irradiated Acetaldehyde from 295 to 335 nm, A. E. Clubb, M. J. T. Jordan, S. H. Kable, and D. L. Osborn, Journal of Physical Chemistry Letters **3**, 3522 (2012).
17) Thermal decomposition of CH_3CHO studied by matrix infrared spectroscopy and photoionization mass spectroscopy, A. K. Vasiliou, K. M. Piech, B. Reed, X. Zhang, M. R. Nimlos, M. Ahmed, A. Golan, O. Kostko, D. L. Osborn, D. E. David, K. N. Urness, J. W. Daily, J. W. Stanton, and G. B. Ellison, Journal of Chemical Physics **137**, 164308 (2012).
18) Synchrotron photoionization measurements of fundamental autoignition reactions: Product formation in low-temperature isobutane oxidation, A. J. Eskola, O. Welz, J. D. Savee, D. L. Osborn, and C. A. Taatjes, Proc. Combust. Inst., **34**, 385 (2013).
19) Low-temperature combustion chemistry of biofuels: Pathways in the low-temperature (550 – 700 K) oxidation chemistry of isobutanol and tert-butanol, O. Welz, J. D. Savee, A. J. Eskola, L. Sheps, D. L. Osborn, and C. A Taatjes, Proc. Combust. Inst., **34**, 493 (2013).
20) Product Detection of the CH Radical Reaction with Acetaldehyde, F. Goulay, A. J. Trevitt, J. D. Savee, J. Bouwman, D. L. Osborn, C. A. Taatjes, K. R. Wilson, and S. R. Leone, Journal of Physical Chemistry A **116**, 6091 (2012).
21) Synchrotron photoionization measurements of OH-initiated cyclohexene oxidation: ring-preserving products in the OH + cyclohexene and hydroxycyclohexyl + O2 reactions, A. W. Ray, C. A. Taatjes, O. Welz, D. L. Osborn, and G. Meloni, Journal of Physical Chemistry A **116**, 6720 (2012).
22) New mechanistic insights to the $O(^3P)$ + propene reaction from multiplexed photoionization mass spectrometry, J. D. Savee, O. Welz, C. A. Taatjes, and D. L. Osborn, Physical Chemistry Chemical Physics **14**, 10410 (2012).
23) Spectroscopy of the simplest Criegee intermediate CH_2OO: simulation of the first bands in its electronic and photoelectron spectra, E. P. F. Lee, D. K. W. Mol, D. E. Shallcross, C. J. Percival, D. L. Osborn, C. A. Taatjes, and J. M. Dyke, Chemistry – A European Journal **18**, 12411 (2012).
24) Direct measurement of Criegee intermediate (CH_2OO) reactions with acetone, acetaldehyde, and hexafluoroacetone, C. A. Taatjes, O. Welz, A. J. Eskola, J. D. Savee, D. L. Osborn, E. P. F. Lee, J. M. Dyke, D. W. K. Mok, D. E. Shallcross, and C. J. Percival, Physical Chemistry Chemical Physics **14**, 10391 (2012).
25) Absolute photoionization cross-section of the propargyl radical, J. D. Savee, S. Soorkia, O. Welz, T. M. Selby, C. A. Taatjes, and D. L. Osborn, Journal of Chemical Physics **136**, 134307 (2012).
26) Ground and low-lying excited states of propadienylidene ($H_2C=C=C:$) obtained by negative ion photoelectron spectroscopy, J. F. Stanton, E. Garand, J. Kim, T.I. Yacovitch, C. Hock, A. S. Case, E. M. Miller, Y. J. Lu, K. M. Vogelhuber, S. W. Wren, T. Ichino, J. P. Maier, R. J. McMahon, D. L. Osborn, D. M. Neumark, and W. C. Lineberger, Journal of Chemical Physics **136**, 134312 (2012).
27) Low-temperature combustion chemistry of biofuels: pathways in the initial low-temperature (550 – 750K) oxidation chemistry of isopentanol, O. Welz, J. Zador, J.D. Savee, M. Y. Ng, G. Meloni, R.X. Fernandes, L. Sheps, B. A. Simmons, T. S. Lee, D. L. Osborn, and C. A. Taatjes, Physical Chemistry Chemical Physics **14**, 3112 (2012).
28) "Direct kinetic measurements of the Criegee intermediate (CH_2OO) formed by reaction of CH_2I with O2" O. Welz, J. D. Savee, D. L. Osborn, S. S. Vasu, C. J. Percival, D. E. Shallcross, and C. A. Taatjes, Science **335**, 204 (2012).
29) "Absolute photoionization cross-sections of some combustion intermediates" B. Yang, J. Wang, T. A. Cool, N. Hansen, S. Skeen, and D. L. Osborn, International Journal of Mass Spectrometry **309**, 118 (2012).

References

[1] I. R. Slagle and D. Gutman, *J. Am. Chem. Soc.* **107**, 5342 (1985).
[2] M. Frenklach, T. Yuan, and M. K. Ramachandra. *Energy Fuels* **2**, 462 (1988).
[3] V. D. Knyazev and I. R. Slagle. *J. Phys. Chem. A* **106**, 5613 (2002).
[4] G. da Silva, J. A. Cole, and J. W. Bozzelli. *J. Phys. Chem. A* **114**, 2275 (2010).
[5] E. Mayer and E. R. Grant. *J. Chem. Phys.* **103**, 10513 (1995).
[6] J. M. Dyke, N. B. H. Jonathan, A. Morris, and M. J. Winter. *Mol. Phys.* **39**, 629 (1980).
[7] V. A. Shubert and S. T. Pratt. *J. Phys. Chem. A* **114**, 11238 (2010).
[8] B. L. FitzPatrick, B. W. Alligood, L. J. Butler, S. H. Lee, and J. J. M. Lin. *J. Chem. Phys.* **133**, (2010).
[9] A. Bodi, P. Hemberger, D. L. Osborn, and B. Sztáray, *J. Phys. Chem. Lett.* **4**, 2948 (2013).

Program Title: A Theoretical Investigation of the Structure and Reactivity of the Molecular Constituents of Oil Sand and Oil Shale

Principle Investigator: Carol Parish

Address: Department of Chemistry, University of Richmond, Richmond, VA 23227
cparish@richmond.edu

PROGRAM SCOPE

Our work focuses on the theoretical characterization of the gas phase structures, energies and reactivities of the molecular constituents of asphaltenes contained in oil sand and oil shale. Asphaltenes represent an untapped source of hydrocarbon fuel in North America; however, information about the molecular nature of these deposits has only recently become available. Theoretical and experimental evidence suggests that asphaltenes are composed of aromatic molecules that contain 4-10 fused ring cores, with alkyl chain arms extending from the core. Sulfur and nitrogen are also present. Very little is known about the reaction pathways, combustion efficiency and reactivity of these heteroaromatic species. We are currently characterizing the combustion and pyrolysis reaction channels available to asphaltene constituents such as thiophene and methyl thiophene.

RECENT PROGRESS - FY 2013 HIGHLIGHTS

Singlet Oxygen (2+4) Cycloaddition to Heteroaromatic Compounds

The 2+4 cycloaddition reactions of singlet molecular oxygen ($^1\triangle_g$) with a series of aromatic heterocyclic compounds were investigated at both the MP2/6-311++G(d, p) and B3LYP/6-311++G(d, p) levels of theory. Several factors related to heteroaromatic ring structure were determined to affect the activation energy of the cycloaddition and the stability of the corresponding endoperoxide products. Such factors include: (1) the position of methyl substitution; (2) the number of methyl substituents; (3) the alkyl chain length of substituents; (4) the electronic structure of substituents and; (5) the type of heteroatom in the ring. In total, fourteen 2+4 cycloaddition routes were examined and in each case the mechanism is concerted. The order of reactivity toward O_2 ($^1\triangle_g$) was determined to be: 2,3,4,5-tetramethylthiophene > 2,3,5-trimethylthiophene > 2,5-dimethylthiophene > 2-methylthiophene > 2-ethylthiophene > 2-propylthiophene > 3-methylthiophene > thiophene > benzothiophene > dibenzothiophene; and furan > pyrrole > thiophene > benzene. The stability of the endoperoxide products follows a similar trend. Each of the reaction pathways is initiated by the formation of a pre-reactive complex, formed by a van der Waals interaction between a C atom on the ring and an O atom on O_2. To the best of our knowledge, this type of VDW pre-

reactive complex has not been identified in previous studies of cycloaddition reactions of singlet oxygen with arenes.

Minding the Gap: Variations on the Bergman Theme. Electrocyclizations of Penta–, Hepta– and Octa–diynes

The electrocyclization reactions of the penta-1,4-diyne anion, the hepta-1,6-diyne cation and the octa-1,7-diyne dication, to form the corresponding aromatic diradicals, were investigated using the BLYP and B3LYP functionals with different basis sets.

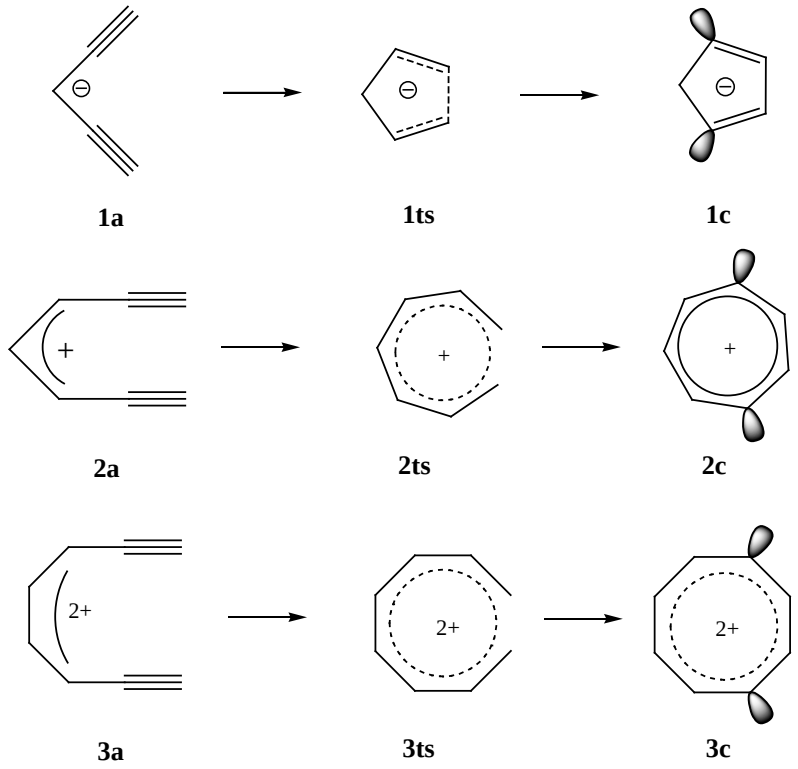

The energetics of these cyclization reactions shed light on the structural factors underlying these important processes. The resultant diradicals provide information regarding through-bond and through-space electron coupling and the role of aromaticity in the energetics of the cyclizations. The geometries obtained at different levels of DFT are quite similar; however, the relative energies depend upon the methodological approach. Therefore, energies were also calculated using the BCCD(T)/cc-pVDZ treatment using BLYP/6-31G* geometries, and compared with the results obtained at DFT levels. The cyclization barrier for the 1,6-heptadiyne cation (25 kcal mol^{-1}) is energetically comparable to that of the Bergman cyclization of (Z)-hexa-3-ene-1, 5-diyne (28 kcal mol^{-1}), while the cyclization barrier for the 1,7-octadiyne dication (15 kcal mol^{-1}) is significantly lower. All three diradicals display aromatic behavior as measured by nucleus independent chemical shifts.

Jahn-Teller Stabilization in POSS Cations: Octatert-butyl and Octachloro silsesquioxanes $Si_8O_{12}(C(CH_3)_3)_8^+$ and $Si_8O_{12}Cl_8^+$

Polyoligomeric silsesquioxanes (POSS) are molecules containing a rigid, cubic inorganic core Si_8O_{12} with Si atoms attached to organic or inorganic peripheral groups. These compounds have found many applications in polymer chemistry as they impart thermal stability when mixed with organic polymers to form nanostructured organic-inorganic hybrids. We have investigate the symmetry breaking mechanism in cubic octatert-butyl silsesquioxane and octachloro silsesquioxane monocations ($Si_8O_{12}(C(CH_3)_3)_8^+$ and $Si_8O_{12}Cl_8^+$) applying density functional theory (DFT) and group theory. Under O_h symmetry, these ions possess $^2T_{2g}$ and ^2E_g electronic states and undergo different symmetry breaking mechanisms. The ground states of $Si_8O_{12}(C(CH_3)_3)_8^+$ and $Si_8O_{12}Cl_8^+$ belong to the C_{3V} and D_{4h} point groups and are characterized by Jahn-Teller stabilization energies of 3959 and 1328 cm^{-1}; respectively, at the B3LYP/def2-SVP level of theory. The symmetry distortion mechanism in $Si_8O_{12}Cl_8^+$ is Jahn-Teller type, whereas in $Si_8O_{12}(C(CH_3)_3)_8^+$ the distortion is a combination of both Jahn-Teller and pseudo-Jahn-Teller effects. The distortion force acting in $Si_8O_{12}(C(CH_3)_3)_8^+$ is mainly localized on one Si-(tert-butyl) group while in $Si_8O_{12}Cl_8^+$ it is concentrated on the oxygen atoms. In these ionic compounds, the main distortion forces acting on the Si_8O_{12} core arise from the coupling between the electronic state and the vibrational modes; identified as $9t_{2g}+1e_g+3a_{2u}$ for the $Si_8O_{12}(C(CH_3)_3)_8^+$ and $1e_g+2e_g$ for $Si_8O_{12}Cl_8^+$. This work has been submitted to the *Journal of Chemical Theory and Computation.*

FUTURE WORK

Work is currently underway to characterize ground and excited states of heteroaromatic diradicals such as thiophene, fulvene and pyrrole. We are also pursuing a complete characterization of the singlet and triplet surfaces of the electrocyclization reaction of (Z)-hexa-1,3,5-triene leading to *p*-benzyne as well as a characterization of the endo and exo-dig radical cyclization reactions.

PUBLICATIONS

1. "Mechanisms for the reaction of thiophene and methylthiophene with singlet and triplet molecular oxygen," Xinli Song, Matthew G. Fanelli, Justin M. Cook, Furong Bai and Carol A. Parish*, *Journal of Physical Chemistry A*, **2012** *116*, 4934-4946.
2. "A Mechanistic Study of the 2-Thienylmethyl + HO_2 Radical Recombination Reaction," Xinli Song and Carol Parish,* *Journal of Physical Chemistry A*, **2011**, *115*, 14546-14557
3. "Pyrolysis Mechanisms of Thiophene and Methylthiophene in Asphaltenes," Xinli Song and Carol Parish,* *Journal of Physical Chemistry A* **2011**, *115*, 2882-2891.

PUBLICATIONS - NOT RELATED TO THE PROJECT

1. “Halogen bonding in DNA base pairs,” Anna J. Parker, John Stewart, Kelling Donald* and Carol Parish,* *Journal of the American Chemical Society*, **2012** *134*, 5165-5172.
2. “Evidence that the kinesin light chain contains tetratricopeptide repeat units.” Sally Q. Fisher, Meredith Weck, Jenna E. Landers, Jeffrey Emrich, Shana A. Middleton, Jordan Cox, Lisa N. Gentile and Carol A. Parish,* *Journal of Structural Biology,* **2012,** *177*, 602-612.
3. “Challenging Disciplinary Boundaries in the First-Year: A New Introductory Integrated Science Course for STEM Majors”, Gentile, L.*; Caudhill, L.; Fetea, M.; Hill, A.; Hoke, K.; Lawson, B.; Lipan, O.; Kerckhove, M.; Parish, C.; Stenger, K.; Szajda, D., *Journal of College Science Teaching*, **2012,** *41(5)*, 24-30.
4. “(*rac*)- 1,1′-Binaphthyl-based simple receptors designed for fluorometric discrimination of maleic and fumaric acids,” Kumaresh Ghosh,* Tanushree Sen, Amarnedra Patra, John S. Mancini, Justin M. Cook and Carol A. Parish,* *Journal of Physical Chemistry B,* **2011**, *115*, 8597-8608.
5. “Oligonucleotide Incorporation and Base Pair Stability of 9-deaza-2’-deoxyguanosine,” Michelle L. Hamm*, Anna J. Parker, Jennifer L. Carman, Tyler W. E. Steele, and Carol A. Parish,* *Journal of Organic Chemistry* **2010**, *75*, 5661-5669.
6. “Conformational Analysis of a Model for the trans-fused FGH Ether Rings in Brevetoxin A,” Evan B. Wang and Carol A. Parish*, *Journal of Organic Chemistry*, **2010** *75***,** 1582-1588.

The Dynamics of Large-Amplitude Motion in Energized Molecules

David S. Perry, Principal Investigator
Department of Chemistry, The University of Akron
Akron OH 44325-3601
DPerry@UAkron.edu

I. Program Scope

Chemical reactions, by definition, involve large-amplitude nuclear motion along the reaction coordinate that serves to distinguish reactants from products. Some reactions, such as roaming reactions and reactions proceeding through a loose transition state, involve more than one large amplitude degree of freedom. In principle, the exact quantum nuclear dynamics may be calculated, but such calculations are limited by practical considerations to a few degrees of freedom. Thus in systems larger than 3 or 4 atoms, one must define the active degrees of freedom and separate them in some way from the other degrees of freedom. In this project, we use large-amplitude motion in bound model systems to investigate the coupling of large-amplitude degrees of freedom to other nuclear degrees of freedom [1-12]. This approach allows us to use the precision and power of high-resolution molecular spectroscopy to probe the specific coupling mechanisms involved, and to apply the associated theoretical tools. In addition to slit-jet spectra at the University of Akron [6, 8], work on this project involves collaboration with Brooks Pate's group at the University of Virginia [1], with Michel Herman of the Université Libre de Bruxelles [2, 5, 7], and with Brant Billinghurst at the Canadian Light Source (torsion-vibration coupling in nitromethane). The concepts developed in this project are finding application to the coupled torsional motions in conjugated organic polymers used in solar photovoltaics [3, 4, 9-11].

II. Recent Progress

A. Vibrational Conical Intersections in Methanol

In this work, a set of seven conical intersections between vibrationally adiabatic surfaces has been found, and the implications for spectroscopy and dynamics are discussed.

Conical intersections (CI's) between electronic potential energy surfaces are widespread throughout electronic spectroscopy and are responsible for ultrafast electronic relaxation in diverse circumstances. Whereas these electronic surfaces represent the adiabatic separation of electronic and nuclear motions under the Born-Oppenheimer approximation, it is also possible in some cases to make an (approximate) adiabatic separation of fast and slow vibrational motions. In such cases, the motion of the high frequency vibrations, which might include hydride stretches, can be solved quantum mechanically at each molecular geometry along the low frequency, large-amplitude torsional or bending coordinates. These slower motions are then solved in the effective potential that is the sum of the electronic potential plus the variation of the high-frequency vibrational energies in the large-amplitude space.

Zwanziger and Grant[1] studied $E\otimes e$ systems in which both Jahn-Teller and Renner-Teller couplings are present, the former scaling linearly with the deviation ρ from the C_{3v} reference geometry and the latter scaling quadratically. They showed that there are necessarily four CI's between the coupled electronic surfaces, one at the C_{3v} reference geometry and three more at distorted geometries of C_s symmetry at the values of ρ where the magnitudes of the linear and quadratic couplings become equal.

This same formalism applies also to the case of methanol, where the adiabatic separation is not between degenerate Born-Oppenheimer electronic states and a degenerate vibrational mode, but now between a high frequency degenerate vibrational state in the electronic ground state and a pair of large-amplitude low-frequency modes. Specifically, we consider the vibronic surfaces formed by considering the energies of the asymmetric CH stretch vibrations as a function of the torsional angle, γ, and the COH bend angle, ρ. The C_{3v} reference geometry occurs at $\rho = 0$ where the COH group is linear. In this reference geometry, the two asymmetric CH stretch vibrations (ν_2 and ν_9) become degenerate (E), and the large-amplitude coordinates ρ and γ together become a degenerate COH bending coordinate (e). One

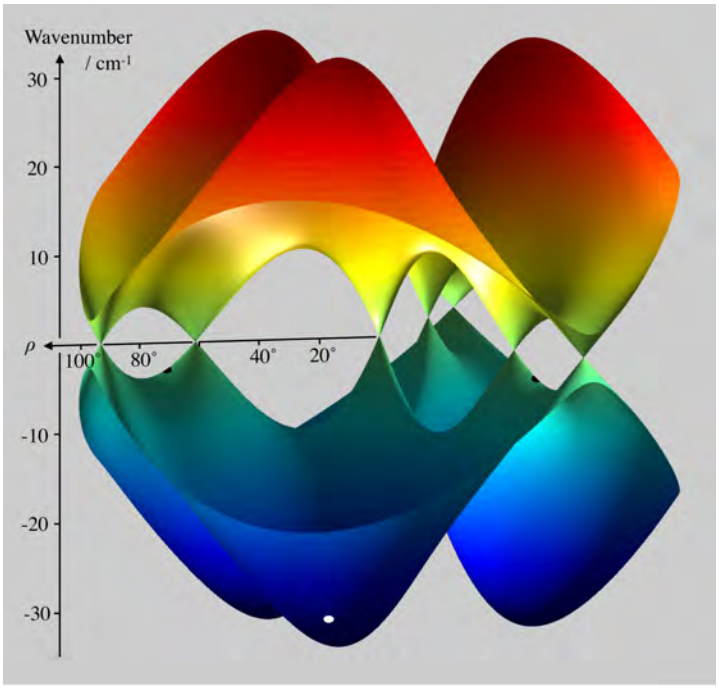

Fig. 1. Relative model frequencies of the two asymmetric CH stretch vibrations in methanol, represented as surfaces in the 2-dimensional coordinate space of the COH bend angle ρ and the torsional angle γ. The model (Eq. (1)) was fit to ab initio frequencies (MP2/6-311+G(3df,2p)) computed at geometries optimized with respect to the other ten internal coordinates. To enhance viewability, the large variations of the average frequency ω_0 and of the underlying electronic energy are suppressed.

significant difference encountered when applying the $E\otimes e$ formalism to the vibrationally adiabatic surfaces in methanol is that the equilibrium geometry is now far from the C_{3v} reference geometry ($\rho = 71^\circ$) rather than close to it as is typically the case for Jahn-Teller coupling between electronic surfaces. In the methanol case, we include higher-order terms in ρ in the Zwanziger and Grant expression[1] for the energies of the intersecting surfaces,

$$\omega_{\pm}^{adiabatic}(\gamma,\rho) = \omega_0(\rho) \pm \tfrac{1}{2}\left[f^2(\rho) + 2f(\rho)g(\rho)\cos 3\gamma + g^2(\rho)\right]^{\frac{1}{2}}. \quad (1)$$

Here both f and g are polynomial expansions in ρ. This analytical form, fitted to ab initio data to ±0.9 cm^{-1}, is shown in Fig. 1 [12]. Fig. 1 reveals the presence of seven conical intersections, one occurring in the C_{3v} reference geometry ($\rho = 0^\circ$), and six more occurring in eclipsed conformations (C_s) at $\rho = 62^\circ$ and 94°. The three CI's at $\rho = 62^\circ$ are close to the torsional saddle point at $\rho = 71^\circ$, within the range of the zero-point COH bending amplitude, and therefore accessible to the dynamics at relatively low energies.

When the dimensionality of the low-frequency coordinate space is 3 or more, then the CI's become seams or hyper-seams of CI's. Now, we include CO stretch coordinate r_{CO} along with γ and ρ to form a 3-dimensional low-frequency coordinate space. Fig. 2 shows that the CI's at $\rho = 62^\circ$ and 94° belong to the same seam of CI's, a significant length of which lies within the range of the zero-point motions of the COH bend and CO stretch.

These conical intersections illuminate the role of geometric phase in methanol. Since four CI's are enclosed by the MEP for a 2π torsional rotation, the Zwanziger and Grant theorem[1] predicts a geometric phase of +1 in agreement with the findings of Xu at al.[2] However, from a semiclassical point of view, one might consider additional classical paths enclosing an odd number of CI's, say 1 or 3. Thus, in a fully coupled treatment, the ν_2 and ν_9 wavefunctions may be linear combinations of basis states of differing geometric phase, with the +1 contribution being dominant.

Since these CI's exist only as an abstraction in the context of an approximate adiabatic separation of high- and low-frequency vibrations, it is relevant to ask, what, if any, impact do they have on the observable energy level structure of methanol? Although physically different models[2-4] predict the inverted torsional tunneling splittings in the CH-stretch fundamentals, the CI's will likely impact the energy level patterns of the higher torsional and COH bending levels built on the CH stretch fundamentals and overtones.

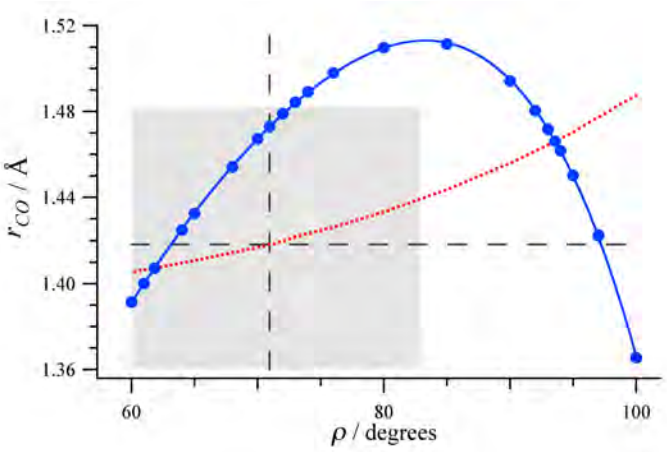

Fig. 2. The location of the seam of conical intersections for eclipsed methanol (markers) and a polynomial fit (solid blue line) is plotted in terms of the CO bond length and the COH bending angle. The red dotted line represents the eclipsed geometries from Fig. 1. and the conical intersections shown in Fig. 1 are located at the intersections of the blue solid and red dotted lines. The dashed lines indicate the zero-point geometries of both coordinates, and the grey shaded area represents the approximate extent of the zero-point amplitudes.

The CI's have the potential to impact both the unimolecular and the intermolecular dynamics of methanol. Xu et al.[2] have shown that the vibrational characters of ν_2 and ν_9 change sharply over a small range of the torsional angle near the eclipsed conformation. The presence of nearby CI's explains this behavior and will allow quantitative predictions of non-adiabatic processes (surface hopping) near the eclipsed geometry. In general, in the context of either intramolecular or collision-induced dynamics, the CI's provide a connection between the vibrationally adiabatic surfaces. Therefore, one should expect acceleration of energy transfer processes in localized regions around the CI's. Just as electronic conical intersections are now known to be ubiquitous throughout electronic spectroscopy, vibrational conical intersections may also be widespread, consequently impacting the vibrational dynamics in diverse chemical systems

B. Six-Fold Internal Rotation

CH_3NO_2 is a benchmark system for nearly free internal rotation in a 6-fold potential and of the coupling to other small-amplitude vibrations. Since many internal rotor states are populated at room temperature, CH_3NO_2 offers an opportunity to study a manifold of large-amplitude states built on the CH stretches. As noted above, such combination states hold the key to unlocking the interactions between large- and small-amplitude degrees of freedom. Rotationally resolved infrared spectra of CH_3NO_2 have been recorded using Far-infrared Beamline at Canadian Light Source on a high resolution Bruker IFS 125HR spectrometer. The observed infrared spectra, in the range 400 - 1000 cm^{-1}, are recorded at a nominal resolution of 0.00096 cm^{-1}. Together with previous spectra from EMSL at the Pacific Northwest National Laboratory, high resolution spectra of five bands have been obtained: the in-plane NO_2 wag (475.2 cm^{-1}), the out-of-plane NO_2 wag (604.9 cm^{-1}), NO symmetric bend (657.1 cm^{-1}) for CN-stretch and at for CN-stretch (917.2 cm^{-1}), and the NO asymmetric stretch (1582.9 cm^{-1}). The analysis is ongoing.

C. Two-Dimensional Large-Amplitude Motion and Coupling to CH Stretches

In molecules with two large-amplitude vibrations (LAV), the LAV's are coupled both to each other and to the other small-amplitude vibrations (SAV) such as CH stretches. Our *ab initio* calculations on CH_3NH_2, $CH_3OH_2^+$, and $CH_3CH_2\cdot$ have shown that the couplings connecting the torsion (α) and inversion (τ) are very similar across these systems despite the wide variation in the tunneling barriers. In all three cases, the dominant torsion-inversion coupling term is $V_{1,3}\tau\cos 3\alpha$ with $V_{1,3}$ in the range 280 to 450 cm^{-1}. For CH_3NH_2 and $CH_3CH_2\cdot$, we find that the torsion-inversion coupling to the CH stretch force constants has a very similar pattern, but that the pattern for the charged species $CH_3OH_2^+$ is very different. The variation of the 2-D tunneling patterns in CH stretch excited states has been investigated across the series methanol, methylamine, 2-methylmalonaldehyde and 5-methyltropolone [6, 9]. In the latter two molecules, the second LAV is proton transfer rather than inversion.

V. Future Plans

The analysis and interpretation of the nitromathane work will continue, focusing on the torsionally excited states, with the purpose of understanding the interactions of the different vibrational modes with the large-amplitude torsional motion. The recently discovered conical vibrational intersections in methanol have implications for both spectroscopy and dynamics. Work in the upcoming period will explore those implications.

VI. Publications from this Project, 2011-2014

[1] S. Twagirayezu, X. Wang, D. S. Perry, J. L. Neill, M. T. Muckle, B. H. Pate, L.-H. Xu, IR and FTMW-IR Spectroscopy and Vibrational Relaxation Pathways in the CH Stretch Region of CH_3OH and CH_3OD, *J. Phys. Chem. A* **115**, 9748-9763 (2011). http://dx.doi.org/10.1021/jp202020u.

[2] D. S. Perry, J. Martens, B. Amyay, and M. Herman, Hierarchies of Intramolecular Vibration-Rotation Dynamical Processes in Acetylene up to 13,000 cm^{-1}, *Mol. Phys.* **110**, 2687-2705 (2012). http://dx.doi.org/10.1080/00268976.2012.711493.

[3] R. S. Bhatta, Y. Yimer, M. Tsige, and D. S. Perry, Nonplanar Conformations and Torsional Potentials of Poly(3-hexylthiophene) Oligomers: Density Functional Calculations up to the Dodecamer, *Computational and Theoretical Chemistry* **995**, 36-42 (2012). http://dx.doi.org/10.1016/j.comptc.2012.06.026.

[4] R. S. Bhatta and D. S. Perry, Correlated backbone torsional potentials in poly(3-methylthiophene), *Computational and Theoretical Chemistry* **1008**, 90-95 (2013). http://dx.doi.org/10.1016/j.comptc.2013.01.003.

[5] K. Prozument, R. G. Shaver, M. Ciuba, J. S. Muenter, G. B. Park, J. F. Stanton, H. Guo, B. M. Wong, D. S. Perry, and R. W. Field, A New Approach toward Transition State Spectroscopy, *Faraday Discuss*. **163**, 33-57 (2013). http://dx.doi.org/10.1039/C3FD20160K.

[6] M. B Dawadi, C. M. Lindsay, A. Chirokolava, D. S. Perry and L.-H. Xu, Novel patterns of torsion-inversion-rotation energy levels in the ν_{11} asymmetric CH-stretch spectrum of methylamine, *J. Chem. Phys*. **138**, 104305 (2013). http://dx.doi.org/10.1063/1.4794157.

[7] M. Herman and D. S. Perry, Molecular spectroscopy and dynamics: A polyad-based perspective, *Phys. Chem. Chem. Phys.* **15**, 9970-9993 (2013). http://dx.doi.org/10.1039/C3CP50463H.

[8] M. B Dawadi, R. S. Bhatta and D. S Perry, Torsion-Inversion Tunneling Patterns in the CH-Stretch Vibrationally Excited States of the G_{12} Family of Molecules Including Methylamine, *J. Phys. Chem. A*. (2013). http://dx.doi.org/10.1021/jp406668w.

[9] R. S. Bhatta, Y. Yimer, D. S. Perry and M. Tsige, Improved force field for molecular modeling of poly(3-hexyl thiophene), *J. Phys. Chem. B.* **117**, 10035-10045 (2013). http://dx.doi.org/10.1021/jp404629a.

[10] R. Bhatta, D. Perry and M. Tsige, Nanostructures and Electronic Properties of a High-Efficiency Electron-Donating Polymer, *J. Phys. Chem. A* (2013). http://pubs.acs.org/doi/pdf/10.1021/jp409069d.

[11] R. Bhatta, M. Tsige, and D. Perry, Torsionally-induced blue-shift of the band gap in poly(3-hexylthiophene), *J. Compt. Theor. Nanosc*. **11**, 1-8 (2014). http://dx.doi.org/10.1166/jctn.2014.3621.

[12] Mahesh B. Dawadi and David S. Perry, Conical Intersections between Vibrationally Adiabatic Surfaces in Methanol, *J. Chem. Phys.*, *accepted for publication* (2014).

VII. Other References

[1] J. W. Zwanziger, and E. R. Grant, J. Chem. Phys. **87**, 2954 (1987).
[2] L.-H. Xu, J. T. Hougen, and R. M. Lees, J. Mol. Spectrosc. **293-294**, 38 (2013).
[3] B. Fehrensen, D. Luckhaus, M. Quack, M. Willeke, and T. R. Rizzo, J. Chem. Phys. **119**, 5534 (2003).
[4] X. Wang, and D. S. Perry, J. Chem. Phys. **109**, 10795 (1998).

New Single- and Multi-Reference Coupled-Cluster Methods for High Accuracy Calculations of Ground and Excited States

Piotr Piecuch
Department of Chemistry, Michigan State University, East Lansing, MI 48824
piecuch@chemistry.msu.edu

I. Program Scope

This research program focuses on new generations of *ab initio* electronic structure methods and computer codes exploiting the exponential wave function ansätze of single- and multi-reference coupled-cluster (CC) theories, which can provide an accurate description of chemical reaction pathways, particularly those involving radicals and biradicals, molecular electronic excitations involving one- and many-electron transitions, including challenging cases of electronic near-degeneracies, and properties other than energy. The goal is to design and apply affordable approaches that enable precise modeling of molecular processes and properties relevant to combustion, catalysis, and photochemistry. The emphasis is on methods that offer high accuracy, ease of use, and lower computational costs compared to other approaches that aim at similar precision, so that one can study complex molecular problems with dozens or hundreds of atoms, in addition to smaller systems, in a predictive manner, supporting existing experiments or in the absence of experimental information. Methods pursued in this program can effectively utilize modern multi-node computer architectures and are well suited for pursuing novel coding strategies, such as automated and parallel computer implementations. The most promising electronic structure approaches developed in this program are shared at no cost with the community by incorporating them into the widely used GAMESS package.

II. Recent Progress (2011 – 2013 and January 1 – April 3, 2014)

We have generalized the previously developed biorthogonal moment expansions, which in the past resulted in the left-eigenstate completely renormalized (CR) CC and equation-of-motion (EOM) CC approaches [1,3,6,17,19,20], so that we can now correct the CC/EOMCC energies obtained with the conventional as well as unconventional truncations in the cluster operator T and the EOM excitation operator R_μ for essentially any category of electron correlation effects of interest [6,7,10]. The resulting CC(P;Q) formalism [6,7,10] enables us to contemplate a wide variety of computationally efficient *ab initio* schemes for high accuracy calculations of ground- and excited-state molecular potential energy surfaces (PESs). Among them is the CC(t;3), CC(t,q;3), CC(t,q;3,4), etc. hierarchy, in which energies obtained in the active-space CC/EOMCC calculations, such as CCSDt/EOMCCSDt or CCSDtq/EOMCCSDtq, which recover much of the non-dynamical and some dynamical electron correlation effects, are corrected for the higher-order, primarily dynamical, correlations, such as certain classes of triples ('3') or triples and quadruples ('3,4') missing in the active-space CC/EOMCC considerations [6,7,10]. Potential advantages of the CC(P;Q) formalism were illustrated by the CC(t;3) calculations for several multi-reference (MR) problems, including bond breaking in HF, F_2, and F_2^+, automerization of cyclobutadiene, isomerization of bicyclo[1.1.0]butane to trans-buta-1,3-diene, and singlet-triplet gaps in the methylene, trimethylenemethane (TMM), and $(HFH)^-$ biradicals [6,7,10]. We showed that CC(t;3) greatly improves the CCSD(T), CCSD(2)$_T$, Λ-CCSD(T), CR-CC(2,3), CCSDt, and CCSD(T)-h results, providing PESs and singlet-triplet gaps that agree with the full CCSDT data to within small fractions of a millihartree for total energies and small fractions of kcal/mol for relative energies at the tiny fraction of the costs of the CCSDT computations, which are competitive with the MRCC and Quantum Monte Carlo calculations for the benchmarked systems.

We have extended the active-space EOMCC methods to the doubly electron-attached (DEA) and doubly ionized (DIP) formalisms, which are applicable to open-shell species with two electrons outside the closed-shell cores, particularly to the electronic spectra of biradicals and single bond breaking, without invoking complicated steps of genuine MRCC theories. The initial papers reporting the development of the full and active-space DEA- and DIP-EOMCC methods with up to 4-particle–2-hole (4p2h) and 4-hole–2-particle (4h2p) excitations have already been published [12,18]. By examining bond breaking in F_2 and low-lying singlet and triplet states in CH_2, $(HFH)^-$, and TMM, we

showed that the DEA- and DIP-EOMCC methods with an active-space treatment of 4p2h and 4h2p excitations reproduce the results of the analogous full calculations at the tiny fraction of the computer effort, allowing us to calculate the singlet-triplet and singlet-singlet gaps in biradicals to within fractions of kcal/mol [12,18]. We also demonstrated that the DEA- and DIP-EOMCC approaches with the full and active-space treatments of 4p2h and 4h2p excitations provide results which are practically insensitive to the choice of the underlying molecular orbital basis, including orbitals of the target *N*-electron species and their (*N*–/+2)-electron counterparts [18]. This should be contrasted with the DEA/DIP EOMCC methods truncated at 3*p*1*h*/3*h*1*p* excitations, which are less accurate and more sensitive to the choice of orbitals [18]. We have also continued working on the active-space EA/IP EOMCC methodology [2,4]. In particular, we demonstrated an excellent performance, in terms of accuracy and computational efficiency, of the active-space EA-EOMCCSD(3p2h) and IP-EOMCCSD(3h2p) approaches in calculations of the excitation energies of CNC, C_2N, N_3, and NCO, where some of the low-lying excited states have a significant MR character, causing problems to EOMCC. We showed that the active-space EA/IP EOMCC schemes, which use small subsets of 3p2h and 3h2p excitations and which we incorporated some time ago in GAMESS, reproduce the results of their parent methods, while requiring a computational effort similar to CCSD. This applies to adiabatic excitation energies and ground- and excited-state geometries [2]. We also performed the scalar relativistic IP- and EA-EOMCC calculations with up to 3h2p and 3p2h excitations, using the second-order Douglass-Kroll-Hess Hamiltonian, along with the SAC-CI calculations, for the electronic spectra of the $CuCl_4^{2-}$ and $CuBr_4^{2-}$ complexes [4], providing an assignment of the observed strong bands and weaker shoulder transitions, and showing how relativity affects excitation energies and geometries.

We implemented the rigorously size-intensive modification of the previously developed (see [6,20] for reviews) CR-EOMCC(2,3) approach, termed δ-CR-EOMCC(2,3) [1,3], which corrects the EOMCCSD energies for the effects of triple excitations using the non-iterative N^7 steps similar to CCSD(T), CR-CC(2,3), and CC(t;3), offering great improvements in the EOMCCSD results. The δ-CR-EOMCC(2,3) codes, along with the extension of the EOMCCSD routines to open shells, have been incorporated in GAMESS as additions to a variety of the CC and EOMCC options that we developed for GAMESS in the past. We used the δ-CR-EOMCC(2,3) approach to examine shifts in the $\pi\rightarrow\pi^*$ excitation energy in cis-7-hydroxyquinoline (cis-7HQ) induced by hydrogen bonding with environment, on the order of 500-2000 cm^{-1}, along with the corresponding excitation energies, on the order of 30,000 cm^{-1}, obtained in the frozen-density embedding theory (FDET) and supermolecular time-dependent density functional theory (TDDFT) calculations, and in experiment [1,3]. We demonstrated that the δ-CR-EOMCC(2,3) and FDET spectral shifts agree with one another and with experiment to within 100 cm^{-1} or 15 % on average, whereas the analogous shifts obtained in the supermolecular TDDFT calculations do not agree with the δ-CR-EOMCC(2,3) data, producing large errors (39% on average). We also reported the unprecedented δ-CR-EOMCC(2,3) computations showing that the previously postulated doubly excited state of azulene below the ionization threshold and mediating the 1+2'multi-photon ionization that leads to a clear Rydberg fingerprint exists [13], proving a crucial role of doubly excited states in the Rydberg fingerprint spectroscopy. We also applied CR-EOMCC(2,3) and its ground-state CR-CC(2,3) counterpart to several singlet and triplet PESs corresponding to the dissociation of the water molecule into OH and H [19], showing that the black-box CR-CC(2,3) and CR-EOMCC(2,3) methods are as accurate as or more accurate than the expert MRCC approaches [19].

We have continued applying our CR-CC methods to important chemical problems relevant to combustion and catalysis, including accurate modeling of JP-10 (*exo*-tetrahydrodicyclopentadiene) high temperature oxidation, which has benefitted from the use of CR-CC(2,3) [5], and unprecedented scalar relativistic CR-CC(2,3) computations for the aerobic oxidation of methanol to formic acid on the Au_8^- nano-particles [15]. In the latter case, we did not only obtain a definitive description of the relevant catalytic reaction pathway, but we also used the CR-CC(2,3) results to benchmark representative DFT approaches, demonstrating that many of them fail. In the same spirit, we used parallel CCSD(T) codes in GAMESS based on our algorithms to evaluate the performance of various DFT

functionals in the examination of reaction mechanisms of Cu(I)-catalyzed indole synthesis and click chemistry of iodoalkynes and azides [16]. We have also helped to incorporate CR-CC(2,3), as a substitute for CCSD(T), into a correlation consistent composite approach (ccCA) for thermodynamic properties and reaction paths [8]. The new ccCA-CC(2,3) method, implemented in GAMESS, produces a mean absolute deviation of 1.7 kcal/mol for predicted heats of formation at 298 K, based on calibration with the G2/97 set of 148 molecules, while significantly improving the performance of the CCSD(T)-based ccCA approaches in calculations for the more demanding radical and biradical species [8]. We also used our EOMCCSD codes, along with the MC-QDPT2 approach and TDDFT, to provide insights into the electronic structure of the low-lying excited states of methylcobalamin, showing that its S_1 state should be interpreted as a metal-to-ligand charge transfer transition [11].

Some additional algorithmic advances in the reporting period include the development of efficient parallel numerical derivatives for fast geometry optimizations and vibrational frequency calculations at any level of CC/EOMCC theory through the utilization of modern multi-node, multi-core computer architectures. We used the resulting codes, combined with a parallel implementation of CCSD(T) in GAMESS, to optimize the geometries of the low-energy structures of the neutral Au_8 particle, answering one of the key questions in catalysis involving smaller gold nano-particles, which is their planar vs. non-planar shape [14]. We examined the effects of geometry relaxation at the high *ab initio* CCSD(T) level and of the combined effects of the basis set and core-valence correlations, comparing the results with MP2 and DFT. Our best CCSD(T) computations favor the planar configuration of Au_8, with the next three non-planar structures separated by 4–6 kcal/mol [14]. We also demonstrated how our CR-CC ideas and algorithms, developed in the context of quantum chemistry, can be used to extend the CC theory with singles, doubles, and a non-iterative treatment of triples to the three-body interactions emerging in the nuclear structure considerations [17].

We have continued our work on the development and applications of the local correlation CCSD, CCSD(T), and CR-CC(2,3) approaches, and their multi-level extensions, which exist under the common term of 'cluster-in-molecule' (CIM) methods [9]. The resulting CIM-CCSD, CIM-CCSD(T), and CIM-CR-CC(2,3) methods, and their CIM-MP*n* analogs enable high-accuracy calculations for systems with hundreds of correlated electrons. Our CIM-CC and CIM-MP2 codes in GAMESS were officially released in May 2013. They are characterized by the linear scaling of the CPU time with the system size, when a single-level CIM-CC or CIM-MP2 approach is used, memory requirements that do not grow with the size of the system, coarse-grain parallelism, which can be further enhanced by the fine-grain parallelism of each CIM subsystem calculation, and the purely non-iterative character of the local triples and other perturbative corrections to correlation energy. They enable one to fuse high- and low-level CC and MP*n* calculations without splitting large molecular systems into *ad hoc* fragments and saturating dangling bonds. Among the most successful recent applications of the CIM methodology are the unprecedented CR-CC(2,3)-level calculations for the Co-methyl bond dissociation in methylcobalamin [9]. Our local CIM-CR-CC(2,3) method combined with canonical CCSD allowed us to produce the entire Co-methyl bond breaking curve and the dissociation energy of 37-38 kcal/mol, where experiment gives 37±3 or 36±4 kcal/mol. DFT gave all kinds of values between -2 and 41 kcal/mol and the largest MR-level CASPT2 calculation we could afford 54 kcal/mol [9].

III. Immediate Future Plans (2014/2015)

- Development of the active-space DEA and DIP EOMCC methods by examining various ways of selecting 3p1h/3h1p and 4p2h/4h2p excitations to further lower computer costs.
- Further development of the CC(*P*;*Q*) formalism, particularly, the CC(t;3) approach for excited states and the CC(t,q;3) and CC(t,q;3,4) methods with connected triple and quadruple excitations.
- New studies of radical, biradical, and catalytic reactions and electronic and photo-detachment spectra, including systems relevant to combustion and nano-particles and complexes relevant to catalysis.

IV. Publications supported by DOE: 2011 – present (April 3, 2014)

[1] G. Fradelos, J.J. Lutz, T.A. Wesołowski, P. Piecuch, M. Włoch, "Embedding vs Supermolecular Strategies in Evaluating the Hydrogen-Bonding-Induced Shifts of Excitation Energies," *J. Chem. Theory Comput.* **7**, 1647-1666 (2011).

[2] J.A. Hansen, P. Piecuch, J.J. Lutz, J.R. Gour, "Geometries and Adiabatic Excitation Energies of the Low-Lying Valence States of CNC, C_2N, N_3, and NCO Studied with the Electron-Attached and Ionized Equation-of-Motion Coupled-Cluster Methodologies," *Phys. Scr*. **84**, 028110 (2011) (17 pp).
[3] G. Fradelos, J.J. Lutz, T.A. Wesołowski, P. Piecuch, M. Włoch, "Shifts in Excitation Energies Induced by Hydrogen Bonding: A Comparison of the Embedding and Supermolecular Time-Dependent Density Functional Theory Calculations with the Equation-of-Motion Coupled-Cluster Results," in: *Progress in Theoretical Chemistry and Physics*, Vol. 22, edited by P.E. Hoggan, E. Brändas, J. Maruani, P. Piecuch, and G. Delgado-Barrio (Springer, Dordrecht, 2012), pp. 219-248.
[4] M. Ehara, P. Piecuch, J.J. Lutz, J.R. Gour, "Symmetry-Adapted-Cluster Configuration-Interaction and Equation-of-Motion Coupled-Cluster Studies of Electronically Excited States of Copper Tetrachloride and Copper Tetrabromide Dianions," *Chem. Phys*. **399**, 94-110 (2012).
[5] G.R. Magoon, J. Aguilera-Iparraguirre, W.H. Green, J.J. Lutz, P. Piecuch, H.-W. Wong, O.O. Oluwole, "Detailed Chemical Modeling of JP-10 (*exo*-tetrahydrodicyclopentadiene) High Temperature Oxidation: Exploring the Role of Biradical Species in Initial Decomposition Steps," *Int. J. Chem. Kin*. **44**, 179-193 (2012).
[6] J. Shen, P. Piecuch, "Biorthogonal Moment Expansions in Coupled-Cluster Theory: Review of Key Concepts and Merging the Renormalized and Active-Space Coupled-Cluster Methods," *Chem. Phys.* **401**, 180-202 (2012).
[7] J. Shen, P. Piecuch, "Combining Active-Space Coupled-Cluster Methods with Moment Energy Corrections via the CC(*P*;*Q*) Methodology, with Benchmark Calculations for Biradical Transition States," *J. Chem. Phys.* **136**, 144104 (2012) (16 pp).
[8] S.A. Nedd, N.J. De Yonker, A.K. Wilson, P. Piecuch, M.S. Gordon, "Incorporating a Completely Renormalized Coupled Cluster Approach into a Composite Method for Thermodynamic Properties and Reaction Paths," *J. Chem. Phys.* **136**, 144109 (2012) (13 pp).
[9] P.M. Kozłowski, M. Kumar, P. Piecuch, W. Li, N.P. Bauman, J.A. Hansen, P. Lodowski, M. Jaworska, "The Cobalt-Methyl Bond Dissociation in Methylcobalamin: New Benchmark Analysis Based on Density Functional Theory and Completely Renormalized Coupled-Cluster Calculations," *J. Chem. Theory Comput.* **8**, 1870-1894 (2012).
[10] J. Shen, P. Piecuch, "Merging Active-Space and Renormalized Coupled-Cluster Methods via the CC(P;Q) Formalism, with Benchmark Calculations for Singlet-Triplet Gaps in Biradical Systems," *J. Chem. Theory Comput.* **8**, 4968-4988 (2012).
[11] K. Kornobis, N. Kumar, P. Lodowski, M. Jaworska, P. Piecuch, J.J. Lutz, B.M. Wong, P.M. Kozłowski, "Electronic Structure of the S_1 State in Methylcobalamin: Insight from CASSCF/MC-XQDPT2, EOM-CCSD, and TD-DFT Calculations," *J. Comp. Chem.* **34**, 987-1004 (2013).
[12] J. Shen, P. Piecuch, "Doubly Electron-Attached and Doubly Ionized Equation of- Motion Coupled-Cluster Methods with 4-particle-2-hole and 4-hole-2-particle Excitations and their Active-Space Extensions," *J. Chem. Phys.* **138**, 194102 (2013) (16 pp).
[13] P. Piecuch, J.A. Hansen, D. Staedter, S. Faure, V. Blanchet, "Communication: Existence of the Doubly Excited State that Mediates the Photoionization of Azulene," *J. Chem. Phys.* **138**, 201102 (2013) (4 pp).
[14] J.A. Hansen, P. Piecuch, B.G. Levine, "Communication: Determining the Lowest-Energy Isomer of Au_8: 2D, or not 2D," *J. Chem. Phys.* **139**, 091101 (2013) (4 pp).
[15] J.A. Hansen, M. Ehara, P. Piecuch, "Aerobic Oxidation of Methanol to Formic Acid on Au_8^-: Benchmark Analysis Based on Completely Renormalized Coupled-Cluster and Density Functional Theory Calculations," *J. Phys. Chem. A* **117**, 10416-10427 (2013).
[16] C.E.P. Bernardo, N.P. Bauman, P. Piecuch, P.J. Silva, "Evaluation of Density Functional Methods on the Geometric and Energetic Descriptions of Species Involved in Cu^+-Promoted Catalysis," *J. Mol. Model.* **19**, 5457-5467 (2013).
[17] S. Binder, P. Piecuch, A. Calci, J. Langhammer, P. Navrátil, R. Roth, "Extension of Coupled-Cluster Theory with a Non-iterative Treatment of Connected Triply Excited Clusters to Three-Body Hamiltonians," *Phys. Rev. C* 88, 054319 (2013) (21 pp).
[18] J. Shen, P. Piecuch, "Doubly Electron-Attached and Doubly Ionised Equation-of-Motion Coupled-Cluster Methods with Full and Active-Space Treatments of 4-particle-2-hole and 4-hole-2-particle Excitations: The Role of Orbital Choices," *Mol. Phys.* **112**, 868-885 (2014).
[19] J.J. Lutz, P. Piecuch, "Performance of the Completely Renormalized Equation-of-Motion Coupled-Cluster Method in Calculations of Excited-State Potential Cuts of Water," *Comput. Theor. Chem.*, submitted.
[20] P. Piecuch, M. Włoch, J.R. Gour, W. Li, J.J. Lutz, "Dealing with Chemical Reaction Pathways and Electronic Excitations in Molecular Systems via Renormalized and Active-Space Coupled-Cluster Methods," in: AIP Conf. Proc., edited by T.E. Simos and G. Maroulis, in press.

Kinetic Modeling of Combustion Chemistry

W.J. Pitz and C. K. Westbrook
Physical and Life Sciences Directorate
Lawrence Livermore National Laboratory
Livermore, CA 94550
pitz1@llnl.gov

I. Program Scope

We develop chemical kinetic reaction mechanisms to describe the combustion of hydrocarbons and biofuels. These mechanisms are validated through comparisons between computations and experiments in carefully-controlled laboratory-scale facilities including laminar flames, shock tubes, stirred reactors and rapid compression machines, and then are used to understand more complex combustion phenomena in practical engines and other combustion systems. Chemical systems and fuels are chosen for analysis because they represent practical fuels used in transportation and other energy devices. We strive to identify key reactions that need further study by DOE BES researchers. We do attempt to anticipate kinetic modeling needs of the DOE combustion community, so other researchers can have useful reaction mechanisms to use in their programs. Our resulting kinetic mechanisms are routinely available on the LLNL web page at https://www-pls.llnl.gov/?url=science_and_technology-chemistry-combustion and provide a valuable service to the combustion community.

II. Recent Progress

A. Low temperature chemistry of n-heptane

Villano et al.[1-3] have developed new *ab initio* RO_2 and QOOH reaction rate rules for a wide variety of molecular structures for C4 to C8 alkanes. Recently, the LLNL researchers have incorporated these new *ab initio* rate rules into an updated n-heptane mechanism [4]. The predictions of this model were compared to stirred reactor and rapid compression machine experiments that measured the concentrations of important intermediate species in n-heptane oxidation. The theoretically-derived rates lead to predicted ignition delay times and intermediate species concentrations that were in much better agreement with the experimental data than those of the previous mechanism. Perhaps the most important observation was that the updated rate constants provided significant improvements for the heptenes (see Fig. 1) and C5 and C6 olefin profiles.

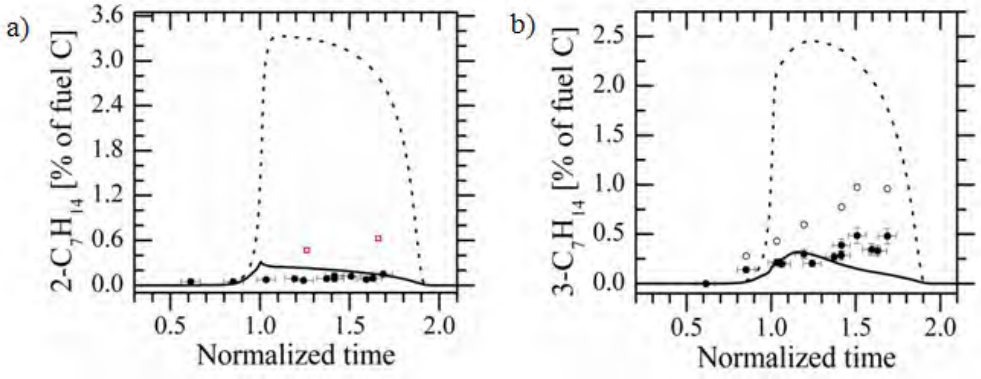

Figure 1: Concentration-time profiles for a) 2-heptene and b) 3-heptene. The symbols correspond to rapid compression machine measurements, the dotted line to the first generation LLNL heptane mechanism predictions, and the solid line to the updated heptane mechanism predictions [4].

B. Modeling of low temperature ignition of methyl cyclohexane

Cycloalkanes are important components in gasoline, jet, and diesel fuels. During the last year, LLNL researchers have updated the low temperature chemistry in their methylcyclohexane (MCH) chemical kinetic model to better predict low temperature ignition relevant to internal combustion engines. The RO_2

isomerizations rates on the cyclic ring structure were based on the *ab initio* rates computed by Zador and coworkers [5]. Recently, Davis and coworkers [6] computed an *ab initio* isomerization rate for the special case of an RO_2 isomerization from the cyclohexane ring to the methyl group and found it to be one of the fastest RO_2 isomerization rates in MCH. Using these new rate constants and many other mechanism updates [6], computed ignition delay times from the model were compared to those measured in shock tubes [7, 8] and RCMs [6].

C. New mechanism for aromatics and alkyl-benzenes

Aromatics and alkyl-aromatics are an important chemical class in gasoline, jet and diesel fuels. When present in real fuels, they play a key role in controlling ignition behavior in internal combustion engines. In collaboration with National University of Ireland, Galway (NUIG), new detailed chemical kinetic mechanisms for alkyl-benzenes were developed, including n-propyl benzene and n-butyl benzene and validated by comparison of predicted results to laminar burning velocity experiments, and ignition measurements from shock tubes and rapid compression machines [9-12]. Additionally, a mechanism for the two-ring aromatic α-methyl naphthalene (AMN) has been developed as a surrogate component to represent this chemical class in diesel fuel. The AMN mechanism was validated by comparison to flow reactor speciation data, laminar burning velocities and shock tube ignition data.

D. Surrogate mixture models for gasoline

We have developed gasoline surrogate mixture models to represent FACE [13] (Fuels for Advanced Combustion Engines) gasoline fuels. These FACE fuels represent a range of possible chemical properties of gasoline fuels. Two FACE fuels, A and C, were compared, which differed in the relative amounts of n-alkanes, iso-alkanes, and aromatics, but had the same gasoline ignition properties based on their octane numbers. Gasoline surrogate model calculations have been compared to ignition experiments in shock tubes and RCMs with encouraging results [14].

E. Biofuels/alternative fuels/oxygenated fuels

We have continued to develop detailed kinetic reaction mechanisms for large methyl esters, the largest of which are the major components of current biodiesel fuels produced from soy and rapeseed plant oils [15]. While we have published several initial reaction mechanisms, recent advances in reaction rate studies have required mechanism modifications. In particular, consideration of the *bis*-allyl CH_2 groups in methyl linoleate and methyl linolenate have been shown to affect strongly the rates of low temperature reactivities, due to the extremely low bond energy between fuel chain C atoms and both H and O_2 at these *bis*-allyl sites [16]. Continual mechanism refinements are in progress to address these effects. In addition, kinetic modeling projects have addressed oxidation and pyrolysis of smaller alkyl esters, in an attempt to improve our understanding of the kinetics of both saturated and unsaturated methyl esters.

Future Work

We will continue to incorporate into our mechanisms more accurate reaction rate constants and product paths becoming available from fundamental theoretical and experimental studies. These changes will be validated by comparing predictions from the updated mechanisms with fundamental combustion data from shock tubes, laminar flames, rapid compression machines, stirred reactors and flow reactors.

Acknowledgements: This work was performed under the auspices of the U.S. Department of Energy by Lawrence Livermore National Laboratory under Contract DE-AC52-07NA27344.

III. References

1. S. M. Villano, H.-H. Carstensen, A. M. Dean, The Journal of Physical Chemistry A (2013).
2. S. M. Villano, L. K. Huynh, H. H. Carstensen, A. M. Dean, J. Phys. Chem. A 116 (21) (2012) 5068-5089.
3. S. M. Villano, L. K. Huynh, H.-H. Carstensen, A. M. Dean, The Journal of Physical Chemistry A 115 (46) (2011) 13425-13442.

4. See Paper 8 in Section IV below.
5. R. X. Fernandes, J. Zador, L. E. Jusinski, J. A. Miller, C. A. Taatjes, Physical Chemistry Chemical Physics 11 (9) (2009) 1320-1327.
6. B. W. Weber, W. J. Pitz, M. Mehl, E. J. Silke, A. C. Davis, C.-J. Sung, Combust. Flame (2014).
7. S. S. Vasu, D. F. Davidson, Z. Hong, R. K. Hanson, Energy & Fuels 23 (1) (2009) 175-185.
8. J. Vanderover, M. A. Oehlschlaeger, Int. J. Che
m. Kinet. 41 (2) (2009) 82-91.
9. See Paper 5 in Section IV below.
10. See Paper 6 in Section IV below.
11. See Paper 7 in Section IV below.
12. M. Mehl, O. Herbinet, P. Dirrenberger, R. Bounaceur, P.-A. Glaude, F. Battin-Leclerc, W. J. Pitz, Proceedings of The Combustion Insitute (2014) Accepted for presentation.
13. FACE, *CRC Fuels for Advanced Combustion Engines Working Group (FACE)*, http://www.crcao.org/publications/advancedVehiclesFuelsLubricants/FACE/index.html, 2013.
14. S. M. Sarathy, G. Kukkadap, M. Mehl, W. Wang, T. Javed, S. Park, M. A. Oehlschlaeger, A. Farooq, W. J. Pitz, C.-J. Sung, Proc. Combust. Inst. Submitted (accepted for presentation) (2014).
15. C. K. Westbrook, C. V. Naik, O. Herbinet, W. J. Pitz, M. Mehl, S. M. Sarathy, H. J. Curran, Combust. Flame 158 (4) (2011) 742-755.
16. See Paper 15 in Section IV below.

IV. References and Journal articles supported by this project 2012-2014

1. Cai, L., Sudholt, A., Lee, D.J., Egolfopoulos, F.N., Pitsch, H., Westbrook, C.K., Sarathy, S. M., "Chemical kinetic study of a novel lignocellulosic biofuel: Di-n-butyl ether oxidation in a laminar flow reactor and flames", Combust. Flame 161, 798-809 (2014).
2. Wang, Y.L., Lee, D.J., Westbrook, C.K., Egolfopoulos, F.N., and Tsotsis, T.T., "Oxidation of Small Alkyl Esters in Flames", Combust. Flame 161, 810-817 (2014).
3. Sarathy, S. M., Javed, T., Karsenty, F., Heufer, A., Wang, W., Park, S., Elwardany, A., Farooq, A., Westbrook, C. K., Pitz, W. J., Oehlschlaeger, M. A., Dayma, G., Curran, H. J. and Dagaut, P., "A Comprehensive Combustion Chemistry Study of 2,5-Dimethylhexane," Combustion and Flame (2014). http://dx.doi.org/10.1016/j.combustflame.2013.12.010
4. Weber, B. W., W. J. Pitz, M. Mehl, E. J. Silke, A. C. Davis and C.-J. Sung (2014). "Experiments and Modeling of the Autoignition of Methylcyclohexane at High Pressure." Combustion and Flame, http://dx.doi.org/10.1016/j.combustflame.2014.01.018.
5. Darcy, D., Nakamura, H., Tobin, C. J., Mehl, M., Metcalfe, W. K., Pitz, W. J., Westbrook, C. K. and Curran, H. J., (2014). "An Experimental and Modeling Study of a Surrogate Mixtures of n-Propyl-

and n-Butylbenzene in n-Heptane to Simulate n-Decylbenzene Ignition," Combustion and Flame, http://dx.doi.org/10.1016/j.combustflame.2013.12.006.
6. Darcy, D., Nakamura, H., Tobin, C. J., Mehl, M., Metcalfe, W. K., Pitz, W. J., Westbrook, C. K. and Curran, H. J., "A High-Pressure Rapid Compression Machine Study of n-Propylbenzene Ignition," Combustion and Flame 161 (1) (2014) 65-74.
7. Nakamura, H., Darcy, D., Mehl, M., Tobin, C. J., Metcalfe, W. K., Pitz, W. J., Westbrook, C. K. and Curran, H. J., "An Experimental and Modeling Study of Shock Tube and Rapid Compression Machine Ignition of n-Butylbenzene/Air Mixtures," Combustion and Flame 161 (1) (2014) 49-64.
8. Karwat, D. M. A., Wagnon, S. W., Wooldridge, M. S. and Westbrook, C. K., "Low-Temperature Speciation and Chemical Kinetic Studies of n-Heptane," Combustion and Flame 160 (12) (2013) 2693-2706.
9. Prager, J., Najm, H. N., Sargsyan, K., Safta, C. and Pitz, W. J., "Uncertainty Quantification of Reaction Mechanisms Accounting for Correlations Introduced by Rate Rules and Fitted Arrhenius Parameters," Combustion and Flame 160 (9) (2013) 1583-1593.
10. Veloo, P.S., Dagaut, P., Togbe, C., Dayma, G., Sarathy, S.M., Westbrook, C.K., Egolfopoulos, F.N., "Experimental and Modeling Study of the Oxidation of n- and iso-Butanal", Combust. Flame 160, 1609-1626 (2013).
11. Westbrook, C.K., "Combustion of Biodiesel Fuel Made from Soybean Oil", Ch. 16 in Soy: Nutrition, Consumption and Health", Aamir Ahmad, editor. New York: Nova Science Publishers, Inc., 2013.
12. Sarathy, S.M., Niemann, U., Yeung, C., Gehmlich, R., Westbrook, C.K., Plomer, M., Luo, Z., Mehl, M., Pitz, W.J., Seshadri, K., Thomson, M.J., and Lu, T., "A counterflow diffusion flame study of branched octane isomers", Proc. Combust. Inst. 34, 1015-1023 (2013).
13. Liu, N., Sarathy, S.M., Westbrook, C.K., and Egolfopoulos, F.N., "Ignition of non-premixed counterflow flames of octane and decane isomers", Proc. Combust. Inst. 34, 903-910 (2013).
14. MacDonald, M.E., Davidson, D.F., Hanson, R.K., Pitz, W.J., Mehl, M., and Westbrook, C.K., "Formulation of an RP-1 pyrolysis surrogate from shock tube measurements of fuel and ethylene time histories", Fuel 103 (2013) 1051-1509.
15. Westbrook, C. K., Pitz, W. J., Sarathy, S. M. and Mehl, M., "Detailed Chemical Kinetic Modeling of the Effects of C-C Double Bonds on the Ignition of Biodiesel Fuels," Proceedings of The Combustion Institute, 34 (2) (2013) 3049-3056.
16. B. Yang, C. K. Westbrook, T. A. Cool, N. Hansen and K. Kohse-Höinghaus, "Photoionization mass spectrometry and modeling study of premixed flames of three unsaturated $C_5H_8O_2$ esters," *Proc. Combust. Inst.* 34 (1) (2013) 443-451.
17. Campbell, M. F., Davidson, D. F., Hanson, R. K. and Westbrook, C. K., "Ignition Delay Times of Methyl Oleate and Methyl Linoleate Behind Reflected Shock Waves," Proceedings of the Combustion Institute 34 (1) (2013) 419-425.
18. Sarathy, S.M., Park, S., Weber, B.W., Wang, W., Veloo, P.S., Davis, A.C., Togbe, C., Westbrook, C.K., Park, O., Dayma, G., Luo, Z., Oehlschlaeger, M.A., Egolfopoulos, F.N., Lu, T., Pitz, W.J., Sung, C.-J., and Dagaut, P., "A comprehensive experimental and modeling study of iso-pentanol combustion", Combust. Flame 160, 2712-2728 (2013).
19. W. Wang, Z. Li, M. A. Oehlschlaeger, D. Healy, H. J. Curran, S. M. Sarathy, M. Mehl, W. J. Pitz and C. K. Westbrook, "An experimental and modeling study of the autoignition of 3-methylheptane," Proc. Combust. Inst. 34 (1) (2013) 335-343.
20. MacDonald, M.E., Davidson, D.F., Hanson, R.K., Pitz, W.J., Mehl, M., and Westbrook, C.K., "Formulation of an RP-1 pyrolysis surrogate from shock tube measurements of fuel and ethylene time histories", Fuel 103 (2013) 1051-1509.
21. Keromnes, A., Metcalfe, W. K., Heufer, K. A., Donohoe, N., Das, A. K., Sung, C. J., Herzler, J., Naumann, C., Griebeld, P., O. Mathieue, Krejci, M. C., Petersen, E. L., Pitz, W. J. and Curran, H. J., "An Experimental and Detailed Chemical Kinetic Modelling Study of Hydrogen and Syngas Mixtures at Elevated Pressures," Combustion and Flame 160 (6) (2013) 995-1011.

INVESTIGATION OF NON-PREMIXED TURBULENT COMBUSTION

Grant: DE-FG02-90ER14128

Stephen B. Pope & Perrine Pepiot
Sibley School of Mechanical & Aerospace Engineering
Cornell University
Ithaca, NY 14853
s.b.pope@cornell.edu, pp427@cornell.edu

1 Scope of the Research Program

The focus of the current work is on the development of computational approaches which allow our detailed knowledge of the chemical kinetics of combustion to be applied to the modeling and simulation of combustion devices. The principal modeling approaches used are large-eddy simulation (LES) to describe the flow and turbulence, and probability density function (PDF) methods to treat the turbulence-chemistry interactions. The chemistry is handled efficiently using different combinations of *in situ* adaptive tabulation (ISAT), rate-controlled constrained equilibrium (RCCE), and directed relation graphs with error propagation (DRG-EP). In the past year, the research has focused on the development of a methodology for adaptive chemistry, and on the investigation of different RCCE implementations in the framework of adaptive chemistry.

2 Recent Progress

The principal research results from this program are described in the publications listed in Section 4. The following subsections detail the progress made on the focused topics mentioned above.

2.1 An Adaptive Methodology to Implement Detailed Chemistry in LES/PDF

The basic observation motivating adaptive chemistry is that, in any small region of the composition space, many species have negligible concentration, and only a few are chemically active. Hence, the chemistry in the small region can be described by a kinetic model involving many fewer species and reactions than a more detailed model applicable over the entire composition space. In Liang *et al.* (Proceedings of the 8th U.S. National Combustion Meeting, 2013, corresponding paper in preparation), we proposed a novel adaptive chemistry strategy specifically designed for LES/particle PDF simulations of non-premixed turbulent flames with the following key ingredients: (i) using a recursive cutting plane algorithm, the composition space is partitioned *a priori* into a user-specified number of regions, over which suitable reduced chemical representations and chemical models are identified; (ii) in contrast to the vast majority of published adaptive chemistry strategies, the computational particles used in the PDF framework carry only the variables present in the reduced representations, also referred to as "active" species; and (iii) the region to which a given particle belongs is identified using a low-dimensional binary tree search algorithm, thereby keeping the run-time overhead associated with the adaptive approach to a minimum. The feasibility of the adaptive

approach was successfully demonstrated for propane/air non-premixed flame in a partially stirred reactor (PaSR) with pair-wise mixing.

For this preliminary assessment of our strategy, chemistry simplification was carried out based on both species and reaction eliminations, using the Directed Relation Graph with Error Propagation (DRGEP, [1]) method. Typical results are displayed in Fig. 1, showing that:

- For a given model size, the root-mean-square (rms) errors introduced in the PaSR particle compositions due to the reduction were much smaller in the adaptive case, compared to the standard, non-adaptive approach (Fig. 1, blue and red solid lines with open symbols.)
- The computational overhead of the additional steps required by the adaptive procedure, namely identifying the correct reduced model to use (classification) and mapping particle compositions from one model to another (conversion) is *negligible* compared to the PaSR mixing and reaction steps. This is illustrated in Fig. 1 by the alignement of the blue (non-adaptive) and red (adaptive) dotted lines with filled symbols: the gain in computational time scales linearly with the number of active species in both cases.
- For the conditions tested, and when using the conventional, non-adaptive approach, there exists a critical model size below which no burning solution can be obtained in the PaSR. No such critical threshold is observed when the adaptive treatment is adopted, and much smaller models can be used while maintaining rms error at acceptable levels (around 1%).
- For a given rms error tolerance, using a more refined partition of the composition space (and therefore, a larger library of reduced models) consistently decreases the overall computational cost.

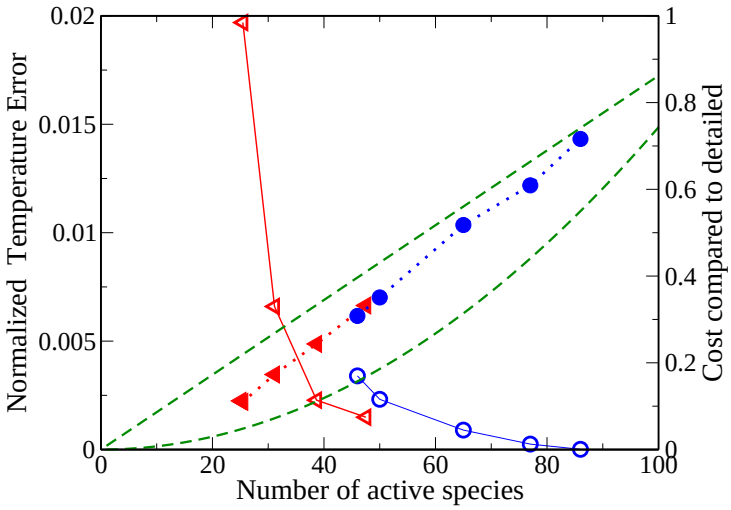

Figure 1: Comparison between non-adaptive (blue circles) and adaptive (red triangles) PaSR computations. Open symbols show rms error in temperature as function of the average model size. Filled symbols indicate computational gains compared to detailed model. Dashed lines indicate linear (top) and quadratic (bottom) cost dependency on model size.

Much effort has been devoted to optimizing the algorithms used to obtain the reduced model library, thereby enabling the extension of the technique to much larger detailed kinetic models ($\mathcal{O}(10^3)$ species). Furthermore, the adaptive strategy has been formulated to be directly compatible with previously developed dimension-reduction and tabulation techniques such as ISAT/RCCE.

2.2 Investigation of RCCE implementations in the framework of adaptive chemistry

Rate-Controlled Constrained Equilibrium (RCCE) is a thermodynamic based dimension reduction method which enables the representation of chemistry involving N_s active species in terms of fewer N_r constraints. We

focus on the application of the RCCE in the framework of adaptive chemistry, as presented above, to complement and further improve the DRGEP-based reduction technique. The cost vs. benefits of four different strategies to identify the best N_r represented species set for each reduced model in the adaptive database have been evaluated: the RCCE/GALI implementation presented in Hiremath & Pope (2011) [2], two RCCE/Greedy (A and R) algorithms, and a DRGEP-based ranking of suitable represented species. The main conclusions at this point are:

- For a given error tolerance, RCCE/GALI provides the most compact set of represented species, but at a much higher computational cost than the other methods.
- Because it is using the DREGP importance indices to choose the represented species, RCCE coupled with DRGEP is the cheapest method of all four, but retains a larger number of represented species for the same accuracy.
- RCCE/R-Greedy, which iteratively discards species from the represented species set using a simple greedy algorithm, consistently decreased the number of represented species by a factor of 2 (Fig. 2) at moderate cost, and was therefore identified as the most promising option when considering large detailed kinetic scheme.

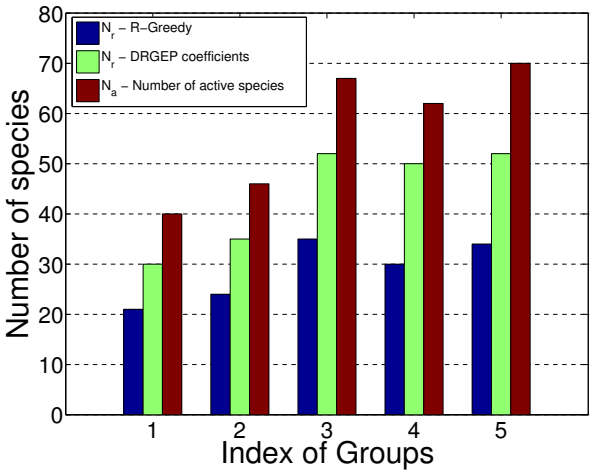

Figure 2: Number of active and represented species in each model of a small model library for adaptive propane/air non-premixed combustion. Comparison between the number of active species obtained after DREGP reduction (N_a), and the number of represented species that can be achieved using (i) RCCE/R-Greedy; and (ii) RCCE/DRGEP. An error tolerance (relative to detailed results) of 10^{-4} has been set for the selection of active species, while the errors introduced by RCCE have been capped to an additional 10^{-5}.

3 Future Plans

The work in the next year will focus on the integration of the adaptive chemistry strategy into a LES/PDF code for turbulent flame simulation, and subsequent assessment of the strategy in large scale flame computations.

4 Publications from DOE Research 2011-2013

1. D.C. Haworth and S.B. Pope (2011) "Transported Probability Density Function and Filtered Density Function Methods," in *Turbulent Combustion Modeling: Advances, New Trends and Perspectives*, eds. T. Echekki, E. Mastorakos, Springer.
2. V. Hiremath, Z. Ren and S.B. Pope (2011) "Combined Dimension Reduction and Tabulation Strategy using ISAT-RCCE-GALI for the Efficient Implementation of Combustion Chemistry", Combustion and Flame, **158**, 2113–2127.
3. S.B. Pope (2011) "Simple Models of Turbulent Flows", Physics of Fluids **23**, 011301.
4. Z. Ren, G.M. Goldin, V. Hiremath and S.B. Pope (2011) "Reduced Description of Reactive Flows with Tabulated Chemistry", Combustion Theory and Modelling, **15**, 827–848.
5. S. Viswanathan, H. Wang and S.B. Pope (2011) "Numerical Implementation of Mixing and Molecular Transport in LES/PDF Studies of Turbulent Reacting Flows", Journal of Computational Physics, **230** 6916–6957.
6. V. Hiremath, S.R. Lantz, H. Wang and S.B. Pope (2012) "Computationally-Efficient and Scalable Parallel Implementation of Chemistry in Simulations of Turbulent Combustion", Combustion and Flame, **159**, 3096–3109.
7. A.Y. Klimenko and S.B. Pope (2012) "Propagation Speed of Combustion and Invasion Waves in Stochastic Simulations with Competitive Mixing, Combustion Theory and Modelling, **16**, 679–714.
8. V. Hiremath, S.R. Lantz, H. Wang and S.B. Pope (2013) "Large-Scale Parallel Simulations of Turbulent Combustion using Combined Dimension Reduction and Tabulation of Chemistry", Proceedings of the Combustion Institute, **34**, 205–215.
9. Z. Ren, G. M. Goldin, V. Hiremath, S. B. Pope (2013) "Simulations of a Turbulent non-Premixed Flame Using Combined Dimension Reduction and Tabulation for Combustion Chemistry", Fuel, **105**, 636–644.
10. V. Hiremath and S.B. Pope (2013) "A Study of the Rate-Controlled Constrained-Equilibrium Dimension Reduction Method and its Different Implementations", Combustion Theory and Modelling, **17**, 260-293.
11. K. Narayanaswamy, P. Pepiot, and P. Pitsch. (2013) "A chemical mechanism for low to high temperature oxidation of *n*-dodecane as a component of transportation fuel surrogates." Combust. Flame, **161**, 866–884.
12. S.B. Pope (2013) "Small Scales, Many Species and the Manifold Challenges of Turbulent Combustion", Proceedings of the Combustion Institute, **34**, 1-31.
13. S.B. Pope (2013) "A model for turbulent mixing based on shadow-position conditioning", Physics of Fluids, **25**, 110803, DOI: 10.1063/1.4818981
14. P.P. Popov and S.B. Pope (2013) "Large Eddy Simulation/Probability Density Function Simulations of Bluff Body Stabilized Flames", Combustion & Flame (to be published).

References

[1] P. Pepiot and H. Pitsch, Combust. Flame **154** (2008) 67–81.

[2] V. Hiremath, Z. Ren, and S.B. Pope, Combust. Flame **158** (2011) 2113-2127.

OPTICAL PROBES OF ATOMIC AND MOLECULAR DECAY PROCESSES

S.T. Pratt
Building 200, B-125
Argonne National Laboratory
9700 South Cass Avenue
Argonne, Illinois 60439
E-mail: stpratt@anl.gov

PROGRAM SCOPE

Molecular photoabsorption, photoionization, and photodissociation dynamics can provide considerable insight into how energy and angular momentum flow among the electronic, vibrational, and rotational degrees of freedom in isolated, highly energized molecules. This project involves the study of these dynamics in small molecules, with an emphasis on understanding the mechanisms of intramolecular energy flow and determining how these mechanisms influence decay rates and product branching ratios. Such studies also provide insight into related collision processes such as dissociative recombination, providing a connection between spectroscopy and dynamics. In recent years, the project has also been aimed at understanding the factors that determine and influence photoabsorption and photoionization cross sections, as well as dissociative ionization processes. The experimental approach combines a variety of laser-based techniques, including nonlinear methods to generate tunable vacuum ultraviolet light, and double-resonance methods to prepare selected excited states of the species of interest. The detection methods include mass spectrometry, photoion- and photoelectron-imaging, and high-resolution photoelectron spectroscopy, which are used to characterize the decay processes of the selected excited states. In addition, synchrotron-based photoabsorption spectroscopy is now being used to provide high resolution spectra both above and below the ionization threshold.

RECENT PROGRESS

Photoionization studies and absolute photoionization cross sections

We are continuing to use photoion and photoelectron imaging, vacuum-ultraviolet (vuv) single-photon ionization, and resonant multiphoton ionization to probe the photodissociation dynamics of small polyatomic molecules, and to characterize the photoionization dynamics of combustion-relevant species. One aspect of this work is to determine the absolute photoionization cross sections of radicals and other reactive species. In the past year we performed a determination of the absolute photoionization cross section of the phenoxy radical, which was produced by the photodissociation of anisole. We determined the absolute photoionization cross section of the phenoxy radical at 118.2 nm (10.486 eV) relative to that of the methyl radical co-fragment. Even at this energy, there is extensive fragmentation of the phenoxy radical upon photoionization, which is attributed to ionizing transitions that populate low-lying excited electronic states of the cation. For phenoxy radicals with less than ~1 eV of internal energy, we find a cross section for the production of the phenoxy cation of 14.8 ± 3.8 Mb. For radicals with higher internal energy, dissociative ionization is the dominant process, and for internal energies of ~2.7 - 3.7 eV, we find a total cross section (photoionization plus dissociative ionization) of 22.3 ± 4.1 Mb. These values are in reasonably good agreement with the cross section estimated by using information on the cross section for phenol. We have recently performed preliminary experiments to determine the photoionization cross section of the phenyl and benzyl radicals, which can be produced by the photodissociation of iodobenzene and ethylbenzene, respectively, along with the co-fragments I and CH_3.

High-Resolution Photoabsorption Studies of Alkynes

This past year, we have initiated a new project to study the photoabsorption spectra of a series of alkyne molecules using the Fourier-transform vacuum-ultraviolet spectrometer at the Soleil Synchrotron facility. This spectrometer offers resolving powers of up to 1,000,000, with extremely high wavelength precision, as well as the ability to record both room-temperature and jet-cooled absorption spectra. The aim of this work is study shape resonant features close to the ionization threshold, and to investigate how these resonances influence the bound portion of the spectra. Because shape resonances often involve the trapping of relatively high-ℓ states (leading to enhanced core penetration by these states), they should be

manifest in the bound portion of the absorption spectrum as transitions to high-ℓ Rydberg series from the ground state. Owing to the non-penetrating nature of high-ℓ states in atoms, such transitions are generally thought to be very weak, but in molecules, the situation can clearly change. For example, in 2-butyne there is a very strong shape resonance just above the lowest ionization threshold that results from trapping of g (ℓ = 4) partial waves. This observation would suggest that transitions to ℓ = 4 Rydberg series should also be observed just below threshold. This expectation is also supported by the nodal structure of the 2-butyne ground state HOMO, which has significant f (ℓ = 3) character.

In our first beamtime at Soleil, room-temperature photoabsorption spectra were recorded in the energy range 6 - 12 eV for acetylene, propyne, 1-butyne, and 2-butyne. In addition, jet-cooled spectra with an estimated rotational temperature of ~100 K were recorded for acetylene and propyne. The analysis initially focused on the propyne spectra. In propyne, the ground state HOMO has significant d character, suggesting that transitions to nf Rydberg series might be important. However, previous work on the absorption spectrum did not seriously consider this possibility, and although there have been calculations of the excited states of propyne in the relevant energy region, these calculations ignored the possibility of nf states. [See, for example, M. H. Palmer et al., Chem. Phys. **249**, 129-144 (1999) and J. C. Shieh et al., J. Chem. Phys. **112**, 7384-7393 (2000).] To assess the role of nf states, our collaborator, R. R. Lucchese, calculated the photoabsorption cross section just above the ionization threshold, and provided a partial wave decomposition of the result. As expected, absorption to εf continua is significant, suggesting that nf series should be observed below threshold as well. Examination of the new spectra, particularly the jet-cooled results, did indeed show evidence for a previously unassigned nf Rydberg series. Going forward, the use of continuum photoabsorption cross section calculations to inform the analysis of below threshold spectra should prove useful in a variety of other systems. We are currently applying this approach to the analysis of the 1-butyne and 2-butyne data, where even higher ℓ Rydberg series are expected. A manuscript on the propyne spectra is nearly complete.

Photodissociation via the B state of methyl iodide

The photodissociation of CH_3I at 193 nm has been the source of some controversy for many years. The earliest studies using translational spectroscopy indicated the branching fraction for producing excited iodine atoms ($I\ ^2P_{1/2}$, or I*) was essentially unity [G. N. A. van Veen et al. Chem. Phys. 97, 179-186 (1985)]. However, studies using direct infrared absorption spectroscopy on the iodine atoms indicated this branching fraction was only 0.7 [W. P. Hess et al., J. Phys. Chem. 91, 6085-6087 (1987)]. A recent study reproduced this latter result, but found a quantum yield of unity when a technique using Doppler spectroscopy was employed [A. Gilchrist et al., J. Phys. Chem. A 112, 4531-4536 (2008)]. These authors suggested that the non-unity quantum yield in the absorption measurements was due to I_2 build-up in the absorption cell. On the other hand, a recent velocity map imaging study at 199.11 nm (accessing a different vibronic level of the B state) displayed convincing evidence for an I* branching fraction less than one [M. G. González et al., J. Chem. Phys. 135, 021102 (2011)]. We re-examined the photodissociation dynamics at 193 nm by using velocity map imaging and single-photon vuv ionization of the iodine atoms just above and below the $I\ ^2P_{3/2}$ ionization threshold (well above the I* threshold). Our detection sensitivity in this region is very high for the I atoms relative to the I* atoms. Using this approach, we determined a branching fraction for I* of 0.93. Surprisingly, we found that the I atoms actually had a lower velocity than the I* atoms, explaining their absence in the Doppler measurements. We are now performing a more comprehensive study of the photodissociation of CH_3I in this region.

Dissociative recombination of small polyatomic ions

In collaboration with Christian Jungen, I have continued to work on theoretical models of dissociative recombination and vibrational autoionization. In the past year, we developed some general ideas about the behavior of low-energy dissociative recombination cross sections, and we reached the conclusion that indirect dissociative recombination via electronically core-excited Rydberg states could play a significant role at relatively low collision energies (< 2-3 eV) in many larger polyatomic ions. We also began to develop some ideas about how to treat the dissociative recombination of $H_3^+ + e^-$ in a simplified manner that would also allow the treatment of individual rotational levels. This work will be pursued in the coming year.

FUTURE PLANS

I plan on continuing studies of the photodissociation and photoionization of combustion-relevant radicals by using ion-imaging techniques, vacuum-ultraviolet single-photon ionization, and resonant multiphoton ionization techniques. The studies of the absolute photoionization cross sections for the phenyl and benzyl radicals will be completed and extended to studies to other systems such as the CH_2CH_2OH, CH_2CH, and CH_3O. My postdoc, Hong Xu, and I will complete our more detailed study of the photodissociation of methyl iodide via the B state. Specifically, we are using tunable ultraviolet light between 193 nm and 200 nm and velocity map imaging to study the dependence of the photodissociation process on the specific resonances excited within the B state. We hope that this will help unravel the details of the dissociation dynamics in this prototypical system. We are also investigating two different radical sources (jet-cooled photolysis and discharge sources) to be used as sources for spectroscopic and photoionization studies of selected reactive species. We will use a combination of single-photon vuv techniques and multiphoton double-resonance techniques to study the photoionization dynamics, and in particular electronic autoionization, in some simpler systems such as N_2 and OH.

I will complete the analysis of the photoabsorption data on acetylene, 1-butyne, and 2-butyne from my initial experiments using Fourier-transform vacuum-ultraviolet spectroscopy. I have successfully applied for additional beamtime at the Soleil Synchrotron. The beamtime will be used to explore the photoabsorption spectra of larger alkyne molecules, including 1-pentyne, 2-pentyne, 1-hexyne, 2-hexyne, and 3-hexyne. In particular, the extent to which the near-threshold shape resonance observed in 2-butyne is preserved in the larger alkynes will be examined, as well as the dependence of this shape resonance on the position of the triple bond. Some evidence (for example, the comparison of 1-butyne and 2-butyne) indicates that the symmetry of the location of the triple bond is important, suggesting that the spectrum of 3-hexyne will be particularly interesting. This beamtime is scheduled for late July, 2014. I have also applied for beamtime to investigate the high-resolution, near-threshold photoionization dynamics of N_2, which would provide insight into the dynamics of electronic autoionization processes. I note that these experiments will be performed at the Soleil Synchrotron because there are currently no very high resolution beamlines (resolving power of 100,000 - 1,000,000) available for vacuum ultraviolet work in the US.

I will continue to collaborate with Christian Jungen on theoretical models of vibrational autoionization and dissociative recombination in polyatomic molecules. Our efforts will focus on an attempt to identify the resonances observed in the low-energy dissociative recombination of $H_3^+ + e^-$. Specifically, the experimental cross sections show a number of strong resonances at low energy that almost certainly must be associated with capture into specific Rydberg states based of rovibrationally excited H_3^+ in its electronic ground state. Although this is the simplest triatomic molecule, no convincing assignments of these resonances in the experimental spectrum have been made to date.

I am collaborating with the Atomic Physics Group at Argonne on a project that will be carried out at the Linac Coherent Light Source. These experiments will use a two-color, time-resolved x-ray technique to study the dynamics and electron transfer processes occurring during the relaxation following inner-shell excitation. The beamtime is scheduled for May, 2014. These experiments will be performed on xenon difluoride, and will follow the decay of a core hole generated on the Xe atom and the electronic relaxation that involves both the outer shells of the Xe atom as well as the electrons on the F atoms. These studies will make use of a unique two-color operating mode of the LCLS, and lay the groundwork for a wide range of related studies.

ACKNOWLEDGEMENTS

This work was performed in collaboration with my postdoc Hong Xu. Work at Soleil was performed in collaboration with S. Boyé-Péronne (Institut des Sciences Moléculaires d'Orsay, France), D. M. P. Holland (STFC, Daresbury, UK), U. Jacovella (ETH-Zürich, Switzerland), R. R. Lucchese (Texas A&M), and N. de Oliveira (Soleil, France). Work on dissociative recombination was performed in collaboration with Ch. Jungen (Laboratoire Aime Cotton, France). This work was supported by the U.S. Department of

Energy, Office of Science, Office of Basic Energy Sciences, Division of Chemical Sciences, Geosciences, and Biological Sciences under contract No. DE-AC02-06CH11357.

DOE-SPONSORED PUBLICATIONS SINCE 2011

1. S. T. Pratt
HIGH-RESOLUTION VALENCE-SHELL PHOTOIONIZATION
in *Handbook of High-Resolution Spectroscopies*, edited by M. Quack and F. Merkt (Wiley, New York, 2011), pp 1595-1616. (October 18, 2011).

2. S. T. Pratt and Ch. Jungen
DISSOCIATIVE RECOMBINATION OF SMALL POLYATOMIC MOLECULES
J. Phys. Conf. Ser. **300**, 012109 (8 pages) (2011).

3. V. A. Shubert and S. T. Pratt
PHOTOELECTRON IMAGING OF SEVERAL 5d AND 6p RYDBERG STATES Xe_2 AND IMPROVING THE Xe_2^+ I(1/2g) POTENTIAL
J. Chem. Phys. **134**, 044315 (12 pages) (2011).

4. N. Thiré, R. Cireasa, D. Staedter, V. Blanchet, and S. T. Pratt
TIME-RESOLVED PREDISSOCIATION OF THE VIBRATIONLESS LEVEL OF THE B STATE OF CH_3I
Phys. Chem. Chem. Phys. **13**, 18485-18496 (2011).

5. V. Alvin Shubert and S. T. Pratt
PHOTOELECTRON IMAGING OF AUTOIONIZING STATES OF XENON: THE EFFECT OF EXTERNAL ELECTRIC FIELDS
Phys. Rev. A, **84**, 053413 (10 pages) (2011).

6. H. Xu, U. Jacovella, B. Ruscic, S. T. Pratt, and R. R. Lucchese
NEAR-THRESHOLD SHAPE RESONANCE IN THE PHOTOIONIZATION OF 2-BUTYNE
J. Chem. Phys., **136**, 154303 (10 pages) (2012).

7. Ch. Jungen, M. Jungen, and S. T. Pratt
THE JAHN-TELLER EFFECT IN THE 3pe' RYDBERG STATE OF H_3. REVIEW OF EXPERIMENTAL AND AB INITIO DETERMINATIONS
Phil. Trans. Roy. Soc. London, **370**, 5074-5087 (2012).

8. S. T. Pratt and Ch. Jungen
THE ISOTOPE DEPENDENCE OF DISSOCIATIVE RECOMBINATION VIA THE INDIRECT MECHANISM
J. Chem. Phys. **137**, 174306 (6 pages) (2012).

9. H. Xu and S. T. Pratt
THE PHOTOIONIZATION CROSS SECTION OF PROPARGYL RADICAL AND SOME GENERAL IDEAS FOR ESTIMATING RADICAL CROSS SECTIONS
J. Phys. Chem. A **117**, 9331-9342 (2013).

10. H. Xu and S. T. Pratt
THE PHOTODISSOCIATION OF ANISOLE AND THE ABSOLUTE PHOTOIONIZATION CROSS SECTION OF THE PHENOXY RADICAL
J. Phys. Chem. A **117**, 12075-12081 (2013).

11. H. Xu and S. T. Pratt
A NEW LOOK AT THE PHOTODISSOCIATION OF METHYL IODIDE AT 193 NM
J. Chem. Phys. **139**, 214310 (2013).

Photoinitiated Reactions of Radicals and Diradicals in Molecular Beams

Hanna Reisler
Department of Chemistry, University of Southern California
Los Angeles, CA 90089-0482
reisler@usc.edu

Program Scope

Open shell species such as radicals and diradicals are central to reactive processes in combustion and environmental chemistry. Our program is concerned with photoinitiated reactions of hydroxyalkyl radicals and carbenes. The goal is to investigate the detailed dynamics of dissociation of free radicals and diradicals in which multiple pathways participate, including molecular rearrangements, and compare them with high-level calculations. Studies include unimolecular reactions on the ground state as well as photodissociation dynamics on excited Rydberg and valence states that involve multiple potential energy surfaces.

Recent Progress

Excited States of the Hydroxymethylene Radical (HCOH, HCOD)

Our current experiments on the photodissociation of the hydroxymethyl radical focus on the hydroxymethylene product, an elusive intermediate implicated in the unimolecular decomposition of formaldehyde. We provide new information on the *trans*- and *cis*-isomers of HCOH(D) with internal energies that extend all the way up to and above their dissociation thresholds to H(D) + H(D)CO. We also determine the singelt-triplet gap in HCOH. This information is derived from sliced velocity map imaging experiments, in which we measure the velocity distributions of H and D photofragments. Below we summarize our major findings.

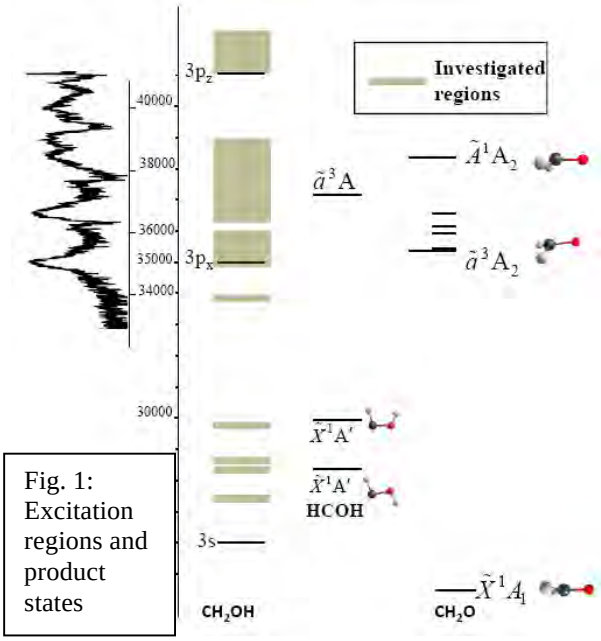

Fig. 1: Excitation regions and product states

One of the advantages of using the hydroxymethyl radical as a source of hydroxymethyelene is that it has continuous absorption over a broad wavelength range, and thus the internal energy of HCOH can be increased gradually. Figure 1 shows the excitation energies that were interrogated so far, which include regions on the 3s, 3p$_x$ and 3p$_z$ surfaces of $CH_2OH(D)$. Absorption to 3s is structureless, whereas absorption to 3p$_x$ exhibits broad vibronic bands, and the vibronic bands of 3p$_z$ are much sharper (See Figure 1, left panel; the origin band of 3p$_z$ is the sharp line at the very top). By monitoring the velocity and kinetic energy release (KER) of H photofragments generated by C-H bond breaking we gain information on HCOH(D) products.

Near the threshold of breaking the C-H bond of $CH_2OH(D)$, we observe a small new feature at low KEs region, which is correlated with formation of HCOH(D). The lowest energy isomer is *trans*-HCOH and it appears first but with low yield. The yields of both *trans*- and *cis*-HCOH remain relatively low until the origin band of the 3p$_x$ state is reached. At this energy, which is above the calculated barrier for the conical intersection leading to C-H bond breaking,

[1] the yield increases sharply, the rotational excitation of the products *decreases*, and it is possible to establish that the dominant product is the *cis* isomer. The distinction between the *cis* and *trans* isomers becomes clearer when using different H/D isotopologs, because their vibrational frequencies are different. This can be seen in Figure 2, which displays H/D photofragment KER plots correlated with hydroxymethylene. The H signal correlated with HCOH exhibits good vibrational resolution, and shows the ground vibrational state of *trans*-HCOH and the ground and first vibrational levels of *cis*-HCOH. The D signal correlated with DCOD, on the other hand, has the best separation between the ground states of the *trans* and *cis* isomers, but the vibrational states of *cis*-DCOD are clustered together and cannot be resolved. The preference for generating the higher-lying *cis* isomer in CH_2OH photodissociation has been predicted by Yarkony [1]. The observed~ 1550 cm^{-1} *cis-trans* separation in HCOH is very close to the calculated value [2]. We note that this is the first time that the *cis* isomer of hydroxymethylene has been observed.

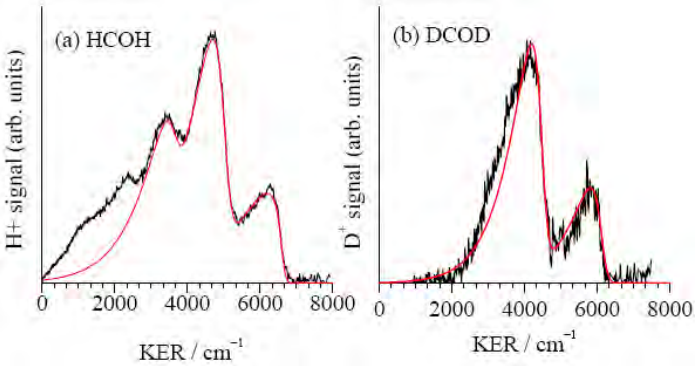

Fig. 2: KER plots (black curves) obtained from images in which the low KE region was expanded to fill the detector. Excitation to the origin band of the $3p_x$ transition (35,053 cm^{-1}) was used in (a) CH_2OH, and (b) CD_2OD. The red curves show best fits using vibrational levels of *trans* and *cis* hydroxymethylene. The two highest KE peaks are assigned as the ground states of the *trans* and *cis* isomers. The next peak in part (a) is fit by assuming excitation to the CO stretch ν_4 of HCOH(D).

Next we increased the $CH_2OH(D)$ excitation energy to regions where the triplet states of formaldehyde and hydroxymethelene were accessible (see Figure 1). The triplet state of H_2CO is well characterized, and indeed we are able to identify its vibrationless and 4^2 levels in the H photofragment velocity distribution from CH_2OH (Figure 3).

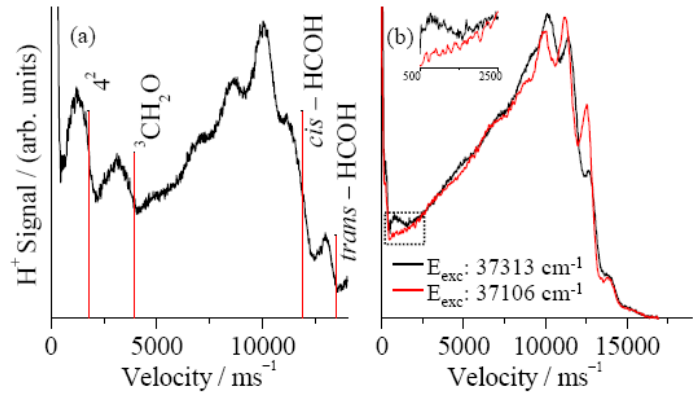

Fig. 3. (a) H fragment velocity distribution obtained in the photodissociation of CH_2OH above the energetic threshold for formation of triplet formaldehyde. (b) Comparison of H fragment velocity distributions obtained in the photodissociation of CH_2OD just below (red) and just above (black) the calculated threshold for triplet HCOD. The inset shows the expanded low-velocity region, which highlights the appearance of the new feature. The sliced velocity map images were taken such that only the velocity region correlated with HCOH(D) is recorded.

The situation is much less clear when searching for the triplet state of HCOH. Note that whereas the S-T gap in formaldehyde is ~25,194 cm^{-1}, the corresponding gap for HCOH is only ~ 8700 cm^{-1} [3], and thus any new peak must rise above a substantial background of high vibrational levels of *cis*-HCOH(D). Our experiment indeed shows a small new feature rising above a fairly large background at CH_2OD excitation energy just above the expected threshold

for the triplet state of HCOD (Figure 3). The observed threshold is assigned tentatively as the triplet state of HCOD, which gives $\Delta E_{S-T} = 8817 \pm 200$ cm^{-1} (25.21 kcal/mol), in good agreement with calculations [3]. Unfortunately, higher vibrational levels of triplet HCOD could not be resolved, but it appears that the fraction of triplet products increases with increasing excitation energy.

Lastly, we investigated the fate of the HCOD radicals when their internal energy exceeded their dissociation energy. In the photodissociation of CH_2OD the two product isomers, H_2CO and HCOD, are generated with similar yields, and we can follow their subsequent dissociation by observing the appearance of low-KE D and H fragments generated when the internal energies of the molecular products exceed their dissociation energies to H(D) + D(H)CO (Figure 4). Both H and D KEDs show new, low KE features that first appear at energies corresponding to dissociation of "hot" photofragments. These features grow in intensity and expand in kinetic energy with further increase in the dissociation energy. The KED plots of the D fragments show that the H_2CO co-fragments have only a very small component with internal energies high enough to allow for secondary dissociation (right panel of Figure 4), and therefore H_2CO contributes only a minor fraction to the slow H fragments. On the other hand, a considerable fraction of HCOD fragments has sufficient internal energy to dissociate (left panel of Figure 4), and these fragments appear to be the major source of secondary dissociation to H and D atoms. Because we see both slow H and D products with comparable populations, the most plausible dissociation mechanism is first isomerization of HCOD to HDCO followed by dissociation: HCOD → HDCO → H/D + H/DCO. Bowman and coworkers have calculated a global potential energy surface for the H_2CO/HCOH system, and thus it should be possible to carry out trajectory calculations starting from the HCOH global minimum to confirm the dissociation mechanism.

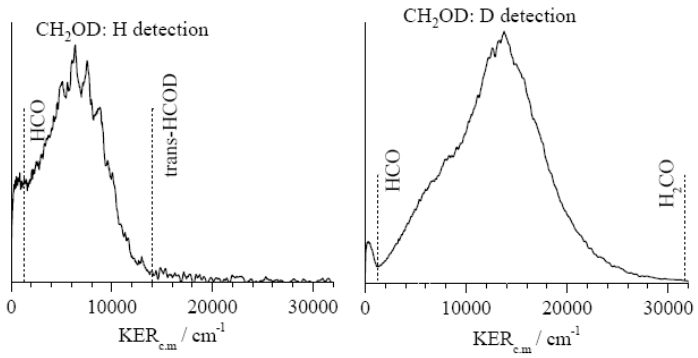

Fig. 4. KER plots of H and D fragments generated in the dissociation of CH_2OD at the 4_0^1 band of the transition to $3p_z$. The right panel shows the D signal, which is mostly correlated with H_2CO. The small peak at low KEs is correlated with secondary dissociation of HCOD to D + HCO. The left panel shows the corresponding KER obtained by monitoring H photoproducts, which is mostly correlated with HCOD. The small increase in signal at low KEs is associated with secondary dissociation to H + DCO.

Future Work

We plan to continue our H-atom sliced velocity map imaging studies by examining the photodissociation of hydroxyethyl and hydroxypropyl radicals, as well as state-specific studies of the hydroxymethelene radical. We are also planning to study how reaching different regions of the excited states affects conical intersections. This will be achieved by first exciting OH-stretch vibrations of CH_2OH and its isotopologs followed by photodissociation.

References

1. B. C. Hoffman and D. R. Yarkony, J. Chem. Phys. **116**:8300 (2002); D. R. Yarkony, J. Chem. Phys. **122**, 084316 (2005).

2. (a) L. Koziol, Y. M. Wang, B. J. Braams, J. M. Bowman, and A. I. Krylov, J. Chem. Phys. 2008, 128, 4310; (b) P. R. Schreiner, H. P. Reisenauer, F. C. Pickard, A. C. Simmonett, W. D. Allen, E. Matyus, and A. G. Csaszar, Nature 2008, 453, 906-909.

3. M. H. Matus, M. T. Nguyen and D. A. Dixon, *J. Phys. Chem. A*, 2006, **110**, 8864–8871.

Publications, 2012-2013

1. E. Kamarchik, C. Rodrigo, J.M. Bowman, H. Reisler, and A. I. Krylov, "Overtone-induced dissociation and isomerization dynamics of the hydroxymethyl radical (CH_2OH and CD_2OH). I. A theoretical study", J. Chem. Phys. 136, 084304 (2012).

2. M. Ryazanov, C. Rodrigo and H. Reisler, "Overtone-induced dissociation and isomerization dynamics of the hydroxymethyl radical (CH_2OH and CD_2OH). II. Velocity map imaging studies", J. Chem. Phys. 136, 084305 (2012).

3. M. Ryazanov and H. Reisler, "Improved sliced velocity map imaging apparatus optimized for H photofragments", J. Chem. Phys. 138, 144201 (2013).

4. C. Rodrigo, C. Zhou, and H. Reisler, "Accessing multiple conical intersections in the 3s and $3p_x$ photodissociation of the hydroxymethyl radical", J. Phys. Chem. A (Wittig Festschrift) 117, 12049-12059 (2013).

Accurate Calculations and Analyses of Electronic Structure, Molecular Bonding and Potential Energy Surfaces

Klaus Ruedenberg
Ames Laboratory USDOE, Iowa State University, Ames, Iowa, 50011
ruedenberg@iastate.edu

Scope

Theoretical treatments of molecular reactions and their kinetics require accurate potential energy surfaces in non-equilibrium regions of coordinate space. A challenge is the accurate description of the non-relativistic electron correlations in the presence of a multi-configurational dominant zeroth-order component in the electronic wave function along reaction paths. An advance towards this goal has been made through the correlation energy extrapolation by intrinsic scaling (CEEIS) method, developed in this group. By combining it with the extrapolation to the complete basis limit, potential energy curves were obtained within about 0.1 kcal/mol for ground and excited states of diatomic molecules.

Recent Work

The formalism of Correlation Energy Extrapolation by Intrinsic Scaling (CEEIS) has been extended to the simultaneously determination of several electronic states. Starting with state-averaged reference states, a state averaged first order density kernel and a state averaged virtual orbital space are determined. Each state is then independently extrapolated to approximate its complete basis set limit of the full configuration interaction. Weights introduced in the state averaging were shown to have no effect on the final CEEIS results.

With this generalized method, the potential energy curves of the four lowest lying singlet states of the C_2 molecule, *viz.* ($X^1\Sigma^+_g$, $A^1\Pi_u$, $B^1\Delta_g$ and $B'^1\Sigma^+_g$) have been obtained to high accuracy. The valence electron correlations were accounted for by the CEEIS approach. Core-valence correlation, relativistic effects and. spin-orbit coupling were added by corrections of commensurate accuracy. Spin-orbit coupling was found to be insignificant. The $B^1\Delta_g$ was found to cross the lower states. A narrowly avoided crossing exists between the $X^1\Sigma^+_g$ state and the $B'^1\Sigma^+_g$ state. The potential energy curves are displayed in the figure. The equilibrium bond distances are reproduced within 0.05%. The dissociation energies of the

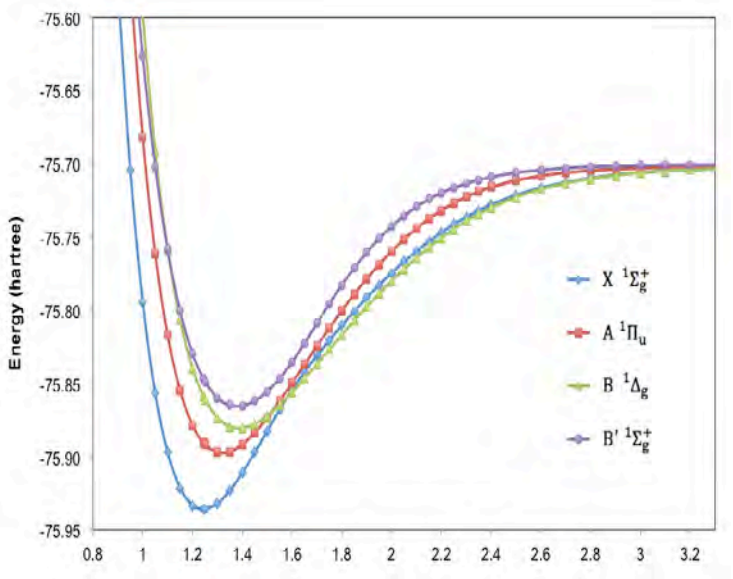

states agree with experiment to within ~0.5 kcal/mol. Spectroscopic constants exhibit very good agreement with experiment. Vibrational energy levels show average deviations of ~20 cm^{-1} or less. In the $B^1\Delta g$ state, the mean absolute deviation from experiment is 2.41 cm^{-1}. Rotational constants agree very well with experiment.

The CEEIS method is also used to obtain energies of milli-hartree accuracy for the critical points on the ground state surface (1^1A_1) of ozone, *viz*. the open equilibrium structure, the ring equilibrium structure, the transition state between these structures and the conical intersection with the next surface of like symmetry (2^1A_1), as well as the minimum of the 2^1A_1 state. The energy differences between these points on the potential energy surface are not yet known experimentally. Calculations at lower levels of correlation have yielded a range of values for them. The prediction of credible values for these energies requires therefore high accuracy calculations. Work on this system is in progress. In this context, new linear relations of the type used in the CEEIS method were discovered that pertain to the correlation contributions generated by localized orbitals.

The described work on C_2 and O_3 are joint projects of Professor Ruedenberg and Professor Theresa L. Windus at the Ames Laboratory.

An analysis of accurate calculations on the basis of the variation principle has shown that the covalent bonds in the molecules H_2^+, H_2, B_2, C_2, N_2, O_2 and F_2 result from the drive of electron waves to lower their kinetic energy by expanding in space. In particular, it has been found that this delocalization involves not only the superposition of partially filled orbitals from different atoms, but the drive towards delocalization also causes the contraction of the atomic orbitals at closer distances, even though this may seem counter-intuitive because it decreases the overlap. The fact that the intra-atomic contraction renders the molecular potential binding energy negative does not alter the facts that the total intra-atomic energy change is anti-bonding and that it is the inter-atomic kinetic delocalization energy that drives the bond formation.

Future Work

The high-accuracy CEEIS calculation on the ozone ground state and the lowest excited state of like symmetry ($^1A_1$) will be completed. Accurate potential energy curves will be determined for excited states of C_2 with higher multiplicities. Since the success of the CEEIS method appears to be based on the randomness of the small contributions from higher correlating excitations, the linear relations that have been found for correlation contributions from localized orbitals will be explored with the aim of developing CEEIS-type extrapolations within the context of many-body expansions.

Publications in 2011, 2012, 2013

Accurate potential energy curve for B_2. Ab initio elucidation of the experimentally elusive ground state rotation-vibration spectrum.
L. Bytautas, N.Matsunaga , G. Scuseria , K. Ruedenberg, *J. Phy. Chem.* A., **116**, 1717-1729 (2012)

The dispersion interaction between quantum mechanics and effective fragment potential molecules.
Q.A. Smith, K. Ruedenberg, M.S. Gordon, L.V. Slipchenko, *J. Chem. Phys*. **136**, 244107 (2012)

Three Millennia of Atoms and Molecules.
K. Ruedenberg and W.H.E. Schwarz, Invited Chapter 1, pages 1-45, in the book *Pioneers of Quantum Chemistry* (T. Strom and A. Wilson Editors, American Chemical Society, ACS Symposium Series **1122**, 2013)

Unusual Inorganic Biradicals: A Theoretical Analysis.
E. Miliordos, K. Ruedenberg, S. S. Xantheas, *Angewandte Chemie, International Edition* **52**, (Issue 22) 5736–5739 (2013)

A comprehensive analysis of molecule-intrinsic quasi-atomic, bonding, and correlating orbitals. I. Hartree-Fock wave functions.
A. C. West, M. W. Schmidt, M. S. Gordon, and K. Ruedenberg, *J. Chem. Phys*. **139**, 234107, 18 pages (2013)

Accurate ab initio potential energy curves and spectroscopic properties of the four lowest singlet states of C_2.
J. S. Boschen, D. Theis, K. Ruedenberg, T.L. Windus, *Theor Chem Acc* **33**, 1425, 12 pages

The Physical Origin of Covalent Binding.
K. Ruedenberg, M. W. Schmidt, J. Ivanic, Chapter 1, pp. 1-67 of the book *The Chemical Bond* (G. Frenking and S. Shaik Editors, Wiley-VCH, 2013) in production

Covalent bonds are created by the drive of electron waves to lower their kinetic energy by expansion.
M. W. Schmidt, J. Ivanic, K. Ruedenberg, *J. Chem. Phys*., accepted

Active Thermochemical Tables

Branko Ruscic
Chemical Sciences and Engineering Division, Argonne National Laboratory,
9700 South Cass Avenue, Argonne, IL 60439
ruscic@anl.gov

Program Scope

The *spiritus movens* of this program is the need to provide the scientific community with accurate and reliable thermochemical information on chemical species that are relevant in combustion, or play prominent roles in related post–combustion environmental chemistry. Detailed knowledge of thermodynamic parameters for a broad array of chemical stable and ephemeral species is pivotal to chemistry and essential in many industries. In particular, the availability of accurate, reliable, and internally consistent thermochemical values is a *conditio sine qua non* in kinetics, reaction dynamics, formulation of plausible reaction mechanisms, and construction of predictive models of complex chemical environments. Furthermore, the appearance of accurate thermochemical values has historically been the prime driver for steady advancement of increasingly sophisticated electronic structure theories.

The focus of this program is on bringing substantial innovations to the field of thermochemistry through the development of new methodologies, and utilizing them to systematically improve both the quality and quantity of available thermochemical data relevant to energy–producing processes. In order to achieve the stated goals, this program has developed a novel approach that is centered on analyzing and optimally utilizing the information content of *all available* thermochemically relevant determinations. The aim is not only to dynamically produce the best currently possible thermochemical parameters for the targeted chemical species, but also to allow efficient updates with new knowledge, properly propagating its consequences through all affected chemical species, as well as to provide critical tests of new experimental or theoretical data, and, when possible, to develop pointers to future determinations that are most likely to efficiently improve the overall thermochemical knowledge base. In order to provide a broad perspective of this area of science, the effort of this program is synergistically coordinated with related experimental and theoretical efforts within the Gas-phase Chemical Dynamics Group at Argonne.

Recent Progress

Over the past year we have continued the development of various methodological aspects of Active Thermochemical Tables (ATcT), together with improving both the quantity and quality of the resulting thermochemical values. ATcT are a new paradigm of how to develop thermochemical values for stable, reactive, and transient chemical species by utilizing to the fullest all available experimental measurements as well as state-of-the-art theoretical data. Intertwined dependencies that underpin virtually all thermochemistry were historically considered to be an intractable complication, leading to the adoption of a simplified sequential approach to thermochemistry (A begets B, which begets C, etc), which produces sets of values that are plagued by hidden progenitor-progeny relationships and thus are impossible to update with new knowledge without introducing serious inconsistencies. The success of ATcT is rooted in readdressing the problem of intertwined dependencies by expressing them as a network of relationships that is amenable to explicit and comprehensive mathematical and statistical manipulation. This did not merely make an intractable problem tractable, but it effectively transformed the original nuisance into a valuable asset that can be credited for the quantum leap in the quality and reliability of the resulting thermochemical values. ATcT analyzes the Thermochemical Network (TN) that (typically) involves a large number of species and attempts to bring it into self consistency by identifying determinations that have ‘optimistic’ uncertainties, and then finds a solution that maximizes the number of the underlying interdependencies that are simultaneously satisfied.

The ATcT effort has two fronts: the development of the ATcT methodology and the development of the Thermochemical Network and other thermochemically-relevant data on which ATcT operates. On the methodology front, we are in the process of exploring the capabilities of the recently developed variance/covariance decomposition procedure, which partitions the final covariance matrix into

contributions associated with individual determinations present in the TN (currently containing ~1000 species and ~15000 determinations). Though the full potentialt of this new capability is not yet clear, it currently provides an accurate account of the provenance of the optimized thermochemical value for any chosen species. In sequential thermochemistry, the provenance is typically linked to one particular determination (the 'best' available measurement). A characteristic of ATcT is that the provenances of the results are normally quite distributed, enhancing their 'robustness'. In fact, tests suggest that if the provenance analysis indicates that some ATcT value critically depends on a single determination, than that determination corresponds to a 'weak link' and the corresponding TN section should be earmarked for improvement. Current tests also suggest that provenance delocalization - one of the inherent consequences of the TN approach - reduces both the variance and covariance of the involved species, and is thus responsible for the increased accuracy and reliability compared to traditional sequential thermochemistry, even when both approaches use the exact same set of thermochemical measurements.

The new provenance analysis capability has been recently used to analyze the ATcT dissociation energies of several homonuclear diatomics that are responsible for producing the CODATA 'key' values for the enthalpies of formation of the corresponding atoms. The analysis helped in resolving a controversy surrounding the correct dissociation energy of F_2, by demonstrating that the current ATcT result is quite robust because it has a very distributed provenance, and that it is not affected at all by the recently postulated small dissociation barrier in this molecule. The conclusion is that the recent ion-pair formation threshold (that in principle would not be affected by such a barrier, but implies a higher dissociation energy, which - incidentally - would be a change in the wrong direction if the barrier were the culprit) must be in error by more than its declared uncertainty. We have further pursued this question in a theoretical collaboration with D. Feller and K. Peterson (WSU), and are currently attempting to develop an additional collaboration that will experimentally re-verify $D_0(F_2)$ by photoionization spectrometry.

Properties that are directly derived from partition functions, such as enthalpy increments, entropy, and heat capacity, depend on species-specific quantities, such as spectroscopic constants, and are largely untouched by the knowledge content encapsulated in the species-interrelating determination that are included in the TN. However, they crucially affect the conversion of ATcT enthalpies of formation from 298 K to combustion temperatures. There is every reason to believe that with the currently achieved accuracies of ATcT enthalpies of formation, the traditional run-of-the-mill RRHO (rigid rotor, harmonic oscillator) partition functions are a major and poorly controlled source of error when ATcT thermochemistry is used at combustion temperatures. We have previously reported on the development of various software tools that enable us to gradually replace the respective RRHO partition functions with NRRAO (nonrigid rotor, anharmonic oscillator) partition functions, either by including corrections for anharmonicity, centrifugal stretching, internal rotation, etc., or by replacing the related RRHO contribution with contributions obtained by level counting. We are in the process of replacing the existing partition functions with improved NRRAO versions for species involved in C_0 and C_1 mechanisms. However, we found cases where there are reasons to suspect even the improved NRRAO partition functions, particularly when the species in question has a low dissociation energy, as is typically the case for many radicals, indicating that further developments may be necessary. We have also recently explored $(H_2O)_2$ as a prototype species related to correct thermochemical description of real gases.

In an effort to accelerate the expansion of the number of species described by the TN, we are involved in a long-term collaboration with S. Klippenstein and L. Harding to systematically produce reliable thermochemistry for all chemical species involved in the C_0 through C_4 hierarchy of combustion chemical mechanisms by synergistically fusing the best aspects of highly accurate theoretical results and ATcT.

We recently had a collaborative effort (E. Goos, DLR) that addressed the species involved in NO_x formation mechanisms and showed the importance of the NCN species, casting serious questions both about the thermochemistry of NCN and the underlying chemical mechanism. In a new collaboration with Peter Glarborg (DTU), we are currently attempting a refined analysis of NO_x formation that uses the latest available thermochemistry and an improved chemical mechanism. As a follow-up on our recently published work analyzing the inhibition of combustion by bromine (which impacts a multi-billion industry of flame retardants and has netted us the Sugden Award of the British Section of the Combustion

Institute), we are currently involved in another international collaborative effort (involving both P. Glarborg, DTU, and E. Goos, DLR) that is analyzing the analogous combustion processes in the presence of chlorine. We are also currently intensely working with A. Burcat (Technion) and E. Goos (DLR) on continuous updates of the widely used Goos/Burcat/Ruscic database with available ATcT results.

The accuracy of ATcT results continues to make them highly desirable quantities for developing, improving, and benchmarking state-of-the-art electronic structure methods. In a recent invited Perspective for Int. J. Quantum Chem., we have emphasized the importance of accompanying measured or computed quantities with properly quantified and unambiguous uncertainties, revisited some frequently confused terms (such as accuracy, precision, and trueness, see Fig. 1), and outlined the frameworks for two basically different approaches to quantifying the accuracy of virtual measurements (i.e. theoretical results). One of the current sources of confusion is the fundamental difference between the accepted standard (IUPAC, CODATA, all thermochemical tables) for expressing uncertainties of thermochemical results (95% confidence intervals, $u_{95\%}$) and the prevailing approach for expressing the fidelity of electronic structure methods (mean absolute deviation, MAD). MAD effectively underestimates $u_{95\%}$ by a factor of 2.5 in a Gaussian distribution (see Fig. 2), and in practice frequently by a factor of ~3 or even more, thus vitiating many claims that 'chemical accuracy' or 'near chemical accuracy' has been achieved.

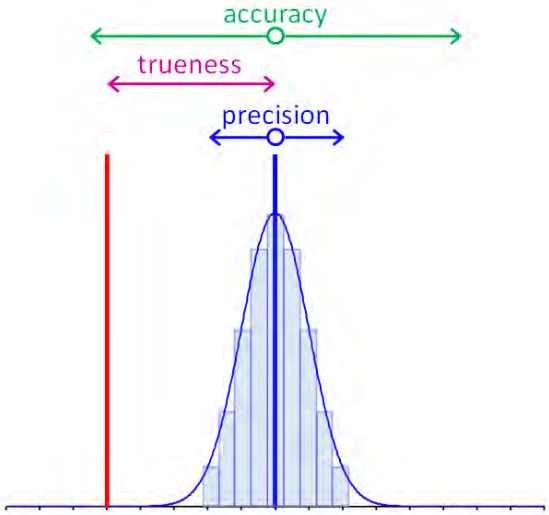

Figure 1. Relationship between accuracy, precision, and trueness. The blue vertical line is the mean of a series of measurements; the red line is the (unknown) true value of the measurand. The blue double arrow is the spread in the measurements (expressed here as 2σ) and reflects precision. The purple double arrow is the bias between the mean and the unknown true value, and reflects trueness. The green horizontal double arrow assesses accuracy, and the corresponding uncertainty is obtained by combining in quadrature the spread in the determinations and the estimated bias.

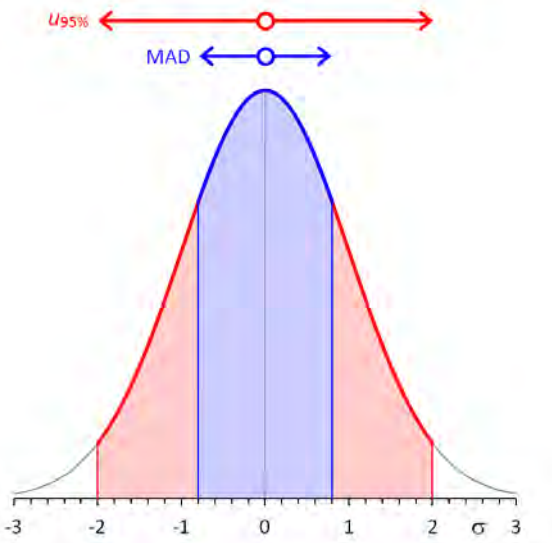

Figure 2. Mean absolute deviation (MAD) seriously underestimates the conventional uncertainty expected in thermochemistry. The relationship between MAD (blue) and the standard deviation σ is distribution-dependent, but MAD is always smaller than σ. In a Gaussian distribution (gray underlying curve), MAD = 0.79σ. The conventional uncertainty associated with thermochemical quantities (red) is expected to correspond to a 95% confidence interval, $u_{95\%} = 2\sigma$. Thus, in a Gaussian distribution, $u_{95\%} = 2.51$ MAD.

Future Plans

Future plans of this program pivot around further developing and expanding the Active Thermochemical Tables approach, continuing to provide accurate thermochemistry, and driving targeted thermochemically-relevant theoretical and experimental investigations of radicals and transient species that are intimately related to combustion processes as well as post-combustion atmospheric processes. A significant part of the effort during the forthcoming period will be devoted to continued 'finalization' and dissemination of the resulting ATcT thermochemistry. A crucial component of the 'finalization' of results for groups of related chemical species consists of testing and analyzing their TN dependencies (in part by using the newly developed variance/covariance decomposition approach) as well as enhancing the

accuracy of their partition functions (by gradually replacing them with new NRRAO partition functions), and, when suggested by ATcT analyses, adding new high-quality results (either virtual, i.e. computational, or actual, i.e. experimental) to coerce the resulting thermochemistry toward stable, 'release quality' values. This iterative process frequently results in an expansion of the number of species that are described by the current TN, which is an added benefit. Another important component in the future plans is the continuation of the current effort of designing and producing an entirely computer–generated web site that will display the current ATcT thermochemistry. Besides full automation with rigorous archival capability, an additional desideratum for the website development is the automatic inclusion of sufficient background information that will sufficiently document the provenance for every recommended thermochemical value, providing proper credit to the actual original (experimental and/or theoretical) determination(s) that are responsible for the final ATcT value. Finally, a signifant long-term component of future progress consists in developing a second generation of ATcT software. This will be based on a thorough redesign of the current ATcT kernel, with the aim of making the sotware not only streamlined and more efficient, but also allowing sufficient flexibility that will enable the adoption and utilization of emerging computing technologies as they become available.

This work is supported by the U.S. Department of Energy, Office of Basic Energy Sciences, Division of Chemical Sciences, Geosciences, and Biosciences, under Contract No. DE–AC02–06CH11357.

Publications resulting from DOE sponsored research (2012 – present)

- *Inhibition of Hydrogen Oxidation by HBr and Br_2*, G. Dixon-Lewis, P. Marshall, B. Ruscic, A. Burcat, E. Goos, A. Cuoci, A. Frassoldati, T. Faravelli, and P. Glarborg, *Combust. Flame* **159**, 528-540 (2012), DOI: 10.1021/jp2006205 (*this work was awarded the Sugden Prize by the British Section of The Combustion Institute*)
- *High-Temperature Rate Constants for H/D + C_2H_6 and C_3H_8*, R. Sivaramakrishnan, J. V. Michael, and B. Ruscic, *Int. J. Chem. Kin.* **44**, 194-205 (2012), DOI: 10.1002/kin.20607
- *Near-threshold shape resonance in the photoionization of 2-butyne*, H. Xu, U. Jacovella, B. Ruscic, S. T. Pratt, and R. R. Lucchese, *J. Chem. Phys.* **136**, 154303/1-10 (2012), DOI: 10.1063/1.3701762
- *Extended Third Millennium Ideal Gas and Condensed Phase Thermochemical Database for Combustion with updates from Active Thermochemical Tables*, E. Goos, A. Burcat, and B. Ruscic (2012-2013)*; (includes complete ATcT values ver. 1.112); progressive updates of thermochemical polynomials are currently available at* http://burcat.technion.ac.il/dir/ (*see also* http://www.technion.ac.il/~aer0201/), *mirrored at* http://garfield.chem.elte.hu/Burcat/burcat.html
- *Prompt NO formation in flames: The influence of NCN thermochemistry*, E. Goos, C. Sickfeld, F. Mauss, L. Seidel, B. Ruscic, A. Burcat, and T. Zeuch, *Proc. Comb. Inst.* **34**, 657-666 (2013), DOI: 10.1016/j.proci.2012.06.128
- *Active Thermochemical Tables: Water and Water Dimer*, B. Ruscic, *J. Phys. Chem. A* **117**, 11940-11953 (2013), DOI: 10.1021/jp403197t
- *Active Thermochemical Tables enthalpies of formation based on ver. 1.110 of the Thermochemical Network*, B. Ruscic, http://atct.anl.gov/Thermochemical%20Data/version%201.110/ (2013)
- *Improved Accuracy Benchmarks of Small Molecules Using Correlation Consistent Basis Sets*, D. Feller, K. A. Peterson, and B. Ruscic, *Theor. Chem. Acc.* **133**, 1407/1-16 (2014), DOI: 10.1007/s00214-013-1407-z
- *Active Thermochemical Tables: Dissociation Energies of Several Homonuclear First-Row Diatomics and Related Thermochemical Values*, B. Ruscic, D. Feller, and K. A. Peterson, *Theor. Chem. Acc.* **133**, 1415/1-12 (2014), DOI: 10.1007/s00214-013-1415-z
- *Uncertainty Quantification in Thermochemistry, Benchmarking Electronic Structure Computations, and Active Thermochemical Tables*, B. Ruscic, *Int. J. Quantum Chem*. **114**, *in press* (2014), DOI: 10.1002/qua.24605

GAS-PHASE MOLECULAR DYNAMICS: HIGH RESOLUTION SPECTROSCOPY AND COLLISION DYNAMICS OF TRANSIENT SPECIES

Trevor J. Sears
Department of Chemistry, Brookhaven National Laboratory
Upton, NY 11973-5000
sears@bnl.gov

Program Scope

This research is carried out as part of the Gas-Phase Molecular Dynamics program in the Chemistry Department at Brookhaven National Laboratory. High-resolution spectroscopic methods, augmented by theoretical and computational work, are used to investigate the structure, collision dynamics and chemical behavior of intermediates in the elementary gas-phase reactions involved in combustion chemistry. There is an emphasis on new technique development with the aim of improving both the sensitivity and resolution of spectroscopic measurements.

I Recent Progress

A. Sub-Doppler spectroscopy of CN

Hyperfine-resolved saturation spectra were measured for a selection of low and medium J rotational lines in the $A\ ^2\Pi - X\ ^2\Sigma$ system of CN using two copropagating laser beams tuned to transitions in the (2-0) and (1-0) bands. A bleach laser was amplitude modulated and fixed in frequency near the center of a rotational line of the (2-0) vibrational band, while a probe laser was frequency-modulated and scanned across selected lines of the (1-0) vibrational band, sharing a common lower state with the bleach laser. To avoid drifting away from the sharp double-resonant condition while signal averaging during slow scans with repetitive photolytic sample preparation, the relative frequency of the two lasers was stabilized using a single confocal cavity. High resolution, low noise, sub-Doppler saturation spectra can in this way be acquired in a two-color, collinear geometry. The resulting resolution and precision of the measured hyperfine splittings is significantly superior to our earlier measurements in the A– X (1-0) band, which used counterpropagating bleach and probe beams from a single laser. The sub-Doppler resonances were fitted with Lorentzian line shapes having a typical full-width at half maximum of 2-3 MHz. Some results are shown in figure 1. The hyperfine spectra observed depend on the hyperfine structure within both rovibronic transitions excited, permitting the determination of hyperfine molecular constants in the v'=2 state and the refinement of previously published values in the v'=1 state. The ground state hyperfine splittings are well known from previous microwave spectroscopic work. Four nuclear magnetic dipole and two electric quadrupole

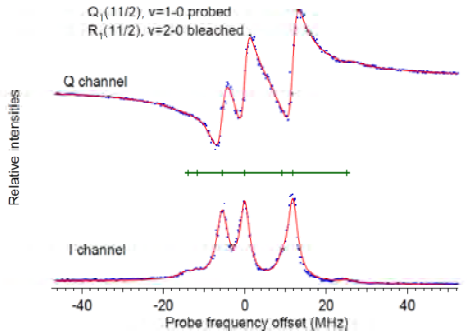

Figure 1: Absorption and dispersion (I and Q) saturation spectra, simultaneously observed by scanning the FM probe laser in the $Q_1(11/2)$ line of the (1–0) band with the bleach laser fixed in the $R_1(11/2)$ line of the (2–0) band. Three strong peaks and four weak lines (an isolated line, a shoulder, and a blended pair of lines) are observed at the offset frequencies depicted between the spectra, determined by fitting the data (blue points) with a sum of Lorentzians (smooth red lines).

hyperfine constants were determined for each of the upper states from a fit with a weighted root mean squared error of 0.5 MHz. The vibrational dependence of these constants is weak or negligible.

B. Frequency comb-stabilized laser spectroscopy

We have continued to develop and refine the comb-stabilized diode laser spectrometer and recently completed a series of measurements of pressure broadening and shift in acetylene spectra perturbed by collisions with nitrogen as a function of temperature. Signal-to-noise ratios of strong lines the $\nu_1+\nu_3$ band of acetylene are now close to 10^5 in a dual beam transmission measurement, and baseline drift has been improved by the use of larger area detectors and temperature stabilization of the beam splitter. In particular, we developed computer codes allowing all the data to be simultaneously fitted to speed-dependent line shape models in both the frequency and time domains. The latter formulation has conceptual advantages in that the observed pressure broadening, narrowing, shift and asymmetry are represented by the real and imaginary parts of the complex relaxation rate which contains both an average and a speed-dependent term. Details are given in some of our recent publications, listed below. From the analysis of this large dataset, we derived line shape parameters applicable to dilute mixtures of acetylene in nitrogen at pressures up to an atmosphere and temperatures between approximately 120 K and 300 K. More recent measurements have concentrated on assessing the applicability of these sophisticated line shape models to mixtures where the absorber is not in low concentration. The analysis of these new data is discussed below

Measurements of sub-Doppler rest frequency line positions using the comb-referenced spectrometer have also continued. The tunable extended cavity diode laser (ECDL) used has insufficient power to saturate transitions without the use of a high finesse cavity, and much recent work has been devoted to improving the stabilization of the ECDL to the cavity, which is itself referenced to the comb via a fixed sideband offset. A new cavity design and work on the tuning of the comb has resulted in greater sensitivity for the saturation dip measurements and also vastly increased the range over which the comb can be scanned without a reset. This will also have benefits in future broadening measurements. An example of a recent measurement of a hot band line in the acetylene $\nu_1+\nu_3$ band is shown in figure 2. The strongest hot band lines in the region derive from levels with $v_4=1$ or $v_5=1$ and are 10-100× weaker than the main lines. Their positions have not previously been frequency measured and we have found systematic discrepancies of up to 20 MHz when compared to entries in the HITRAN database used by thousands of researchers world-wide. Such errors cause problems when the database is applied to extraction of information from remote sensing data, resulting in poor species concentration and temperature profile estimates. We are currently measuring a representative selection of these hot band lines and will analyze the data in combination with the original

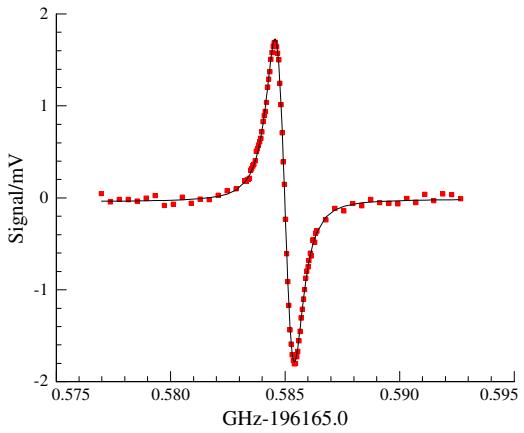

Figure 2: Saturation dip spectrum of the $R(5)_e$ $v_4=1$ hot band line in the $\nu_1+\nu_3$ spectrum of C_2H_2. Data points are in red, the line is a fit assuming a line shape function that is the derivative of a Lorentzian. The rest frequency is measured to be 196165.58489(1) GHz *i.e.* an estimated statistical error of 10 kHz. Sample pressure was 15 mT.

Fourier Transform spectrometer measurements on which the HITRAN tabulation is based, in order to rectify the present database shortcomings.

II. Future Work

A. Spectroscopy and dynamics of transient species

The laboratory at BNL has been in temporary accommodation for approximately two years and it is planned that the spectrometers will be moved to refurbished space during spring and summer of 2014. However, new sub-Doppler measurements of spectroscopic transitions in methylene, CH_2, are planned in the existing space during the move. These are targeted at the identification of singlet rotational levels in the first excited bending vibrational level (0,1,0) of the low-lying $\tilde{a}\ ^1A_1$ state of the radical that are perturbed by accidentally nearly degenerate rotational levels in vibrationally excited levels of the ground $\tilde{X}\ ^3B_1$ state. In the zero point level of the singlet, much previous work by ourselves and others has shown there are just five rotational levels that are strongly perturbed, and collision-induced intersystem crossing (CIISC) between the singlet and triplet states passes through these gateway levels at rates mediated by collisional rotational energy transfer (RET) rates. The rates of CIISC are practically important because of the markedly different reactivities of the singlet and triplet variants of the molecule, as well as providing a well-defined test case for models of RET in polyatomic collisions. In CH_2, the different nuclear spin modifications (ortho- and para-) provide two different sets of non-interacting levels that are otherwise chemically indistinguishable. These sets of levels are expected to exhibit different CIISC rates because of the different patterns of perturbing triplet levels and these expectations are qualitatively in agreement with the experimental observations.

Preliminary work several years ago suggested that no such difference appeared in (0,1,0), despite the fact that spectroscopic measurements of level shifts suggested that more para- levels were strongly perturbed than ortho- ones. Sub-Doppler measurements of hyperfine splittings in those levels identified as likely perturbed by spectroscopic shifts were not carried out at the time the most recent spectroscopic measurements of $\tilde{a}(0,1,0)$ made because the spectrometer did not have sufficient frequency stability. Our work during the past few years has opened the way to make such measurements and these splitting give a direct window into the amount of triplet contamination of the singlet wavefunction and hence the CIISC rates involving the level.

In the refurbished laboratory space, initial experiments will concentrate on sub-Doppler dynamics experiments as outlined in G. Hall's abstract elsewhere in the proceedings. Work on new near-IR radical spectroscopy following the predictions by H. –G Yu described in last year's abstract will also be set up in the new laboratory space.

B. Line shape and sub-Doppler measurements

We are currently analyzing a set of data in which the relative concentrations of the absorber (acetylene) and perturber (nitrogen) molecules are varied. In practically all work to date, the absorber molecule is assumed to be in concentrations low enough that contributions to the line broadening, narrowing, and shifts from absorber-absorber collisions may be neglected in modeling the observed line profiles. Where such effects are included, they are assumed to be additive in ratios of the partial pressures of the components in the mixture. This assumption has been brought into question following work on acetylene-nitrogen mixtures at high acetylene mixing ratios. The newly acquired data explores mixtures of

1, 5 and 10% acetylene from low pressures to up to an atmosphere. There are clear differences in line profiles recorded at identical total pressures but containing different mixture ratios. Analysis has been complicated by the fact that very weak hot band lines (some 1000× weaker than the main line) cause measureable perturbations to the line profile that are difficult to separate from the desired concentration dependences. Some of these underlying lines are not present in the HITRAN database, and where they are included, their rest frequencies are not known to sufficient accuracy. Our lineshape analysis codes will be modified to accommodate these lines with shifts determined from the new data.

The stability of the spectrometer has been significantly improved by the use of a direct digital frequency synthesis board that can synthesize tunable radio frequencies with lower phase noise than was available previously. This, together with improvements in the stability of the cavity absorption cells used for the saturation dip experiments has been crucial to the advances in data quality we have been able to make during the past year. The concepts behind these improvements will be carried over to the radical spectroscopy experiments during the coming year, while further investigations of pressure effects on sub-Doppler saturation dips will be made to investigate the relationship between collisional broadening and shift observed in a saturation dip spectrum and those measured in a Doppler-broadened sample.

III. Publications supported by this project since 2012

Temperature-dependent pressure broadened line shape measurements of self- and nitrogen-broadening in the $\nu_1 + \nu_3$ band of acetylene, M. J. Cich, C. P. McRaven, G. V. Lopez, T. J. Sears, D. Hurtmans and A. W. Mantz, *Appl. Phys. B.* **109**, 373-384 (2012).

What is the best DFT function for vibronic calculations? A comparison of the calculated vibronic structure of the $S_1 - S_0$ transition of phenylacetylene with accurate experimental band intensities, G. V. Lopez, C.-H. Chang, P. M. Johnson, G. E. Hall, T. J. Sears, B. Markiewicz, M. Milan and A. Teslja, *J. Phys. Chem .**A*** **116**, 6750-6758 (2012).

Hyperfine structures in the v=1-0 vibrational band of the $B^3\Pi_g - A^3\Sigma^+_u$ of N_2, D. Forthomme, C. P. McRaven, G. E. Hall, and T. J. Sears. *J. Molec. Spectrosc.* **282**, 50-55 (2012).

Enhancement of Triplet Stability in Benzene by Substituents with Triple Bonds, P. M. Johnson, T. J. Sears, *J. Phys. Chem. A* **117** 7786-7793 (2013) DOI: 10.1021/jp403727f

Argon-induced pressure broadening, shifting and narrowing in the CN $A^2\Pi - X^2\Sigma^+$ (1-0) band, D. Forthomme, C. P. McRaven, T. J. Sears, and G. E. Hall. *J. Phys. Chem A*. **117**, 11837-11846 (2013) DOI: 10.1021/jp4030359

An experimental and theoretical study of the electronic spectrum of HPS, a second row HNO analog, R. Grimminger, D. J. Clouthier, R. Tarroni, Z. Wang and T. J. Sears. *J. Chem. Phys*. **139** 174306 (2013) DOI: 10.1063/1.4827099

Temperature-Dependent, Nitrogen-Perturbed Line Shape Measurements in the $\nu_1 + \nu_3$ Band of Acetylene Using a Diode Laser Referenced to a Frequency Comb, M. J. Cich, D. Forthomme, C. P. McRaven, G. V. Lopez, G. E. Hall, T. J. Sears, and A. W. Mantz, *J. Phys. Chem. A*., **117**, 13908−13918 (2013). DOI:10.1021/jp408960e

Collinear two-color saturation spectroscopy in CN A–X (1–0) and (2–0) bands, D. Forthomme, C. P. McRaven, T. J. Sears, and G. E. Hall, *J. Molec. Spectrosc*. **296** (2014) 36–42.

Theoretical Studies of Potential Energy Surfaces and Computational Methods

Ron Shepard
Chemical Sciences and Engineering Division,
Argonne National Laboratory, Argonne, IL 60439
[email: shepard@tcg.anl.gov]

Program Scope: This project involves the development, implementation, and application of theoretical methods for the calculation and characterization of potential energy surfaces (PES) involving molecular species that occur in hydrocarbon combustion. These potential energy surfaces require an accurate and balanced treatment of reactants, intermediates, and products. This difficult challenge is met with general multiconfiguration self-consistent field (MCSCF) and multireference single- and double-excitation configuration interaction (MR-SDCI) methods. In contrast to the more common single-reference electronic structure methods, this approach is capable of describing accurately molecular systems that are highly distorted away from their equilibrium geometries, including reactant, fragment, and transition-state geometries, and of describing regions of the potential surface that are associated with electronic wave functions of widely varying nature. The MCSCF reference wave functions are designed to be sufficiently flexible to describe qualitatively the changes in the electronic structure over the broad range of molecular geometries of interest. The necessary mixing of ionic, covalent, and Rydberg contributions, along with the appropriate treatment of the different electron-spin components (e.g. closed shell, high-spin open-shell, low-spin open-shell, radical, diradical, etc.) of the wave functions are treated correctly at this level. Further treatment of electron correlation effects is included using large-scale multireference CI wave functions, particularly including the single and double excitations relative to the MCSCF reference space.

Recent Progress: ELECTRONIC STRUCTURE CODE MAINTENANCE, DEVELOPMENT, AND APPLICATIONS: A major component of this project is the development and maintenance of the COLUMBUS Program System. The COLUMBUS Program System computes MCSCF and MR-SDCI wave functions, MR-ACPF (averaged coupled-pair functional) energies, MR-AQCC (averaged quadratic coupled cluster) energies, spin-orbit CI energies, analytic energy gradients, and nonadiabatic coupling. Geometry optimizations to equilibrium and saddle-point structures can be done automatically for both ground and excited electronic states. The COLUMBUS Program System is maintained and developed collaboratively with several researchers including Isaiah Shavitt (University of Illinois, deceased December 2012), Russell M. Pitzer (Ohio State University), Thomas Mueller (Jülich Supercomputer Center, Germany), and Hans Lischka (University of Vienna, Austria, and Texas Tech University). The nonadiabatic coupling and geometry optimizations for conical intersections is done in collaboration with David R. Yarkony (Johns Hopkins University). The distributed development effort and software coordination uses an svn repository of source code. The parallel sections of the code are based on the single-program multiple-data (SPMD) programming model with explicit message passing using the portable MPI library, and the portable Global

This work was performed under the auspices of the Office of Basic Energy Sciences, Division of Chemical Sciences, Geosciences, and Biosciences, U.S. Department of Energy, under contract number DE-AC02-06CH11357.

Array Library (distributed from PNNL) is used for data distribution. The COLUMBUS codes incorporate several of the newer language features of F90 and later in order to facilitate future development and maintenance efforts.

GRAPHICALLY CONTRACTED FUNCTION METHOD: We have developed a novel expansion basis for electronic wave functions [see *Mol. Phys.* **108**, 2717 (2010) and references therein]. In this approach, the wave function is written as a linear combination of *graphically contracted functions* (GCF), and each GCF in turn is formally equivalent to a linear combination of configuration state functions (CSFs) that comprise an underlying full-CI linear expansion space of dimension N_{csf}. The CSF coefficients that define the GCFs are nonlinear functions of a smaller number of variables $N_{\varphi} \ll N_{\mathrm{csf}}$. GCF expansions with N_{GCF}=10 to 20 basis functions can approach the full-CI PES to within chemical accuracy (1 kcal/mole or better) [*Int. J. Quantum Chem.* **107**, 3203 (2007)]. The method is formulated in terms of spin-eigenfunctions using the Graphical Unitary Group Approach (GUGA) of Shavitt, thereby eliminating artifacts that result from spin contamination or spin instability. No intrinsic restrictions are imposed on the orbital occupations, and in particular there are no artificial excitation-level or occupation restrictions with respect to a reference function or reference space; in this sense, the method is more correctly characterized as a multiconfiguratonal method rather than a multireference method. Because the wave function is a linear combinations of N_{GCF} basis functions rather than a single expansion term, the method is variational and may be applied to both ground and excited electronic states.

Our recent focus has been on the development and implementation of a *multifacet* generalization of the GCF method. In the previous implementations, a single lower- or upper-walk, recursively contracted wave function is associated with each node of the Shavitt graph within a GCF basis function; we now term this the *single-facet* GCF approach. With the multifacet approach, each node k of the Shavitt graph may be associated with some larger number f_k^P of lower- and upper-walk contracted wave functions within the GCF $|P\rangle$; each MFGCF thereby has more flexibility than a SFGCF. A general feature of the new method is that arithmetic operations that previously involved scalars are replaced with matrix-vector and matrix-matrix products. The efficient recursive algorithms developed previously for the SFGCF approach carry over in a straightforward way for MFGCF expansions. The individual CSF coefficients within an MFGCF are given by an ordered product of rectangular arc factor arrays; this means that it is formally a *matrix product state* (MPS), and our wave function corresponds to a linear combination of such MPSs.

One of the useful features of the MFGCF expansion form is the ability to optimize the arc factors in order to minimize the energy of the ground state, of an excited state, or of a weighted average of multiple states. This last approach is an example of *state averaging*, and it allows for the balanced descriptions of multiple electronic states. Fig. 1 shows the results of this state averaging approach for the C_{2v} insertion of Be into H_2 for the lowest two $^1A_1$ electronic states. The ground state corresponds to the reaction $Be(^1S)+H_2(^1\Sigma_g^+) \rightarrow BeH_2(^1A_1)$ and the excited state corresponds to $Be(^1P)+H_2(^1\Sigma_g^+) \rightarrow BeH_2(^1A_1)$. This is a challenging electronic structure problem because flexible multiconfigurational wave function expansions are required to describe curve crossings in both states. The ground state barrier results from the avoided crossing of the closed-shell configurations $1a_1^2 2a_1^2 3a_1^2$, dominant at long distances, and $1a_1^2 2a_1^2 1b_2^2$, dominant near

the 1^1A_1 collinear equilibrium conformation. The minimum of the excited state curve also derives from that avoided crossing, but there are additional avoided crossings with the open-shell configurations $1a_1^2 2a_1^1 3a_1^1 1b_1^2$, dominant near the collinear conformation, and $1a_1^2 2a_1^2 3a_1^1 4a_1^1$, dominant at long distances. Fig. 1 shows the SFGCF energy curves (open red symbols) along with those of the more flexible MFGCF expansion (solid blue symbols) with the maximum facet count f_{max}=2. Because these are all variational wave functions, the more flexible MFGCF wave function results in energies that are bounded from above by the SFGCF energies. The black lines in Fig. 1 are the valence full-CI PESs for the two states, which correspond to the exact results in this model calculation. Fig. 2 shows the maximum deviations from the valence full-CI energy curves for a sequence of SFGCF and MFGCF expansions. The SFGCF errors (open red symbols) are plotted as a function of the basis expansion dimension $X=N_{GCF}$, and the MFGCF errors (solid blue symbols) for the fixed dimension N_{GCF}=2 are plotted as a function of $X=f_{max}$. It is observed that the MFGCF errors are not only smaller, but the slopes of the two MFGCF error curves are noticeably different than the SFGCF error curves; this is a consequence of the enhanced flexibility of the MFGCF expansion. The errors of the individual states are comparable as a function of X, demonstrating that balanced descriptions of multiple electronic states may be achieved with the state-averaging procedure even prior to convergence of the wave function to the full-CI limit which is achieved with f_{max}=4.

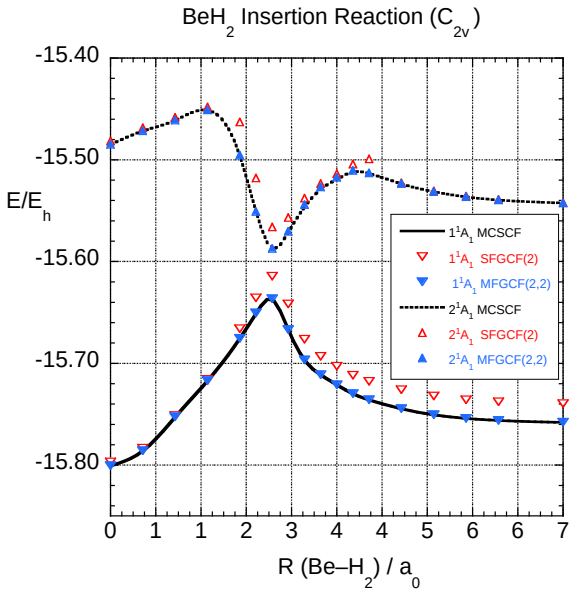

Fig. 1. Potential energy curves in E_h for the 1-2^1A_1 electronic states for the C_{2v} insertion of Be into H_2. The black lines are the $(\mathbf{6})^4$ valence full-CI energies. The open red symbols are the state-averaged SFGCF results with N_{GCF}=2. The solid blue symbols are the state-averaged MFGCF results with N_{GCF}=2 and f_{max}=2.

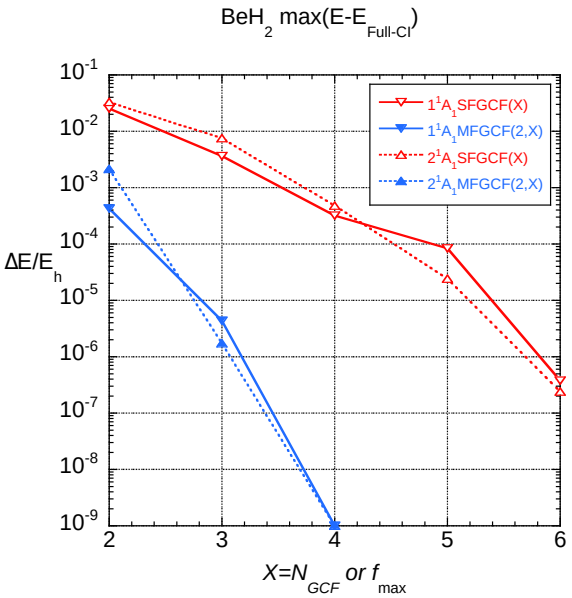

Fig. 2. Maximum energy errors in E_h for the 1-2^1A_1 electronic states for the C_{2v} insertion of Be into H_2 relative to the $(\mathbf{6})^4$ valence full-CI. The open red symbols are the state-averaged SFGCF results as a function of N_{GCF}. The solid blue symbols are the state-averaged MFGCF results with N_{GCF}=2 as a function of f_{max}.

Future Plans: Our MFGCF implementation has so far used single-headed Shavitt graphs appropriate for describing individual molecular states with a given number of electrons, with a particular spin state, and that belong to a particular point group irreducible representation (irrep). We will generalize this in several respects. First, we will introduce state averaging over multiple irreps. This will allow the computation of several molecular states with essentially no additional effort over single-irrep calculations. Next, we will employ multiheaded Shavitt graphs in the state-averaging procedure. This will allow the computation of Hamiltonian matrix elements corresponding to states with different numbers of electrons, different spin values, and different irreps simultaneously with only a relatively small increase in effort over the current single-state approach. The computation of transition properties is facilitated by the fact that all states are described with the same set of arc factors.

The GCF code has now been placed in a development branch of the COLUMBUS svn repository. In this way the code is now available for a wider range of inspection and scrutiny by COLUMBUS developers. We hope to develop a robust implementation and incorporate the GCF method into the standard distribution version of COLUMBUS for even wider use by the broader user community for general chemical applications in the near future.

Publications:

"COLUMBUS–A Program System for Advanced Multireference Theory Calculations," H. Lischka, T. Müller, P. G. Szalay, I. Shavitt, R. M. Pitzer, R. Shepard, *WIREs Comput. Mol. Sci.* **1**, 191 (2011).

"Computational and Methodological Elements for Nonadiabatic Trajectory Dynamics Simulations of Molecules," M. Barbatti, R. Shepard, and H. Lischka, in "Conical Intersections: Theory, Computation and Experiment", W. Domcke, D.R. Yarkony and H. Köppel, Eds., *Advanced Series in Physical Chemistry*, **17** (World Scientific, Singapore, 2011) pp. 415-462.

"Reduced Density Matrices Within the Graphically Contracted Function Method," R. L. Shepard, *Abstracts of Papers of the American Chemical Society* **242**, 278-PHYS (2011).

"Multiconfiguration Self-Consistent Field and Multireference Configuration Interaction Methods and Applications," P. G. Szalay, T. Mueller, G. Gidofalvi, H. Lischka, R. Shepard, *Chem. Rev.* **112**, 108-181 (2012).

"The Multiradical Character of One- and Two-Dimensional Graphene Nanoribbons," F. Plasser, H. Pašalić, M. H. Gerzabek, F. Libisch, R. Reiter, J. Burgdörfer, T. Müller, R. Shepard, and H. Lischka, *Angewandte Chemie International Edition* **52**, 2581-2584 (2013).

"Der Multiradikalcharakter ein- und zweidimensionaler Graphen-Nanobänder," F. Plasser, H. Pašalić, M. H. Gerzabek, F. Libisch, R. Reiter, J. Burgdörfer, T. Müller, R. Shepard, and H. Lischka, *Angewandte Chemie* **125**, 2641-2644 (2013).

"Graphically Contracted Function Electronic Structure Method," R. L. Shepard, G. Gidofalvi, and S. R. Brozell, *Abstracts of Papers of the American Chemical Society* **246**, 159-PHYS (2013).

"Comparison of Multireference Configuration Interaction Potential Energy Surfaces for $H+O_2 \rightarrow HO_2$: The Effect Of Internal Contraction," L. B. Harding, S. J. Klippenstein, H. Lischka, and R. Shepard, *Theor. Chem. Acc.* **133**, 1429 (2014). DOI 10.1007/s00214-013-1429-6.

Mechanisms and Models for Combustion Simulations

Raghu Sivaramakrishnan
Chemical Dynamics Group, Chemical Sciences & Engineering Division
Argonne National Laboratory, Argonne, IL 60439
raghu@anl.gov

I. Program Scope

Mechanisms describing the combustion chemistry of even simple fuels can be complex involving a myriad of unimolecular and bimolecular elementary steps. The primary scope of this program is to develop and validate detailed chemical kinetics mechanisms and models for use in combustion simulations.

The kinetics models will be developed on the basis of a consistent framework incorporating theoretical predictions, experimental measurements, and evaluations of elementary reaction rate coefficients including feedback loops between them. The detailed models will subsequently be used for simulations of data from reactors, shock-tubes, rapid compression machines, and flames, the aim being the validation the mechanistic and kinetic aspects of these models over practical combustion regimes.

II. Recent Progress

A. Radical-Radical Addition-Elimination Reactions are Important in Oxygenate Flames

In the pursuit of developing chemical kinetic mechanisms and models for the purpose of simulating combustion systems, low-pressure flame experiments [1-3] have become popular benchmarks over the past few years. Mechanistic studies that interpret the speciation data from these premixed flames assume a nearly homologous sequence of steps that begin with fuel destruction largely due to hydrogen abstraction reactions. Fuel radicals then mostly decompose by β-scission reactions, forming an unsaturated molecule and a radical species that then helps to perpetuate this abstraction and β-scission sequence. For example, mechanistic interpretations of a recent MBMS-flame study on ethanol [4] suggest that 95% of the fuel is consumed by abstraction reactions, primarily forming CH_3CHOH, with a smaller fraction yielding the other two fuel radicals, CH_2CH_2OH and CH_3CH_2O. The dominant fuel radical, CH_3CHOH, is then consumed exclusively by β-scission to form acetaldehyde and H-atoms. In this particular case [4], unimolecular decomposition was shown to contribute only a minor fraction (5%) to fuel decay. But in other cases, unimolecular decompositions can play a larger role as was shown in a recent study [5] of a methylformate flame where 41% of the fuel decomposition was attributed to unimolecular pathways. However, hydrogen abstractions still played the dominant role in contributing to methylformate destruction.

With most models relying on this sequence of abstraction followed by subsequent β-scission to describe fuel decomposition, predicted radical pools and intermediate products then become sensitive to the rate constants and, of course, branching ratios to various channels for these reactions. A recent ethanol flame study by Tran et al. [6], in predicting intermediate formations, emphasized the sensitivity to rate constants and branching ratios for the OH + C_2H_5OH reaction. In this study, C_2H_4 formation was improved by adjusting the branching ratios to abstraction at the primary C-H bond in ethanol giving CH_2CH_2OH, which then subsequently decomposes rapidly by β-scission forming OH + C_2H_4. Interestingly, in order to match C_2H_4 profiles, the rate constant used in this study [6] for this abstraction channel is approximately a factor of 5 larger than the prediction from a recent experimental/theoretical study on OH + C_2H_5OH [7]. We conclude that if indeed the rate constants from these theoretical predictions [7] are accurate to within a factor of 2 then there must be an alternative source for C_2H_4 in these flames. Relatively stable fuel radicals (such as CH_3CHOH in the case of ethanol) can build up to substantial concentrations in these flames simply because unimolecular pressure fall-off inhibits β-scissions of these radicals in the low-pressure (<0.1 atm) environment. Consequently, bimolecular reactions of the relatively stable fuel radicals with dominant radicals present in the flame, such as H, CH_3,

and OH, might provide a more direct prompt source for intermediates. A probable candidate is the bimolecular reaction, H + CH_3CHOH, which can directly lead to well-skipping products C_2H_4 + H_2O.

Well-skipping radical-molecule reactions such as OH + C_2H_4 have been shown to be the root cause for the elusive enol-intermediates in the trailblazing flame studies of Taatjes et al. [8]. In contrast, there are limited theoretical/modeling studies on the role of radical-radical well-skipping reactions in small oxygenates, particularly if the two radicals are energetically high-lying (from the well) such as the radicals (fuel radical and H-atoms) produced in C-H bond fissions. Of course, the contributions of such fuel radical + H/CH_3/OH reactions need to be assessed, relative to fuel radical + O_2, which is a sink for the fuel-radicals. In the particular case of ethanol radicals, reaction with O_2 has been well characterized in a recent experiment/theory study [9].

In collaboration with N. J. Labbe and S. J. Klippenstein, ab-initio electronic structure theory based kinetics predictions were obtained for radical-radical reactions of relevance to low-pressure ethanol [10] and methyl formate [5] flames. These theoretical rate constants are then used in an in-house kinetic model to assess their potential contributions to C_2H_4 formation at low pressures [5,10]. In particular, it is observed that H + CH_3CHOH (relatively most stable ethanol radical) provides a competing source (see Fig. 1 for Arrhenius plot) for C_2H_4 formation in an ethanol low pressure flame [10]. On the other hand, CH_3 + CH_3CHOH provides a direct route to C_3H_6 in this ethanol flame [10]. For the methyl formate flame [5], we predict that H + CH_2OCHO provides a direct source for CH_3OH formation that competes with unimolecular decomposition. The present simulations also indicate CH_3 + CH_2OCHO recombination is a minor channel in this low-pressure methylformate flame, contradicting Ref. 5 which presumed dominance of this channel. Instead, the present simulations indicate that that the direct well-skipping reaction, CH_3 + CH_2OCHO → C_2H_4 + HCOOH, is the dominant channel and the source for the observed C_2H_4 under the low-pressure flame conditions. Figure 2 depicts the substantial effect of incorporating these addition-elimination reactions into the mechanism. The present results indicate that such addition-elimination reactions of stable fuel radicals with H, CH_3, and OH are expected to be an important sink for fuel radicals and provide additional routes to numerous other intermediates observed in low-pressure flames.

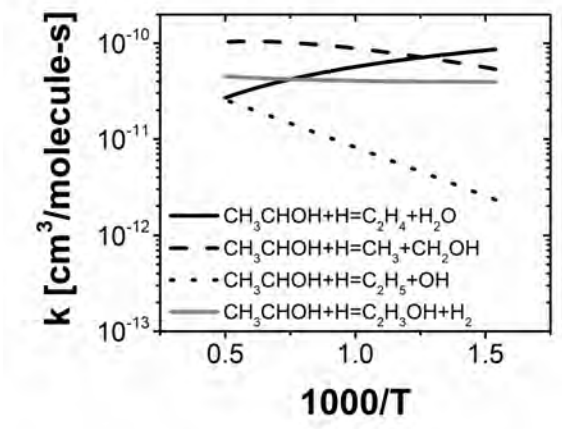

Fig. 1: Kinetics for CH_3CHOH + H at 0.1 atm

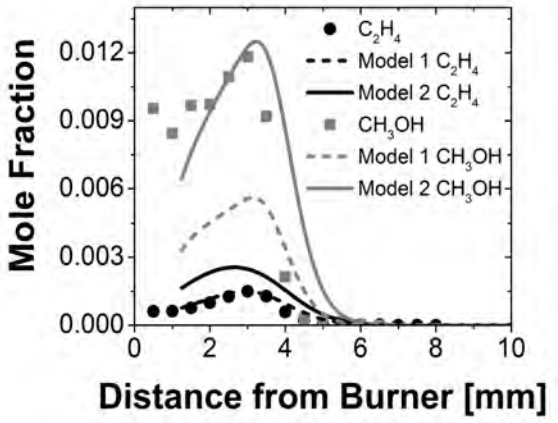

Fig. 2: Simulations of Phi 1.6 MF low-pressure flame [5]. Model 1: Without H/CH_3 + CH_2OCHO addition-eliminations; Model 2: With addition-eliminations.

B. Thermal decompositions of iso-propanol, xylyl radicals

We continue our experiment/theory collaborations with J. V. Michael and S. J. Klippenstein. In the past year we have extended our thermal decomposition studies to higher alcohols such as iso-propanol. Selectively deuterated iso-propanol decomposition experiments were also performed to characterize the contributions of the various dissociation channels and to gain mechanistic insights into the decomposition of the CH_3CHOH-radical formed by the dominant bond-dissociation, i-C_3H_7OH → CH_3CHOH + CH_3. Theoretical predictions for this bond fission are found to be in good agreement with the present experimental data.

In collaboration with J.V. Michael, S.J. Klippenstein, D. Polino and C. Cavallotti (Politechnico Milano), we have initiated a joint experiment-theory study of o-xylylbromide dissociation as a source for o-xylyl radicals and the subsequent dissociation kinetics of o-xylyl. The experimental studies probe the H-atom forming channel with theory providing a more complete description of the mechanistic features of o-xylyl decomposition.

C. Developing detailed and reduced chemical kinetics models for engine simulations

We continue our collaborations with M.J. Davis (Argonne), S. Som, D.E. Longman and S. Goldsborough (Engines & Emissions group at Argonne) on developing reduced and detailed kinetics models and their subsequent analyses for realistic engine modeling studies of diesel and biodiesel surrogates. We propose to test effects of varying the reactivity for diesel and gasoline surrogates by doping cetane enhancers and inhibitors. We also propose to initiate kinetics modeling studies on dimethylether, DME, as a simple real fuel. Detailed kinetics without model reduction can be directly applied for DME in engine simulations and offers a test for the chemistry under practical conditions.

D. A detailed analysis of methanol combustion kinetics

In collaboration with N.J. Labbe, S.J. Klippenstein, and the group of Y. Ju (Princeton University), an updated model for methanol combustion was developed. This joint effort was initiated to probe the kinetics of the simplest methylester, methylformate. Initial simulations indicated that methanol (as the dominant intermediate from methylformate) and its sub-set mechanisms required a substantial update. In particular, the methanol model includes new theoretical kinetics predictions for the decomposition of CH_2OH, CH_3O, with a re-analysis of the numerous H-atom abstractions from methanol by H, OH, CH_3, HO_2, and O_2. Simulations with the model indicate good agreement with literature data from shock-tubes, reactors, and flames. Recommendations for methanol kinetics and combustion studies are also presented.

III. Future work

We have completed our small alcohol (C_1-C_2) combustion modeling/theoretical studies and plan to use this kinetics experiment/theory based methodology to develop kinetics models for selected C_3-C_4 alcohols. We also propose to initiate joint experiment/theory studies on C_3-C_4 aldehydes. Our current efforts on modeling methylformate combustion are expected to lead into systematic modeling studies of larger C_2-C_4 methylesters. The effects of stable fuel-radical + H/CH_3/OH reactions will be systematically explored for larger oxygenated molecules.

IV. References

1. C.A. Taatjes, N. Hansen, D.L. Osborn, K. Kohse-Höinghaus, T.A. Cool, P.R. Westmoreland, Phys. Chem. Chem. Phys. **2008**, 10 (1), 20-34.
2. N. Hansen, T.A. Cool, P.R. Westmoreland, K. Kohse-Höinghaus, Prog. Energy Combust. Sci. **2009**, 35, 168-191.
3. F. Qi, Proc. Combust. Inst. **2013**, 34, 33-63.
4. N. Leplat, P. Dagaut, C. Togbé, J. Vandooren, Combust. Flame **2011**, 158, 705-725.
5. S. Dooley, F.L. Dryer, B. Yang, J. Wang, T.A. Cool, T. Kasper, N. Hansen, Combust. Flame **2011**, 158, 732-741.
6. L.-S. Tran, P.-A. Glaude, R. Fournet, F. Battin-Leclerc, Energy and Fuels **2013**, 27, 2226-2245.
7. R. Sivaramakrishnan, M.-C. Su, J.V. Michael, S.J. Klippenstein, L.B. Harding, B. Ruscic, J. Phys. Chem. A **2010**, 114, 9425-9439.
8. C.A. Taatjes, N. Hansen, J.A. Miller, T.A. Cool, J. Wang, P.R. Westmoreland, M.E. Law, T. Kasper, K. Kohse-Höinghaus, J. Phys. Chem. A **2006**, 110, 3254-3260.
9. J. Zador, R.X. Fernandes, Y. Georgievskii, G. Meloni, C.A. Taatjes, J.A. Miller, Proc. Combust. Inst. **2009**, 32, 271-277.
10. H. Xu, C. Yao, T. Yuan, K. Zhang, H. Guo, Combust. Flame **2011**, 158, 1673-1681.

V. Journal articles supported by this project 2012-2014

1. S. L. Peukert, R. Sivaramakrishnan, M.-C. Su, and J. V. Michael, "Experiment and theory on methylformate and methylacetate kinetics at high temperatures: Rate constants for H-atom abstraction and thermal decomposition", Comb. and Flame **159**, 2312-2323 (2012).
2. S. L. Peukert, R. Sivaramakrishnan, M.-C. Su, and J. V. Michael, "High temperature rate constants for H/D + methylformate and methylacetate", Proc. Combust. Inst. **34**, 463-471 (2013).
3. R. Sivaramakrishnan, W. Liu, M. J. Davis, S. Som, D. E. Longman, and T. F. Lu, "Development of a reduced biodiesel surrogate model for compression ignition engine modeling", Proc. Combust. Inst. **34**, 401-409 (2013).
4. S. L. Peukert, R. Sivaramakrishnan, and J. V. Michael, "High temperature shock tube and theoretical studies on the thermal decomposition of dimethylcarbonate and its bimolecular reactions with H and D-Atoms", J. Phys. Chem. A **117**, 3718-3728 (2013).
5. S. L. Peukert, R. Sivaramakrishnan, and J. V. Michael, "High temperature shock tube studies on the thermal dissociation of O_3 and the reaction of dimethyl carbonate with O-atoms", J. Phys. Chem. A **117**, 3729-3738 (2013).
6. S. Som, W. Liu, D. D. Y. Zhou, G. M. Magnotti, R. Sivaramakrishnan, D. E. Longman, R. T. Skodje, and M. J. Davis "Quantum Tunneling Affects Engine Performance", J. Phys. Chem. Lett. **4**, 2021-2025 (2013).
7. N. J. Labbe, R. Sivaramakrishnan, S. J. Klippenstein, "The role of prompt reactions in ethanol and methylformate low-pressure flames", Accepted, Proc. Combust. Inst. **35** (2014).
8. N. J. Labbe, P. Dievart, X. L. Yang, R. Sivaramakrishnan, S. J. Klippenstein, Y. Ju, "A detail analysis of the kinetics of methanol combustion", In Preparation, Comb. And Flame (2014).
9. R. Sivaramakrishnan, J. V. Michael, L. B. Harding and S. J. Klippenstein, "Revisiting the thermal decomposition mechanism of CH_3CHO", In Preparation, J. Phys. Chem. A (2014).
10. D. Polino, C. Cavallotti, R. Sivaramakrishnan, S. J. Klippenstein, J. V. Michael, "The thermal decomposition kinetics of o-xylylbromide and o-xylyl", In Preparation, J. Phys. Chem. A (2014).

Other Publications and Presentations supported by this project 2012-2014

1. R. Sivaramakrishnan, J. V. Michael, L. B. Harding and S. J. Klippenstein, "Revisiting the Thermal Decomposition of CH_3CHO", 22nd International Symposium on Gas Kinetics, Boulder, CO, 2012.
2. S. L. Peukert, R. Sivaramakrishnan, M.-C. Su, and J. V. Michael, "Experiment and Theory on methylformate and methylacetate kinetics at high temperatures: Rate constants for H-atom abstraction and thermal decomposition", 22nd International Symposium on Gas Kinetics, Boulder, CO, 2012.
3. S. L. Peukert, R. Sivaramakrishnan, J. V. Michael, "Shock tube and modeling study on the pyrolysis of dimethyl carbonate and its reaction with D- and O-atoms", 8th US National Combustion Meeting, Park City, UT, May 19-22, 2013.
4. R. Sivaramakrishnan, N. J. Labbe, W Liu, M. J. Davis, "A high temperature mechanism for methylformate combustion", 8th US National Combustion Meeting, Park City, UT, May 19-22, 2013.
5. W. Liu, S. Som, D. D. Y. Zhou, R. Sivaramakrishnan, D. E. Longman, R. T. Skodje, M. J. Davis, "The role of individual rate coefficients in the performance of compression ignition engine models", 8th US National Combustion Meeting, Park City, UT, May 19-22, 2013.
6. D. Polino, C. Cavallotti, R. Sivaramakrishnan, S. J. Klippenstein, J. V. Michael, "The decomposition kinetics of xylyl radicals", 8th International Conference on Chemical Kinetics, Seville, Spain, July 8-12, 2013.
7. S. L. Peukert, R. Sivaramakrishnan, S. J. Klippenstein, J. V. Michael, "A shock tube and modeling study on the thermal decomposition of iso-propanol and its reaction with D-atoms", 8th International Conference on Chemical Kinetics, Seville, Spain, July 8-12, 2013.
8. N. J. Labbe, R. Sivaramakrishnan, S. J. Klippenstein, "The role of addition-elimination reactions in small oxygenate flames" Central States Section of the Combustion Institute, Mar 16-18, Tulsa, OK.

COMPUTATIONAL AND EXPERIMENTAL STUDY OF LAMINAR FLAMES

M. D. Smooke and M. B. Long
Department of Mechanical Engineering
Yale University
New Haven, CT 06520
mitchell.smooke@yale.edu

Program Scope

Our research has centered on an investigation of the effects of complex chemistry and detailed transport on the structure and extinction of hydrocarbon flames in coflowing axisymmetric configurations. We have pursued both computational and experimental aspects of the research in parallel. The computational work has focused on the application of accurate and efficient numerical methods for the solution of the boundary value problems describing the various reacting systems. Detailed experimental measurements were performed on axisymmetric coflow flames using two-dimensional imaging techniques. Spontaneous Raman scattering and laser-induced fluorescence were used to measure the temperature, and major and minor species profiles. Laser-induced incandescence (LII) has been used to measure soot volume fractions and particle sizes. A new approach to optical pyrometry has been developed to measure temperatures where the other techniques fail due to the presence of soot. Our goal has been to obtain a more fundamental understanding of the important fluid dynamic and chemical interactions in these flames so that this information can be used effectively in combustion modeling.

Recent Progress

Radiative Power Loss

Radiative power loss can be considerable in sooting flames so that the gas temperature and soot formation rates themselves can be significantly altered. In an optically thin approximation the power radiated from soot and gas bands (CO_2, H_2O, and CO, using the exponential wideband model) has been computed using the expressions in [1]. A more sophisticated analysis to assess the importance of optical thickness or radiative re-absorption effects is needed, especially as the soot loadings increase. Recently, we have combined the discrete ordinates approximation [2] with a gas and soot radiation model that uses either Planck Mean or wavelength-dependent absorption coefficients from the RADCAL program [3]. The discrete ordinates algorithm solves the radiative transfer equation (RTE) along a limited number of discrete ray directions, with a solid angle associated with each ray. For axisymmetric cylindrical problems, we have used the S4 approximation, which solves the RTE along 12 ray directions after the calculation is initiated by solution along four special directions. The intensities at the boundaries of the computational domain are calculated, as well as the radiative dissipation, which appears as a source/sink term in the flow energy equation and is responsible for the coupling between radiation and the flow field. The Planck Mean option, which assumes a grey gas, uses curve fits given in [3]. The wavelength-dependent absorption coefficients extracted from the RADCAL program are consistent with the Planck Mean curve fits, and both options give the same predicted radiated power in the optically thin limit, as they must. The wavelength-dependent option, which involves summation over several hundred discrete wavelengths, provides a more exact calculation of radiative emission/absorption effects. When reabsorption effects are important, there can be significant differences between calculations based on Planck Mean and wavelength-dependent absorption coefficients. The most recent beta-version of RADCAL [4] contains absorption

coefficient data for more hydrocarbons fuels so that a precise investigation of the possible interactions of fuel with radiation can be made.

Time-Varying Flames

The extension of a low order implicit solver to model time-dependent chemically reacting flows is hindered by the presence of large artificial diffusion, in particular from the first-order upwind discretizations of the convective terms in the governing equations. As in the steady-state problem, this can be reduced through grid refinement. In a time-evolving flow, however, node clustering must be adjusted dynamically to follow the movement of flow structures such as vortices. Otherwise, during some stages of the computations, important flow nonuniformities may penetrate regions of the domain having insufficient grid resolution and experience a significant amount of artificial diffusion, thus spuriously altering the flow dynamics. As an alternative approach, high order discretization schemes with negligible numerical diffusion can be used for flame computations.

We are applying high order compact spatial discretizations in a fully implicit framework that avoid these problems, and offer many advantages over other current approaches to solving reacting flow problems. Compact schemes are well suited to the simulation of time-dependent flows with complicated structures due to their excellent resolution characteristics [5,6]. Their integration into an efficient Newton-based flame code is an extremely challenging problem requiring research in modern iterative linear algebra solvers and preconditioning, novel storage/retrieval methodologies, fast Jacobian matrix algorithms, and domain decomposition methods. The necessity of implementing all these numerical techniques on message-passing parallel architectures only compounds the difficulty. However, efficiency arguments indicate that the use of compact spatial discretizations with implicit time stepping may be able to reduce overall computation times dramatically compared to other numerical methods commonly employed in detailed-chemistry combustion simulations [7].

Full Field Temperature Measurements in Sooting Coflow Diffusion Flames

The availability of temperature maps over the entire flow field of sooting coflow diffusion flames would allow significant simplifications to the radiation corrections in our computational work. Mapping temperature over the entire flow field involves measurement over a wide range of temperatures, flow velocities, and scattering characteristics. For this reason, three different techniques were selected and spatially overlaid in order to map the entire flow region. A two-color ratio soot pyrometry technique was used in the sooting region [8], thin-filament pyrometry captured the gas temperature adjacent to the sooting region of the flame [9], and a new Rayleigh scattering technique based on Structured Laser Illumination Planar Imaging (SLIPI) was used in the regions below 1150 K. The advantage of the SLIPI approach is that for experiments that involve high background levels (as in the sooting flames), an intensity modulated light sheet serves as a signature that can be used to separate light scattered from within the sheet from background scattering. Our approach involves splitting the output of an Nd:YAG and propagating two beams over 6.9 meters before interfering them above the burner. Relay imaging the signal to the camera and implementation of SLIPI was necessary due to orders of magnitude difference in signal strength between scattering from soot and Rayleigh scattering. Four ethylene flames diluted to various levels with nitrogen were studied. Figure 1 shows the combined temperature measurements from the three different techniques.

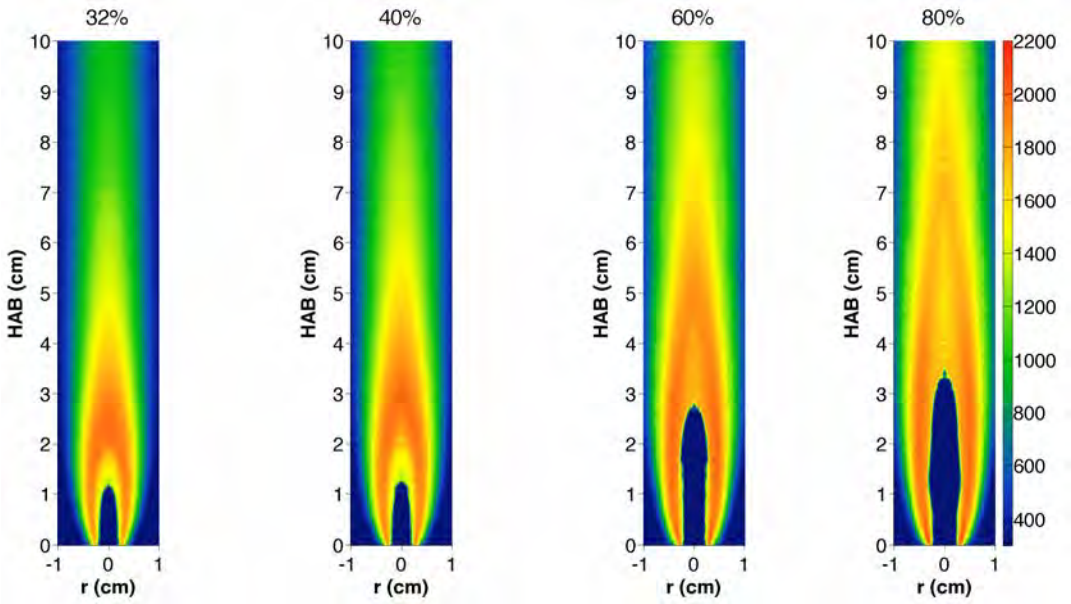

Figure 1. Full field temperature maps for 32, 40, 60, and 80% ethylene flames.

Quantitative CO LIF measurements in steady and time-varying coflow laminar diffusion flames

The ongoing experimental measurement of absolute carbon monoxide concentration in steady and time-varying methane coflow laminar diffusion flames has undergone refinement by modifying the post-processing done to the acquired data. An unpublished work by Settersten and coworkers was used to model and describe CO laser-induced fluorescence with better accuracy. The added improvement allowed for a better agreement between measured and computed fluorescence, taking into account contributions from quenching and photoionization rates, line broadening effects as well as Boltzmann population distribution. Quantitative measurements performed with high laser fluences in the linear/photoionization-dominant regime were found to simplify CO measurement by reducing the uncertainties associated with the quenching rate evaluation. Compared to Raman, LIF CO measurements improved the SNR by a factor of five and the higher sensitivity of the technique allowed for results with better spatial resolution.

Future Plans

During the next year we will continue our study of time varying flames with the goal of fully implementing higher order compact-based methods. We plan to study both sooting and nonsooting hydrocarbon flames. Experimentally, we plan to add minor species measurements (*OH*, *CH* and *NO*) with laser-induced fluorescence to complete the characterization of species in these time-varying flames. Further, we will perform phase-resolved PIV measurements of the velocity profiles within the flames and, using the same techniques that we have developed for the steady sooting flames, we will perform phase-averaged measurements to characterize the soot in the time-varying flames. We will also continue our studies of coflow flames at higher pressures.

References

1. R.J. Hall, M.D. Smooke and M.B. Colket, "Predictions of soot dynamics in opposed jet diffusion flames," Combustion Science and Technology Book Series, 4, 189-230 (1997).
2. HTFS RS 189: The Discrete Ordinates Approximation for Multidimensional Radiant Heat Transfer in

Furnaces, Harwell, Oxfordshire, February, 1977.
3. U.S.G.P. Office, RADCAL: A Narrow-Band Model for Radiation Calculations in a Combustion Environment, Washington, D.C., NIST Technical Note 1402, http://fire.nist.gov/bfrlpubs/fire93/PDF/f93096.pdf, April 1993, 1993.
4. V. Lecoustre, University of Maryland/National Institute of Standards and Technology, private communication, October 1, 2013.
5. S.K. Lele, "Compact Finite Difference Schemes with Spectral-Like Resolution," J. Comput. Phys., **103**, (1992).
6. R.V. Wilson, A.O. Demuren, and M. Carpenter, "Higher-Order Compact Schemes for Numerical Simulation of Incompressible Flows, Part II: Applications," Numer. Heat Transfer, Part B, **39**, (2001).
7. M. Noskov, Ph.D. Thesis, Yale University, 2004.
8. P. B. Kuhn, B. Ma, B. C. Connelly, M. D. Smooke, and M. B. Long, *Proc. Combust. Inst.* **33**, (2011).
9. B. Ma, G. Wang, G. Magnotti, R. S. Barlow and M. B. Long, *Combust. Flame,* **161**, (2014).

DOE Sponsored Publications since 2012

1. L. Tosatto, F. Mella, M. B. Long, and M. D. Smooke, "A Study of JP-8 Scoflow Flame Structure by Combined Use of Laser Diagnostics and Numerical Simulation," Combust. Flame, **159**, (2012).
2. J. Cancian, B. A. V. Bennett, M. B. Colket, and M. D. Smooke, "Prediction of Electron and Ion Concentrations in Low-Pressure Premixed Acetylene and Ethylene Flames," Comb. Theory and Modelling, **17**, (2013).
3. L. Tosatto, B. A. V. Bennett, and M. D. Smooke, "Comparison of Different DRG-Based Methods for the Skeletal Reduction of JP-8 Surrogate Mechanisms," Combust. Flame, **160**, (2013).
4. M. D. Smooke, "The Computation of Laminar Flames," Proceedings of the Combustion Institute, **34**, 2013.
5. B. Ma and M.B. Long, "Absolute light calibration using S-type thermocouples," Proceedings of the Combustion Institute, **34**, 2013.
6. S. Cao, B. Ma, B. A. V. Bennett, D. Giassi, D. P. Stocker, F. Takahashi, M. B. Long, and M. D. Smooke, "A Computational and Experimental Study of Coflow Laminar Methane/Air Diffusion Flames: Effects of Fuel Dilution, Inlet Velocity and Gravity," submitted Proceedings of the Combustion Institute, **35**, 2013.
7. B. Ma, S. Cao, D. Giassi, D. P. Stocker, F. Takahashi, B. A. V. Bennett, M. D. Smooke, and M. B. Long, "An Experimental and Computational Study on Soot Formation in a Coflow Jet Flame under Microgravity and Normal Gravity," submitted Proceedings of the Combustion Institute, **35**, 2013.
8. D. Giassi and M.B. Long, "Quantitative Two-Photon Laser-Induced Fluorescence of CO in a Time-Varying Coflow Methane/Air Flame," submitted Proceedings of the Combustion Institute, **35**, 2013.
9. B. Ma, G. Wang, G. Magnotti, R. S. Barlow and M. B. Long, "Intensity-ratio and color-ratio thin-filament pyrometry: Uncertainties and accuracy," Combust. Flame, **161**, (2014).
10. B. Ma and M. B. Long, "Combined soot optical characterization using 2-D multi-angle light scattering and spectrally resolved line-of-sight attenuation and its implication on soot color-ratio pyrometry," submitted to Appl. Phys B, (2014).

Quantum Chemistry of Radicals and Reactive Intermediates

John F. Stanton
Institute for Theoretical Chemistry
University of Texas
Austin, TX 78712
jfstanton@mail.utexas.edu

Scope of Research

My research group works in the area of theoretical chemical physics, especially on the thermodynamic properties, spectra, and reactions of organic radicals and other transient intermediates. In addition, we are active developers of software for both computational electronic structure and what might be termed computational spectroscopy. Our quantum chemistry research follows a number of paths, including first-principles calculations of bond energies and other thermochemical information (as well as development of methodology for such calculations), methods for the simulation and analysis of molecular spectroscopy, especially those relevant to experiments that can be used to glean thermochemical information, and the development of *ab initio* methods needed for the accurate treatment of transient organic molecules.

Summary of Recent Accomplishments

We have continued our work using the HEAT protocol[1] for the study of transition states, research that was part of our previous renewal proposal. To summarize, the HEAT protocol is a strategy for the computation of molecular energies (both adiabatic electronic energies and zero-point corrections) that is designed to be as accurate as possible, and to involve – apart from basis set extrapolation methods – no "empirical" corrections or assumptions. A number of calibration studies established HEAT to be accurate to within 1 kJ mol^{-1} (*ca.* 80 cm^{-1}) in the calculation of enthalpies of formation for molecules containing four and fewer atoms (a necessary restriction in the scope of applicability of the method at the time of the studies); more recent work has suggested that a high level of accuracy is maintained for larger molecules[2] that are now accessible due to advances in both algorithmic development and available computational resources. In thermochemistry, the quantities of interest are well-defined quantum mechanically, but the relevant quantity in reaction dynamics – the activation energy – is not similarly well-defined and therefore not amenable to comparable calibration studies. However, for those cases in which the electronic structure of the activated complex is similarly "complicated" to those molecules in the calibration set, a similar level of accuracy can be expected for the corresponding electronic energies and zero-point corrections. In the last year, we have applied HEAT and other high-level quantum chemistry to a number of different reaction systems that are relevant to environments involving combustion of fuel or biomaterials: the water-catalyzed and uncatalyzed hydration of ketene; the formation of Creigee intermediates in a methane-oxygen environment (still unpublished); the reaction of fluorine atoms

[1] A. Tajti *et al. J. Chem. Phys.* 121, 11599 (2004).

[2] This statement refers more to bond energies, for which the error does not grow with the size of the system, as opposed to absolute energies or heats of formation, errors for which will tend to grow with system size. The fact that coupled-cluster theory – the workhorse for the HEAT methods – is size-extensive is vital for maintaining the former.

with water; and the self-reaction of hydroxy radicals, for which the quality of our results have recently been confirmed experimentally by other members of the DOE Combustion program[3]. For all reactions where appropriate data is available, the calculated barriers and rates are in good agreement with experimental data, which attests to both the accuracy of the quantum chemistry part – HEAT – and our master-equation based kinetic treatments.

We have continued our work on the applications of semiclassical transition state theory (SCTST) to chemical reactions and the algorithmic improvement of SCTST. SCTST is a method that was conceived of some time ago[4] and provides rate constants that incorporate effects of both quantum-mechanical tunneling and reaction path curvature. However, unlike formally exact quantum calculations that require extensive information about the potential energy surface, efficient realizations of SCTST can be formulated which use only local information (derivatives through fourth-order in displacement) in regions of the potential surface around the transition state, which is an extremely attractive feature of the method. With advances in quantum chemical methodology – particularly the calculation of analytic derivatives of the potential surface – the ability of SCTST to determine reaction rates for reactive molecular systems was first realized some time ago[5], but only with our recent work has SCTST been put together with very accurate quantum chemistry and detailed kinetic models. Our major research effort in SCTST during the past year has been twofold. The fact that this theory is virtually always based on second-order vibrational perturbation theory (VPT2) is generally ignored or unknown, and – as A.F. Wagner has pointed out[6] – the theory can fail when the potential surface for the reaction coordinate deviates significantly from that of an inverted Morse oscillator (VPT2 is exact for the Morse potential in its application to bound-state problems). It is of fundamental interest to see how the theory performs when a better treatment of the "vibrational" states associated with the activated complex is used. This has formed part (but not all) of our motivation to extend the perturbation treatment of the Watson Hamiltonian to the next level: VPT4[7]. In the past year, we have succeeded in deriving and verifying equations for the VPT4 treatment of the rovibrational problem, in the context of the Watson Hamiltonian. An analysis similar to that which is needed to modify bound-state VPT2 into a form amenable to SCTST is underway, but thus far not completed. However, vibrational levels of water are shown below as calculated with VPT2 and VPT4 for the potential of Tennyson and coworkers[8], which demonstrate a systematic improvement of the latter with respect to VPT2. In addition to working on development of SCTST, standard (VPT2-based) SCTST calculations have been used in all of our kinetic studies, recently modified by an *ad hoc* algorithm modification to crudely account for the problems noted by Wagner[9].

---

[3] G. Altinay and R.G. Macdonald *J. Phys. Chem. A* 118, 38 (2014).

[4] W.H. Miller *Faraday Transactions* 62, 40 (1977).

[5] M.J. Cohen, N.C. Handy, R. Hernandez and W.H. Miller *Chem. Phys. Lett.* 192, 407 (1992).

[6] A.F. Wagner *J. Phys. Chem. A* 49, 13089 (2013).

[7] By virtue of how the orders of perturbation are defined,and the use of a harmonic oscillator zeroth-order function, odd orders of VPT vanish.

[8] P. Barletta, S.V. Shirin, N.F. Zobov, O.L. Polyansky, J. Tennyson, E.F. Valeev and A.G. Csaszar *J. Chem. Phys.* 124, 124307 (2006).

[9] J.F. Stanton, unpublished.

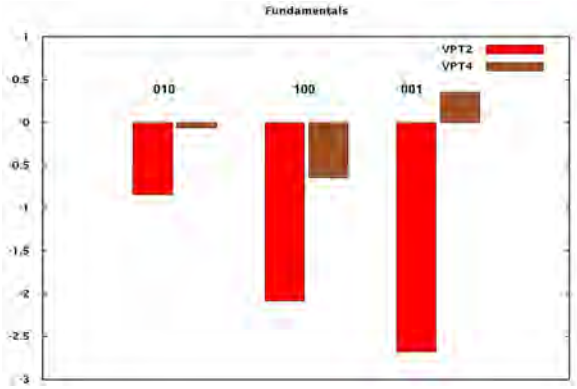

Errors in the calculation of fundamental vibrational levels of water (cm^{-1}) at the VPT2 and VPT4 levels, as compared to exact variational calculations. The potential surface and variational results are taken from P. Barletta, S.V. Shirin, N.F. Zobov, O.L. Polyansky, J. Tennyson, E.F. Valeev and A.G. Csaszar *J. Chem. Phys.* 124, 124307 (2006).

A major accomplishment in the last year has been an initial implementation of the highly-accurate CCSDTQ and CCSDT(Q) treatments of electron correlation in an entirely new, and parallelized, code known as NCC (which is a part of the CFOUR package that is maintained and developed by my group, along with J. Gauss in Mainz, Germany and P.G. Szalay in Budapest, Hungary. At present, this code can do energy calculations for closed-shell systems, using a spin-adaptation scheme developed by myself and Gauss in the last 1990s for triple excitations, but generalized, systematized and published in just the last year. This code is roughly two *orders of magnitude* faster (even on a single processor) than other codes that have implemented these methods, and will be an integral part of our future calculations of high-accuracy thermochemistry and kinetics.

In other work published in the past year, we have worked on special cases of the two-dimensional master equation (energy and angular momentum), applying this to the OH + CO reaction that we studied previously in the low and high-pressure limits; the thermochemistry of the acetylene vinylidene rearrangement and predictions that are relevant to efforts to detect the latter by means of chirped-pulse microwave experiments; and a joint experimental-theoretical study of the simplest Criegee intermediate (H_2C=O-O), which has been produced with very high selectivity in a discharge of molecular oxygen and methane. We have characterized the structure of this famous and elusive molecule at a level of precision that is uncommon even for stable molecules; we also continue to study the global potential energy surface of H_2CO_2, as is mentioned below.

Ongoing Research and Future Plans

Work is underway along several different fronts. In terms of program development, the NCC module mentioned above will soon be capable of gradient calculations at the CCSDT and CCSDT(Q) levels (with closed-shell reference functions; CCSD gradients are already working). As is well-known, the computational infrastructure needed for coupled-cluster gradients is largely equivalent (and sufficient) to that for studying excited, ionized and electron-attached states with equation-of-motion coupled cluster theory. We therefore hope to have gradients *and* equation-of-motion capabilties at the CCSDT and CCSDTQ levels in NCC within a year. All of these developments will go into the CFOUR package, which is freely available to the computational chemistry community.

We are currently engaged in a detailed and through study of the CH_2O_2 potential energy surface (see below). This particular stoichiometry is clearly important for combustion, and the exciting new developments of the past few years regarding the Creigee species[10] (amongst the least stable forms of this molecule) have helped to make this system a much-studied topic in gas-phase chemical physics. We have nearly completed characterizing all stationary points at the HEAT level of theory, and will soon begin kinetic modeling of relevant reactions. In addition, we plan to study the ozonlysis of ethylene, which has been a reaction of great interest to my associate T.L. Nguyen for many years.

[10]O. Welz, J.D. Savee, D.L. Osborn, S.S. Vasu, C.J. Percival, D.E. Shallcross, C.A. Taatjes *Science* 335, 204 (2012).

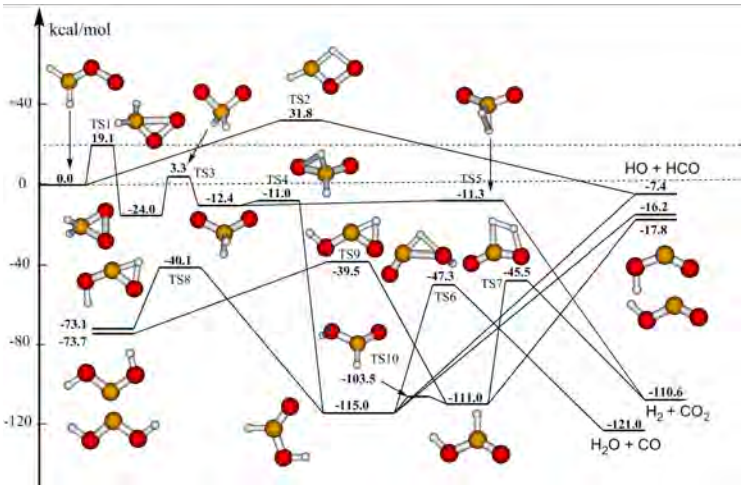

Energies (most calculated at the HEAT-345(Q) level of theory) of isomers and transition states for isomerization pathways on the CH_2O_2 potential energy surface. The Criegee intermediate is at the upper left.

Students and Postdoctoral Supported:

T.L. Nguyen (postdoc) B. Xue (undergrad) H. Lee (undergrad)

References supported by DE-FG02-07ER15884 (2013)

T.L. Nguyen and J.F. Stanton "Theoretical Determination of the Potential Energy Surfaces and Reaction Rates of HO + HO —¿ H2O + O(3P) and its Isotopic Variants, J. Phys. Chem. A 117, 2678 (2013).

D.A. Matthews, J.F. Stanton and J. Gauss "A Revisitation of Non-Orthogonal Spin-Adaptation in Coupled Cluster Theory, J. Chem. Theo. Comput. 9, 2567 (2013).

H. Lee, J.H. Baraban, R.W. Field and J.F. Stanton "High-Accuracy Estimates for the Vinylidene-Acetylene Isomerization Energy and the Ground State Rotational Constants of H2C=C:, J. Phys. Chem. A 117, 11679 (2013).

T.L. Nguyen, J. Li, R. Dawes, J.F. Stanton and H. Guo "Accurate Determination of Barrier Height and Kinetics for the F + H_2O → HF + OH Reaction *J. Phys. Chem. A* 117, 10997 (2013).

T.L. Nguyen, B.C. Xue, G.B. Ellison and J.F. Stanton "Theoretical Study of Ketene Hydration in the Gas Phase: Formation of Acetic Acid?" *J. Phys. Chem. A* 117, 8864 (2013).

M.C. McCarthy, L. Cheng, K.N. Crabtree, O. Martinez, T.L. Nguyen, C.C. Womack and J.F. Stanton "The Simplest Criegee Intermediate (H2C=OO): Isotopic Spectroscopy Equilibrium Structure and Possible Formation from Atmospheric Lightning, J. Phys. Chem. Lett. 4, 4133 (2013).

R.E. Weston, T.L. Nguyen, J.R. Barker and J.F. Stanton "HO + CO Reaction Rates and H/D Kinetic Isotope Effects: Master Equation Models using ab initio SCTST Rate Constants *J. Phys. Chem. A* 117, 821 (2013).

Universal and State-Resolved Imaging Studies of Chemical Dynamics

Arthur G. Suits
Department of Chemistry, Wayne State University
5101 Cass Ave
Detroit, MI 48202
asuits@chem.wayne.edu

I. Program Scope

The focus of this program is on combining universal ion imaging probes providing global insight, with high-resolution state-resolved probes providing quantum mechanical detail, to develop a molecular-level understanding of chemical phenomena. Particular emphasis is placed upon elementary reactions important in understanding and predicting combustion chemistry. This research is conducted using state-of-the-art molecular beam machines, photodissociation, reactive scattering, and vacuum ultraviolet lasers in conjunction with ion imaging technqiues. An ongoing parallel effort is made to develop new tools and experimental methods with which to achieve these goals.

II. Recent Progress

Systematic studies of polyatomic reaction dynamics. We continue to exploit the powerful combination of slice imaging with VUV ionization to pursue systematic studies of polyatomic reaction dynamics in crossed beams.

Roaming in radical addition/elimination. One important direction for our work in the past year has been studies of radical addition/elimination in alkenes in collaboration with the Mebel group. Our experimental results for Cl + butenes show evidence for the addition/elimination reactions prevailing over direct reaction in these systems. Reaction proceeds through a long-lived complex in which the Cl addition to the double bond is followed by HCl elimination from the adjacent methyl groups. No evidence for a 3-center or 4-center transition state is seen in the experimental results, nor in a careful analysis of the ground-state potential energy surface. Instead we find a roaming-type transition state located 1-2 kcal·mol^{-1} below the energy of the reactant asymptote with greatly extended C-Cl and Cl-H bond distances and vibrational frequencies very similar to the reactants. The picture is therefore analogous to the roaming mechanism observed previously in unimolecular reactions.. In this case the roaming dynamics are central to the addition/elimination reaction mechanism: Although abstraction is the only pathway to products as dictated by orbital symmetry considerations, an indirect reaction can occur mediated by the strong electrophilic interaction of the Cl atom with the alkene π cloud. The reactions remain fast and HCl elimination can compete with the Cl loss because of the loose roaming transition state combined with the slight enthalpic advantage.

Reaction of selectively deuterated propane and butane. In the past year we have extended our studies of Cl atom reactions with C-3 and C-4 alkanes this using our intense Cl atom ablation source. In this case our unfocused 157nm probe is not sensitive to the primary radical, whose ionization energy is above the energy of the probe photon. This gives us the unique opportunity to study reaction at a particular site (the central, secondary C atom) with no deuteration or with deuteration on the primary or secondary sites. The results are presented in Fig. 1 for selectively deuterated propane. Reactive scattering images and their derived double differential cross sections are presented for a number of Cl + alkane abstraction reactions involving propane and its two partially deuterated isotopologues, namely 1,1,1,3,3,3-propane-d6 ($CD_3CH_2CD_3$, hereafter **D1**) and 2,2-propane-d2 ($CH_3CD_2CH_3$, **D2**), as well as n-butane and isobutane. Reactive scattering images of the Cl+alkane reactions overlaid

with their Newton diagrams are presented in Fig. 2. Scattering is seen broadly in all regions, with a tendency for peaking in the backward and forward directions. Propane images show strong photochemical background interferences although the integrations are done with signed data after subtraction. For butane, background is readily subtracted and the full scattering distributions can be analyzed.

As mentioned above, it is important to address the question of detection efficiency depending on the different radical products for each reaction. In this study, no primary abstraction products were detected for selectively deuterated propane, whether labeled at the primary or secondary site. This is consistent with the calculated ionization energies. This is an indirect consequence of the radical source improvement that makes possible the use of an *unfocused* probe laser beam: although we could have access to primary abstraction products as already shown by multiphoton ionization with a focused VUV probe, we believe our results here are now site-selective even in the case of non-labeled butanes, given the similarity in the vertical IEs of propane and butane.For all systems, the translational energy of the FW component peaks at higher energy than the SW/BW component. As seen in Fig. 3, the scattering signal is therefore maximal at low angles, then reaches a minimum in the 60-90° range, and increases steadily over 180°. Overall, the distributions for the **D1** and **D2** reactions show the same features as for the reaction with normal propane but significant differences can however be seen. Concerning translational energy recoil, FW and SW **D1** distributions peak at lower E_T^* than regular propane and **D2**, while all FW distributions peak at similar E_T^*. This reflects a more effective energy disposal into the CD_3CHCD_3 propyl degrees of freedom for the "rebound-like" mechanism. Among the systems studied here, the most similar distributions are those of propane **D1** and isobutane. These systems have a unique H abstraction site, and **D1** is the propane system with the highest vibrational density-of-states. The observed progression of translational energy release with hydrocarbon mass seems to indicate that C3 and C4 hydrocarbons are the last steps before convergence toward

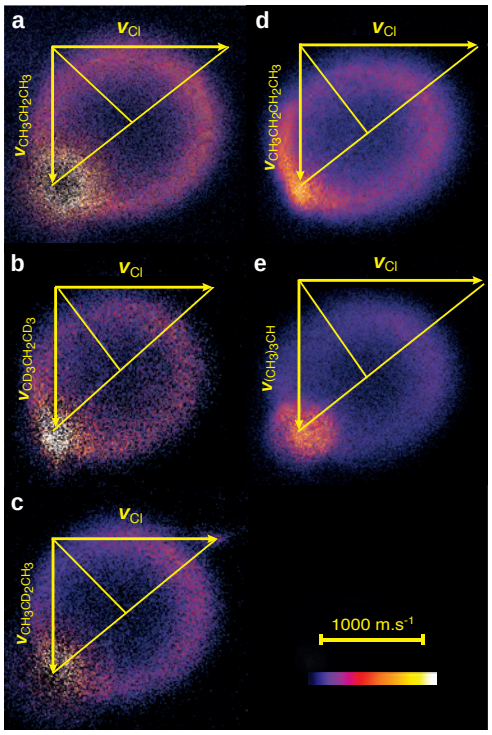

Figure 1. DC sliced raw images of reactive scattering and Newton diagrams for the reactions of chlorine with propane and butane: a) propane, E_C = 11.6 kcal.mol^{-1} b) propane D1, probe at m/z=49 (CD_3CHCD_3) E_C = 11.8 kcal.mol^{-1}, c) propane D2, probe at m/z=46, (CH_3CDCH_3) E_C = 12.1 kcal.mol^{-1}, d) n-butane, probe at m/z=57, E_C = 13.4 kcal.mol^{-1}, and e) isobutane, probe at m/z=57, E_C = 13.6 kcal.mol^{-1}.1

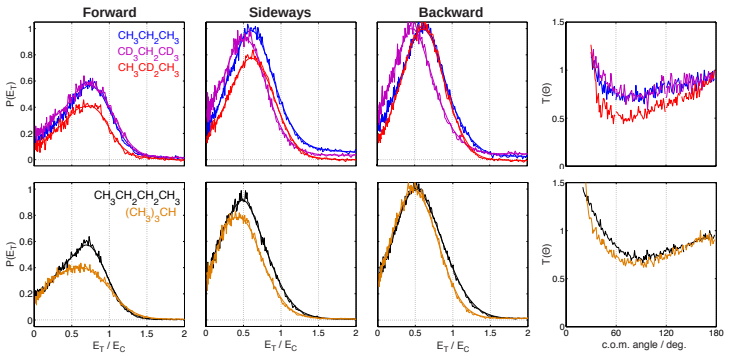

Figure 2. Reduced translational energy distributions for forward (30-60°), sideways (60-120°), and backward (120-180°) scattered products and the center-of-mass angular distributions. Top panel corresponds to propane reactions with propane in blue, **D1** in purple and **D2** in red. Bottom panel corresponds to butane reactions with n-butane in black and isobutane in gold.

the internal energy transfer seen for larger saturated systems.

Isomer-specific detection and imaging via "semi-soft" ionization. We have reported the use of strong-field non-resonant ionization, in conjunction with the "fingerprint" mass spectra, to identify and quantify product molecules and distinct isomers in a way somewhat analogous to tunable VUV ionization. The strong-field ionization probe shows great promise in a wide range of potential applications. Its advantages are its universality (any molecule may be ionized in a field of 1.5×10^{14} W/cm^2), its detection limit (There may be a dozen molecules in the focal volume, all ionized and counted) and the selectivity of its detection in mass spectrometry, which we have begun to demonstrate. We note, however, that although it has near unit detection efficiency, this is only in an extremely small probe volume. It is not suitable for detection of very dilute or low number density samples. We are currently investigating strong-field probes of radicals produced in flash pyrolysis. This is illustrated in Fig 3 for isoprene pyrolysis. In the upper panels we show strong-field ionization of isoprene at modest laser power contrasted with electron impact ionization from the NIST database. At $2x10^{13}$ W/cm^2, almost no fragmentation is seen, while in the electron impact spectrum the parent ion is only about 15% of the total ion yield. In the lower panel we show the mass spectra in the 2-4 carbon region at a laser power above the saturation intensity both with and without the flash pyrolysis. Here the dominant pyrolysis product is C_4H_4 from loss of CH_4 (m/z=52), in addition to which strong signals are seen at C_3H_3 and C_3H_4. These preliminary results simply showcase the potential of strong-field ionization as a versatile, universal probe technique. Using the measured saturation intensities we can evaluate the possible product isomers to assign the most likely candidate product.

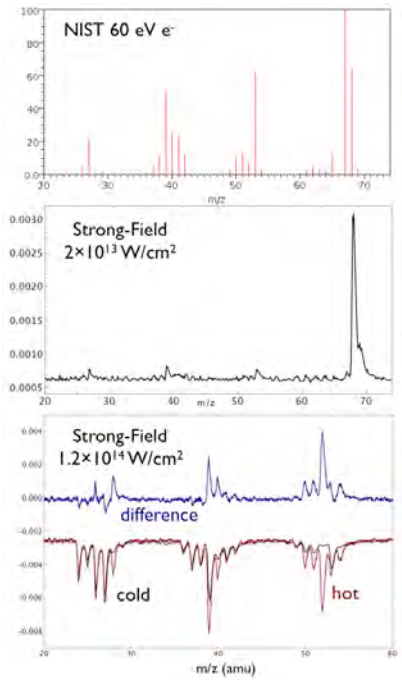

Figure 3. Electron impact (top) and strong-field mass spectra of isoprene. Bottom panel shows strong field ionization following flash pyrolysis.

III. Selected Future Plans

State-resolved and universal crossed-beam DC slice imaging. We have plans to continue exploring a range of systems using our crossed-beam sliced imaging approach. We have increased the radical beam intensity another four-fold, so our background problems should be greatly reduced. Then we can go to lower collision energy and revisit a number of systems mentioned above. One promising direction with the new radical source will be CH reactions. These are very fast, and give branching both to CH_2 and H elimination. For the latter pathways we will have near-zero background. These offer the opportunity for "chemical activation" investigation of roaming systems. These radicals can insert directly into bonds, forming highly energetic ground state systems at a well-defined total energy. This is ideal for probing roaming reactions quite generally.

Roaming dynamics probed with IRMPD. Our earlier studies that first documented roaming did so in formaldehyde, but we were confined to coarse sampling of the excitation energy through metastable levels of S_1. We have recently reported the first study to combine IRMPD with ion imaging. This combination is ideal to probe roaming phenomena which are expected to be favored by ground state

processes. Using IRMPD with DC slice imaging detection of the CO product we can look close to the roaming threshold and tune the excitation by adjusting the CO_2 laser fluence. We can monitor both the overall rotational distributions, which are bimodal owing to the presence of roaming and conventional TS pathways, and we can also record images on the intermediate levels that have both channels present. This will allow us to look at the roaming branching continuously, in steps of the CO_2 laser photon energy, in the threshold region. In fact, this combination of IRMPD with state-correlated imaging offers the possibility of seeing discrete excitation even in this multiphoton excitation process: each additional IR photon will give a new set of correlated states displaced by the photon energy of ~1000 cm^{-1}. These will be clearly resolvable in the images, so the usual critique of IRMPD that the excitation energy is not well-defined will not hold in high-resolution imaging. Similar considerations will apply to acetaldehyde, the second-most studied roaming system, and another likely target for IRMPD-imaging.

Chirped-pulse mm-wave detection in uniform supersonic flows. In collaboration with Bob Field, we are developing a unique and powerful new instrument that will combine two uniquely well-matched, emerging technologies: chirped-pulse Fourier-transform micro/mm-wave spectroscopy developed by Brooks Pate and pulsed uniform supersonic flows as developed by Rowe et al. This combination promises a nearly *universal detection method that can deliver isomer and conformer specific, quantitative detection and spectroscopic characterization* of unstable reaction products and intermediates, product vibrational distributions, and molecular excited states. The proposed technique will be suitable for application in diverse fields including fundamental studies in spectroscopy and reaction dynamics, kinetics, and combustion. The instrument is being developed with NSF funds, but DOE related work will be one of the principal applications of the apparatus.

IV. DOE Publications 2011-present

N. Herath and A. G. Suits, "Roaming radical reactions," *J. Phys. Chem. Lett.*, **2** 642 (2011).

J.M. Bowman and A. G. Suits, "Roaming reactions: The Third Way," *Phys. Today*, **64** 33 (2011).

A. D. Estillore, L. M. Visger-Kiefer, A. G. Suits, "Reaction dynamics of Cl + butanol isomers by crossed-beam sliced ion imaging," *Faraday Discussion 157*, (2012). DOI:10.1039/C2FD20059G.

L. Yan, F. Cudry, W. Li, and A. G. Suits, "Isomer-Specific Mass Spectrometric Detection Via Semi-Soft Strong-Field Ionization," *J. Phys. Chem. A* (2013) DOI: 10.1021/jp403118c.

Joalland, B., Van Camp, R. D., Shi, Y., Patel, N., & Suits, A. G., "Crossed-Beam Slice Imaging of Cl Reaction Dynamics with Butene Isomers." *The Journal of Physical Chemistry A.* (2013) DOI: 10.1021/jp403030s.

B. Joalland, Y. Shi, Patel, N., R. Van Camp, & A. G. Suits, "Dynamics of Cl+ Propane, Butanes Revisited: A Crossed Beam Slice Imaging Study." *Phys. Chem. Chem. Phys.* (2014) DOI: 10.1039/C3CP51785C.

B. Joalland, Y. Shi, A. G. Suits and A. M. Mebel, "Roaming dynamics in radical addition/elimination reactions," *(submitted).*

An Update on the Implementation of a Novel Multiscale Simulation Strategy

PI: James C. Sutherland
Department of Chemical Engineering, The University of Utah
Salt Lake City, UT 84112-9203
James.Sutherland@utah.edu
Project start date: October, 2012

I. Lattice Based Multiscale Simulation

A. Introduction

Direct Numerical Simluation (DNS) of turbulent flows, particularly at high Reynold's numbers, is prohibitively expensive due to the range of length scales present. The One-Dimensional Turbulence (ODT) model is a cost effective alternative that fully resolves length scales down to the Kolmorogov length scales in a single dimension while using a stochastic model to account for turbulence. Although ODT has been shown to capture buoyant flows, stratified flows and, of most interest to us, combusting flows [1–3] accurately, it fails to capture some large scale phenomena such as vortex pairing, recirculation or three dimensional flows that cannot easily be reduced to lower dimensions such as asymmetric geometries.

We have previously proposed a new methodology to bridge the gap between Large Eddy Simulation (LES) and DNS. This methodology, termed Lattice-Based Multiscale Simulation (LBMS), creates a system of ODT models that overcomes the shortcomings of ODT at a cost significantly cheaper than DNS. Furthermore, by fully solving all governing equations at the smallest scales, all phenomena associated with turbulent combustion can be accurately captured.

B. Basic Formulation

The LBMS model is a lattice like structure of ODT models, as depicted in Figure 1. The governing equations take the form of

$$\int_{\mathsf{V}(t)} \frac{\partial \rho\psi}{\partial t}\,\mathrm{d}\mathsf{V} = -\int_{\mathsf{S}(t)} \boldsymbol{\Theta}_\psi \cdot \mathbf{n}\,\mathrm{d}\mathsf{S} + \int_{V(t)} R_\psi\,\mathrm{d}\mathsf{V}, \qquad (1)$$

where ψ is the transported variable, $\boldsymbol{\Theta}_\psi$ is the flux through surface S and R_ψ are source terms. Table 1 defines these quantities for the mass, momentum, species and total internal energy equations.

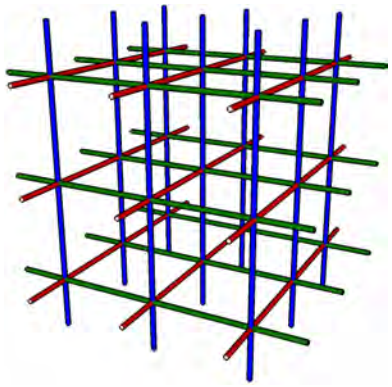

Figure 1: Representation of a 3D LBMS mesh. Each color denotes a different directional bundle. Lines are fully resolved.

The fine spacing, δx_i, where i denotes a cartesian direction, is the resolution required for the smallest spatial structures in the flow field. The coarse spacing, Δx_i, is the spacing between each individual line (on the order of the integral length scale), and all lines in a given direction form a *bundle*.

Fluxes between ODT lines (*i.e.* perpendicular to the bundle direction they are calculated on) are under-resolved due to the coarse spacing Δx_i. This issue is resolved in one of two ways, both of which interpolate a fully resolved flux from the bundle parallel to said flux direction to the other

Table 1: Definitions of ψ, $\mathbf{\Theta}_\psi$ and σ_ψ for Equation (1) for a non-reacting, single-phase system. $\boldsymbol{u}$ represents the velocity, ρ the density, $\boldsymbol{\tau}$ is the stress tensor, P represents the pressure, $\boldsymbol{g}$ the gravitational acceleration, e_0 the total internal energy and $\boldsymbol{q}$ the energy diffusive flux, Y_i the mass fraction of species i, $\boldsymbol{j_i}$ the diffusive flux of species i and R_i the reaction rate of species i.

Equation	ψ	Total Flux, $\mathbf{\Theta}_\psi$	Source Term, σ_ψ
Mass	1	$\rho\mathbf{u}$	0
Momentum	$\mathbf{v}$	$P\mathbf{I} + \boldsymbol{\tau} + \rho\mathbf{u}\mathbf{u}$	$\rho\mathbf{g}$
Total Internal Energy	e_0	$e_0\mathbf{u} - p\mathbf{u} - \boldsymbol{\tau}\cdot\mathbf{u} + \mathbf{q}$	$\rho\mathbf{g}\cdot\mathbf{u}$
Species	Y_i	$\rho Y_i\mathbf{u} + \mathbf{j}_i$	R_i

bundles. In the first method, flux interpolation is completed by imposing the fluxes that live on other bundles. In the second, the flux is reconstructed by setting the high wave number but underresolved flux information from the bundle that is receiving the fully resolved flux to the integral of the fully resolved flux to ensure conservation across control volumes. This is shown for a two dimensional case in Figure 2, where $\mathbf{\Theta}$ represents the total flux, the subscript represents the flux direction and the superscript represents the bundle in which the flux lives on.

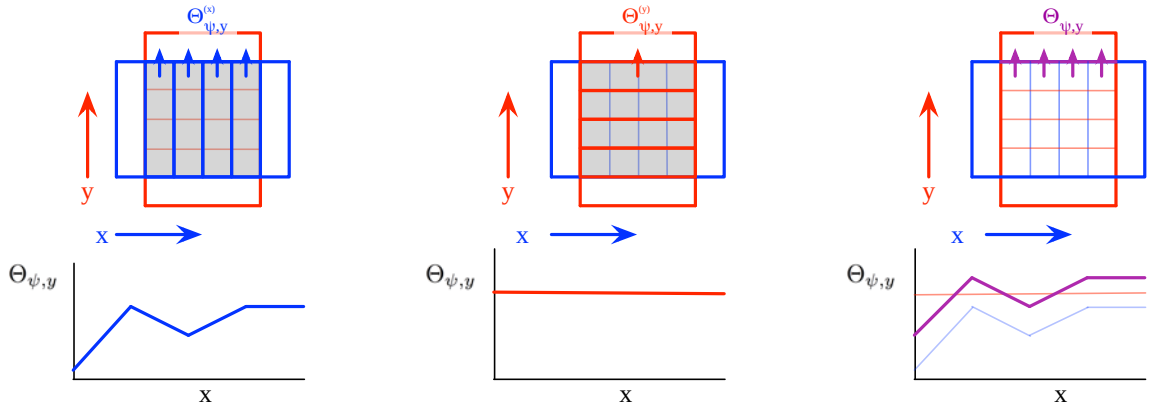

(a) Under resolved high information flux in the y-direction on the x-bundle

(b) Fully resolved, low information flux in the y-direction on the y-bundle

(c) Fully resolved, high information flux reconstruction

Figure 2: Two dimensional flux reconstruction

II. Recent Progress

A. Convergence Studies

An important test for verification is a convergence study. The schemes utilized by LBMS are a second order central differencing scheme in space and a first order forward marching scheme in time (which will be extended to second order soon). As shown in Figure 3, LBMS converges to second order spatially and first order temporally.

These cases were run on advecting scalar transport and compared to analytical solutions. For

the temporal accuracy, the mesh size was maintained and time step size was maintained to calculate spatial convergence. Verification is still being completed on the full system of transport equations, as the coupling increases the complexity of the code.

B. Parallelization and Scaling Results

Domain-decomposition of ODT is challenging because of the stochastic occurrence of eddies, which may act at random locations and sizes. LBMS is parallelized using domain decomposition at two levels: the bundle and the line. Given that bundles couple through coarse fluxes, communication between bundles is not as intensive as it can be between patches in traditional domain-decomposition approaches for Computational Fluid Dynamics. Thus, bundles are first distributed across processors and then lines within each bundle are distributed across processors. This results in two distinct communication patterns occurring: one between bundles (volumetric communication on coarse volumes) and one between lines within a bundle.

Figure 4 shows preliminary scaling results from a simple test case of the LBMS code on a local cluster up to around 2000 MPI processes. These are preliminary results, but indicate that the parallelization strategy is showing promise in both strong and weak scaling regimes, with parallel efficiencies consistently above 70% even at the highest processor counts. As more physics are added, we anticipate that scalability may improve since we will be increasing the workload relative to the amount of communication that will occur. Some of the "chatter" in the scalability is due to the domain decomposition strategy, which can result in minor load imbalances for some processor counts.

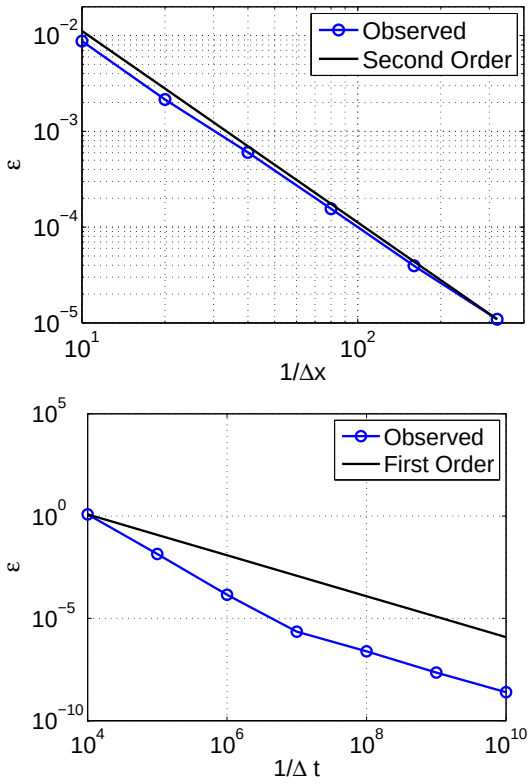

Figure 3: Top: spatial convergence (second order). Bottom: temporal convergence (first order).

III. Future Plans

A. Parameter Studies

As of now, the LBMS code has triplet map permutations associated with the ODT code implemented into the LBMS framework. Our next step is to consider isotropic turbulence decay to evaluate the model's ability to capture the $-5/3$ scaling law as well as the temporal decay of the power spectrum from experimental data [4].

Two parameters of particular importance are the eddy rate constant and the ratio of coarse to fine scales, Δ/δ. The eddy rate constant affects the number of eddies and thus, the transfer of momentum to thermal energy through viscous dissipation. The eddy rate constant must be tuned appropriately to ensure that the kinetic energy decay in time matches DNS, experimental or model data sets. The coarse to fine ratio, Δ/δ, directly affects the scale at which three-dimensional affects are directly resolved (Δ). Scales between Δ and δ are resolved along individual lines in each direction, but turbulent mixing in this range of length scales is modeled through ODT. We

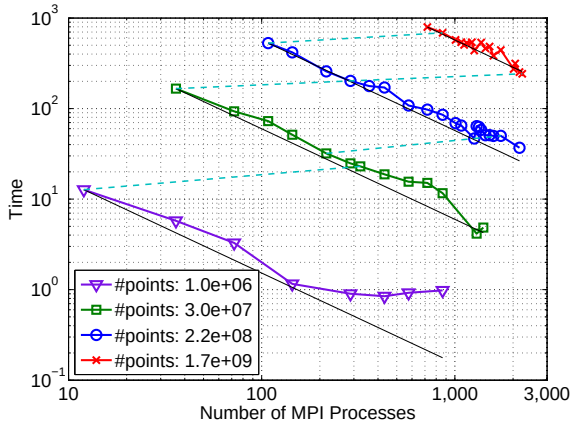

(a) Strong and weak scaling of the LBMS simulation code up to 2100 MPI processes with $\Delta/\delta = 1$. Teal dashed lines indicate weak scaling and solid black lines indicate perfect strong scaling.

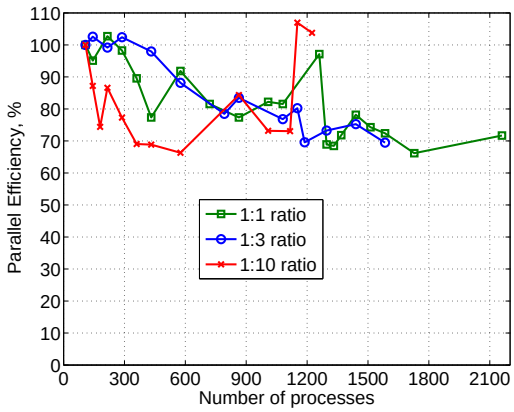

(b) Parallel efficiency for strong scaling for $\Delta/\delta = 1, 3, 10$ on problems with 200 million total grid points.

Figure 4: Preliminary scalability of the LBMS code on a local cluster up to 2100 MPI processes.

expect that, for isotropic turbulence, large Δ/δ will be feasible, but for other flows involving strong recirculations such as confined jets will require smaller Δ/δ. However, this must be quantified through validation studies.

B. Species Transport and Source Term Closure

The next objective in turbulent combustion simulation is including species transport and chemical reactions. Source term closure will need to be addressed. Ultimately, as $\Delta x \gg \delta x$, there will be a wealth of information on the fine mesh that will need to be interpolated from each bundle to the coarse mesh to integrate the source terms over the control volumes. This will be particularly important for species source terms during combustion as flame fronts tend to be highly reactive but at small length scales. Various interpolation/reconstruction methods have been tested on the unique LBMS mesh with simple configurations to explore their efficacy, and this work will continue through the next year as we move toward highly reactive flows.

References

[1] Wm. T. Ashurst and Alan R. Kerstein. One-dimensional turbulence: Variable-density formulation and application to mixing layers. *Physics of Fluids*, 17(2):025107, 2005.

[2] J C Hewson and A R Kerstein. Stochastic simulation of transport and chemical kinetics in turbulent CO/H2/N2 flames. *Combust. Theory Modelling*, 5:669–697, 2001.

[3] Naveen Punati, James C. Sutherland, Alan R. Kerstein, Evatt R. Hawkes, and Jacqueline H. Chen. An evaluation of the one-dimensional turbulence model: Comparison with direct numerical simulations of CO/H2 jets with extinction and reignition. *Proceedings of the Combustion Institute*, 33(1):1515–1522, 2011.

[4] Stanley Corrsin. Simple Eulerian time correlation of full- and narrow-band velocity signals in grid-generated, isotropicâ turbulence. 48, 1971.

Elementary Reaction Kinetics of Combustion Species

Craig A. Taatjes
Combustion Research Facility, Mail Stop 9055, Sandia National Laboratories, Livermore, CA 94551-0969
cataatj@sandia.gov

SCOPE OF THE PROGRAM

This program aims to develop new methods for studying chemical kinetics and to apply these methods to the investigation of fundamental chemistry relevant to combustion science. One central goal is to perform accurate measurements of the rates at which important free radicals react with each other and with stable molecules. Another goal is to characterize complex reactions that occur via multiple potential wells by investigating the formation of products. These investigations employ simultaneous time-resolved detection of multiple species in well-characterized photolytically-initiated reaction systems where multiple consecutive and competing reactions may occur. Understanding the reactions in as much detail as possible under accessible experimental conditions increases the confidence with which modelers can treat the inevitable extrapolation to the conditions of real-world devices. This research often requires the development and application of new detection methods for precise and accurate kinetics measurements. Absorption-based techniques and mass-spectrometric methods have been emphasized, because many radicals critical to combustion are not amenable to fluorescence detection.

An important part of our strategy, especially for complex reaction systems, is using experimental data to test and refine detailed calculations (working in close cooperation with Stephen Klippenstein at Argonne and Ahren Jasper and Judit Zádor at Sandia), where the theory offers insight into the interpretation of experimental results and guides new measurements that will probe key aspects of potential energy surfaces. This methodology has been applied in our investigations of the reactions of fuel radicals with O_2. The combination of rigorous theory and validation by detailed experiments has made great strides toward a general quantitative model for alkyl oxidation, and now extends to reactions of oxygenated molecules relevant to biofuel combustion and to the effects of unsaturation on the chemistry leading to autoignition. Moreover, we have increasingly aimed at producing species that are intermediates in oxidation systems (e.g., Criegee intermediates, hydroperoxyalkyl radicals) and directly probing their reaction kinetics.

RECENT PROGRESS

We continue to apply frequency-modulation and direct absorption spectroscopy to measurements of product formation in reactions of alkyl radicals with O_2 and kinetics of unsaturated hydrocarbon radicals. In addition, the multiplexed photoionization mass spectrometric reactor at the Advanced Light Source (ALS), an experimental effort led by David Osborn (see his abstract), has become a major part of our investigations of low-temperature hydrocarbon oxidation chemistry. In the past year we have been largely occupied with expanding our understanding of the fundamental chemistry of carbonyl oxides (Criegee intermediates), but our attention is returning to details of reactions that are important in the ignition chemistry of biofuels, such as the reactions of molecular oxygen with fuel radicals obtained by H atom abstraction from cyclic ethers and ketones.

Chemistry of carbonyl oxides. Carbonyl oxides ("Criegee intermediates") are produced in ozonolysis, and are hence important intermediates in tropospheric hydrocarbon oxidation. They are also the intermediates in combustion reactions of carbenes with O_2, and calculations suggest that they may also be products of QOOH + O_2 reactions.[1] The carbonyl oxides have an electronic structure that includes closed-shell zwitterion and singlet biradical character, and their reactivity is of considerable fundamental interest. However, they have been difficult to detect and study in the gas phase, before our detection of CH_2OO[2] and measurement of its reaction kinetics by photoionization mass spectrometry. We have continued to measure reactions of CH_2OO, and have also measured larger carbonyl oxides acetaldehyde oxide (CH_3CHOO) and acetone oxide ($(CH_3)_2COO$).

Conformer-dependent reactions of acetaldehyde oxide.[(l)] We succeeded in producing the second-smallest carbonyl oxide, acetaldehyde oxide, from the reaction of 1-iodoethyl radicals with O_2. Acetaldehyde oxide exists as two conformers, *syn* (with the O–O group pointing towards the methyl group) and *anti* (with the O–O group pointing away from the methyl group. These two conformers have slightly different photoionization spectra and can be separately probed. We showed that *anti*-CH_3CHOO is substantially more reactive toward water and SO_2 than is *syn*-CH_3CHOO, making the first direct determination of a rate coefficient for reaction of a carbonyl oxide with water.

Correction to third-body effect of O_2 on $CH_2I + O_2$ reaction.[(q)] We reinvestigated the apparent collision efficiency of helium, O_2, N_2, and SF_6 in stabilizing CH_2IOO in the reaction of $CH_2I + O_2$ and now find no substantially larger stabilization efficiency of O_2 than that of N_2. The error in the initial report was caused by an incorrect treatment of the instrumental response function of the detection system in previous data processing.

Reactions of carbonyl oxides with acids.[(b)] We directly measured rate coefficients for the reactions of the CH_2OO and CH_3CHOO with the two simplest carboxylic acids, formic acid (HCOOH) and acetic acid (CH_3COOH). The measured rate coefficients are in excess of 1×10^{-10} cm^3 s^{-1}, several orders of magnitude larger than those suggested from indirect experiments. The slower CI reactions with aldehydes and ketones exhibit reactant van der Waals complexes that may affect the overall kinetics.[3] The large rate coefficients suggest that the bottlenecks to reaction of CI with carbonyls are absent in reaction of CI with acids. Facile transfer of the acidic –OH hydrogen to the basic terminal O atom of the CI, forming the hydroperoxyalkyl carboxylate, may act to prevent any kinetically significant entrance-channel complex.

Stark effect in formaldehyde oxide.[(a)] With collaborators in Europe and China, ab-initio calculations of geometries and dipole moments were used to compute the Stark effect on the lowest rotational levels of CH_2OO. The hexapole transmission spectra for the low-field seeking states are sensitive to the details of the dipole moment, suggesting that the hexapole can potentially be useful to study the molecular properties of CH_2OO, or to select CH_2OO for molecular beam scattering or photodissociation measurements.

FUTURE DIRECTIONS

We will continue our exceptionally productive collaboration with David Osborn using the photoionization mass spectrometry machine at the Advanced Light Source, as well as expanding to higher pressure operation in conjunction with Lenny Sheps and the Argonne-Sandia Consortium on High-Pressure Combustion Chemistry (see ASC-HPCC

abstract). The effects of unsaturation and oxygenation on low-temperature oxidation chemistry will be further explored, with further measurements of elementary oxidation reactions of representative biofuel molecules in the temperature region 500 K – 800 K. This work is part of a continuing goal of developing a more general understanding of the ignition chemistry of alternative fuels. For example, in work from a Sandia Laboratory-Directed Research and Development project on fungal biofuels,[4] we found that vinoxylic resonance stabilization in QOOH radicals can play an important role in guiding the course of low-temperature oxidation chemistry.[5] The further exploration of resonance-stabilization effect in the fundamental oxidation chemistry of unsaturated esters and ketones will be an immediate goal of the present program, as will investigations of resonance stabilization in oxidation reactions of substituted aromatics.

Our study of QOOH reactions will continue the longstanding quest to directly detect QOOH. One key difficulty has been simply making a high enough concentration of QOOH, and we have recently shown that the reactions of Cl with alkyl hydroperoxides offer a path to overcome this difficulty. Reactions of QOOH with molecular oxygen remain the most important unmapped area in autoignition chemistry. Ketohydroperoxides, which are products of these critical reactions, have recently been detected in photolytically initiated oxidation experiments,[6] and we will employ photoionization mass spectrometry and infrared absorption methods to characterize formation and decomposition reactions of ketohydroperoxide intermediates. As advanced theoretical kinetics develops rigorous predictions for these reactions, experiment must be able to detect products of these reactions for validation of theory.

References

1 Andersen, A. & Carter, E. A. Hybrid density functional theory predictions of low-temperature dimethyl ether combustion pathways. II. Chain-branching energetics and possible role of the Criegee intermediate. *J. Phys. Chem. A* **107**, 9463-9478 (2003).

2 Taatjes, C. A. *et al.* Direct Observation of the Gas-Phase Criegee Intermediate (CH_2OO). *J. Am. Chem. Soc.* **130**, 11883-11885 (2008).

3 Jalan, A., Allen, J. W. & Green, W. H. Chemically activated formation of organic acids in reactions of the Criegee intermediate with aldehydes and ketones. *Phys. Chem. Chem. Phys.* **15**, 16841-16852, doi:10.1039/c3cp52598h (2013).

4 Gladden, J. M. *et al.* Tailoring Next-Generation Biofuels and their Combustion in Next-Generation Engines. Report No. SAND2013-10094, 100 pp (Sandia National Laboratories, Livermore, California, 2013).

5 Scheer, A. M., Welz, O., Zádor, J., Osborn, D. L. & Taatjes, C. A. Low-Temperature Combustion Chemistry of Novel Biofuels: Resonance-Stabilized QOOH in the Oxidation of Diethyl Ketone. *Phys. Chem. Chem. Phys.* **in press** doi:10.1039/C3CP55468F (2014).

6 Eskola, A. J., Welz, O., Savee, J. D., Osborn, D. L. & Taatjes, C. A. Measurements of product formation in low-temperature n-butane oxidation: Towards fundamental understanding of autoignition and n-C_4H_9 + O_2 / sec-C_4H_9 + O_2 reactions. *J. Phys. Chem. A* **117**, 12216-12235 (2013).

Publications acknowledging BES support for C.A.T., 2012 –

a. Oliver Welz, Arkke J. Eskola, Leonid Sheps, Brandon Rotavera, John D. Savee, Adam M. Scheer, David L. Osborn, Douglas Lowe, A. Murray Booth, Ping Xiao, M. Anwar H. Khan, Carl J. Percival, Dudley E. Shallcross, and Craig A. Taatjes, "Rate Coefficients of C1 and C2 Criegee Intermediate Reactions with Formic and Acetic Acid Near the Collision Limit: Direct Kinetics Measurements and Atmospheric Implications," *Angew. Chem.* **in press** doi:10.1002/anie.201400964 (2014).

b. D. E. Shallcross, C. A. Taatjes, C. J. Percival, "Criegee intermediates in the indoor environment: new insights," *Indoor Air*, **in press** doi:10.1111/ina.12102 (2014).

c. W. G. Roeterdink, J. Bulthuis, E. P. F. Lee, D. Ding, and C. A. Taatjes, "Hexapole transmission spectrum of formaldehyde oxide," Chem. Phys. Lett. **598**, 96–101 (2014).

d. Craig A. Taatjes, Dudley E. Shallcross, and Carl J. Percival, "Research frontiers in the chemistry of Criegee intermediates and tropospheric ozonolysis," *Phys. Chem. Chem. Phys.* **16**, 1704–1718 (2014).

e. John D. Savee, Jessica F. Lockyear, Sampada Borkar, Arkke J. Eskola, Oliver Welz, Craig A. Taatjes and David L. Osborn, "Absolute photoionization cross-section of the vinyl radical," *J. Chem. Phys.* **139**, 056101 (2013).
f. Oliver Welz, Judit Zádor, John D. Savee, Leonid Sheps, David L. Osborn, and Craig A. Taatjes, "Low-Temperature Combustion Chemistry of Biofuels: Principal Oxidation Pathways for Hydroxybutyl Radicals Derived from n-Butanol," *J. Phys. Chem. A* **117**, 11983–12001 (2013).
g. Jessica F Lockyear, Oliver Welz, John D. Savee, Fabien Goulay, Adam J. Trevitt, Craig A. Taatjes, David L. Osborn, and Stephen R Leone, "Isomer Specific Product Detection in the Reaction of CH with Acrolein," *J. Phys. Chem. A* **117**, 11013–11026 (2013).
h. Carl Percival, Oliver Welz, Arkke J. Eskola, John D. Savee, David L. Osborn, David O. Topping, Doug Lowe, Steve Utembe, Asan Bacak, Gordon McFiggans, Mike Cooke, Alexander T. Archibald, Michael Jenkin, R. G. Derwent, Ilona Riipinen, Daniel Mok, Edmond P. F. Lee, John Dyke, Craig A. Taatjes and Dudley E. Shallcross, "Regional and Global Impacts of Criegee Intermediates on Atmospheric Sulphuric Acid Concentrations and First Steps of Aerosol Formation," *Faraday Discuss.* **165**, 45–73 (2013).
i. Adam J. Trevitt, Matthew B. Prendergast, Fabien Goulay, John D. Savee, David L. Osborn, Craig A. Taatjes, and Stephen R. Leone, "Product Branching Fractions of the CH + Propene Reaction from Synchrotron Photoionization Mass Spectrometry," *J. Phys. Chem. A* **117** 6450–6457 (2013).
j. Joseph Czekner, Craig A. Taatjes, David L. Osborn, and Giovanni Meloni, "Absolute Photoionization Cross-Sections of Selected Furanic and Lactonic Potential Biofuels," *Int. J. Mass Spectrom.* **348**, 39–46 (2013).
k. Judit Zádor, Haifeng Huang, Oliver Welz, Johan Zetterberg, David L Osborn and Craig A Taatjes, "Directly Measuring Reaction Kinetics of QOOH – a Crucial but Elusive Intermediate in Hydrocarbon Autoignition," *Phys. Chem. Chem. Phys.* **15**, 10753-10760 (2013).
l. Craig A. Taatjes, Oliver Welz, Arkke J. Eskola, John D. Savee, Dudley E. Shallcross, Adam M. Scheer, Brandon Rotavera, Edmond P. F. Lee, John M. Dyke, Daniel K. W. Mok, David L. Osborn, and Carl J. Percival, "Direct Measurements of Conformer-Dependent Reactivity of the Criegee intermediate CH_3CHOO," *Science* **340**, 177-180 (2013).
m. Xia Zhang, Chris J. Eyles, Craig A. Taatjes, Dajun Ding and Steven Stolte, "A general scaling rule for the collision energy dependence of a rotationally inelastic differential cross-section and its application to NO(X) + He," *Phys. Chem. Chem. Phys.* **15**, 5620-5635 (2013).
n. Fabien Goulay, Adeeb Derakhshan, Eamonn Maher, Adam J. Trevitt, John D. Savee, Adam M. Scheer, David L. Osborn, and Craig A. Taatjes, "Formation of dimethylketene and methacrolein by reaction of the CH radical with acetone," *Phys. Chem. Chem. Phys.* **15**, 4049–4058 (2013).
o. Oliver Welz, Stephen J. Klippenstein, Lawrence B. Harding, Craig A. Taatjes and Judit Zádor "Unconventional Peroxy Chemistry in Alcohol Oxidation – The Water Elimination Pathway," *J. Phys. Chem. Lett.* **4**, 350−354 (2013).
p. Oliver Welz, John D. Savee, Arkke J. Eskola, Leonid Sheps, David L. Osborn, and Craig A. Taatjes, "Low-Temperature Combustion Chemistry of Biofuels: Pathways in the Low-Temperature (550–700 K) Oxidation Chemistry of Isobutanol and tert-Butanol," *Proc. Combust. Inst.* **34**, 493-500 (2013).
q. i.) Haifeng Huang, Arkke J. Eskola, and Craig A. Taatjes, "Pressure-dependent I atom yield in the reaction of CH_2I with O_2 shows a remarkable apparent third-body efficiency for O_2," J. Phys. Chem. Lett. **3**, 3399–3403 (2012); ii). Haifeng Huang, Brandon Rotavera, Arkke J. Eskola and Craig A. Taatjes, "Correction to Pressure-dependent I atom yield in the reaction of CH_2I with O_2 shows a remarkable apparent third-body efficiency for O_2," *J. Phys. Chem. Lett.* **4**,3824–3824 (2013).
r. Edmond P. F. Lee, Daniel K. W. Mok, Dudley E. Shallcross, Carl J. Percival, David L. Osborn, Craig A. Taatjes, and John M. Dyke, "Spectroscopy of the simplest Criegee intermediate CH_2OO: Simulation of the first bands in its electronic and photoelectron spectra," *Chem.–Eur. J.* **18**, 12411–12423 (2012).
s. Amelia W. Ray, Craig A. Taatjes, Oliver Welz, David L. Osborn, and Giovanni Meloni, "Synchrotron Photoionization Measurements of OH-initiated Cyclohexene Oxidation: Ring-Preserving Products in OH + Cyclohexene and 2-Hydroxycyclohexyl + O_2 Reactions," *J. Phys. Chem. A.* **116**, 6720–6730 (2012).
t. Fabien Goulay, Adam J. Trevitt, John D. Savee, Jordy Bouwman, David L. Osborn, Craig A. Taatjes, Kevin R. Wilson, and Stephen R. Leone, "Product detection of the CH radical reaction with acetaldehyde," *J. Phys. Chem. A* **116**, 6091–6106 (2012).
u. Craig A. Taatjes, Oliver Welz, Arkke J. Eskola, John D. Savee, David L. Osborn, Edmond P.F. Lee, John M. Dyke, Daniel W. K. Mok, Dudley E. Shallcross, and Carl J. Percival, "Direct Measurement of Criegee Intermediate (CH_2OO) Reactions with Acetone, Acetaldehyde, and Hexafluoroacetone," *Phys. Chem. Chem. Phys.* **14**, 10391–10400 (2012).
v. John D. Savee, Oliver Welz, Craig A. Taatjes, and David L. Osborn, "New Mechanistic Insights to the $O(^3P)$ + Propene Reaction from Multiplexed Photoionization Mass Spectrometry," *Phys. Chem. Chem. Phys.* **14**, 10410–10423 (2012).
w. John D. Savee, Satchin Soorkia, Oliver Welz, Talitha M. Selby, Craig A. Taatjes, and David L. Osborn, "Absolute Photoionization Cross-Section of the Propargyl Radical," J. Chem. Phys. **136**, 134307 (2012).
x. Oliver Welz, John D. Savee, David L. Osborn, Subith S. Vasu, Carl J. Percival, Dudley E. Shallcross, and Craig A. Taatjes, "Direct Kinetic Measurements of Criegee Intermediate (CH_2OO) Formed by Reaction of CH_2I with O_2," *Science*, **335**, 204–207 (2012).

Elementary Reactions of PAH Formation

Robert S. Tranter
Chemical Sciences and Engineering Division, Argonne National Laboratory
Argonne, Il-60439
tranter@anl.gov

I. Program Scope

This program is focused on the experimental determination of kinetic and mechanistic parameters of elementary reactions, in particular those involved in the formation and destruction of the building blocks for aromatic species. The program also encompasses dissociation of novel fuels such as ethers and cyclic species and their dissociation products that are representative of oxygenated intermediates in combustion mechanisms. Thermal sources of radicals are also investigated and characterized for use in more complex reaction systems where secondary chemistry can be significant. Recently, the scope has been increased to include thermally initiated roaming reactions. The approach involves a diaphragmless shock tube (DFST) equipped with laser schlieren (LS) and a time-of-flight mass spectrometer (TOF-MS) and low pressure, fast flow, reactor equipped with a quadrupole MS. The combination of these techniques accesses a wide range of reaction temperatures and pressures.

II. Recent Progress

A. Recombination of Allyl Radicals

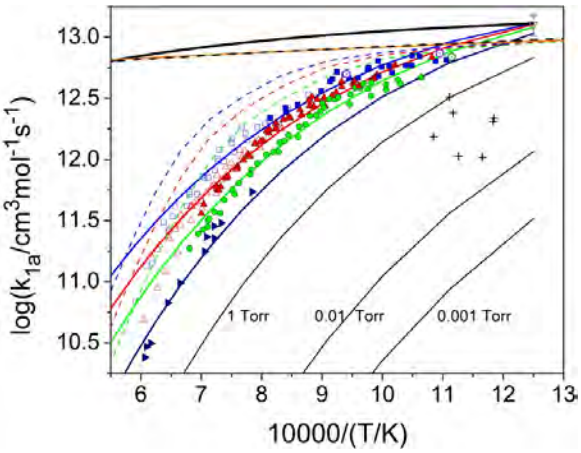

Figure 1: $k_{(2\ C3H5 \rightarrow C6H10)}$. Blue, red, green and dark blue respectively refer to respectively to123, 57, 30 and 10 Torr experiments and calculations. Filled symbols C_3H_5I/Kr (LS), open symbols 1,5-hexadiene/Kr (LS). Crosses VLPP results from Rossi et al.[ix] Solid lines: current RRKM model. The heavy solid line is k_∞ from the LS experiments. Orange/black line: k_∞ Georgievskii et al.[ii] Dashed lines: RRKM calculations from Matsugi et al.[i] Inverted triangle, Matsugi et al. 800 K.[i]

Resonantly stabilized radicals such as propargyl (C_3H_3) and allyl (C_3H_5) can reach relatively high concentrations in flames. In sooting regions recombination reactions can compete with pyrolysis, oxidation and addition. For instance, recombination of propargyl is generally accepted as a major source of single ring aromatics. By contrast recombination of allyl radicals predominantly forms 1,5-hexadiene which cannot readily cyclize but at modest temperatures acts as a sink for C_3H_5. Recombination of allyl radicals has been studied experimentally at low temperatures, T<800 K, by several groups and the most recent measurement by Matsugi et al.[i] is within 30% of theoretical estimates of k_∞.[i,ii] Matsugi et al. also predicted that above ~800 K C_3H_5 recombination would show strong falloff, Fig. 1, but no experimental studies were available to verify this.

In addition to its significance in combustion the allyl radical is also a key dissociation product in several ongoing and planned LS experiments, and a reliable mechanism describing recombination and dissociation of allyl radicals at the conditions of LS experiments is necessary to further these studies. Consequently, the recombination of C_3H_5 radicals was investigated in the DFST with LS and TOF-MS.[iii] In addition, complementary single pulse shock tube experiments[iv] were carried out in collaboration with Brezinsky (University of Illinois at Chicago) to expand the experimental space and

$$C_3H_5 + C_3H_5 \rightarrow H_2C{=}CHCH_2CH_2CH{=}CH_2 \qquad \Delta H_{r,298K} = -60.5 \text{ kcal/mol} \qquad (1a)$$

$$C_3H_5 + C_3H_5 \rightarrow C_3H_6 + C_3H_4 \qquad \Delta H_{r,298K} = -30.2 \text{ kcal/mol} \qquad (1b)$$

obtain detailed analysis of stable products. The combined study spanned 650-1700 K and 10 Torr -10 bar. Two precursors, allyl iodide and 1,5-hexadiene (15HD) were used to generate C_3H_5, and RRKM models for their dissociations were obtained. The self-reaction proceeds mainly by recombination, reaction (1a), with <6% of the flux going through a disproportionation channel, reaction (1b) in good agreement with the literature.[V] The recombination reaction shows considerably more fall off than predicted by Matsugi et al.[i] However, an RRKM model derived from the LS results is in good agreement with both the current work and the limited experimental literature, and the calculated k_∞ is in good agreement with the literature, Fig. 1. Furthermore, the RRKM model results are completely consistent with the single pulse shock tube results.

The equilibrium constant, $K_{(2C3H5\leftrightarrow 15HD)}$, strongly favors recombination at the conditions of the LS experiments. As a consequence the LS experiments that used 1,5-hexadiene as the precursor were very sensitive to $K_{(2\ C3H5\leftrightarrow\ 15HD)}$, and hence the entropies of the reagents. Initial attempts to simulate the density gradient profiles from the LS experiments were unsuccessful which, for a system where essentially only one reaction occurs, is indicative of an underlying problem in the thermochemical properties in the model. Fitting the LS profiles successfully revealed an error in the literature S_{298K} for 1,5-hexadiene and a new value of S_{298K} = 87.3 cal mol^{-1} K^{-1} has been estimated which is ~7 cal mol^{-1} K^{-1} larger than the literature. In collaboration with Ruscic, this difference was traced to an inadequate treatment of internal rotors in theoretical treatments of 1,5-hexadiene.

B. Methyl Acetate

Long chain methyl esters have received considerable attention due to their prevalence in biofuels. However, development of accurate models for the pyrolysis and combustion of these species is hampered by a lack of rigorous experimental and theoretical data. Experimentally, large methyl esters are difficult to study due to their low volatility and the large number of sites for bond scission or radical attack. Furthermore, such large molecules cannot be studied at the desired level of theory. Small methyl esters

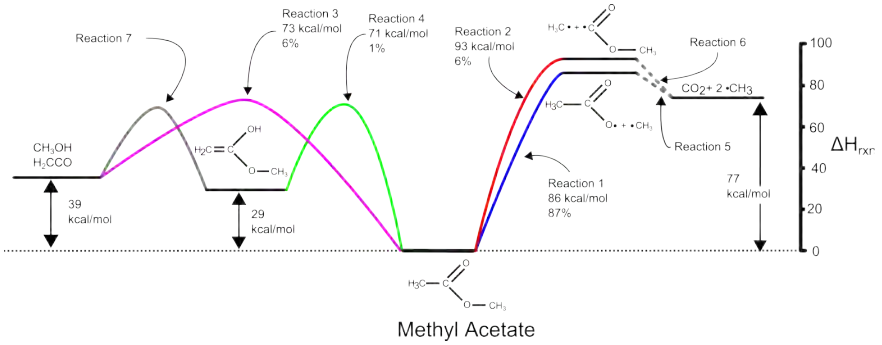

Figure 2: Reaction scheme of the four primary dissociation channels of methyl acetate following Peukert et al.[vi] For each channel the barrier recommended in this work, as well as the loss of methyl acetate at a temperature of 1750 K and 120 Torr through the given channel is shown.

serve as prototypes for the large esters and can be studied experimentally and theoretically in sufficient detail. Methyl acetate is the smallest methyl ester with an alkyl backbone and can dissociate as shown in Fig.2. To extend the range of conditions examined by Michael and co-workers[vi] in shock tube H-ARAS experiments a series of LS experiments were performed at 122±3 and 63±2 Torr and 1492-2266 K. The LS experiments clearly resolved falloff in the high temperature rate coefficients and allowed the master equation model of Michael et al. to be refined. The density gradients from the LS experiments are consistent with scission of the H_3C-O bond (reaction 1, Fig. 2) being the dominant dissociation route as suggested by Michael and co-workers. However, at these reaction conditions the remaining channels are

note entirely negligible, as shown in Fig. 2. However, due to the small flux and low rates of reaction for the molecular channels the LS experiments show little sensitivity to them and the rate parameters were obtained from master equation modeling rather than experiment. In Fig. 3 rate coefficients from LS experiments for reaction (1) are shown along with the results of the master equation modeling. The model also resolves an apparent disagreement between Sulzmann et al.[vii] and Carlsen et al.[viii] as to whether MA dissociates predominantly by molecular channels (Carlsen) or the radical channels (Sulzmann). The master equation model shows the branching between these pathways is strongly pressure and temperature dependent and that at very low pressures (Carlsen) the molecular paths dominate with the reverse being true at high pressures.

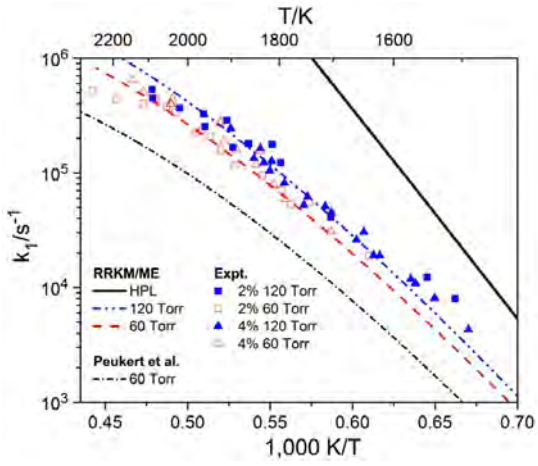

Figure 3: $k_{(MA \rightarrow CH3C(O)O + CH3)}$ and the master equation model. Also shown is k calculated for 60 Torr with the model of Peukert et al.[vi]

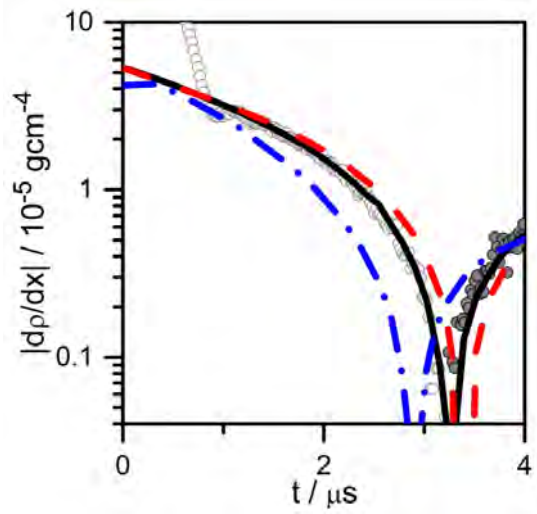

Figure 4: Sensitivity to $k_{2b}/(k_{2a}+k_{2b})$, BR, for 2% nitromethane in krypton at P_2= 118 Torr, T_2= 1476 K. Open symbols +ve density gradients; closed symbols –ve. Lines simulations: Black solid, BR=0.2; Red dashed BR=0; Blue dash dot, BR=0.5.

C. Nitromethane

Thermally initiated roaming reactions have been studied in shock tube experiments and typically the roaming channel created two stable molecular products rather than radical products from the simple bond scission channel. Recently, it has been shown theoretically[x,xi] that roaming may occur in pyrolysis of nitromethane but rather than dissociating the molecule isomerizes to methyl nitrite. Dissociation of methyl nitrite creates methoxy radicals that subsequently lose an H-atom. Thus the roaming path in nitromethane can lead to more reactive species rather than less as seen in other molecules.

The large difference in heats of reaction makes LS experiments quite sensitive to the branching ratio B.R. = $k_{2b}/(k_{2a}+k_{2b})$. A series of experiments at nominal incident shock pressures, P_2, of 60 and 120 Torr have been performed with mixtures of 1% and 2% nitromethane in krypton. For the simulations in Fig. 4 ($k_{2a}+k_{2b}$) was fixed and B.R. varied between 0 and 0.5.

Not including the roaming channel, B.R.= 0, results in simulations that are too positive relative to the experimental results. Whereas B.R. = 0.5 yields results that are too negative. Simply increasing k_{2a} with B.R.=0 does not produce results that are consistent across the complete dataset. Considering all of the 120 Torr experiments results in B.R. = 0.25 which is somewhat higher than the theoretical calculation of Zhu et al.[xi] of 0.07. The differences in B.R. are quite significant and the underlying reasons are being investigated. Initial analysis of the 60 Torr LS experiments indicates that there is a small pressure dependence in B.R. and that lower pressures favour higher branching ratios. This trend is consistent with that predicted by Zhu et al.

$$CH_3NO_2 \rightarrow CH_3 + NO_2 \qquad \Delta H_{r,298K} = 60 \text{ kcal/mol} \qquad (2a)$$

$$CH_3NO_2 \rightarrow CH_3ONO \qquad \Delta H_{r,298K} = 3 \text{ kcal/mol} \qquad (2b)$$

III. Future Work

The DFST/TOF-MS/LS studies of aromatics and resonantly stabilized radicals are being expanded to include reactions between radicals and oxygen molecules. These represent a new application of the LS technique and initial efforts are focusing on phenyl + O_2. Further investigations of PAH formation are planned with studies of the H-atom catalyzed conversion of fulvene to benzene and dimethyl fulvenes to xylenes. Additional experiments are planned to study reactions of phenyl and *o*-benzyne radicals with small molecules such as C_2H_2 and CH_3 The study of roaming reactions in nitromethane will be expanded to include methyl nitrite which is expected to show similar behavior to nitromethane. Investigations of the mechanisms and kinetics of high temperature dissociation of cyclic molecules are ongoing and will include dissociation of cycloheptane and 2-DMF.

IV. References

i. Matsugi A., Suma K. and Miyoshi A., J. Phys. Chem. A **2011,** 115**,** 7610
ii. Georgievskii Y., Miller J. A. and Klippenstein S. J., Phys. Chem. Chem. Phys. **2007**, 9, 4259
iii. Lynch P. T., Annesley C. J., Aul C. J., Yang X. and Tranter R. S., *J. Phys, Chem. A.,* **2013**, 117, 4750
iv. Fridlyand A., Lynch P. T., Tranter R. S. and Brezinsky K., *J. Phys. Chem. A*, **2013**, 117, 4762
v. Selby, T.; Meloni, G.; Goulay, F.; Leone, S.; Fahr, A.; Taatjes, C.; Osborn, D. *J. Phys. Chem. A* **2008**, 112, 9366
vi. Peukert S., Sivaramakrishnan R., Su M.-C. and Michael J. V., *Combust. Flame*, **2012**, 159, 2312
vii. Sulzmann K. G. P., Baxte D. E.r, Khazra M. and Lund T. S., *J. Phys.Chem*., **1985**, 89, 3561
viii. Carlsen L., Egsgaard H. and Pagsberg P., *J. Chem. Soc., Perkin Transactions 2*, **1981**, 1256
ix. Rossi, M.; King, K.; Golden, D, *J. Am. Chem. Soc.* **1979**, 101, 1223
x. Homayoon Z. and Bowman J. M., *J. Phys. Chem. A*, **2013**, 10.1021/jp312076z
xi. Zhu R. S.; Raghunath P.; Lin M. C., *J. Phys. Chem. A*, **2013**, 117, 7308

V. Publications and submitted journal articles supported by this project 2012-2014

1 Lynch P. T., Annesley C. J. and Tranter R. S. 'Dissociation of *ortho*-Benzyne Radicals in the High Temperature Fall-off Regime' Accepted for presentation at the 35th Combustion Symposium.
2 Annesley C. J., Goldsmith C. F. and Tranter R. S. 'A shock tube laser schlieren study of methyl acetate dissociation in the fall-off regime' Phys. Chem. Chem. Phys. **2014**, 16, 7241-7250
3 Tranter R. S. and Brezinsky K., 'Shock tube studies of combustion relevant elementary chemical reactions and sub-mechanisms' in Cleaner Combustion: Developing Detailed Chemical Kinetic Models ISBN - 978-1-4471-5306-1 **2013**
4 Yasunaga K. and Tranter R. S., 'Speciation in shock tubes' in Cleaner Combustion: Developing Detailed Chemical Kinetic Models ISBN - 978-1-4471-5306-1 **2013**
5 Tranter R. S. and Lynch P. T., 'A miniature high repetition rate shock tube' Rev. Sci. Instrum. DOI:10.1063/1.4820917 **2013**
6 Lynch P. T., Annesley C. J., Aul C. J., Yang X. and Tranter R. S., 'Recombination of allyl radicals in the high temperature fall-off regime' J. Phys, Chem. A.: **2013**, 117, 4750-4761
7 Fridlyand A., Lynch P. T., Tranter R. S. and Brezinsky K., 'Single pulse shock tube study of allyl radical recombination' J. Phys. Chem. A, **2013**, 117, 4762-4776
8 Tranter R. S., Lynch P. T., Yang X., 'Dissociation of dimethyl ether at high temperatures' Proc. Combust. Inst. **2013,** 34, 591-598
9 Tranter R. S., Lynch P. T., Annesley C. J., 'Shock tube investigation of CH_3 + CH_3OCH_3' J. Phys Chem. A, 116, **2012**, 7287-7292
10 Yang. X., Tranter R. S. 'High temperature dissociation of ethyl radicals and ethyl iodide' Intl. J. Chem. Kinet. **2012**, 44, 433-443

Variational Transition State Theory

Donald G. Truhlar
Department of Chemistry, University of Minnesota
207 Pleasant Street SE, Minneapolis, Minnesota 55455
truhlar@umn.edu

Program scope

This project involves the development of variational transition state theory (VTST) including optimized multidimensional tunneling (OMT) contributions and the application of this theory to gas-phase reactions with a special emphasis on developing reaction rate theory in directions that are important for applications to combustion. The further development of VTST/OMT as a useful tool for combustion kinetics also involves (i) developing and applying new methods of electronic structure calculations for the input potential energy surface, which is typically an implicit surface ("direct dynamics") defined by a level of electronic structure theory, (ii) methods to interface reaction-path and reaction-swath dynamics calculations with electronic structure theory, and (iii) methods to treat vibrational anharmonicity and vibration–rotation coupling. The project also involves the development and implementation of practical techniques and software for applying the theory to various classes of reactions and transition states and applications to specific reactions, with special emphasis on combustion reactions and reactions that provide good test cases for methods needed to study combustion reactions.

The direct dynamics approach to gas-phase reactions in this project involves electronic structure calculations of potential energy surfaces and the use of these surfaces to calculate generalized free energies of activation and multidimensional tunneling probabilities. A key emphasis is the interface of electronic structure calculations with dynamics algorithms as achieved in the POLYRATE computer program and its various RATE interfaces to electronic structure packages.

Recent progress

The atomistic simulation of reactions of complex molecules, such as those involved in combustion, requires one to treat anharmonic, coupled torsions in both reactants and transition states, along with the accompanying torsional anharmonicity, and to consider reaction along more than one reaction path. Our major recent theoretical accomplishment is the development of an internal coordinate method for including multiple structures and torsional anharmonicity of torsions coupled to each other and to overall rotation and for including multiple reaction paths in reaction rate calculations that include both variationally optimized transition states and multi-dimensional tunneling. Our original version used an uncoupled torsional potential, and we have recently extended that to a coupled torsional potential as required to treat anharmonicity all along the reaction path of a low-barrier bimolecular reaction. These methods have been incorporated in a computer code called *MSTor* that is now available to the community at no charge in an international program library and on our Web site. We have applied the method to calculate thermochemical quantities for many molecules, radicals, and transition states, and to calculate reaction rates of combustion reactions. Examples are given in the references below.

Software distribution

We have developed several software packages for applying variational transition state theory with optimized multidimensional tunneling coefficients to chemical reactions. These packages are well documented and distributed with manuals, installation scripts, and test suites. The license requests that we fulfilled during the period Jan. 1, 2011–March 22, 2014, for RATE packages developed under DOE support is as follows:

	Total	*academic*	*government//DoD/non-profit/industry*
POLYRATE	457	421	36
GAUSSRATE	262	247	15
6 other RATE programs	72	62	20

The total number of requests fulfilled for all RATE programs since we began keeping statistics in 1995 is 2816. Beginning with version 2011, we have distributed *MSTor* through both the *Computer Physics Communications* web site (http://www.cpc.cs.qub.ac.uk) and own web site (t1.chem.umn.edu/truhlar/index.htm#software). So far 124 requests have been fulfilled by the former (100 for v1 and 24 for v2) and 40 by the latter.

Future plans

The general objective of this project is to develop and employ improved methods for calculating the rate constants of gas-phase chemical reactions. Our current plans are as follows:

(1) We are presently working on extended versions of POLYRATE and GAUSSRATE with new capabilities for microcanonical rate constants and pressure dependence.

(2) We are extending our tunneling methods molecular dynamics simulations as required to predict certain product distributions.

(3) We will calculate rate constants for specific applications that are important in combustion. This will include reactions of complex and unsaturated and aromatic organic molecules and radicals of interest for modeling combustion of combustion of real fuels, fuel additives, and their combustion-generated intermediates.

Publications supported by this grant, 2011-present

1. "Minimally Augmented Karlsruhe Basis Sets," J. Zheng, X. Xu, and D. G. Truhlar, Theoretical Chemistry Accounts 128, 295-305 (2011). dx.doi.org/10.1007/s00214-010-0846-z
2. "Convergent Partially Augmented Basis Sets for Post-Hartree-Fock Calculations of Molecular Properties and Reaction Barrier Heights," E. Papajak and D. G. Truhlar, Journal of Chemical Theory and Computation **7**, 10-18 (2011). dx.doi.org/10.1021/ct1005533
3. "Kinetic Isotope Effects for the Reactions of Muonic Helium and Muonium with H_2," D. G. Fleming, D. J. Arseneau, O. Sukhorukov, J. H. Brewer, S. L. Mielke, G. C. Schatz, B. C. Garrett, K. A. Peterson, and D. G. Truhlar, Science 331, 448-450 (2011). dx.doi.org/10.1126/science.1199421
4. "Computational Study of the Reactions of Methanol with the Hydroperoxyl and Methyl Radicals. Part I: Accurate Thermochemistry and Barrier Heights," I. M. Alecu and D..G. Truhlar, Journal of Physical Chemistry A 115, 2811–2829 (2011). dx.doi.org/dx.doi.org/10.1021/jp110024

5. “High-Level Direct-Dynamics Variational Transition State Theory Calculations Including Multidimensional Tunneling of the Thermal Rate Constants, Branching Ratios, and Kinetic Isotope Effects of the Hydrogen Abstraction Reactions from Methanol by Atomic Hydrogen,” R. Meana-Pañeda, D. G. Truhlar and A. Fernández-Ramos, Journal of Chemical Physics 134, 094302/1-14. dx.doi.org/10.1063/1.3555763
6. “Practical Methods for Including Torsional Anharmonicity in Thermochemical Calculations of Complex Molecules: The Internal-Coordinate Multi-Structural Approximation,” J. Zheng, T. Yu, E. Papajak, I, M. Alecu, S. L. Mielke, and D. G. Truhlar, Physical Chemistry Chemical Physics **13**, 10885-10907 (2011). dx.doi.org/10.1039/C0CP02644A
7. “How Well Can Modern Density Functionals Predict Transition State Bond Distances?” X. Xu, I. M. Alecu, and D. G. Truhlar, Journal of Chemical Theory and Computation **7**, 1667-1676 (2011). dx.doi.org/10.1021/ct2001057.
8. Multi-Structural Variational Transition State Theory. Kinetics of the 1,4-Hydrogen Shift Isomerization of the Pentyl Radical with Torsional Anharmonicity,” T. Yu, J. Zheng, and D. G. Truhlar, Chemical Science **2**, 2199-2213 (2011). dx.doi.org/10.1039/ C1SC00225B
9. “Thermodynamics of C–H Bond Dissociation in Hexane and Isohexane Yielding Seven Isomeric Hexyl Radicals,” J. Zheng, T. Yu, and D. G. Truhlar, Physical Chemistry Chemical Physics **13**, 19318-19324 (2011). dx.doi.org/10.1039/C1CP21829H
10. “Statistical Thermodynamics of the Isomerization Reaction Between n-Heptane and Isoheptane,” T. Yu, J. Zheng, and D. G. Truhlar, Physical Chemistry Chemical Physics **14**, 482-494 (2011). dx.doi.org/10.1039/c1cp22578b.
11. “Kinetics of the Reaction of the Heaviest Hydrogen Atom with H_2, the $^4He\mu + H_2 \rightarrow {}^4He\mu H + H$ reaction: Experiments, Accurate Quantal Calculations, and Variational Transition State Theory, Including Kinetic Isotope Effects for a Factor of 36.1 in Isotopic Mass,” D. G. Fleming, D. J. Arseneau, O. Sukhorukov, J. H. Brewer, S. L. Mielke, D. G. Truhlar, George C. Schatz, B. C. Garrett, and K. A. Peterson, Journal of Chemical Physics **135**, 184310/1–18 (2011). dx.doi.org/10.1063/1.3657440
12. “Computational Study of the Reactions of Methanol with the Hydroperoxyl and Methyl Radicals. 2. Accurate Thermal Rate Constants,” I. M. Alecu, and D. G. Truhlar, Journal of Physical Chemistry A **115**, 14599-14611 (2011). dx.doi.org/10.1021/jp209029p
13. “Multipath Variational Transition State Theory. Rate Constant of the 1,4-Hydrogen Shift Isomerization of the 2-Cyclohexylethyl Radical,” T. Yu, J. Zheng, and D. G. Truhlar, Journal of Physical Chemistry A **116**, 297-308 (2012). dx.doi.org/10.1021/jp209146b
14. "Multi-Structural Variational Transition State Theory: Kinetics of the 1,5-Hydrogen Shift Isomerization of 1-Butoxyl Radical Including All Structures and Torsional Anharmonicity," X. Xu, E. Papajak, J. Zheng, and D. G. Truhlar, Physical Chemistry Chemical Physics **14**, 4204-4216 (2012). dx.doi.org/10.1039/c2cp23692c.
15. “Multi-path Variational Transition State Theory for Chemical Reaction Rates of Complex Polyatomic Species: Ethanol + OH Reactions,” J. Zheng and D. G. Truhlar, Faraday Discussions **157**, 59-88 (2012). dx.doi.org/10.1039/C2FD20012K.
16. “MSTor: A program for calculating partition functions, free energies, enthalpies, entropies, and heat capacities of complex molecules including torsional anharmonicity,” J. Zheng, S. L Mielke, K. L Clarkson, and D. G. Truhlar, Computer Physics Communications **183**, 1803-1812 (2012). dx.doi.org/10.1016/j.cpc.2012.03.007

17. “A Product Branching Ratio Controlled by Vibrational Adiabaticity and Variational Effects: Kinetics of the H + trans-N_2H_2 Reactions,” J. Zheng, R. J. Rocha, M. Pelegrini, L. F. A. Ferrão, E. F. V. Carvalho, O. Roberto-Neto, F. B. C. Machado, and D. G. Truhlar, Journal of Chemical Physics **136**, 184310/1-10 (2012). dx.doi.org/10.1063/1.4707734
18. “What are the Most Efficient Basis Set Strategies for Correlated Wave Function Calculations of Reaction Energies and Barrier Heights?” E. Papajak and D. G. Truhlar, Journal of Chemical Physics **137**, 064110/1–8 (2012). dx.doi.org/ 10.1063/1.4738980
19. “Thermochemistry of Radicals Formed by Hydrogen Abstraction from 1-Butanol, 2-Methyl-1-propanol, and Butanal,” E. Papajak, P. Seal, X. Xu, and D. G. Truhlar, Journal of Chemical Physics **137**, 104314/1-13 (2012). dx.doi.org/10.1063/1.4742968
20. "Role of Conformational Structures and Torsional Anharmonicity in Controlling Chemical Reaction Rates and Relative Yields: Butanal + HO_2 Reactions," J. Zheng, P. Seal, and D. G. Truhlar, Chemical Science **4**, 200-212 (2013). dx.doi.org/10.1039/c2sc21090h
21. "Multi-Structural Variational Transition State Theory: Kinetics of the Hydrogen Abstraction from Carbon-2 of 2-Methyl-1-propanol by Hydroperoxyl Radical Including All Structures and Torsional Anharmonicity," X. Xu, T. Yu, E. Papajak, and D. G. Truhlar, Journal of Physical Chemistry A **116**, 10480-10487 (2012). dx.doi.org/10.1021/jp307504
22. "Biofuel Combustion. Energetics and Kinetics of Hydrogen Abstraction from Carbon-1 in *n*-Butanol by the Hydroperoxyl Radical Calculated by Coupled Cluster and Density Functional Theories and Multi-Structural Variational Transition State Theory with Multidimensional Tunneling," I. M. Alecu, J. Zheng, E. Papajak, T. Yu, and D. G. Truhlar, Journal of Physical Chemistry A **116**, 12206-12213 (2012). dx.doi.org/10.1021/jp308460y
23. "Quantum Thermochemistry: Multi-Structural Method with Torsional Anharmonicity Based on a Coupled Torsional Potential," J. Zheng and D. G. Truhlar, Journal of Chemical Theory and Computation **9**, 1356-1367 (2013). dx.doi.org/10.1021/ct3010722
24. “Including Torsional Anharmonicity in Canonical and Microcanonical Reaction Path Calculations,” J. Zheng and D. G. Truhlar, Journal of Chemical Theory and Computation **9**, 2875-2881(2013). dx.doi.org/10.1021/ct400231q
25. "Chemical Kinetics and Mechanisms of Complex Systems: A Perspective on Recent Theoretical Advances," S. J. Klippenstein, V. Pande, and D. G. Truhlar, Journal of the American Chemical Society **136**, 528-546 (2014). (Perspective Article) dx.doi.org/10.1021/ja408723a
26. "Army Ants Tunneling for Classical Simulations," J. Zheng, X. Xu, R. Meana-Pañeda, and D. G. Truhlar, Chemical Science, accepted Dec. 24, 2013. Published online on Feb. 7, 2014 as an Advance Article at dx.doi.org/10.1039/C3SC53290a
27. "Anchor Points Reactive Potential for Bond-Breaking Reactions," K. R. Yang, X. Xu, and D. G. Truhlar, Journal of Chemical Theory and Computation **10**, 924-933 (2014). dx.doi.org/10.1021/ct401074s
28. “Prediction of Experimentally Unavailable Product Branching Ratios for Biofuel Combustion: The Role of Anharmonicity,” by J. Zheng, R. Meana-Pañeda, and D. G. Truhlar, Journal of the American Chemical Society, online as Article ASAP as of March 20, 2014. dx.doi.org/10.1021/ja5011288

Developing a predictive model for the chemical composition of soot nanoparticles: Integrating Model and Experiment

Lead PI: Angela Violi, University of Michigan, Ann Arbor avioli@umich.edu

Collaborating Institutions:
Combustion Research Facility - Sandia National Laboratories Livermore: PIs: Dr. N. Hansen and Dr. H. Michelsen
Lawrence Berkeley National Laboratory: PI: Dr. K. Wilson

Program Scope / Definition

The goal of this proposal is to develop a validated predictive model to describe the chemical composition of soot nanoparticles in premixed and diffusion flames. The collaborative nature of the proposed study combines expertise in computational and experimental areas to tackle the complex problem of soot nucleation and growth at the molecular level. The computational effort will be tightly coupled to experimental data produced by the research groups of Michelsen and Hansen at Sandia National Laboratories and Wilson at Lawrence Berkeley National Laboratory. The studies proposed herein will address several key questions concerning soot nanoparticle formation and growth with an array of state-ofthe-art computational and experimental approaches. The research will provide critical insights for the development of the next generation of soot models with the capability to predict the nucleation process, and hence the number of nanoparticles, together with the evolution of their chemical composition.

Recent Progress

Recent progress has involved both experimental and theoretical investigations as well as the integration of these respective studies to create insight composition of nascent PAHs in counterflow flames. This project closely couples experimental investigations of soot precursors and incipient particle characteristics with the development of a predictive model for the chemical composition of soot nanoparticles.

The goal of these studies was to measure incipient soot particle sizes and composition in a counterflow diffusion flame at atmospheric pressure. These measurements were intended to inform, constrain, and test the nanoparticle formation model. We designed and built a counterflow burner for measurements of incipient soot particle distributions in these flames at pressures close to atmospheric. We also designed and built a microprobe that would allow dilution of the flow after sampling from the flame to reduce particle coagulation. We coupled this extraction line to the aerosol mass spectrometer (AMS) developed at the ALS by Kevin Wilson and coworkers. This AMS uses an aerodynamic-lens system to focus an ensemble of particles, sampled at atmospheric pressure, into the high vacuum region of a time-of-flight mass spectrometer. The particle beam is directed onto a heated target, which flash vaporizes the non-refractory components of the particle beam. The resulting vapor plume is photoionized by high-flux tunable VUV radiation (~1016 photons/s) produced by the ALS, and the ions are detected with a time-of-flight mass spectrometer. As with the gas-phase experiments above, the burner was translated relative to the sampling probe for particle

profile measurements in the flame, and we scanned the VUV photon energy to measure photoionization efficiency (PIE) curves for isomer identification. We also performed experiments in which we diverted the extraction line to a Scanning Mobility Particle Sizer (SMPS) for particle size distribution measurements. The experimental setup has been described in further detail in a recent publication.

We recently developed new software for simulating gas-phase nanoparticle growth named SNAPS (Stochastic Nanoparticle Simulator). This software was used for stochastic simulation of PAH growth in the acetylene flame, in order to elucidate the chemical composition of species associated with peaks in experimentally measured mass spectra. SNAPS, along with an accompanying PAH chemical growth mechanism, has been described in detail elsewhere. Briefly, SNAPS uses an algorithm based on kinetic Monte Carlo to generate stochastic trajectories of the growth of an initial "seed" molecule in a given gas-phase environment, governed by a given reaction mechanism. Additionally, a PAH growth model was formulated and includes addition of major proposed PAH-growth pathways, including HACA, addition of ethylene and benzene, and addition of vinyl, methyl, propargyl, cyclopentadienyl, and phenyl radicals. Due to the probabilistic nature of the method, a typical SNAPS trajectory represents one of many possible growth trajectories. Therefore an ensemble of trajectories can be used to glean macroscopic information about particle growth. These trajectories can then be analyzed to compare with experimental measurements, and provide additional molecular detail. For example, Figure 1 shows a comparison between experimentally measured and computed mass spectra for an acetylene/oxygen flame at a distance of 5.75 mm from the fuel outlet, showing good reproduction of the experimental data. This comparison corroborates the validity of SNAPS simulations and the credibility of further detailed analysis of the simulation trajectories.

SNAPS simulations were analyzed to classify the most important PAH structures for specific mass ranges. To simplify analysis of the vast amount of potential structures, PAHs were classified by carbon configuration using social permutation invariant topological (SPRINT) coordinates, which utilize graph theory to describe the connectivity of an isomer. SPRINT coordinates were computed for each SNAPS trajectory.

Importantly, PAHs with equivalent connectivity will have almost identical SPRINT coordinates, which are invariant under all permutations of a set of N atoms. Isomers with specific carbon numbers were grouped, focusing specifically on carbon-carbon connectivity, by placing a limit on the p-2 norm of the difference between the vectors representing the SPRINT coordinates of each pair of PAHs in the target ensemble. This p-2 norm threshold was adjusted to produce distinct carbon configurations for the top five most frequently observed PAH structures.

SNAPS simulations provide molecular structures associated with mass distribution peaks. Figure 2 shows the most commonly observed structures for carbon numbers between 12 and 18 at a distance of 5.75 mm from the fuel outlet. These structures account for the cluster of masses associated with peaks that differ by hydrogen content. These hydrogens were neglected to focus specifically on carbon structure, as some hydrogen addition or abstraction is expected within the sampling line. Experimental analysis compares photoionization efficiency (PIE) curves of known species to those measured on sampled PAH mass to conjecture about the types of PAH species associated with a given peak. Aiding this approach, the simulations allow the evaluation of the plausibility of such conjecture and elucidate molecular detail about peaks in mass spectra. In this way, we can achieve synergy between experimental and theory to further drive our collective efforts and create deeper insight into the PAH growth process.

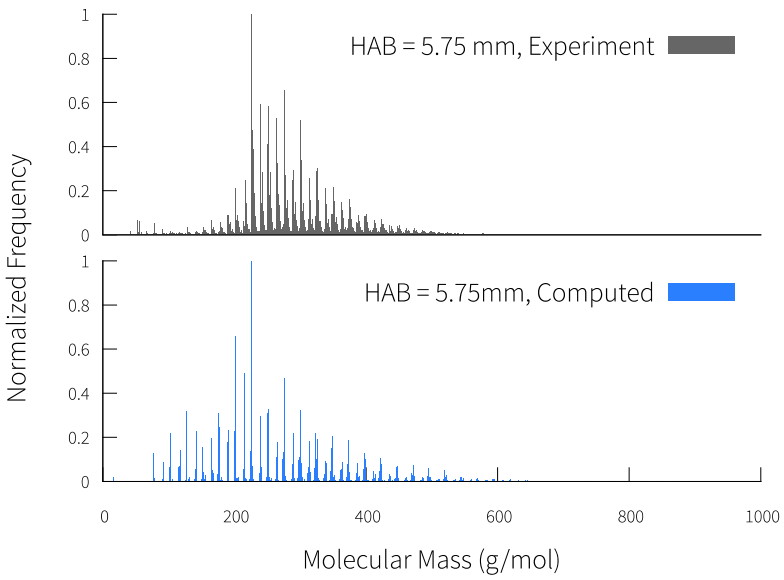

Figure 1: Comparison of ensemble-averaged mass distributions computed by SNAPS (2000 trajectories) compared with experimentally measured values in the counterflow acetylene/oxygen flame at a height of 5.75 mm above burner.

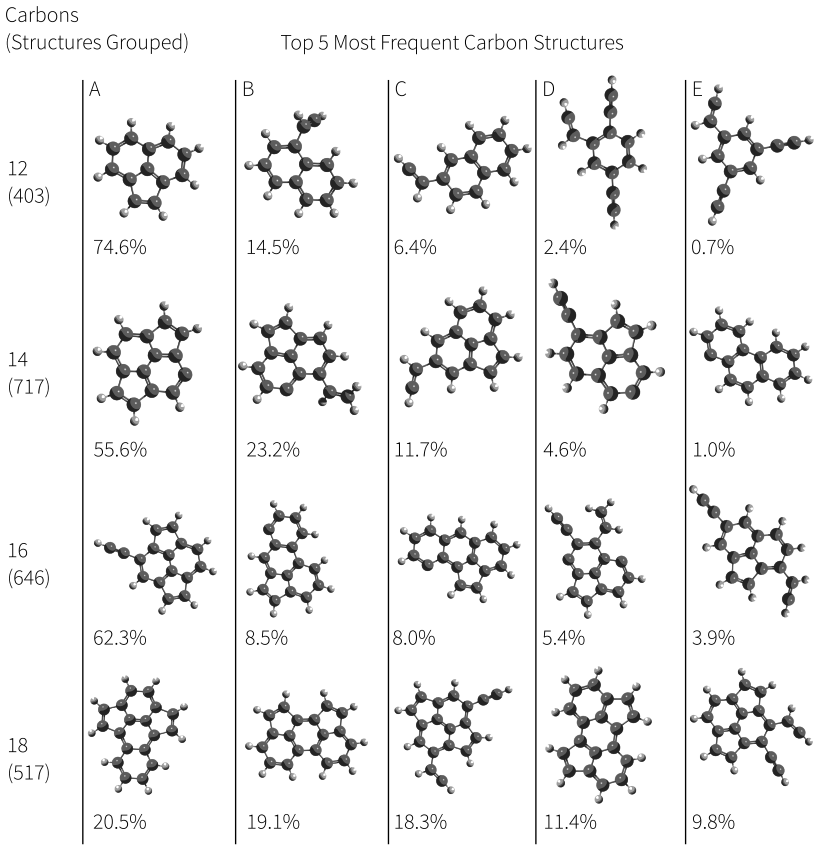

Figure 2: Top 5 most frequent carbon structures observed at 5.75 mm from the fuel outlet in 20000 simulations for varying number of carbons. The value ``Structures Grouped'', shown in parenthesis on the left below the number of carbons in each row, represents the quantity of trajectories with structures matching the specified number of carbons at this distance.

Future Work

Future work will involve close coupling experimental and modeling efforts, towards further characterizing PAH growth in a variety of flame environments. These efforts will involve further experimental probing of soot precursors, searching in particular for species predicted by simulations. The success or failure of these predictions will further enable refinement of the simulation methodology, thus building a strong description of this part of the soot formation process.

References DOE sponsored research appeared since 2011

1. S.H. Chung, A. Violi "Pericondensed aromatics with aliphatic chains as key intermediates for the nucleation of aromatic hydrocarbons" Proc. Combust. Inst. 33(1), 693-700, (2011).
2. S. A. Skeen, H. A. Michelsen, K. R. Wilson, D. M. Popolan, A. Violi, and N. Hansen, "Near-threshold photoionization mass spectra of combustion-generated high-molecular-weight soot precursors," *J. Aerosol Sci.*, vol. 58, pp. 86–102, Apr. 2013.
3. S.A. Skeen, B. Yang, H.A. Michelsen, J.A. Miller, A. Violi, N. Hansen "Studies of laminar opposed-flow diffusion flames of acetylene at low-pressures with photoionization mass spectrometry", Proceedings of the Combustion Institute 34 (2013), pp. 1067-1075.
4. P. Elvati, A. Violi "Thermodynamics of poly-aromatic hydrocarbon clustering and the effects of substituted aliphatic chains" Proceedings of the Combustion Institute 34 (2013), pp. 1837-1843.
5. K.O. Johansson, J. Lai, S.A. Skeen, K.R. Wilson, N. Hansen, A. Violi and H.A. Michelsen "Soot precursor formation and the breakdown of the stabilomer concept" Proc. Combust. Inst.: 35, submitted, accepted for oral presentation.
6. J.Y. Lai, P. Elvati, A. Violi, "Stochastic Atomistic Simulation of Polycyclic Aromatic Hydrocarbon Growth in Combustion", Phys. Chem. Chem. Phys., 16 (17), 7969 – 7979 (2014).
7. J.S. Lowe, J.Y.W. Lai, P. Elvati and A. Violi. "Towards a predictive model for polycyclic aromatic hydrocarbon dimerization propensity" Proc. Combust. Inst.: 35, submitted, accepted for oral presentation.

PRESSURE DEPENDENCE OF COMBUSTION REACTIONS: QUANTUM INELASTIC DYNAMICS ON AUTOMATICALLY GENERATED POTENTIAL ENERGY SURFACES

Albert Wagner
Chemical Sciences and Engineering Division
Argonne National Laboratory
9700 South Cass Avenue
Argonne, IL 60439
Email: wagner@anl.gov

PROJECT SCOPE

This program is aimed both at developing improved ways to automatically construct a reliable potential energy surface (PES) and at using such surfaces to carry out inelastic quantum dynamics studies on pressure effects. In this last year, opportunities in tunneling and its connection to PESs were pursued.

RECENT PROGRESS

The analytic multidimensional semiclassical tunneling formula of Miller et al.[1] is based on second order vibrational perturbation theory (VPT2) and is a reliable tunneling option in the Multiwell[2] suite of codes for thermal kinetics. However it is qualitatively incorrect for deep tunneling at energies well below the top of the barrier. The reason is that the formula uses an effective barrier weakly related to the true energetics but correctly adjusted to reproduce the VPT2 anharmonic description of the saddle point. We have developed an analytic improved semiclassical formula that correctly includes energetic information and allows a qualitatively correct representation of deep tunneling. This is done by a VPT2-modified, effective, three-segment Eckart potential continuous everywhere in value and derivative. Figure 1a displays a series of composite potentials with a common VPT2 saddle point description but different barriers. The dotted black line in the figure is the barrier that un-improved theory assumes from saddle point properties alone. This composite potential has an analytic barrier penetration integral leading

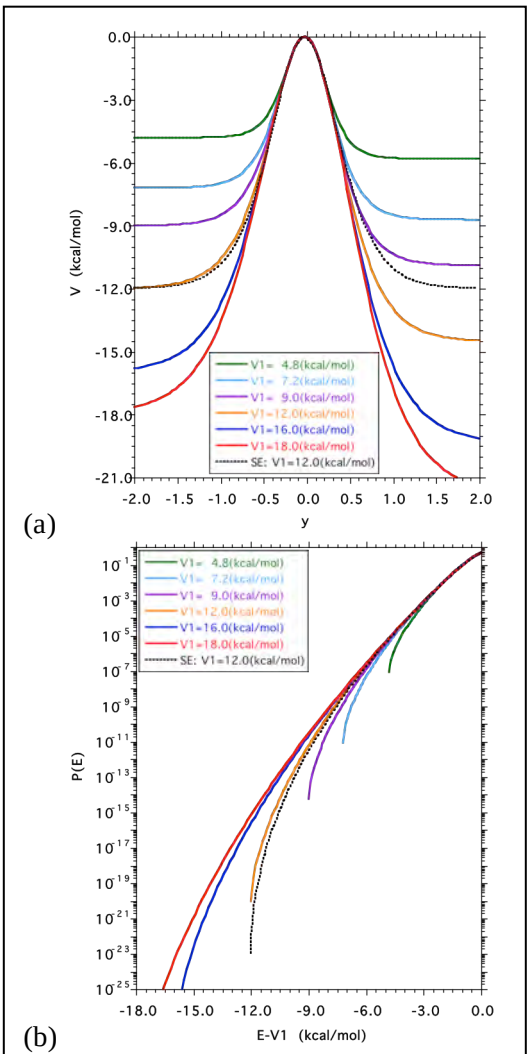

Figure 1: (a) A family of composite potentials all with the same VPT2 description of the saddle point. (b) Tunneling probabilities color coded as in (a) using the improved semiclassical tunneling formula.

to a new analytic semiclassical tunneling formula. Figure 1b shows the calculated tunneling probability from the potentials in Fig. 1a. The black dotted line is the tunneling probability the un-improved theory would give for all the potentials in panel (a). The middle segment of the composite potential is by itself somewhat superior to the original formulation because it incorporates the asymmetry of the reaction barrier produced by the known reaction exoergicity. The limitations of the original formula are echoed in high-energy descriptions of bound vibrational states perpendicular to the reaction path but typically the necessary corrective ab initio information is not available.

In collaboration with the Dawes group (Missouri U. of Science and Technology), H. Guo (U. New Mexico), and R. Continetti (UC San Diego), the measured H(D)OCO survival fractions of the photodetachment-photofragment coincidence experiments by the Continetti group[3] have been qualitatively reproduced by tunneling calculations to H(D) + CO_2 on several recent ab initio PESs for the HOCO system. The tunneling calculations involve effective one-dimensional barriers based on steepest descent paths computed on each PES. The resulting tunneling probabilities are converted into H(D)OCO survival fractions using a model developed by the Continetti group[3] in which every oscillation of the H(D)-OCO stretch provides an opportunity to tunnel. Four different PESs are examined with the best qualitative agreement with experiment occurring for the PIP-NN PES based on UCCSD(T)-F12a/AVTZ electronic structure calculations and also a partial

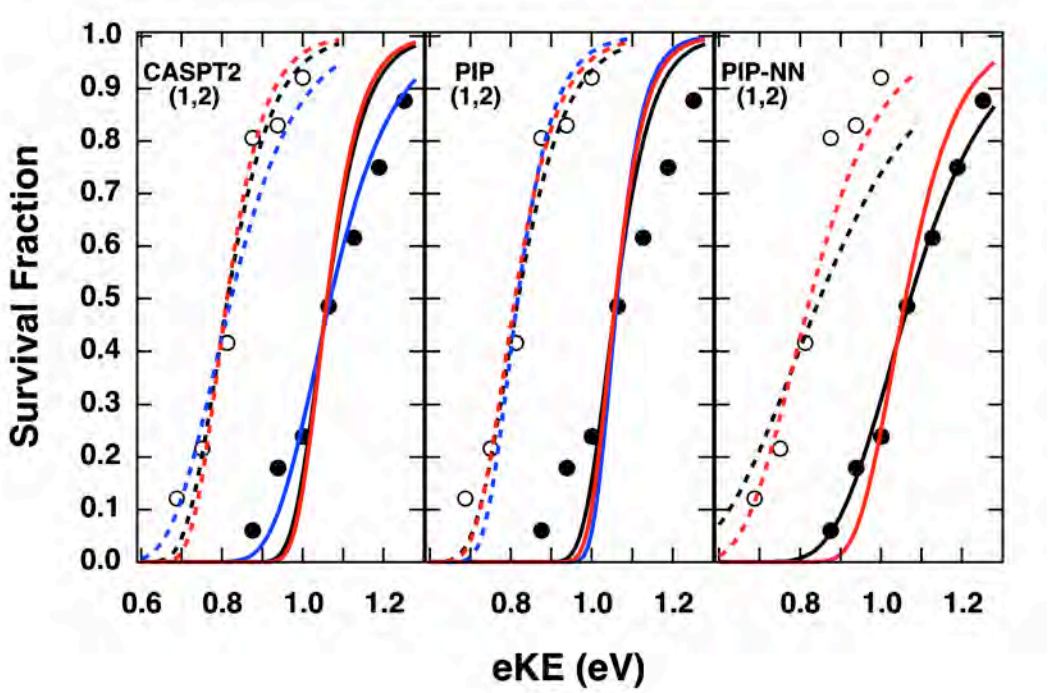

Figure 2. Measured and computed H(D)OCO survival fractions versus kinetic energy of the detached electron (eKE). Solid symbols or lines for HOCO; open symbols and dashed lines for DOCO. The PES for each panel is indicated. Black (SCT), red (iSCTST), and blue (Eckart) indicate different tunneling methods.

PES constructed for this study based on CASPT2/AVDZ electronic structure

calculations. These two PESs differ in barrier height by 1.6 kcal/mol but when matched at the saddle point have an almost identical shape along their reaction paths. The PIP PES is a less accurate fit to a smaller ab intio data set than that used for PIP-NN and its computed survival fractions are somewhat inferior to PIP-NN. The LTSH PES is the oldest surface examined and is qualitatively *in*compatible with experiment. On each PES, four different approximate tunneling methods are compared but only the small curvature tunneling (SCT) method of POLYRARTE[4] and the improved semiclassical transition state method (iSCTST and discussed above) produce useful results on all four PESs. In Fig. 2, the best results on the CASPT2, PIP, and PIP-NN PESs are compared for SCT (black), iSCTST (red), and Eckart (blue). The Eckart is qualitatively incorrect on the PIP-NN PES and is not included in the figure. The SCT and iSCTST results are generally comparable and in qualitative agreement with experiment, especially for the PIP-NN and CASPT2 PESs. For reason previously mentioned, the original SCTST method produces incorrect tunneling probabilities on CASPT2 and PIP-NN PESs. The SCT method requires following the reaction path down far enough to capture the tunneling process under investigation. The iSCTST avoids following reaction paths at the price of a VPT2 calculation at the saddle point, although that calculation can be done in parallel and is a built-in option in some electronic structure codes.

FUTURE PLANS

In collaboration with the Thompson group (University of Missouri), we are examining with classical trajectories the vibrational and rotational relaxation of initially excited molecules in a thermal Ar bath gas at pressures that range over two orders of magnitude from ~10 atm to ~1000 atm. In this study the bath gas motion is explicitly followed using either periodic boundary conditions or containment within a soft-wall rigid sphere too large to perturb results. With parallel computational resources, relaxation of complicated molecules up to nanoseconds can be followed. Three species are under study: OH, HO_2, and CH_3NO_2 where in all cases pairwise additive potentials for the molecule-Ar interaction are added to the molecule's internal potential. Figure 3

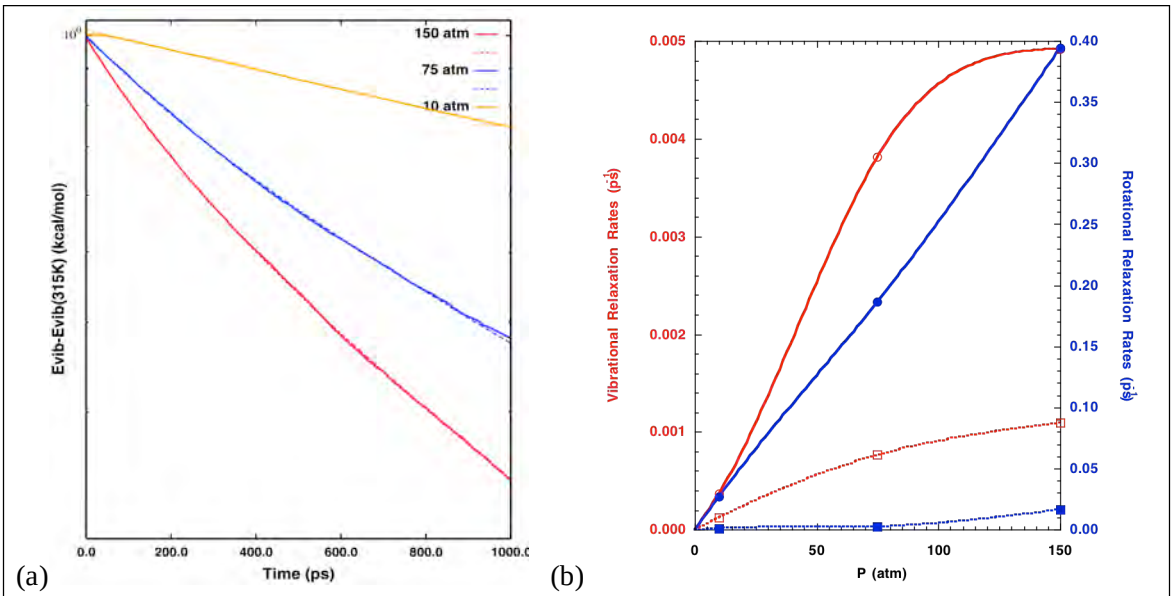

Figure 3. (a) Computed and fitted relaxation of excess energy above thermal for CH_3NO_2 in an Ar bath. (b) Plot of vibrational (red) and rotational (blue) relaxation rates as a function of pressure.

illustrates some initial results, in this case for CH_3NO_2 at room temperature where 1000 Ar atoms were followed. Panel (a) displays vibrational relaxation over 1 nsec at pressures from 10 atm to 150 atm. Clearly multiple-rate relaxation grows in at the higher pressures. The barely visible dashed lines are a bi-exponential fit to the trajectory results. Panel (b) displays a spline through the fitted vibrational relaxation rates in red and fitted rotational relaxation rates in blue. At low pressures, relaxation rates are directly proportional to pressure because isolated collisions occur with a pressure dependent frequency. At high pressures, collisions are no longer isolated and the collision rate – pressure relationship breaks down. Figure 3 shows that extrapolation of low pressure (< 10 atm) vibration relaxation rates overestimates the relaxation at pressures > ~100 atm and misses the development of multiple rates at high pressures. However, for rotations low-pressure extrapolations are reasonably reliable. Preliminary results for HO_2 show similar behavior while OH show rates directly proportional to pressure over large variations in pressure. The mechanisms behind these behaviors are being investigated.

Concerning the development of PESs, in collaboration with the Dawes group and the Thompson group, we are developing a permutational invariant IMLS PES for C_2H_5 based on 235,000 M05 DFT calculations of the PES produced by ab initio trajectories and saved during a previous study.[5] In collaboration with Y. Suleymanov and W. Green (MIT), we are pursuing the application of IMLS methods to automatically grow that portion of the PES needed for ring polymer molecular dynamics (RPMD) calculations of abstraction and insertion rate constants.

---

[1] W. H. Miller, R. Hernandez, N. C. Handy, D. Jayatilaka, and A. Willets, *Chem. Phys. Lets.* **1990**, *172*, 62.

[2] As developed by T. L. Nguyen, J. F. Stanton, and J. R. Barker and contained in Multiwell at http://aoss-research.engin.umich.edu/multiwell/

[3] C. J. Johnson, B. L. J. Poad, B. B. Shen and R. E. Continetti, *J. Chem. Phys.* **134**, 171106 (2011).

[4] D. G. Truhlar et al., POLYRATE–version 2010, University of Minnesota, Minneapolis, 2010. See http://comp.chem.umn.edu/polyrate/.

[5] A. F. Wagner, L. A. Rivera, D. Bachellerie, J. W. Perry, and D. L. Thompson, *J. Phys. Chem. A.* **117**, 11624-11639 (2013)

DOE-SPONSORED PUBLICATIONS SINCE 2012

1. A. F. Wagner, R. Dawes, R. E. Continetti, and H. Guo, THEORETICAL/EXPERIMENTAL COMPARISON OF DEEP TUNNELING DECAY OF QUASI-BOUND H(D)OCO TO H(D)+CO_2, submitted to *J. Chem. Phys.*
2. A. F. Wagner, IMPROVED MULTIDIMENSIONAL SEMICLASSICAL TUNNELING THEORY, *J. Phys. Chem. A* **117**, 13089-13100 (2013).
3. J. W. Perry, R. Dawes, A. F. Wagner, and D. L. Thompson, CLASSICAL TRAJECTORY STUDY OF THE INTRAMOLECULAR DYNAMICS, ISOMERIZATION, AND UNIMOLECULAR DISSOCIATION OF HO_2, *J. Chem. Phys.* **139**, 084319 (2013)
4. A. F. Wagner, L. A. Rivera, D. Bachellerie, J. W. Perry, and D. L. Thompson, A CLASSICAL TRAJECTORY STUDY OF THE DISSOCIATION AND ISOMERIZATION OF C_2H_5, *J. Phys. Chem. A.* **117**, 11624-11639 (2013)

Low Temperature Combustion Chemistry and Fuel Component Interactions

Margaret S. Wooldridge
Departments of Mechanical and Aerospace Engineering, University of Michigan
2350 Hayward Street, Ann Arbor, MI 48109-2121
mswool@umich.edu

I. Program Scope

Recent research into combustion chemistry has shown that reactions at "low temperatures" (700 – 1100 K) have a dramatic influence on ignition and combustion of fuels in virtually every practical combustion system. A powerful class of laboratory-scale experimental facilities that can focus on fuel chemistry in this temperature regime is the rapid compression facility (RCF), which has shown a remarkable ability to examine the details of fuel chemistry in this important regime. Our past studies have advanced our understanding of low temperature chemistry of important fuel compounds and has identified areas of high uncertainty for further research. In particular, we have shown how factors including fuel molecular structure, the presence of unsaturated C=C bonds, and the presence of alkyl ester groups influence fuel auto-ignition and produce variable amounts of negative temperature coefficient behavior of fuel ignition. We have also reported new discoveries of synergistic ignition interactions between alkane and alcohol fuels, with both experimental and kinetic modeling studies of these complex interactions.

This project focuses on further clarifying the effects of molecular structure including carbon bond saturation, through low temperature combustion chemistry studies of esters, alkanes, alkenes, and alcohols. Studies of synergistic fuel component interactions are also of interest in this project. Gas-speciation analysis is applied to directly identify decomposition and oxidation pathways and to measure sentinel species for particulate production (e.g. propene).

During the past year, we completed ignition and speciation studies of n-heptane, methyl trans-3-hexanoate, and started new studies of hexene isomers. We also started studies of ethanol/iso-octane interactions by establishing baseline ethanol experiments. Iso-octane reference experiments have been completed in previous studies. Ignition delay time data were acquired using the University of Michigan rapid compression facility (UM RCF) over a range of state and mixture conditions for each of these fuels. Mass sampling and gas chromatography were applied to quantify the stable intermediates present during ignition of n-heptane, methyl trans-3 hexanoate and the hexene isomers. We also completed a computational study of the effects of buffer gas composition on ignition behavior. Details of the studies of buffer gas composition are not presented here, but can be found in Wagnon and Wooldridge [1].

II. Recent Progress

The UM RCF is an innovative and robust experimental apparatus that can be used to isolate reaction kinetics by creating uniform conditions over a broad range of temperatures (T = 500-3000 K) and pressures (P = 0.5-60 atm). The long test times of the UM RCF allow application of rapid gas sampling methods to simultaneously measure a large number of stable species during ignition experiments. Details on the dimensions, components and performance characterization of the UM RCF can be found in Donovan *et al.* [2]. Previous UM RCF studies have considered ignition chemistry of numerous important reference fuel compounds including iso-octane [3], n-heptane [4], n-butanol [5], H_2/CO mixtures [6], and C_5 esters [7,8]. UM RCF studies include continuous absolute measurements of OH radicals during iso-octane ignition [9], as well as discrete measurements of intermediate species formed during ignition for several different fuel compounds [4,5,8,10].

This report presents a brief summary of the results of the n-heptane study published this past year [4]. Although there have been many studies of *n*-heptane ignition, few studies have provided detailed insights into the low-temperature chemistry of *n*-heptane—a primary reference fuel—through direct measurements of intermediate species formed during ignition. In the study by Karwat et al. [4], new ignition and speciation data for n-heptane ignition were presented for high pressure (9 atm), low

temperatures (660-710 K) conditions. The time-histories of seventeen species, including large alkenes, aldehydes, carbon monoxide, and *n*-heptane were quantified using gas chromatography, and the experimental data are presented in **Figure 1**. A detailed chemical kinetic mechanism developed previously for oxidation of *n*-heptane [11,12] reproduced experimentally observed ignition delay times reasonably well, but predicted levels of some important intermediate chemical species that were significantly different from measured values as shown in **Figure 1**. Results from recent theoretical studies of low temperature hydrocarbon oxidation reaction rates by Villano et al. [13,14] were used to upgrade the chemical kinetic mechanism for *n*-heptane, leading to much better agreement between experimental and computed intermediate species concentrations as seen in **Figure 1**. However, the mechanism predicts higher consumption of *n*-C_7H_{16} at the first stage of ignition and predicts more heat release at the first stage of ignition than observed experimentally.

While previous *n*-C_7H_{16} ignition studies have provided remarkable understanding of the effects of a broad range of temperatures and pressures on ignition delay times, few experimental studies have interrogated the reaction pathways proposed and represented in chemical kinetic mechanisms in the form of intermediate chemical species concentrations. The UM RCF ignition study provided new measurements of intermediate species levels during *n*-C_7H_{16} ignition in the low-temperature regime that could not be reproduced using currently available kinetic mechanisms. The discrepancies are largely due to poorly known reaction rates of alkylperoxy radicals and other species produced via alkylperoxy isomerization reactions. New theory results by Villano et al. [13,14] reduced these uncertainties, and improvements in the mechanism made possible by these new studies were key to improving the agreement between computed and measured intermediate species concentrations. Previous rates for alkylperoxy and alkylperoxy isomerization reactions had been based primarily on well-intentioned estimates, so the new rate information, based on established theoretical principles, are a significant upgrade to current kinetic models. New studies of these reactions, particularly including experiments that address oxidation reactions and rates in the low temperature range are critical to making further mechanism refinements in this very important temperature regime.

III. Future Work

Our future work includes ignition and speciation studies of unsaturated hydrocarbons to clarify the uncertainties raised in this class of compounds during our previous studies. Specifically, we have started ignition and speciation studies of several hexene isomers to compare the effect of the double bond on the reaction pathways [15]. We have also started baseline studies to examine the fuel interaction effects between iso-octane and ethanol [16]. We continue to work with Dr. Charles Westbrook to develop a more accurate understanding of the intermediates formed during ignition of hydrocarbons and oxygenated hydrocarbons. During this past year we also worked with Dr. Robert Tranter of Argonne National Laboratories (ANL) to create a new sampling valve system to allow studies at higher pressures based on his valve designs used at ANL. Further, Dr. Tranter hosted Mr. Scott Wagnon a University of Michigan doctoral student for two visits to ANL as part of a student exchange. We hope to continue this exchange into the future. Lastly, we collaborated this past year with Dr. Stephen Klippenstein and Dr. Michael Davis, also of ANL, to revisit UM RCF ignition data on n-butanol in light of new studies of elementary chemical reactions important in n-butanol combustion. We plan to complete this study in the coming year.

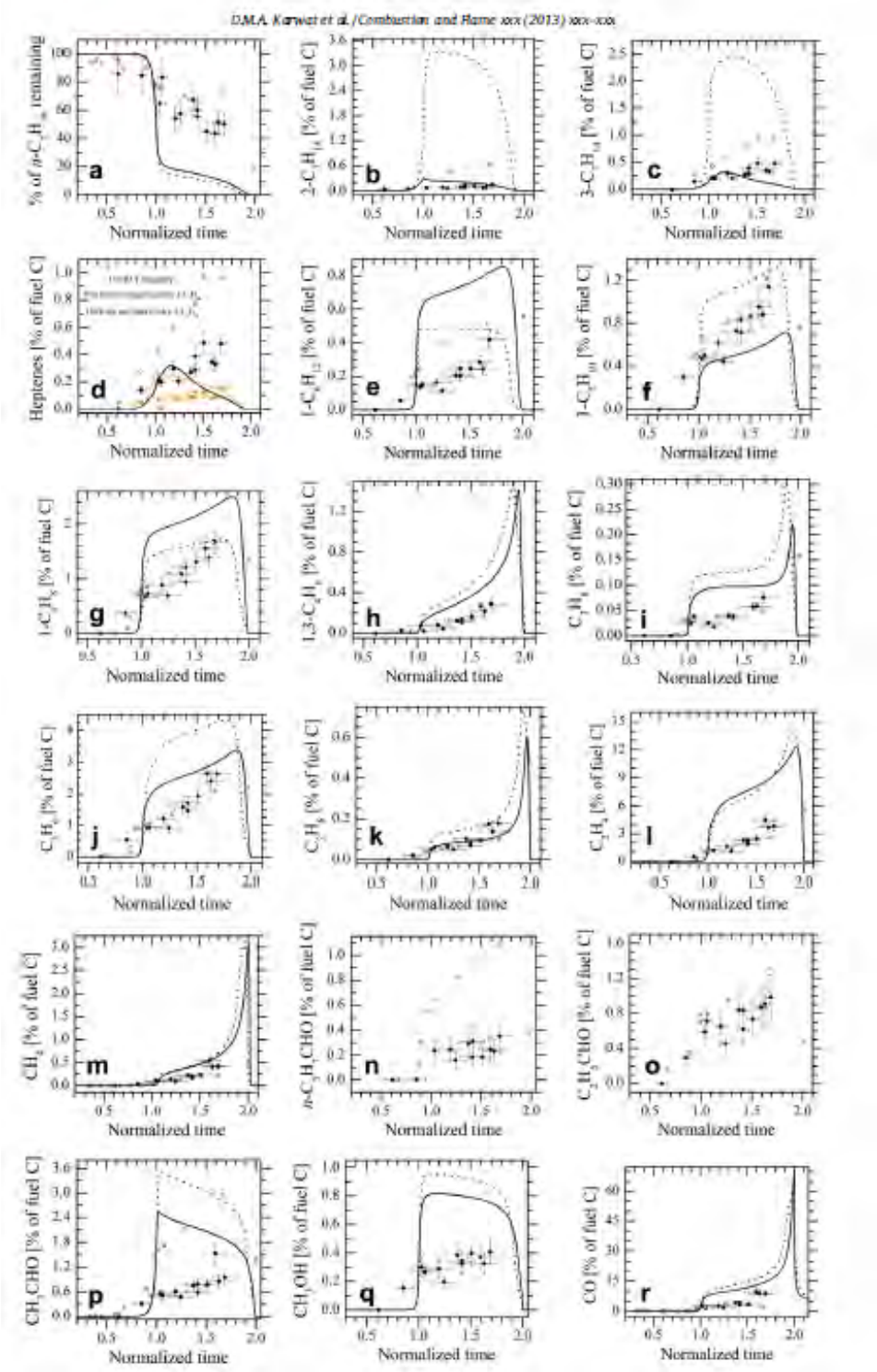

Figure 1: Species concentration time-histories from n-heptane ignition UM RCF sampling experiments (solid black circles), from the Minetti et al. [17] study (open red squares), and from the model predictions for the UM RCF data based on the current reaction mechanism (solid line) and the Mehl et al. [12] mechanism (dashed line). (Note the unique symbols for **Fig. 1d**.) The model predictions are shown for constant volume, adiabatic conditions with P_0 = 9 atm, T_0 = 700 K, n-C_7H_{16} = 0.0134, O_2 = 0.149, N_2 = 0.2336, and CO_2 = 0.6040 (mole fraction). All data are presented as normalized to the % of fuel carbon in the initial reactant mixture. Further discussion of these results can be found in Karwat et al. [4].

IV. References

1. Wagnon, S. W., Wooldridge, M. S., accepted to *Combust. Flame*, September 2013, in press.
2. Donovan, M.T., He, X., Zigler, B.T., Palmer, T.R., Wooldridge, M.S., Atreya, A. (2004) *Combust. Flame* **137** 351.
3. He, X., Donovan, M.T., Zigler, B.T., Palmer, T.R., Walton, S.M., Wooldridge, M.S., Atreya, A. (2005) *Combust. Flame* **142** 266.
4. Karwat, D. M. A., Wagnon, S., Wooldridge, M. S., Westbrook, C. K. (2013) *Combust. Flame* **160** 2693.
5. Karwat, D. M. A., Wagnon, S., Teini, P. D., Wooldridge, M. S. (2011) *J. Phys. Chem. A* **115** 4909.
6. Walton, S.M., He, X., Zigler, B.T., Wooldridge, M.S. (2007) *Proc. Combust. Inst.* **31** 3147.
7. Walton, S. M., Wooldridge, M. S., and Westbrook, C. K. (2009) *Proc. Combust. Inst.* **32** 255.
8. Walton, S.M., Karwat, D.M., Teini, P.D., Gorny, A., Wooldridge, M.S. (2011) *Fuel* **90** 1796.
9. He, X., Zigler, B.T., Walton, S.M., Wooldridge, M.S., Atreya, A. (2006) *Combust. Flame* **145** 552.
10. He, X., Walton, S.M., Zigler, B.T., Wooldridge, M.S., Atreya, A. (2007) *Int. J. Chem. Kinet.* **39** 498.
11 Curran, H. J., Gaffuri, P., Pitz, W. J., Westbrook, C. K. (1998) Combust. Flame **114** 149.
12. Mehl, M. Pitz, W.J. Westbrook, C.K. Curran, H.J. (2011) *Proc. Combust. Inst.* **33** 193.
13 Villano, S. M., Huynh, L. K., Carstensen, H.-H., Dean, A. M. (2011) *J. Phys. Chem. A* **115** 13425.
14 Villano, S. M., Huynh, L. K., Carstensen, H.-H., Dean, A. M. (2012) *J. Phys. Chem. A* **116** 5068.
15 Wagnon, S., Wooldridge M. S., (2014) "Auto-Ignition and Speciation Studies of Trans-Hexene Isomers in a Rapid Compression Facility," Spring Meeting of the Canadian Section of the Combustion Institute, May 2014.
16 Barraza-Botet, C., Wagnon, S., Wooldridge M. S., (2014) "Ignition Delay Time Measurements and High-speed Imaging Analysis for Ethanol-Air Mixtures in a Rapid Compression Facility," Spring Meeting of the Canadian Section of the Combustion Institute, May 2014.
17. Minetti, R. Carlier, M. Ribaucour, M. Therssen, E. Sochet, L.R. (1995) *Combust. Flame* **102** 298.

V. Publications and submitted journal articles supported by this project 2011-2013

1. Barraza-Botet, C., Wagnon, S., Wooldridge M. S., (2014) "Ignition Delay Time Measurements and High-speed Imaging Analysis for Ethanol-Air Mixtures in a Rapid Compression Facility," Spring Meeting of the Canadian Section of the Combustion Institute, May 2014.
2. Wagnon, S., Wooldridge M. S., (2014) "Auto-Ignition and Speciation Studies of Trans-Hexene Isomers in a Rapid Compression Facility," Spring Meeting of the Canadian Section of the Combustion Institute, May 2014.
3. Wagnon, S. W., Karwat, D. M. A., Wooldridge, M. S., and Westbrook, C. K. "On the Ignition Chemistry of Methyl Trans-3-Hexenoate," submitted to the *35th Intl. Symp. on Comb.*, December 2013.
4. Wagnon, S. W., Wooldridge, M. S., (2014) "Effects of Diluent Gas Composition on Autoignition," accepted to *Combustion and Flame*, September 2013, in press.
5. Karwat, D. M. A., Wagnon, S., Wooldridge, M. S., Westbrook, C. K. (2013) "Low Temperature Speciation and Chemical Kinetic Studies of n-Heptane," *Combustion and Flame* **160**, pp. 2693-2706.
6. Karwat, D. M. A., Wagnon, S., Wooldridge, M. S., Westbrook, C. K., (2012) "On the Combustion Chemistry of n-Heptane and n-Butanol Blends," *Journal of Physical Chemistry A*, DOI 10.1021/jp3093 58h, **116**, pp. 12406-12421.
7. Karwat, D. M. A., Wagnon, S., Teini, P. D., Wooldridge, M. S. (2011) "On the Chemical Kinetics of n-Butanol: Ignition and Speciation Studies," *Journal of Physical Chemistry A*, **115**, pp. 4909-4921.
8. Walton, S. M., Karwat, D. M., Teini, P. D., Gorny, A., and Wooldridge, M. S. (2011) "Speciation Studies of Methyl Butanoate Ignition," *Fuel*, 90, pp. 1796-1804.

THEORETICAL STUDIES OF THE REACTIONS AND SPECTROSCOPY OF RADICAL SPECIES RELEVANT TO COMBUSTION REACTIONS AND DIAGNOSTICS

DAVID R. YARKONY, DEPARTMENT OF CHEMISTRY, JOHNS HOPKINS UNIVERSITY, BALTIMORE, MD 21218
yarkony@jhu.edu

Overview

A. Photoionization Spectra

We continued our work on photoionization spectra that reveal the spectrum of a residual molecule (the species left after the electron is removed) whose states are strongly coupled by conical intersections, completing of our simulation of the photoionization spectrum of propyne, where the experimentally measured combined effects of the Jahn-Teller and spin-orbit interactions required clarification.

B. Nonadiabatic Dynamics

While electronic structure is essential to explain chemical mechanisms, quantification of those results requires nuclear dynamics. Recently we reported, as part of other funded research, an algorithm to construct coupled diabatic states representations, $\mathbf{H}^{d}$, of adiabatic potential energy surfaces (PESs) coupled by conical intersections based on electronic structure data, energies, energy gradients and derivative couplings obtained from multireference configuration interaction single and double excitation (MRCISD) wave functions, where large amplitude nuclear motions including dissociation are possible.[1] The electronic structure data are calculated at points determined by quasi classical surface hopping trajectories (QCT) obtained using Truhlar's ANT program. The resulting quasi diabatic representations of coupled adiabatic PESs will enable accurate dynamics studies while avoiding the accuracy limitations inherent in the dynamics on the fly approach usually used. We have completed a coupled quasi diabatic state representation of the coupled adiabatic PESs that describe photodissociation of NH_3, and are constructing such representations for CH_2OH, and C_6H_5OH and the reactive quenching reaction, $OH(A)+H_2 \rightarrow OH(X)+H_2$ or H_2O+H.

WORK COMPLETED.

A. Propyne Photoionization spectrum. Clarifying experiments. [2]

Propyne, $CH_3C \equiv CH$ is an important intermediate in combustion chemistry being known to participate in the formation of polycyclic aromatic hydrocarbons.[3] Propyne has an $\tilde{X}^1A_1$ (C_{3v}) ground electronic state, whereas the ionized species, the propyne cation has an $\tilde{X}^2E$ ground state, which exhibits a Jahn-Teller distortion. The ^2E state is also split by the spin-orbit interaction, producing $^2E_{1/2}$ and $^2E_{3/2}$ states. Grant and coworkers[4] have recorded and successfully analyzed a nonresonant two-photon pulsed field ionization-photoelectron (PFI-PE) spectrum of propyne, $C_3H_4^+(\tilde{X}^2E_{1/2,3/2}) \leftarrow C_3H_4(\tilde{X}^1A_1)$ using the spin-orbit (A) constant for the acetylene cation $^2\Pi_{1/2,3/2}$, A = -30.9 cm^{-1} (Ref. [5]) for the ^2E state, with a structure very little altered by Jahn-Teller distortion.

More recently Ng and coworkers, have used the IR-VUV-PFI-PE method, to analyze the $C_3H_4^+(\tilde{X}^2E, \nu_1^+) \leftarrow C_3H_4(\tilde{X}^1A_1, \nu_1)$. These authors compared, measured and simulated spectra and find A = -13.9±0.2 cm^{-1} and a ratio of the photoionization cross sections $E_{1/2}$:$E_{3/2}$ = 4:1. These results are not consistent with those of Grant and coworkers. [4].

We used KDC vibronic coupling theory,[6] to simulate the near threshold region of the photoionization spectrum of propyne including spin-orbit coupling. The analysis predicts an 18.7 (13.9) cm^{-1} fine structure splitting of the $^2E_{3/2} - {}^2E_{1/2}$ states. This represents a 36 (57) percent Ham reduction[7] of the spin-orbit coupling. These results are in reasonable accord with the experimental results of Ng,[3] given parenthetically, but contradict those of Ref. [4], where the spin-orbit interaction was assumed to be completely unquenched. However, we predicted that the cross sections for producing $C_3H_4^+(^2E_{3/2},v^+=0)$ and $C_3H_4^+(^2E_{1/2},v^+=0)$ by ionizing propyne, which are equal by symmetry in the nonrelativistic limit, remain equal when the spin-orbit interaction is included. This result is at odds with the conclusion of Ref. [3] that the

cross section ratio ($^2E_{1/2}$,v^+=0):($^2E_{3/2}$,v^+=0) = 4:1. However, discussions with Cheuk Ng, based on a preprint of our work, have determined that the conclusion of Ref.[3] is incorrect and the predicted 1-1 ratio is quite reasonable.

Finally we considered the lowest vibronic levels above threshold in the photoionization spectrum of propyne reported in Ref. [8]. Our analysis suggests hot bands, rather than the experimentally proposed explanation, are responsible for the observed features. In future work this spectrum will be analyzed in greater detail.

B. $NH_3(X)+hv \rightarrow NH_3(A) \rightarrow NH_2(A,X)+H$[9]

We have, in collaboration with Hua Guo(University of New Mexico), extended our **H**[d] representing the 1,2^{1}A states of NH_3 and used it to simulate the kinetic energy release spectrum with rotational resolution following excitation to the A^{1}A state of NH_3.[9] The excellent agreement between the experimental and simulated spectrum is pictured below. These results provide the foundation for the description of the vibrationally mediated photodissociation of NH_3 obtained with DoE funding in Crim's laboratory almost a decade ago[10] which to date have resisted explanation.

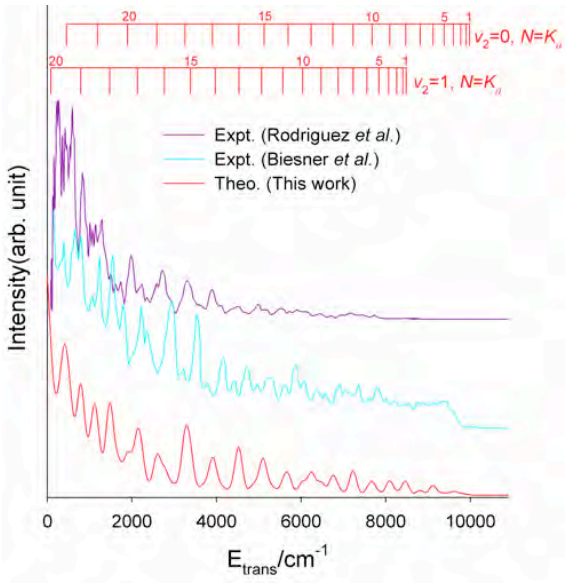

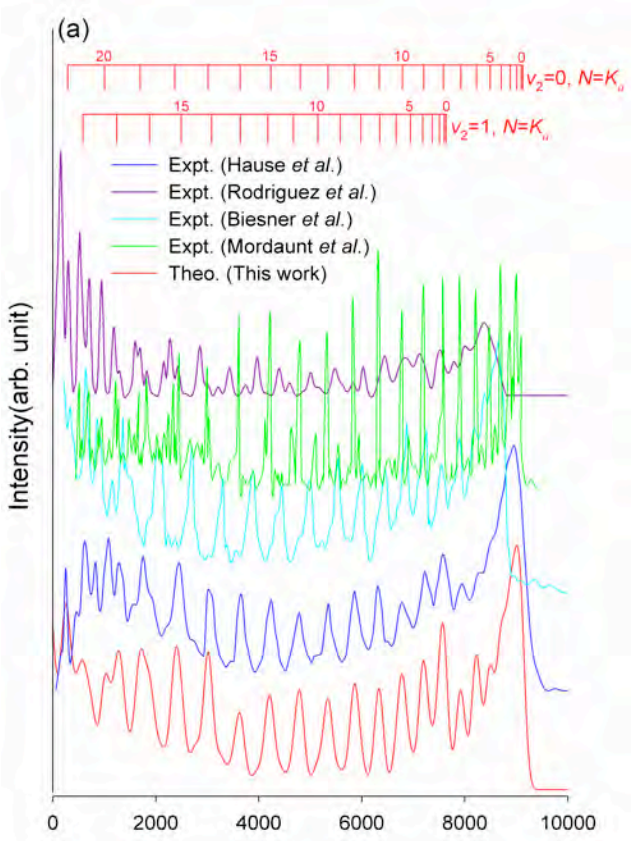

Figure: Comparison of the calculated H-translational energy distribution of the $NH_2(\tilde{X}\,^2B_1)$ product with experimental results at the total energy of (bottom plate) 6.55 eV (the 0^0 state) and (top plate) 6.66 eV (the 2^1 state). The calculated N=K_a energy levels of $NH_2(\tilde{X}\,^2B_1)$ are also included. Individual results are shifited for clarity with the results of theory below those of experiment

C. $OD(A^2\Sigma^+) + H_2 \rightarrow H_2O + D$(insertion), HOD + H(abstraction), $OD(X^2\Pi)+H_2$, Part 1- A Reaction Mechanism[11]

The captioned reaction is of fundamental importance as an archetypical nonadiabatic reaction involving more than one exit channel, and has been studied in the DoE supported laboratories of Lester(University of Pennsylvania)[12] and Davis(Cornell).[13] In the captioned work we have proposed a new mechanism for the collisional deactivation of $OH(A^2\Sigma^+)$ involving an intermediate complex formed on the 2^2A PES in a region of nuclear coordinate space where the wave functions are Rydberg in character.

Energetically accessible paths to this Rydberg region on the 2^2A PES involve passage through a linking region, where the electronic structure changes from valence to Rydberg in character. The important structures for this mechanism are nonplanar and the described pathways are a major departure from current models of this reaction. The mechanism provides an explanation for the broad H-atom kinetic energy distributions measured by Lester and coworkers[12] for the insertion channel, which needs to be confirmed by dynamics calculations.

Work in Progress

A. $OD(A^2\Sigma^+) + H_2 \rightarrow H_2O + D$(insertion), HOD + H(abstraction), $OD(X^2\Pi)+H_2$, Part 2- Representing the coupled PESs

Based on the above results, we are currently constructing a coupled four quasi diabatic state representation of the captioned reaction, at the MRCISD level. The representation of the skeletal data, a coarse representation of key regions of the PESs, described in our previous mechanistic work is now complete. We will use QCT to complete the definition of the domain required to describe the electronic quenching processes. Nonadiabatic dynamics on these coupled PESs will enable us to understand the origin of the insertion products which to date have resisted theoretical explanation.

B. Multichannel PESs coupled by conical intersections: The photodissociation $CH_2OH(X) + hv \rightarrow CH_2OH^* \rightarrow CH_2O(X)+H$, CHOH(X) [cis/trans] +H, CH_3O

For these reactions, studied in Reisler's laboratory,[14] we have developed an MRCISD expansion of greater than 60 million CSFs which is capable of describing all channels in the above captioned reaction. We are in the process of using that description to construct a coupled state quasi-diabatic representation of the 1,2,3 ^{2}A coupled adiabatic states that can be used to simulate the captioned reactions. We have completed the representation of the skeletal data, the asymptotes, local minima and low energy portions of the $1,2^2$A and $2,3^2$A conical intersection seams. We are currently using QCT to complete the definition of the domain required for dynamics simulations of these processes. Because of the size of the MRCISD expansion these calculations are only possible with a grant of computer time on the NERSC computer platforms.

C. Representing PESs coupled by conical intersections for significantly larger molecules: $C_6H_5OH(\tilde{X}) + hv \rightarrow C_6H_5OH(\tilde{A}) \rightarrow C_6H_5O(\tilde{X}, \tilde{A}) + H$

As part of other funded research our algorithm for representing adiabatic states coupled by conical intersections using an $\mathbf{H}^d$ has been extended to treat nonadiabatic processes in considerably larger molecules.[15] The method treats all internal degrees of freedom and uses electronic structure data from *ab initio* MRCISD calculations with nuclear configuration selection based on QCT. It treats all (so far 33 is our largest) internal degrees of freedom including dissociative and large amplitude internal motion. Two procedures are essential to the algorithm, a null space projector which removes basis functions from the fitting process until they are needed and a partial diagonalization technique which allows for automated, but accurate, treatment of the vicinity of extended seams of conical intersections of two or more states. The $\mathbf{H}^d$ can smooth the irregularities in the electronic energies attributable to the orbital changes in the active space that are inherent to nonadiabatic processes.

As part of our DoE funded research we are taking this method beyond the proof of principle stage treating the photodissociaton of phenol, $C_6H_5OH(\tilde{X}^1A')+hv \rightarrow C_6H_5OH^* \rightarrow C_6H_5O(\tilde{X}^2B_1,\tilde{A}^2B_2) + H$ using *ab initio* electronic structure data for the $1,2,3,4^1$A states. This reaction has been the focus of DoE funded computational[16] and experimental[17] work. Our representation is based on an MRCISD level expansion

comprised of 200 million CSFs! Based on the preliminary representation using first order CI wave functions, we have determined that electronic structure data at ~4700 (predetermined) nuclear configurations will be required to construct this representation. To date calculations at ~1200 geometries are complete and we average ~500 geometries/week. This **H**^{d}, which will define the state of the art in representing coupled adiabatic PESs, is only possible because of a generous grant of computer time on the NERSC computing platforms.

References

[1]X. Zhu, and D. R. Yarkony, J. Chem. Phys. **137,** 22A511(2012).
[2]S. Marquez, J. Dillon, and D. R. Yarkony, J. Phys. Chem A. **117,** 12002(2013).
[3]X. Xing, M.-K. Bahng, B. Reed, C. S. Lam, K.-C. Lau, and C. Y. Ng, J. Chem. Phys. **128,** 094311(2008).
[4]H. Matsui, Y.-F. Zhu, and E. R. Grant, Laser Chem. **16,** 161(1996).
[5]S. T. Pratt, P. M. Dehmer, and J. L. Dehmer, J. Chem. Phys. **99,** 6233(1993).
[6]H. Köppel, W. Domcke, and L. S. Cederbaum, Adv. Chem. Phys. **57,** 59(1984).
[7]F. S. Ham, Phys. Rev. **166,** 307(1968).
[8]G. H. Ho, M. S. Lin, Y. L. Wang, and T. W. Chang, J. Chem. Phys. **109,** 5868(1998).
[9]C. Xie, J. Ma, X. Zhu, D. H. Zhang, D. R. Yarkony, D. Xie, and H. Guo, J. Phys. Chem. Lett **5,** 1055(2014).
[10]M. L. Hause, Y. H. Yoon, and F. F. Crim, J. Chem. Phys. **125,** 174309(2006).
[11]J. Dillon, and D. R. Yarkony, J. Phys. Chem. A **117,** 7344(2013).
[12]J. H. Lehman, J. L. Bertrand, T. A. Stephenson, and M. I. Lester, J. Chem. Phys. **135,** 144303(2011).
[13]M. Ortiz-Suárez, M. F. Witinski, and H. F. Davis, J. Chem. Phys. **124,** 201106(2006).
[14]C. P. Rodrigo, C. Zhou, and H. Reisler, J. Phys. Chem. A **117,** 12049(2013).
[15]X. Zhu, and D. R. Yarkony, J. Chem. Phys. **140,** 024112 (2014).
[16]X. Xu, K. R. Yang, and D. G. Truhlar, J. Chem. Theory and Computation **9,** 3612(2013).
[17]M. L. Hause, Y. H. Yoon, A. S. Case, and F. F. Crim, J. Chem. Phys. **128,** 104307(2008).

PUBLICATIONS ACKNOWLEDGING (EXCLUSIVELY) CURRENT DOE SUPPORT (2011-2014)

1. *A Lippmann – Schwinger Approach for the Determination of Photoionization and Photodetachment Cross Sections Based on a Partial Wave Green's Function Expansion and Configuration Interaction Wave Functions.*
Seungsuk Han and David R. Yarkony, Mol. Phys. 110, 845-859 (2012).

2. *Nonadiabatic Effects in Substitutional Isomers of Jahn-Teller Molecules. The Strange Case of Hydroxymethoxy*
Joseph Dillon and David R. Yarkony, J. Chem. Phys. **137**, 154315 (2012)

3. *Reactive quenching of OH A $^2S^+$ by O_2 and CO: Experimental and nonadiabatic theoretical studies of H- and O-atom product channels*
Julia H. Lehman, Marsha I. Lester, and David R. Yarkony, J. Chem. Phys. 137, 094312 (2012)

4.*Seams of Conical Intersections Relevant to the Quenching of OH($A^2\Sigma^+$) by Collisions with H_2.*
Joseph Dillon and David R. Yarkony, J. Phys. Chem. A, 117 , 7344-7355 (2013)

5. *On the Mechanism for the Nonadiabatic Reactive Quenching of OH($A^2\Sigma^+$) by $H_2(^1\Sigma^+_g)$. The Role of the 2^2A State*
Joseph Dillon and David R. Yarkony, J. Chem. Phys. **139**, 064314 (2013).

6. *On the Photoionization Spectrum of Propyne. A fully ab initio Simulation of the Low-Energy Spectrum including the Jahn-Teller Effect and the Spin-Orbit Interaction*
Sara Marquez, Joseph Dillon and David R. Yarkony, J. Phys. Chem A. 117, 12002-12010 (2013)

7. *Full-dimensional quantum state-to-state non-adiabatic dynamics for photodissociation of ammonia in its A-band* Changjian Xie, Jianyi Ma, Xiaolei Zhu, Dong Hui Zhang, David R. Yarkony Daiqian Xie, and Hua Guo, J. Phys. Chem. Lett. 5,1055-1060 (2014).

GAS-PHASE MOLECULAR DYNAMICS: THEORETICAL STUDIES IN SPECTROSCOPY AND CHEMICAL DYNAMICS

Hua-Gen Yu (hgy@bnl.gov)
Chemistry Department, Brookhaven National Laboratory, Upton, NY 11973-5000

Program Scope

The main goal of this program is the development and application of computational methods for studying chemical reaction dynamics and molecular spectroscopy in the gas phase. We are interested in developing rigorous quantum dynamics algorithms for small polyatomic systems and in implementing approximate approaches for complex ones. Particular focus is on the dynamics and kinetics of chemical reactions and on the rovibrational spectra of species involved in combustion processes. This research also explores the potential energy surfaces of these systems of interest using state-of-the-art quantum chemistry methods, and extends them to understand some important properties of materials in condensed phases and interstellar medium as well as in combustion environments.

Recent Progress

Structure and TD wavepacket study of photo-initiated dissociation of O_2 on TiO_2

The O_2/Rutile TiO_2 system is a benchmark system for molecular photochemistry on semiconductor surfaces. It has been the subject of extensive experimental and theoretical studies, yet the mechanisms of photoinduced desorption and dissociation of O_2 on TiO_2 are still controversial. Motivated by the research in the BNL Surface Chemical Dynamics Group, we have carried out a theoretical study of electronic structure and quantum wavepacket dynamics of oxygen molecule adsorption and photo-initiated dissociateion of O_2 on a rutile TiO_2 nanocluster. The orientation of O_2 adsorbed parallel to the reduced TiO_2 cluster at the bridging row vacancy site was found to be the most favorable, in a charge state of O_2^{2-}. Natural transition orbital analysis for TiO_2-O_2 system shows that photon absorption injects an electron from the O_2 molecule back into the TiO_2 surface. This corresponds to a hole-mediated dissociation mechanism, in contrast to a previously advocated electron-mediated mechanism. The configuration with O_2 adsorbed perpendicular to the surface was found to be a transition state with a low barrier from the parallel configuration via a tilted local minimum. Stable configuration for $2O_2$ molecules

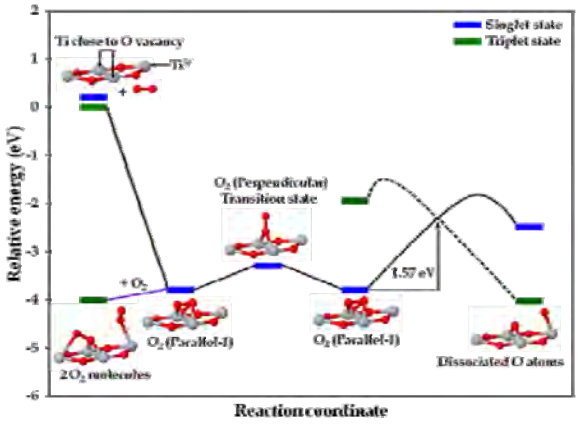

Figure 1: Relative energy diagram for the O_2/TiO_2 interaction system, the lowest crossing point between S_0 and T_0 is reduced to be about 0.6 eV in full dimensionality.

adsorbed on the reduced TiO_2 cluster was identified. It was found that adsorption of the second O_2 molecule stabilizes the energy. A stable configuration for the formation of tetraoxygen species at the bridging row oxygen vacancy site could not be identified. Calculated density of states and electronic spectra for various systems were found in good agreement. The relative energy diagram is shown in Figure 1.

Subsequently, O_2 dissociation starting from the most stable parallel orientation was studied. After dissociation, one O atom was found to heal the bridging row oxygen vacancy, whereas the other was deposited on the neighboring Ti^{5f} atom. The entire dissociation process on the ground state was found to involve an intersystem crossing (ISC) and has to overcome a large activation energy barrier. Using TDDFT potential energy surfaces for O_2 dissociation, a time-dependent wavepacket dynamics model was developed. The time-dependent wavepacket calculations show that the photo-initiated dissociation of O_2 at TiO_2 occurs via a direct dissociation mechanism. The lifetime of excited O_2 molecules was predicted to be about 266 fs. It was noticed that the non-adiabatic effects among the singlet electronic states play an important role in the dissociation reaction. However, the spin-orbit effect on the dynamics was found to be negligible. In near future, we plan to model the dynamics of the photoinduced O_2 desorption processes from TiO_2 surfaces, in particular, the translational distribution of O_2 as measured by White's group at BNL.

Development of linearly scaled quantum scattering dynamics method for polyatomic reactions

We (with Nyman at Gothenburg, Sweden) have summarized a nearly linearly scaled quantum scattering method for studying polyatomic molecular reactions, mainly based on our own developed two-layer Lanczos algorithm in the past years. Basically, the adiabatic functions at each scattering coordinate sector are computed using the two-layer Lanczos algorithm in a DVR or FBR basis set instead of the direct diagonalization (DD) method. The DD method has a cubic cpu-time scaling with the basis size *N* whereas the two-layer Lanczos algorithm has a nearly linear cup-time scaling owing to the use of the guided spectral transformation and iterative diagonalization techniques.

Future Plans

Kinetics and dynamics study of combustion-related reactions

Electronically excited species such as $^1CH_2$ also play an important role in combustion chemistry. However, the studies of their reactivity are rather limited, partially due to the non-adiabatic dynamics effects because those reactions often occur on multiple potential energy surfaces. In this research, we will extend the surface hopping direct *ab initio* molecular dynamics algorithm, developed for the SECH MD studies, to simulate the bimolecular reactions and the photo-dissociation chemistry. The first application would be the photodissociation dynamics of acetone at 193-230 nm. This system has been investigated by Suits et al. using a universal ion imaging technique. The photon excited acetones produce two major types of products: $CH_3CO + CH_3$ and $CO + 2CH_3$. The latter products result from poorly understood dissociation mechanisms. Here we will attempt to explore the dissociation pathways of acetone on its three low-lying electronic states. Here, we also propose to develop a zero-point energies-constrained NA-AIMD algorithm.

Development of a general program for calculating vibrational spectra of polyatomic systems

In this proposal, we aim to develop computational algorithms to accurately calculate the vibrational spectra of polyatomic molecules, and to assist experimentalists to understand their observed spectra. For polyatomic systems beyond six-atom, the challenge in rigorous quantum dynamics calculations comes from the huge basis size owing to high-dimensional problems. The Lanczos method is an iterative eigensolver capable of solving the eigenvalue problem of a large sparse matrix with a size up to $N \sim 10^7$, which might be equivalent to a chemical system with six degrees of freedom. In order to overcome this difficulty, we may try to reduce the basis size by using a compact basis set. The reduction of the basis size is the crucial idea of the sequential truncation approach widely used in direct diagonalization methods. This approach however requires too much CPU time and fast memory to be tractable for polyatomic molecules beyond five-atom molecules. During the past decade, several methods to obtain a compact basis set have been developed, e.g., the pruned basis functions.

Instead, in this proposal, we will use our recently developed ZDVR method to build a compact basis set. The ZDVR is a multi-dimensional PO-DVR method so that the ZDVR basis is very compact, which can substantially reduce the basis size. Numerical tests also demonstrated that it has the Gauss convergence speed with the basis size. Importantly, the ZDVR is a grid basis representation. As a result, the matrix representation of system Hamiltonian in ZDVR is often very sparse, which guarantees the efficiency of an iterative diagonalization method as well as the low memory requirement. The new algorithm will be called ZDVRMode.

We will apply the ZDVRMode program to study the vibrational spectra of combustion-related radicals such as vinyl (C_2H_3) and propargyl (C_2H_5) radicals, in collaboration with Sears and Hall in the GPMD group of BNL They are going to measure the overtones of both radicals using high-resolution near infrared spectroscopy. Currently, the Hamiltonian in normal mode coordinates has been numerically tested with propargyl radical in full dimension. The full coupled potential energy surface is used. Results obtained are very promising.

Publications since 2011

T.V. Tscherbul, H.-G. Yu, and A. Dalgarno, *Sympathetic cooling of polyatomic molecules with S-state atoms in a magnetic trap*, Phys. Rev. Lett. **106**, 073201 (2011).

H.-G. Yu, *An ab initio molecular dynamics study of the roaming mechanism of the H_2 + HOC^+ reaction*, Physica Scripta **84**, 028104 (2011).

S.-Y. Du, T. Germann, J. Francisco, K. Peterson, H.-G. Yu, and J. Lyons, *The kinetics study of the $S + S_2 \rightarrow S_3$ reaction by the Chaperon mechanism*, J. Chem. Phys. **134**, 154508 (2011).

H.-G. Yu, *An optimal density functional theory method for GaN and ZnO,* Chem. Phys. Lett. **512**, 231 (2011).

W.-Q. Han, H.-G. Yu, Z. Liu, *Convert graphene sheets to boron nitride and boron nitride-carbon sheets via a carbon-substitution reaction*, App. Phys. Lett. **98**, 203112 (2011).

H.-G. Yu and G. Nyman, *The infrared and UV-visible spectra of polycyclic aromatic hydrocarbons containing (5,7)-member ring defects: A theoretical study*, Astrophys. J., **751**, 3 (2012).

P.P Dholabhai and H.-G. Yu, *Exploring the ring opening pathways in the reaction of morpholinyl radicals with oxygen molecule*, J. Phys. Chem. A, **116**, 7123 (2012).

T.V. Tscherbul, T.A. Grinev, H.-G. Yu, A. Dalgarno, J. Klos, L. Ma and M.H. Alexander, *Cold collisions of polyatomic molecular radicals with S-state atoms in a magnetic field: An ab initio study of He + $CH_2(X^3B_1)$*, J. Chem. Phys. **137**, 104302 (2012).

G. Nyman and H.-G. Yu, *Quantum approaches to polyatomic reaction dynamics*, Int. Rev. Phys. Chem., **32**, 39 (2013).

P.P Dholabhai and H.-G. Yu, *Electronic structure and quantum dynamics of photoinitiated dissociation of O_2 on rutile TiO_2 nanocluster*, J. Chem. Phys., **138**, 194705 (2013).

Chemical Kinetics of Elementary Reactions

Judit Zádor
Combustion Research Facility, Mail Stop 9055, Sandia National Laboratories
Livermore, CA 94551-0969
jzador@sandia.gov

I. PROGRAM SCOPE

My program focuses on the theoretical determination of rate coefficients and branching fractions relevant to combustion chemistry. Specifically, the formation and dissociation of primary radicals derived from various fuel molecules, and the pressure- and temperature-dependent formation and reactions of peroxyalkyl radicals associated with low-temperature autoignition processes are studied. The work involves quantum chemical calculations, application of transition-state theory, solution of the master equation, and modeling of small reaction systems related to the experimental conditions. My recent focus is the automatic exploration of reactive potential energy surfaces to systematize and significantly accelerate research in elementary chemical kinetics. A particular aspect of the program is the close collaboration with experimental PIs (Taatjes, Sheps, Osborn) to minimize the effects of inherent uncertainties in the theoretical methods, and also to reveal the parts of our current theoretical models that cause most of these uncertainties.

II. RECENT PROGRESS

A. Primary fuel radicals

Unsaturated hydrocarbon + OH reactions. We calculated the unimolecular dissociation and isomerization rate coefficients of C_3H_7O isomers based on our previously published[i] propene + OH PES. The C_3H_7O isomers found on this surface correspond to the isomers obtained from propanol by H-abstraction, and are inherently important in setting the stage for propanol combustion. All rate coefficients were obtained with internal consistency with particular attention paid to shallow wells. After minor adjustments, very good agreement with the experimental results on *i*-propoxy dissociation[ii] was obtained. Several interesting pathways were uncovered, such as the catalytic dehydration, well-skipping reactions, and reactions forming enols. Our work quantitatively described the dissociation pathways from the radicals derived from propanol, which can be used for both the improvement of propanol models as well as to make better predictions for larger alcohols.

We mapped out the stationary points and the corresponding conformational space on the C_3H_5O potential energy surface relevant for the OH + allene and OH + propyne reactions systematically and automatically using our KinBot

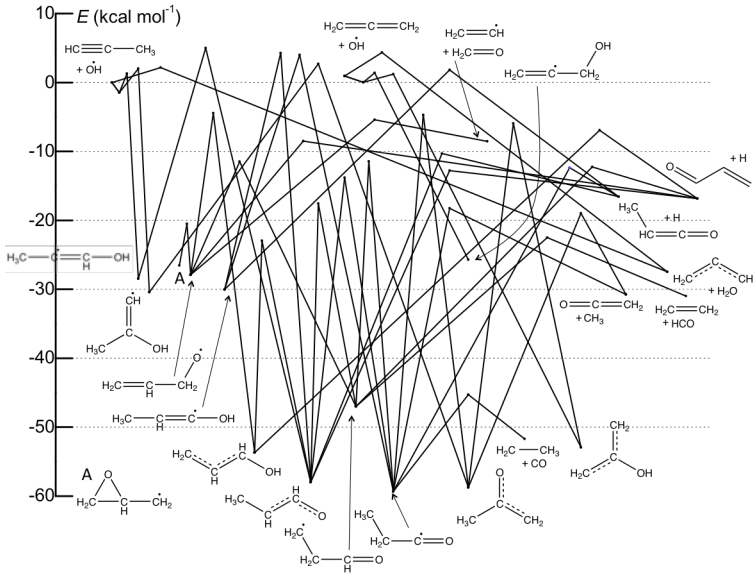

The ZPE-corrected C_3H_5O PES, showing all channels with 5 kcal mol^{-1} threshold above the propyne + OH reactants except a few "cul-de-sac" pathways. The pathways were found automatically using the KinBot software.

software at the UCCSD(T)-F12b/cc-pVQZ-F12//M06-2X/6-311++G(d,p) level of theory. Using RRKM-based 1-D master equations we calculated pressure- and temperature-dependent, channel-specific phenomenological rate coefficients for the bimolecular reactions propyne + OH and allene + OH, and for the unimolecular decomposition of the CH_3CCHOH, $CH_3C(OH)CH$, CH_2CCH_2OH, $CH_2C(OH)CH_2$ primary adducts, and also for the related acetonyl, propionyl, 2-methylvinoxy, and 3-oxo-1-propyl radicals. The major channel of the bimolecular reactions at high temperatures is the formation propargyl + H_2O, which makes the title reactions important players in soot formation at high temperatures. However, below ~1000 K the chemistry is more complex, involving the competition of stabilization, isomerization and dissociation processes. We found that the OH addition to the central carbon of allene has a particularly interesting and complex pressure dependence, caused by the low-lying exit channel to form ketene + CH_3 bimolecular products. We compared our results to a wide range of experimental data and assessed possible uncertainties arising from certain aspects of the theoretical framework.

B. Low-temperature autoignition chemistry

Direct investigation of QOOH radicals The single largest obstacle when studying ephemeral species such as QOOH radicals is their generation in sufficient quantities and purity. QOOH radicals are very short-lived transients in the R + O_2 → ROO → QOOH → P sequence, and, therefore, are never present in high enough concentrations when starting with an alkyl radical. We devised a new experimental strategy to make QOOH radicals: we reacted stable tert-butyl hydroperoxide (TBHP) molecules with photolytically generated Cl atoms at room temperature.

The QOOH radical that is produced, 2-hydroperoxy-2-methylprop-1-yl, dissociates exclusively to form the corresponding cyclic ether (2,2-dimethyl oxirane) + OH. The formation of QOOH was indeed demonstrated by multiplexed photoionization mass spectrometry (MPIMS) measurements by observing the formation of this cyclic ether as the major product species. However, we did not observe the PIE spectrum of this QOOH radical itself, because the structure of the neutral and cation are very different, leading to a poor Frank-Condon overlap. In the presence of oxygen, however, we were able to detect the related OOQOOH radical and record its PI spectrum. This is the first such PIE spectra in the literature. We have also determined the ionization mechanism of this substituted alkylperoxy radical, which was found to be fundamentally different from that of small unsubstituted alkylperoxy radicals.

In another set of experiments we measured OH concentration–time profiles using direct absorption, and were able to derive directly from the experiments rate coefficients for both the pressure dependent decomposition of this QOOH radical as well as for its association reaction with oxygen. The results were compared to, and confirmed by high-level theoretical kinetics calculations. This work breaks fresh ground for further studies on QOOH radicals, and helps build more accurate autoignition models, which critically depend on the chemistry of these short-lived species.

Unconventional peroxy chemistry and the role of low-lying zwitterionic states. For the detailed modeling of combustion chemistry the possibility of unknown pathways is of continual concern, especially for biofuels, where the presence of oxygen atoms can significantly alter the chemical pathways. In our recent work we characterized a low-lying water elimination pathway from key QOOH radicals derived from alcohols. The corresponding saddle-point structure involves the interaction of radical and zwitterionic electronic states. This interaction presents extreme difficulties for electronic structure characterizations, as most standard methods produce two completely different potential curves depending on whether one starts with the corresponding orbital guesses from the reactant side or the product side. On the reactant side, the ROHF HOMO has the character of a carbon-centered radical orbital, while on the product side the HOMO has the character of an OO σ* orbital associated with the breaking OO bond. The latter is a zwitterionic state and has a large dipole moment.

We demonstrated that the properties of this saddle point can be well captured by M06-2X and CCSD(T) methods, which methods produce comparable and low barrier heights. In the HF, MP2, CCSD and CCSD(T) progression the character of the calculated radical and zwitterionic states converge to each other, indicating the importance of excited states.

Experimental evidence for the existence and relevance of this pathway was shown using recently reported MPIMS data from our group on the low-temperature oxidation of isopentanol and isobutanol. In these systems, water elimination is a major pathway, and is likely ubiquitous in low-temperature alcohol oxidation. These findings will substantially alter current alcohol oxidation mechanisms. Moreover, the methods described will be useful for the more general phenomenon of interacting radical and zwitterionic states. More recently, in collaboration with Taatjes, we have investigated the importance of water elimination pathways in QOOH radicals derived from diethyl ketone. However, we found that these QOOHs display a large barrier to eliminate water, and, therefore, it is not important pathway in this case.

Peroxy chemistry plays also an important role in the degradation of organic polymers in the condensed phase. In collaboration with Kevin Leung, we investigated the degradation mechanisms of poly(3-hexylthiophene) (P3HT) theoretically and explored reaction pathways that may lead to the oxidation of the thiophene backbone as a critical step toward disrupting the polymer conjugation. We calculated barrier heights for reactions of the P3HT backbone with oxidizing agents including the hydroxyl radical (OH), hydroperoxide (ROOH), and the peroxyl radical (ROO). We found that an attack of a peroxyl radical on the side chain on the P3HT backbone may provide low barrier reaction pathways to photodegradation of P3HT and other similar polymers with side chains.

C. Uncertainty analysis

Theoretical methods to obtain rate coefficients are essential to fundamental combustion chemistry research, yet the associated uncertainties are greatly unexplored in a systematic manner. In an exploratory work, in collaboration with Najm, we focused on the parametric uncertainties for the hydrogen-atom-abstraction reaction, $CH_3CH(OH)CH_3 + OH \rightarrow CH_3C(OH)CH_3 + H_2O$. The barrier height, one of the lowest vibrational frequencies at the transition state, and the imaginary frequency were identified as the parameters causing the most significant uncertainty in the rate-coefficient calculations. Bayesian inference was employed to determine the joint probability distribution function of these parameters using the experimental data of Dunlop and Tully on isopropanol + OH.[iii]

We found that although most of the commonly used high-level ab initio calculations result in not more than a factor of two difference in the rate coefficient for this specific reaction in the 293 – 745 K temperature range, significant uncertainties remain in these types of calculations. We have clearly demonstrated that it is not necessarily true that the lion's share of the uncertainty in the calculated rate coefficient arises solely due to the uncertainties in the barrier height, and the presented methodology provided a transparent way of assessing the various quantum chemical methods.

III. FUTURE WORK

As a natural continuation of our work on propene + OH,[i,iv] we are currently investigating the OH + 2-butene reaction in collaboration with Sheps. The initial adduct is one of the primary radicals from 2-butanol, therefore, this study will extend our knowledge on butanol chemistry as well. The reaction pathways and conformational space is explored automatically using KinBot to accelerate and systematize the procedure. Our goal is to quantitatively characterize this reaction in the important intermediate (~500 – 700 K) range. The possibility to conduct this reaction both with cis- and trans-butene offers a unique confirmation for the dissociation rate coefficients of 3-hydroxy-2-butyl radicals. Another area of recent interest that we plan to contribute to is the oxidation of heterocycles,[v] where ring-opening pathways can result in significantly different reactivity compared to acyclic compounds.

The past work on uncertainty was only a first step towards understanding the uncertainty in the currently used models. It would be important to explore the inherent correlation of the molecular parameters as obtained from electronic structure calculations better, and if possible, use this information both in the forward uncertainty propagation and the inference step. These correlations would be employed in the construction of the joint prior on the parameters. Such correlation will reduce the uncertainty predictions, and also point to weak points in the model more directly. We recently started to explore the aspects of the isobutyl + O_2 reaction, comparing the effects on the rate coefficients of various electronic

structure methods and hindered rotor treatments, with particular emphasis on many, often ignored details of these calculations. This study will help develop methods for larger molecules, where the most important challenges include the large number of reactive pathways, the computational cost of the electronic structure theory calculations, and the internal motion complexity of the large carbon chains.

We continue to develop the KinBot code to enable fast and systematic exploration of reactive potential energy surfaces, including the conformational space. KinBot is currently being applied to the butyl isomers + O_2, C_2H_4 + $O(^3P)$, cyclopentene + $O(^3P)$, and 2,5-dimethyl-1-hexyl reactive potential energy surfaces.

IV. References

i. Zádor, J.; Jasper, A. W.; Miller, J. A., *Phys. Chem. Chem. Phys.* **2009**, *11*, 11040-11053.
ii. Devolder, P.; Fittschen, C.; Frenzel, A.; Hippler, H.; Poskrebyshev, G.; Striebel, F.; Viskolcz, B., *Phys. Chem. Chem. Phys.* **1999**, *1*, 675-681.
iii. Dunlop, J. R.; Tully, F. P., *J. Phys. Chem.* **1993**, *97*, 6457-6464.
iv. Kappler, C.; Zádor, J.; Welz, O.; Fernandes, R. X.; Olzmann, M.; Taatjes, C. A., *Z. Phys. Chem.* **2011**, *225*, 1271-1293.
v. Roman-Leshkov, Y.; Barrett, C. J.; Liu, Z. Y.; Dumesic, J. A., *Nature* **2007**, *447*, 982-U985.

V. DOE supported publications, 2012-present

1. Zádor, J.; Miller, J. A., Adventures on the C_3H_5O potential energy surface: OH + propyne, OH + allene and related reactions. *Proc. Combust. Inst.* accepted.
2. Eskola, A. J.; Welz, O.; Zádor, J.; Antonov, I. O.; Sheps, L.; Savee, J. D.; Osborn, D. L.; Taatjes, C. A., Probing the low-temperature chain-branching mechanism for n-butane autoignition chemistry via time-resolved measurements of ketohydroperoxide formation in photolytically initiated *n*-C_4H_{10} oxidation. *Proc. Combust. Inst.* accepted.
3. Scheer, A. M.; Welz, O.; Zádor, J.; Osborn, D. L.; Taatjes, C. A., Low-temperature combustion chemistry of novel biofuels: Resonance-stabilized QOOH in the oxidation of diethyl ketone. *Phys. Chem. Chem. Phys.* **2014**, *Online*.
4. Sai, N.; Leung, K.; Zádor, J.; Graeme, H., First principles study of photo-oxidation degradation mechanisms in P3HT for organic solar cells. *Phys. Chem. Chem. Phys.* **2014**, *Online*.
5. Zádor, J.; Huang, H.; Welz, O.; Zetterberg, J.; Osborn, D. L.; Taatjes, C. A., Directly measuring reaction kinetics of QOOH – a crucial but elusive intermediate in hydrocarbon autoignition. *Phys. Chem. Chem. Phys.* **2013**, *15*, 10753-10760.
6. Welz, O.; Klippenstein, S. J.; Harding, L. B.; Taatjes, C. A.; Zádor, J. Unconventional peroxy chemistry in alcohol oxidation: The water elimination pathway. *J. Phys. Chem. Lett.* **2013**, *4*, 350.
7. Zádor, J.; Miller, J. A., Unimolecular dissociation of hydroxypropyl and propoxy radicals. *Proc. Combust. Inst.* **2013**, *34*, 519-526.
8. Welz, O.; Zádor, J.; Savee, J. D.; Sheps, L.; Osborn, D. L.; Taatjes, C. A., Low-temperature combustion chemistry of n-butanol: Principal oxidation pathways of hydroxybutyl radicals. *J. Phys. Chem. A* **2013**, *117*, 11983−12001.
9. Prager, J.; Najm, N. H.; Zádor, J., Uncertainty quantification in the ab initio rate-coefficient calculation for the $CH_3CH(OH)CH_3$ + OH → $CH_3C(OH)CH_3$ + H_2O reaction. *Proc. Combust. Inst.* **2013**, *34*, 583-590.
10. Welz, O.; Zádor, J.; Savee, J. D.; Ng, M. Y.; Meloni, G.; Fernandes, R. X.; Sheps, L.; Simmons, B. A.; Lee, T. S.; Osborn, D. L.; Taatjes, C. A., Low-temperature combustion chemistry of biofuels: pathways in the initial low-temperature (550 K-750 K) oxidation chemistry of isopentanol. *Phys. Chem. Chem. Phys.* **2012**, *14*, 3112-3127.

Isomer-specific Spectroscopy and Pyrolysis of Model Aromatic Fuels

Timothy S. Zwier
Department of Chemistry, Purdue University, West Lafayette, IN 47907-2084
zwier@purdue.edu

Program Definition and Scope

The chemical complexity of hydrocarbon fuels and the fast-expanding list of potential plant-derived biofuels offer a challenge to the scientific community seeking to provide a molecular-scale understanding of their combustion. The development of accurate combustion models stands on a foundation of experimental data on the kinetics and product branching ratios of individual reaction steps. Spectroscopic tools need to continue to be developed to selectively detect and characterize the widening array of fuel components and the reactive intermediates they generate upon pyrolysis and combustion. There is growing recognition that a key component of future progress in the field is the development of detection schemes that are isomer-specific and even conformation-specific. This project uses an array of laser-based and broadband microwave methods to carry out isomer-specific and conformation-specific spectroscopy on key fuel components and the reactive intermediates formed during their pyrolysis and combustion.

Recent Progress

A. Toward a first principles model of the alkyl CH stretch region (ref. 7, 13)

The alkyl CH stretch region of the infrared is a region rich in information content, but a challenge to assign, due to the ubiquitous presence of strong Fermi resonance mixing between the alkyl CH stretch and CH bend overtone levels. Conformational assignments based on a comparison of the observed alkyl CH stretch spectra with *ab initio* predictions of harmonic frequencies often fail in spectacular fashion due to these Fermi resonances, which shift and split bands to the point that comparison with harmonic calculations is fruitless. Working in collaboration with Ned Sibert (UW-Madison), we are developing a first-principles model of the alkyl CH stretch region built around a reduced dimension Hamiltonian in which anharmonic CH stretches and scissor modes are Fermi coupled. The phenyl capped alkyl and ether chains present in 1,2-diphenylethane (C_6H_2-CH_2-CH_2-C_6H_5, DPE, ref. 6) and 1,2-diphenoxyethane (C_6H_5-O-CH_2-CH_2-O-C_6H_5, DPOE, ref. 7) served as initial model conformationally flexible chains that contain only CH_2 groups, and therefore are easier to model theoretically.

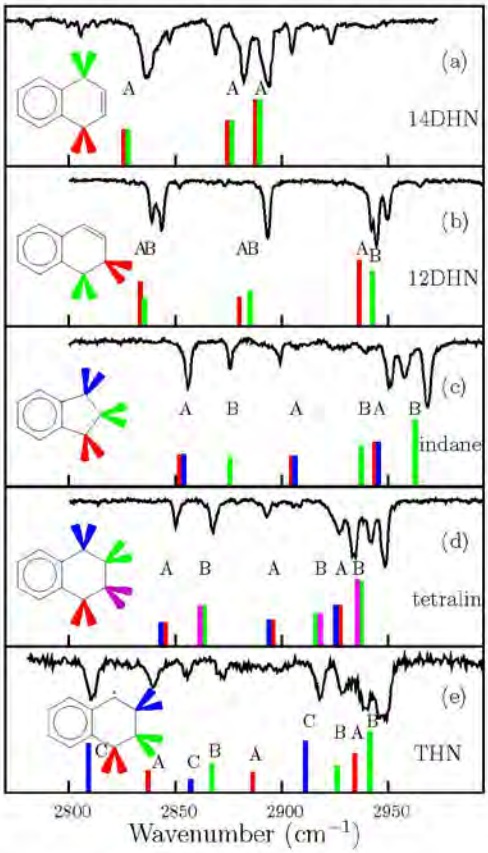

Figure 1: Experimental ground state infrared spectra in the alkyl CH stretch region, compared with the results of the decoupled CH_2 model.

During the past year we have extended the model to a series of hydrogenated naphthalene derivatives including tetralin, 1,2-dihydronaphthalene, 1,4-dihydronaphthalene, indene, and indane. Similar data on the trihydronaphthyl radical and

inden-2-ylmethyl radicals completed the series. Despite the fact that the individual spectra are quite different in appearance from one another, the theoretical model developed by Sibert is able to account for the experimental CH stretch spectra of the entire set of molecules in significant detail. Figure 1 shows the alkyl CH stretch spectra of key members of that series, with sticks presenting the predictions of a simplified version of the model in which the CH_2 groups are decoupled from one another. This simplified model makes it possible to assign and understand the individual spectra, and led to a prediction for the spectrum of cyclohexane, which awaits experimental verification. A manuscript describing this work is accepted in JPCA (ref. 13).

B. Vibronic coupling in near-degenerate excited states (ref. 8)

Beyond their role in modeling alkyl CH stretch spectra, the flexible bichromophore DPOE has served a dual purpose as a benchmark system in which to study vibronic coupling involving the two aromatic chromophores. We have carried out a detailed spectroscopic characterization of DPOE in the region of its S_1/S_2 states, and have proven that they are separated from one another by ~1 cm^{-1} out of 36000, putting the molecule in the extreme case of weak vibronic coupling. This work was described in some detail in last year's abstract, which has now been published (8).

C. Resonance-stabilized radicals (ref. 9, 12)

We also continue to pursue isomer-specific and conformation-specific spectroscopy of resonance-stabilized radicals. During the past year, we completed our analysis and published a detailed study of the R2PI, LIF excitation, dispersed fluorescence, and alkyl CH stretch infrared spectra of α–methylbenzyl radical C_6H_5-ĊH-CH_3 (ref. 9). Our interest in this radical is fueled by the fact that the methyl radical rocks against the primary radical site of this resonance-stabilized radicals. The excited state calculations, carried out in collaboration with Lyudmila Slipchenko, show that benzyl-type radicals continue to be an exceptional challenge to theory, with two close-lying excited states, open-shell character, and strong vibronic coupling.

We have followed up this study with an analogous one on the CH stretch infrared spectra of trihydronaphthyl (THN) radical and inden-2-ylmethyl (I2M) radicals, two resonance-stabilized radicals of some interest in pathways that lead towards PAHs in flames. Like the work on α–methylbenzyl, a unique aspect of this study is its inclusion of infrared spectra in both ground and excited electronic states. Sibert's first-principles model of the alkyl CH stretch region of THN (Fig. 1e) and I2M (not shown) works equally well for radicals as for stable molecules (Figure 1a-d). Interestingly, in the excited state, parts of the spectrum are seemingly missing, leading us to postulate the presence of dissociative pathways along certain CH bonds that broaden or shift the spectrum. A manuscript describing this work has just been submitted (12).

D. Model lignin compounds and biofuels (ref. 10, 11)

Among the important degradation products in the combustion and pyrolysis of wood are methoxyphenols, the aromatic chromophore pervasive to lignin, shared by the three monolignols. The UV spectroscopy of a series of simple methoxyphenols shows a striking sensitivity to the position and number of OH and/or OCH_3 groups on the aromatic ring.

We also have just completed a study of the UV spectroscopy of two model lignin dimers, in which the prototypical guaiacyl chromophores are connected to one another by two of the most abundant and important chemical linkages in lignin, the β-O-4 and β–β linkages (ref. 11). These linkages are very different in their conformational landscapes, with the former much more flexible than the latter. Intramolecular H-bonds along the β-O-4 linkages and between the linkage and the aromatic rings are present.

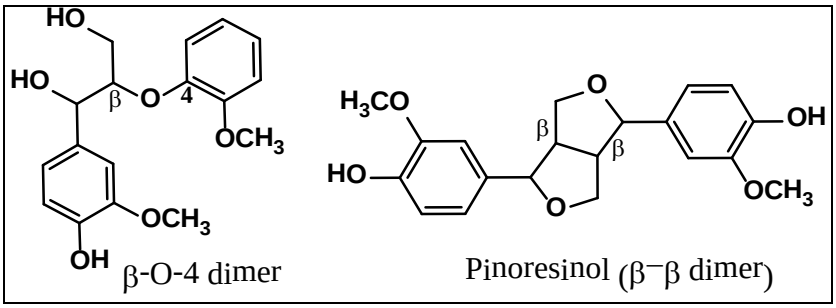

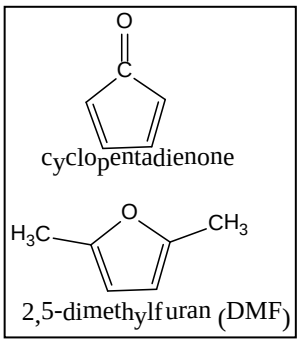

E. Broadband microwave spectroscopy of intermediates formed in flash pyrolysis (ref. 12)

Over the past year, we have set off in a new direction that will serve as an important launch point for our future work, involving the use of a hyperthermal nozzle (or Chen nozzle) to create reactive intermediates from pyrolysis or combustion for spectroscopic interrogation. This interrogation will involve either of two complementary detection schemes: mass-resolved detection in our molecular beam time-of-flight mass spectrometer, or via chirped-pulse Fourier transform microwave (CP-FTMW) spectroscopy.

As an illustration, Figure 3 displays a 200 MHz portion of the full spectrum of the pyrolysis of phenylene sulfite, a molecule synthesized by the Ellison group at CU-Boulder, which is known to undergo efficient thermal degradation to form cyclopentadienone, a prototypical "anti-aromatic". The 2_{02}-1_{01} rotational transition of the all ^{12}C isotopomer of cyclopentadienone (CPD) is identified in red in the computed spectrum below experiment. Its intensity is 50- or 100-fold greater than the transitions marked by green, brown, and blue sticks that locate the corresponding transitions of the single ^{13}C isotopomers of CPD in natural abundance. All other transitions are due to the precursor. Such isotopic data are being used to locate the positions of these atoms to high precision, obtaining r_0 and r_e structures. This analysis is being carried out in collaboration with John Stanton at UT-Austin.

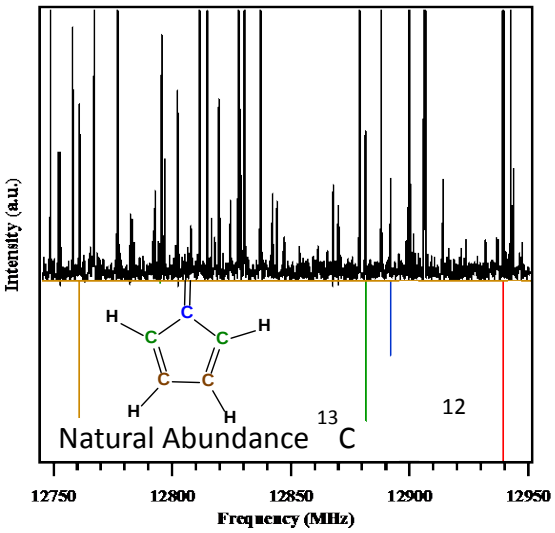

Figure 3: 200 MHz portion of the CP-FTMW spectrum of the pyrolysis effluent from the hyperthermal nozzle using phenylene sulfite as precursor. Calculated frequencies and intensities of 2_{02}-1_{01} transitions of CPD due to natural-abundance ^{13}C are shown as sticks below.

Future Work

In collaboration with Ned Sibert, we are extending our CH stretch model to include methyl groups, and plan to study the alkyl CH stretch spectroscopy of a series of phenyl alkanes and methoxyphenols. We also will study the R2PI and IR spectroscopy of phenylalkyl radicals with radical sites along the alkyl chain. R2PI, IR, and CP-FTMW spectra of key pyrolysis intermediates from methylfuran and 2,5-dimethylfuran will also be subjects of future work. Finally, one of the directions we hope to explore is the production of two-dimensional CP-FTMW spectra that show off-diagonal couplings connecting microwave transitions due to a single species in the pyrolysis sample. Such 2D spectra will be extraordinarily powerful means of deciphering which microwave transitions are shared by a single species, aiding in their assignment, much as is done in NMR spectroscopy.

Publications acknowledging DOE support, 2011-present

1. Joshua A. Sebree, Nathan Kidwell, Evan G. Buchanan, Marek Zgierski, and Timothy S. Zwier, "Spectroscopy and Ionization Thresholds of π-Isoelectronic 1-Phenylallyl and Benzylallenyl Resonance Stabilized Radicals", Chemical Science, **2**, 1746-1754 (2011).

2. Chirantha P. Rodrigo, William H. James III, and Timothy S. Zwier, "Single-conformation ultraviolet and infrared spectra of jet-cooled monolignols: p-coumaryl alcohol, coniferyl alcohol, and sinapyl alcohol", J. Am. Chem. Soc. **133**, 2632-2641 (2011).

3. Chirantha P. Rodrigo, Christian W. Müller, Nathan R. Pillsbury, William H. James III, Timothy S. Zwier, and David F. Plusquellic, "Conformer-specific vibronic spectroscopy and vibronic coupling in a flexible bichromophore: bis-(4-hydroxyphenyl)methane", J. Chem. Phys. **134**, 164312 (2011).

4. Shin G. Chou, Chirantha P. Rodrigo, Christian W. Müller, Kevin O. Douglass, Timothy S. Zwier, and David F. Plusquellic, "Rotationally resolved C_2 symmetric conformers of bis-(4-hydroxyphenyl)-methane: Prototypical examples of Excitonic coupling in the S_1 and S_2 Electronic States, J. Phys. Chem. A **115**, 9643-9652 (2011).

5. Jacob C. Dean, Deepali Mehta, William H. James III, and Timothy S. Zwier, "Conformation-specific spectroscopy and populations of diastereomers of a model monolignol derivative: Chiral effects in a triol chain", J. Phys. Chem. A **115**, 8464-8478 (2011).

6. Evan G. Buchanan, Jacob C. Dean, Timothy S. Zwier, and Edwin L. Sibert III, "Towards a first-principles model of Fermi resonances in the alkyl CH stretch region: Application to 1,2-diphenylethane and 2,2,2-paracyclophane", J. Chem. Phys. **134**, 064308 (2013). 11 pages.

7. Evan G. Buchanan, Edwin L. Sibert III, and Timothy S. Zwier, Ground state Conformational Preferences and CH stretch-bend coupling in a model alkoxy chain: 1,2-diphenoxyethane", J. Phys. Chem. A **117**, 2800-2811 (2013).

8. Evan G. Buchanan, David F. Plusquellic, and Timothy S. Zwier, "Excitonic splitting and vibronic coupling in 1,2-diphenoxyethane: Conformation-specific effects in the weak coupling limit", J. Chem. Phys. **138** 204313 (2013). 11 pages.

9. Nathanael M. Kidwell, Neil J. Reilly, Ben Nebgen, Deepali N. Mehta-Hurt, Ross D. Hoehn, Damian L. Kokkin, Michael C. McCarthy, Lyudmila V. Slipchenko, and Timothy S. Zwier, "Jet-cooled Spectroscopy of the α–Methylbenzyl Radical: Probing the State-Dependent Effects of Methyl Rocking against a Radical Site", *J. Phys. Chem. A*, **117**, 13465-80 (2013).

10. Jacob C. Dean, Polina Navotnaya, Alexander P. Parobek, Rachel M. Clayton, and Timothy S. Zwier, "Ultraviolet spectroscopy of fundamental Lignin sub-units: Guaiacol, 4-methylguaiacol, syringol, and 4-methylsyringol", **139**, 144313 (2013). (16 pages)

11. Jacob C. Dean, Patrick S. Walsh, Bidyut Biswas, P. V. Ramachandran, and Timothy S. Zwier, "Single-conformation UV and IR spectroscopy of model G-type lignin dilignols: the β-O-4 and β–β linkages", Chem. Sci., **5**, 1940 – 1955 (2014).

12. Edwin L. Sibert III, Nathanael M. Kidwell, and Timothy S. Zwier, "A First-Principles Model of Fermi Resonance in the Alkyl CH Stretch Region: Application to Hydronaphthalenes, Indanes, and Cyclohexane", J. Phys. Chem. A **DOI:** 10.1021/jp5014048.

Participant List

34th Annual Combustion Research Meeting Participation List

Last Name	First Name	Organization	Email
Ahmed	Musahid	Lawrence Berkeley National Laboratory	mahmed@lbl.gov
Alexander	millard	University of Maryland	mha@umd.edu
Allen	Wesley	University of Georgia	wdallen@uga.edu
Barlow	Robert	Sandia National Laboratories	barlow@sandia.gov
Belkacem	Ali	Lawrence Berkeley National Laboratory	abelkacem@lbl.gov
Bellan	Josette	California Institute of Technology, Jet Propulsion Laboratory	Josette.Bellan@jpl.nasa.gov
Blanquart	Guillaume	California Institute of Technology, Jet Propulsion Laboratory	g.blanquart@caltech.edu
Bowman	Joel	Emory University	jmbowma@emory.edu
Bunel	Emilio	Argonne National Laboratory	ebunel@anl.gov
Butler	Laurie	The University of Chicago	L-Butler@uchicago.edu
Chandler	David	Sandia National Laboratories	gdecast@sandia.gov
Chen	Jacqueline	Sandia National Laboratories	jhchen@sandia.gov
Continetti	Robert	UC San Diego	rcontinetti@ucsd.edu
Crim	Fleming	University of Wisconsin	fcrim@chem.wisc.edu
Dagdigian	Paul	Johns Hopkins University	pjdagdigian@jhu.edu
Dahms	Rainer	Sandia National Laboratories	Rndahms@sandia.gov
Davis	Michael	Argonne National Laboratory	davis@tcg.anl.gov
Davis	H. Floyd	Cornell University	hfd1@cornell.edu
Dawes	Richard	Missouri University of Science and Technology	dawesr@mst.edu
Dibble	Theodore	SUNY-Env. Sci. & Forestry	tsdibble@esf.edu
Douberly	Gary	University of Georgia	douberly@uga.edu
Field	Robert	MIT	rwfield@mit.edu
Frank	Jonathan	Sandia National Laboratories	jhfrank@sandia.gov
Green	William	Massachusetts Institute of Technology	whgreen@mit.edu
Guo	Hua	University of New Mexico	hguo@unm.edu

Hall	Gregory	Brookhaven National Lab	gehall@bnl.gov
Hanson	Ronald	Stanford University	rkhanson@stanford.edu
Harding	Lawrence	Argonne National Laboratory	harding@anl.gov
Harris	Alexander	Brookhaven National Laboratory	alexh@bnl.gov
Head-Gordon	Martin	Lawrence Berkeley National Laboratory	mhg@cchem.berkeley.edu
Hershberger	John	North Dakota State University	john.hershberger@ndsu.edu
Hirata	So	University of Illinois at Urbana-Champaign	sohirata@illinois.edu
Hoffmann	Mark	University of North Dakota	mark.hoffmann@email.und.edu
Hwang	Robert	Sandia National Laboratories	gdecast@sandia.gov
Jasper	Ahren	Sandia National Laboratories	ajasper@sandia.gov
Kaiser	Ralf	University of Hawaii	ralfk@hawaii.edu
Kellman	Michael	University of Oregon	kellman@uoregon.edu
Kirchhoff	William	DOE/BES (RET)	william.kirchhoff@att.net
Kliewer	Christopher	Sandia National Laboratories	cjkliew@sandia.gov
Klippenstein	Stephen	Argonne National Laboratory	sjk@anl.gov
Kostko	Oleg	Lawrence Berkeley National Lab	okostko@lbl.gov
Krause	Jeffrey	Department of Energy	jeff.krause@science.doe.gov
Krylov	Anna	USC	krylov@usc.edu
Leone	Stephen	Univ. of California and LBNL	srl@berkeley.edu
Lester	Marsha	University of Pennsylvania	milester@sas.upenn.edu
Lester Jr.	William A.	University of California Lawrence Berkeley Laboratory	walester@lbl.gov
Long	Marshall	Yale University	marshall.long@yale.edu
Lu	Tianfeng	University of Connecticut	tlu@engr.uconn.edu
Manley	Dawn	Sandia National Laboratories	dmanley@sandia.gov
Marceau	Diane	Department of Energy	diane.marceau@science.doe.doe
Mebel	Alexander	Florida International University	mebela@fiu.edu
Michael	Joe	Argonne National Laboratory	jmichael@anl.gov
Michelsen	Hope	Sandia National Labs	hamiche@sandia.gov
Miller	William H.	University of California Lawrence Berkeley Laboratory	millerwh@berkeley.edu
Miller	James	Argonne National Laboratory	jim.miller1946@gmail.com
Miller	Terry	The Ohio State University	miller.104@osu.edu
Mullin	Amy	University of Maryland	mullin@umd.edu

Najm	Habib	Sandia National Laboratories	hnnajm@sandia.gov
Nesbitt	David	JILA/University of Colorado	djn@jila.colorado.edu
Ng	Cheuk-Yiu	University of California, Davis	cyng@ucdavis.edu
Oefelein	Joseph	Sandia National Laboratories	oefelei@sandia.gov
Oran	Elaine	University of Maryland	eoran@umd.edu
Osborn	David	Sandia National Laboratories	dlosbor@sandia.gov
Parish	Carol	University of Richmond	cparish@richmond.edu
Pederson	Mark	Department of Energy	mark.pederson@science.doe.gov
Pepiot	Perrine	Cornell University	pp427@cornell.edu
Perry	David	The University of Akron	dperry@uakron.edu
Piecuch	Piotr	Michigan State University, Department of Chemistry	piecuch@chemistry.msu.edu
Pitz	William	Lawrence Livermore National Laboratory	pitz1@llnl.gov
Pope	Stephen	Cornell University	s.b.pope@cornell.edu
Pratt	Stephen	Argonne National Laboratory	stpratt@anl.gov
Reisler	Hanna	University of Southern California	reisler@usc.edu
Robert	Lucht	Purdue University	lucht@purdue.edu
Ruscic	Branko	Argonne National Laboratory	ruscic@anl.gov
Schaefer	Henry	Center for Computational Quantum Chemistry	qc@uga.edu
Sears	Trevor	Brookhaven National Laboratory	sears@bnl.gov
Settersten	Thomas	Department of Energy	thomas.settersten@Science.Doe.gov
Shaddix	Christopher	Sandia National Labs	crshadd@sandia.gov
Shepard	Ron	Argonne National Laboratory	shepard@tcg.anl.gov
Sheps	Leonid	Sandia National Laboratories	lsheps@sandia.gov
Sisk	Wade	Department of Energy	Wade.Sisk@science.doe.gov
Sivaramakrishnan	Raghu	Argonne National Laboratory	raghu@anl.gov
Smooke	Mitchell	Yale University	mitchell.smooke@yale.edu
Som	Sibendu	Argonne National Laboratory	ssom@anl.gov
Stanton	John	University of Texas	jfstanton@mail.utexas.edu
Suits	Arthur	Wayne State University	asuits@wayne.edu
Sutherland	James	University of Utah	James.Sutherland@utah.edu
Taatjes	Craig	Sandia National Labs	cataatj@sandia.gov
Tranter	Robert	Argonne National Laboratory	tranter@anl.gov

Truhlar	Donald	University of Minnesota	truhlar@umn.edu
Violi	Angela	University of Michigan	avioli@umich.edu
Wagner	Albert	Argonne National Laboratory	wagner@anl.gov
Westbrook	Charles	Lawrence Berkeley National Lab	westbrookck@earthlink.net
Wilson	Kevin	Lawrence Berkeley National Lab	krwilson@lbl.gov
Wittig	Curt	University of Southern California	wittig@usc.edu
Wooldridge	Margaret	University of Michigan	mswool@umich.edu
Yarkony	David	Johns Hopkins University	yarkony@jhu.edu
Yu	Hua-Gen	Brookhaven National Laboratory	hgy@bnl.gov
Zádor	Judit	Sandia National Laboratories	jzador@sandia.gov
Zwier	Timothy	Purdue University	zwier@purdue.edu